Dolomite Recrystallization Along the Rimbey-Meadowbrook Reef Trend, Western Canada Sedimentary Basin, Alberta, Canada

by

Sergey Kuflevskiy

A thesis submitted in partial fulfillment of the requirements for the degree of

Master of Science

Department of Earth and Atmospheric Sciences
University of Alberta

ABSTRACT

Three theoretical alternatives of what can happen to dolomite when it recrystallizes (steady recrystallization, stepwise recrystallization, or no recognizable signs of recrystallization) were tested on Leduc dolomites of the Devonian Rimbey–Meadowbrook reef trend located in Alberta, Canada.

Four textural types of matrix dolomite, R1, R2, R3 and R4, were distinguished based on crystal size distribution and crystal geometry.

Stabilization from initially formed replacive, metastable dolomite to well-ordered, nearly stoichiometric, and stable dolomite in the reef trend likely took place within a very short time after initial formation, analogous to experimental results in which initially formed metastable (proto-) dolomite recrystallizes via Ostwald's step rule very soon after the initial calcite replacement. However this process is not recognizable in these ancient dolomites. Rather, initial dolomitization with ensuing recrystallization via Ostwald's step rule appear as one process.

Fine crystalline matrix dolomite R1 is interpreted as the 'least-altered' dolomite phase that is geochemically and petrographically the closest to the initial replacive dolomite. The fluids responsible for initial dolomitization and early recrystallization appear to be normal to near-normal marine waters. Dolomitization with ensuing early recrystallization likely occurred during Late Devonian to Early Carboniferous times.

At least some medium crystalline matrix dolomite R2 and coarsely crystalline porous R3 are interpreted to have formed by further recrystallization of a microcrystalline R1 precursor at deeper burial by warmer connate formation fluids. Mixing of dense brines of the Cooking Lake aquifer and meteoric waters of the Lower Mannville aquifer significantly affected the region north from township 44, causing depletion of $\delta^{18}O$ values and enrichment in $\delta^{13}C$, $^{87}Sr/^{86}Sr$, trace elements and REE compositions.

In loving memory of my father Vladimir Kuflevskiy.

ACKNOWLEDGEMENTS

TABLE OF CONTENTS

APPENDICIES

LIST OF TABLES

CHAPTER 8

LIST OF FIGURES

Page

CHAPTER 4

CHAPTER 5

CHAPTER 6

CHAPTER 7

CHAPTER 8

LIST OF PLATES

CHAPTER 1

INTRODUCTION

1.1 Introduction

The Upper Devonian Rimbey–Meadowbrook reef trend located in Central Alberta, Canada (Figure 1.1.1) has received great attention because of considerable economic interest towards its hydrocarbon reservoirs. This "Golden Trend" was the source of the first oil discovered in central Alberta and is still an active exploration target today (Dembicki and Podivinsky, 2012).

The petroleum reservoirs along the Rimbey-Meadowbrook reef trend belong to the Upper Devonian Woodbend Group (Figure 1.1.2), which consists of a thick sequence of shallow-water platform carbonates (Cooking Lake Formation), numerous platform margin reef buildups (Leduc Formation), and basin-filling shales and limestones (Majeau Lake Member, Duvernay and Ireton Formations). The Cooking Lake and Leduc Formations along the reef trend are extensively dolomitized. The origin of the Leduc replacement dolomites, the source of dolomitizing fluids, and the mechanisms responsible for transporting and moving these fluids, as well as the degree of recrystallization remain uncertain. Burial compaction or some form of relatively shallow-intermediate (~500 – 1500 m) seawater convection have been previously identified as the most likely alternatives (Amthor *et al.*, 1993, 1994; Drivet, 1993; Drivet and Mountjoy, 1997; Mountjoy *et al.*, 1999).
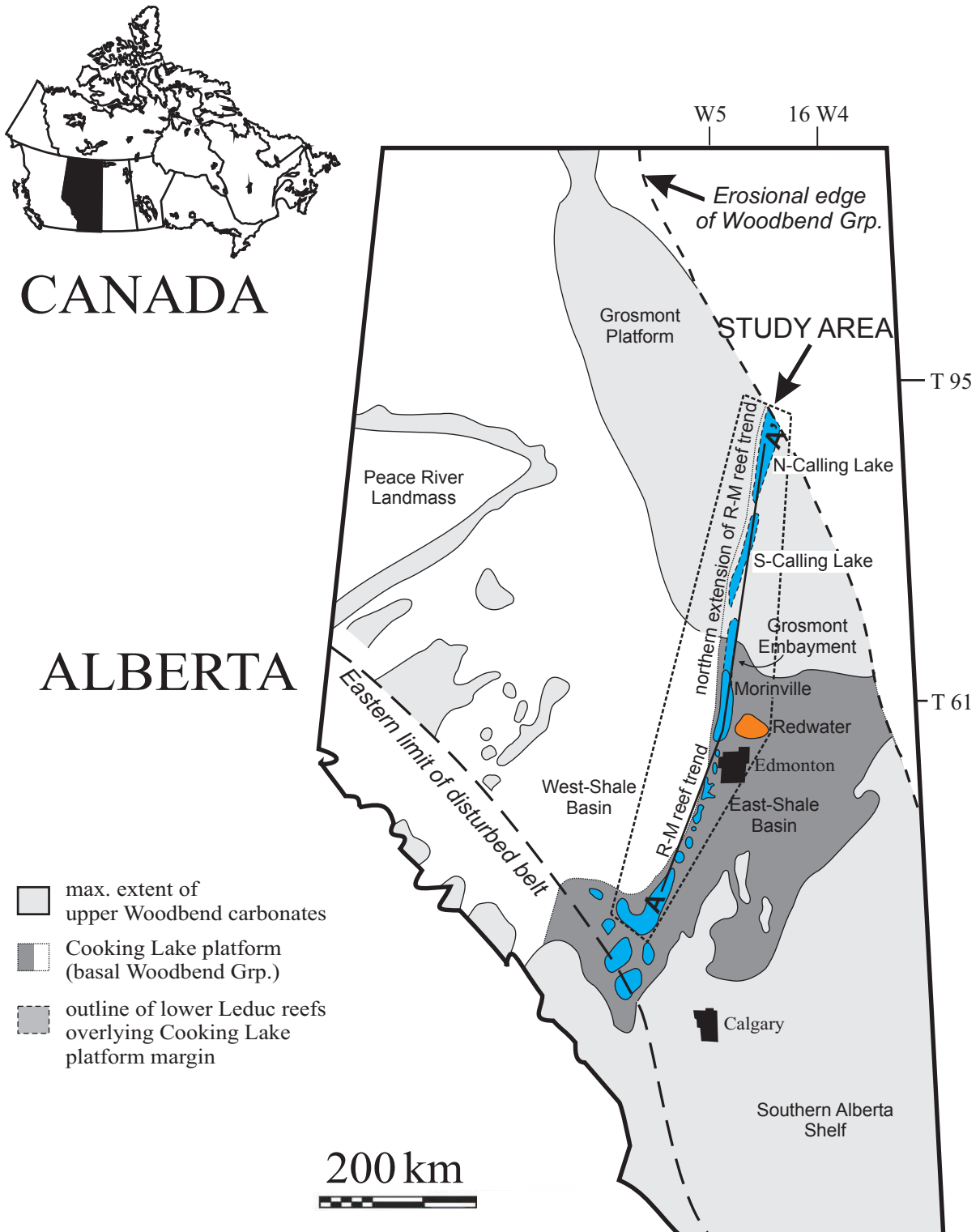
Figure 1.1.1. Location map of the study area in Alberta, Canada.
R-M reef trend = Rimbey-Meadowbrook reef trend. Modified from Huebscher, 1996.

The map contains the following labels:

W5   16 W4

Erosional edge
of Woodbend Grp.

Grosmont
Platform

STUDY AREA

T 95

N-Calling Lake

Peace River
Landmass

S-Calling Lake

Grosmont
Embayment

ALBERTA

Morinville

T 61

Redwater

Edmonton

West-Shale
Basin

East-Shale
Basin

northern extension of R-M reef trend

R-M reef trend

Eastern limit of disturbed belt

CANADA

max. extent of
upper Woodbend carbonates

Cooking Lake platform
(basal Woodbend Grp.)

outline of lower Leduc reefs
overlying Cooking Lake
platform margin

200 km

Calgary

Southern Alberta
Shelf

Figure 1.1.2. Schematic subsurface lithostratigraphy of the Upper Devonian in central Alberta. (Modified from Horrigan, 1996)

A clear understanding of the outlined aspects is important for the oil industry because diagenetic processes, particularly dolomite recrystallization in these reefs, were closely related to and had a strong influence on the accumulation and migration of petroleum. The porosity, permeability, and, hence, the oil- and gas- bearing potential of these carbonate reservoirs might have been diagenetically affected by the dolomitization of this trend (Horrigan, 1996).

The primary purpose of this chapter is to define the term 'recrystallization' and to discuss possible alternatives of what can happen to dolomite when it starts recrystallizing.

The term 'recrystallization' was initially proposed by Sorby in the mid-to-late 1800s as a "reorganization of the mineral or metallic constituents". Folk (1965) substituted it with the term 'neomorphism' which did not gain much attention and was essentially

abandoned. Machel (1997) suggested an extended definition of the term 'recrystallization' and included the following characteristics: textural changes in crystal size and shapes; structural changes in ordering and in strain; compositional changes in stoichiometry, trace elements, isotopic ratios, and fluid inclusion properties; and changes in the paleomagnetic properties. He also established two categories: '*significant recrystallization*' when at least "*one of the measurable properties is modified to a range larger than that in the original crystals*"; and '*insignificant recrystallization*' when "*the changes are so small that the total range of properties after recrystallization is the same as when the dolomite first formed*" (Machel, 1997).

There are differing opinions on what happens to dolomite when it starts recrystallizing. Some authors claim that most dolomites recrystallize during burial forming a gradual trend with depth (Sperber *et al.*, 1984). Others, like Land (1992) and Kaczmarek and Sibley (2007, 2011, 2012, 2014), suggest that initially metastable (proto-) dolomite recrystallizes to stable dolomite via Ostwald's step rule (Ostwald, 1897). Neither of these hypotheses has been proven.

Due to its considerable length and commensurate depth variation, the Rimbey-Meadowbrook reef trend provides an excellent opportunity to test these hypotheses. A specific petrographic type of dolomite, matrix-replacive dolomite, at a specific stratigraphic level can be traced from one end of the trend to the other. The Cooking Lake and Leduc Formations are appropriate for this purpose because they were formed at about the same time, and then buried to depths ranging from ~200m to about 6-8 km (Switzer *et al.*, 1994). The best petrographic choice for testing these hypotheses would be grey matrix

replacement dolomite, which occurs in several sub-types that appear to be genetically related, and which are almost ubiquitous along the entire reef trend.

There are at least three theoretical outcomes of this research (Figure 1.1.3):

1) no measurable signs of recrystallization;

2) recrystallization with depth in a more or less steady form – steady recrystallization;

3) recrystallization with depth in a stepwise manner – stepwise recrystallization;

4) something "other".
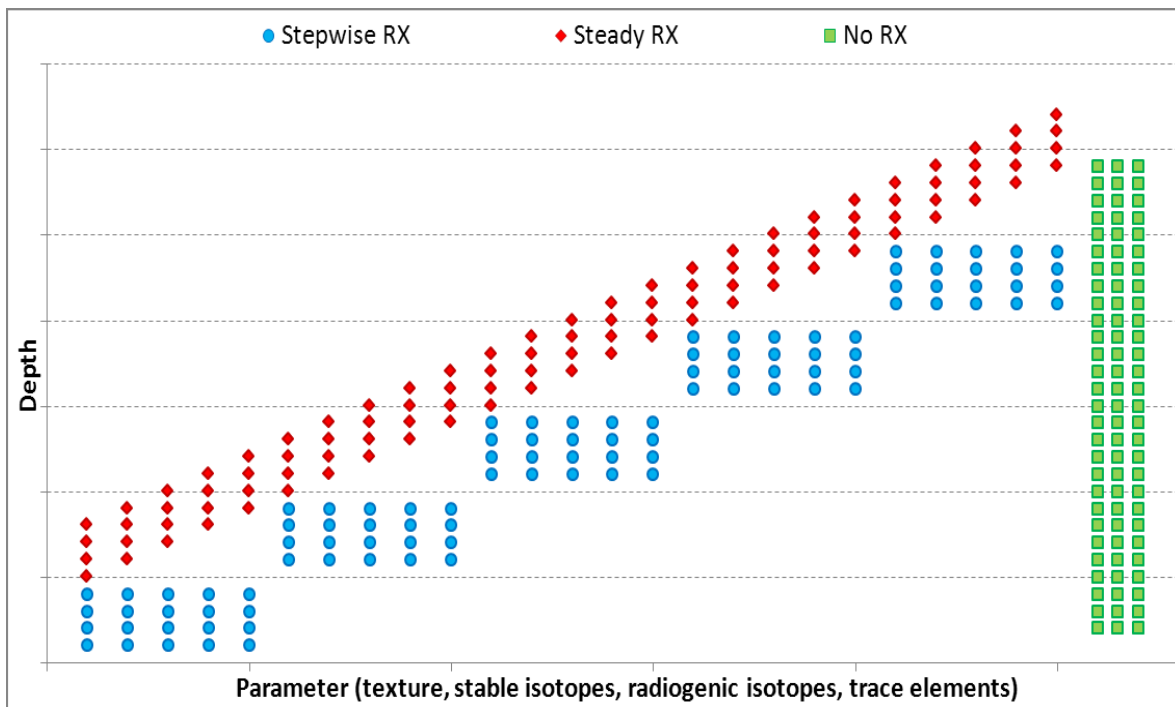
Figure 1.1.3. Possible alternatives of dolomite recrystallization (RX = recrystallization).

1.2 Previous work

Although there had been some discoveries of oil and gas in southern Alberta in 1904 and 1914 near Waterton and Turner Valley in Southern Alberta (Mossop and Shetsen, 1994), work on the Rimbey-Meadowbrook reef trend was begun by Imperial Oil Limited, who discovered oil near the town of Leduc in 1947 (Imperial Oil Limited, Geological Staff, 1950). In later papers (Baugh, 1950; Waring and Layer, 1950; Andrichuk, 1958a, b) it was pointed out that all the Leduc reefs of this trend are located along the western margin of the underlying Cooking Lake platform, and that most of them are completely dolomitized.

The reason for extensive dolomitization of these Leduc reefs is still unclear. Illing (1959) proposed that the fluids for dolomitization were derived via compaction from the adjacent Ireton, Duvernay and Cooking Lake strata. Stoakes and Creaney (1984) suggested that the Cooking Lake platform functioned as a "pipeline" for the migration of oil (Figure 1.2.1), and that this "pipeline" acted as a conduit for earlier compactional dewatering of the adjacent basin. Later it was suggested that this conduit was also responsible for funnelling the dolomitizing fluids into the Leduc buildups (Machel and Mountjoy, 1987; Machel and Anderson, 1989; Amthor *et al.*, 1993, 1994).

Drivet (1993), Marquez (1994) and Horrigan (1996) worked on the southern part of the reef trend in order to assess the validity of the regional fluid flow hypothesis of Amthor *et al*. (1993), who questioned the burial compaction model of dolomitization
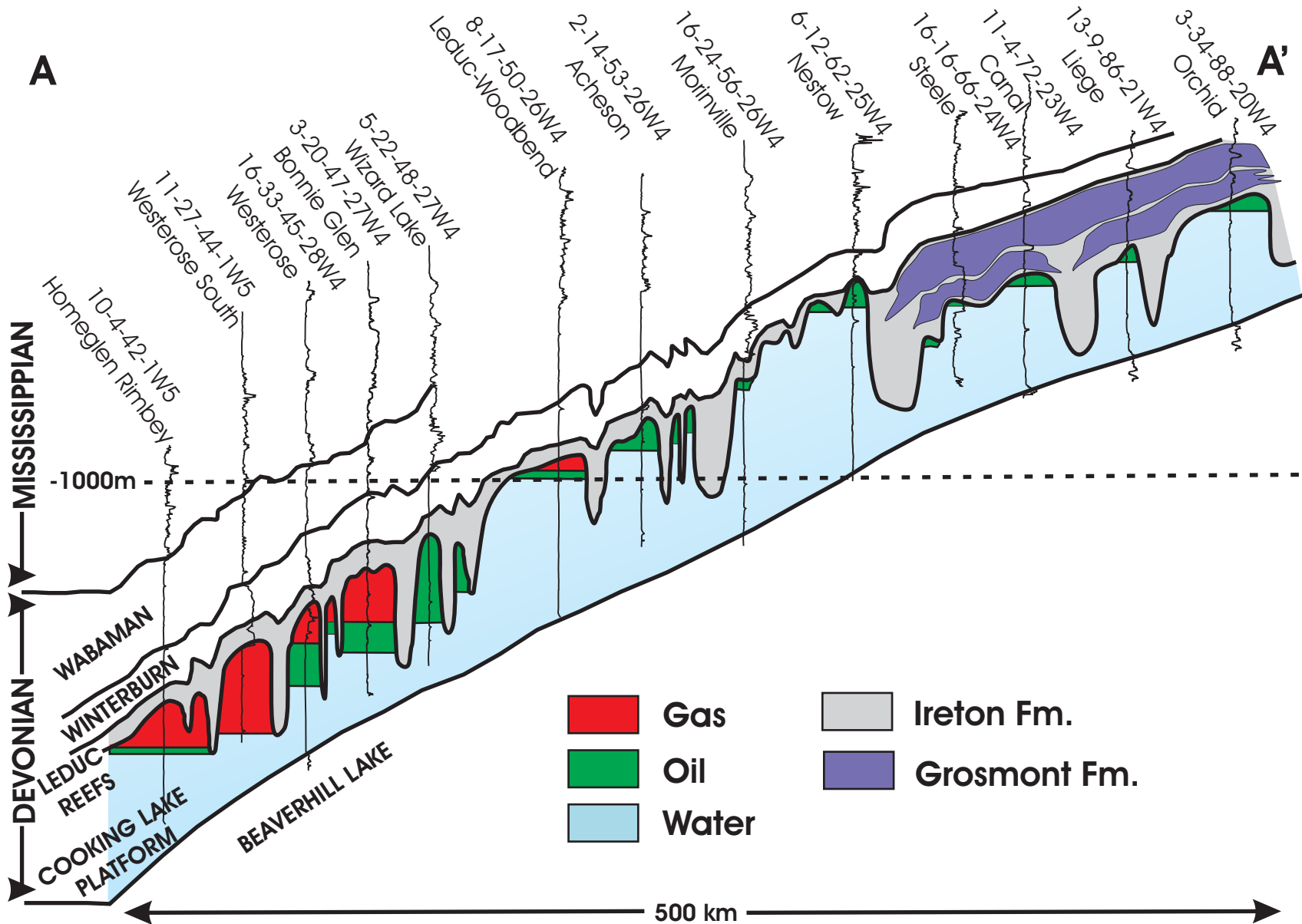
Figure 1.2.1. Schematic structural gamma ray cross section showing distribution of oil, gas and water in the Leduc reefs of Alberta. For location of cross section A -A' see Figure 1.1.1.Modified from Stoakes and Creaney (1984).

due to the insufficient amount of Mg derived from compaction fluids. Rostron (1995) and Horrigan (1996) suggested that additional Mg could have been supplied from undefined fluids derived through cross-formation flow entering the reef trend at its southwesternend, similarly to the adjacent Bashaw Complex. Anfort *et al.* (2001) and Bachu *et al.* (2008) later supported this idea. However, a driving mechanism of this type of cross-formation flow has not been identified in the study area.

The northeasternmost part of the trend was investigated by Huebscher (1996) who worked with Grosmont and Leduc Formation dolomites and considered regional-scale fluid flow to be the best explanation for the pervasive dolomitization of the reef trend, with the Cooking Lake platform beneath the Leduc buildups acting as a conduit system linking individual reefs.

Al-Aasm and Packard (2000), who worked with Mississippian dolomites of the Mount Head Formation, suggested recrystallization by warmer basinal fluids and re-equilibration during progressive burial. Potma *et al.* (2001) proposed that the initial conditions of dolomite formation cannot be characterized using the data available. They argued that the matrix dolomites were initially formed from a reflux of an evaporitic fluid of a marine parentage and subsequently recrystallized at greater burial depths and higher temperatures obscuring the original geochemical signatures.

Symons *et al.* (1999) and Lewchuk *et al.* (2000), in their paleomagnetic studies, discovered that all Middle Devonian to Mississippian matrix dolomites on the western side of the Western Canada Sedimentary Basin became remagnetized during deep burial associated with the late Laramide Orogenic event, thereby erasing any earlier paleomagnetic signature. They suggested that this was caused by a massive fluid flow

event, which recrystallized preexisting dolomites by increasing their crystal sizes, changing the crystal geometry, and negatively shifting oxygen isotope values.

Grasby and Chen (2005), Gue (2012), and Gibson *et al.* (2013) proposed that the fluid movements along the reef trend have changed their direction multiple times throughout the basin history (see sections 2.4 and 8.5).

1.3 Study area

The study area is situated in the subsurface of south-central Alberta, Canada (Figures 1.1.1). The Upper Devonian Rimbey-Meadowbrook reef trend extends for more than 600 km from the NE near the Athabasca river towards the Canadian Rockies over an area defined by Townships 33 to 95 and Ranges 27 west of the fourth Meridian to 12 west of the fifth Meridian. The trend is buried at a depth of about 200 m at its North-Eastern part, reaching a depth of about 6-8 km at its south-western end (Figure 1.2.1). This trend contains a series of reefs, which vary in size from less than 1 to several tens of square kilometres in area, with thicknesses ranging from 150 m to around 300 m (Barfoot and Ko, 1987; Machel and Mountjoy, 1987; Rostron *et al.*, 1997).

Almost all of these reefs are gas, oil, or gas + oil pools, and include the South-Calling Lake, North-Calling Lake, Morinville, St. Albert, Acheson, Leduc-Woodbend, Wizard Lake, Bonnie Glen, Westerose, Westerose South, Homeglen Rimbey, Gilby, Medicine River, Sylvan Lake, Lanaway, Garrington, Bearberry, and Harmattan reefs

(Figure 1.3.1). Furthermore, most reefs are completely dolomitized. Exceptions include the limestone Golden Spike, Redwater, and partly dolomitized Phoenix and Strachan buildups.

The present thesis area geographically overlaps with the following study areas: Qiang (1992), Amthor *et al.* (1993, 1994), Drivet (1993), Marquez (1994), Horrigan (1996), and Huebscher (1996). Therefore, this project partially utilizes data compiled from those studies as well as the samples collected by the current author from the townships not previously covered. This study is the first to provide a detailed description and interpretation of dolomite textures and recrystallization of the whole Rimbey–Meadowbrook reef trend (Figure 1.3.1).

Figure 1.3.1. Map of the Rimbey-Meadowbrook reef trend showing the distribution of Leduc buildups. The outlined areas are previous studies.
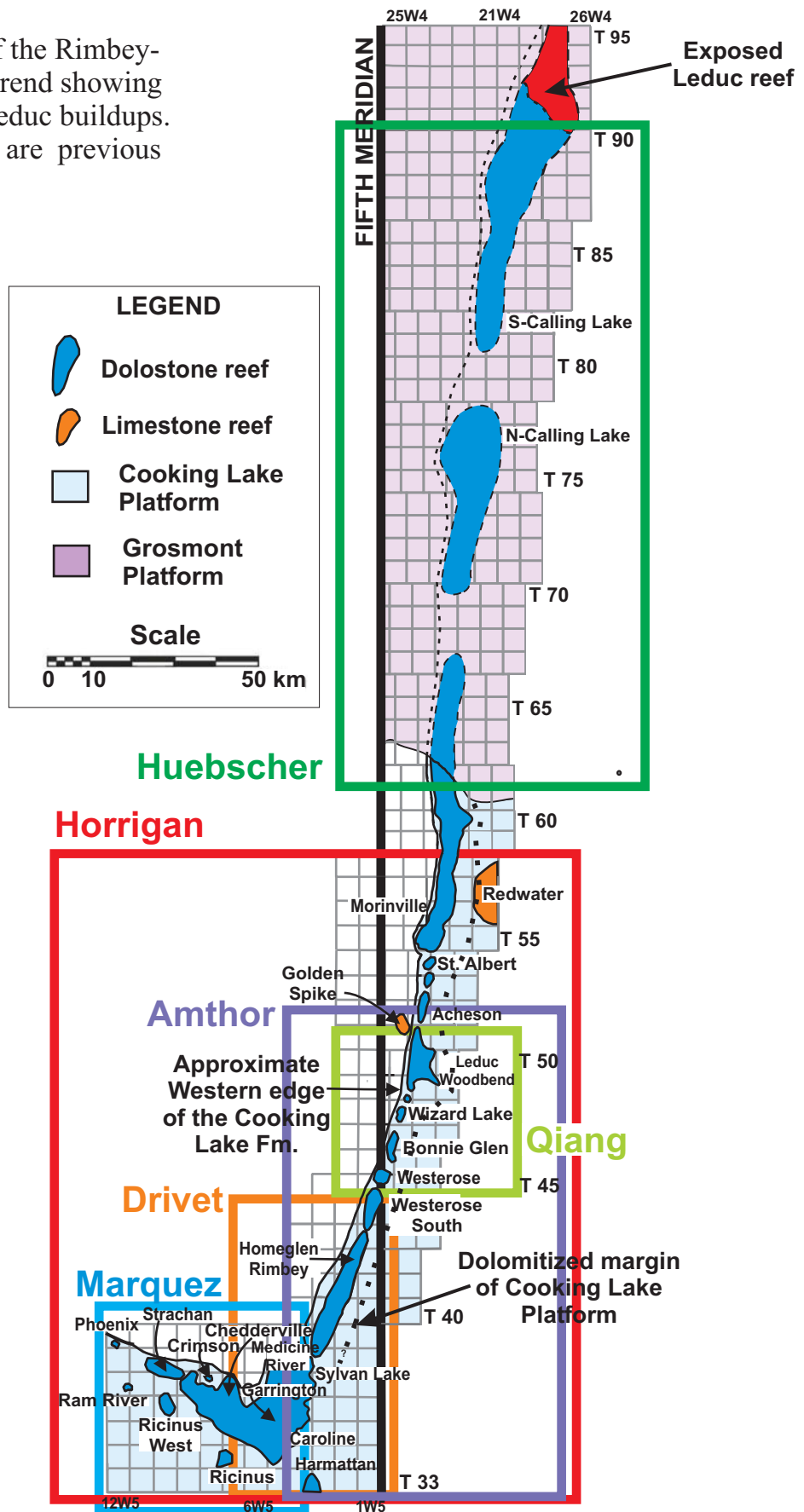
1.4 Objectives

The main objective of this project is to identify and characterize the presence and extent of dolomite recrystallization along the entire Rimbey-Meadowbrook reef trend through selected petrographic and geochemical techniques as follows:

1. establish a paragenetic sequence from the diagenetic textures;

2. determine if there are any significant differences between the dolomites that occur in the Cooking Lake platform and the ones from the overlying Leduc reefs;

3. determine possible sources, timing and temperatures of the dolomitizing fluids from C, O, and Sr isotopes, and major and trace element compositions;

4. elucidate the origin of the dolomites and other diagenetic phases;

5. characterize the extent of dolomite recrystallization;

6. encompassing the previous points and with a reference to Figure 1.1.3, determine which theoretical alternative (steady recrystallization, stepwise recrystallization, no recrystallization, or other) applies to and/or represents these dolomites.

The degree of recrystallization (5) must be understood in order to place tighter constraints on the origin of these dolomites (4). Thus far it is uncertain whether or to which degree the geochemical compositions (δ^{18}O, δ^{13}C, Sr – isotopes, trace elements, etc.) characterize the fluid(s) of dolomitization or that (those) of post-replacement recrystallization.

CHAPTER 2

GEOLOGICAL FRAMEWORK

2.1 Stratigraphy and Geological Setting

The Rimbey-Meadowbrook reef trend was deposited in the south-central part of the Alberta Basin (Figure 2.1.1) during the Upper Devonian (Frasnian). The area of interest contains the units belonging to the Woodbend Group, and in particular the Leduc and Cooking Lake Formations (Figure 1.1.2). This chapter summarizes the stratigraphy and geologic history of the Woodbend Group in south-central Alberta. More detailed geologic information about the Western Canada Sedimentary Basin (WCSB) during the Upper Devonian can be found in the Geological Atlas of the Western Canada Sedimentary Basin (Mossop and Shetsen, 1994).

2.2 General Burial of the Woodbend Group strata

During Frasnian time, an extensive shallow water carbonate platform with approximate thickness of 75 m – the Cooking Lake Formation (Figure 1.1.1) – was deposited in a subtropical epicratonic sea at a latitude of about 30°S (Figure 2.2.1). This was followed by a relative sea level rise, which resulted in the nucleation of Leduc Formation reefs on the western edge of the platform. These reefs developed in three stages – the Lower, the Middle, and Upper Leduc – reaching a maximum thickness of 275 m (Switzer *et al.*, 1994).

13
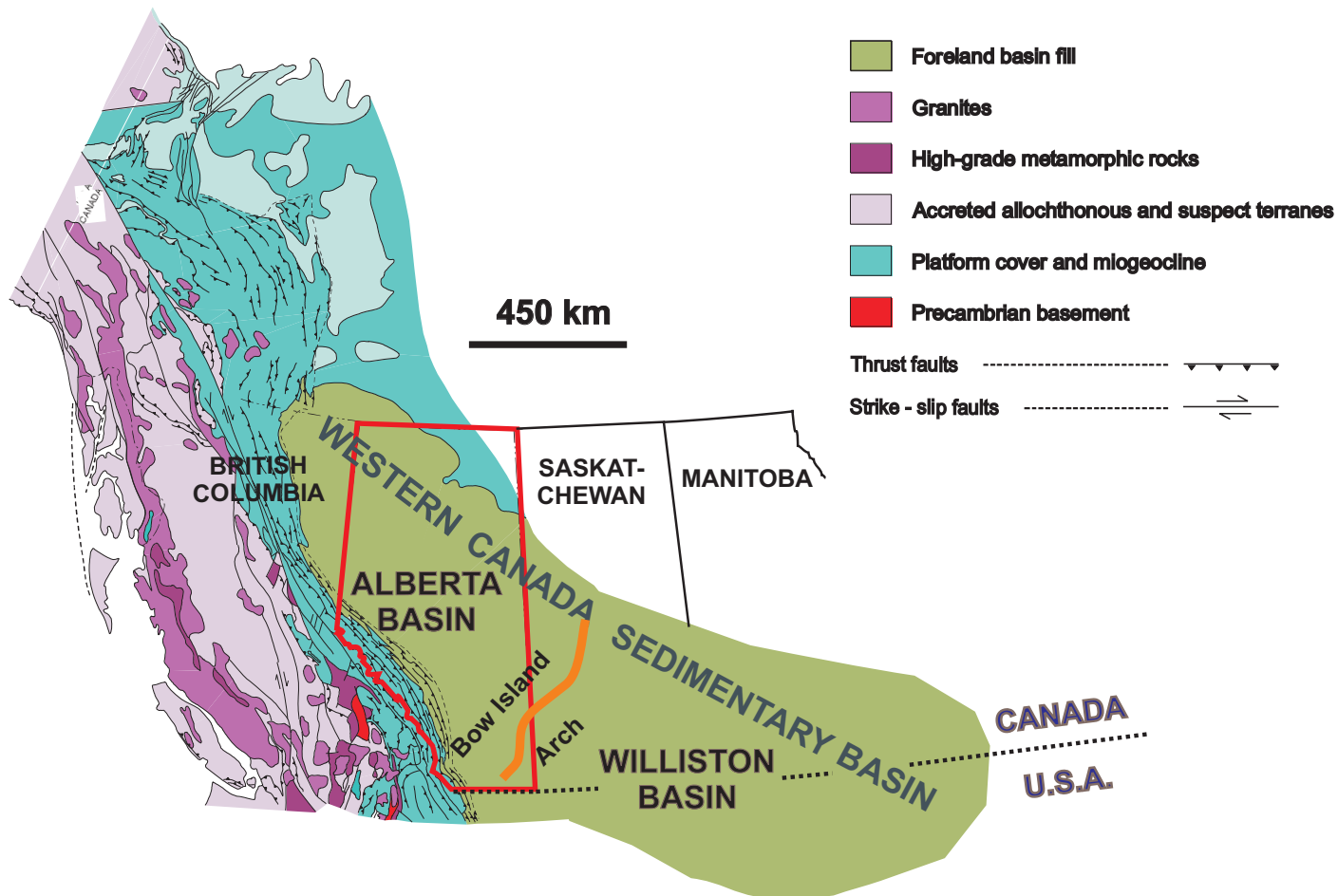
Figure 2.1.1.Structural elements of the Western Canada Sedimentary Basin that extends from the Northwest Territories in the north to the Northern United States in the south. The WCSB is divided into the Alberta Basin and the Williston Basin by the Bow Island Arch. (Modified from Mossop and Shetsen, 1994).

Figure 2.2.1. Paleogeographic representation of Laurussia during Late Devonian (~360 Ma). Today's Province of Alberta (outlined in blue) would have been located south of the paleoequator (white line) and covered by a shallow epicontinental sea. (Modified from Blakey, 2014, http://www2.nau.edu/rcb7/namD360.jpg).

The Cooking Lake Platform extends beneath the East Shale Basin, having its western margin 2 to 10 km to the west of the reef trend. The thickness of this partially dolomitized platform is about 76 m beneath the Leduc reefs, decreasing eastward. The Cooking Lake – Leduc combined comprise one of the main aquifer systems in the WCSB that acted as a regional subsurface conduit for basinal fluids (*e.g.* Rostron *et al.*, 1997; Mountjoy *et al.*, 1999).

During the Late Frasnian, the reef trend along with the underlying platform were surrounded and then covered by the basin-filling shales and argillaceous carbonate muds of the Majeau Lake, Duvernay and Ireton Formations, which stratigraphically

correspond to the Lower, Middle, and Upper Leduc (Switzer *et al.*, 1994). The organic-rich Duvernay Formation was a petroleum source rock responsible for the generation of oil and gas in Leduc reef traps, whereas the overlying Ireton shales completely sealed the reefs at least in the now deeper, southwestern part of the Rimbey-Meadowbrook reef trend.

2.3 Diagenetic Evolution of Woodbend Carbonates

The Rimbey-Meadowbrook Reef Trend underwent a complicated diagenetic history (Amthor *et al.*, 1993, 1994). During the Late Devonian, the Leduc reefs experienced nearly continuous burial to about 500 m. This allowed the lithification of the carbonate sediments to limestones by several types of calcite cements. During deeper burial from about 500 to 1500 m in the Late Devonian and Mississippian, most of these limestones were pervasively dolomitized to so-called 'grey matrix dolomite' that commonly comprises about 85-90 vol % of the rocks (Mountjoy *et al.*, 1999). Exceptions include the Golden Spike, Redwater, and Strachan buildups, which escaped pervasive dolomitization and have only minor amounts of dolomite; and the partially dolomitized Phoenix reef. The Cooking Lake strata underwent dolomitization in the areas beneath the dolomitized Leduc reefs, with significantly decreasing dolomite content to the east and west of the reef trend (Horrigan, 1996).

The source of the dolomitizing fluids remains uncertain. Some authors (Illing 1959, Mountjoy and Amthor 1994, Mountjoy *et al.* 1999) suggested that it was "connate" seawater expelled from compaction of the surrounding shales with estimated temperatures of about 45 to 75°C, based on conventional oxygen isotope geothermometry. Others

(Amthor *et al.*, 1993) argued that these compaction fluids alone did not have enough magnesium, and that additional fluid and magnesium sources were required for pervasive dolomitization.

From the Mississippian until the Late Cretaceous, the region underwent minor deposition, non-deposition and erosion, and the strata were tilted westward causing uplift of the eastern part of the basin and creating the foreland basin in front of the developing Rocky Mountains. During the Late Cretaceous to Eocene, the reefs were buried to maximum depths of about 2000m in the northeast and about 7000m in the southwest. This led to maturation of the organic-rich Duvernay Formation and migration of oil and gas, and also resulted in the formation of late diagenetic saddle dolomite, calcite, and some Fe-sulfides. After maximum burial, there was a gradual uplift of at least 500 m in the updip portion and of at least 1500m in the downdip portion of the study area (Switzer *et al.,* 1994). The Rimbey-Meadowbrook Reef trend with the underlying Cooking Lake platform presently form a structural homocline that crops out around Township 92, dipping for several hundred kilometers southwestward into the deepest part of the basin (Mountjoy *et al.*, 1999) (Figures 1.1.1, 1.2.1, 1.3.1).

2.4 Hydrogeology and hydrocarbon trapping

The Rimbey-Meadowbrook Reef Trend with the underlying Cooking Lake Platform comprises one of the main aquifer systems in the WCSB and is a regional conduit for aqueous and petroliferous fluid migration. The movement of fluids in this aquifer occurs through a relatively narrow conduit defined by a highly permeable dolomitized portion of

the Cooking Lake Platform (Amthor *et al.*, 1993, 1994; Creaney *et al.*, 1994; Rostron *et al.*, 1997).

Formation water flow was channeled updip through this conduit in the northward direction across the entire study area. In the central part, regional fluid flow may have been joined by cross-formation flow facilitated by the erosional surface of the sub-Cretaceous unconformity (Bachu *et al.*, 2008; Figure 2.4.1). This resulted in mixing of diagenetically altered meteoric waters of the Lower Mannville Formation and dense brines of the Cooking Lake Formation and reversed flow directions from the Lower Mannville aquifer into the Cooking Lake aquifer, especially in the places where the Ireton shales thin above Leduc buildups (Anfort, 1998; Anfort *et al.*, 2001; Bachu *et al.*, 2008).

Another meteoric water anomaly was discovered by Grasby and Chen (2005), who suggested that the brines discharging from the northern end of the Rimbey-Meadowbrook Reef Trend do not correlate with the deep-basin formation waters but exhibit mixed signatures of fresh water, dissolved evaporites and deeper basin brines. They proposed that due to the reversed regional topographic gradient and, hence, reversed basin-scale topography driven flow during the Pleistocene, subglacial meltwater intruded through the Northeast into the carbonates of the Rimbey-Meadowbrook Reef Trend deep enough to dissolve Prairie evaporates and that this resulted in Pleistocene-aged collapse features, karstification and calcitization of dolomites. The interpretation of these fluid compositions was also supported by Gue (2012) and Gibson *et al.* (2013), who found that evaporate-enriched meteoric waters are currently discharging into the Athabasca river. Based on these observations, it was proposed that the present-day fluid flow system does not necessarily
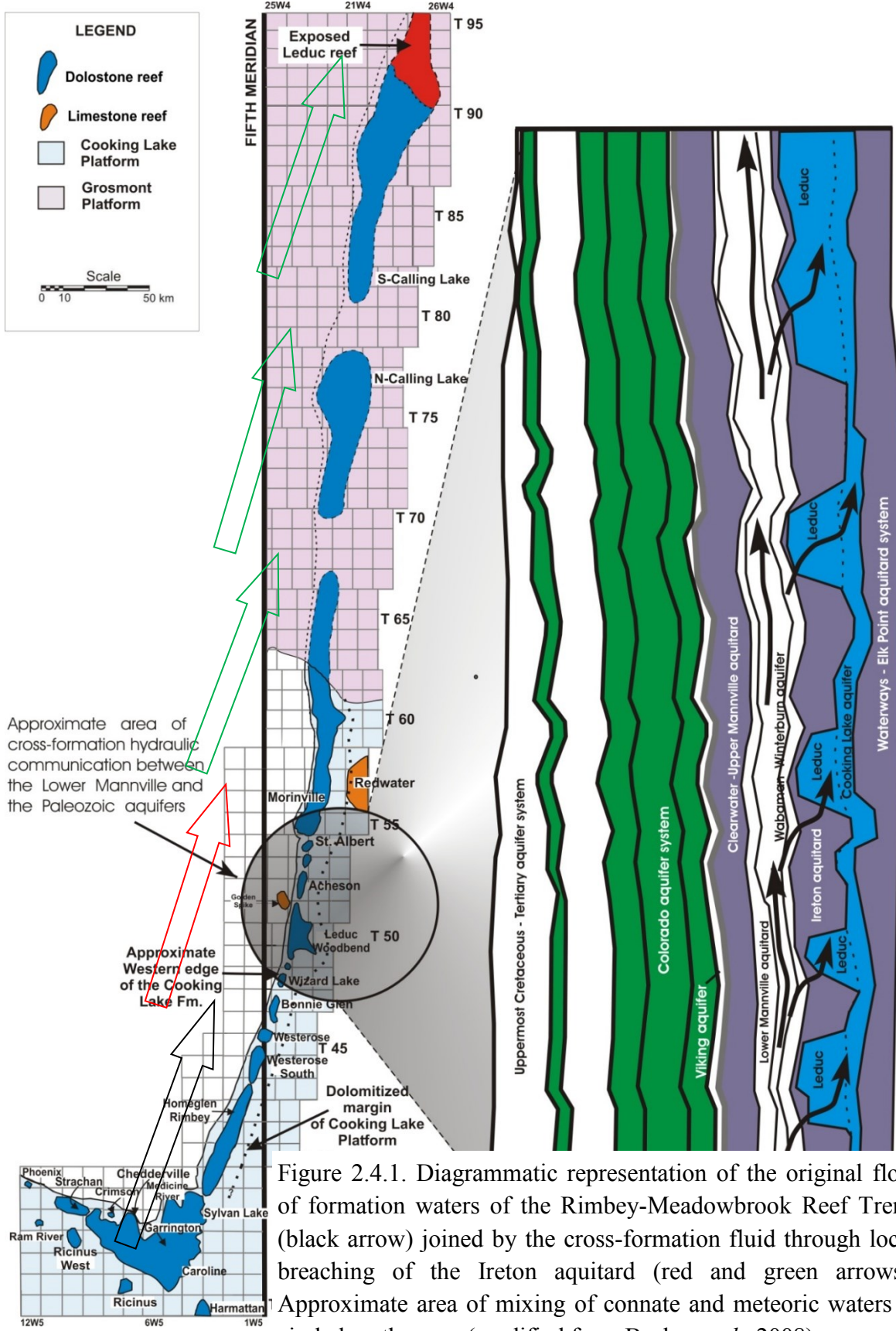
Figure 2.4.1. Diagrammatic representation of the original flow of formation waters of the Rimbey-Meadowbrook Reef Trend (black arrow) joined by the cross-formation fluid through local breaching of the Ireton aquitard (red and green arrows). Approximate area of mixing of connate and meteoric waters is circled on the map (modified from Bachu *et al.*, 2008).

reflect past fluid movements due to multiple changes in direction throughout the basin history.

Based on paragenetic and geochemical data, the major stage of replacive matrix dolomitization in the Rimbey-Meadowbrook reef trend occurred long before oil migration and may have been initiated as early as the Late Devonian (O'Connor and Gretener, 1974; Machel and Mountjoy, 1987). Nevertheless, replacive dolomitization may have played an important role in oil migration and accumulation, because matrix dolomitization may have been the process that generated the highly permeable platform margin conduit later used for oil migration.

Oil migration in the Devonian system was favored by the connection between the Duvernay source rock and the Cooking Lake Platform (Figure 1.1.2), allowing mature hydrocarbons to be expelled directly into the aquifer. As discussed by Rostron *et al.* (1997), oil and gas migration in the reefs occured under the influence of buoyancy and hydrologic flow. When one reef trap was filled to its spill point, excess oil migrated updip to be trapped in the next reef updip in a pattern commonly referred to as "differential entrapment" (Figure 2.4.2). However, in some parts of the basin the aquitards that normally seal the reefs are thin and fractured, hence relatively permeable. This caused leaking of several reef traps along the Rimbey-Meadowbrook Reef Trend after initial oil emplacement (Rostron, 1995; Rostron *et al.,* 1997). For instance, in reefs located north of Township 38, where the Ireton aquitard is at least 35 m in thickness, hydrocarbon columns exceed 200m in height; whereas the ones located below Township 38 are essentially devoid of hydrocarbons because the cap rocks are much thinner (less than 5 m), which permitted escape of oil and gas.
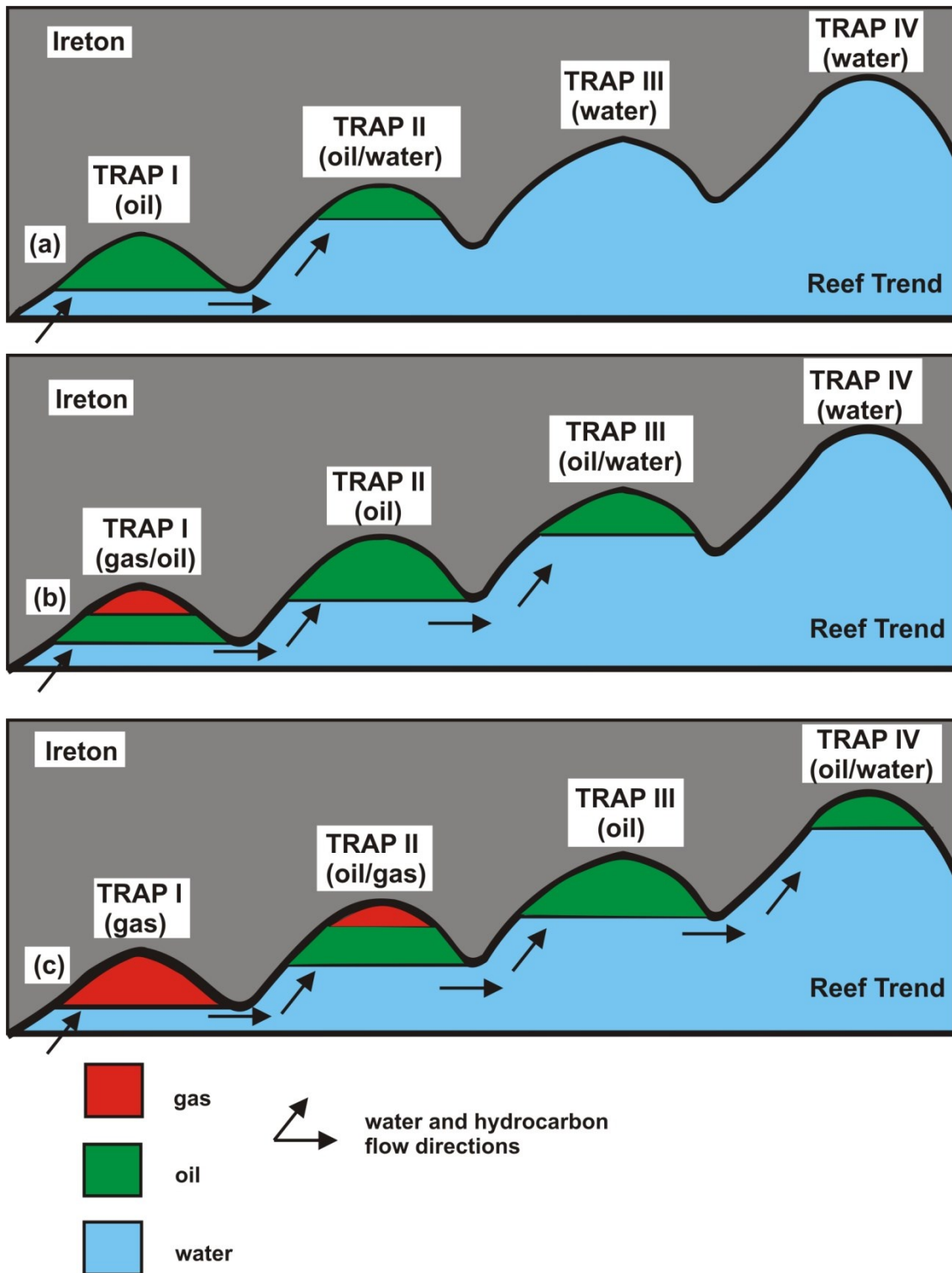
Figure 2.4.2. Model of differential hydrocarbon entrapment. (Modified from Gussow, 1954).

CHAPTER 3

SAMPLE ORIGIN AND ARCHIVING

3.1 Sampling strategy

The primary criterion for the sample selection was to compile a representative set of dolomite samples of a specific petrographic type in a narrow stratigraphic level that could be traced from one end of the Rimbey-Meadowbrook Reef Trend to the other. Matrix dolomites of the Cooking Lake and the overlying Leduc Formations perfectly fit these requirements. These dolomites are the most abundant type of dolomite along the whole trend. They were formed along the reef chain at about the same time and then were buried at a depth ranging from about 1.2 km in the northeast to more than 7 km in the southwest (Amthor *et al.,* 1993). Saddle dolomite is not suitable for this purpose, because it does not spread evenly along the reef trend.

The Cooking Lake Formation is rarely cored. Therefore, core selection primarily focused on wells that perforated the Leduc Formation. In some areas, these two formations could not be distinguished due to the resemblance between the dolomites caused by complete dolomitization and similar well logs. In such cases the choice was limited to those cores with continuous recovery from the Leduc Formation.

The present thesis area geographically overlaps with those of the following studies: Qiang (1990-1992), Amthor *et al.* (1993, 1994), Drivet (1993), Marquez (1994), Horrigan (1996), and Huebscher (1996). Most samples from these studies were available

also for the current study. Thus, this project is based on the samples obtained from these studies supplemented by the ones collected by the current author from the townships not otherwise covered (Figure 1.3.1).

A sample set collected by Qiang (1990-1992) was severely damaged, missing labels and analytical results. Therefore, this collection had to be reorganized and compiled into a new database.

Sampling was guided by the time available to complete this Master's thesis and by the budget provided. For these reasons the number of wells cored per township was limited to 1-2, with 2 to 6 samples per well.

A total of 92 new samples from 17 wells were collected from the Energy Resources Conservation Board (ERCB) Core Research Centre in Calgary; seventy previous samples were used from Horrigan (1996); eighteen - from Qiang (1990-1992); twenty four – from Huebscher (1996); and ten – from Amthor *et al.* (1996). Appendix 1 provides a listing of all samples used in this study.

3.2 Photographic documentation

All cores examined at the Core Research Centre were photographically documented as a series of "posters" including one to four core boxes per 'poster' with close-up photographs of representative specimens from each core interval. Plate 3.2.1 illustrates an example of the "posters" made.

The second archive contains images of the "raw" specimens marked for thin sectioning and microdrilling. These images are beneficial for future reference, especially if samples got damaged during thin section preparation (Plate 3.2.2 a and b).

Archive number 3 is high-resolution scans of each whole thin section that was used for image analysis (Plate 3.2.2 c and d).

The fourth archive is photomicrographs that were taken under the petrographic microscope in various magnifications both in transmitted and crossed-polarized light (Plate 3.2.2 e and f).

The last archive includes cathodoluminescence images coupled with transmitted light photomicrographs in various magnifications (Plate 3.2.2 g and h).

6-14-37-7W5
Core 4
Int 3726 - 3739 m

Box 2 of 9   Box 1 of 9

SK67-1

SK67-2

SK67-3
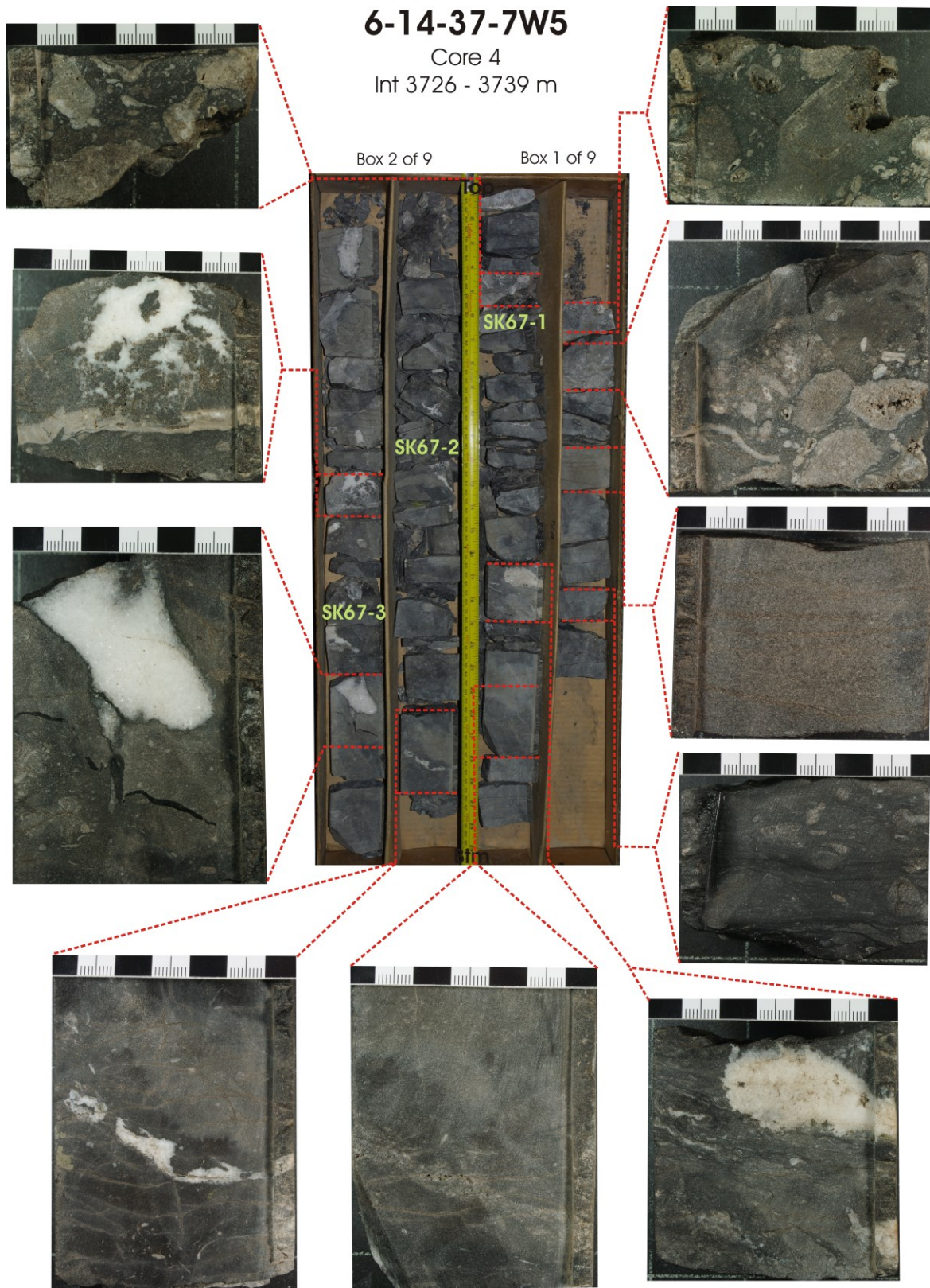
Plate 3.2.1. Examples of core photographic archiving. Each "poster" includes one to four core boxes per 'poster', with close-up photographs of representative specimens from each core interval.

16-24-56-26W4
Core 1
Int 1601.00 - 1603.75 m

Plate 3.2.1. Continued.

16-24-56-26W4
Core 2
Int 1604.5 - 1622.5 m

Box 4 of 16   Box 3 of 16   Box 2 of 16   Box 1 of 16

SK56-3

SK56-4

16-24-56-26W4
Core 2
Int 1604.5 - 1622.5 m

Box 8 of 16   Box 7 of 16   Box 6 of 16   Box 5 of 16

SK 56-5

Plate 3.2.1. Continued.

16-24-56-26W4
Core 2
Int 1604.5 - 1622.5 m
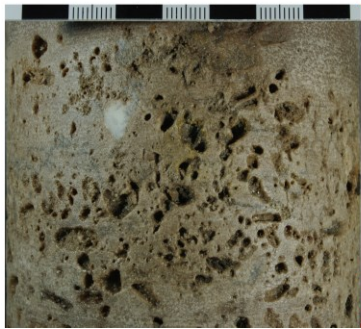
16-24-56-26W4
Core 2
Int 1604.5 - 1622.05 m
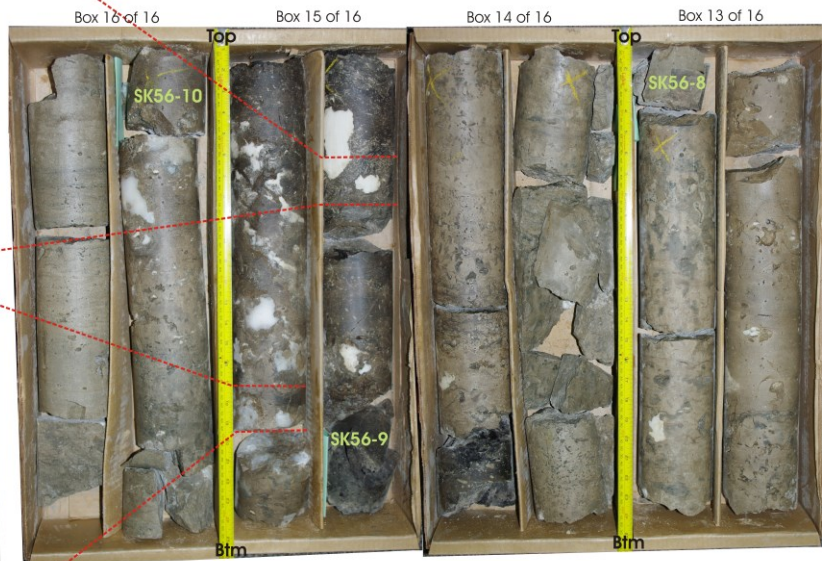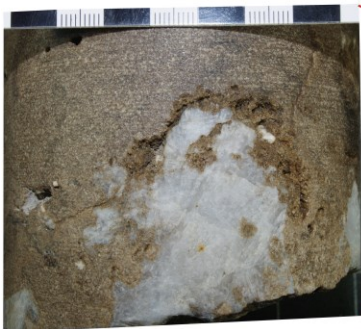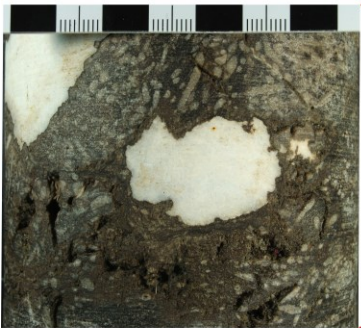
Plate 3.2.1. Continued.
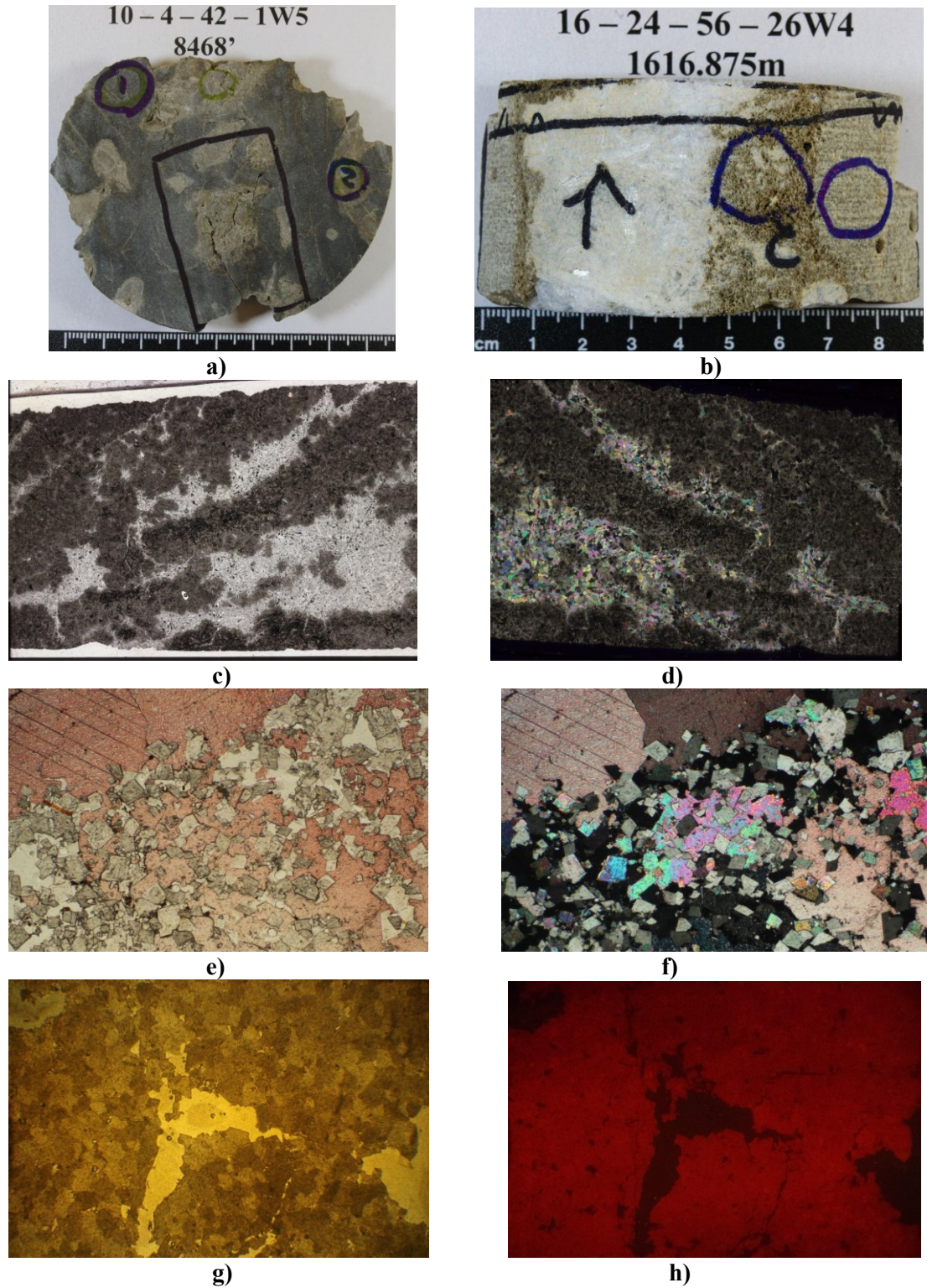
Plate 3.2.2. Examples of photo-archiving. a) and b): Raw hand specimens marked for thin sectioning and microdrilling; c) and d): High-resolution scans of the whole sections in transmitted light vs. polarized light, sample SK-55-4, well 02-16-55-25W4 (4372ft); e) and f): Thin section photomicrographs in transmitted light vs. XPL, sample EH-64, well 15-23-52-26W4 (1547.4 m); g) and h): Thin section photomicrographs in transmitted light vs. cathodoluminescence, sample HH-88-6, well 03-34-88-20W4 (1530 ft).

CHAPTER 4

METHODS

This chapter provides a description of methods applied to study the dolomites of the Rimbey-Meadowbrook Reef Trend. These methods include petrography, cathodoluminescence microscopy and spectroscopy, X-ray diffraction, stable and radiogenic isotope analyses, major and trace element analyses, image analysis, and multivariate statistical analysis.

4.1 Petrography

A total of two hundred and five polished thin sections were investigated using a Zeiss Jenapol Polarizing Microscope to distinguish matrix dolomite types. To determine the carbonate mineral composition, one hundred and eighty sections were stained with Alizarin red-S. This number includes sections that were already stained by previous researchers (Qiang, 1990-1992; Horrigan, 1996; Huebscher, 1996) and the new sections stained by the current author. The unstained sections were either coated (carbon or glass), or they had only one dolomite phase. All the textures observed were documented in a spreadsheet (Appendix 2).

4.2 Cathodoluminescence microscopy and spectroscopy

Cathodoluminescence (CL) of selected samples was studied using a CL microscope (Olympus BH-2) with a cold cathode Premier American Technologies Luminoscope, Model ELM-3R. CL petrography was carried out with a beam voltage of 10-15 kV and a beam current of 0.5 mA in a 40-50 mTorr vacuum. Luminescence images were captured during CL operations using an adapted SLR digital camera (Pentax, K-5).

The CL spectra were measured in the short wave ultraviolet (UV) to infrared (SWIR) region between 380 nm and 1200 nm using a Princeton Instruments PIXIS 100 Fourier Transformed Infrared (FTIR) spectrometer with ST-133 controller and 400*1340 B camera. The procedure was activated through the 'spectra acquisition' tool of the WinSpec/32 software (version 2.5C), which is integrated with the spectrometer, and run for 10 seconds. The dolomite spectra acquired were automatically converted from wave number to wave length and presented as a plot showing wavelength versus intensity (Figure 4.2.1). Neon light was used as a standard for these experiments. The results were tabulated in a spreadsheet presented in Appendix 2.
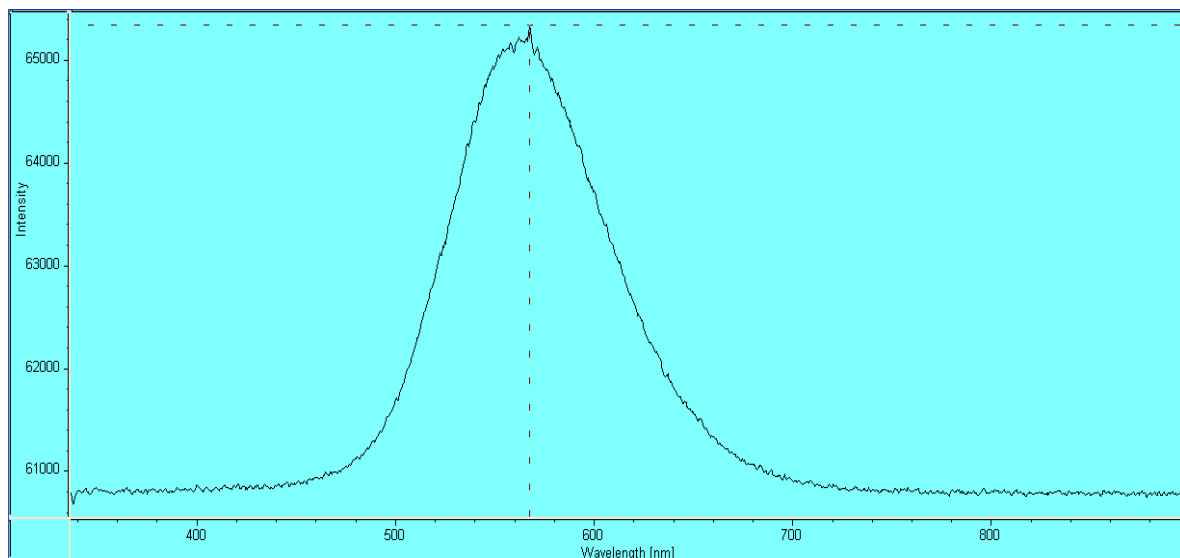
Figure 4.2.1. Example of the WinSpec/32 plot showing wavelength versus intensity.

4.3 Sample preparation

After petrographic examination of the thin sections, 160 powder samples of matrix dolomite were drilled from 98 matching hand specimens (from which the sections had been cut) using a low-speed microdrill. Three sets of powder samples about 15-25 mg each were prepared for (i) X-ray diffraction, (ii) carbon, oxygen, and (iii) strontium isotope analyses, and one additional set of approximately 200 mg powder was drilled for major and trace element analyses.

4.4 X-Ray Diffractometry (XRD)

All powder samples were analyzed by X-ray diffractometry (XRD) in the X-Ray diffractometry laboratory at the University of Alberta. About 10 mg of powder were mixed with an internal quartz standard and then fixed as an ethanol slurry to a silicon plate transparent to X-rays. Samples were run on a Rigaku D/tex Ultra X-ray Diffractometer, using Co $K\alpha$-radiation at 40 kV and 35 mA. The area from 29° to 38° 2θ was scanned using a 0.02° 2θ step size with scan speed 4° 2θ/ minute. Total data collection time was approximately 8 minutes.

The obtained d-spacing was then corrected relative to the internal quartz standard. The mol % $CaCO_3$ was estimated using Lumsden and Chimahusky's (1980) equation:

$$mol \% \ CaCO_3 = 333.33*d - 911.99,$$

where d is the corrected interplanar spacing.

The wt% $CaCO_3$ was calculated based on the calcite and dolomite peak intensities using the technique proposed by Locock (2012). The results are presented in Table 6.1.1.

4.5 Stable isotopes

Powder samples of about 15 mg each were analyzed for carbon and oxygen isotope ratios in the Stable Isotope Laboratory in the Department of Earth and Atmospheric Sciences at the University of Alberta. All dolomite samples were reacted with 5 ml anhydrous phosphoric acid in reaction vessels for 3 to 5 days at a temperature of about 25 °C, following the procedure proposed by Degens and Epstein (1964). CO_2 gas was extracted on a vacuum line by a freezing/warming cycle: water was eliminated from the samples using a mixture of dry ice and ethanol, and the CO_2 was separated using liquid nitrogen. The obtained CO_2 gas was then analyzed for carbon and oxygen isotopes using a Finnigan-Mat 252 mass spectrometer.

Samples containing a mixture of calcite and dolomite were subjected to sequential extraction, whereby the CO_2 from calcite was collected after the first hour of acid digestion, and CO_2 from dolomite was collected at the end of the 3-5 day cycle.

The results are given in the conventional delta (δ) notation in parts per thousand (per mil, ‰) relative to the PeeDee Belemnite (PDB) standard. Two international standards (NBS-18 and NBS-19, both supplied by International Atomic Energy Agency (IAEA) in Vienna) have been run for comparative purposes. Analytical precision for $\delta^{13}C$ and $\delta^{18}O$ values is less than 0.2‰ and 0.3‰, respectively. The $\delta^{18}O$ results were corrected by 0.82 for phosphoric acid fractionation (Sharma and Clayton, 1965; Land, 1980, 1985). Results are shown in the table presented in Appendix 3.

4.6 Radiogenic strontium isotopes

Following petrographic and stable isotope analysis, 42 outliers (samples that gave more positive or negative stable isotope results than the majority of the samples) were picked for strontium (Sr) isotope analysis. These samples were chosen on the expectation that they may contain significant amounts of radiogenic Sr indicative of diagenetic processes, rather than just Devonian 'marine' Sr. Powder samples of about 25 mg each were reacted with 2.25 ml of 1M HCl at a room temperature for about 18 hours. The resulting solutions were diluted to 0.75M HCl by adding 0.75 ml of Millipore water. Sr was separated from the solution using standard cation exchange techniques and loaded as a Sr-chlorite onto the side filament of a double rhenium assembly. Sr isotope ratios were then measured on a VG 354 thermal ionization mass spectrometer (TIMS) at the Radiogenic Isotope Facility in the Department of Earth and Atmospheric Sciences of the University of Alberta. The standard NBS SRM-987 was repeatedly analyzed and yielded a mean of 0.71020. Analytical precision on individual runs was better than 0.000024 (2σ). The results are shown in the overview table presented in Appendix 3.

4.7 Major and trace element analyses

One hundred and fifty selected powder-samples were analyzed for major and trace element concentrations in the Canadian Centre for Isotopic Microanalysis at the University of Alberta. The measurements were carried out using a Perkin-Elmer Elan 6000 Inductively Coupled Plasma – Mass Spectrometer (ICP-MS) with a cross-flow nebulizer, a 40 MHz RF-generator and a working power between 600 and 1600 W.

Powdered samples weighing 200 mg each were digested in 10 ml of 8M HNO_3 for 4 hours. Then 1 ml of this solution was mixed with 0.1 ml of HNO_3 and 8.8 ml of deionized water. Additionally, 0.1 ml of internal standards (Bi, Sc, and In) were added to correct the matrix differences. Concentrations were determined for 61 elements: Ag, Al, As, B, Ba, Be, Ca, Cd, Ce, Co, Cr, Cs, Cu, Dy, Er, Eu, Fe, Ga, Gd, Ge, Hf, Ho, Ir, K, La, Li, Lu, Mg, Mn, Mo, Na, Nb, Nd, Ni, P, Pd, Pb, Pr, Pt, Rb, Re, Ru b, Se, Sm, Sn, Sr, Ta, Tb, Te, Th, Ti, Tl, Tm, U, V, W, Y, Yb, Zn and Zr. The results are presented in Appendix 3.

4.8 Image analysis

Image analysis was conducted on two hundred and five thin section scans using the Assess 2.0 software (Lamari, 2008). Petrographic phases in the slides were selected based on their color, textural or brightness differences and run through the software. The results are reported as percentages of dolomite types, calcite and anhydrite cements, pyrite and bitumen, and porosity. In most cases, the program could not tell the various types of matrix dolomite apart from each other, nor pyrite from bitumen, because these phases have a very similar color. Where the process was impossible to perform automatically, these features were traced manually and then run through the program. An example showing a step-by-step process of image analysis is illustrated on Figure 4.8.1.
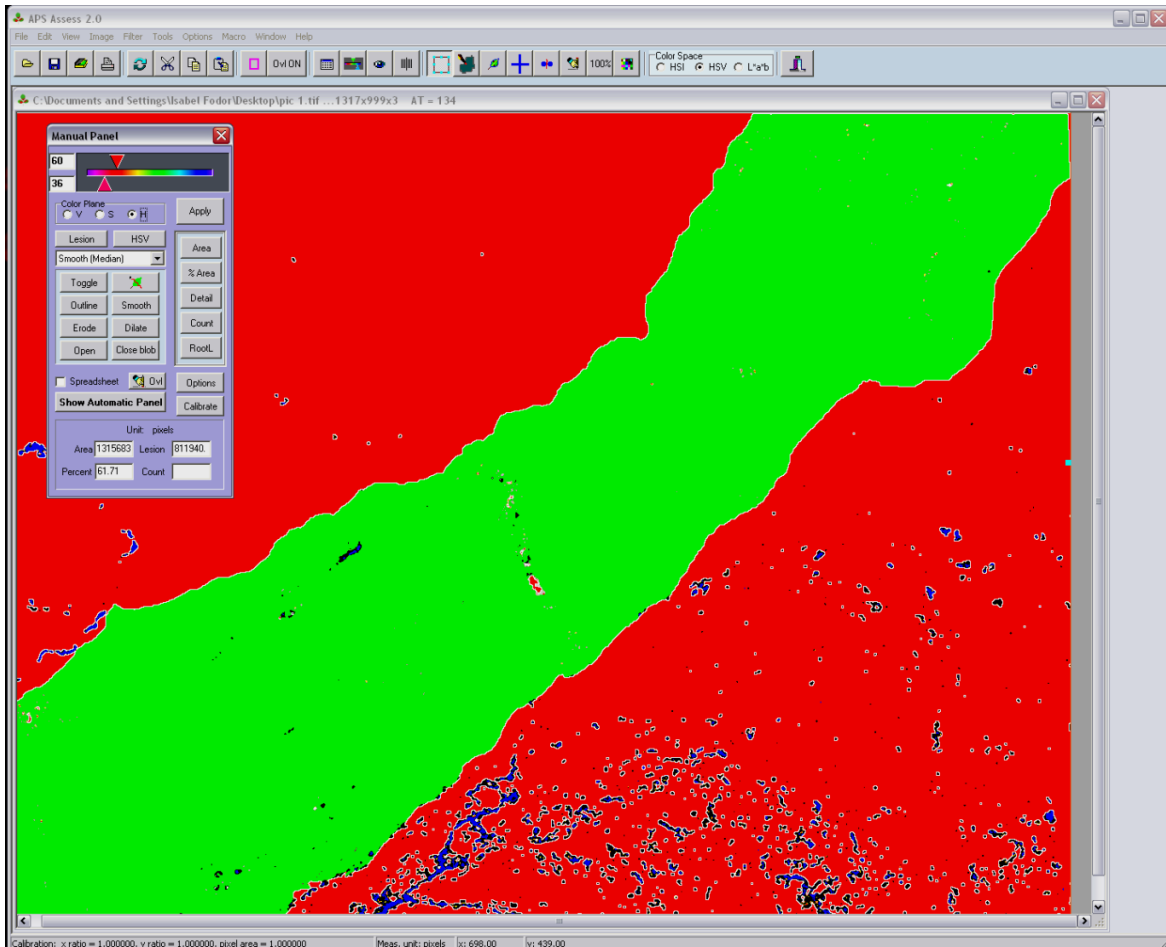
a)
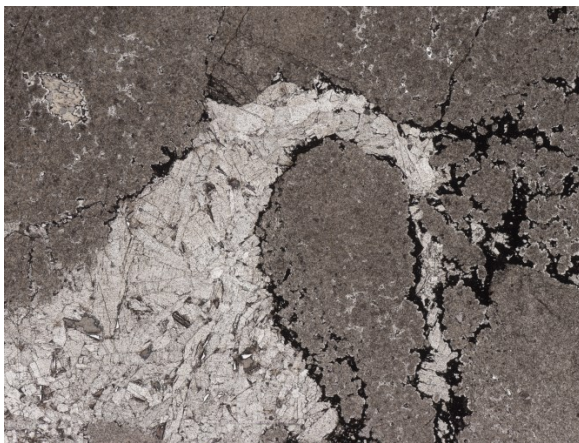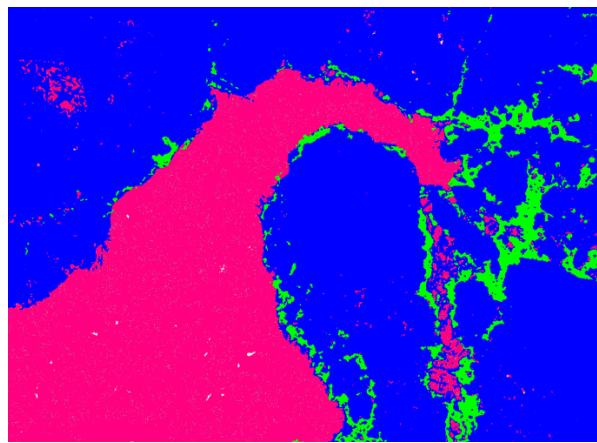
b)   **c)**

Figure 4.8.1. Step-by-step process of image analysis.
a) Using the automatic feature, the threshold levels were set as seen on the slider. Red color outlines the matrix dolomite R2, the green one is anhydrite, and the blue one fills the porosity. The program automatically calculates the percentage of selected phase out of the whole section and shows the result in the '%Area' box.
b) and c) Three different petrographic features – anhydrite (pink), bitumen (green) and matrix dolomite (blue) - were outlined in different colors and run through the program to calculate their percentages.

4.9 Multivariate Statistical Analysis

The geochemical data acquired by this study were combined with the previously reported data from Qiang (1990-1992), Amthor *et al.* (1993, 1994), Drivet (1993), Marquez (1994), Horrigan (1996), and Huebscher (1996) into a single EXCEL spreadsheet consisting of three hundred and sixty samples. Most of these samples were tested only for carbon and oxygen isotopes; one hundred and forty six of them had results from XRD and major and trace element analyses, and only sixty had $^{87}Sr/^{86}Sr$ isotope values. Therefore, for multivariate statistics this data set was reduced to those one hundred and forty six samples for which stable isotope, XRD and major and trace element data are available. The number of variables in this dataset was narrowed down to a total of fifty, discarding trace elements that had insignificant values (close to the detection limit or missing most of the data). Be, Si, Sc, Nb, Pd, Cd, Sb, Cs, Ho, Tm, Lu, Hf, Ta, Os, Bi were thus eliminated.

The reduced set of data was then divided into two subsets: the larger one has one hundred and forty six samples with fifty variables (but excluding $^{87}Sr/^{86}Sr$ isotopes), and the smaller one consists of sixty samples with fifty one variables that included $^{87}Sr/^{86}Sr$ isotopes. For each cell having a value less than the detection limit a new value equal to half of the detection limit was assigned in order to avoid the presence of empty cells. This worksheet was then imported into statistical software programs, MINITAB version 17.1.0 (Minitab Inc, 2014), IBM SPSS (Statistical Package for the Social Sciences) version 22.0 (IBM Corporation, 2013), and R version 3.1.2 (R Development Core Team, 2014), to conduct the analysis of patterns in the data.

4.9.1 Factor analysis (FA)

Factor analysis (FA) was used to examine relationships between variables in the dataset in order to reduce them to a limited number of interpretable factors or components that capture the maximum possible information (variation) from the original variables.

Factor analysis was carried out using the Stat-Multivariate and Analyze-Dimension reduction toolboxes of MINITAB and IBM SPSS, respectively, with VARIMAX rotation of factors (orthogonal rotation considering uncorrelated factors). VARIMAX is the most widely used algorithm that maximizes variance of the squared loadings in the factor matrix and minimizes correlation of variable loads between different factors (MINITAB User's Guide, 2014).

Factor analysis was performed on both subsets of data. The number of factors applied varied from five to fifteen but was finally set to five as the most efficient number for these subsets. Principal component analysis was performed only on the larger subset of data.

In computer output, the variables had different loadings for each factor or component. Loadings represent the correlation between the components and original variable. Loadings can range from -1 to 1 with values close to -1 or 1 showing that the factor has a significant influence on the variable, and values close to 0 showing that the factor has a weak influence on the variable (MINITAB User's Guide, 2014). Loadings in computer output were classified as strong (>0.75), moderate (0.4-0.75), or weak (<0.4).

4.9.2 Cluster analysis

Cluster analysis was used to condense the dataset into small separated groups, so that the attributes (*i.e.* chemical composition) of the samples were similar to each other within each group but different from those in other groups. This technique was carried out in a Q-mode comparing the samples between each other. A variety of different methods of cluster analysis (K-means, model-based and hierarchical clustering algorithms) was applied to both subsets of data, but the hierarchical Ward's linkage method and Euclidian distance between the observations were chosen as the most suitable combination.

Euclidian distance measures the separation between two similar samples in variable space and is represented by the difference between analytical values from these objects. Ward's linkage method controls how the similarity measurements are calculated aiming to minimize the sum of squares of two clusters. (Singh *et al,* 2011). Nonhierarchical K-means method is one of the simplest algorithms that separates the data set into a certain number of clusters based on the k centers defined for each cluster.

The outcome of hierarchical cluster analysis was graphically presented as a dendrogram grouping variables in a hierarchical manner.

4.9.4 Discriminant analysis

Discriminant analysis was used to distinguish different kinds of samples in the collection based on previously defined classes. Four petrographic and four geographic groups were imposed on the dataset to distinguish chemistry based on spatial distribution and types of dolomite. Two additional columns with the numbers assigned to each sample were added to the spreadsheet; the first one was to classify the samples according to the predominant petrographic type of dolomite in each sample (one to four). The second one was to classify them according to the geographic location: "1" for townships 33 – 40, "2" for townships 41 – 61, "3" for townships 62-78, and "4" for townships 79 – 95. Linear discriminant analysis was applied to the larger subset of data using these columns as predictors. The results are presented as discriminant function coefficients (similar to regressional coefficients) reflecting how much discriminating ability the function has.

CHAPTER 5

PETROGRAPHIC OBSERVATIONS

This chapter introduces the detailed petrographic characteristics of dolomites in the Leduc and Cooking Lake Formations. Some observations from the geographically overlapping previous studies are included for comparison. The data reported here represents the first thorough petrographic study covering the entire Rimbey-Meadowbrook reef trend.

The Cooking Lake and Leduc Formations of this reef trend are pervasively dolomitized. Minor occurrences of undolomitized limestones in several buildups (Golden Spike, Red Water, Strachan, and Phoenix) were defined as volumetrically insignificant and are, therefore, not discussed in this study. However, some of their characteristics were used as a baseline for comparison with the dolostones. The following petrographic information on various dolomite types is based on detailed core and thin section analysis using a combination of light and cathodoluminescence (CL) microscopy, CL spectroscopy, and image analysis.

Several textural types of dolomite were distinguished based on crystal size, crystal size distribution (unimodal or polymodal), and crystal geometry (planar-e [euhedral], planar-s [subhedral], or nonplanar), following Sibley and Gregg's (1987) classification system (Figure 5.1). Several scales for representing crystal size in carbonate rocks were considered (Folk, 1962; Friedman, 1965; Lucia, 2007). Folk's (1962) scale was chosen as the most suitable for this set of samples (Figure 5.2). The eight types thus identified are
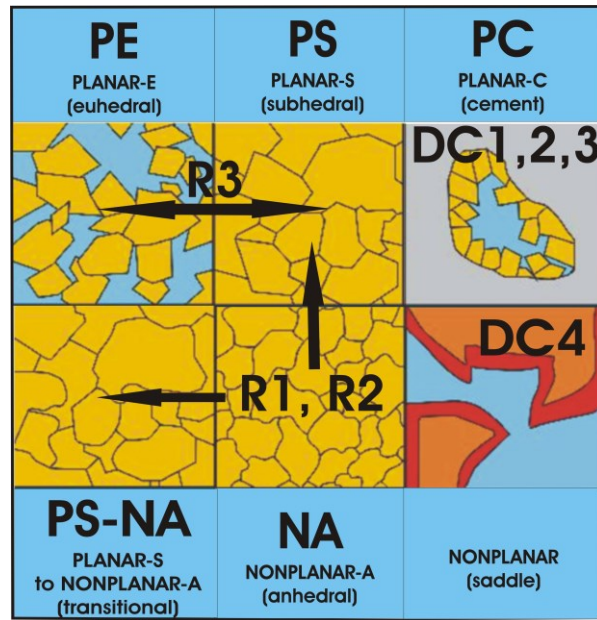
Figure 5.1. Textural classification of dolomites according to Sibley and Gregg (1987) (modified from Machel, 2004). Dolomite types R1, R2, R3, DC1, DC2, DC3, and DC4 are described in Figures 5.3a,b.

Figure 5.2. Terminology for grain sizes in carbonate rocks. The 'medium crystalline' class was chosen to fall between 0.062 and 0.25mm, as most dolomite crystals appear to correspond to this diameter range (modified from Folk, 1962).

fine-crystalline grey matrix dolomite (R1), medium- to coarse-crystalline grey matrix

dolomite (R2), brown porous matrix dolomite (R3), mimetic dolomite (R4), unzoned

dolomite cement (DC1), zoned dolomite cement (DC2), Fe-dolomite cement (DC3), and

saddle dolomite (DC4). These types have been correlated with the ones from the previously

reported classifications (Table 5.1, Figures 5.3a,b).

Table 5.1. Dolomite textures of the Rimbey-Meadowbrook Reef Trend according to previous studies: Sibley and Gregg (1987), Machel (1985), Amthor *et al.* (1993), Drivet (1993), Marquez (1994), Horrigan (1996), and Huebscher (1996). See Figures 5.1 and 5.3a,b for letter codes and Figure 5.2 for crystal size ranges.

DOLOMITE TEXTURES										
Sibley + Gregg	Machel	Amthor et al	Drivet	Marquez	Horrigan	Huebscher	Kuflevskiy		Dominance (see Figure 5.1)	Crystal size (see Figure 5.2)
PS+ (PS+NA) + NA	GMD	—	R1	R1	R1	R1	R1		PS -- NA	Fine < 62 µm
PS+ (PS+NA) + NA	GMD	D1	R2	R2	R2	R2	R2		PS -- NA	Micro-medium to macro-coarse (62 - 700 µm)
PE + PS	BPMD	D2	R3	R3	R3	—	R3		PE -- PS + NA	Micro- to macro-coarse (250 - 1,000 µm)
—	—	D4	R4	R4	R4	—	R4		Mimetic	Fine to macro-medium (62 - 250 µm)
PC	—	—	—	—	—	DC1	DC1		PC	Micro- to macro-coarse (250 - 1,000 µm)
PC	LD	D3	C1	C1	—	DC2	DC2		PC	Micro- to very coarse, zoned (250 - 1,500 µm)
PC	—	—	—	—	—	FeDC	DC3		PC	Micro- to very coarse, zoned (250 - 1,500 µm)
NP	—	D5	C2	C2	—	—	DC4		NP	Very to extremely coarse (up to 5,000 µm)

Matrix Replacement Dolomite Types

R1
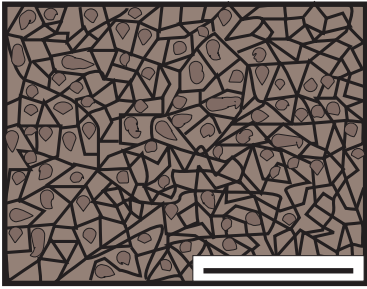
Fine-crystalline grey matrix dolomite (GMD)

- fine crystalline
- planar-subhedral (PS) to non-planar (NA)
- dense mosaic
- unimodal
- grey to beige
- dull orange-red luminescence

R2
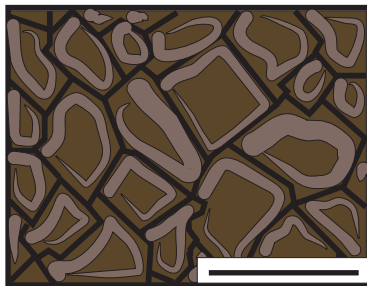
Micro-medium to macro-coarse crystalline grey matrix dolomite (GMD)

- micro-medium to macro-coarse crystalline
- planar-subhedral (PS) to non-planar (NA)
- dense mosaic
- unimodal
- grey to beige
- dull orange-red luminescence

R3
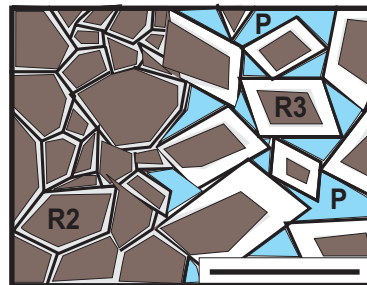
Brown porous matrix dolomite (BPMD)

- micro- to macro-coarse crystalline
- planar-euhedral (PE) to planar-subhedral (PS)
- porous mosaic
- polymodal
- clear to brown
- blotchy orange-red luminescence

R4
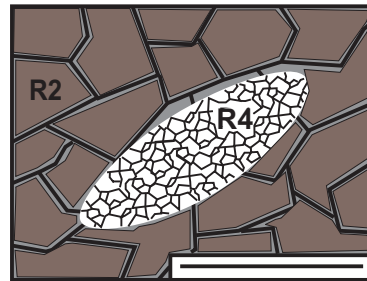
Mimetic dolomite

- fine to macro-medium crystalline
- planar-subhedral (PS) to non-planar (NA)
- dense mosaic
- usually surrounded by R2
- clear to grey
- dull orange-red luminescence

KD
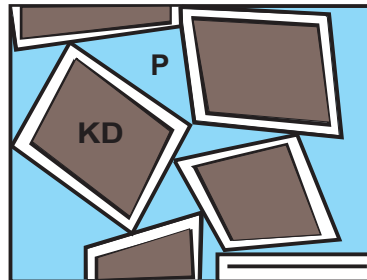
Karst or dedolomite

- micro-medium to macro-coarse crystalline
- planar-euhedral (PE)
- porous, partly calcitized mosaic
- clear to brown
- mottled to blotchy orange-red luminescence

Figure 5.3a. Matrix replacement dolomites observed in the Rimbey-Meadowbrook Reef Trend. "P" is an abbreviation for porosity. Scale bars = 500 μm.

Dolomite Cement Types

C1
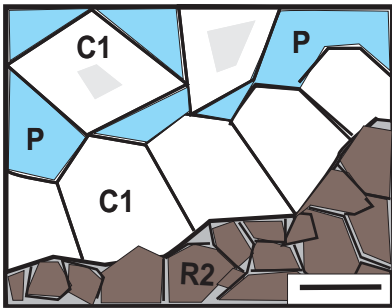
Unzoned dolomite cement (DC)

- micro- to macro-coarse crystalline
- planar-subhedral to planar-euhedral (PC)
- clear to cloudy white
- dull orange-red luminescence

C2
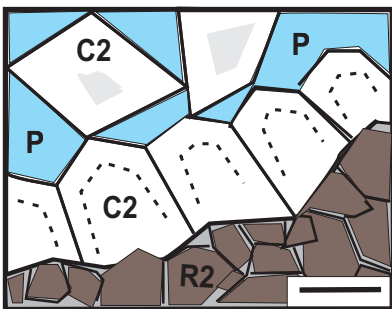
Zoned dolomite cement (limpid dolomite, LD)

- micro- to very coarse crystalline
- planar-subhedral to planar-euhedral (PC)
- zoned
- clear to cloudy white
- orange-red zoned luminescence

C3
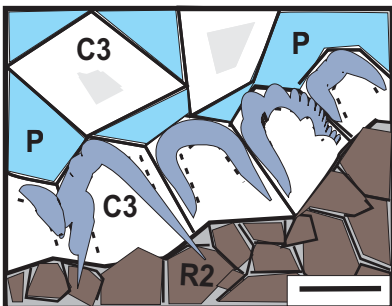
Fe-dolomite cement (FeDC)

- micro- to very coarse crystalline
- planar-subhedral to planar-euhedral (PC)
- zoned
- clear to cloudy white
- no luminescence

C4
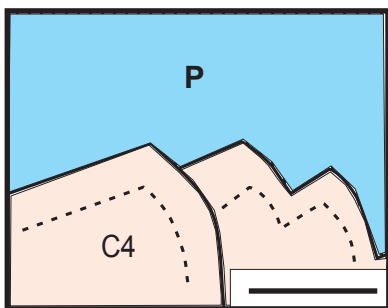
Saddle dolomite (SD)

- very to extremely coarse crystalline
- non-planar (NP)
- curved crystal faces with sweeping extinction
- homogeneous red luminescence

Figure 5.3b. Pore-lining dolomite cement types anticipated to be observed in the Rimbey-Meadowbrook Reef Trend. "P" is an abbreviation for porosity. Scale bars = 500 μm.

5.1 Matrix replacement dolomites

Matrix replacement dolomites are the most abundant diagenetic phase in the study area, making up at least 95% of all dolomites in the Woodbend Group (Huebscher, 1996). A few buildups, notably Golden Spike, Red Water, Strachan, and Phoenix, largely escaped dolomitization and the limestones are still preserved. In the Leduc Formation reefs, the matrix consists of two main types of dolomite: grey matrix dolomite and brown porous matrix dolomite. Both types are mostly fabric destructive on a microscopic scale (Amthor *et al.,* 1993).

Petrographically, these two types can be further divided into four types: R1, R3, R4, and R2 (Figure 5.3a). These types are listed in order of increasing abundance, with R2 being the most abundant one, reaching up to 90% of total volume of Leduc Formation dolomites. This number classification is adopted from Amthor *et al.* (1993) and enhanced by adding one additional type, R1, as a fine-crystalline version of R2. The letter 'R' in these abbreviations stands for 'replacement'.

5.1.1 Fine-crystalline grey matrix dolomite (R1)

Fine-crystalline grey matrix dolomite (R1) is brown to medium grey colored in hand specimens, forms densely packed planar subhedral to nonplanar anhedral crystal mosaics, with the average diameter varying between 30 and 62 micrometres (Plate 5.1.1.1, Plate 5.1.1.2a-f) and no visible porosity. Crystal sizes slightly increase toward the deeper part of the reef trend, coinciding with a gradual increase in the abundance of nonplanar

crystal boundaries. These "dirty" brown and cloudy crystals exhibit sharp extinction and dull red homogeneous or speckled orange-red cathodoluminescence (Plate 5.1.1.2f). In some sections, the crystals appear accumulated along stylolites and are coated by organic material.

R1 is the least abundant type in the study area. It is common in the Cooking Lake Formation and is relatively abundant in the Leduc Formation in the northern part of the Rimbey-Meadowbrook reef trend. R1 is rare or absent in the deeper parts of the reef trend (Strachan, Phoenix, Ricinus, Chedderville, Ram River and Crimson buildups).

R1 is also called R1 in Drivet (1993), Marquez (1994), Horrigan (1996) and Huebscher (1996). It was not included in Amthor's classification (Amthor *et al.,* 1993).

In addition, Horrigan (1996) reported some of what is classified here as R4 matrix dolomites as matrix dolomite R1. However, it makes more sense to keep all the fossil-replacive material in one group.

Huebscher (1996) slightly expanded the crystal size range for this type to 20 to 100 micrometres. In this study, this type refers only to matrices of up to 62 micrometres in diameter, and the larger fraction of Huebscher's R1 would be reclassified as a micro-medium crystalline subclass of R2.

Plate 5.1.1.1. Photograph of a 20 m Leduc core section from well 1AA/ 2-28-95-18W4 showing distribution of matrix dolomite R1. Scales are in cm at stratigraphic top. (A) Photograph of a core slab illustrating partially bitumen-stained dolomudstone. (B), (C), (D) Core photographs illustrating tight dolomite matrix with nodular/lenticular fabric. The original depositional texture appears to have been a floatstone dominated by crinoid and coral fragments.
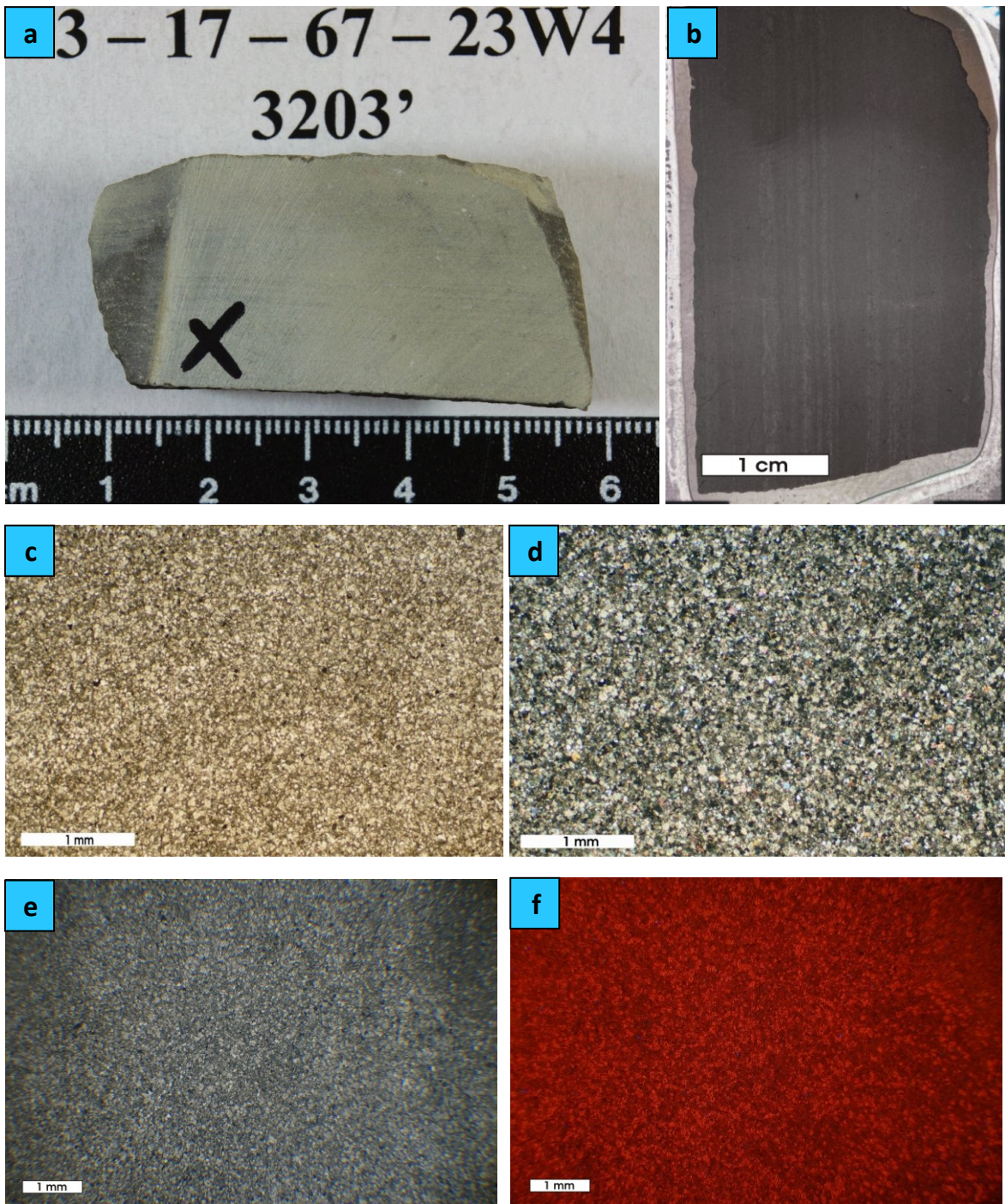
Plate 5.1.1.2. Examples of matrix replacement dolomite R1 in hand sample and thin sections. a) Hand specimen showing fine-crystalline grey matrix dolomite in sample SK-67-3, well 13-17-67-23W4 (3203ft); b) thin sections scan of sample SK-67-3; c) photomicrograph illustrating fine-crystalline matrix R1 in sample SK-67-3, plane polarized light; d) photomicrograph illustrating fine-crystalline matrix R1 in sample SK-67-3, cross-polarized light; e) photomicrograph of matrix R1 in sample SK-95-12, well 02-28-95-18W4 (434.77m); f) cathodoluminescence photomicrograph of matrix dolomite R1 of sample shown in (e) displaying speckled CL pattern.

49

5.1.2 Micro-medium- to macro-coarse crystalline grey matrix dolomite (R2)

Micro-medium- to macro-coarse crystalline grey matrix dolomite (R2) is grey – beige colored in hand specimens and forms dense, planar subhedral to nonplanar anhedral interlocking crystal mosaics with low or no visible intercrystalline porosity (Plate 5.1.2.1a-d). Individual crystals commonly display cloudy brown inclusion-rich cores and clear outer rims, with irregular boundaries between core and rim. Compared to R1 the average diameter is larger, ranging from 62 to 700 micrometres. Typically, the larger crystals of R2 occur along boundaries of vugs and molds, filling these voids to variable degrees, rarely completely. R2 exhibits straight, sometimes weakly undulose extinction, and is characterized by a homogeneous to blotchy dull orange-red cathodoluminescence (Plate 5.1.2.1d-f). Ghosts of original textures are uncommon in this matrix type. Low to high amplitude (cm-dimensions) stylolites pre- and postdate this dolomite type.

R2 is the most abundant type of dolomite in the Leduc Formation and often appears with other matrix dolomites (Plate 5.1.2.2A-F; Plate 5.1.3a, c and d). It was defined as "grey matrix dolomite" by Machel (1985), corresponds to type 1 of Amthor *et al.* (1993), and has the same designation (R2) in Drivet (1993), Marquez (1994), Horrigan (1996), and Huebscher (1996) (Table 5.1).
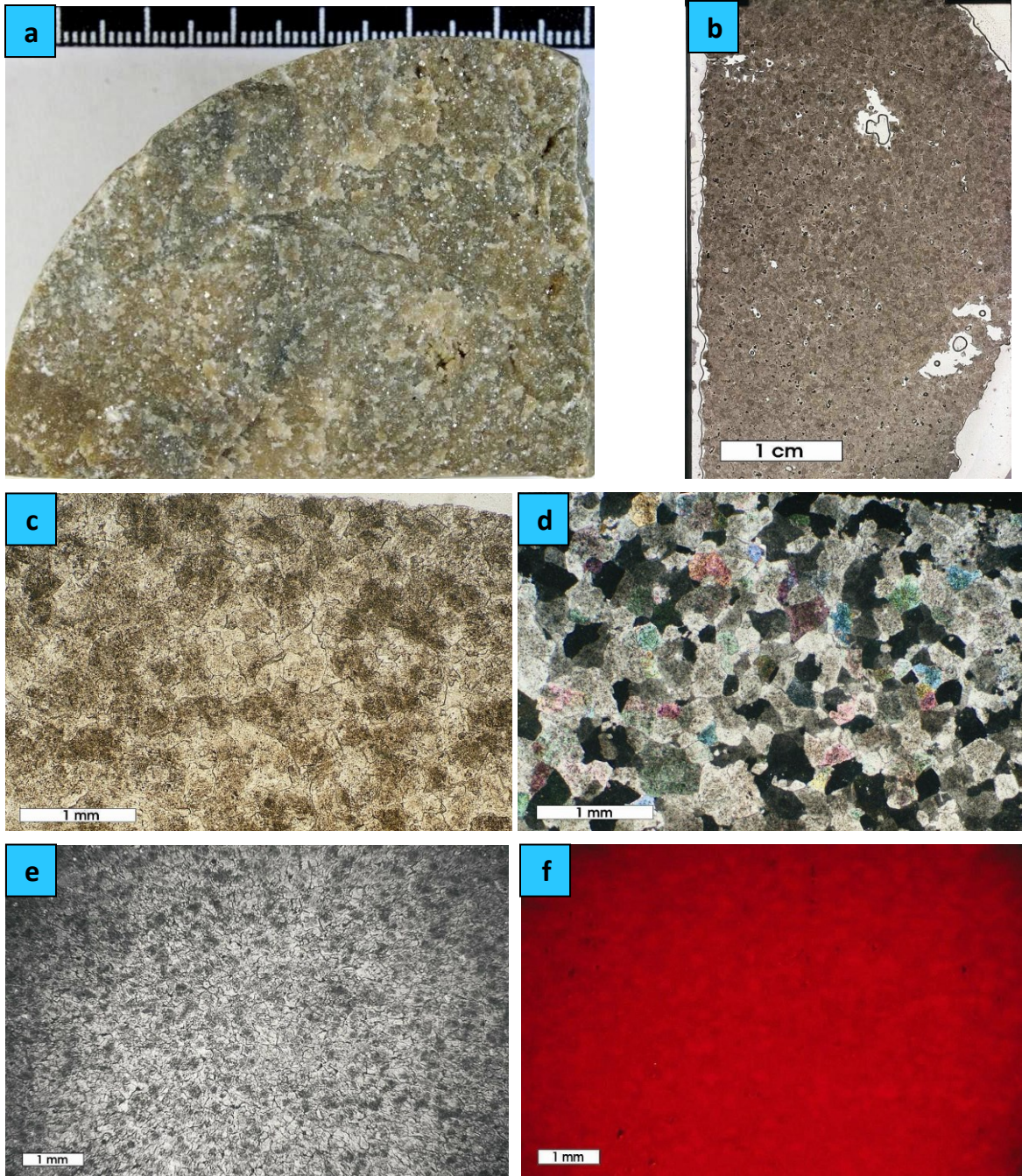
Plate 5.1.2.1. Examples of matrix dolomite R2 in hand sample and thin sections.
a) Hand specimen showing macro-coarse crystalline grey matrix dolomite R2 in sample SK-56-5, scale is in cm at stratigraphic top, well 16-24-56-26W4 (5279.8ft); b) thin section scan of sample EH-32 displaying association of R2 with vugs, well 10-31-37-09W5 (4325ft); c) photomicrograph illustrating macro-coarse crystalline matrix dolomite R2 in sample SK-54(2)-5, plane polarized light; d) photomicrograph of (b) in cross-polarized light; e) photomicrograph of micro-medium crystalline matrix dolomite R2 in sample HH-88-6, well 03-34-88-20W4 (1530 ft); f) cathodoluminescence photomicrograph of (e) illustrating blotchy CL pattern.
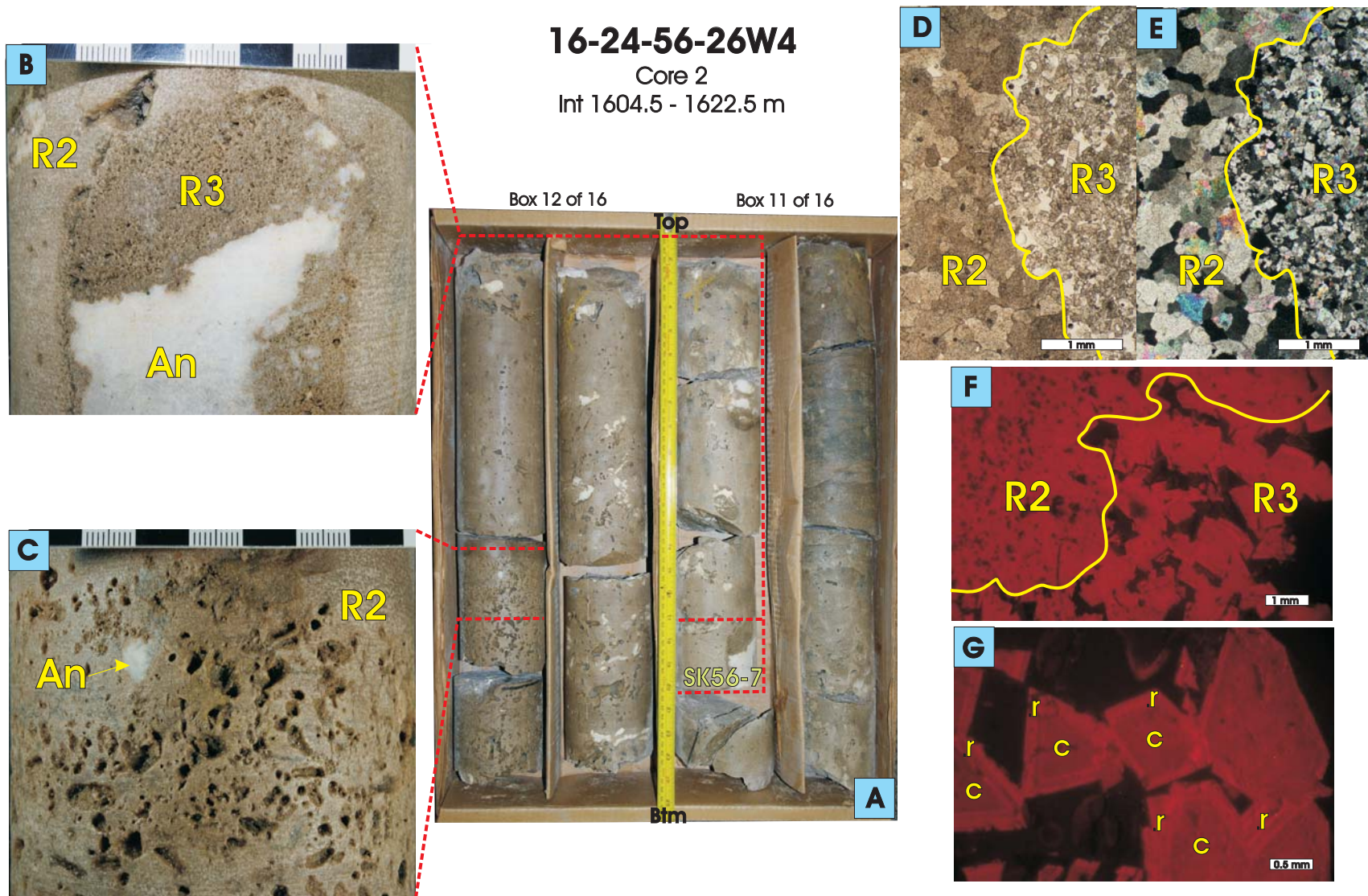
Plate 5.1.2.2. Photograph of an 18 m Leduc core section from well 16-24-56-26W4 (A) with a core slab (B) displaying a sharp contact between matrix dolomites R2 and R3. Anhydrite cement (An) filling vuggy pores also replaces dolomite R3 that itself replaced what appears to be a stromatoporoid. Core photograph (C) illustrates large uncemented moldic pores associated with dolomite R2. Some pores are filled with coarse anhydrite (An). Scales are in cm at stratigraphic top. Photomicrographs in plain- (D), cross-polarized light (E), and CL (F) showing 2 distinct domains with a transitional zone from R2 to R3, contacts between R2 and R3 are outlined in yellow; note the untypically coarse (macro-coarse crystalline) R2 vs. macro-medium crystalline R3 in (D) and (F) (sample EH-9, 5-13-37-12W5, 5047m). (G) Cathodoluminescence photomicrograph of (F) at a higher magnification illustrating zoned coarse dolomite R3 crystals with darker red cores (c) and brighter rims (r).

52

5.1.3 Brown porous matrix dolomite (R3)

Micro- to macro-coarse crystalline brown porous matrix dolomite (R3) appears sucrosic in hand specimens (Plate 5.1.3a). This dolomite is a combination of planar subhedral and planar euhedral crystals with diameters between 250 and 1000 micrometres (Plate 5.1.3b-d) and variable intercrystalline porosity. The crystal sizes tend to increase with increasing depth toward the southern part of the reef trend (Figure 5.5.4, see section 5.5). Euhedral crystals are coated by bitumen in many samples, hence the brown color. Individual crystals have cloudy, inclusion-rich cores (indeterminate amounts of clay minerals, fluid inclusions, and/ or hydrocarbons) surrounded by clear rims, with irregular boundaries between core and rim. Many crystals display well developed cleavage, sharp extinction, and microblotchy cathodoluminescence with orange-red cores and brighter red bands at the rims (Plate 5.1.3e-f, Plate 5.1.2.2G).

This dolomite is relatively common in the Leduc Formation and usually occurs in the areas around vugs and molds destroying all precursor sedimentary textures (Plate 5.1.3a, Plate 5.1.2.2). In some samples it is associated with anhydrite and calcite cements and is clustered along low-amplitude stylolites (Plate 5.1.2.2B).

R3 is more common toward the deeper end of the Rimbey-Meadowbrook reef trend, especially in the Morinville, Strachan, Ricinus, Chedderville, Ram River, and Crimson buildups. It is described as "brown porous matrix dolomite" by Machel (1985) and corresponds to the coarser porous portion of Type 2 dolomite as described by Amthor *et al.* (1993). This dolomite type was not reported by Huebscher (1996). The other previous authors listed earlier used the same designation R3 (Table 5.1).
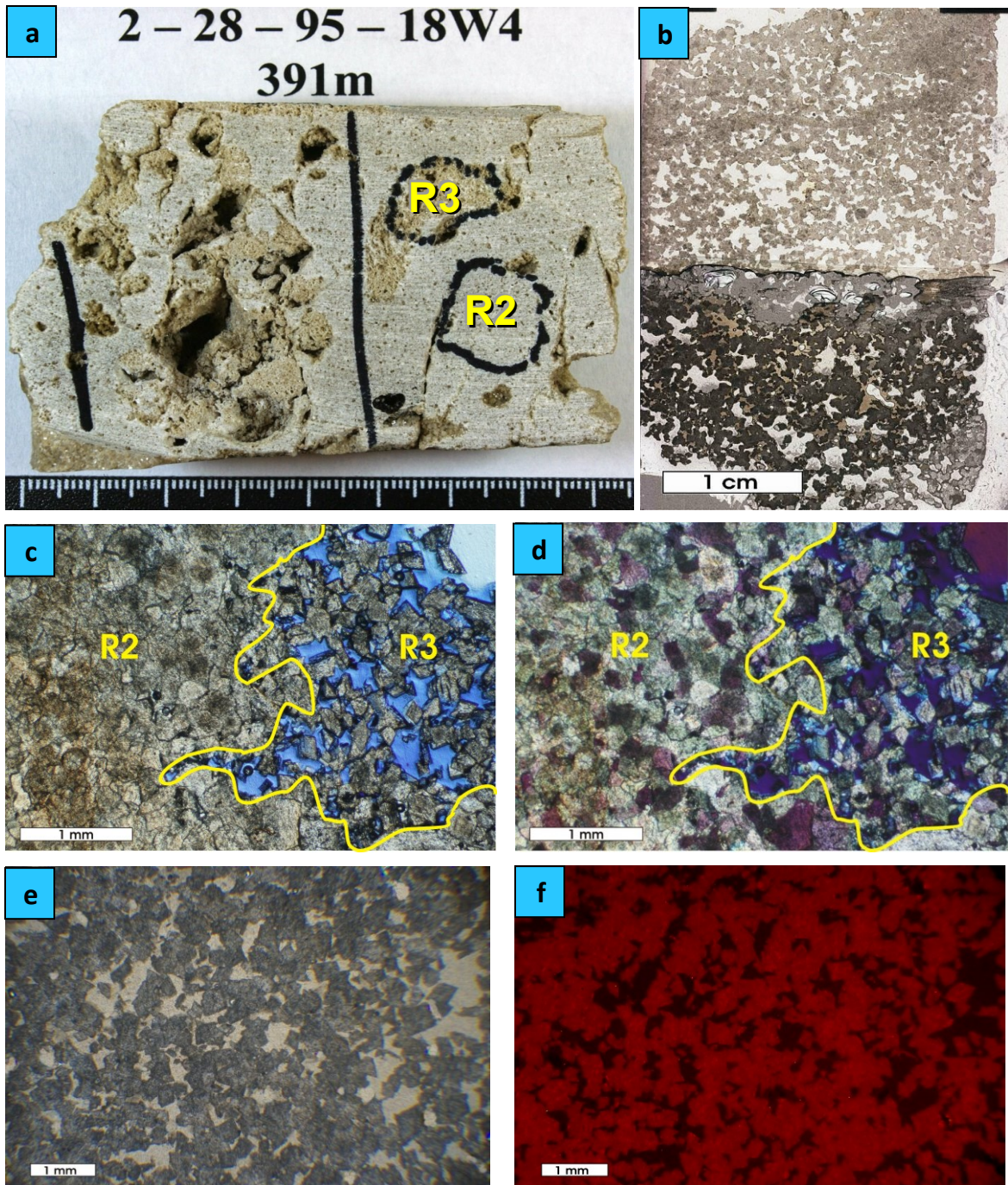
Plate 5.1.3. Examples of matrix replacement dolomite R3 in hand sample and thin sections.
a) Hand specimen showing brown porous matrix dolomite R3 associated with dolomite R2 in sample SK-95-5, well 02-28-95-18W4 (391m); b) thin section scan of sample H-62-5, well 16-22-62-25W4 (3720ft); c) photomicrograph of sample EH-64 illustrating a contact (outlined in yellow) between matrix dolomites R2 and R3 with blue-dye epoxy filled open pores, well 15-23-52-26W4 (1547.4 m), plane polarized light; d) photomicrograph illustrating porous matrix dolomite R3 in sample EH-64, cross-polarized light with a gypsum plate; e) photomicrograph of matrix dolomite R3 in sample SK 95-6, well 02-28-95-18W4 (400.4 m); f) cathodoluminescence photomicrograph of sample shown in (e) displaying zoned and blotchy CL patterns.

5.1.4 Dedolomite and Karst

Dedolomite (partially to completely calcitized dolomite) as found in the Rimbey-Meadowbrook reef trend is essentially matrix dolomites R2 or R3 affected by meteoric/karstic dissolution. Dedolomite occurs exclusively in the drill cores located along the boundary between the Grosmont Platform and the Cooking Lake platform (townships 61, 62, and 63) and below the sub-Cretaceous unconformity (north of township 80), in a region known to be pervasively karstified (*e.g.,* Machel *et al.,* 2012).

Dedolomites occur as micro- to macro-medium euhedral crystals exhibiting mottled orange-red cathodoluminescence (Plarte 5.1.4.1). These crystals are remnants of dolomite matrix largely replaced by calcite. The degree of calcitization ranges from selective (Plate 5.1.4.1c-d), affecting only particular zones of dolomite crystals, to complete (Plate 5.1.4.1f).

Karstified matrix dolomites appear sucrosic in hand specimens (Plate 5.1.4.2a) and form porous, partially calcitized mosaics of planar euhedral crystals, with average diameters varying between 62 and 1000 micrometres (Plate 5.3.6.2b-d). Many crystals display well developed cleavage, sharp extinction, and microblotchy orange-red luminescence (Plate 5.3.6.2e-f).

Crystal size distribution and crystal geometry of the dolomites remaining during dedolomitization and karstification are very similar to the ones of the matrix dolomite R3. These dolomite textures were previously discussed by Machel (2004) and Huebscher (1996) as products of partial dissolution of grey matrix dolomites.
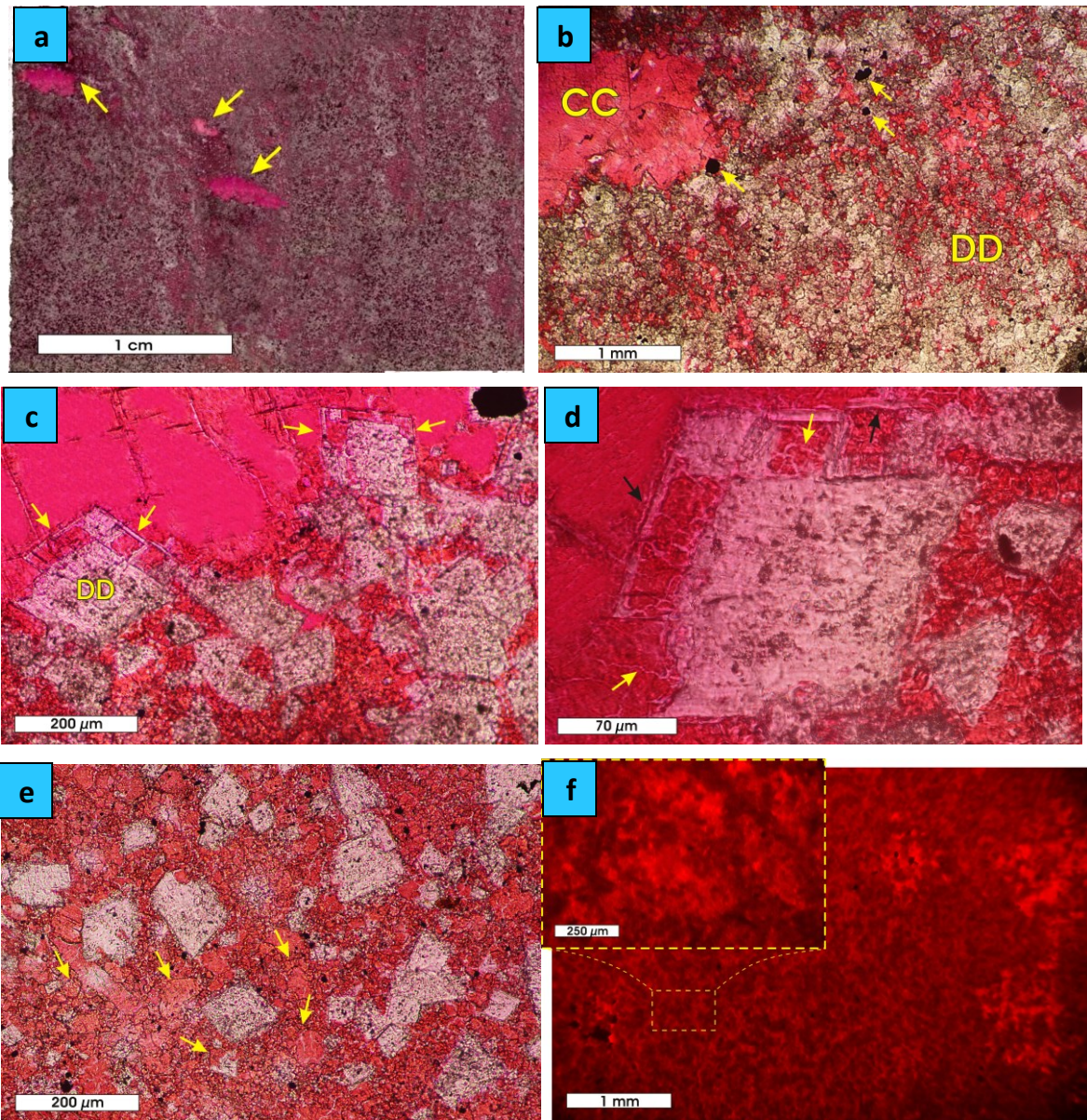
Plate 5.1.4.1. Examples of dedolomite in sample HH-66(2)-9, well 06-16-66-24W4 (1186.6 m).
a) Scan of a thin section stained with alizarin red-S illustrating calcitized dolomite with calcite grown into open voids (yellow arrows); b) plane-polarized light photomicrograph showing dedolomitization of matrix with calcite occluding the void; note opaque pyrite crystals (marked by yellow arrows) disseminated throughout the matrix; c) plane-polarized light photomicrograph illustrating selective calcitization of dolomite crystals (DD); note the remnants of outer parts of crystal rims and the inner parts replaced by calcite (marked by yellow arrows); d) plane-polarized light photomicrograph of calcitized dolomite crystal labled in (c) as DD illustrating preserved outer parts of crystal rim (marked by black arrows) and remnant dolomite veins spreading throughout calcitized parts (marked by yellow arrows); e) plane-polarized light photomicrograph illustrating complete calcitization of dolomite crystals; note the outlines of dolomite rhombs replaced by calcite (marked by yellow arrows) and opaque pyrite crystals disseminated throughout the matrix; f) cathodoluminescence photomicrograph with a close-up (yellow box) showing mottled luminescence of dedolomite.
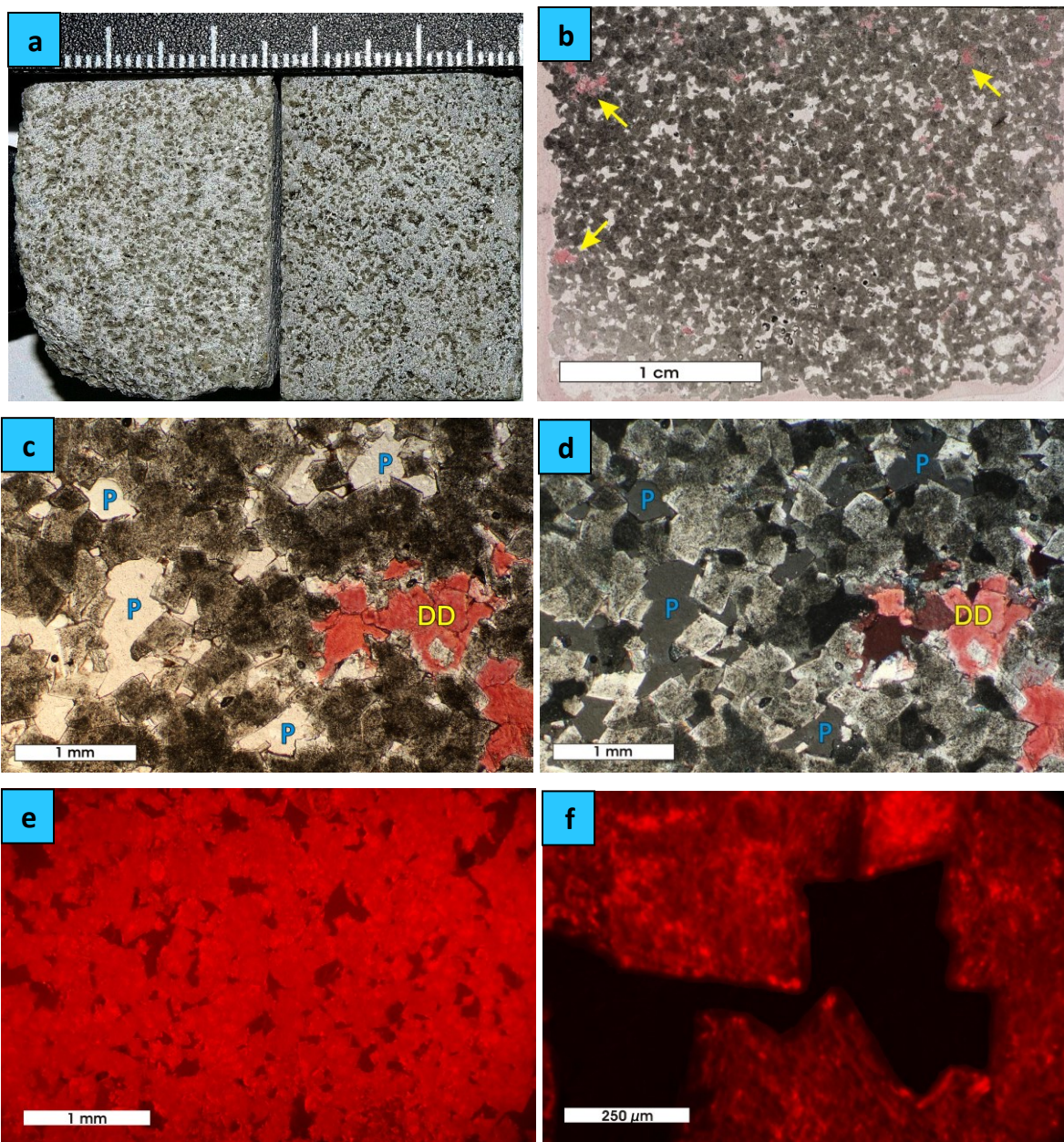
Plate 5.1.4.2. Examples of karstified dolomite in sample HH-61-1, well 07-31-61-24W4 (1064.1m).
a) Core photograph displaying karstification of Leduc Formation dolomite, scale is in cm at stratigraphic top;   b) thin section scan illustrating partial calcitization of karstified matrix dolomite (marked by arrows); c) plane-polarized light photomicrograph showing karst with partially dedolomitized (DD) matrix dolomite, P = porosity; d) photomicrograph of (c) in cross-polarized light; e) and f) cathodoluminescence photomicrographs of karsified sample; note blotchy luminescence of dolomite crystals.

5.1.5 Mimetic dolomite (R4)

Fine- to macro-medium crystalline mimetic dolomite (R4) occurs as planar subhedral to nonplanar anhedral crystals 30 to 250 micrometres in diameter (Plate 5.1.5a-e). In some samples (townships 39, 48, 70 and 88), crystal sizes reach 550 micrometers. This type usually macroscopically mimics the textures of calcite cements and biochems. Individual crystals exhibit straight to weakly undulose extinction and have dull red cathodoluminescence (Plate 5.1.5d,f).

Matrix dolomite R4 appears mostly in *Amphipora* and *Thamnopora* grainstones. Stylolites are commonly associated with this type of dolomite.

This texture was also described by Amthor *et al.* (1993), who called it D4, and by Drivet (1993), Marquez (1994), and Horrigan (1996), who called it R4 (Table 5.1). Horrigan (1996), however, reported some of what is classified here as matrix dolomite R4 as her matrix dolomite R1. In this study, all the fossil-replacive material of Horrigan's R1 is reclassified as the R4 type.
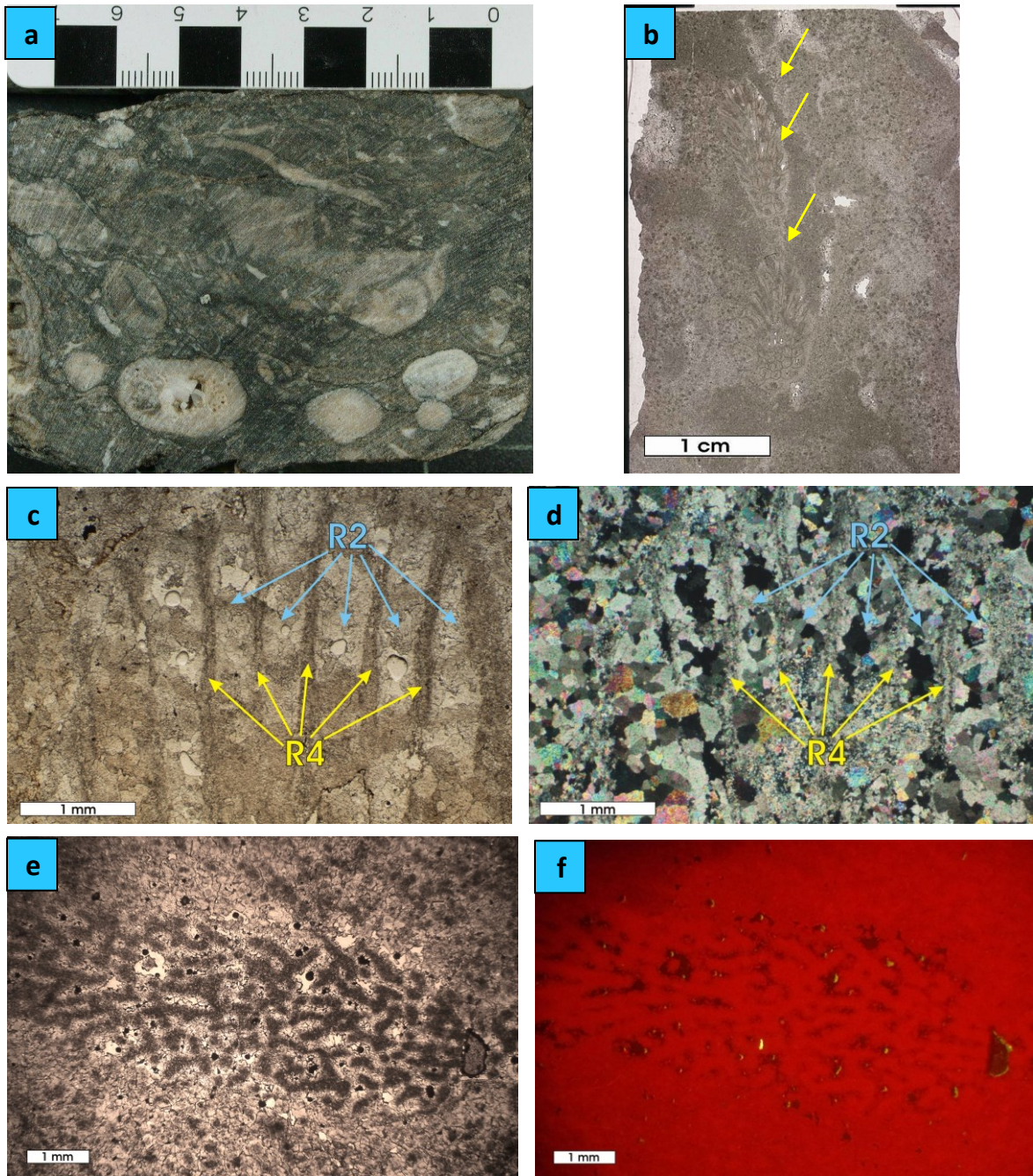
Plate 5.1.5. Examples of matrix replacement dolomite R4 in hand samples and thin sections.
a) Photograph of a core slab illustrating matrix dolomite R4 mimetically replacing allochems, scale is in cm at stratigraphic top, well 12-25-44-1W5 (4908.5 ft); b) thin sections scan of sample SK-55-4 showing longitudinal to oblique view of mimetically replaced *Thamnopora sp.* coral branch with exquisitely preserved septa and tabulae (marked by yellow arrows), well 02-16-55-25W4 (4372ft); c) photomicrograph of sample SK-55-4 illustrating mimetic dolomite replacement of *Thamnopora sp.* coral with well-preserved intercorralite wall structure (marked by yellow arrows) and macro-medium grained sediment dolomitized into R2 that infills the interseptal spaces (marked by blue arrows), plane polarized light; d) photomicrograph of (c) in cross-polarized light; e) photomicrograph of sample HH-88-6 showing mimetic dolomite replacement of *Thamnopora sp.* coral, well 03-34-88-20W4 (1530 ft), plane polarized light; f) cathodoluminescence photomicrograph of (e).

59

5.2 Dolomite cements

Dolomite cements appear in almost every core, albeit in very small percentages (<<5%), typically lining or in some cases occluding smaller pores and larger vugs, thus, reducing remnant porosity. Three types of dolomite cements, DC1, DC2 and DC4, postdating the matrix dolomites, are present in the Leduc reefs (Figure 5.3b). Dolomite cement DC3 was also considered in this study mainly because it was previously reported by Huebscher (1996) in the overlying Grosmont intervals.

5.2.1 Unzoned dolomite cement (DC1)

Unzoned dolomite cement (DC1) forms micro- to macro-coarse crystalline subhedral to euhedral crystals between 250 to 1000 micrometres in size. This type is clear to cloudy white crystals and mottled dull orange-red cathodoluminescence (Plate 5.2.1a-c). This dolomite is equivalent to DC1 of Huebscher (1996) and was not reported by the other previous authors listed earlier (Table 5.1).

5.2.2 Zoned dolomite cement (DC2)

Zoned dolomite cement (DC2) occurs as micro to very coarse, subhedral to euhedral, zoned crystals between 250 to 1500 micrometers in size. This type is clear to cloudy white crystals with cloudy, inclusion-rich cores and clear rims (Plate 5.2.1d). It displays straight extinction and mottled dull orange-red cathodoluminescence with two or more growth zones ranging from bright red and orange to dull red (Plate 5.2.1e-f). This dolomite type occurs as the only cement phase, or associated with later-stage calcite or anhydrite cements (Plate 5.2.1d-e).
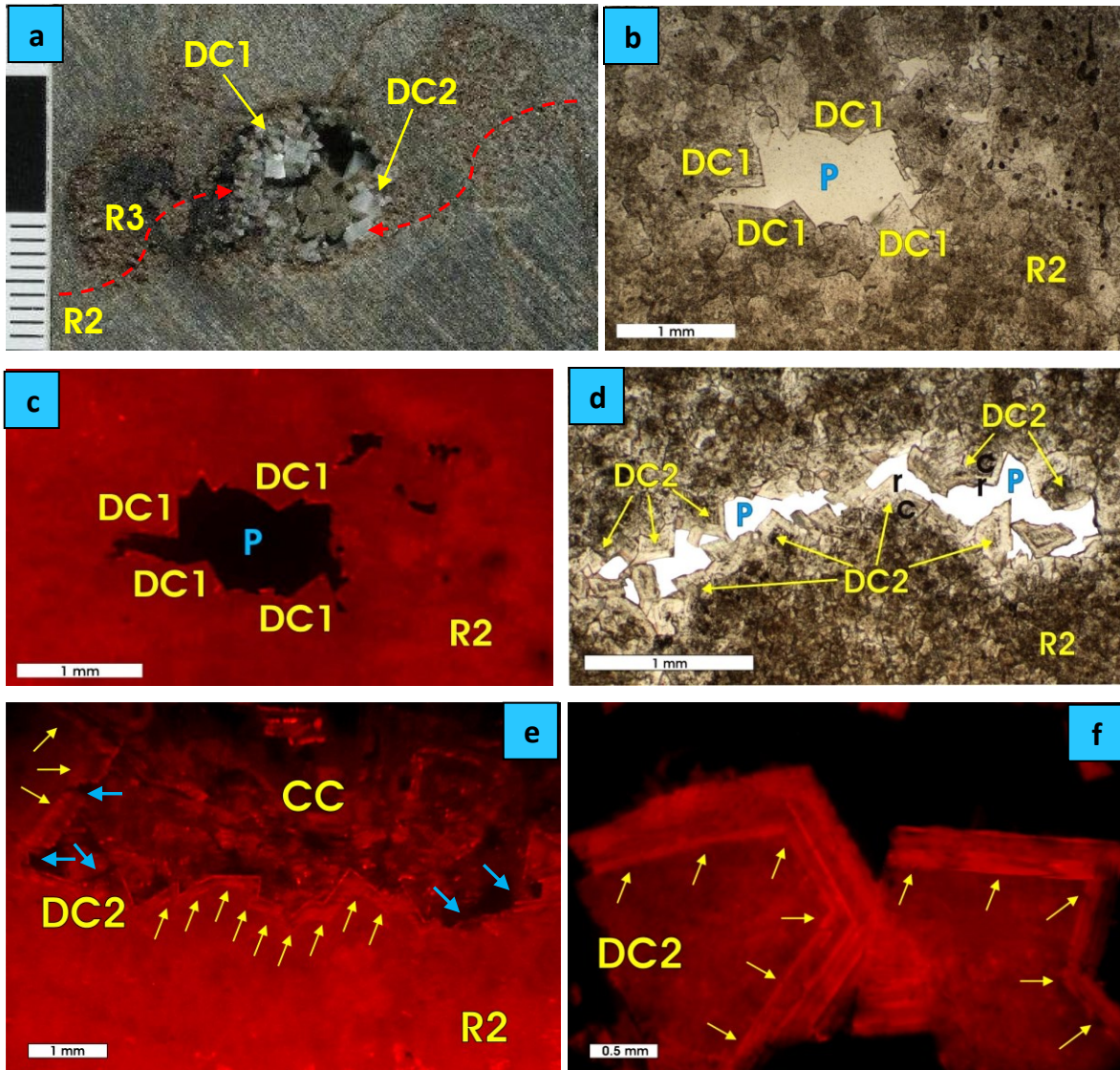
Plate 5.2.1. Examples of dolomite cements DC1 and DC2 in hand specimen and thin sections.
a) Photograph of a core slab illustrating dolomite cements DC1 and DC2 partially filling the vug; note the transition from R2 to R3 and later cementation on top of R3 (red arrows); scale is in cm at stratigraphic top, well 12-25-44-1W5 (7889.9 ft); b) photomicrograph illustrating unzoned cloudy dolomite cement DC1 developed on matrix dolomite R2 in sample EH-50, P = pore space, well 14-05-41-02W5 (8284ft), plane polarized light; c) cathodoluminescence photomicrograph of (b) showing no zonation in DC1 dolomite crystals; d) photomicrograph illustrating zoned dolomite cement DC2 lining moldic porosity (P) in sample HH-70-6; note cloudy cores (c) and clear rims (r), well 03-28-70-24W4 (3568 ft), plane polarized light; e) cathodoluminescence photomicrograph of sample EH-47 displaying zonation (marked by yellow arrows) in dolomite cement DC2, subsequent calcite cement (CC) occludes the pore space, R2 dolomite is present in the periphery; note slightly corroded rims of DC2 in some places (marked by blue arrows) and alternating orange to dull red zones in sparry Fe-calcite crystals, well 03-20-47-27W4 (1998.9m); f) cathodoluminescence photomicrograph illustrating dolomite DC2 rims with an alternation of dark red and orange-red zones (yellow arrows), black area is pore space, sample SK-44(2)-4, well 12-25-44-01W5 (7888.6 ft).

Zoned dolomite cement (DC2) is described as limpid dolomite by Machel (1985) and corresponds to Type 3 dolomite of Amthor *et al.* (1993), C1 in Drivet (1993) and Marquez (1994) and DC2 in Huebscher (1996) (Table 5.1).

5.2.3 Fe-dolomite cement (DC3)

Fe-dolomite cement is similar to zoned dolomite DC2 displaying cloudy inclusion –rich cores with limpid rims (Figure 5.3b). Due to the high content of Fe the clear overgrowths turn turquoise to light blue in thin sections stained with potassium ferricyanide. DC3 is not luminescent.

This is the Fe-dolomite cement of Huebscher (1996), who reported this type in the Lower Grosmont and Upper Grosmont intervals overlying the Leduc Formation in the northern part of the reef trend.

Even though this type was included into the dolomite classification (Figures 5.1 and 5.3b), it was not found in the Rimbey-Meadowbrook Reef Trend. All zoned dolomite cements display bright orange-red to dull red CL zonation (Plate 5.2.1e-f), as opposed to non-luminescent crystal overgrowths typical for DC3.

5.2.4 Saddle dolomite (DC4)

Saddle dolomite (DC4) is very- to extremely-coarse crystalline with diameters ranging between ~1 and 5 mm. Most crystals are cement, white to milky colored, have curved faces, and partially or completely occlude molds and vugs. In some samples they are covered with bitumen. They exhibit sweeping extinction under the cross polarized light and have sharp boundaries to other diagenetic phases (Plate 5.2.2a-e).

This dolomite type displays either a homogeneous dull red, in some samples blotchy, cathodoluminescence with no zonation in the southern part of the reef trend, or a dull red to bright orange-red, zoned cathodoluminescence in the northern part of the reef trend (Plate 5.2.2f).

Saddle dolomite DC4 is less common than DC1, DC2 and DC3, comprising less than 1 vol.% of the rocks (Section 5.5). It postdates all of these cements. Saddle dolomite is present only in the Ram River, Ricinus West, Chedderville, Garrington, Sylvan Lake, Wizard Lake and Leduc Woodbend buildups.

DC4 is equivalent to Type 5 dolomite in Amthor *et al.* (1993), and corresponds to C2 in Drivet (1993) and Marquez (1994). It was not reported by Horrigan (1996) and Huebscher (1996) (Table 5.1).
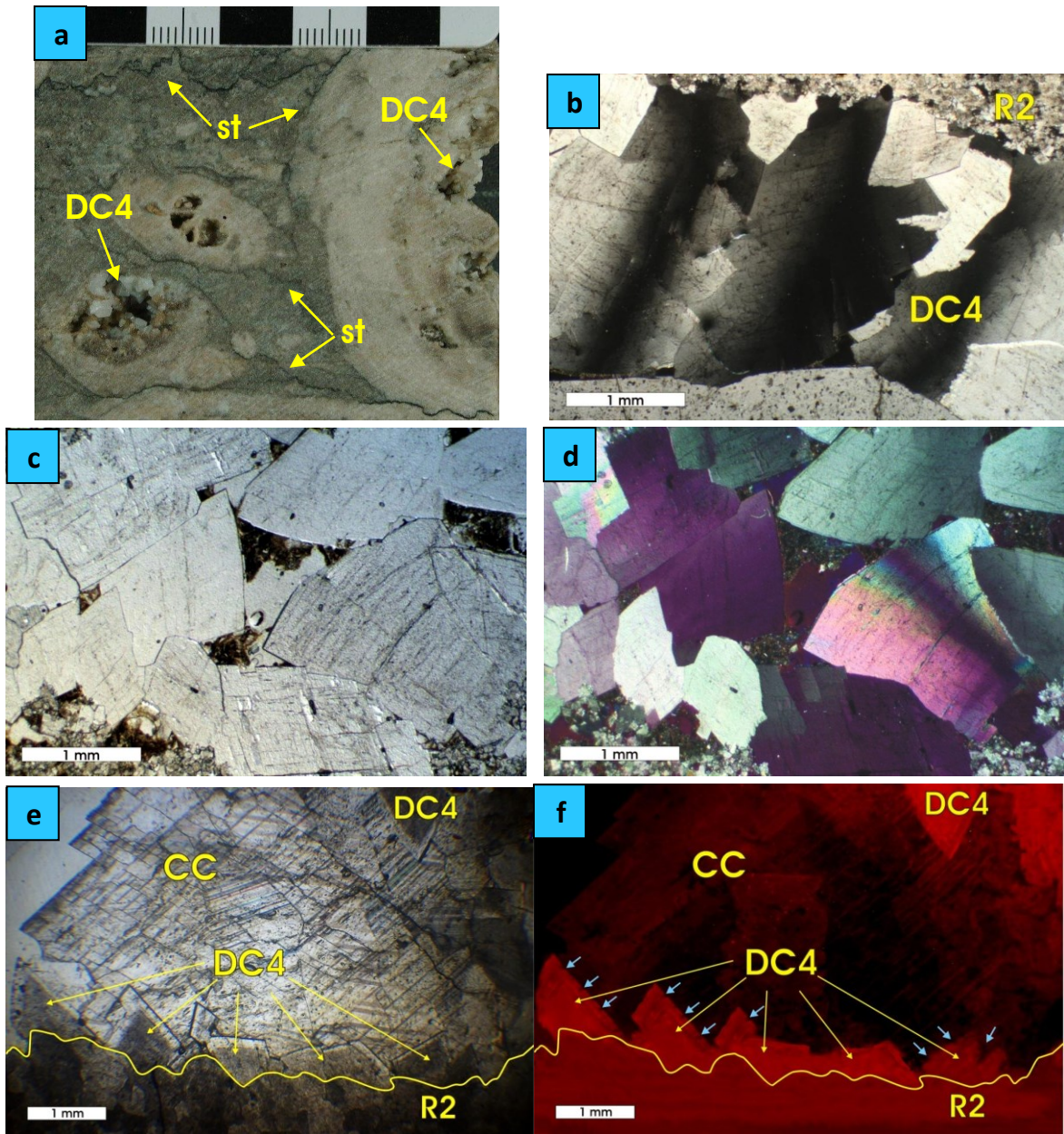
Plate 5.2.2. Examples of saddle dolomite cement DC4.
a) Photograph of a core slab showing saddle dolomite (DC4) cementing vugs left by partial dissolution of stromatoporoid and corals; note stylolites (st) surrounding allochems and cross-cutting the matrix dolomite, well 12-25-44-1W5 (8027.5 ft); b) cross-polarized light photomicrograph of sample EH-39 illustrating sweeping extinction of saddle dolomite; note the distinct contact between saddle (DC4) and matrix (R2) dolomites, well 07-34-33-06W5 (3969.7m); c) photomicrograph of sample N-182 illustrating saddle dolomite crystals lining a large solution-enhanced vug; note coarse crystal size and curved faces of saddle dolomite, well 08-16-51-25W4 (5851ft), plane-polarized light; d) photomicrograph of (c) in cross-polarized light with a gypsum plate; note the sweeping extinction of saddle dolomite; e) photomicrograph of sample EH-9 showing dolomite cement DC4 in pore space later filled by sparry calcite cement (CC); note the curved crystal faces of saddle dolomite and distinct contact between DC4 and matrix dolomite R2 (outlined in yellow), well 5-13-37-12W5 (5047m), plane-polarized light; f) cathodoluminescence photomicrograph of (e) showing the contact (yellow line) between zoned saddle dolomite DC4 and R2, note the nonluminescent calcite cement (CC) and slightly corroded DC4 rims (blue arrows).

5.3 Later diagenetic phases

5.3.1 Pressure solution features

Pressure solution features are present in most samples of the Rimbey-Meadowbrook Reef Trend, mainly as dissolution seams with clay residues, and as wispy stylolites with amplitudes of up to several centimeters (Plates 5.2.2a and 5.3.1a-f). Most stylolites are devoid of hydrocarbons, yet some include black organic residues (Plate 5.3.1d). Stylolites are usually located at the contacts between two different facies types and are more common in fine-grained sediments that contain dark clay minerals, sulfides and organic material (Plate 5.3.1a-b).

Stylolites occur completely undisrupted (forming continuous, often sutured to serrated accumulations of clay minerals) throughout the dolomite framework, crosscutting the matrix with crystals exhibiting different extinction on both sides (Plate 5.3.1e-f). However, locally, microstylolites appear disrupted by dolomite crystals (Plate 5.3.1d). Dissolution seams usually pass around dolomite crystals in anastomosing pattern and do not cut them (Plate 5.3.1c).

5.3.2 Secondary anhydrites

Diagenetic anhydrites in the drill cores occur as a late pore filling cement or replacive phase within Leduc Formation dolostones. Most anhydrites are milky-white to greyish translucent in hand specimens and consist of irregularly shaped clusters with a
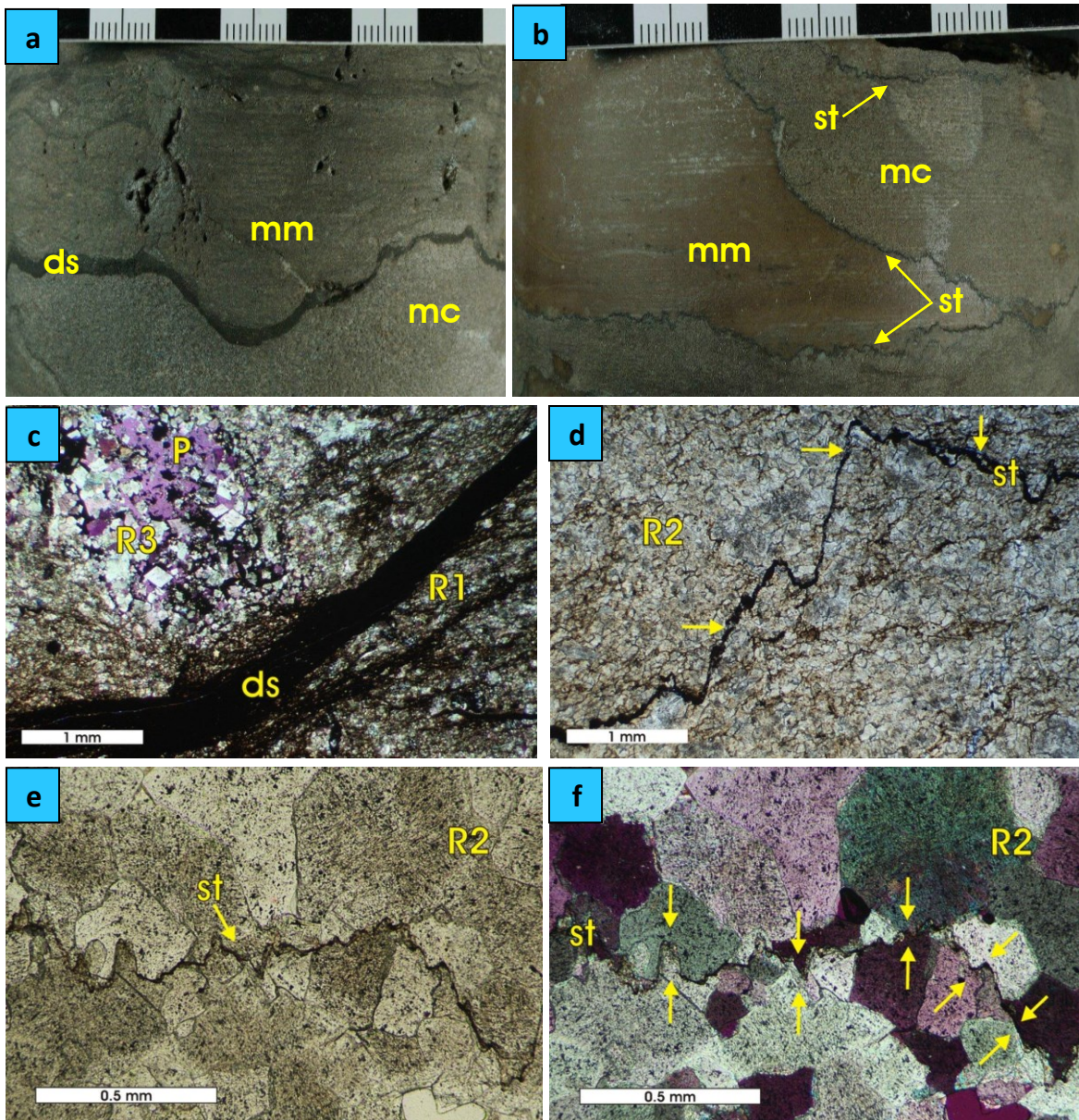
Plate 5.3.1. Examples of solution seams and stylolites.

a) Photograph of a core slab showing matrix dolomite R2 cross-cut by dissolution seam (ds); note crystal size variation from micro-medium crystalline (mm) on one side of solution seam to micro-coarse crystalline (mc) on the other side, scale is in cm at stratigraphic top, well 02-05-58-25W4 (1412.75 ft); b) photograph of a core slab showing low amplitude stylolites (st) located at the contacts between micro-medium (mm) and micro-coarse (mc) crystalline matrix dolomites R2, scale is in cm at stratigraphic top, well 02-05-58-25W4 (7333 ft); c) photomicrograph of sample N-91 illustrating matrix dolomite R1 cross-cut by hydrocarbon filled anastomosing dissolution seams (ds); note bitumen coated dolomite R3 crystals in remnant pore space (P), well 06-11-51-26W4 (1759.3 m), cross-polarized light with a gypsum plate; d) photomicrograph in plane-polarized light illustrating hydrocarbon filled high amplitude stylolite (st), which appears to be locally disrupted by matrix dolomite R2 crystals (marked by yellow arrows), sample EH-61, well 15-23-52-26W4 (1535.4 m); e) photomicrograph of sample N-144 illustrating matrix dolomite R2 cross-cut by clay filled stylolite (st), well 16-07-47-27W4 (2104.4 m), plane-polarized light; f) photomicrograph of (e) in cross-polarized light with a gypsum plate showing dolomite crystals truncated by stylolite (st); note different extinction of dolomite crystals on both sides of stylolite (yellow arrows).

66

range of textures and crystal sizes. Some of these clusters form meshes of felted microcrystalline (about 30 μm long) anhedral fibers (Plate 5.3.2a, c, d), others as very to extremely coarse (up to 2 cm) corrotopic anhydrite (Plate 5.1.2.2.B, plate 5.3.2b, e, f). Both types are non-luminescent.

The replacive nature of felted and corrotopic anhydrites can be seen from the floating remnants of dolomite crystals (some are corroded) and angular clasts of dolomitized host rock within anhydrite aggregates (Plate 5.3.2b-f). Most anhydrites postdate dolomite cements and are associated with stylolites (Plate 5.3.2c, e). Minor amounts of anhydrite are coated with bitumen (Plate 5.3.2e). The relationship between anhydrites and sparry calcite cements is unclear as these diagenetic phases do not occur together in the samples examined.

5.3.3 Sparry calcite cements

Two types of calcite cement, sparry calcite and sparry Fe-calcite, were identified based on their response to staining with potassium ferricyanide and cathodoluminescence. Both types typically occur as coarse poikilotopic crystals (up to 1.5 cm) filling vugs, molds, fenestral pores and fractures (Plate 5.3.3a-c). Both cements are characterized by white to translucent color, distinct crystal planes (subhedral) and inclusion-rich crystals with sharp extinction (Plate 5.3.3c-e). Some crystals contain oil inclusions (Plate 5.3.3d).

Sparry calcite cements exhibit no apparent zonation and display no cathodoluminescence (Plates 5.2.2e-f and 5.3.3c-g). Sparry Fe-calcite cements, however, reveal alternating pink (Fe-poor) and light purple (Fe-enriched) zones when stained with
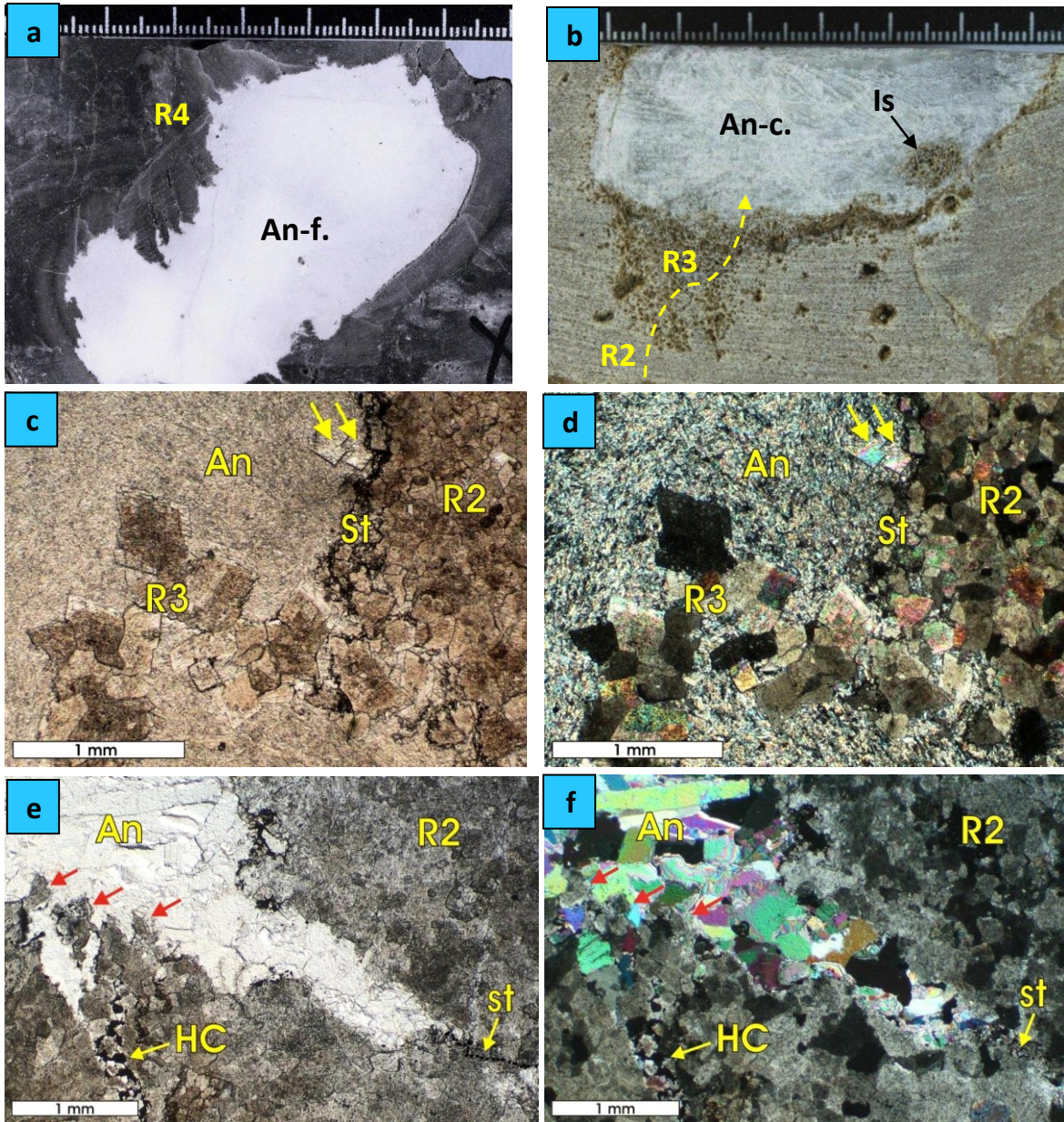
Plate 5.3.2. Examples of anhydrites in study area.
a) Core photograph of sample SK-54-11 displaying felted anhydrite (An-f.) replacing matrix dolomite R4 that has itself replaced what appears to be tabular stromatoporoid, scale is in cm at stratigraphic top, well 14-18-54-25W4 (5347ft); b) core photograph of sample SK-56-07 showing a transition from matrix dolomite R2 to porous matrix dolomite R3 (yellow arrow) and subsequent cementation of the vug/ replacement of R3 by corrotopic anhydrite (An-c.); note the floating 'island' of R3 (Is) within the anhydrite, scale is in cm at stratigraphic top, well 16-24-56-26W4 (1616.875 m); c) photomicrograph of sample SK-42-1 illustrating fine crystalline mesh of felted anhydrite (An) filling vuggy pores and replacing matrix dolomite R3, remnant 'islands' and corroded crystals (marked by yellow arrows) of dolomite R3 are floating within the anhydrite; note stylolite (St) rimming the vug and separating dolomite R2 from anhydrite, well 10-04-42-01W5 (2579.1m), plane-polarized light; d) photomicrograph of (c) in cross-polarized light; e) photomicrograph of sample N-215 illustrating corrotopic anhydrite (An) along stylolite (st); note the floating clasts of dolomitized host rock (marked by red arrows) within the anhydrite and bitumen (HC) coating microvug, well 03-20-47-27W4 (1998.9m), plane-polarized light; f) photomicrograph of (e) in cross-polarized light.
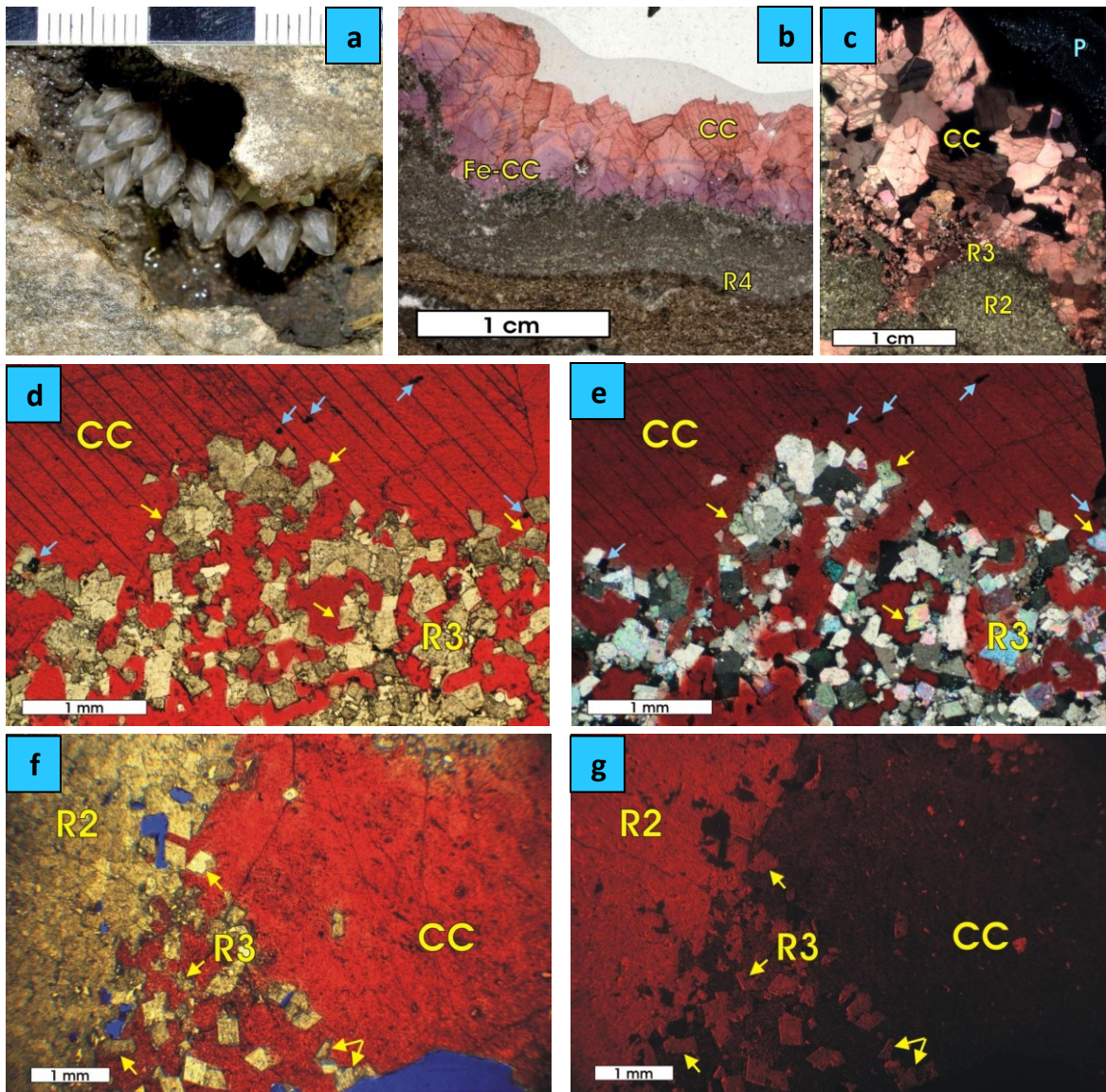
Plate 5.3.3. Examples of later-diagenetic calcite cements.

a) Photograph of a core slab showing calcite crystals grown in a vug, scale is in cm at stratigraphic top, well 02-05-58-25W4 (1409.2 m); b) scan of a thin section stained with potassium ferricyanide showing alternating pink (CC) and light purple (Fe-CC) zones in Fe-rich sparry calcite cement coating a vug, sample HH63-8, well 05-24-63-25W4 (1333.5 m); c) thin section scan of sample HH 88-3 in cross-polarized light showing sparry calcite cement (CC) crystals infilling a vug; note the transition from R2 to R3 and later poikilotopic cementation around the R3 crystals, P=open pore space, well 03-34-88-20W4 (425.5 m); d) photomicrograph of sample SK-58(2)-3 in plane-polarized light illustrating extremely coarse crystalline sparry calcite cement (CC) stained with alizarin red-S poikilotopically filling intercrystal pore spaces between matrix dolomite R3 crystals, excess calcite grown into the open void; note partial replacement of dolomite R3 (corroded R3 crystals marked by yellow arrows) and oil inclusions (marked by blue arrows) within the calcite, well 02-05-58-25W4 (1410.35 m); e) photomicrograph of (d) in cross-polarized light; f) plane-polarized light photomicrograph of sample SK-58(2)-3 showing the transition from dense matrix dolomite R2 to porous dolomite R3 with blue epoxy filled open pores and later cementation by poikilotopic sparry calcite (CC, stained with alizarin red-S); note the corroded crystals of dolomite R3 (marked by yellow arrows) floating within the calcite; g) cathodoluminescence photomicrograph of (f) showing nonluminescent calcite cement (CC) and slightly corroded R3 crystals (yellow arrows).

69

potassium ferricyanide (Plate 5.3.3b). These zones correspond to alternating orange to dull red zones in CL (Plate 5.2.1e).

Sparry calcite cements are generally rare in the Leduc Formation reefs but locally reach up to 24% in some reefs (Appendix 3, Section 5.5). Their distribution roughly coincides with that of saddle dolomite. Sparry Fe-calcite cement occurs only in the northern part of the reef trend beneath the Grosmont heavy oil reservoir (Huebscher, 1996). The relationship between these two phases is unclear as these cements do not occur together. However, both calcite cements postdate all dolomite phases (matrix and cements) (Plates 5.2.1e, 5.2.2f, and 5.3.3, Section 8.1).

5.3.4 Solid bitumen

Solid bitumen, also referred to as 'dead oil', is a frequent component of the Rimbey Meadowbrook Reef Trend. It occurs as both pore-lining and pore-filling substance throughout the study area (Plate 5.3.4.1). According to Lomando's classification (1992), it appears as one of three morphotypes: droplets, carpets, and peanut brittle. The first one is represented by individual rounded "blobs" attached to the pore walls (Plate 5.3.4.1a-b). The second one continuously coats the vug walls (Plate 5.3.4.1c-d). The third one coats the walls discontinuously and has random rounded particles in the intercrystalline porosity (Plate 5.3.4.1e-f).

'Dead oil' stain is found mainly in the southern and northern parts (Plate 5.3.4.2) of the Rimbey-Meadowbrook Reef Trend showing only rare traces or no bitumen between townships 47 and 67 (Plates 3.2.1 and 5.1.2.2A-C).
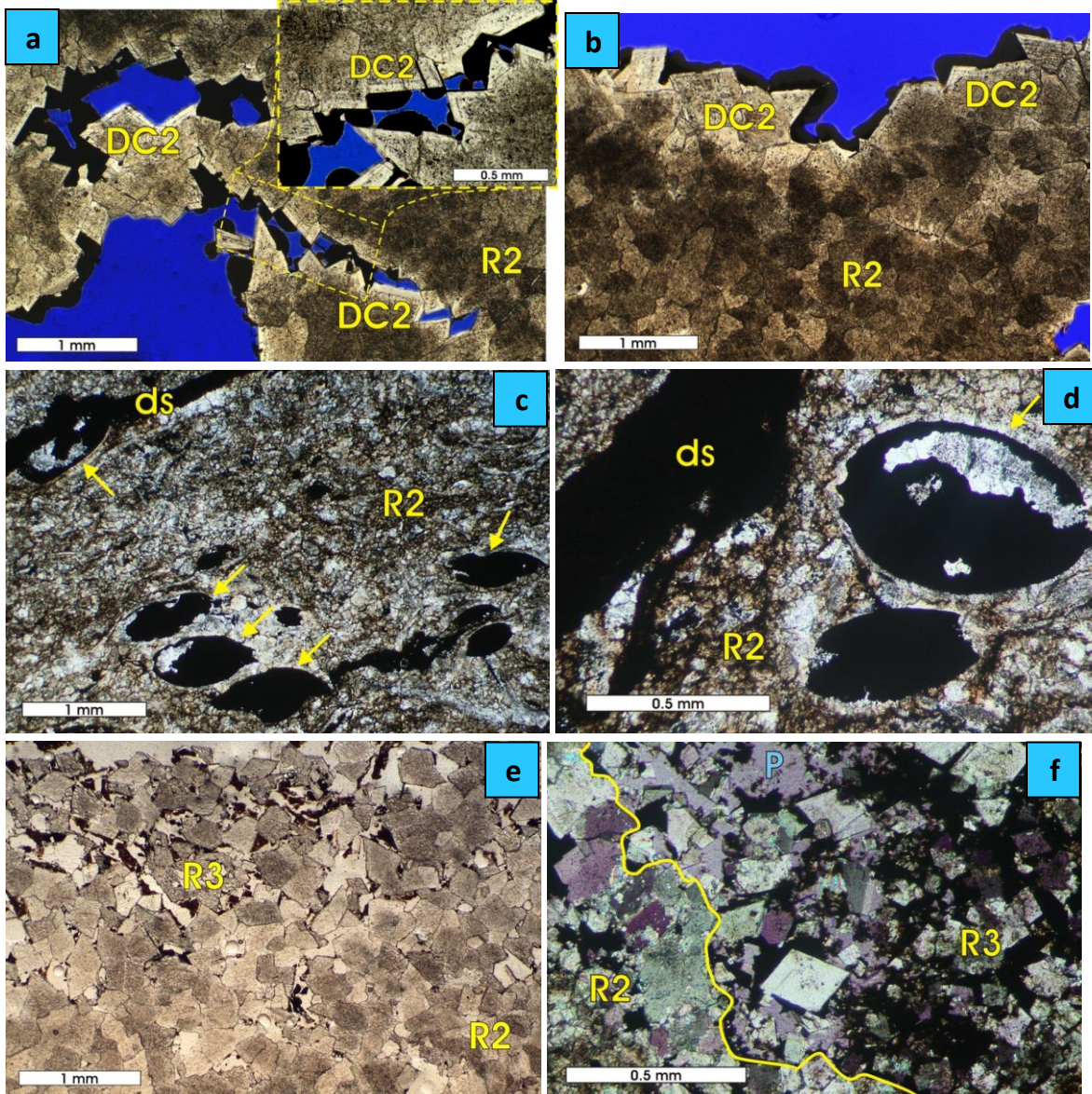
Plate 5.3.4.1. Photomicrographs illustrating solid secondary bitumen in the Leduc reefs.

a) Photomicrograph of sample N-132 showing droplets of bitumen coating zoned dolomite DC2 crystals in open pores; note the close-up photomicrograph of the outlined area (yellow box), well 16-07-47-27W4 (2159.5 m), plane-polarized light, blue-dye epoxy; b) photomicrograph of sample N-132 in plane-polarized light illustrating a thin layer of bitumen droplets almost completely coating blue epoxy filled microvug, note zoned dolomite cement DC2 grown over matrix dolomite R2; c) photomicrograph of sample N-91 illustrating remnants of ostracodes (marked by yellow arrows) that have their outer shells preserved and interiors dissolved and now holding bitumen (carpets); note matrix dolomite R2 cross-cut by hydrocarbon- filled dissolution seam (ds), well 06-11-51-26W4 (1759.3 m), plane-polarized light; d) photomicrograph of sample N-91 in plane-polarized light displaying bitumen-filled remnants of ostracodes with their outer shells replaced by quartz (yellow arrow); note the dissolution seam (ds) passing around R2 dolomite crystals in anastomosing pattern; e) photomicrograph of sample SK44(1)-7 showing peanut brittle bitumen patches in the intercrystalline porosity; note the transition from R2 to R3, well 11-27-44-01W5 (2248.9 m), plane-polarized light, f) photomicrograph of sample N-91 in cross-polarized light with a gypsum plate illustrating peanut brittle bitumen patches in the intercrystalline porosity (P, light purple) between dolomite R3 crystals; note the contact (outlined in yellow) between two distinct domains of dense matrix dolomite R2 mosaic and porous dolomite R3.

71
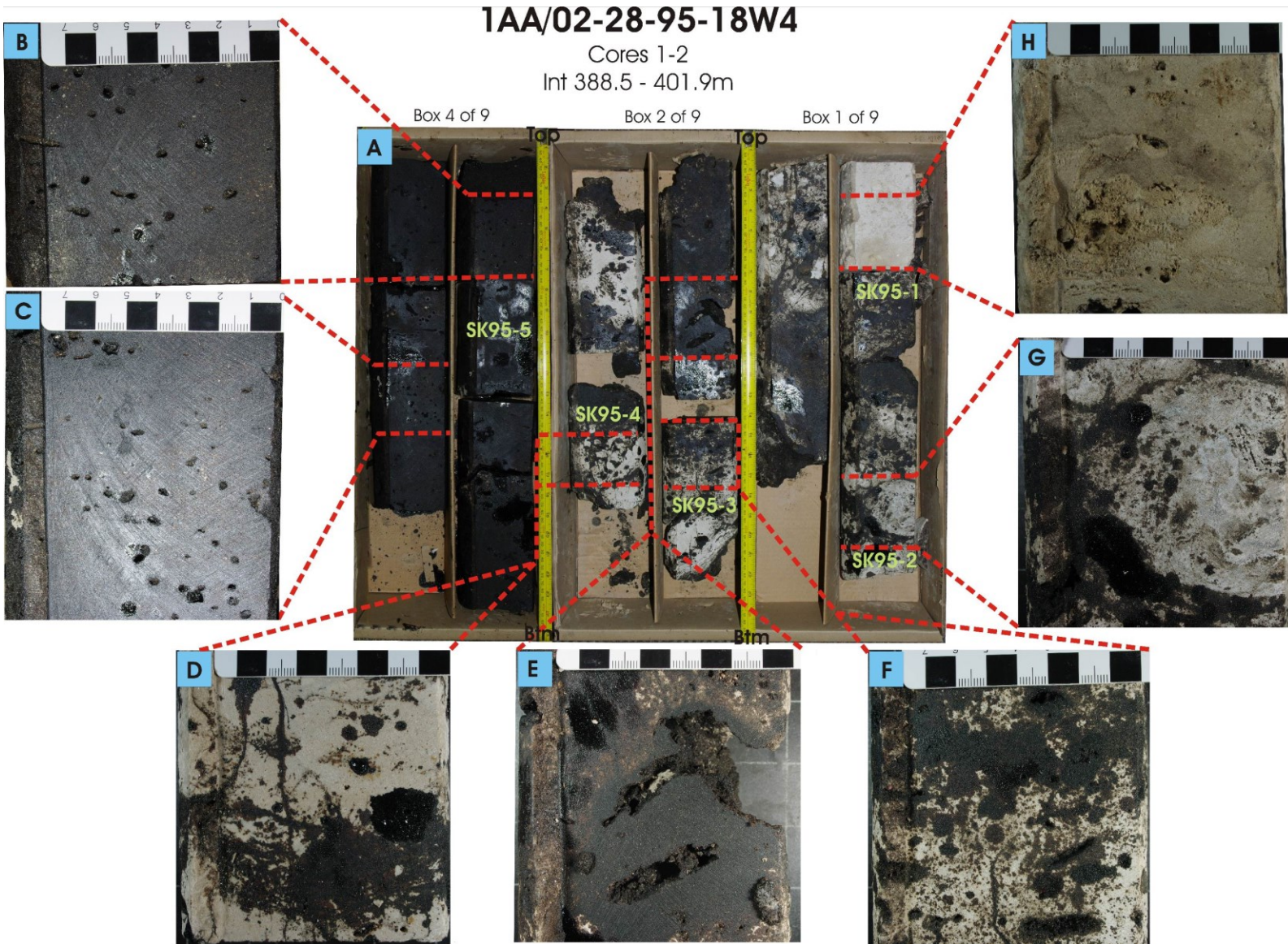
Plate 5.3.4.2. Photograph of a 13 m Leduc core section from well 1AA/2-28-95-18W4 (A) with the close-up photographs of representative specimens partially (D-G) to completely (B,C) stained with bitumen. Scales are in cm at stratigraphic top. The original depositional texture appears to have been a floatstone with a variety of corals and stromatoporoids, although most of these primary features have been obliterated by dolomitization. Note vuggy porosity developed after dissolution of *Amphipora* (B and C) and stromatoporoid (E, G and H).

5.3.5 Other diagenetic products

A few other, volumetrically minor (less than 1 vol. % over any 1m-core interval) cements are present in the Leduc Formation reefs. These cements are mainly a product of sulfate reduction, either by bacteria in the northern part of the trend, or by the TSR-related processes in the southern end.

5.3.5.1 Native sulfur

Elemental sulfur occasionally occurs in sour gas producing wells (5-13-37-12W5 and 7-26-36-10W5) partly to completely filling vugs, pores, and some late-stage fractures that crosscut blocky calcite cements. It appears either as a yellow powder, or as a blotchy yellow, coarse crystalline mineral (Plate 5.3.5a).

5.3.5.2 Metal sulfide minerals

Pyrite is present in minor amounts throughout most wells in the form of medium to coarse euhedral crystals as well as irregular masses disseminated throughout the matrix, or growing on the walls of vugs (Plate 5.3.5b-d). Pyrite is commonly associated with stylolites and late calcite, anhydrite and dolomite cements (Plate 5.3.5c-e).

Sphalerite is less common than pyrite and usually occurs as extremely coarse, translucent dark brown tetrahedral crystals (up to 4 mm), intergrown with sparry calcite or lining the vugs along with pyrite crystals (Plate 5.3.5d).
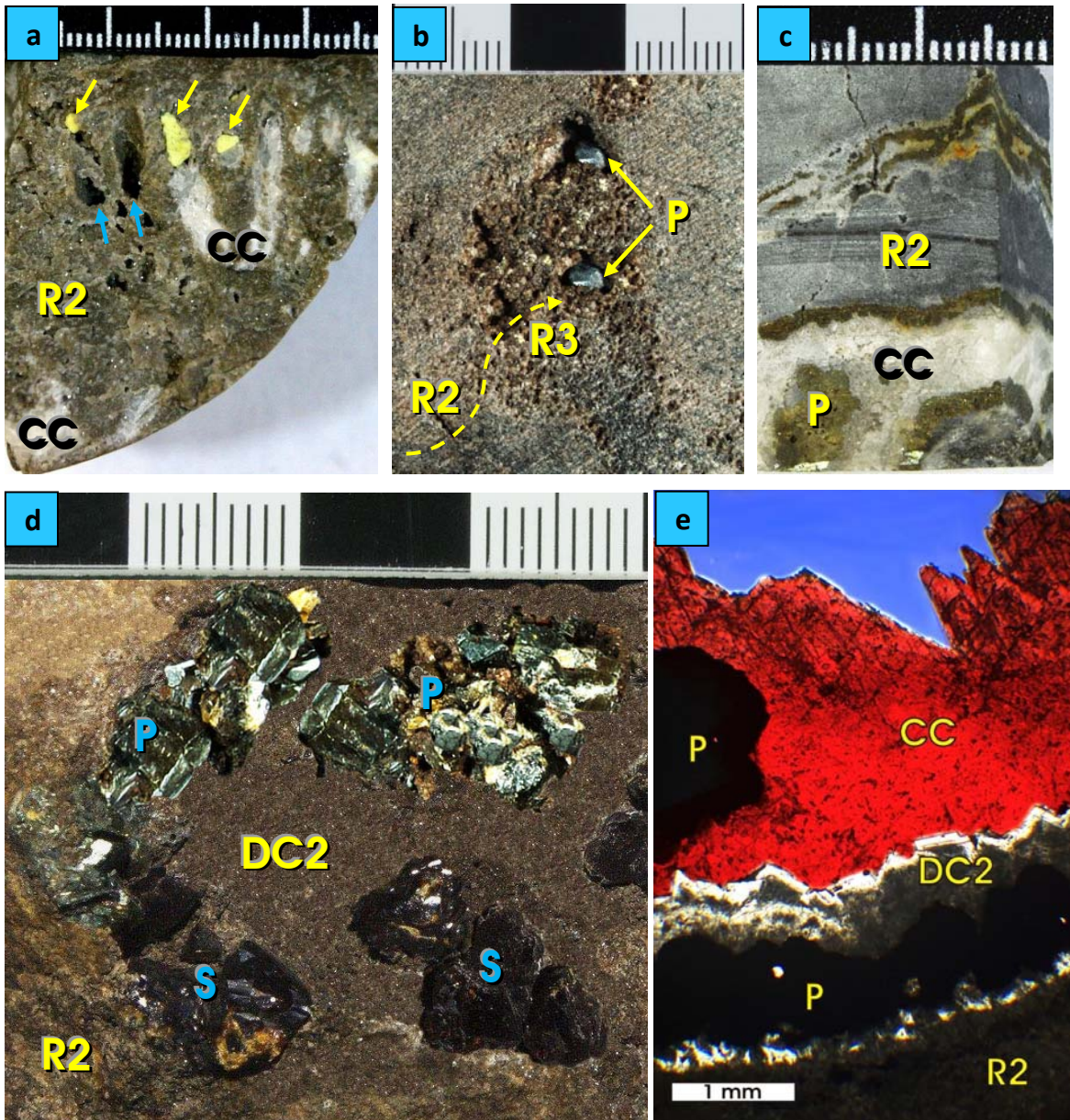
Plate 5.3.5. Examples of later-diagenetic cements in the Leduc reefs, scales are in cm.
a) Core photograph displaying native sulfur (marked by yellow arrows) intergrown with translucent to white calcite cement (CC) infilling remnant porosity (marked by blue arrows) in matrix dolomite R2, sample EH-12, well 06-14-34-08W5 (4286.9 m); b) photograph of a core slab illustrating coarse pyrite crystals (P) grown in the intercrystalline porosity of matrix dolomite R3; note the transition from R2 to R3 and later cementation over R3 (yellow dashed arrow), well 11-27-44-1W5 (7391 ft); c) photograph of sample HH-66(2)-3 showing shiny pyrite crystals (P) intergrown with translucent to white calcite cement (CC) infilling remnant vug space in matrix dolomite R2, well 06-16-66-24W4 (3421 ft); d) photograph of core sample N-228 illustrating extremely coarse crystals of pyrite (P) and sphalerite (S) grown over dolomite cement DC2, which is lining a large solution vug in dolomite R2 matrix, well 09-30-49-25W4 (5246 ft); e) photomicrograph of (c) in plane-polarized light displaying pyrite masses (P) grown over zoned dolomite cement (DC2); note that sparry calcite cement (CC, stained with alizarin red-S) infilling remaining vug space (blue) is intergrown with pyrite.

5.4 Cathodoluminescence microscopy and spectroscopy

Most matrix dolomites exhibit a homogeneous to microblotchy dull orange-red cathodoluminescence (Plates 5.1.1.2f, 5.1.2.1f, 5.1.3f, 5.1.4f), yet some show zonation (Plates 5.1.2.2F-G). Dedolomite and karstified matrix dolomite display mottled to microblotchy orange-red cathodoluminescence (5.3.6.1f, 5.3.6.2e-f).

Dolomite cements DC1 and DC2 are mostly characterized by mottled dull orange-red cathodoluminescence (Plates 5.2.1c,e,f). Dolomite DC4 displays either a homogeneous dull red, in some samples blotchy, cathodoluminescence with no apparent zonation in the southern part of the reef trend, or a dull red to bright orange-red, zoned cathodoluminescence in the northern part (Plate 5.2.2f).

Sparry calcite cements are nonluminescent (Plates 5.2.2f and 5.3.3g). Sparry Fe-calcite cements, however, show orange to dull red cathodoluminescent zoning (Plate 5.2.1e). All anhydrite crystals are non-luminescent.

CL-spectrum measurements were conducted on 80 thin sections. CL spectra for all matrix and cements dolomites had a prominent emission band centered at approximately 570 nm wavelength, which is typical for activation by Mn^{2+} substituting for Ca^{2+} in the lattice (Machel *et al.,* 1991; Figures 5.4.1 and 5.4.2). Samples containing sparry Fe-calcite cement presented a peak at about 615 nm, which is also caused by Mn^{2+} activation (Machel *et al.,* 1991; Figure 5.4.3). Cathodoluminescence activated by Sm^{3+} that is also orange-red
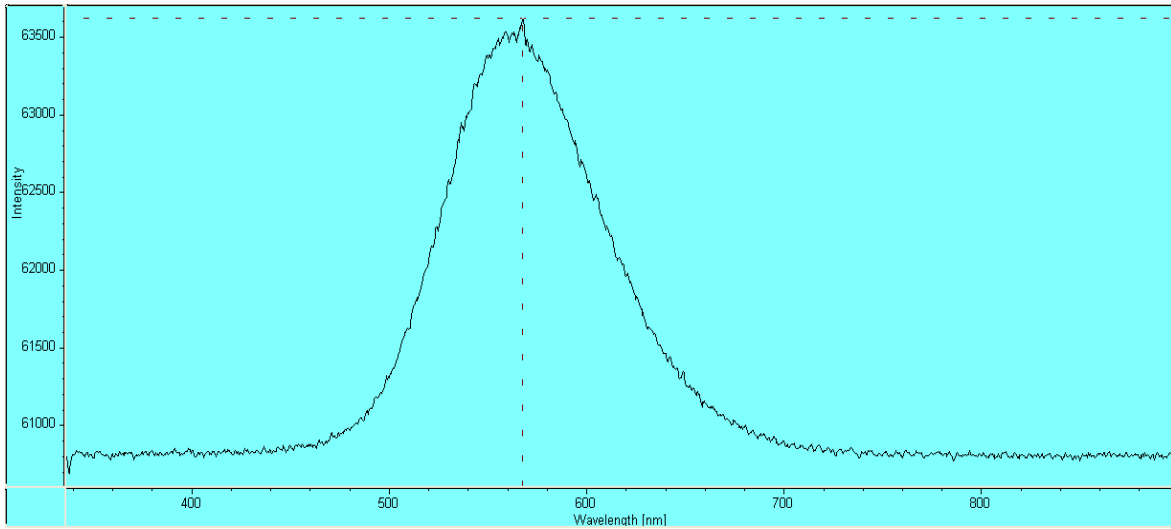
Figure 5.4.1. Mn^{2+} activated CL emission spectra of matrix dolomite R3 in sample EH-9, well 05-13-37-12W5 (5047 m).
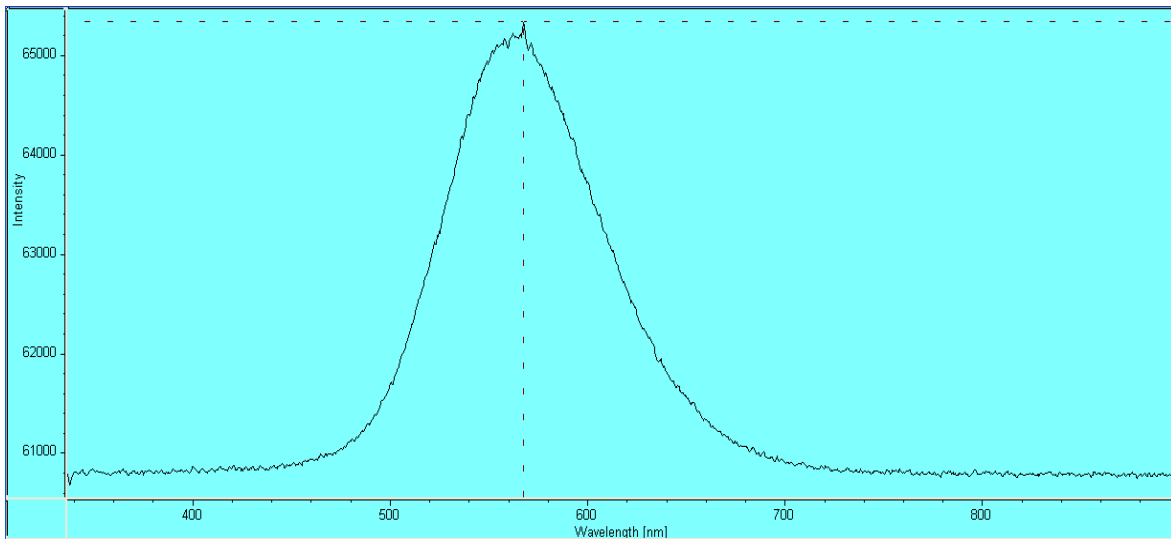
Figure 5.4.2. Mn^{2+} activated CL emission spectra of matrix dolomite R2 in sample EH-9, well 05-13-37-12W5 (5047 m).

and is visually indistinguishable from that of Mn^{2+} (Machel *et al.,* 1991) was not observed in the samples studied.

All attempts to measure a spectrum of zoned areas in dolomite crystals were unsuccessful due to the limited characteristics of the CL microscope. This microscope does not have an objective with sufficient magnification to view the details required. The highest magnification that can be reached is times 40. Magnification needed for measuring spectra of crystal zones should be ten times higher, otherwise the signal will be contaminated by the ones from the neighboring zones.
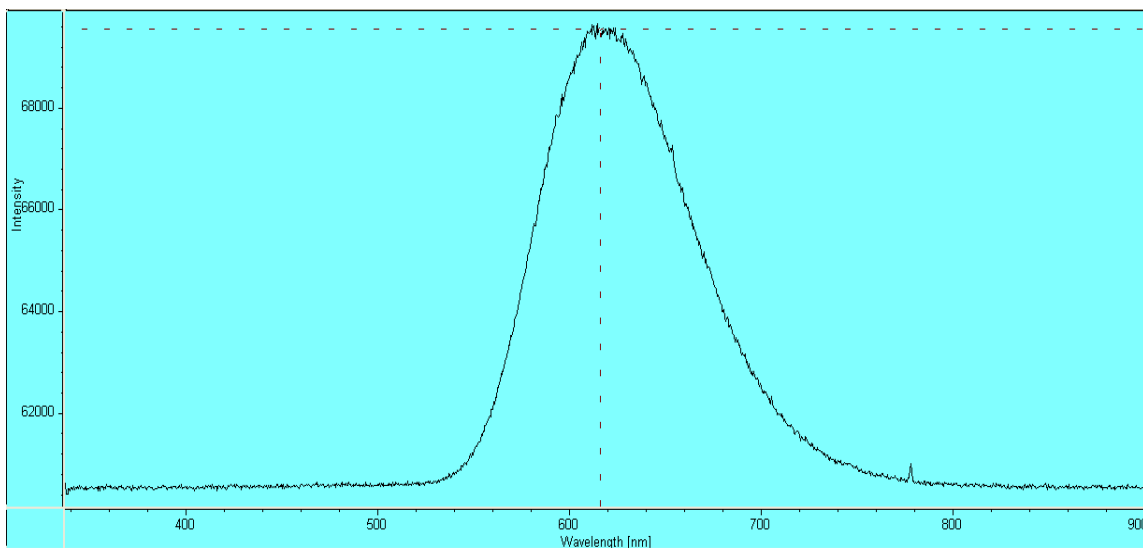
Figure 5.4.3. CL emission spectra of blocky calcite cement in sample SK-58(2)-3, well 02-05-58-25W4 (1410.35 m). The sharp spike at 780 nm is an artifact.

5.5 Distribution of replacement dolomites and later-diagenetic phases

The regional distribution of all diagenetic features along the Rimbey-Meadowbrook Reef trend was determined based on the data obtained from image analysis of thin sections (percentages of the diagenetic phases), visual microscope observations (crystal size and distribution), and the AccuMap database (porosity and permeability). The results of these techniques are presented in Appendix 2 and are similar to those reported in previous studies (Amthor *et al.*, 1993; Drivet, 1993; Marquez, 1994).

Matrix dolomite R1 is most common in the northern (shallow) part of the study area and is almost absent in the deeper end of the reef trend (Figure 5.5.1). The only exception is sample EH-42 (well 11-10-35-5W5, 3365.9m) from the southern part of the reef chain with 94.54% of matrix dolomite R1. Even though there is no apparent correlation between the crystal size and depth on a regional scale, a "local" northward increase in size can be observed between townships 62 and 72 (Figure 5.5.2).

Matrix dolomite R2 is the dominant dolomite type throughout the study area, exhibiting a local trend of increasing crystal size between townships 50 and 36, having extremely coarse crystals (up to 1mm) in the southern (deep) part of the reef chain (Figure 5.5.3). There also are enlarged crystals in the central part of the study area. Generally, most dolomite R2 crystals reach 600 to 1100 micrometres in diameter in the deeper end of the reef chain and are significantly smaller than 600 micrometres near the shallow end.
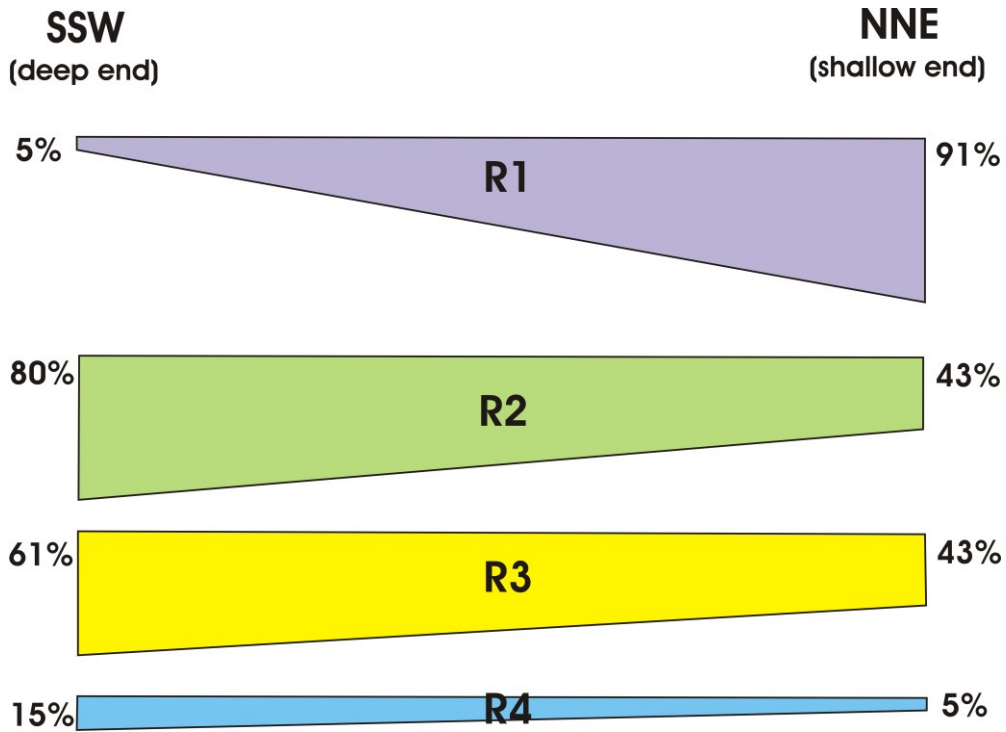
Figure 5.5.1. General distribution and relative abundance of matrix replacement dolomites along the Rimbey-Meadowbrook reef trend. Data is acquired from image analysis. Note that this distribution is an average distribution of matrix dolomites at the extreme ends of the reef trend disregarding the variation in the central part.
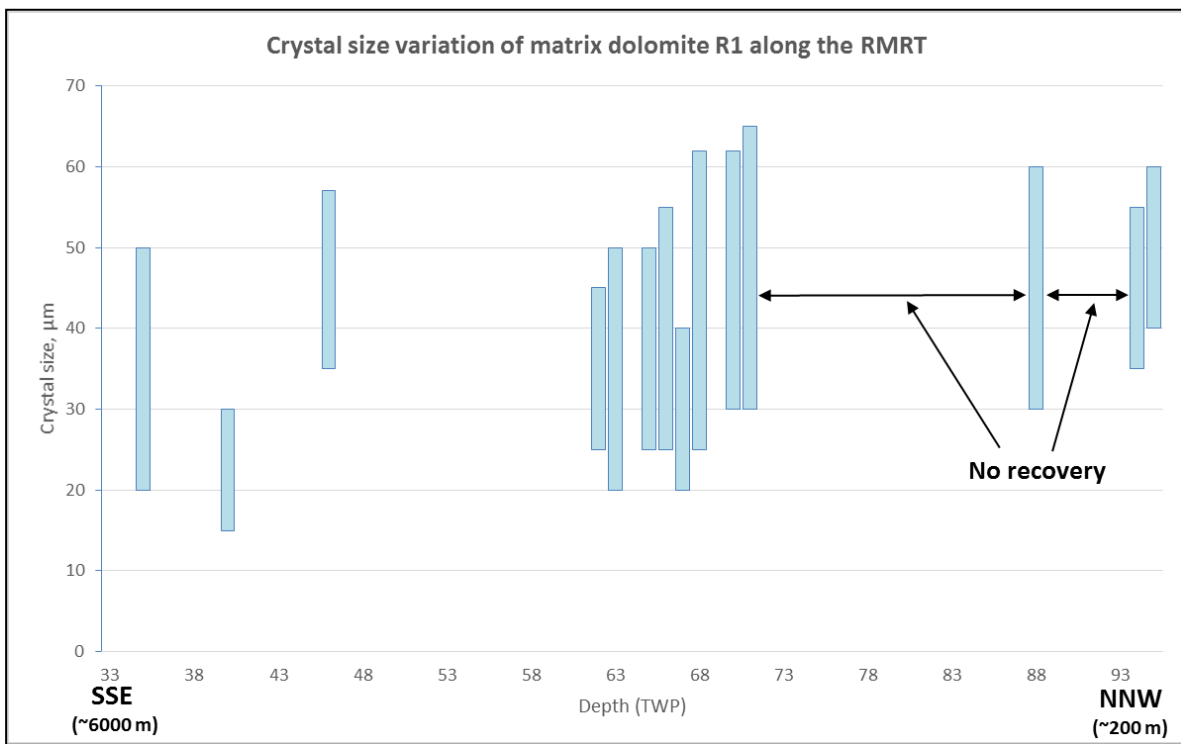
Figure 5.5.2. Crystal size variation of matrix dolomite R1 along the Rimbey-Meadowbrook reef trend.
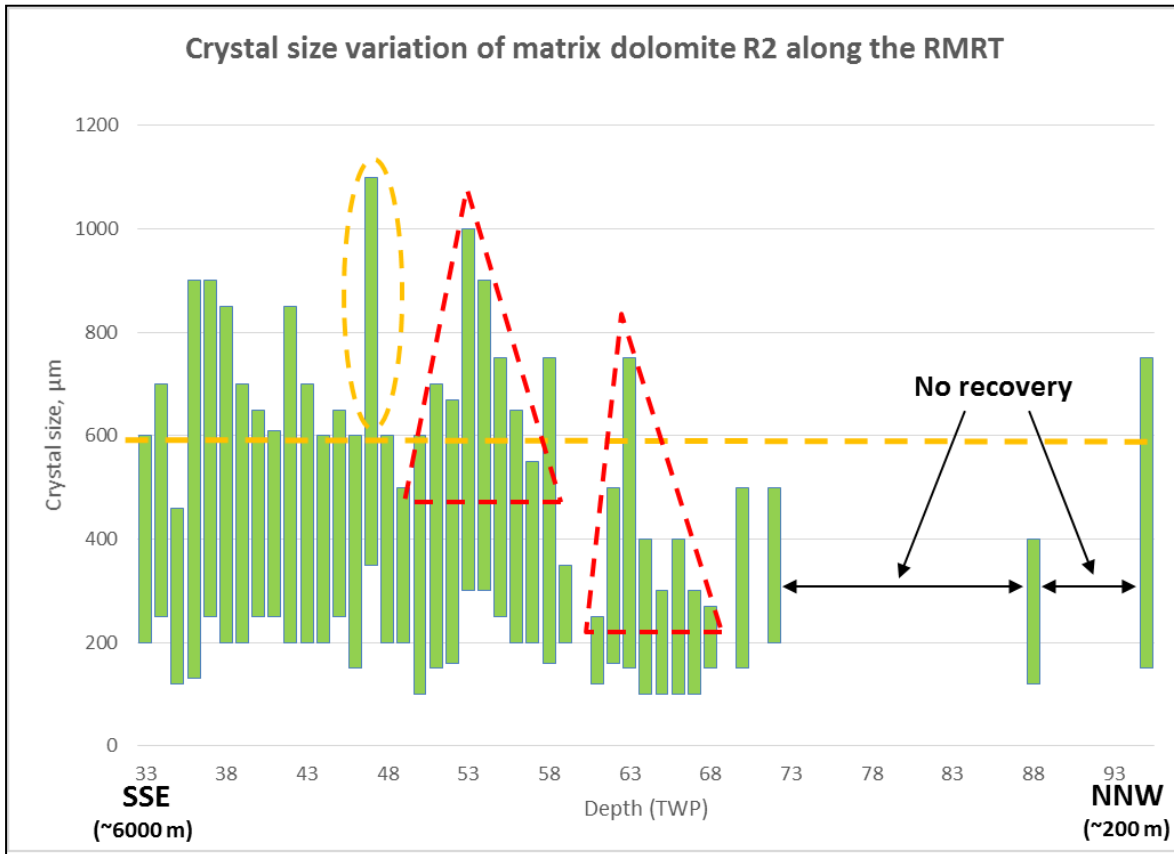
Figure 5.5.3. Crystal size variation of matrix dolomite R2 along the Rimbey-Meadowbrook reef trend showing several domains with enlarged crystals (red triangles and orange circle) in the central part of the study area. Note that most crystals are 600 micrometres or larger (above the dashed line) in the southern part and are smaller than 600 micrometres (below the dashed line) in the northern part.

Brown porous matrix dolomite R3 also occurs throughout the entire reef trend and displays crystal sizes gradually increasing from 100 micrometres in the shallow end to 750 micrometres in the deeper end of the reef trend (Figure 5.5.4). This type appears most abundantly in wackestones and mudstones of the buildup interiors. As with matrix dolomite R2, matrix dolomite R3 has several domains with coarser crystals in the central part of the study area.

As shown in figure 5.5.5, matrix dolomite R3 is considerably more abundant relative to R2 in the deeper part of the reef trend.
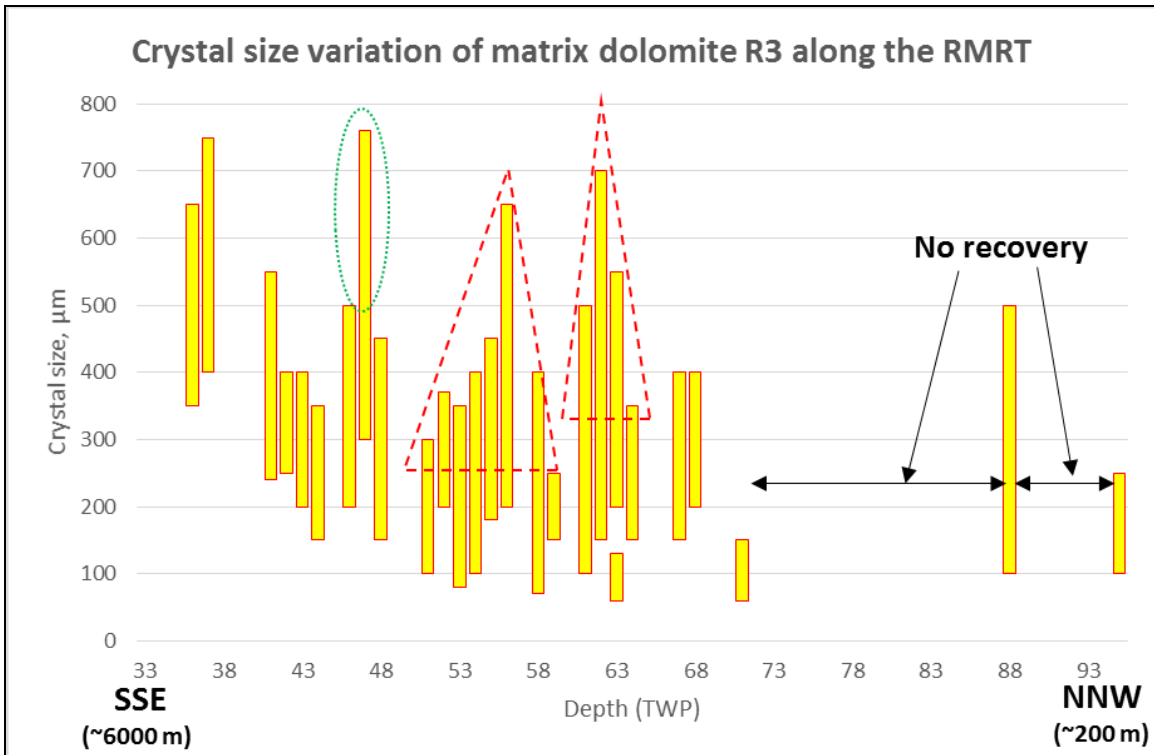
Figure 5.5.4. Crystal size variation of matrix dolomite R3 along the Rimbey-Meadowbrook reef trend showing a weak downdip trend of inceasing crystal sizes. Note several domains with enlarged crystals (red triangles and orange circle) in the central part of the study area.
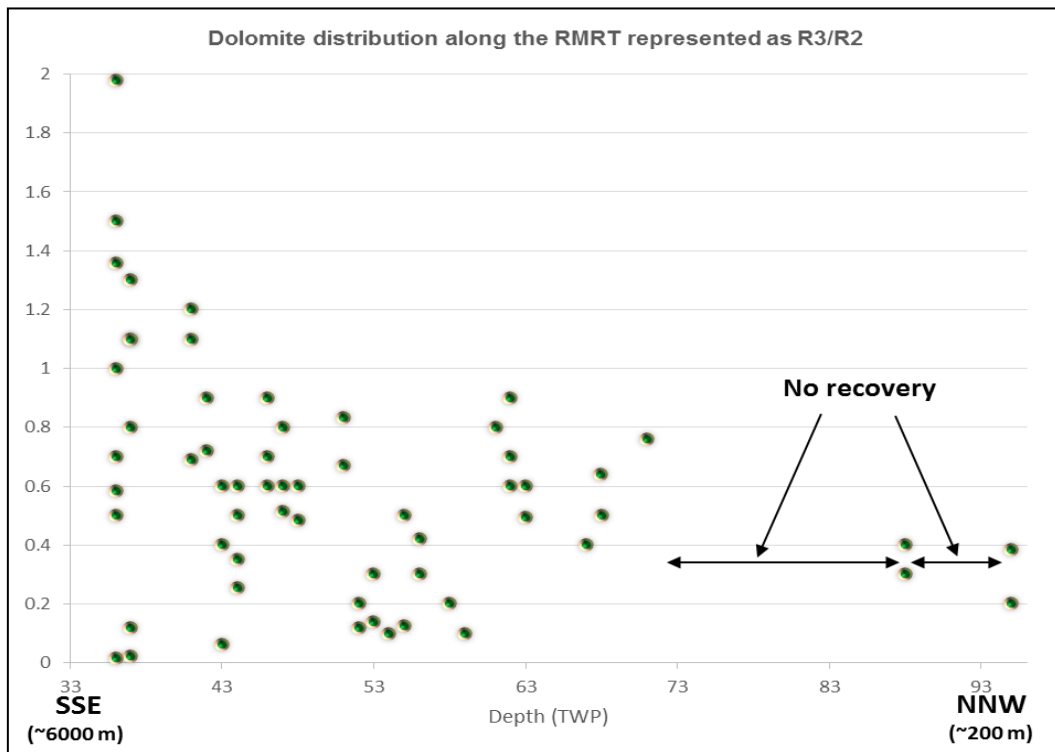
Figure 5.5.5. Relative distribution of matrix dolomite R3 vs. matrix dolomite R2 along the Rimbey Meadowbrook Reef Trend.

Matrix dolomite R4 appears in almost every core sample and is mostly associated with *Amphipora* and *Thamnopora* grainstones (Figure 5.5.6). Unlike matrix dolomites R1, R2 and R3, this type does not show any apparent trend.

Karst and dedolomite are observed only in the northern part of the reef chain in the drill cores located along the boundary between the Grosmont Platform and the Cooking Lake platform (townships 61, 62, and 63) and below the sub-Cretaceous unconformity (north of township 80).
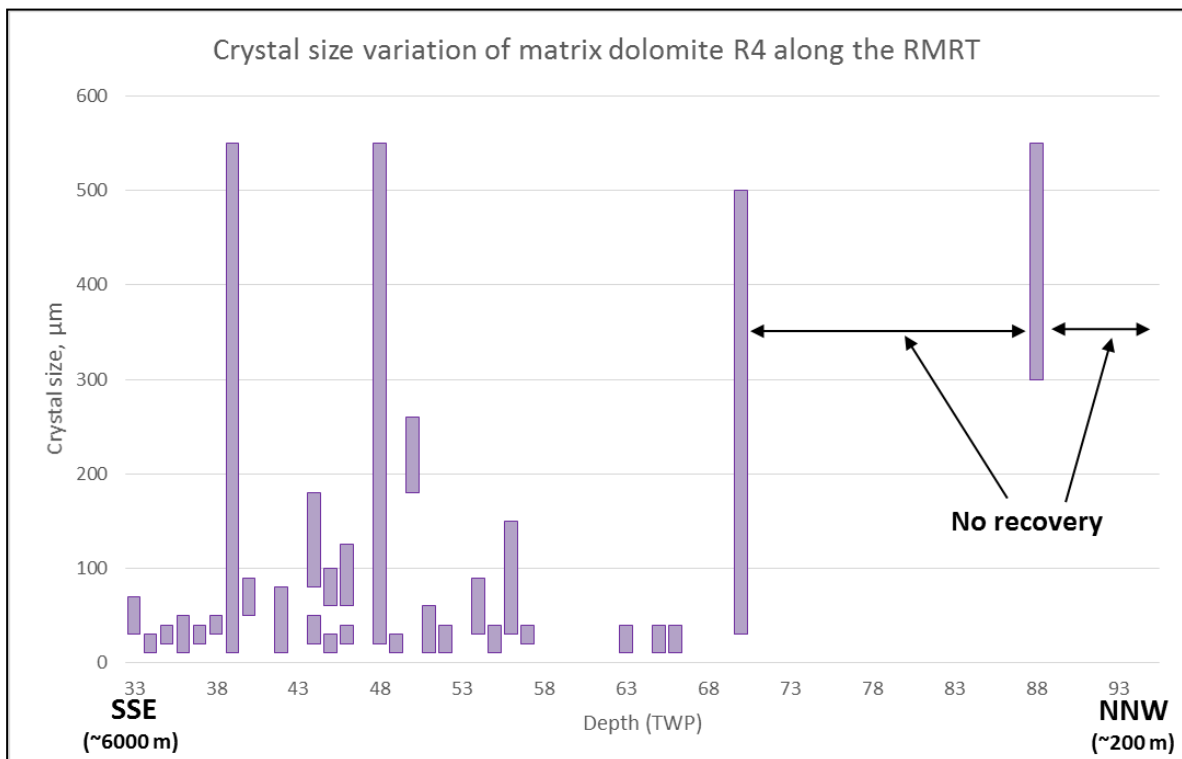
Figure 5.5.6. Crystal size variation of matrix dolomite R4 along the Rimbey-Meadowbrook reef trend showing no apparent trend, but several domains (townships 39, 48, 70 and 88) with much coarser crystals than in the rest of samples.

The general distribution and relative abundances of the later diagenetic phases is presented in Figure 5.5.7. Calcite and dolomite cements, as well as native sulfur and sulfides, generally decrease in volume northward along the trend. Elemental sulfur appears only in a few southern buildups at depths greater than 3000m and is absent toward the northern end of the reef trend. The volumetrically most important pore-occluding phases are anhydrite and bitumen. Anhydrite is more common in the southern (deeper) part of the study area and present only in traces toward the northern (shallow) end. The distributions of dolomite cements DC1, DC2 and DC4 coincides with that of matrix dolomite R3 and decreases in volume with increasing percentage of matrix R2 (Figure 5.5.8).
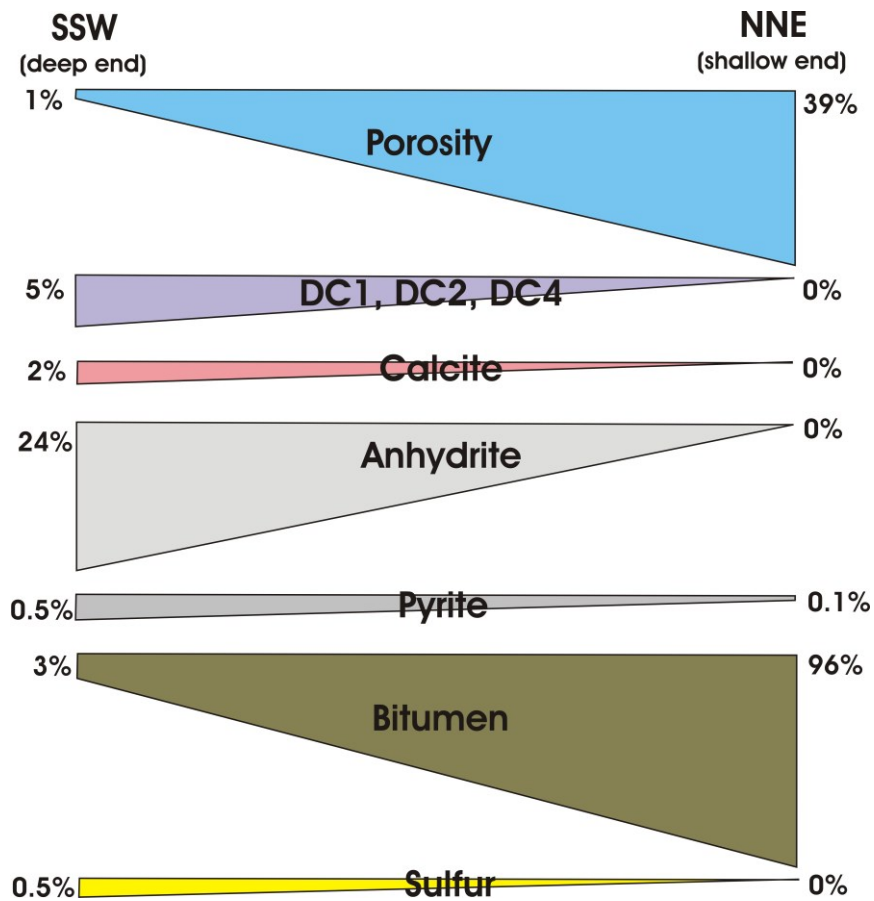
Figure 5.5.7. General distribution and relative abundance of later diagenetic phases along the Rimbey-Meadowbrook reef trend. Data is acquired from image analysis.
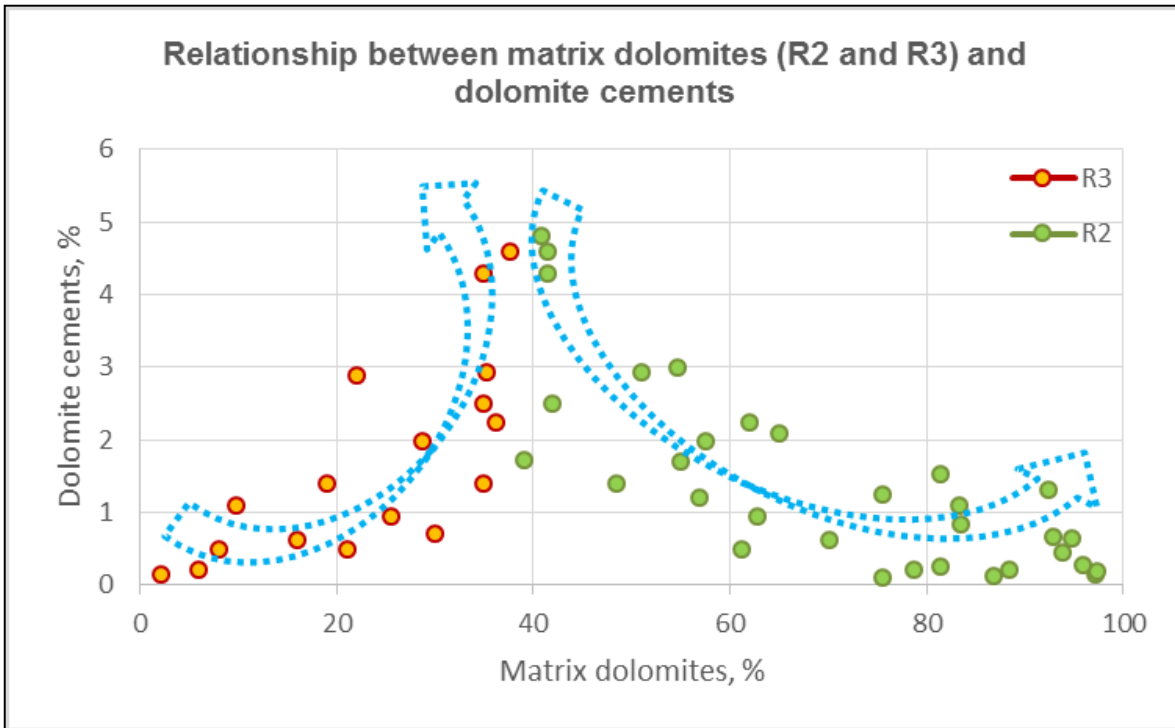
Figure 5.5.8. Relationship between matrix dolomites (R2 and R3) and dolomite cements DC1, DC2 and DC4 along the Rimbey-Meadowbrook Reef Trend showing a positive correlation between distribution of dolomite cements and matrix dolomite R3, and negative correlation between matrix dolomite R2 and dolomite cements.

Porosity and horizontal permeability increase northward along the trend reaching 25 (AccuMap data) to 39% (image analysis) and tens of thousands mD (AccuMap data), respectively (Figures 5.5.9 and 5.5.10). Porosities are positively correlated with the distribution of matrix dolomite R3 and decrease with increasing R2 volume-percentages (Figures 5.5.11 - 5.5.12). Similar relationships were previously reported by Amthor *et al.* (1994). Matrix dolomite R1 does not exhibit any visible porosity.
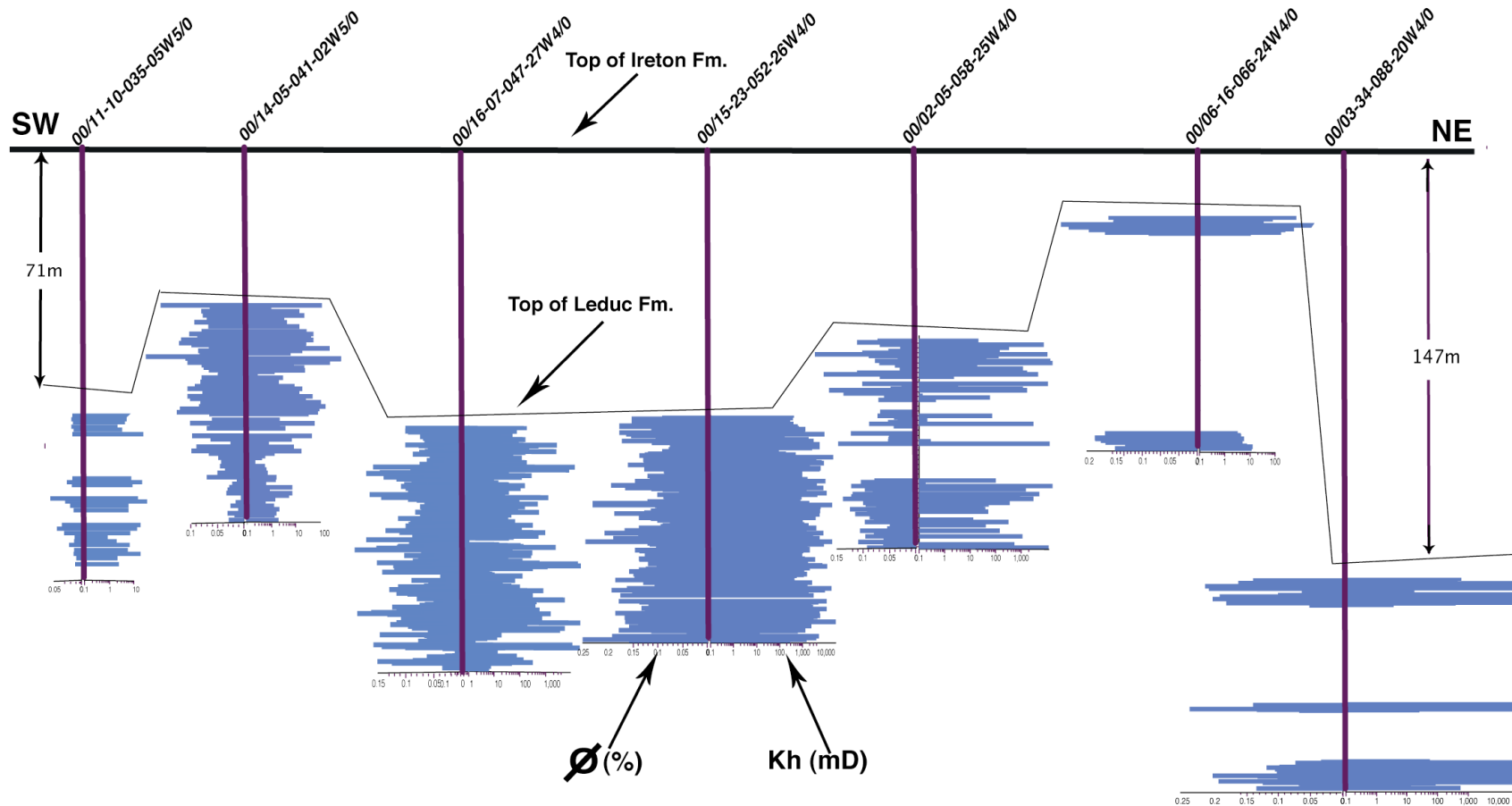
Figure 5.5.9. Cross-section of the Leduc Formation from SW to NE along the Rimbey-Meadowbrook Reef Trend showing percent porosity (ø) and horizontal permeability (Kh) from core analysis (AccuMap). Datum: top of the Ireton Formation. Wells are chosen based on availability of core analysis data in the AccuMap database. Note the northward increase in porosity (ø) and permeability (Kh) along the trend reaching 25% and tens of thousands mD, respectively.
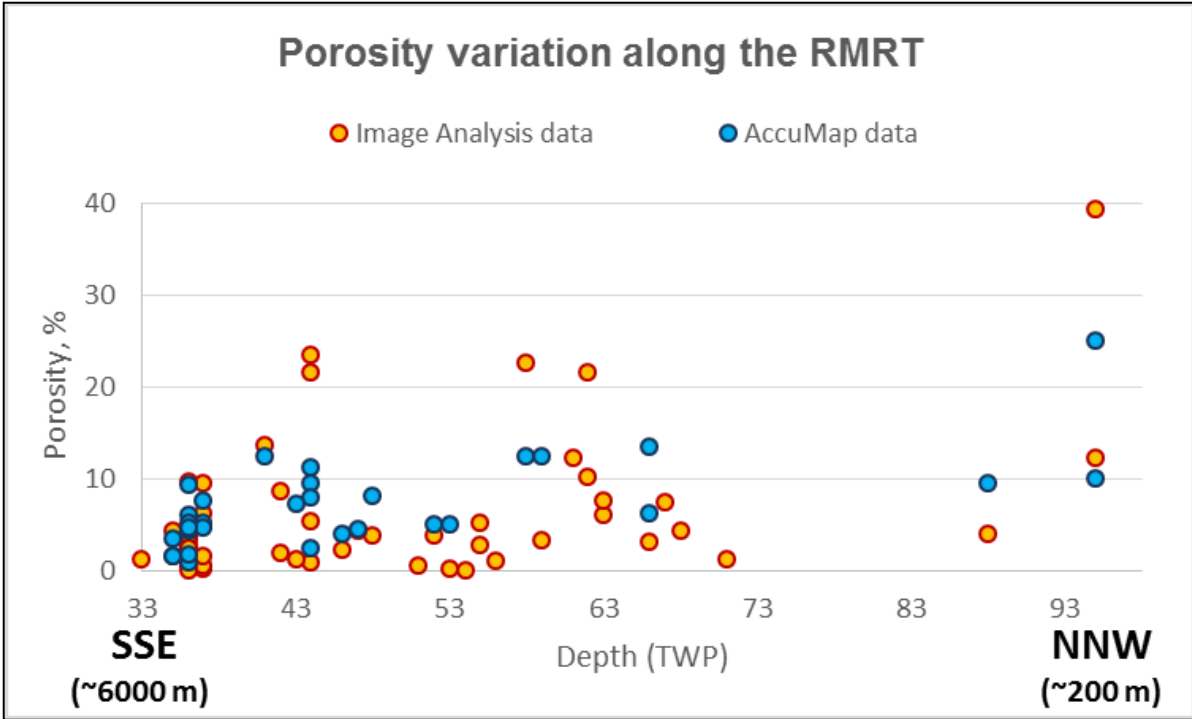
Figure 5.5.10. Porosity variation along the Rimbey-Meadowbrook Reef Trend.
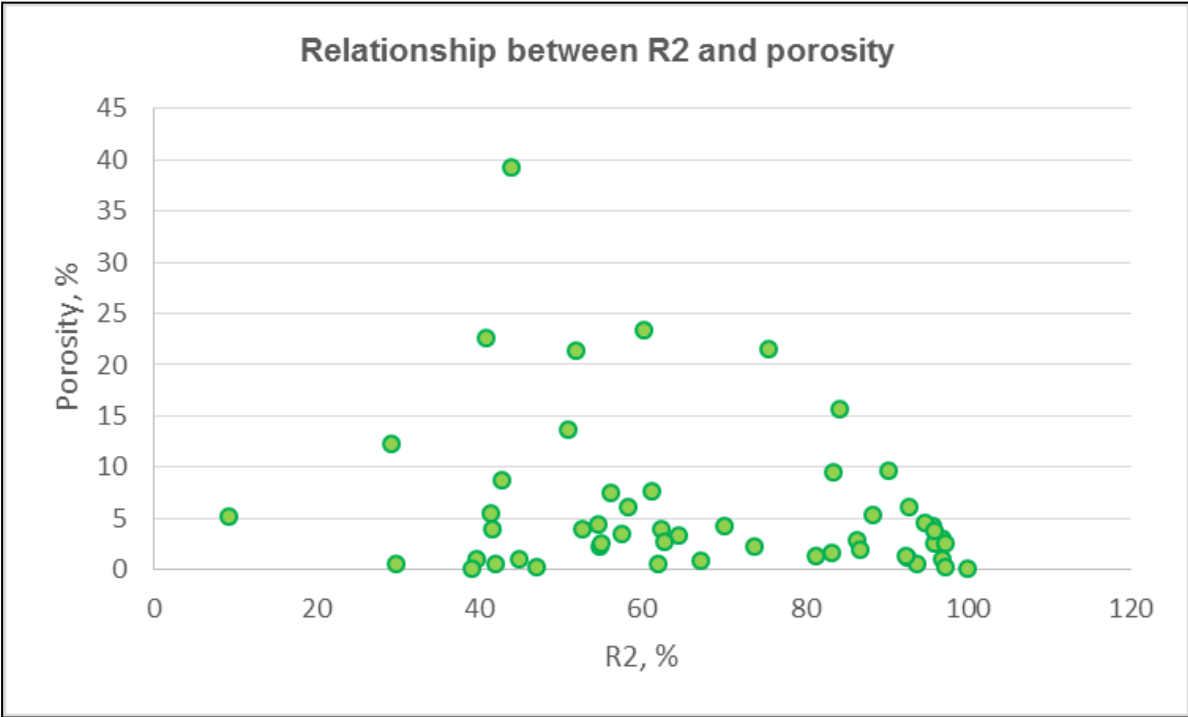
Figure 5.5.11. Relationship between matrix dolomite R2 and porosity along the Rimbey-Meadowbrook Reef Trend.
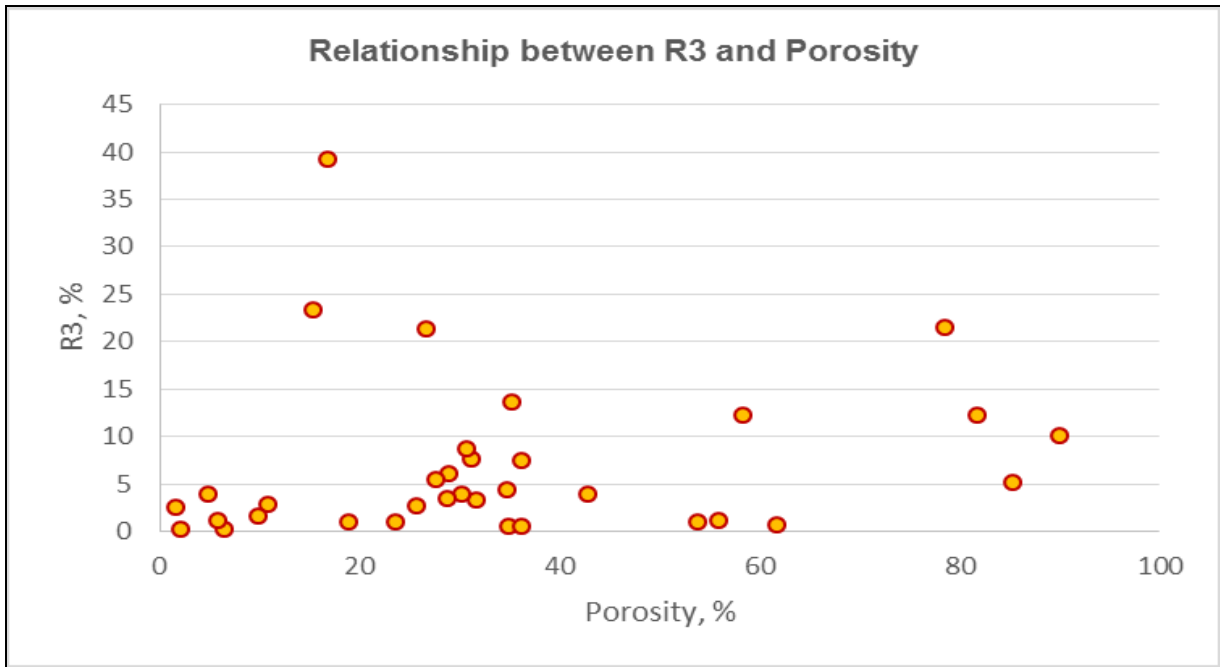
Figure 5.5.11. Relationship between matrix dolomite R3 and porosity along the Rimbey-Meadowbrook Reef Trend.

CHAPTER 6

GEOCHEMISTRY

Following the petrographic classification of matrix dolomites in the Leduc and Cooking Lake Formations, 98 specimens were selected for microsampling for geochemical analysis. The petrographic types chosen were restricted to matrix dolomites R1, R2 and R3, avoiding mimetic dolomite R4 and dolomite cements. Therefore, matrix dolomite R4 will be excluded from further discussions due to the risk of contamination by clay material enclosed in stylolites and solution seams commonly associated with this type of dolomite. Dolomite cements, however, will be discussed based on the geochemical data acquired from the previous studies.

A total of 164 powder samples were drilled focusing on one petrographic type at a time. However, in some cases contamination by other diagenetic phases was unavoidable. Four sets of powder samples were prepared and analysed for x-ray diffraction, stable carbon/ oxygen and radiogenic strontium isotopes, and major and trace elements. The purpose of these analyses was to determine the composition, possible sources and timing of the dolomitizing fluids, especially because obtaining direct information on dolomitizing fluids of matrix dolomites from standard heating-freezing runs was impossible due to small inclusion sizes. Interpretation and discussion of the geochemical results will be presented in Chapter 8.

The main purpose of this section is to describe the chemistry of the major dolomite types of the entire Rimbey-Meadowbrook Reef trend in the townships where Leduc and Cooking Lake Formation cores were available. The samples were analyzed in the townships with no existing data in order to fill the gaps in earlier research (Figure 6.1). The data acquired in this study were
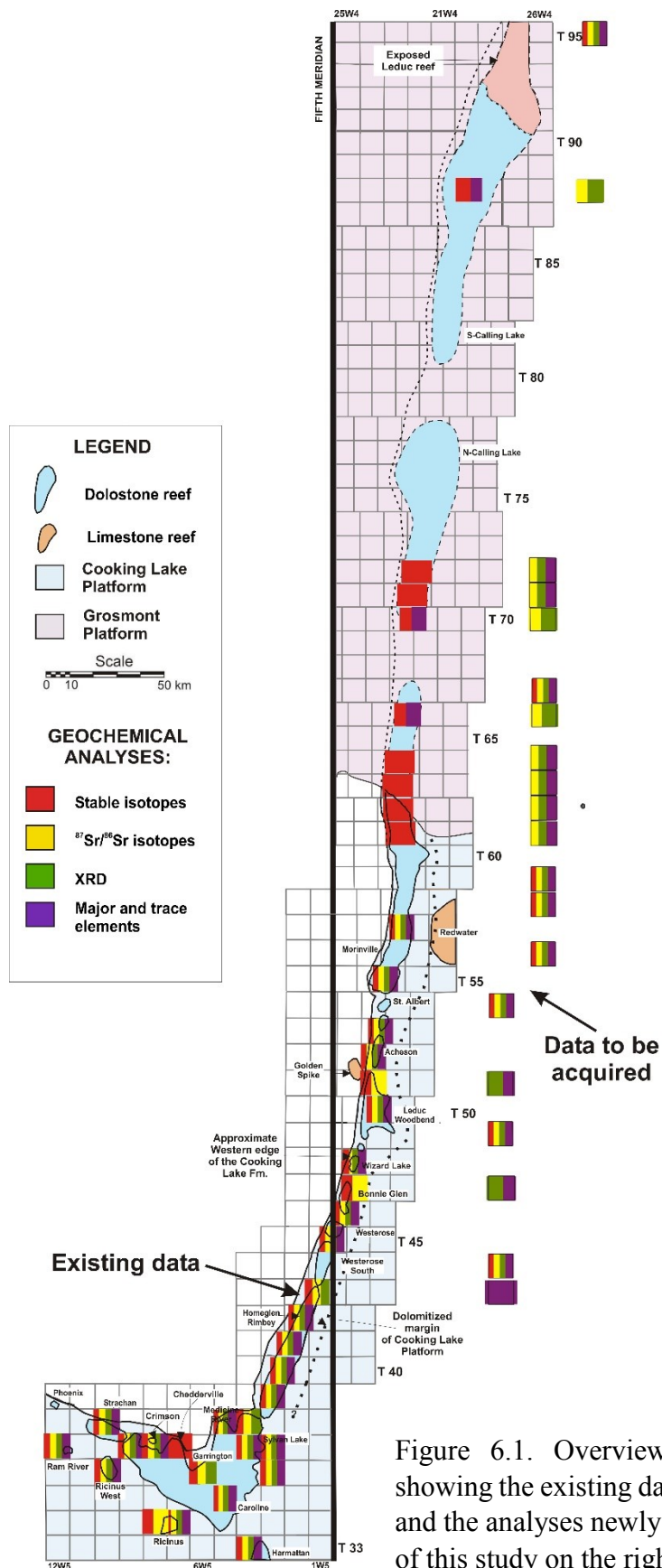
Figure 6.1. Overview geochemistry chart showing the existing data on the left hand side and the analyses newly acquired in the course of this study on the right hand side.

combined with the results from the previous works and compiled into one table (Appendix 3). In some cases (Amthor *et al.*, 1993; Horrigan, 1996; Huebscher, 1996) the data from other authors had to be adjusted for consistency reasons, as discussed in the following sections.

6.1 X-Ray Diffraction (XRD)

XRD analysis was used to determine dolomite stoichiometry, which was calculated using the position of the $d_{(104)}$ peak following the method of Lumsden and Chimahusky (1980):

$$\text{mol \% CaCO}_3 = 333.33 * d_{(104)} - 911.99, \qquad [6.1]$$

where d is an interplanar spacing corrected by the difference between the d-spacing of the internal quartz standard and the theoretical d-spacing for a quartz peak as shown in the following equations:

$$d\ (corrected)_{dolomite} = d_{dolomite} - \Delta\ d_{quartz}$$

Bragg's law: $\qquad \lambda_{CoK\alpha} = 2d * \sin\theta$, where $\lambda_{CoK\alpha}$ – wavelength
$\qquad\qquad\qquad\qquad\qquad\qquad\qquad\qquad\qquad$ d – interplanar spacing
$\qquad\qquad\qquad\qquad\qquad\qquad\qquad\qquad\qquad$ θ – diffraction angle obtained
$\qquad\qquad\qquad\qquad\qquad\qquad\qquad\qquad\qquad\qquad$ from the XRD analysis

$$d = \frac{\lambda_{CoK\alpha}}{2\sin\theta}$$

$\lambda_{CoK\alpha 1} = 1.788996$

$\lambda_{CoK\alpha 2} = 1.792835 \qquad\qquad\qquad \lambda_{CoK\alpha} = \dfrac{2\lambda_{CoK\alpha 1} + \lambda_{CoK\alpha 2}}{3} = 1.790276$

According to Reeder and Sheppard (1984), the above equation [6.1] can lead to inaccuracies of about 2 to 3 mol% $CaCO_3$, especially at lower $CaCO_3$ contents.

In mixed calcite-dolomite samples, the wt % $CaCO_3$ was calculated based on the calcite and dolomite peak intensities using a calcite-dolomite polynomial expression described in the technique proposed by Locock (2012):

$$wt\%CaCO_3 = 9.1926x^2 + 90.8447x$$

$$x = \frac{I_c}{I_c + I_d},$$ where I_c - calcite peak intensity

I_d - dolomite peak intensity

This mathematical procedure was processed in EXCEL and is presented in Table 6.1.1. Additionally, seven powder samples drilled by Horrigan (1996) were run for the purpose of correlation between the two data sets, because her XRD data was consistently too low for mol % $CaCO_3$ with a range of 2.87 mol% $CaCO_3$, which is within the analytical error of 3 mol% $CaCO_3$. Therefore, it was assumed that her XRD results were uncorrected. The new results had normal (credible) values with a much smaller range of 1.73 mol% $CaCO_3$. Based on this comparison, Horrigan's (1996) XRD results listed in Appendix 3 were corrected by +1.01 mol% $CaCO_3$ (Table 6.1.2).

According to the results shown in Figure 6.1.1, most matrix dolomites of the Rimbey-Meadowbrook Reef Trend are of nearly ideal stoichiometric composition varying from 49.25 to 51.87 mol % $CaCO_3$ with an average of 50.43 mol % $CaCO_3$ and d_{104} measurements at 2.884 – 2.892 Å, respectively. Only one matrix dolomite R1 sample (SK95-12) has a non-stoichiometric composition with extremely high $CaCO_3$ concentration (56.25 mol %).

Table 6.1.1. Mol% CaCO$_3$ and wt% CaCO$_3$ calculations from XRD data using the technique proposed by Locock (2012).

Sample ID	Quartz			Dolomite				mol % CaCO3	Ic	Id	Ic/ (Ic+Id)	wt% CaCO3
	2-θ	sin θ	d	2-θ	sin θ	d	d-corrected					
std PDF	31.058	0.267726	3.343484									
K37-2	31.040	0.267575	3.345375	36.100	0.309847	2.888969	2.8870776	50.36	< D.L.	173583	—	< 1
K37-5	31.040	0.267575	3.345375	36.130	0.310096	2.886650	2.8847588	49.59	< D.L.	207808	—	< 1
K42-1	31.050	0.267659	3.344324	36.130	0.310096	2.886650	2.8858097	49.94	< D.L.	178937	—	< 1
K42-31	31.060	0.267743	3.343274	36.130	0.310096	2.886650	2.8868599	50.29	< D.L.	166892	—	< 1
K42-32	30.979	0.267062	3.351801	36.060	0.309515	2.892067	2.8837501	49.25	< D.L.	283150	—	< 1
K441-1	31.010	0.267322	3.348532	36.090	0.309764	2.889743	2.8846946	49.57	< D.L.	214573	—	< 1
K441-4	31.050	0.267659	3.344324	36.130	0.310096	2.886650	2.8858097	49.94	< D.L.	294099	—	< 1
K441-7	31.020	0.267407	3.347479	36.100	0.309847	2.888969	2.8849737	49.66	< D.L.	342666	—	< 1
K442-2	31.070	0.267827	3.342224	36.150	0.310262	2.885106	2.8863657	50.12	< D.L.	192507	—	< 1
K442-4	31.030	0.267491	3.346427	36.080	0.309681	2.890517	2.8875741	50.53	< D.L.	276714	—	< 1
K442-5	31.100	0.268079	3.339080	36.150	0.310262	2.885106	2.8895103	51.17	< D.L.	184187	—	< 1
K442-8	31.059	0.267734	3.343379	36.120	0.310013	2.887422	2.8875275	50.51	< D.L.	223213	—	< 1
K48-1	30.981	0.267079	3.351590	36.020	0.309183	2.895172	2.8870661	50.36	68818	5729	0.923149	91.70
K48-2	31.020	0.267407	3.347479	36.050	0.309432	2.892842	2.8888473	50.95	84884	1838	0.978806	97.73
K49-2	31.060	0.267743	3.343274	36.110	0.309930	2.888195	2.8884054	50.80	< D.L.	156870	—	< 1
K49-3	31.040	0.267575	3.345375	36.110	0.309930	2.888195	2.8863042	50.10	< D.L.	188395	—	< 1
K51-21	31.080	0.267911	3.341175	36.150	0.310262	2.885106	2.8874146	50.47	< D.L.	156584	—	< 1
K51-22	31.040	0.267575	3.345375	36.110	0.309930	2.888195	2.8863042	50.10	< D.L.	246914	—	< 1
K53-1	31.090	0.267995	3.340127	36.140	0.310179	2.885878	2.8892345	51.08	< D.L.	161013	—	< 1
K53-12	31.100	0.268079	3.339080	36.160	0.310345	2.884335	2.8887391	50.91	< D.L.	424313	—	< 1
K54-1	31.040	0.267575	3.345375	36.100	0.309847	2.888969	2.8870776	50.36	< D.L.	182037	—	< 1
K542-1	31.040	0.267575	3.345375	36.120	0.310013	2.887422	2.8855313	49.84	< D.L.	233497	—	< 1
K542-51	30.990	0.267154	3.350640	36.070	0.309598	2.891292	2.8841355	49.38	< D.L.	241764	—	< 1
K55-4	31.020	0.267407	3.347479	36.070	0.309598	2.891292	2.8872965	50.43	95285	177767	0.348963	32.82
K55-5	31.050	0.267659	3.344324	36.140	0.310179	2.885878	2.8850376	49.68	< D.L.	437983	—	< 1
K56-3	31.030	0.267491	3.346427	36.080	0.309681	2.890517	2.8875741	50.53	< D.L.	167661	—	< 1
K56-71	31.040	0.267575	3.345375	36.120	0.310013	2.887422	2.8855313	49.84	< D.L.	223716	—	< 1
K56-72	31.040	0.267575	3.345375	36.090	0.309764	2.889743	2.8878515	50.62	< D.L.	768132	—	< 1
K56-10	31.059	0.267734	3.343379	36.130	0.310096	2.886650	2.8867549	50.25	< D.L.	213569	—	< 1
K581-21	31.100	0.268079	3.339080	36.180	0.310511	2.882794	2.8871980	50.40	< D.L.	234829	—	< 1
K581-22	31.040	0.267575	3.345375	36.110	0.309930	2.888195	2.8863042	50.10	< D.L.	410652	—	< 1
K581-3	31.040	0.267575	3.345375	36.120	0.310013	2.887422	2.8855313	49.84	< D.L.	202807	—	< 1
K582-1	31.050	0.267659	3.344324	36.110	0.309930	2.888195	2.8873552	50.45	< D.L.	156101	—	< 1
K582-3	31.060	0.267743	3.343274	36.100	0.309847	2.888969	2.8891788	51.06	378504	1015	0.997326	99.75
K582-9	31.049	0.26765	3.344429	36.110	0.309930	2.888195	2.8872501	50.42	36882	63451	0.367596	34.64
K59-21	31.010	0.267322	3.348532	36.080	0.309681	2.890517	2.8854688	49.82	< D.L.	193897	—	< 1
K59-22	31.080	0.267911	3.341175	36.120	0.310013	2.887422	2.8897309	51.24	72026	570396	0.112116	10.30
K59-4	30.989	0.267146	3.350746	36.040	0.309349	2.893618	2.8863568	50.12	< D.L.	173650	—	< 1
K67-2	31.050	0.267659	3.344324	36.120	0.310013	2.887422	2.8865822	50.19	< D.L.	237686	—	< 1
K67-3	31.020	0.267407	3.347479	36.090	0.309764	2.889743	2.8857476	49.92	< D.L.	120561	—	< 1
K95-51	31.020	0.267407	3.347479	36.110	0.309930	2.888195	2.8842003	49.40	< D.L.	266436	—	< 1
K95-52	31.090	0.267995	3.340127	36.160	0.310345	2.884335	2.8876916	50.56	< D.L.	585499	—	< 1
K95-12	31.060	0.267743	3.343274	35.900	0.308187	2.904529	2.9047389	56.25	38211	67284	0.362207	34.11
H61-1	31.08	0.267911	3.341175	36.17	0.310428	2.883564	2.8858726	49.96	2130	274829	0.007691	0.70
H61-3	31.11	0.268163	3.338033	36.19	0.310593	2.882024	2.8874749	50.49	< D.L.	64257	—	< 1
H62-2	31.07	0.267827	3.342224	36.14	0.310179	2.885878	2.8871374	50.38	< D.L.	85842	—	< 1
H62-3	31.12	0.268247	3.336987	36.19	0.310593	2.882024	2.888521	50.84	< D.L.	81934	—	< 1
H62-5	31.08	0.267911	3.341175	36.16	0.310345	2.884335	2.8866434	50.21	< D.L.	253929	—	< 1
H63-4	31.089	0.267987	3.340232	36.16	0.310345	2.884335	2.8875868	50.53	< D.L.	96268	—	< 1
H63-5	31.11	0.268163	3.338033	36.19	0.310593	2.882024	2.8874749	50.49	< D.L.	80326	—	< 1
H63-7	31.119	0.268239	3.337091	36.19	0.310593	2.882024	2.8884164	50.81	< D.L.	100363	—	< 1
H63-8	31.04	0.267575	3.345375	36.08	0.309681	2.890517	2.8886258	50.88	< D.L.	83524	—	< 1
H63-11	31.07	0.267827	3.342224	36.14	0.310179	2.885878	2.8871374	50.38	< D.L.	92366	—	< 1
H63-13	31.1	0.268079	3.339080	36.18	0.310511	2.882794	2.887198	50.40	< D.L.	98614	—	< 1
H64-1	31.15	0.2685	3.333852	36.23	0.310925	2.878949	2.88858	50.86	< D.L.	108192	—	< 1
H65-1	31.13	0.268331	3.335941	36.21	0.310759	2.880485	2.8880279	50.68	< D.L.	95373	—	< 1
H65-2	31.09	0.267995	3.340127	36.15	0.310262	2.885106	2.8884628	50.82	< D.L.	102029	—	< 1
H662-5	31.07	0.267827	3.342224	36.14	0.310179	2.885878	2.8871374	50.38	< D.L.	145244	—	< 1
H662-8	31.15	0.2685	3.333852	36.22	0.310842	2.879717	2.8893482	51.12	< D.L.	196821	—	< 1
H662-9	31.08	0.267911	3.341175	36.15	0.310262	2.885106	2.8874146	50.47	21617	55345	0.280879	26.24
H68-1	31.12	0.268247	3.336987	36.15	0.310262	2.885106	2.8916033	51.87	< D.L.	94670	—	< 1

Table 6.1.1. Continued.

Sample ID	Quartz			Dolomite				mol % CaCO3	Ic	Id	Ic/ (Ic+Id)	wt% CaCO3
	2-θ	sin θ	d	2-θ	sin θ	d	d-corrected					
H68-2	31.11	0.268163	3.338033	36.18	0.310511	2.882794	2.8882448	50.75	< D.L.	100477	—	< 1
H71-2	31.12	0.268247	3.336987	36.18	0.310511	2.882794	2.8892909	51.10	< D.L.	53750	—	< 1
H72-1	31.08	0.267911	3.341175	36.16	0.310345	2.884335	2.8866434	50.21	< D.L.	92228	—	< 1
H72-1(B)	31.08	0.267911	3.341175	36.16	0.310345	2.884335	2.8866434	50.21	< D.L.	155284	—	< 1
H72-3	31.07	0.267827	3.342224	36.15	0.310262	2.885106	2.8863657	50.12	15352	93044	0.141629	13.05
H72-5	31.129	0.268323	3.336046	36.21	0.310759	2.880485	2.8879234	50.64	< D.L.	92519	—	< 1
EH-10	31.02	0.267407	3.347479	36.1	0.309847	2.888969	2.8849737	49.66	1011	101032	0.009908	0.90
EH-11	31.09	0.267995	3.340127	36.21	0.310759	2.880485	2.883842	49.28	< D.L.	215435	—	< 1
EH-12	31.069	0.267819	3.342329	36.16	0.310345	2.884335	2.8854896	49.83	< D.L.	85489	—	< 1
EH-45	31.07	0.267827	3.342224	36.15	0.310262	2.885106	2.8863657	50.12	< D.L.	93248	—	< 1
EH-51	31.11	0.268163	3.338033	36.19	0.310593	2.882024	2.8874749	50.49	< D.L.	110946	—	< 1
EH-58	31.11	0.268163	3.338033	36.17	0.310428	2.883564	2.8890151	51.01	< D.L.	81871	—	< 1
EH-60	31.099	0.268071	3.339184	36.18	0.310511	2.882794	2.8870932	50.36	< D.L.	115421	—	< 1

Table 6.1.2. Calculations of the correction factor (CF) for Horrigan's (1996) XRD data. The values are in mol % CaCO$_3$.

Sample ID	Horrigan	Kuflevskiy	Δ
EH-10	49.17	49.66	+0.49
EH-11	48.36	49.28	+0.92
EH-12	47.66	49.83	+2.17
EH-45	49.83	50.12	+0.29
EH-51	49.76	50.49	+0.73
EH-58	50.53	51.01	+0.48
EH-60	48.37	50.36	+1.99
Range (min to max)	2.87	1.73	
Δ mean (CF)			+1.01
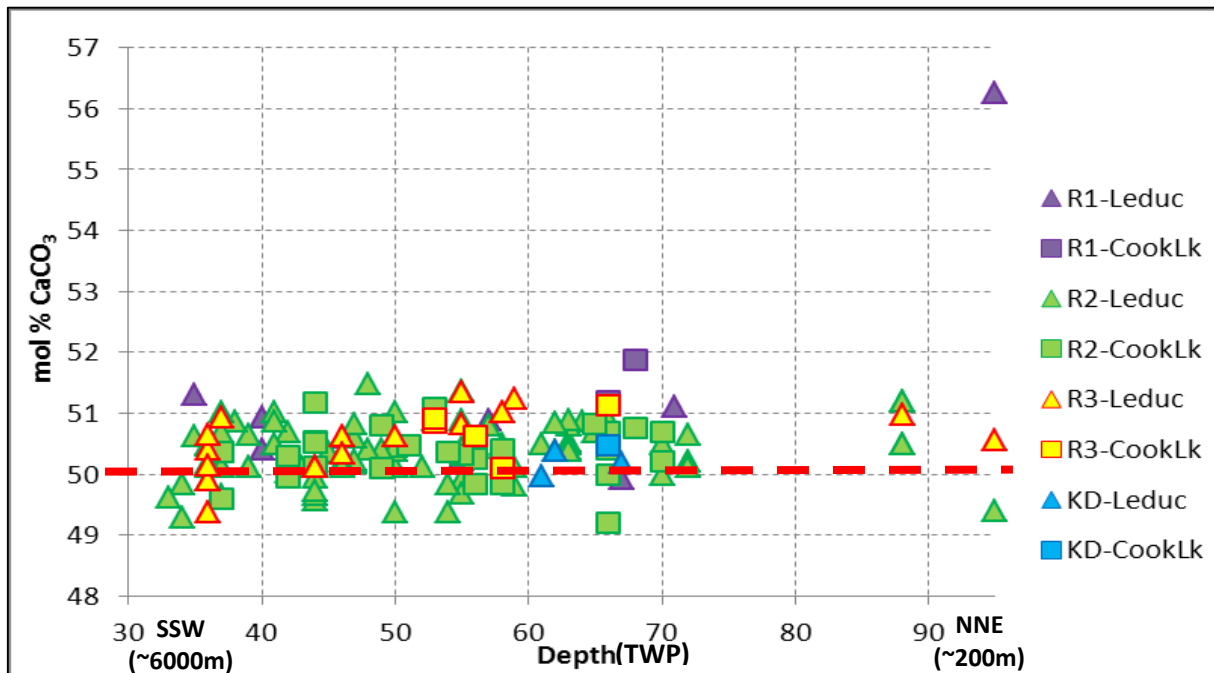
Figure 6.1.1. Chemical composition of different types of matrix dolomite of the Cooking Lake and Leduc Formations in mol% CaCO$_3$ as a function of depth. Note the red line showing the stoichiometric dolomite.

6.2 Stable carbon and oxygen isotopes

Carbon and oxygen isotopic ratios were determined to explain the origin of matrix dolomites in the reef trend. These isotopes are the most frequently used in the study of carbonates due to their abundance and fractionation by a number of physical and chemical processes.

Carbon isotopic compositions reflect the source of carbon involved in dolomite precipitation or recrystallization during diagenesis. Due to the relative insolubility of CO_2 in water, the carbon isotopic compositions of replacement dolomites may be inherited from the precursor limestones, which formed in equilibrium with seawater. These isotopic compositions experience very little temperature-dependent fractionation of ^{13}C and ^{12}C during replacement (Land, 1980; Tucker and Wright, 1990). Typical signatures of the Late Devonian marine dolomites were estimated to lie between +1.5 and +3.5‰ PDB (Hurley and Lohmann, 1989; Carpenter and Lohmann, 1989). Therefore, any deviation from this range could indicate recrystallization associated with a number of diagenetic processes (Figure 6.2.1) or non-marine sources of carbon. More depleted $\delta^{13}C$ values (down to -20‰) signal contributions of organic matter, through processes such as from biogenic or thermogenic oxidation or bacterial (BSR) or thermochemical (TSR) sulfate reduction (Table 6.2.1; Machel *et al.*, 1995). Conversely, more positive values (up to +15‰) indicate microbial reduction of CO_2 to CH_4 and microbial fermentation of organic matter (Claypool and Caplan, 1974; Irwin *et al.,* 1977).

Oxygen isotopes can be used either to determine the nature of the fluid (meteoric, marine or evaporitic) involved in dolomite diagenesis or to estimate the temperature of
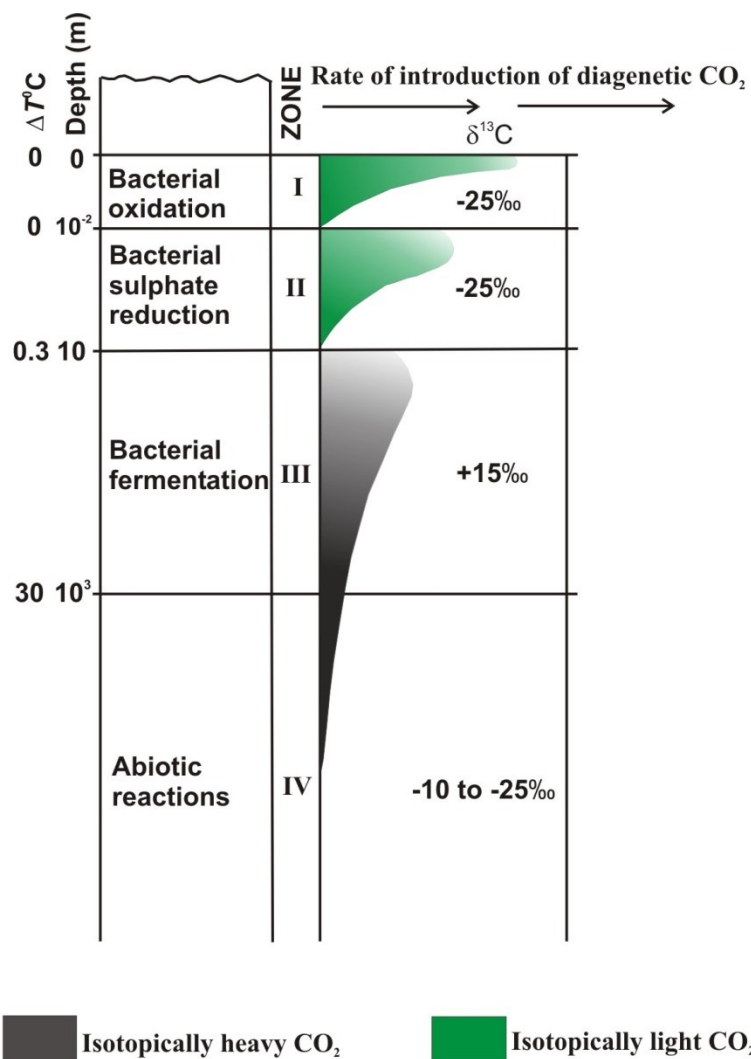
Figure 6.2.1 Model for depth zonation with reference to the diagenetic CO_2 (modified from Irwin et al. 1977).

Table 6.2.1. Carbon isotope composition from different pools of the Upper Devonian Nisku sour gas play, Canada (modified from Machel *et al.,* 1995).

	mol% H₂S	CO₂	CH₄	C₂H₆	C₃H₈
$\delta^{13}C$ ‰ PDB	0.4	-6.9	-41.7	-29.5	-25.8
	0.7	-6.9	-41.5	-29.6	-27.5
	12	-7.1	-38.7	-29.1	-27.5

dolomite formation. Paleotemperatures can be calculated using the equations of [1] Friedman and O'Neil (1977) for calcite and [2] Land (1985) for dolomite:

$$10^3 ln \frac{\delta^{18}O_{calcite}+1000}{\delta^{18}O_{fluid}+1000} = \frac{2.78*10^6}{T^2} -2.89 \qquad [1]$$

where $\delta^{18}O_{calcite}$ – $\delta^{18}O$ value of the precursor calcite (in SMOW),
       $\delta^{18}O_{fluid}$ – $\delta^{18}O$ value of the fluid forming the precursor calcite (in SMOW),
       T – temperature of the parent fluid (in Kelvin);

$$10^3 ln \frac{\delta^{18}O_{dolomite}+1000}{\delta^{18}O_{fluid}+1000} = \frac{2.78*10^6}{T^2} +0.91 \qquad [2]$$

where $\delta^{18}O_{dolomite}$ – measured $\delta^{18}O$ value of the dolomite (in SMOW),
       T – temperature of the fluid from which dolomite formed (in Kelvin).

According to Amthor *et al.* (1993), the Upper Devonian marine baseline values of $\delta^{18}O$ of dolomite are expected to be between 0 and –2.4‰. Any variation from this range may be a result of recrystallization associated with several factors listed below:

- water-to-rock ratio: during high fluid/rock ratio dolomites would be isotopically dominated by the fluid chemistry, but rock-dominated during low fluid/rock ratios;

- the nature of the fluid (*e.g.* meteoric water infiltrating the dolomite system typically results in lower $\delta^{18}O$ values);

- latitude, altitude and seasonal changes (*e.g.* increased latitude and altitude cause lower $\delta^{18}O$ values), in systems with meteoric water input;

- temperature-dependent fractionation causing depleted values during burial diagenesis (Clayton *et al.,* 1966);

- biological fractionation in biogenic carbonates that are not in isotopic equilibrium with seawater (*e.g.* crinoids and rugose corals);

- secular changes in seawater composition that show more depleted $\delta^{18}O$ values with increasing age of dolomites (Anderson and Arthur, 1983; Given and Wilkinson, 1987; Cummins *et al.,* 2014; Veizer and Prokoph, 2015). This statement, however, was disputed by Muehlenbachs (1998), who claimed that the seawater $\delta^{18}O$ values have not changed since the Proterozoic.

6.2.1. Calibration of the previously reported data

One hundred and sixty four carbon and oxygen isotopic analyses acquired in this study were combined with 258 previously reported stable isotope ratios and compiled into one table (Appendix 3). Additionally, cross-study calibration was performed on the datasets with available samples from Qiang (1990-1992), Amthor *et al.* (1993), Horrigan (1996), and Huebscher (1996). Powder samples drilled by the previous authors were re-run by the current author. Where the original powders were unavailable, new microsamples were drilled from the spots marked for sampling by the earlier authors.

A total of 60 powder samples were re-run for calibration purposes. Twenty nine of them were from Horrigan (1996), including nine powders prepared by Horrigan and 20 newly drilled from the areas outlined on the hand specimens. Twenty three microsamples were from Huebscher (1996), including ten of Huebscher's powders along with 13 from the spots marked for drilling. Eight powders were drilled from the samples provided by Amthor *et al.* (1993), and ten from Qiang (1990-1992). Due to the fact that Amthor's and Qiang's specimens were not marked by the authors and most of them were missing, the powders were obtained from the samples with depths closest to the ones with the values presented, usually within five metres.

A few problems arose during this calibration process. Firstly, it was unclear if Qiang (1990-1992), Amthor *et al.* (1993), Drivet (1993), and Marquez (1994) corrected their $\delta^{18}O$ values for phosphoric acid fractionation, as opposed to Huebscher (1996) and Horrigan (1996) who used the correction factor of 0.82‰ proposed by Sharma and Clayton (1965). Secondly, a decision had to be made whether to apply the fractionation factor on the whole data set or leave the data uncorrected.

As discussed by Spőtl and Vennemann (2003), there is no need to use the phosphoric acid fractionation factor for the reactions conducted at high temperatures. Therefore, it is very likely that Drivet (1993) and Marquez (1994) did not correct their $\delta^{18}O$ values due to the temperatures of the reaction (73 ± 2 °C) in their studies. Their data, however, was almost the same as that acquired from exactly the same wells and exactly the same depths in this study (Table 6.2.1.1), even though the experiments were run at a lower temperature of 25°C. Therefore, it was decided to keep the entire dataset uncorrected for phosphoric acid fractionation and adjust the values from Huebscher (1996) and Horrigan (1996) along with

the ones from Amthor *et al.* (1993), who did not specify the conditions at which their reactions were run.

The $\delta^{18}O$ results from Amthor *et al.* (1993), Horrigan (1996), and Huebscher (1996) were revealed to be consistently depleted by 1.3-1.5‰ (Table 6.2.1.2), which is significantly larger than their analytical error of +/- 0.3‰, and 0.5-0.7‰ higher than the 0.82‰ acid fractionation correction factor. This suggests that Amthor *et al.* (1993) probably also corrected their $\delta^{18}O$ values by this factor. Additionally, Horrigan's (1996) stable isotope data were not considered credible, because her results for samples analysed from exactly the same wells and depths as in Drivet (1993) and Marquez (1994) showed a significant difference compared to their results (Table 6.2.1.1).

The $\delta^{18}O$ values of Amthor *et al.* (1993), Horrigan (1996), and Huebscher (1996) were adjusted by the factors presented in Table 6.2.1.2. The cross-plots showing the data before and after adjustments are presented in Figure 6.2.1.1. The $\delta^{13}C$ results from these authors were not corrected as they are consistent with those of all other studies (generally within the analytical error of 0.2‰, Table 6.2.1.2).

The quality control results for the isotope data obtained from Qiang (1990-1992) did not show any significant difference compared to the newly acquired data, having the $\delta^{13}C$ and $\delta^{18}O$ values enriched by only 0.10‰ and 0.24‰, respectively (Table 6.2.1.2), which is within the analytical errors. This suggests that his results were not corrected for the acid fractionation. The enrichment itself might be explained by drilling not from exactly the same but from the neighboring specimens.

Overall, the adjusted results are credible values that are nearly perfectly correlated with the data previously reported by Drivet (1993) and Marquez (1994).

99

Table 6.2.1.1. Comparison of the $\delta^{13}C$ and $\delta^{18}O$ values from Drivet (1993), Marquez (1994) and Horrigan (1996) with those acquired from the same wells and depths in this study (highlighted in blue). Δ mean values (highlighted in red) are mean values of the differences between the newly acquired and original isotope data.

Well ID	Depth, m	Type	δ¹³C ‰ PDB				δ¹⁸O ‰ PDB			
			Kuflevskiy	*Drivet*	*Marquez*	*Horrigan*	*Kuflevskiy*	*Drivet*	*Marquez*	*Horrigan*
11-3-42-2W5	2390	R2	1.63	1.59		1.78	-4.47	-4.80		-5.79
14-5-41-2W5	2514	R2	1.54	1.57			-4.65	-4.27		
16-11-38-5W5	3071	R2	2.63	2.28		2.63	-4.38	-4.48		-6.24
10-17-37-3W5	2863	R2	2.10	2.13		2.22	-4.42	-4.25		-6.17
16-32-37-4W5	2982	R2	1.87	1.29		1.83	-3.68	-4.60		-5.31
10-31-37-9W5	4318.3	R2	3.71		3.54	5.03	-4.24		-4.57	-3.04
10-33-36-10W5	4564	R2	2.4		2.42		-4.6		-4.61	
10-33-36-10W5	4661	R2	2.00		1.94	1.85	-4.99		-4.90	-6.55
11-27-36-10W5	4476.1	R2	2.3		2.39		-4.8		-4.43	
6-14-34-8W5	4286.9	R2	2.40		2.26		-4.62		-4.55	
Δ mean				+0.2	+0.05	+0.4		+0.16	-0.05	+1.41

Table 6.2.1.2. Correction factors (CF) for $\delta^{13}C$ and $\delta^{18}O$ values from Amthor *et al.* (1993), Horrigan (1996), Huebscher (1996) and Qiang (1990-1992). Δ values are the differences between the original and the newly acquired isotope data.

Sample ID	δ¹³C (PDB)			δ¹⁸O (PDB)		
	original	corrected	Δ	original	corrected	Δ
Horrigan						
EH-50a	1.85	1.73	0.12	-4.23	-5.81	1.58
EH-38	1.55	1.78	-0.23	-4.45	-5.79	1.34
EH-42	0.36	0.30	0.06	-3.08	-4.81	1.73
EH-56	2.63	2.63	0	-4.38	-6.24	1.86
EH-50b	1.70	1.48	0.22	-4.60	-6.51	1.91
EH-5	-0.07	-0.20	0.16	-5.12	-7.21	2.09
EH-9	2.06	1.65	0.41	-8.67	-9.87	1.20
EH-24	3.40	3.39	0.01	-4.53	-6.00	1.47
EH-29	2.10	2.22	-0.12	-4.42	-6.17	1.75
EH-19b	2.37	2.44	-0.07	-4.86	-6.54	1.68
EH-49	2.89	2.92	-0.03	-4.42	-5.77	1.35
EH-37	2.07	1.85	0.22	-4.74	-6.55	1.81
EH-32	3.84	5.03	-1.19	-4.08	-3.04	-1.04
EH-32-Erin	3.78	5.03	-1.25	-4.17	-3.04	-1.13
EH-32-Erin	3.71	5.03	-1.32	-4.24	-3.04	-1.20

EH-5-Erin	-0.19	-0.20	0.01	-5.54	-7.21	1.67
EH-49-Erin	2.94	2.92	0.02	-4.29	-5.77	1.48
EH-37-Erin	2.08	1.85	0.23	-4.68	-6.55	1.87
EH-38-Erin	1.63	1.78	-0.15	-4.47	-5.79	1.32
EH-24-Erin	3.45	3.39	0.06	-4.84	-6.00	1.16
EH-37-Erin	2.00	1.85	0.15	-4.99	-6.55	1.56
EH-58	1.87	1.83	0.04	-3.68	-5.31	1.63
EH-60	2.79	2.87	-0.08	-4.43	-5.67	1.24
CF			**+0.04**			**+1.49**
Huebscher						
H71-2	1.29	1.35	-0.06	-4.16	-5.57	1.41
H71-2 Huebscher	1.23	1.35	-0.12	-4.18	-5.57	1.39
H662-81 Huebscher	5.13	5.28	-0.15	-4.54	-5.86	1.32
H88-6 Huebscher	5.79	5.70	0.09	-4.63	-6.14	1.51
H88-1 Huebscher	2.87	2.96	-0.09	-6.22	-7.57	1.35
H68-2	1.56	1.83	-0.27	-5.95	-7.39	1.44
H68-2no extr.	1.46	1.83	-0.37	-6.07	-7.39	1.32
H64-1no extr.	1.37	1.79	-0.42	-4.44	-5.54	1.10
H63-4	1.34	1.62	-0.28	-4.30	-5.86	1.56
H63-4 Huebscher	1.68	1.62	0.06	-4.17	-5.86	1.69
H62-5	1.50	1.85	-0.35	-4.29	-5.52	1.23
H62-5 Huebscher	1.46	1.85	-0.39	-4.28	-5.52	1.24
H61-3	0.57	0.99	-0.42	-4.78	-4.79	0.01
CF			**-0.21**			**+1.28**
Amthor et al.						
A-38	-0.07	-0.20	0.14	-5.12	-7.21	2.09
A-39	2.06	1.65	0.41	-8.67	-9.87	1.20
A41	3.40	3.39	0.01	-4.53	-6.00	1.47
A-42	2.10	2.22	-0.12	-4.42	-6.17	1.75
N-14	3.71	5.03	-1.32	-4.24	-3.04	-1.20
A-125a	-0.19	-0.20	0.01	-5.54	-7.21	1.67
A-125b	2.94	2.92	0.02	-4.29	-5.77	1.48
A-130	1.23	1.35	-0.12	-4.18	-5.57	1.39
CF			**+0.01**			**+1.47**
Qiang						
N-155	2.36	2.17	0.19	-4.64	-4.68	0.04
N-151	3.65	3.46	0.19	-4.49	-4.67	0.18
N-148	2.08	2.39	-0.31	-5.46	-4.26	-1.20
N-146	2.25	2.48	-0.23	-6.16	-4.59	-1.57
N-141	1.63	1.38	0.25	-5.19	-4.42	-0.77
N-140	1.63	2.12	-0.49	-5.19	-4.45	-0.74
N-137	2.85	2.09	0.76	-4.94	-4.29	-0.65
N-135	1.84	1.73	0.11	-4.32	-4.46	0.14
N-133	1.86	1.88	-0.02	-4.37	-4.97	0.60
N-132	1.86	1.87	-0.01	-4.37	-4.57	0.20
CF			**-0.10**			**-0.24**
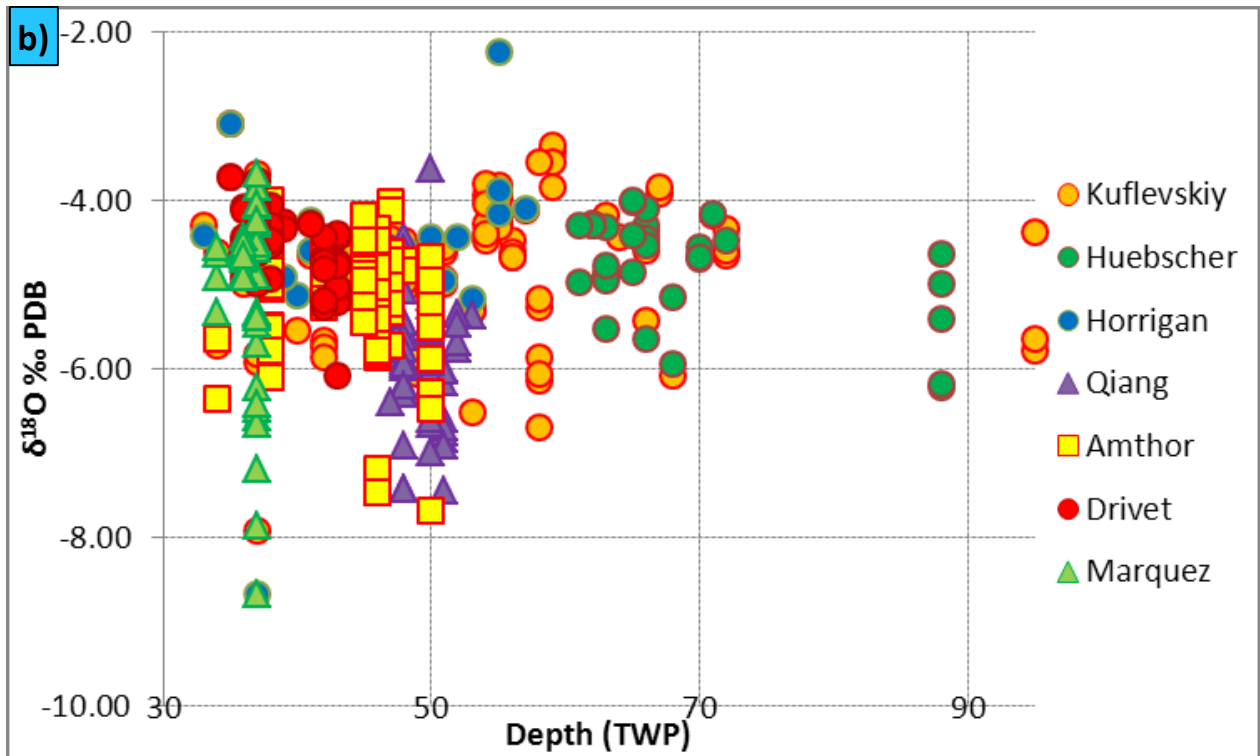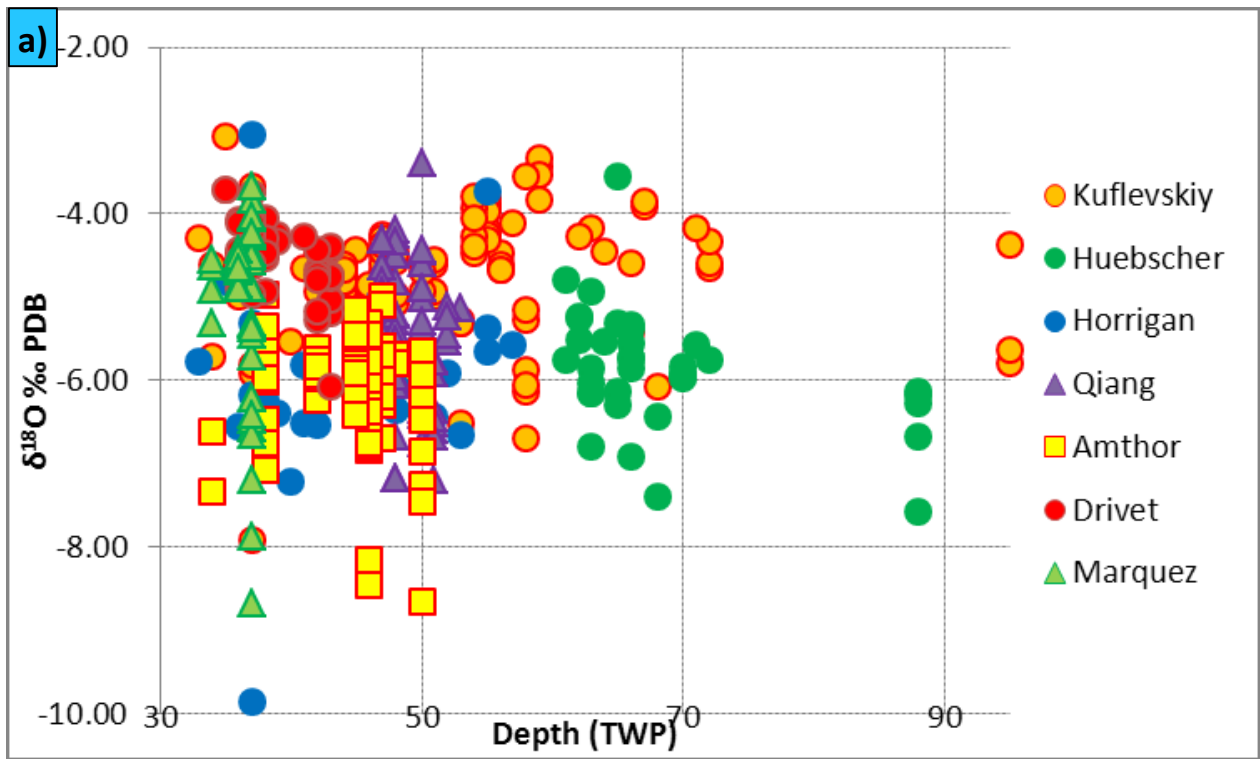
Figure 6.2.1.1. Oxygen isotope values compiled from different studies before (a) and after (b) adjustments.

6.2.2. Stable isotope results

The carbon and oxygen isotopic compositions for all matrix dolomites of the study area range from -0.1‰ to +6.98‰ and from -8.67‰ to -3.14‰, respectively (Figures 6.2.2.1 through 6.2.2.4).

Approximately 300 δ^{13}C values out of a total of 422 fall into the estimated range for Late Devonian marine dolomites (Carpenter and Lohmann, 1989) and are similar to the ones reported for other matrix dolomites across the Western Canada Sedimentary Basin (Mattes and Mountjoy, 1980; Machel and Anderson, 1989; Qing and Mountjoy, 1989; Kaufman *et al.,* 1990; Laflamme, 1990; Patey, 1995; Duggan, 1997; McKenzie, 1999; Keilly, 2004; Green and Mountjoy, 2005; Machel and Buschkuehle, 2008). There are four distinct clusters showing elevated δ^{13}C values from +3.5‰ to +6.98‰ and five Leduc Formation samples that have depleted δ^{13}C values forming a cluster near 0‰ (Figure 6.2.2.1a).

Matrix dolomite R1 exhibits carbon isotopic ratios ranging from -0.19‰ to +5.11‰ with an average of +2.25‰. Matrix dolomites R1 from both Cooking Lake and Leduc Formations show a weak trend of increasing carbon isotopic values with depth with the exception of one outlier (SK95-12) in the northernmost end of the reef trend, and a small cluster with relatively negative δ^{13}C ratios in the southern end (Figure 6.2.2.5).

Matrix dolomite R2 shows carbon ratios ranging between -0.05‰ and +6.85‰ with an average of +2.63‰. Cooking Lake Formation matrix dolomite R2 exhibits a prominent trend of increasing carbon isotopic values with depth despite considerable scatter (Figure 6.2.2.6). Carbon isotopic compositions of matrix dolomites R2 of both Cooking Lake
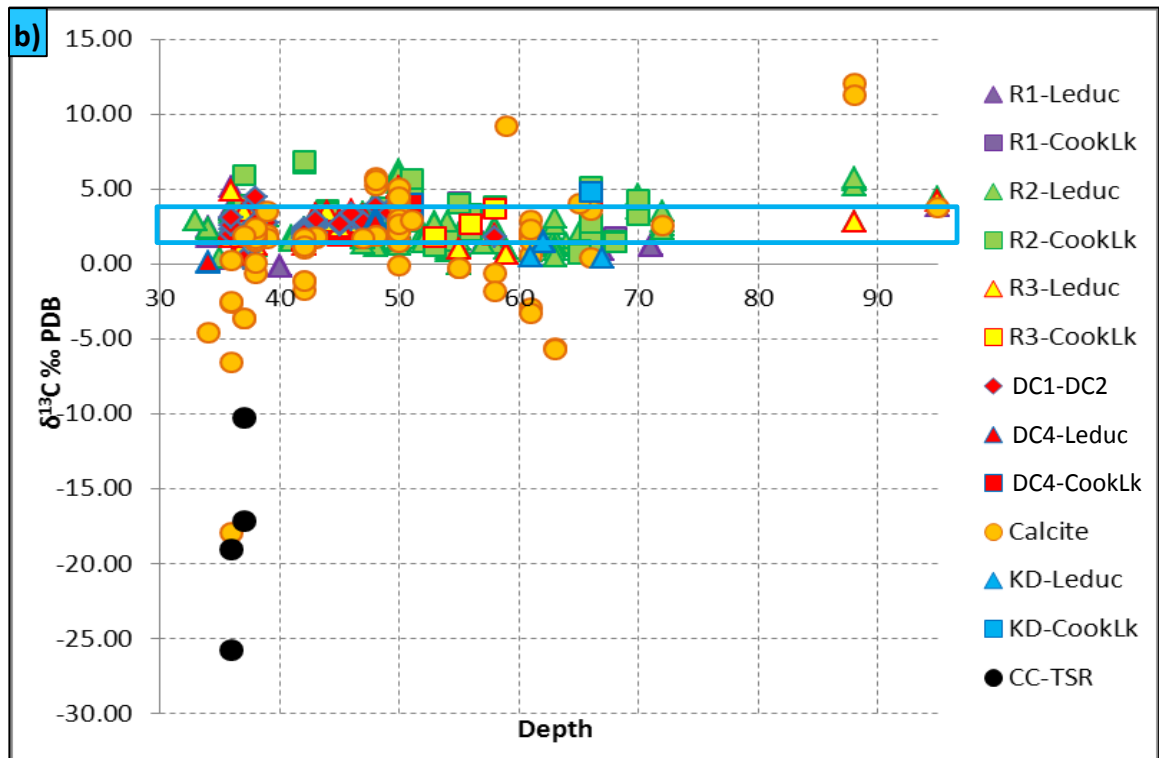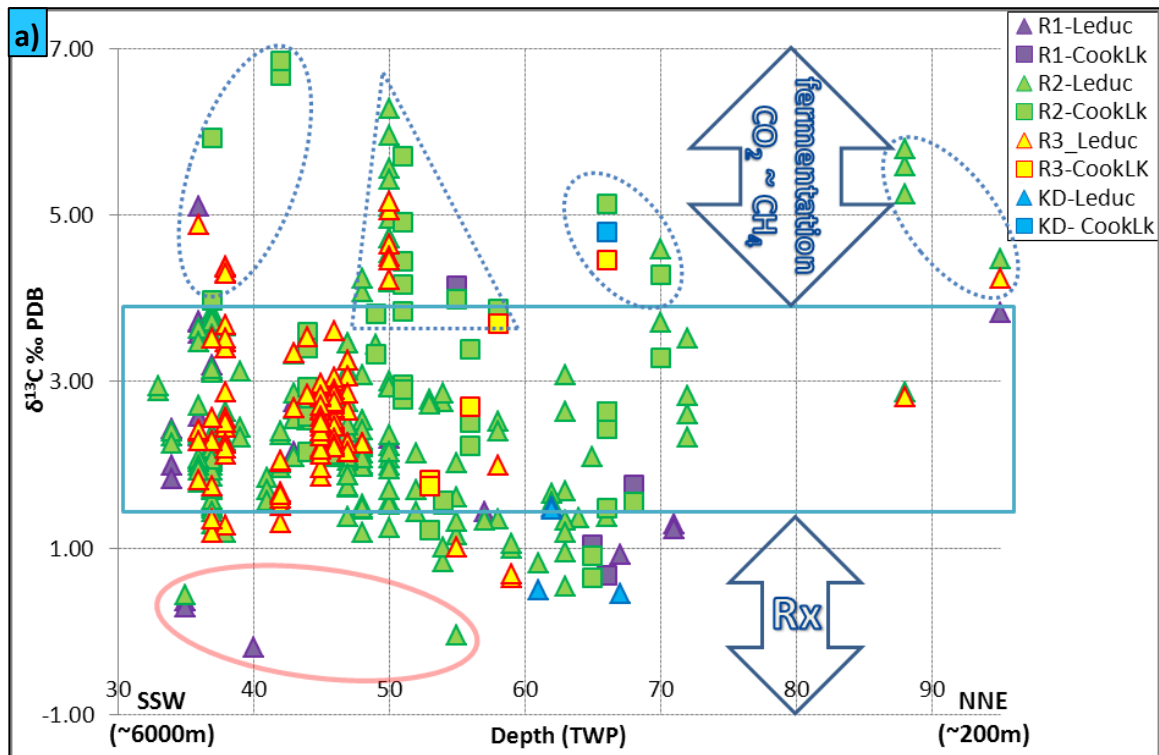
Figure 6.2.2.1. Plot of carbon isotope compositions of Cooking Lake and Leduc Formations (a) matrix dolomites and (b) including dolomite and calcite cements. Note the clusters with outliers circled in red. The blue box indicates estimated ranges for marine dolomite that would have formed in equilibrium with Late Devonian seawater (Carpenter and Lohmann, 1989).
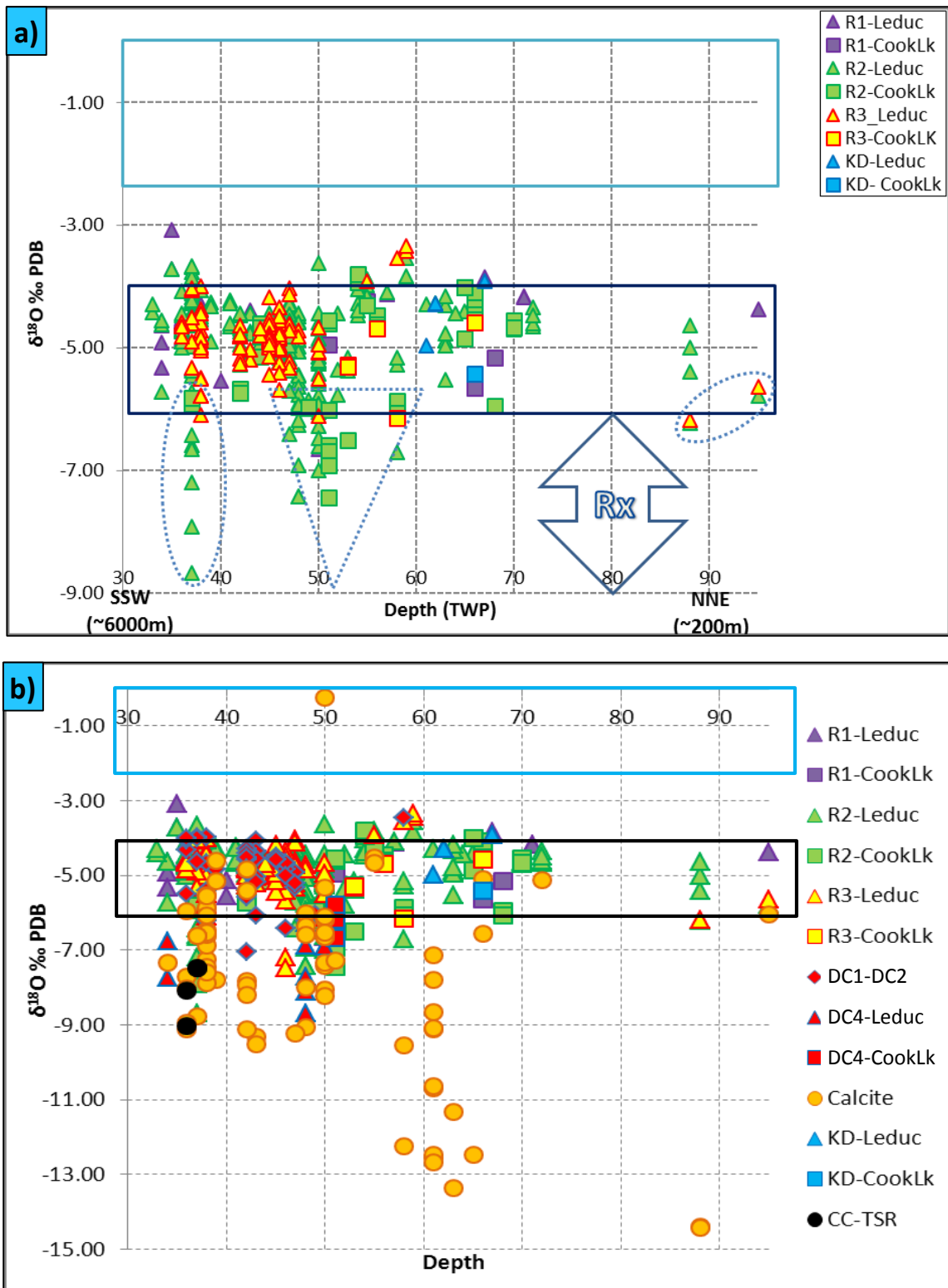
Figure 6.2.2.2. Plot of oxygen isotope compositions of Cooking Lake and Leduc Formations (a) matrix dolomites and (b) including dolomite and calcite cements. Note the clusters with outliers circled in red. The boxes indicate estimated ranges for Late Devonian marine dolomites (blue) and calcites (black) (Amthor *et al.,* 1993).
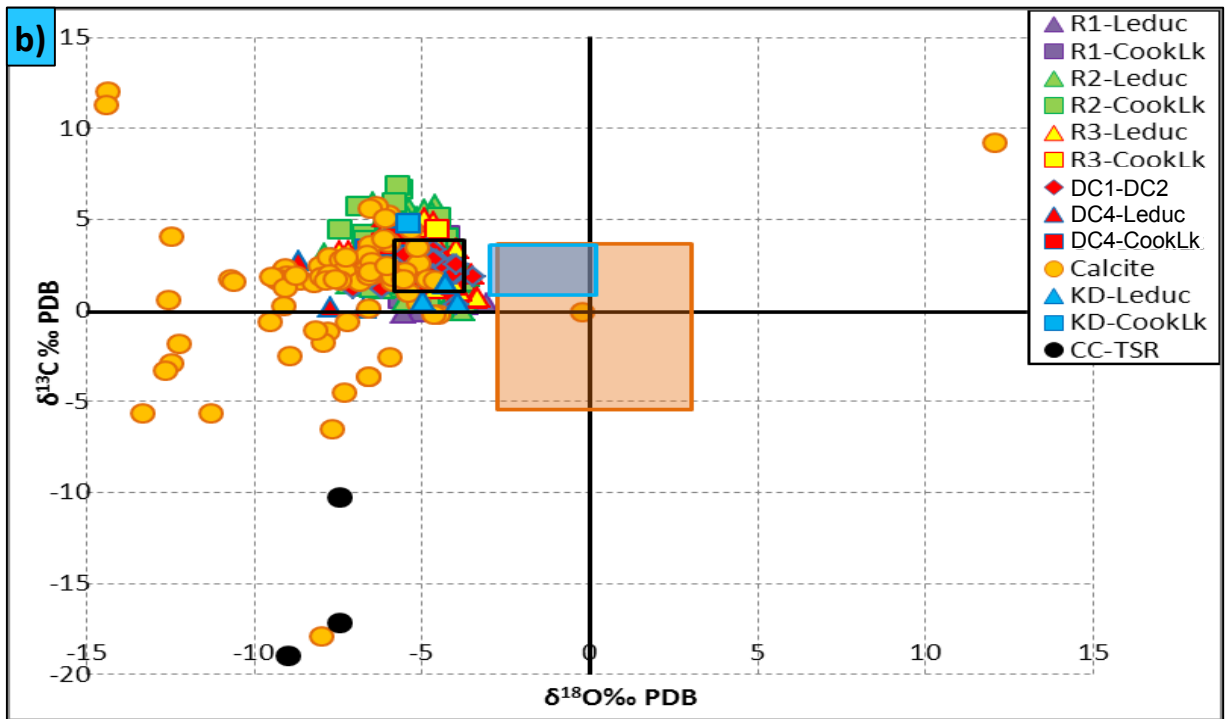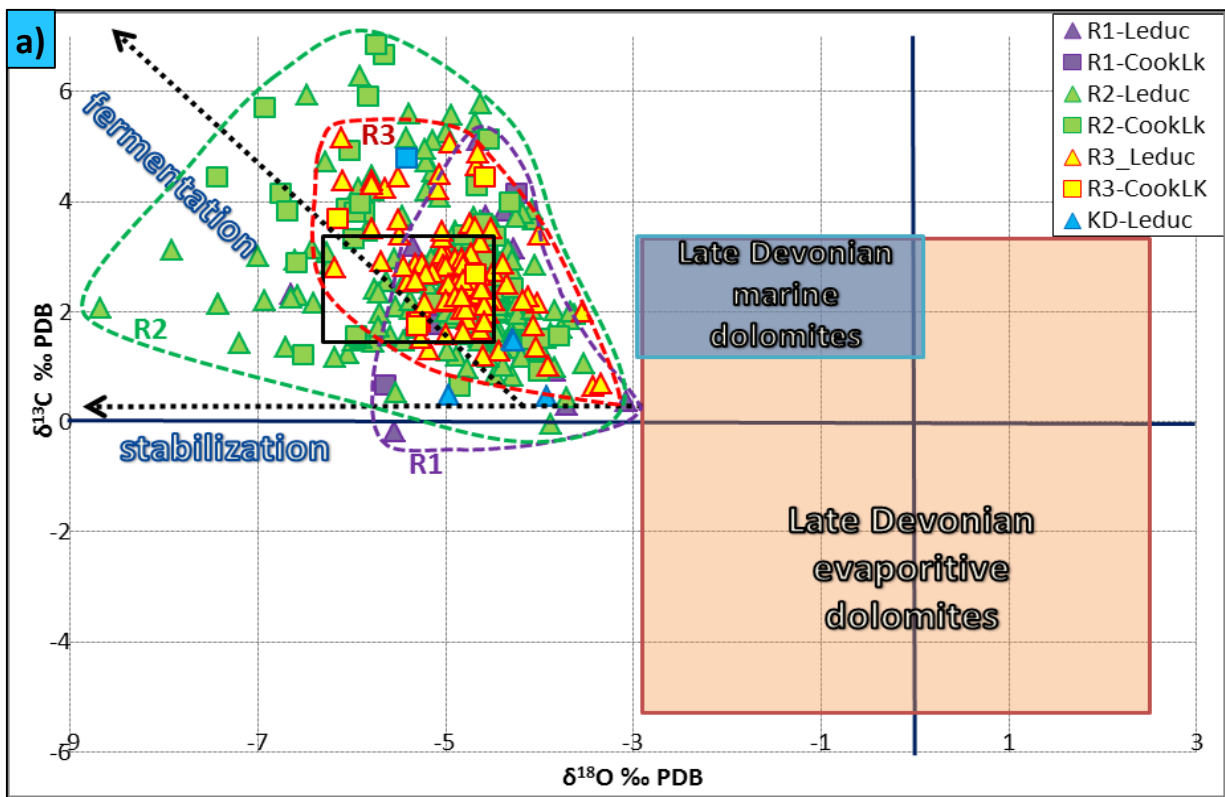
Figure 6.2.2.3. Oxygen versus carbon stable isotope plot for Cooking Lake and Leduc Fm. (a) matrix dolomites and (b) including dolomite and calcite cements. The boxes indicate estimated ranges for Late Devonian marine dolomites (blue) and calcites (black) (Amthor *et al.,* 1993).
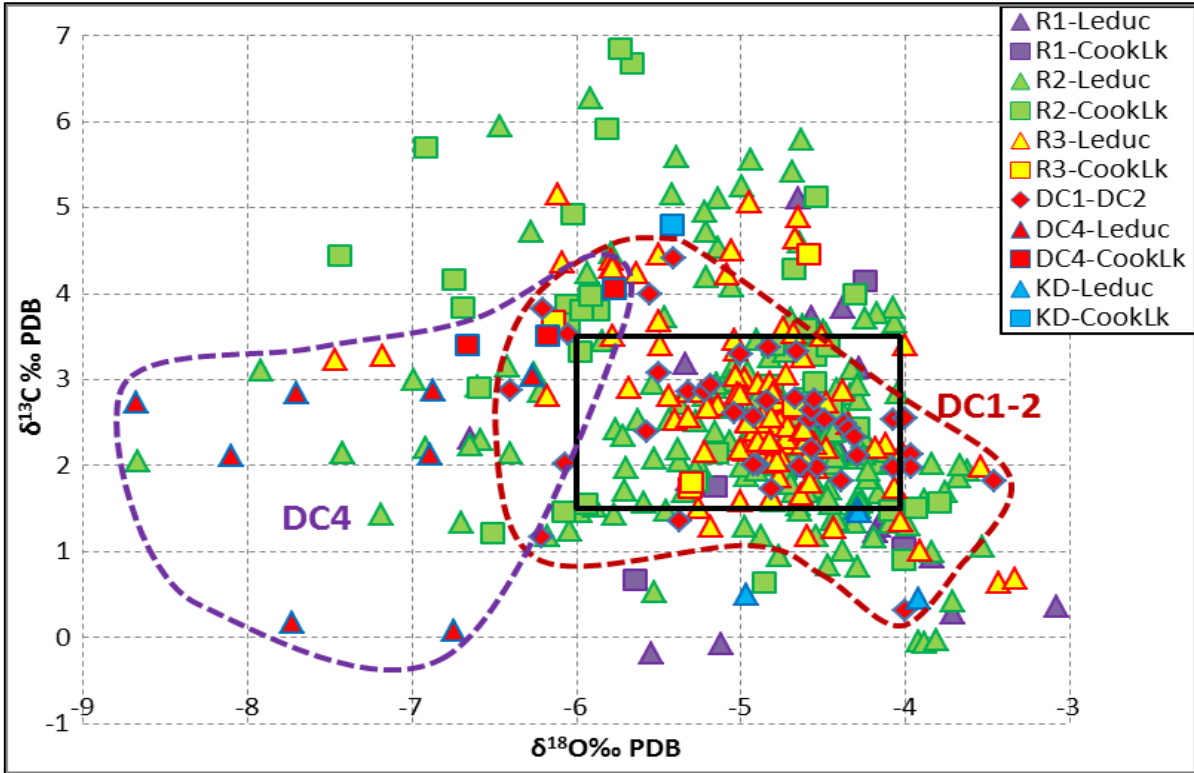
Figure 6.2.2.4. Oxygen versus carbon stable isotope plot for Cooking Lake and Leduc Fm. matrix dolomites and dolomite cements. This plot is an enlarged version of Figure 6.2.2.3b in the data ranges of -3 to -9‰ and -1 to +7‰ for $\delta^{18}O$ and $\delta^{13}C$, respectively. The black box indicates estimated range for Late Devonian marine calcites (Amthor *et al.,* 1993).
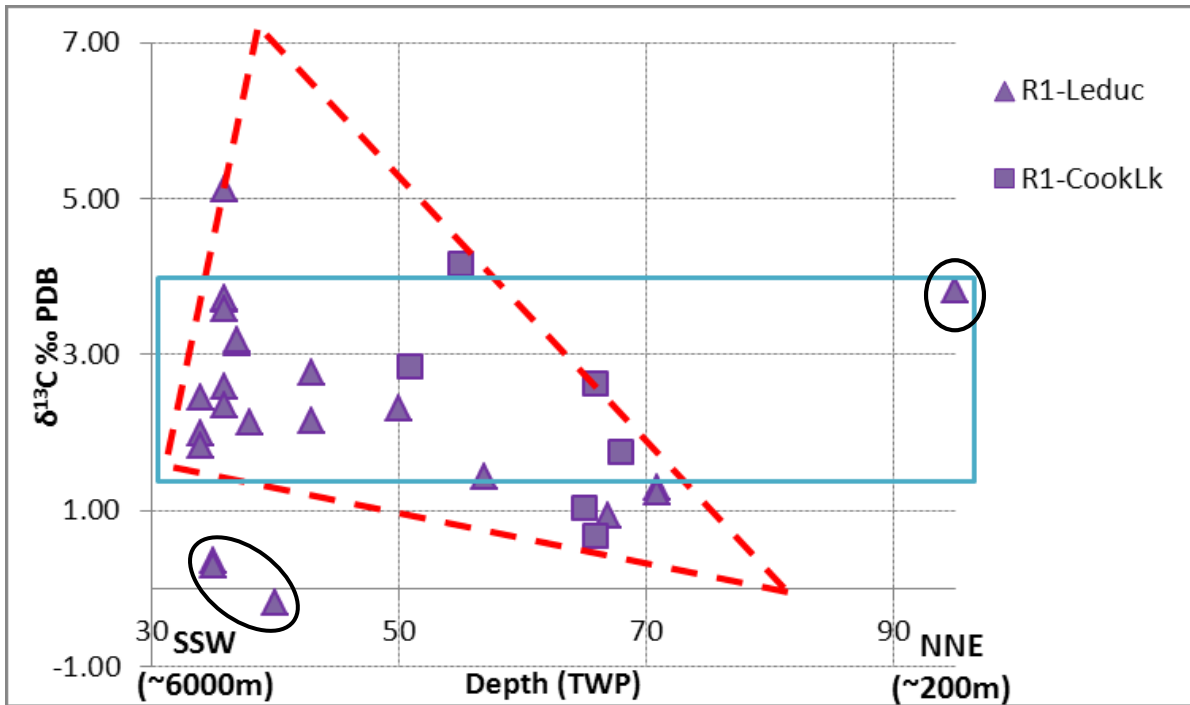
Figure 6.2.2.5. Carbon isotope plot illustrating an updip depletion in $\delta^{13}C$ for fine-crystalline matrix dolomites R1 and a few outliers circled in black. The estimated isotopic range for Late Devonian marine dolomites (blue box) is taken from Carpenter and Lohmann (1989).
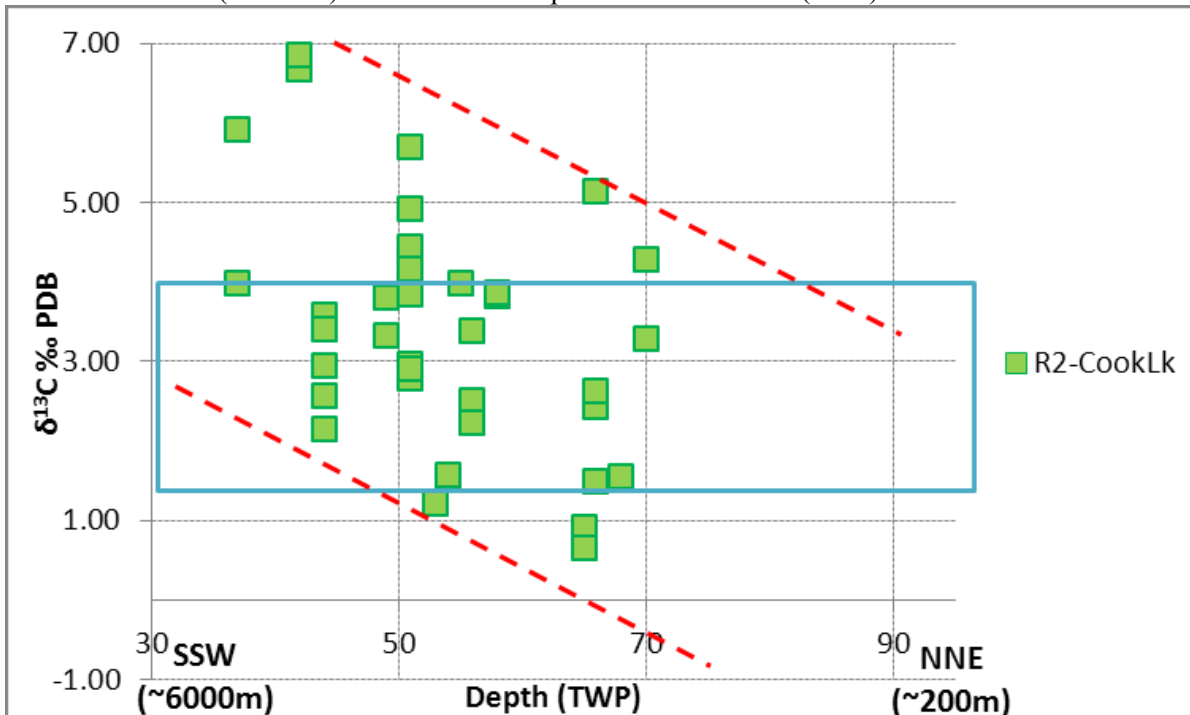
Figure 6.2.2.6. Carbon isotope plot illustrating a weak downdip trend of increasing $\delta^{13}C$ ratios for Cooking Lake matrix dolomite R2. The estimated isotopic range for Late Devonian marine dolomites (blue box) is taken from Carpenter and Lohmann (1989).

and Leduc Formations show no apparent covariant trends with crystal size (Figures 6.2.2.7 and 6.2.2.9).

The carbon isotopic composition of matrix dolomite R3 ranges from +0.64‰ to +5.16‰ with an average of +2.67‰. Three karstified Leduc samples (KD) show carbon ratios ranging between +0.45‰ and +1.50‰ (average +0.98‰), and the only Cooking Lake Formation karstified sample HH66(2)-9 has an elevated carbon ratio of +4.80‰.

All $\delta^{18}O$ values of matrix dolomites R1, R2 and R3 are 1‰ to 5.5‰ more negative than the hypothetical Late Devonian marine dolomites (Amthor *et al.,* 1993). These values are comparable to the ones from most matrix dolomites found elsewhere in the basin. The oxygen isotopic compositions of matrix dolomite R1 vary from -3.08‰ to -6.65‰, with an average of -4.62‰. $\delta^{18}O$ values of matrix dolomite R2 range from -3.53‰ to -8.67‰ (average -4.99‰), and the values of R3 range from -3.34‰ to -6.18‰ (average -4.87‰). Three karstified Leduc Formation samples KD fall into the range from -3.92‰ to -4.96‰ (average -4.36‰), and the karstified Cooking Lake Formation sample HH66(2)-9 is slightly depleted in oxygen (-5.42‰) relative to the rest of the KD samples. There are three clusters showing more negative oxygen ratios than the majority of the analyzed samples (Figure 6.2.2.2a).

Generally, the $\delta^{18}O$ isotopes show no covariant trends with crystal size (Figures 6.2.2.8 and 6.2.2.9).

The isotope values of dolomite cements DC1, DC2 and DC4 generally overlap with those of matrix dolomites R1, R2 and R3. There is no apparent data separation in oxygen versus carbon isotope plots for matrix dolomite R1, R2 and R3 (Figure 6.2.2.3a). Rather, there is a general overlap between these data, with dolomite R3 exhibiting a tighter cluster and dolomite R2 showing a larger spread and "consuming' the smaller ones (R3 and R1). There are two distinct clusters separating dolomite cements DC1 and DC2 from saddle dolomite DC4 (Figure 6.2.2.4).
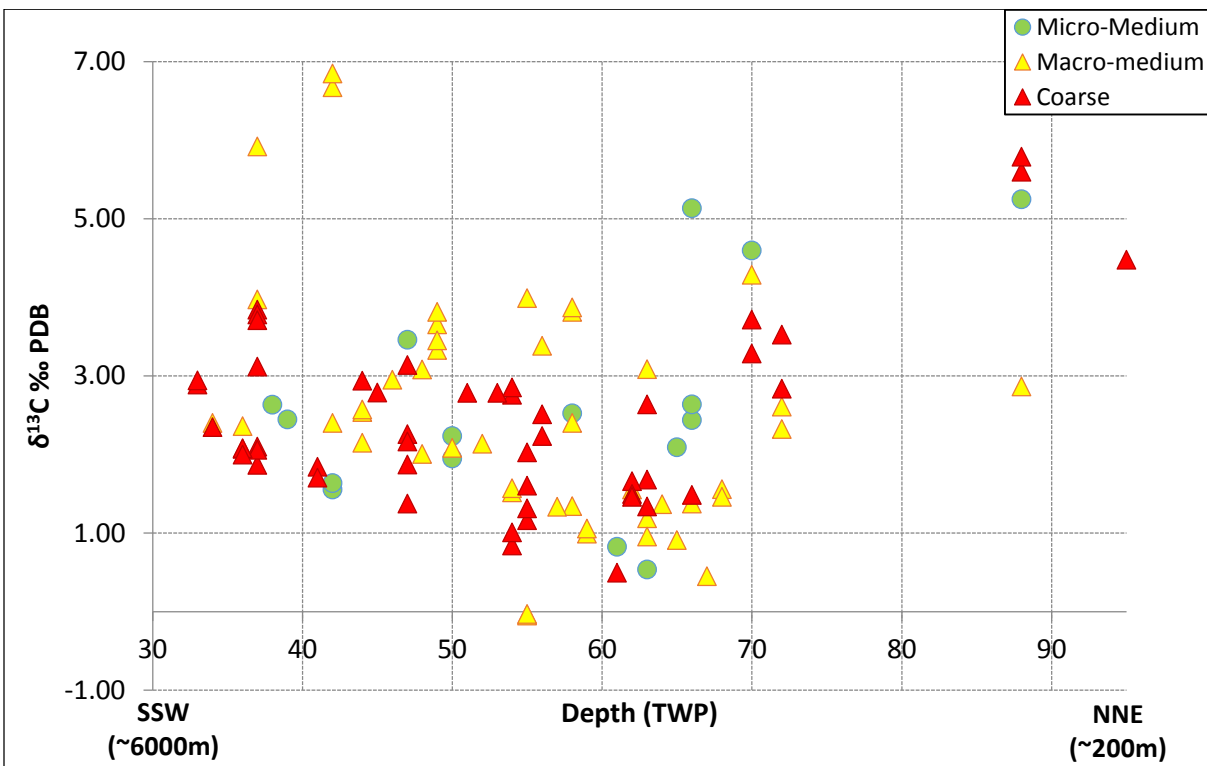
Figure 6.2.2.7. Regional distribution of carbon isotope ratios of matrix dolomite R2 with varying crystal sizes.
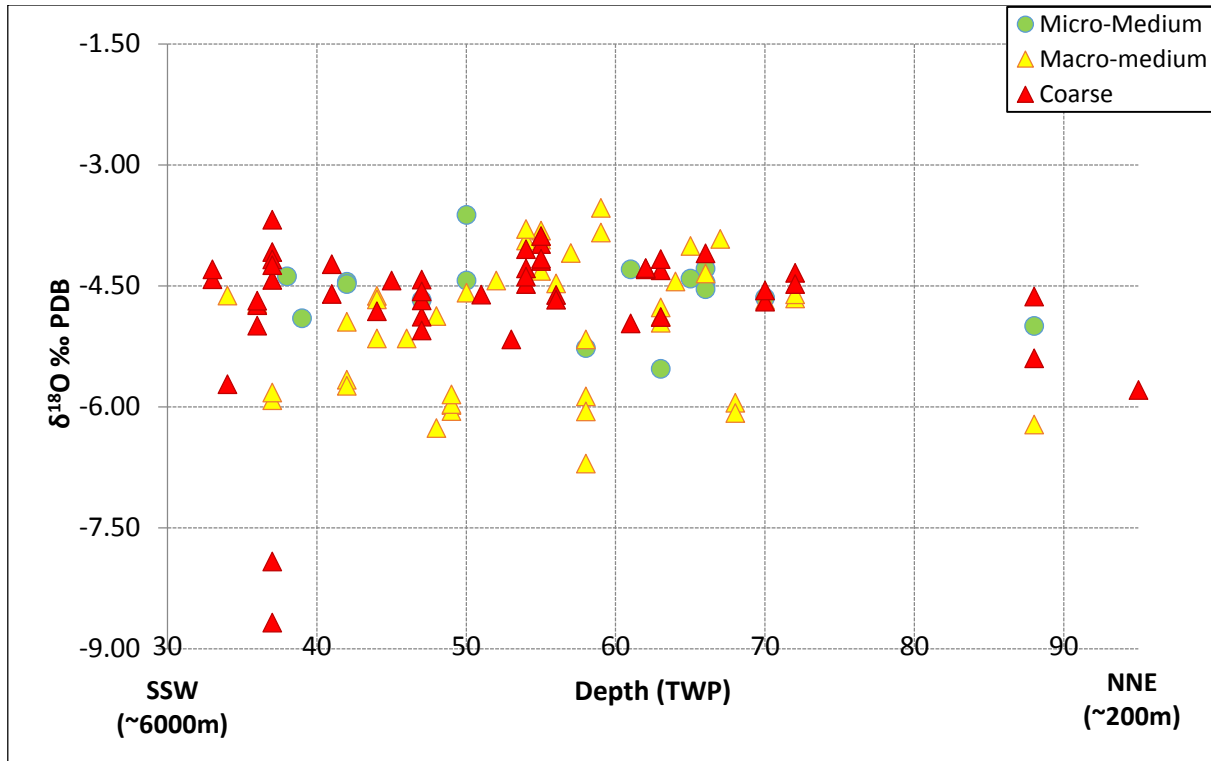
Figure 6.2.2.8. Regional distribution of oxygen isotope ratios of matrix dolomite R2 with varying crystal sizes.
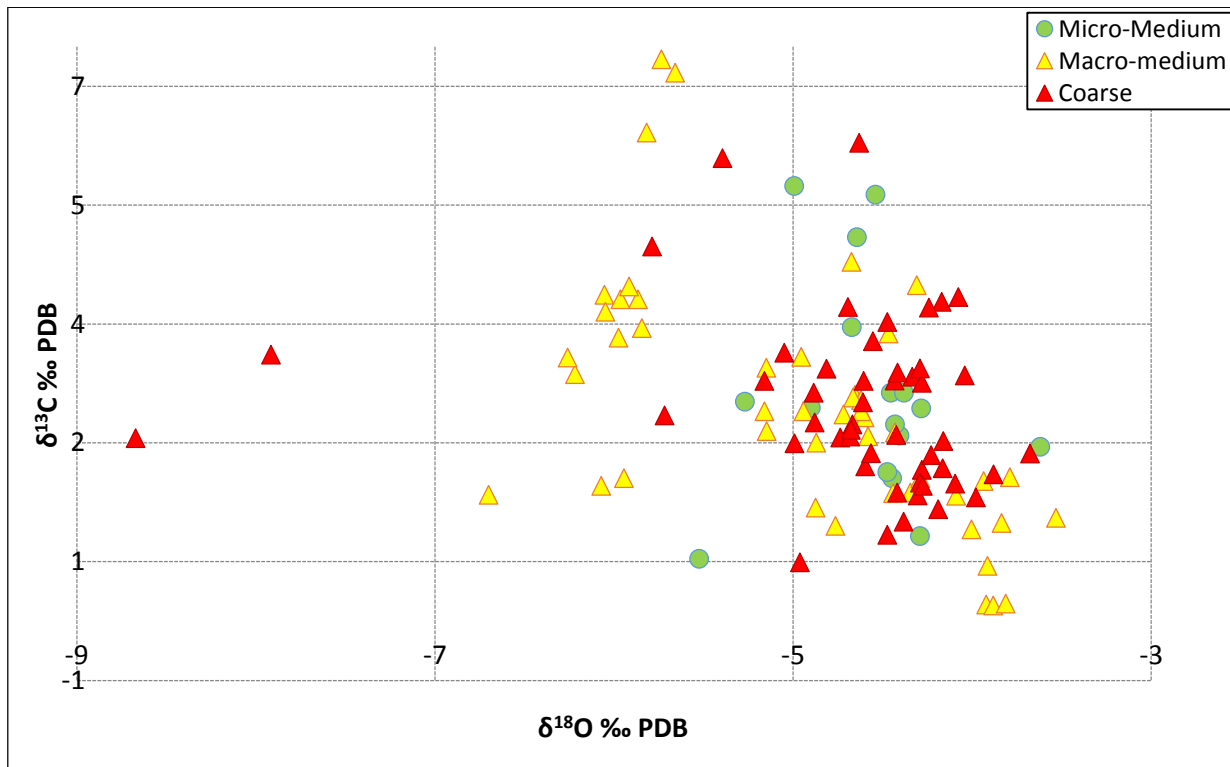
Figure 6.2.2.9. Cross-plot of oxygen and carbon isotope ratios with varying crystal sizes.

111

6.3 Radiogenic (Sr) isotopes

Due to the insignificant fractionation by variations in the temperature and pressure conditions during precipitation and recrystallization, the $^{87}Sr/^{86}Sr$ isotopic ratio of carbonate minerals is assumed to be a reflection of the isotopic composition of the fluid (Banner, 1995). Therefore, strontium isotopes can be used as a geochemical tracer for changes in fluid compositions. The estimated $^{87}Sr/^{86}Sr$ values of the Late Devonian seawater lie between 0.7078 and 0.7085 (Figure 6.3.1; Burke *et al*., 1982; Smalley *et al.,* 1994). Any elevated $^{87}Sr/^{86}Sr$ signatures could be contributed from interaction with Rb-rich minerals or basinal fluids from the Western Canada Sedimentary Basin that are enriched in ^{87}Sr (Mountjoy *et al.,* 1992). The $^{87}Sr/^{86}Sr$ isotopic ratios can be also compared to the **Ma**ximum **S**r **I**sotope **R**atio of **Ba**sinal **S**hales (MASIRBAS) defined by Machel and Cavell (1999) as 0.7120. Any value higher than this signature may reflect an influence of metamorphic (extra-basinal) formation waters.

A total of 46 samples were analyzed for strontium isotopic ratios. The subset of data acquired from the previous studies did not vary from the current study's results and, therefore, did not require adjustment (Appendix 3).

As shown in Figure 6.3.2, all matrix dolomites of the Rimbey-Meadowbrook Reef trend fall below MASIRBAS ranging from 0.7082 to 0.7090, which is slightly above the theoretical marine values of the Late Devonian. These results fall into the same range as the previously reported matrix dolomites across the Western Canada Sedimentary Basin (Qing and Mountjoy, 1989; Kaufman *et al.,* 1990; Laflamme, 1990; Patey, 1995; Duggan, 1997; McKenzie, 1999; Keilly, 2004; Green and Mountjoy, 2005).
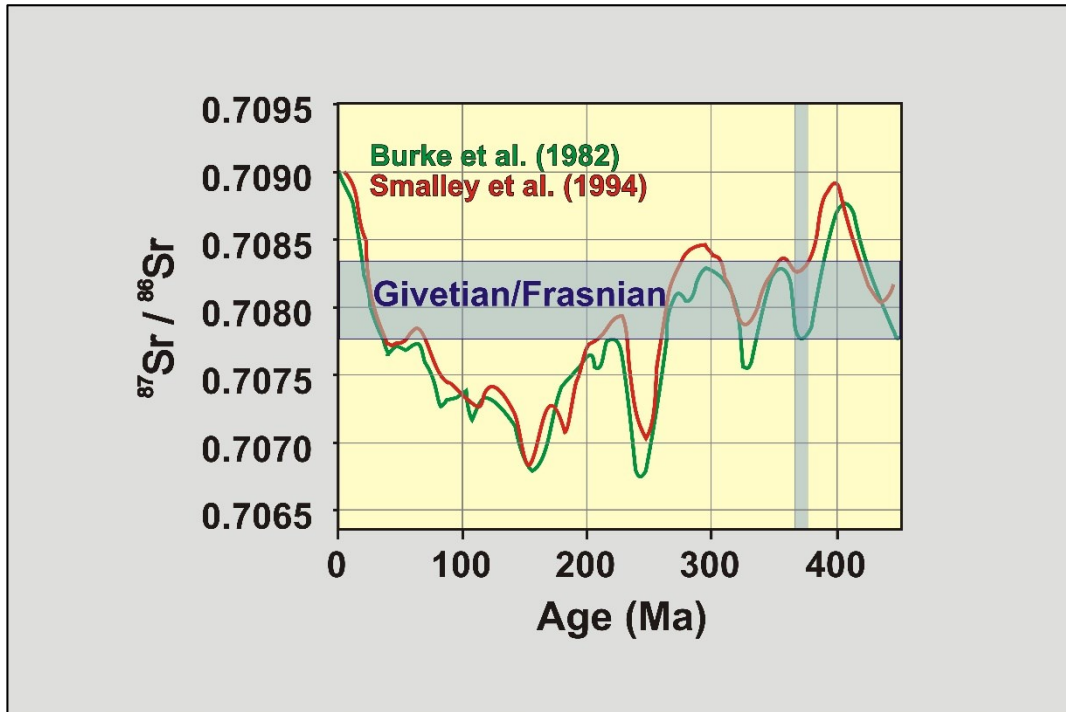
Figure 6.3.1. $^{87}Sr/^{86}Sr$ secular curve for seawater during the Phanerozoic. The vertical bar represents the time interval of the Late Devonian. The horizontal shaded area represents the best estimate for the Sr-isotope values of Givetian/ Frasnian sea water (modified from Veizer *et al.,* 1999).
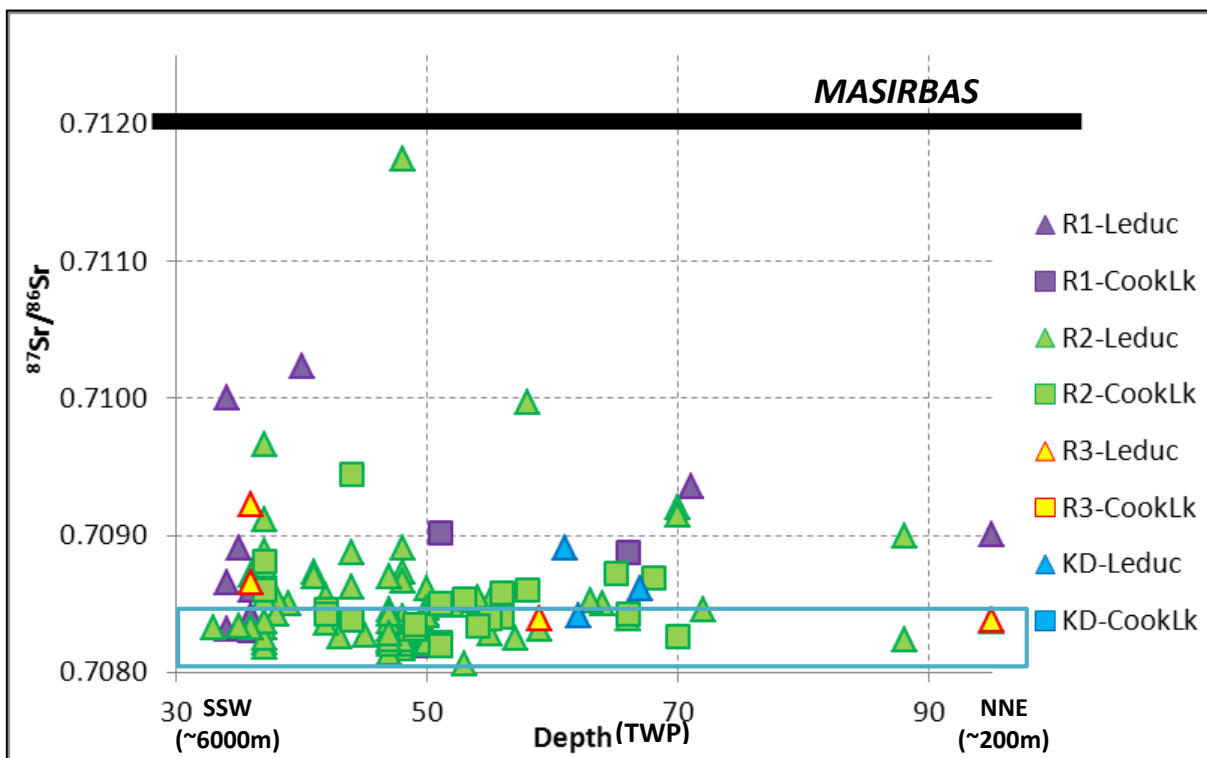
Figure 6.3.2. Strontium isotope distribution along the Rimbey-Meadowbrook reef trend. The Maximum Strontium Isotope Ratio in Basinal Shales (MASIRBAS) = 0.7120. The blue box indicates estimated ranges for marine dolomite that would have formed in equilibrium with Late Devonian seawater (Veizer *et al.,* 1999).

Generally, matrix dolomites R1 exhibit slightly enriched strontium isotope values, varying from 0.710 to 0.7082, compared to the majority of the samples. Six R1 and R2 specimens have more radiogenic $^{87}Sr/^{86}Sr$ ratios up to 0.7102, which is still below MASIRBAS, and one R2 sample almost reaches MASIRBAS at 0.71174 (Figure 6.3.2). When plotted against the $\delta^{18}O$ values, the strontium isotopes do not show any apparent correlation (Figure 6.6.3).

Dolomite cements DC1, DC2 and DC4 and sparry calcite cements, even the ones that were identified by Marquez (1994) as TSR-calcite cements (CC-TSR, Figure 6.3.3), fall below MASIRBAS.
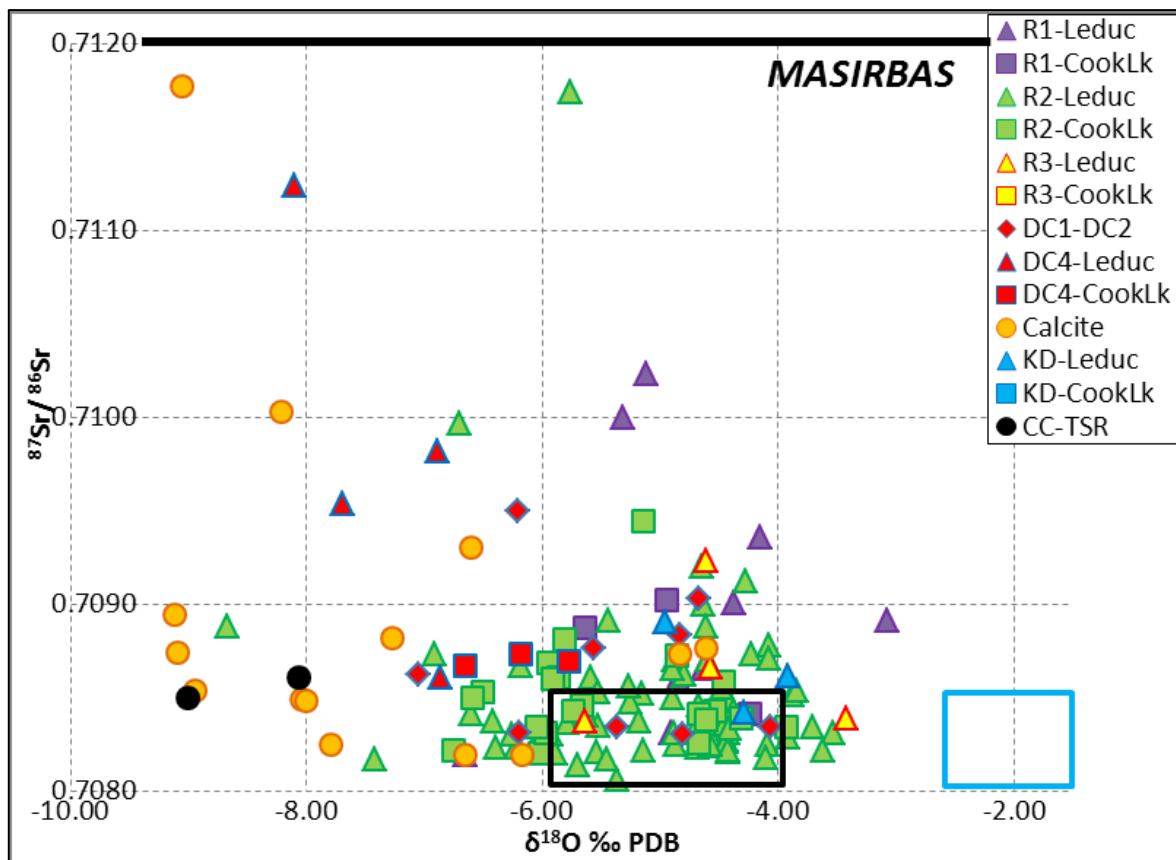
Figure 6.3.3. Oxygen versus radiogenic strontium isotope plot of Cooking Lake and Leduc Fm. matrix dolomites and dolomite and calcite cements. The Maximum Strontium Isotope Ratio in Basinal Shales (MASIRBAS) = 0.7120. The boxes indicate estimated ranges for Late Devonian marine dolomites (blue) and calcites (black) (Amthor *et al.*, 1993) using the Late Devonian marine Sr-isotope value (Veizer *et al.*, 1999).

6.4 Element compositions

The results for major and trace element analyses acquired from 109 samples were combined with those sixty one samples of Horrigan (1996) and tabulated in Appendix 3. Additionally, eighteen powders prepared by the author were rerun for quality control purposes. Where the original microsamples were too small, additional powders were drilled from the spots marked for sampling by the author and added to the existing powders. The correction factors are presented in table 6.4.1.

Aluminum was used to indicate the clay content in dolomite samples due to partial dissolution of clay "impurities" during sample analysis. A weak northward trend of increasing Al concentrations in matrix dolomites R2 and R3 is observed in the study area. These concentrations shift from 50 to 480 ppm, with nine samples enriched (up to 33000 ppm) in clays (Figure 6.4.1). Generally, the highest concentrations are noted in finer grained dolomites varying from 12 to 7120 ppm (average 1325 ppm). Brown porous matrix dolomite R3 exhibits the lowest aluminum contents of approximately 128 ppm on average ranging between 12 and 348 ppm.

Iron and manganese can both be used as indicators for redox conditions of the fluids involved in dolomite precipitation and recrystallization. Due to the similarity of the radii of iron and manganese to magnesium (Fe^{2+} and Mn^{2+} ions have radii of 0.083 and 0.091 nm, respectively; whereas Ca^{2+} and Mg^{2+} are 0.106 and 0.078 nm, respectively) they tend to substitute the Mg^{2+} ion in dolomites (Machel, 1989).

Table 6.4.1. Correction factors for the elemental compositions reported in Horrigan (1996). The original data is highlighted in blue, quality control (QC) data acquired in this study is highlighted in purple.

Sample ID	Li	B	Na	Mg	Al	K	Ca	V	Cr	Fe	Mn	Co	Ni	Cu	Zn	Ga
EH-5	3.79	13.49	224.50	48300	1558.59	1322.28	78800	34.83	4.29	5567.19	174.48	0.08		5.18	8.28	2.02
QC	5.29	29	317	88333	2838	2678	124906	7.37	9.88	10222	361	4.21	12.6	5.39	7.84	1.14
delta	1.50	15.66	92.85	40032.86	1279.72	1355.59	46105.79	-27.46	5.58	4654.36	186.91	4.13	12.56	0.22	-0.44	-0.88
EH-9	0.93	2.86	539.64	145800	200.93	202.08	215400	26.32	1.85	2892.96	347.17			2.31	6.90	12.87
QC	0.75	<DL	452	107026	66.7	115	156060	1.05	4.36	1962	304	1.58	9.37	2.20	7.18	<DL
delta	-0.18		-88.00	-38773.69	-134.24	-86.74	-59339.78	-25.28	2.50	-931.16	-42.99	1.58	9.37	-0.10	0.27	
EH-10	0.39	1.86	315.42	145100	66.68	126.25	211300	25.33	1.53	2474.80	284.82			2.25	6.60	2.69
QC	0.36	<DL	226	103755	67.3	86	150590	0.53	3.19	1860	284	1.54	8.50	0.52	3.67	<DL
delta	-0.04		-88.97	-41344.51	0.64	-40.30	-60709.82	-24.80	1.66	-615.30	-0.93	1.54	8.50	-1.73	-2.92	-2.69
EH-11	0.63	7.52	164.85	100300	7.32	88.15	198700	33.70	3.48	1019.15	72.14			1.46	11.06	2.12
QC	0.80	4	185	91683	19.3	83	134907	0.77	2.93	624	81.7	1.25	8.00	0.41	1.54	<DL
delta	0.17	-3.34	20.42	-8616.73	11.95	-5.55	-63793.37	-32.94	-0.55	-395.13	9.52	1.25	8.00	-1.05	-9.52	-2.12
EH-12	0.63	4.90	327.26	114900		87.91	172300	34.54	0.73	1046.80	71.12			0.63	3.74	0.35
QC	0.81	<DL	280	103751	26.5	118	142911	0.77	3.05	520	74.7	1.31	9.56	0.21	1.15	<DL
delta	0.18	-2.90	-47.44	-11149.41	26.46	30.25	-29389.41	-33.77	2.32	-526.99	3.55	1.31	9.56	-0.42	-2.59	-0.35
EH-29	0.05	0.38	24.90	72300	1.95	14.49	134600	3.43	103.00	88.08	4.17			0.40	0.76	0.03
QC	1.23	35	453	107786	30.6	119	153334	0.49	3.93	573	72.4	1.45	9.21	0.47	1.68	<DL
delta	1.18	34.20	427.91	35485.68	28.60	104.06	18734.29	-2.94	0.00	485.12	68.22	1.45	9.21	0.08	0.92	
EH-35	0.61	5.96	205.03	126900	53.95	38.44	187600	6.46	0.82	919.55	155.58			1.66	4.00	0.52
QC	0.65	<DL	184	97341	83.4	125	149713	0.77	3.48	1060	143	1.26	9.34	0.87	2.38	<DL
delta	0.03	3.96	-20.89	-29558.76	29.45	86.40	-37887.07	-5.68	2.66	140.22	-12.37	1.26	9.34	-0.80	-1.62	-0.52
EH-37	0.77	9.39	160.77	112400	28.27	43.05	174900	7.43	1.17	510.57	97.46			0.64	4.47	21.54
QC	1.02	20	227	113659	60.1	115	161809	0.94	6.60	728	114	1.39	22.7	0.61	1.71	<DL
delta	0.24	10.86	66.05	1259.40	31.86	72.23	-13091.32	-6.49	5.43	217.28	16.93	1.39	22.68	-0.03	-2.75	
EH-41b	2.24	8.36	417.07	114400	1194.24	1238.02	176100	13.93	3.74	4203.08	79.75	1.81		6.28	5.43	1.13
QC	1.88	11	394	80859	800	1124	117981	4.25	5.08	3627	65.7	4.06	38.5	4.45	2.06	0.35
delta	-0.35	2.85	-22.99	-33540.99	-393.90	-114.30	-58119.41	-9.68	1.34	-576.55	-14.06	2.25	38.47	-1.83	-3.37	-0.78
EH-42	2.58	11.16	502.56	141000	1509.45	1182.44	206800	29.24	2.79	1979.69	72.53			2.01	5.54	0.92
QC	2.37	22	363	103719	741	798	149534	2.00	5.83	1460	70.7	1.96	10.9	1.06	2.42	0.23
delta	-0.21	10.92	-139.22	-37281.12	-768.90	-384.58	-57265.83	-27.23	3.04	-519.54	-1.83	1.96	10.91	-0.95	-3.12	-0.69
EH-45	0.73	5.91	195.73	149600	176.92	185.23	210200	31.13	0.71	1139.97	95.45				3.91	1.47
QC	1.07	3	231	111656	473	483	156396	2.21	7.27	1188	107	1.62	9.83	0.39	2.71	0.17
delta	0.33	-2.71	35.71	-37943.91	295.85	297.53	-53804.41	-28.92	6.55	48.34	11.06	1.62	9.83	0.39	-1.20	-1.30
EH-51	0.76	4.97	516.02	127400	50.92	159.27	177600	31.03	1.22	1637.98	88.17			1.73	6.66	3.12
QC	0.71	2	443	100062	29.04	159	144641	0.76	3.93	973	88.3	1.39	9.09	0.53	3.26	<DL
delta	-0.05	-2.69	-72.93	-27338.38	-21.88	-0.59	-32959.03	-30.26	2.71	-664.64	0.12	1.39	9.09	-1.19	-3.40	-3.12
EH-56	0.85	8.62	245.74	125200	32.28	72.51	176500	35.32	0.89	828.53	58.73			2.08	4.40	0.27
QC	1.31	5	278	104600	216	255	154869	1.15	4.88	891	67.8	1.58	9.48	0.65	2.02	0.12
delta	0.46	-3.42	32.10	-20599.73	184.18	182.75	-21631.36	-34.17	3.99	62.61	9.04	1.58	9.48	-1.43	-2.38	-0.15
EH-58	0.75	6.21	247.44	96600	22.90		159000	5.69	0.33	50.78	66.76			0.73	2.80	0.29
QC	1.05	<DL	245	98093	56.2	142	153883	1.13	6.40	804	76.6	1.40	11.9	0.47	3.31	<DL
delta	0.30	4.21	-2.41	1492.98	33.27	142.40	-5116.89	-4.56	6.07	753.32	9.82	1.40	11.88	-0.26	0.51	-0.29
EH-60	0.60	3.29	265.48	147100		26.14	206700	25.67		468.45	69.15			2.46	5.11	0.15
QC	0.86	5	426	108052	13.5	254	168671	1.16	4.84	1028	78.8	1.42	9.79	0.51	2.06	<DL
delta	0.27	2.03	160.14	-39047.88	13.52	228.19	-38028.55	-24.51	4.84	559.67	9.63	1.42	9.79	-1.94	-3.04	-0.15
EH-75	0.85	4.98	396.71	126900	17.71	54.72	196100	12.59	0.43	590.21	73.58			4.40	6.18	0.16
QC	2.80	5	2299	108467	241	232	181942	7.26	5.73	2851	138	0.94	3.10	1.73	5.07	<DL
delta	1.95	0.16	1901.91	-18432.72	223.61	177.63	-14158.07	-5.33	5.30	2260.51	64.70	0.94	3.10	-2.67	-1.10	-0.16
delta	0.25621	5.80038	23.48772	-28635.6531	-47.36676	36.553728	-38949.5939	-21.2462	3.21065	-140.1965	4.693179	1.70188		-0.80557	-2.3104	-0.8699

Table 6.4.1. Continued.

Sample ID	As	Se	Rb	Sr	Y	Zr	Ag	Sn	Ba	La	Ce	Pr	Nd	Sm	Gd	Dy	Pb	Bi	Th	U
EH-5	4.71		6.22	34.41	2.07	0.51	0.32		12.39	2.17	4.63	0.55	2.35	0.44	0.48	0.40	0.95		0.36	0.08
QC	0.60	0.6	13.8	73.8	4.71	1.00	<DL	0.32	21.2	3.71	8.68	1.16	5.01	1.12	1.23	0.83	6.04		0.76	0.20
delta	*-4.11*		*7.53*	*39.43*	*2.64*	*0.49*	*-0.32*		*8.78*	*1.54*	*4.04*	*0.61*	*2.66*	*0.68*	*0.75*	*0.43*	*5.09*	*0.00*	*0.40*	*0.11*
EH-9	5.13		0.33	63.54	1.42	0.54	0.67	3.93	319.32	0.55	0.42	0.10	0.37	0.11	0.10	0.09	2.04	0.07	0.08	0.15
QC	0.18	0.3	0.26	65.5	1.54	0.20	<DL	<DL	848	0.65	0.53	0.10	0.45	0.11	0.16	0.12	3.32		0.05	0.09
delta	*-4.95*	*0.30*	*-0.08*	*1.94*	*0.11*	*-0.34*	*-0.67*	*-3.90*		*0.10*	*0.10*	*0.00*	*0.09*	*0.00*	*0.06*	*0.03*	*1.28*	*-0.07*	*-0.03*	*-0.06*
EH-10	4.92		0.16	33.24	1.37	0.60	0.61	4.01	58.65	0.50	0.37	0.08	0.29	0.06	0.08	0.08	1.46	0.03		0.06
QC	0.18	0.4	0.16	35.4	1.53	0.11	<DL	<DL	20.1	0.65	0.54	0.10	0.42	0.08	0.13	0.11	0.71		0.02	0.04
delta	*-4.75*	*0.40*	*0.00*	*2.14*	*0.16*	*-0.49*	*-0.61*	*-4.00*	*-38.51*	*0.15*	*0.18*	*0.02*	*0.13*	*0.02*	*0.05*	*0.03*	*-0.75*	*-0.03*	*0.02*	*-0.02*
EH-11	11.51		0.09	236.03	1.42	0.69	0.94		21.44	0.46	0.44	0.07	0.29	0.10	0.08	0.07	1.30	0.03		0.23
QC	0.21	0.3	0.06	139	1.14	<DL	<DL	<DL	8.13	0.57	0.63	0.09	0.38	0.07	0.11	0.08	0.85		0.01	0.20
delta			*-0.03*	*-96.85*	*-0.28*	*-0.60*	*-0.94*		*-13.32*	*0.12*	*0.20*	*0.02*	*0.09*	*-0.03*	*0.03*	*0.02*	*-0.45*	*-0.03*	*0.01*	*-0.02*
EH-12	5.52		0.07	28.48	0.64	0.24	0.38			0.44	0.36	0.05	0.20	0.04	0.04	0.04	0.32			0.18
QC	0.18	0.3	0.14	43.1	1.09	<DL	<DL	<DL	3.40	0.57	0.57	0.08	0.31	<DL	0.09	0.07	0.58		0.01	0.26
delta	*-5.34*	*0.30*	*0.07*	*14.64*	*0.45*	*-0.20*	*-0.38*		*3.40*	*0.13*	*0.21*	*0.04*	*0.11*		*0.05*	*0.03*	*0.26*	*0.00*	*0.01*	*0.08*
EH-29	0.59		0.01	9.83	0.05	0.04	0.04		0.09	0.03	0.03	0.00	0.02	0.00	0.00	0.00	0.20			0.01
QC	0.27	0.3	0.12	96.8	1.06	<DL	<DL	<DL	2.21	0.60	0.60	0.09	0.34	<DL	0.10	0.08	1.10		0.06	0.14
delta	*-0.32*	*0.30*	*0.11*	*86.99*	*1.01*				*2.11*	*0.57*	*0.57*	*0.08*	*0.32*		*0.10*	*0.08*	*0.90*	*0.00*	*0.06*	*0.13*
EH-35	0.99	0.02	0.21	32.70	0.87	0.36	0.43		7.83	0.58	0.61	0.10	0.42	0.12	0.09	0.07	4.84	0.03	0.06	0.14
QC	0.38	0.5	0.27	37.2	1.14	0.14	<DL	0.33	5.34	0.57	0.73	0.10	0.45	0.09	0.12	0.09	3.75		0.10	0.11
delta	*-0.61*	*0.44*	*0.06*	*4.51*	*0.27*	*-0.21*	*-0.43*		*-2.49*	*-0.01*	*0.13*	*0.00*	*0.03*	*-0.02*	*0.04*	*0.03*	*-1.09*	*-0.03*	*0.04*	*-0.04*
EH-37	1.29	0.02	0.17	49.92	1.10	0.27	0.45		347.64	0.48	0.42	0.10	0.42	0.07	0.10	0.08	0.84	0.04	0.03	0.88
QC	0.21	0.3	0.20	49.7	1.39	0.10	1.07	<DL	36.6	0.59	0.58	0.10	0.44	0.09	0.16	0.12	0.34		0.02	0.08
delta	*-1.08*	*0.28*	*0.03*	*-0.20*	*0.29*	*-0.17*	*0.63*		*-310.99*	*0.11*	*0.16*	*0.00*	*0.01*	*0.02*	*0.05*	*0.04*	*-0.50*	*-0.04*	*-0.01*	*-0.80*
EH-41b	3.90		5.25	58.39	2.74	0.37	0.50		12.05	1.21	3.08	0.43	1.99	0.76	0.83	0.56	11.10	0.06	0.84	1.03
QC	2.94	0.5	5.35	61.5	3.10	0.52	<DL	<DL	8.59	1.16	3.20	0.45	2.33	0.85	0.88	0.61	8.50		0.69	0.49
delta	*-0.96*	*0.50*	*0.09*	*3.11*	*0.35*	*0.15*	*-0.50*		*-3.46*	*-0.06*	*0.12*	*0.01*	*0.34*	*0.09*	*0.06*	*0.05*	*-2.59*	*-0.06*	*-0.14*	*-0.54*
EH-42	6.02		4.16	58.97	1.52	0.73	0.47		5.86	0.83	2.00	0.28	1.26	0.27	0.26	0.18	2.13	0.02	0.27	0.36
QC	1.00	0.3	3.35	68.1	1.59	0.57	<DL	0.40	7.22	0.76	1.95	0.27	1.10	0.25	0.29	0.22	2.44		0.27	0.29
delta	*-5.02*	*0.30*	*-0.80*	*9.13*	*0.06*	*-0.16*	*-0.47*	*0.34*	*1.36*	*-0.07*	*-0.05*	*-0.01*	*-0.16*	*-0.02*	*0.03*	*0.03*	*0.31*	*-0.02*	*0.00*	*-0.07*
EH-45	5.06		0.95	28.88	0.76	0.03	0.32		9.82	0.48	0.82	0.07	0.44	0.03	0.02	0.07				0.08
QC	0.24	0.3	1.67	36.7	1.13	0.35	<DL	0.09	9.05	0.63	1.05	0.15	0.68	0.13	0.13	0.13	1.04		0.14	0.17
delta	*-4.82*	*0.30*	*0.72*	*7.83*	*0.37*	*0.32*	*-0.32*		*-0.78*	*0.15*	*0.23*	*0.09*	*0.24*	*0.10*	*0.13*	*0.06*	*1.04*	*0.00*	*0.14*	*0.09*
EH-51	6.48		0.26	45.11	1.50	0.55	0.55		38.36	1.20	1.01	0.17	0.58	0.14	0.16	0.12	2.20	0.04	0.10	0.36
QC	0.36	0.3	0.17	49.8	1.75	0.10	<DL	0.11	8.49	1.20	1.02	0.15	0.66	0.12	0.18	0.13	1.41		0.02	0.29
delta	*-6.12*	*0.30*	*-0.09*	*4.71*	*0.25*	*-0.45*	*-0.55*		*-29.87*	*-0.01*	*0.01*	*-0.02*	*0.08*	*-0.03*	*0.02*	*0.01*	*-0.80*	*-0.04*	*-0.08*	*-0.06*
EH-56	5.87		0.24	29.42	0.96	0.25	0.38		1.05	0.57	0.59	0.08	0.41	0.03	0.07	0.09	1.56			0.32
QC	0.32	0.4	0.73	44.3	1.68	0.27	<DL	<DL	2.86	0.77	1.05	0.13	0.57	0.12	0.17	0.14	2.99		0.08	0.53
delta	*-5.55*	*0.40*	*0.48*	*14.93*	*0.72*	*0.01*	*-0.38*		*1.81*	*0.21*	*0.47*	*0.05*	*0.16*	*0.08*	*0.09*	*0.05*	*1.43*	*0.00*	*0.08*	*0.21*
EH-58	0.67	0.02	0.06	50.05	0.62	0.16	0.33		4.21	0.44	0.61	0.05	0.29	0.04	0.05	0.08	0.47			0.12
QC	0.34	0.8	0.17	75.2	0.99	<DL	<DL	<DL	8.65	0.56	0.87	0.11	0.44	0.09	0.10	0.10	1.10		0.03	0.15
delta	*-0.33*		*0.11*	*25.19*	*0.37*	*-0.16*	*-0.33*		*4.44*	*0.12*	*0.26*	*0.06*	*0.14*	*0.06*	*0.05*	*0.02*	*0.63*	*0.00*	*0.03*	*0.03*
EH-60	3.99			35.25	0.54		0.26		0.78	0.29	0.25		0.13							0.15
QC	0.27	0.4	0.20	55.0	0.89	<DL	<DL	0.10	1.67	0.42	0.40	0.07	0.28	<DL	0.09	0.07	0.82		0.01	0.25
delta	*-3.72*	*0.40*	*0.20*	*19.79*	*0.35*		*-0.26*		*0.88*	*0.13*	*0.15*	*0.07*	*0.15*		*0.09*	*0.07*	*0.82*	*0.00*	*0.01*	*0.10*
EH-75	1.30	0.02	0.07	50.07	2.40	0.07	0.53		2.05	0.98	1.10	0.16	0.73	0.14	0.25	0.25	0.83			0.58
QC	0.64	0.3	1.06	53.2	2.17	0.56	<DL	0.14	382	1.02	1.82	0.26	1.08	0.25	0.30	0.24	10.4		0.41	0.45
delta	*-0.66*	*0.29*	*0.99*	*3.16*	*-0.23*	*0.49*	*-0.53*		*380.34*	*0.05*	*0.72*	*0.10*	*0.35*	*0.12*	*0.04*	*-0.01*	*9.58*	*0.00*	*0.41*	*-0.13*
delta	-3.17976	0.28137	0.06241	9.1535	0.31919	-0.1205	-0.3688	-2.52	-25.108	0.11667	0.19509	0.02836	0.124491	0.0201	0.0602	0.03829	0.0353	-0.0217	0.03665	-0.0572

In most samples, Fe^{2+} and Mn^{2+} concentrations are less than 5000 ppm and less than 200 ppm, respectively (Figures 6.4.2 and 6.4.3). Matrix dolomite R1 shows significantly higher average Fe^{2+} and Mn^{2+} contents of 4555 and 176 ppm, Fe^{2+} ranging from 786 to 14049 ppm and Mn^{2+} ranging from 70.7 to 412.6 ppm, whereas R2 and R3 dolomites have lower concentrations of 203 to 32978 ppm (average 1597) and 5 to 1463.8 ppm (average 115.6 ppm) for iron, and 466 to 7500 ppm (average 2256 ppm) and 72.6 to 292 ppm (average 146.6 ppm) for manganese. The elevated concentrations are observed in the same outliers as in the Al plot suggesting that Fe^{2+} and Mn^{2+} were derived from partial dissolution of clay "impurities". Iron and manganese can also be used for correlation with the CL data. All examined specimens, except for sample N-155, fall into the zone of dull luminescence (Figure 6.4.5).

Strontium content can reflect paleoenvironments of dolomite formation with Sr concentration of Paleozoic dolomites reaching 200 ppm, whereas modern dolomites have about 550 to 700 ppm (Land, 1980; Banner, 1995). Matrix dolomites R1 and R3 have 33-130 ppm (average 73 ppm) and 30-183 ppm Sr (average 64 ppm), respectively (Figure 6.4.4). Matrix dolomite R2 is more enriched in Sr varying between 23 and 336 ppm (average 65 ppm) and reaching 1346 and 4588 ppm in two samples. There is cluster in the southern part of the reef chain and a triangle-shaped zone in the central part exhibiting significantly elevated Sr concentrations (up to 4700 ppm, Figure 6.4.4).

Sodium also has a distribution coefficient smaller than 1. It is commonly used as an indicator of the degree of salinity under which dolomites are formed. Na contents of about 13 ppm are usually a sign of dolomites formed in hypersaline environments, whereas marine

to mesohaline dolomites show higher concentrations of 110-160 ppm Na (Bein and Land, 1983; Veizer, 1983). However, special preparation procedures should be used in order to avoid contamination from fluid inclusions, otherwise the salinity interpretations become nearly impossible (Machel, 1989). According to Veizer *et al.* (1999) Na also exhibits a positive correlation with the clay content in carbonates. A gradual northward trend of increasing Na concentrations is observed in the study area increasing from 10 to 640 ppm (Figure 6.4.6). Two Leduc matrix dolomite R3 samples show extremely high contents of sodium (>2000 ppm).

Copper, lead and zinc usually indicate a hydrothermal influence on dolomite formation (Leach *et al.,* 2010). In the study area, these two elements show a triangle-shaped zone with significantly increased concentrations in the central part of the reef trend (Figures 6.4.6 through 6.4.8).

Rare earth elements (REE) include 15 lanthanide elements with similar ion radius and, therefore, similar geochemical characteristics. They are usually subdivided into light (LREE: La to Nd), medium (MREE: Sm to Dy) and heavy (HREE: Ho to Lu) rare earth elements, all of which are trivalent (with an exception of Ce^{+4} and Eu^{+2} in certain environments) and generally occur together in nature (Azomani *et al.,* 2013). Similar to strontium isotopes, the REE compositions of dolomites can be used as potential indicators of changes in fluid chemistry (Shields and Stille, 2001; Azmy *et al.,* 2011). However, several recent studies showed that some diagenetic environments, such as meteoric and mixed water

setting, have no effect on the composition and distribution of these elements in carbonates except in fluid dominated systems (Nothdurft *et al.,* 2004; Barton *et al.,* 2006; Webb *et al.,* 2009).

Two of these elements, Ce and La, were plotted against depth and showed increased concentrations in the same townships where Fe^{2+} and Mn^{2+} have outliers and triangle-shaped zones with significantly increased concentrations similar to the ones in the Sr, Cu, Pb and Zn plots (Figures 6.4.9 and 6.4.10).
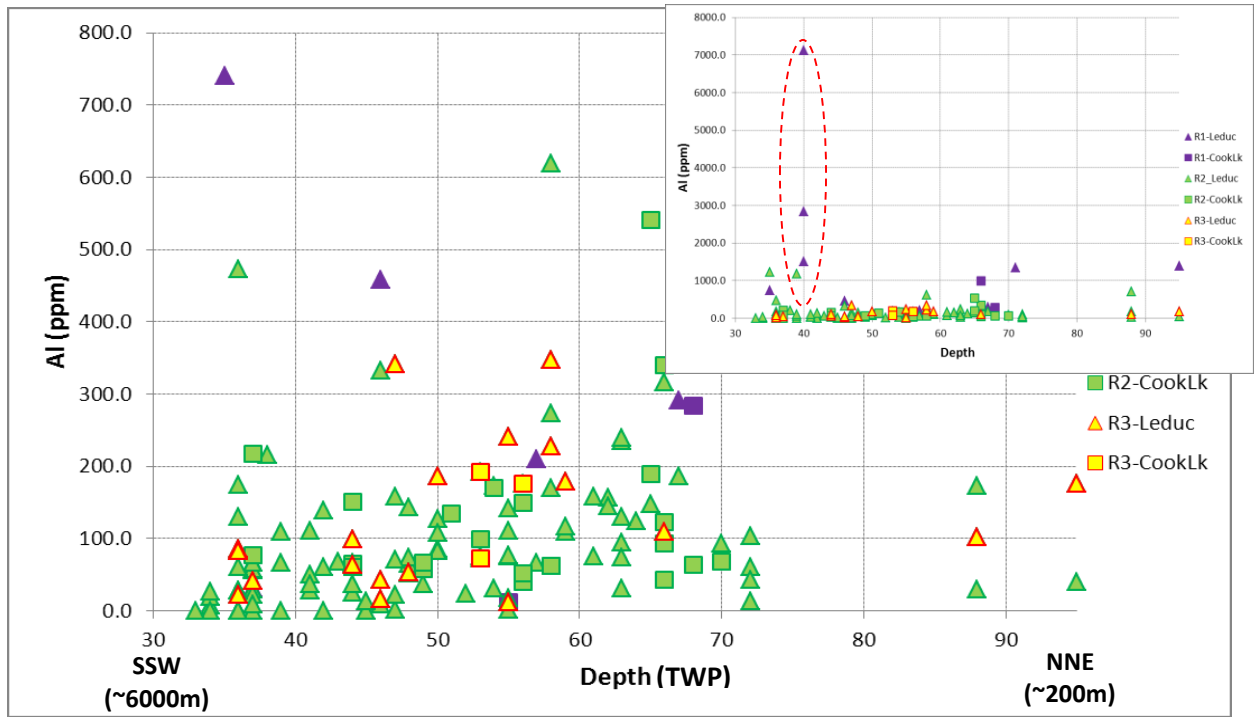
Figure 6.4.1. Regional distribution of Al.
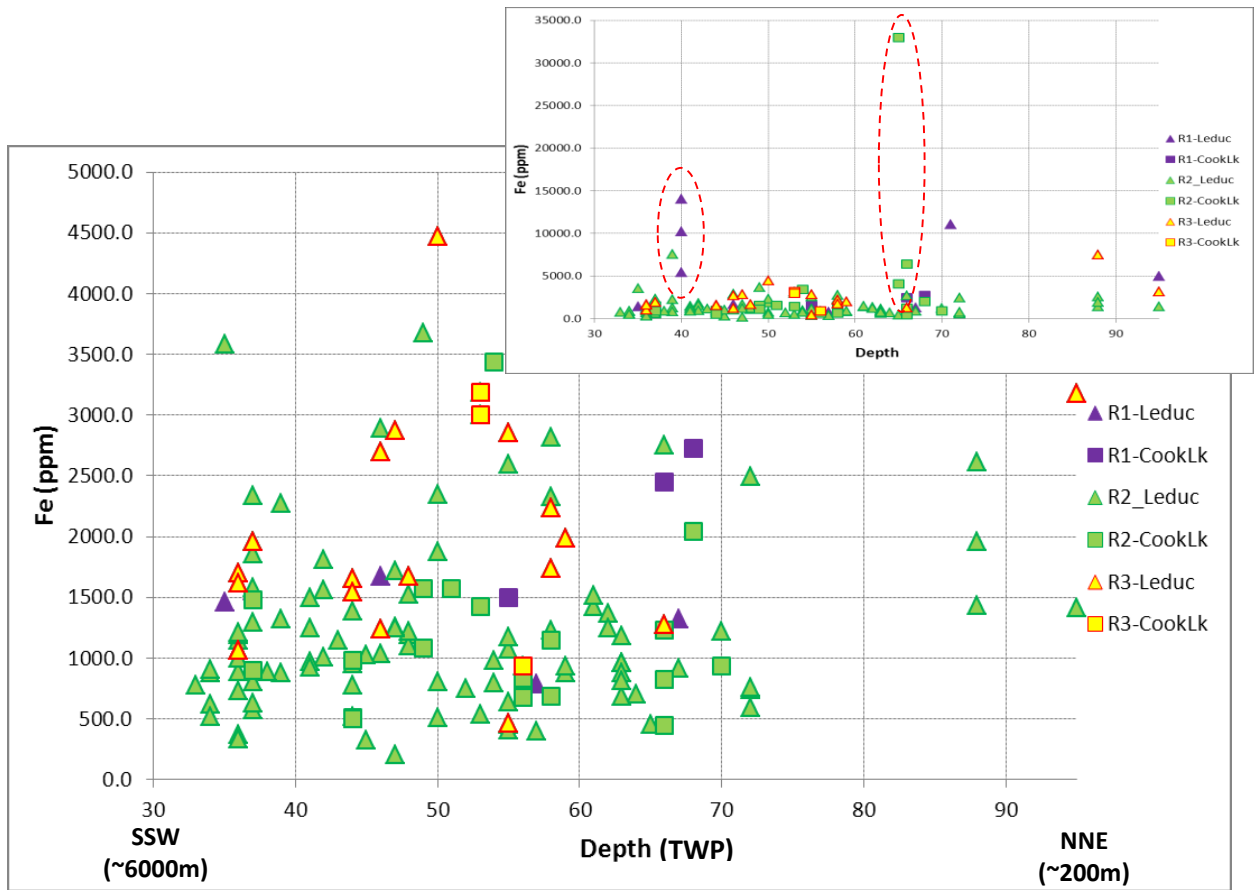
Figure 6.4.2. Regional distribution of Fe.
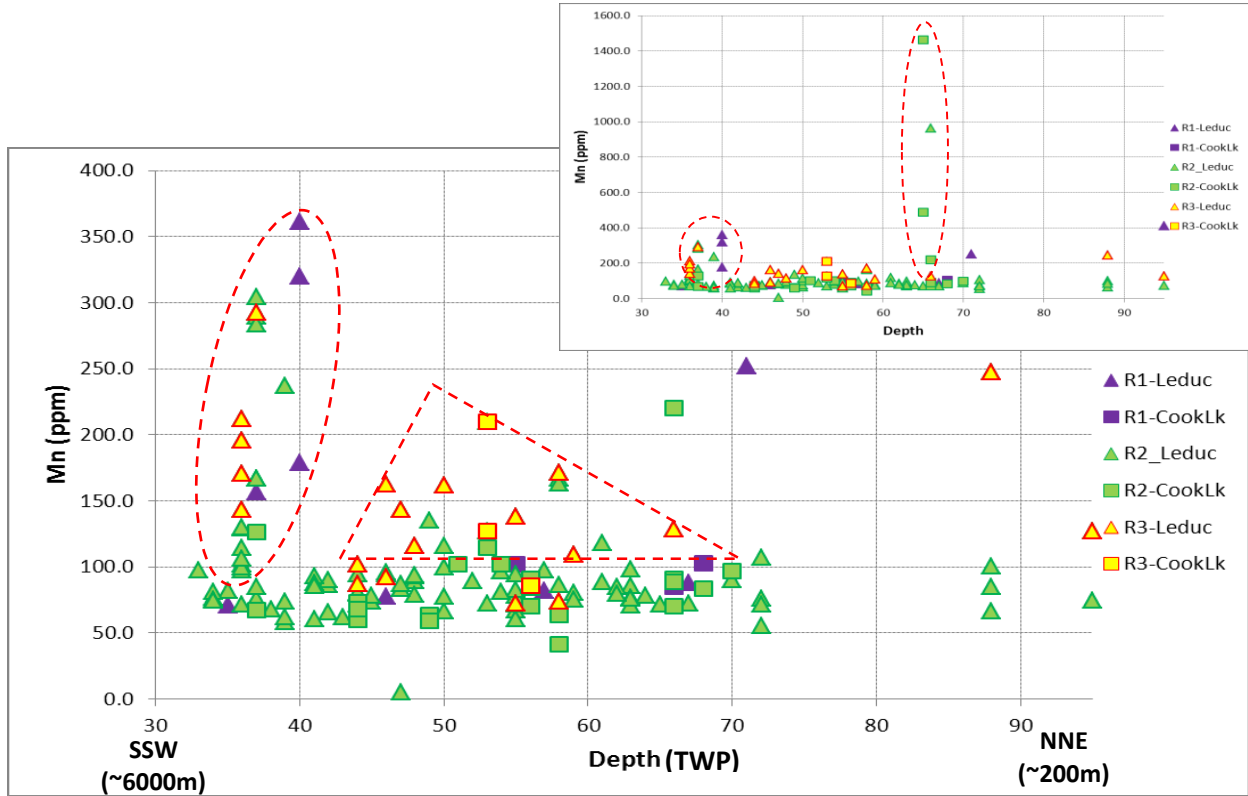
Figure 6.4.3. Regional distribution of Mn.
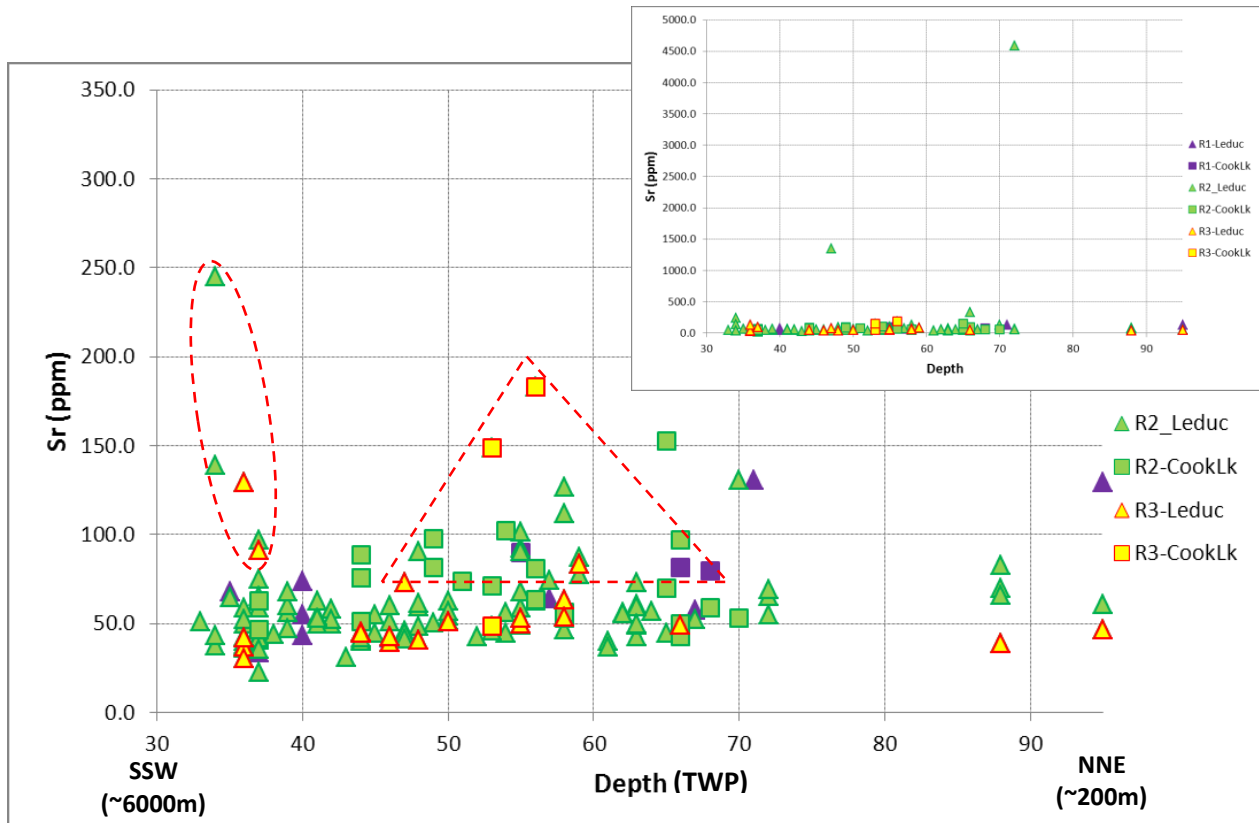
Figure 6.4.4. Regional distribution of Sr.
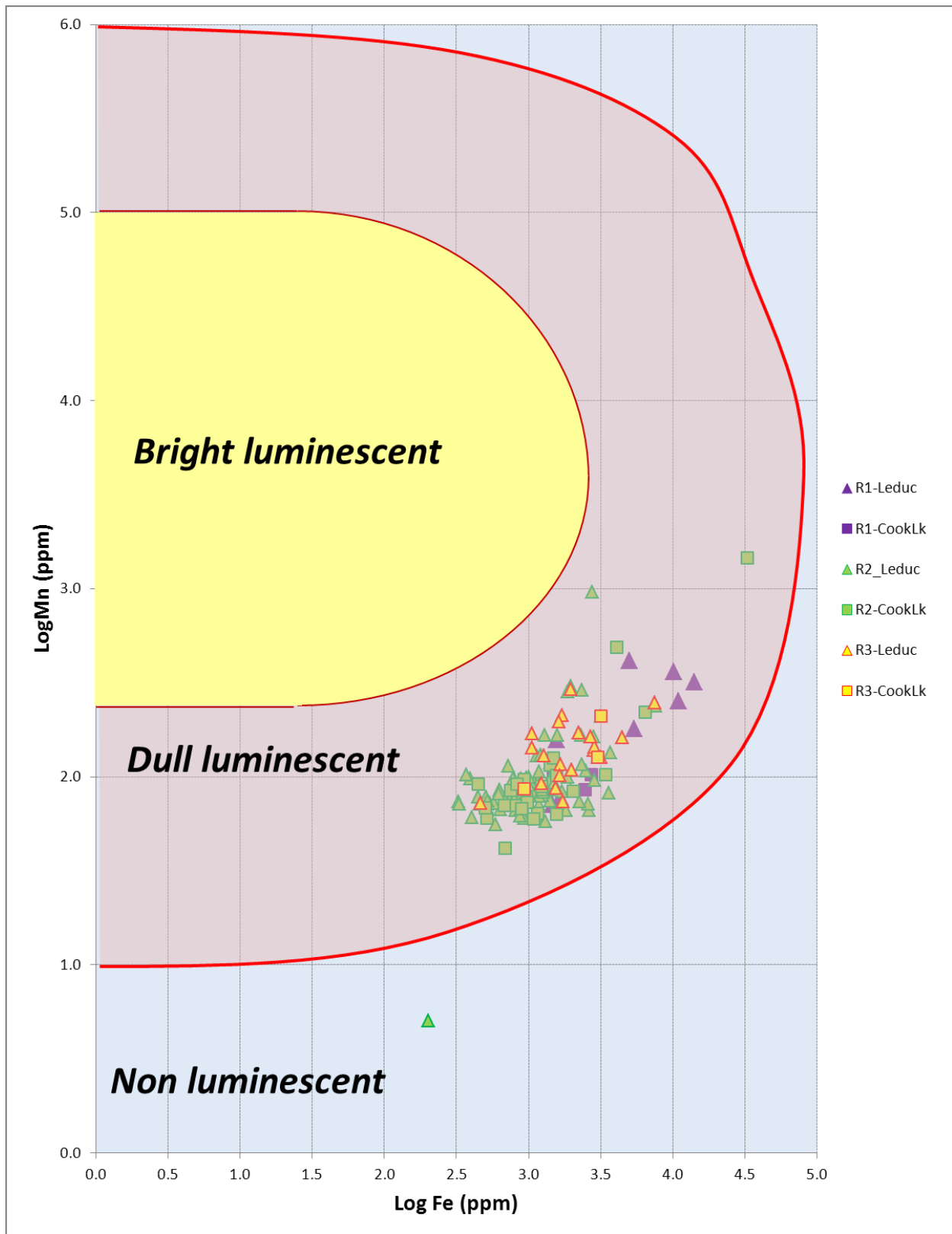
Figure 6.4.5. Cross-plot of Log Mn vs. Log Fe illustrating the CL properties of matrix dolomites in the study area (modified from Machel *et al.,* 1991).
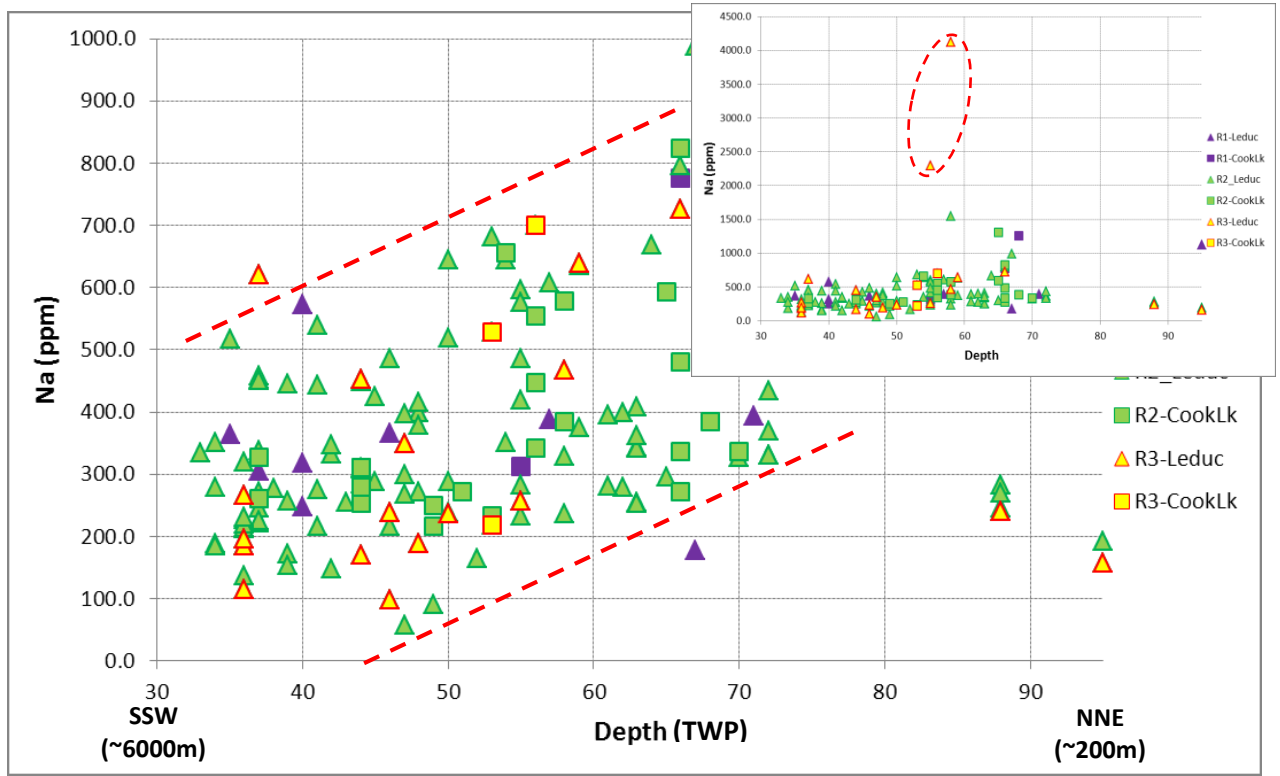
Figure 6.4.6. Regional distribution of Na.
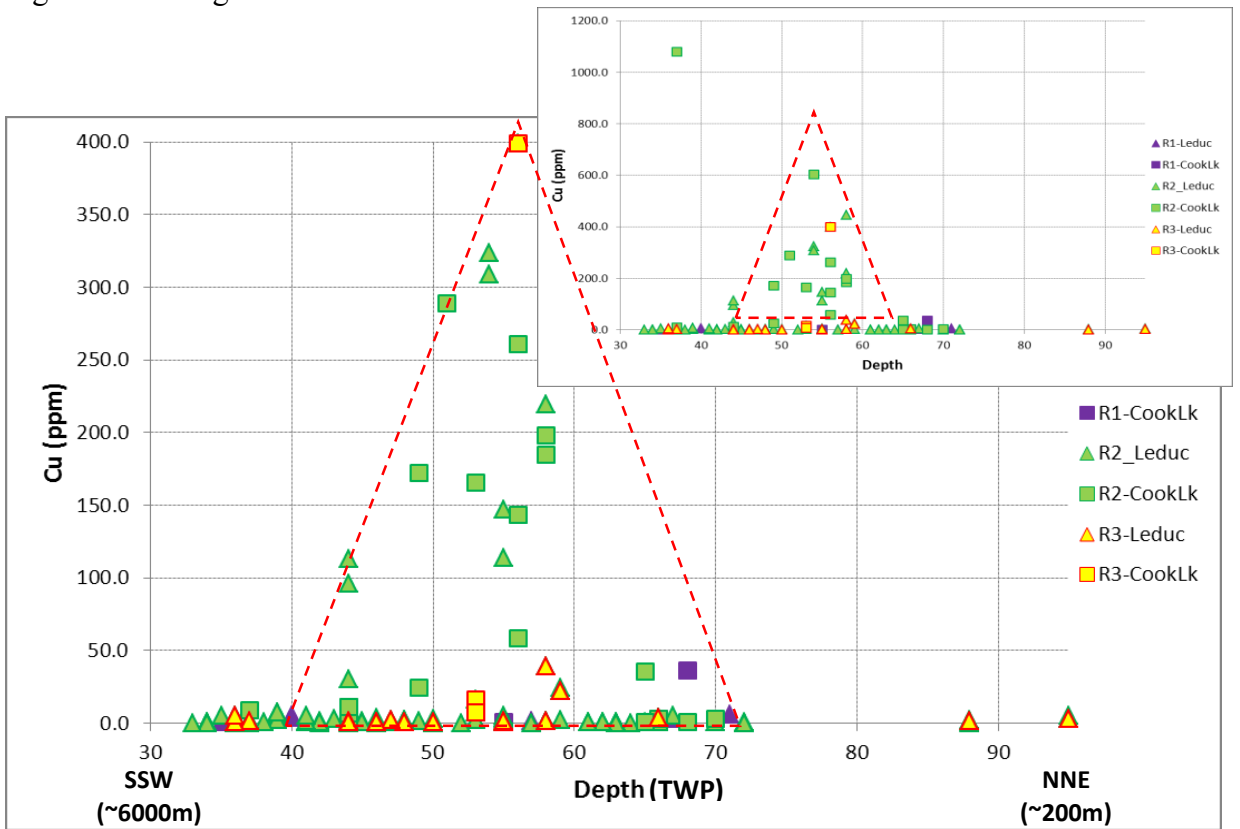
Figure 6.4.7. Regional distribution of Cu.
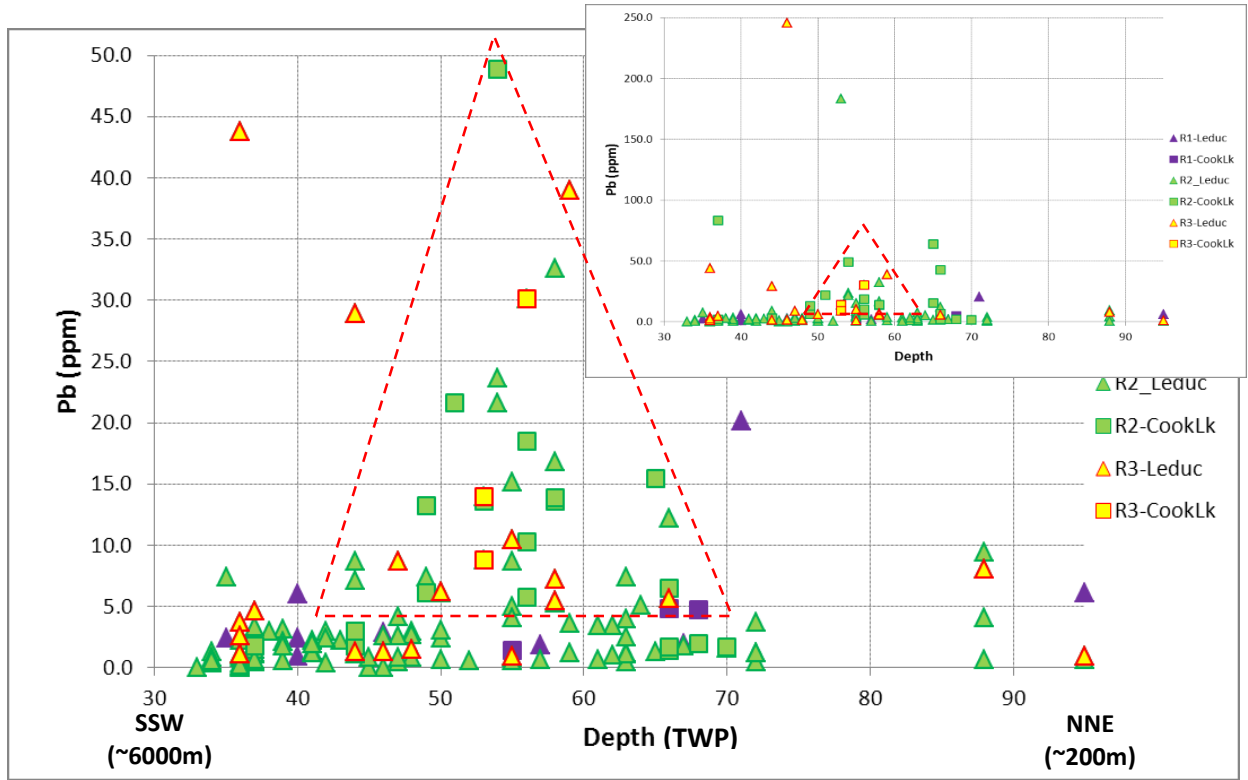
Figure 6.4.8. Regional distribution of Pb.
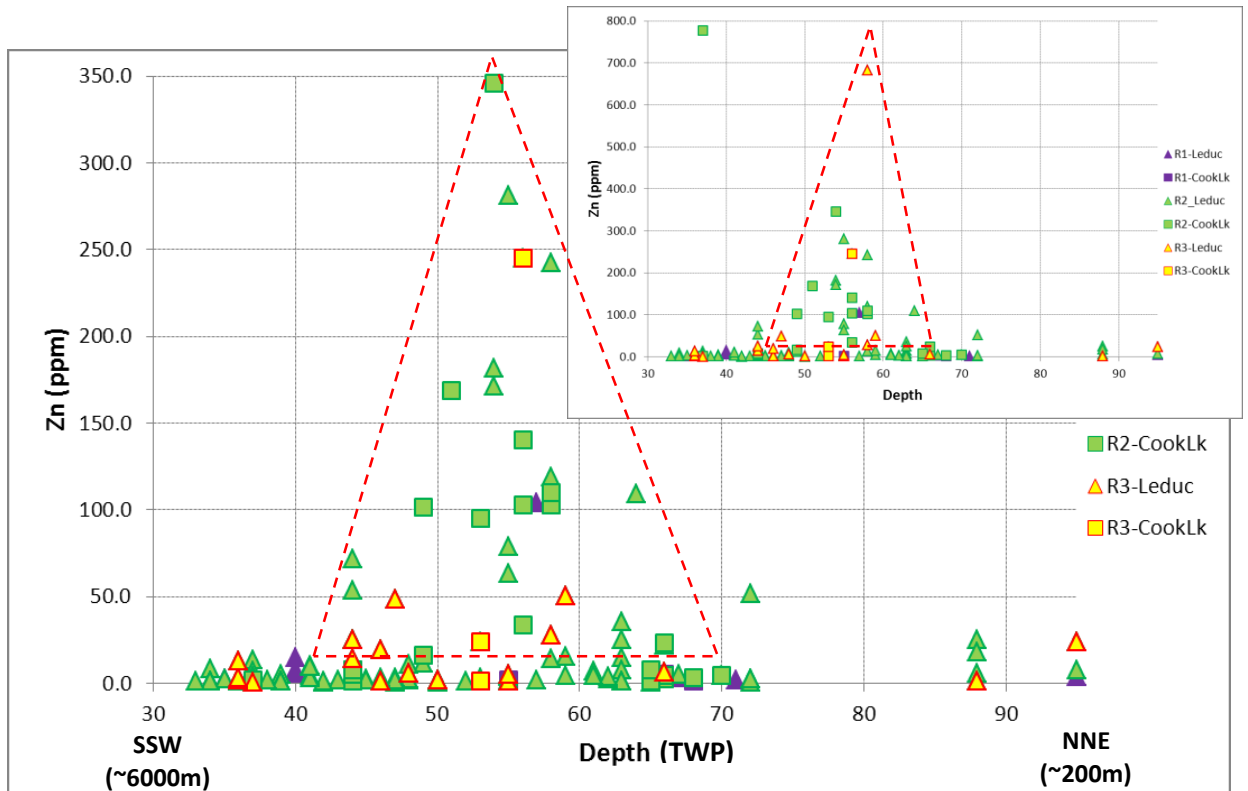
Figure 6.4.9. Regional distribution of Zn.
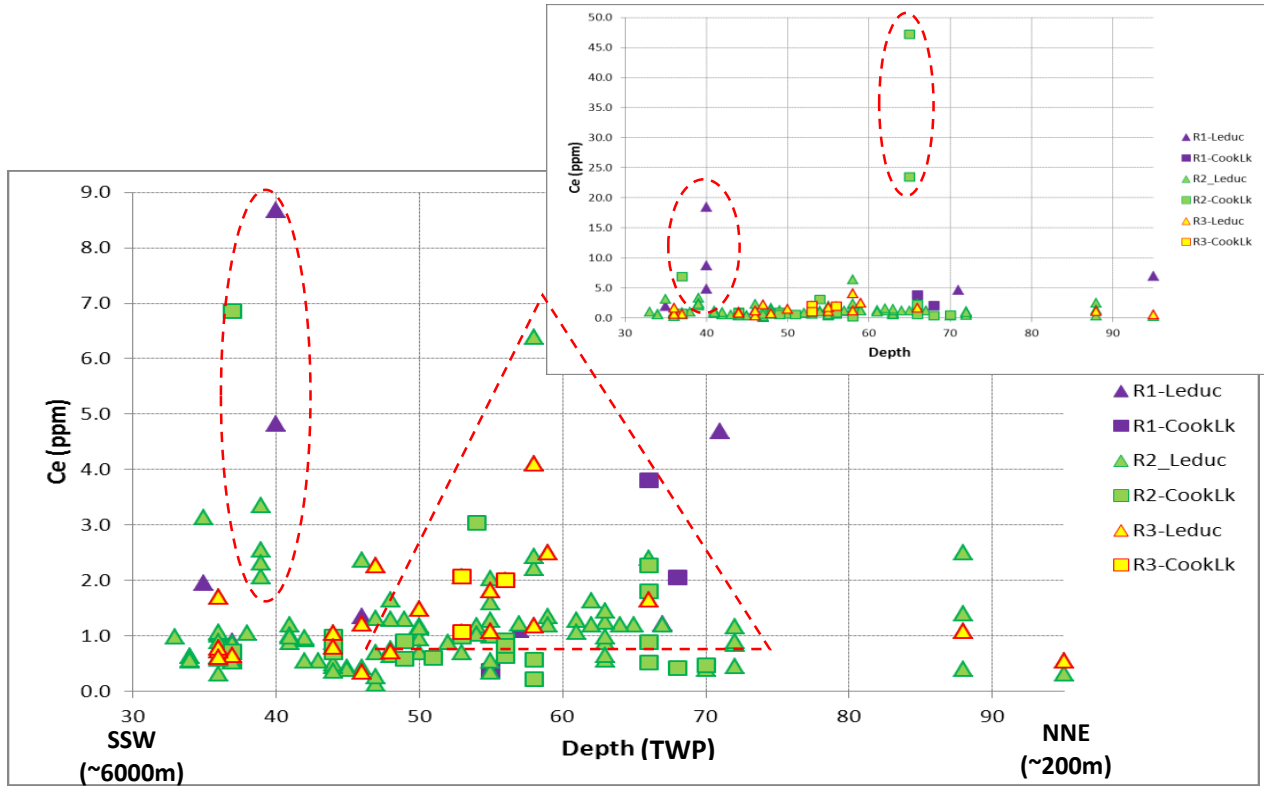
Figure 6.4.10. Regional distribution of Ce.
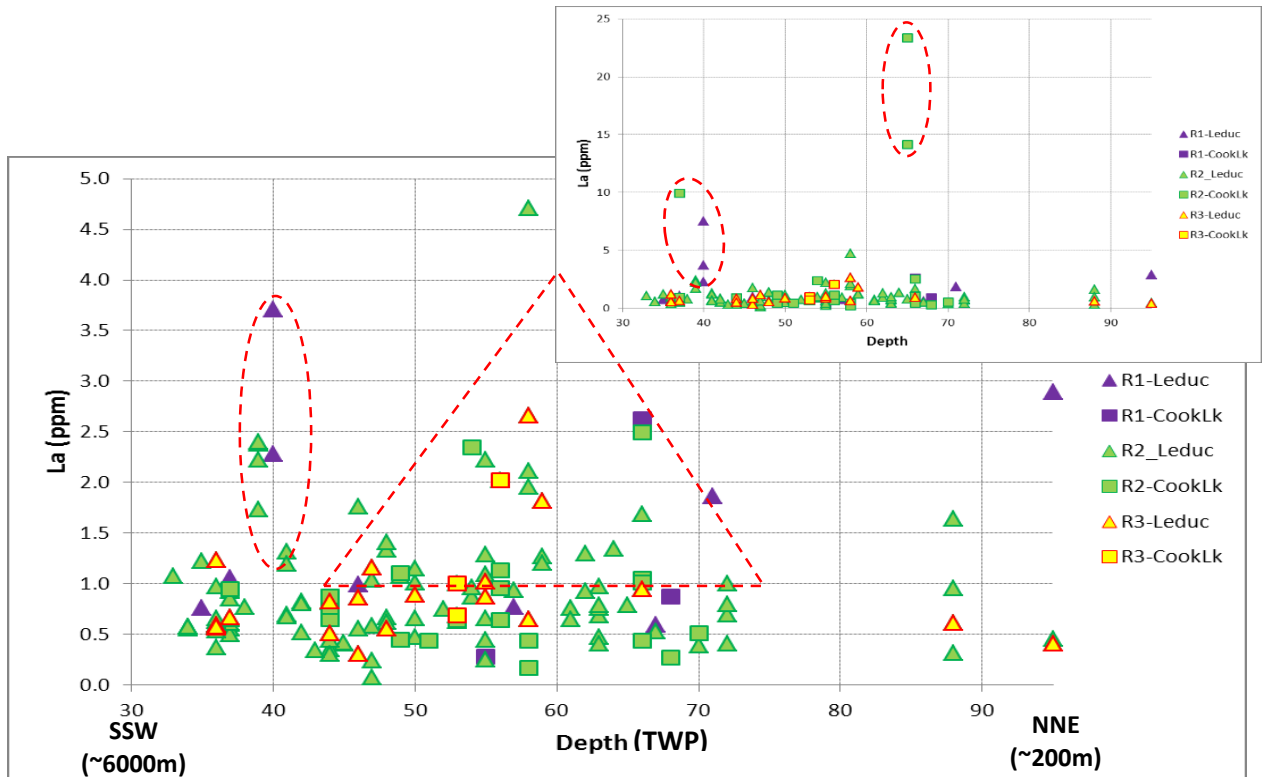
Figure 6.4.11. Regional distribution of La.

CHAPTER 7

STATISTICAL RESULTS

7.1 Factor analysis

In this study, factor analysis was used to examine relationships between variables in the dataset in order to reduce them to a limited number of interpretable factors with a minimum loss of information. This exercise was intended to find statistical associations among the chemical variables that can identify or elucidate the main geochemical processes explaining significant spread in geochemistry of dolomites along the Rimbey-Meadowbrook Reef Trend.

The dataset was divided into two subsets: the smaller one that consisted of 60 samples with 51 variables including $^{87}Sr/^{86}Sr$ isotopes, and the larger one that had 146 samples with 50 variables (excluding $^{87}Sr/^{86}Sr$ isotopes). Loadings in computer output were classified as strong (>0.75), moderate (0.45-0.75), or weak (<0.45).

The smaller subset of data was initially examined using five factors. The results revealed five dominant associations that can explain 77.9% of the total variance (Table 7.1.1). Increasing the number of factors to ten and fifteen raised the variance explained by the selected factors by only approximately 13 to 15% (Table 7.1.2). Additionally, the dominant geochemical variables contributing to the first five factors in Table 7.1.2 are essentially the same as the ones highlighted in Table 7.1.1, which considers only five factors. Therefore, it was decided to keep the number of factors at five.

Table 7.1.1. VARIMAX rotated factors (five factors) for the smaller subset of data explaining 77.9% of the total variance. The highlighted loadings indicate dominant geochemical variables contributing to each factor (green for strong loadings, orange for moderate loadings).

Variable	Factor1	Factor2	Factor3	Factor4	Factor5	Communality
TWP	0.062	-0.14	-0.129	-0.256	-0.616	0.485
Type	0.021	0.403	0.019	-0.033	0.079	0.17
^{13}C	-0.201	0.243	-0.115	0.667	-0.18	0.59
^{18}O	-0.009	0.036	-0.035	-0.16	-0.498	0.277
$^{87/86}$Sr	0.078	-0.645	-0.016	0.005	0.363	0.554
CaCO$_3$	0.092	-0.549	-0.005	-0.297	-0.419	0.573
Ca	-0.065	0.466	0.175	0.468	0.157	0.496
Mg	-0.149	0.606	0.096	0.566	0.06	0.723
Li	0.532	-0.502	0.072	0.106	-0.453	0.757
B	0.178	-0.276	-0.012	0.348	-0.557	0.54
Na	0.472	-0.152	0.096	-0.154	-0.31	0.375
Al	0.14	-0.964	-0.041	0.016	0.049	0.953
P	0.992	0.033	0.008	0.013	-0.07	0.99
K	0.139	-0.959	-0.048	-0.004	0.007	0.942
Ti	0.119	-0.955	-0.069	-0.1	-0.083	0.948
V	0.907	-0.316	0.018	0.036	-0.036	0.926
Cr	0.849	-0.291	-0.085	0.072	0.032	0.82
Fe	0.933	-0.299	-0.022	0.049	-0.016	0.963
Mn	0.938	-0.205	-0.016	-0.041	0.065	0.928
Co	0.971	-0.149	-0.029	-0.042	-0.065	0.973
Ni	0.287	-0.01	0.152	0.097	0.019	0.115
Cu	-0.012	0.022	0.972	0.138	0.017	0.966
Zn	-0.034	0.026	0.968	0.126	0.024	0.956
Ga	0.583	-0.775	-0.048	-0.069	-0.021	0.947
As	0.958	-0.047	0.144	0.043	-0.071	0.948
Se	0.273	0.114	0.404	0.677	0.173	0.739
Rb	0.11	-0.955	-0.055	0.017	0.062	0.932
Sr	0.448	-0.4	0.139	-0.011	-0.423	0.558
Y	0.993	-0.014	0.056	0.011	-0.033	0.991
Zr	0.112	-0.717	-0.007	-0.195	-0.369	0.701
Mo	0.916	-0.153	0.005	0.011	-0.077	0.869
Ru	-0.247	0.116	-0.147	-0.739	-0.111	0.655
Ag	0.1	0.121	0.285	-0.077	0.015	0.112
Sn	-0.012	0.029	0.959	0.105	-0.002	0.932
Ba	0.022	-0.014	-0.045	-0.162	0.486	0.265
La	0.911	-0.135	0.321	0.058	-0.002	0.955
Ce	0.97	-0.189	0.103	0.01	-0.036	0.989
Pr	0.972	-0.16	0.13	0.023	-0.03	0.988
Nd	0.983	-0.12	0.094	0.021	-0.034	0.991
Sm	0.99	-0.1	0.048	0.011	-0.034	0.994
Eu	0.968	-0.105	0.039	-0.019	0.075	0.956
Gd	0.992	-0.077	0.048	0.008	-0.038	0.994
Tb	0.991	-0.081	0.027	0.017	-0.033	0.99
Dy	0.993	-0.07	0.034	0	-0.041	0.994
Er	0.992	-0.073	0.038	-0.003	-0.037	0.991
Yb	0.984	-0.127	0.035	0.001	-0.047	0.988
W	0.966	-0.082	-0.064	0.031	-0.061	0.949
Pb	0.504	-0.048	0.804	0.109	-0.063	0.919
Th	0.441	-0.804	0.087	-0.099	-0.179	0.891
U	0.774	0.066	0.16	-0.14	-0.247	0.709
Variance	21.922	8.065	4.082	2.53	2.367	38.966
% Var	0.438	0.161	0.082	0.051	0.047	**0.779**

Table 7.1.2. VARIMAX rotated factors (ten factors) for the smaller subset of data explaining 90.5% of the total variance. The highlighted loadings indicate dominant geochemical variables contributing to each factor (green for strong loadings, orange for moderate loadings).

Variable	Factor1	Factor2	Factor3	Factor4	Factor5	Factor6	Factor7	Factor8	Factor9	Factor10	Communality
TWP	0.063	0.025	-0.116	-0.585	-0.308	-0.326	-0.115	0.108	0.15	0.286	0.691
Type	-0.006	0.275	0.007	0.147	0.044	0.155	-0.005	-0.749	0.097	0.208	0.737
^{13}C	-0.216	0.359	-0.097	-0.183	0.652	-0.187	0.094	0.145	0.184	0.34	0.856
^{18}O	0.006	-0.009	-0.059	-0.089	-0.117	-0.035	-0.798	-0.175	-0.104	-0.323	0.808
$^{87/86}$Sr	0.092	-0.646	0.009	0.096	-0.035	0.161	0.154	0.458	0.045	0.106	0.709
CaCO$_3$	0.092	-0.372	-0.023	-0.817	-0.093	-0.014	0	0.067	0.015	-0.059	0.831
Ca	-0.045	0.489	0.182	0.177	0.481	0.172	-0.06	0.344	0.053	-0.125	0.707
Mg	-0.158	0.554	0.088	0.474	0.418	-0.236	-0.02	0.027	-0.168	-0.021	0.825
Li	0.522	-0.423	0.093	-0.163	-0.071	-0.649	-0.057	0.009	-0.032	0.092	0.925
B	0.168	-0.18	0.028	-0.038	0.08	-0.894	-0.065	0.054	-0.015	-0.063	0.881
Na	0.446	-0.099	0.004	-0.47	0.079	-0.033	-0.041	-0.285	-0.444	-0.143	0.738
Al	0.137	-0.964	-0.017	-0.073	0.001	-0.112	-0.002	0.096	0.021	-0.011	0.977
P	0.99	0.041	-0.009	-0.027	0.014	-0.07	-0.013	-0.012	-0.043	0.031	0.991
K	0.133	-0.963	-0.028	-0.109	-0.001	-0.116	-0.03	0.022	0.015	-0.018	0.973
Ti	0.114	-0.922	-0.056	-0.254	-0.073	-0.118	-0.021	0.063	0	0	0.954
V	0.905	-0.324	0.011	-0.016	0.034	-0.088	-0.056	-0.002	-0.044	0.004	0.939
Cr	0.848	-0.284	-0.097	-0.101	0.164	0.054	-0.006	0.009	-0.006	-0.089	0.857
Fe	0.93	-0.293	-0.024	-0.038	0.045	-0.088	0.014	0.02	0.005	0.045	0.965
Mn	0.937	-0.175	-0.03	-0.129	0.024	0.04	0.152	0.063	-0.022	0.002	0.956
Co	0.969	-0.145	-0.038	-0.049	-0.05	-0.087	-0.007	-0.022	-0.015	0.056	0.978
Ni	0.255	-0.055	0.112	0.009	0.074	0.046	0.004	-0.192	-0.135	0.734	0.683
Cu	0.001	0.044	0.981	0.041	0.091	-0.026	0.01	0.027	-0.044	0.046	0.979
Zn	-0.021	0.05	0.977	0.027	0.089	-0.002	0.014	0.027	-0.035	0.039	0.969
Ga	0.581	-0.762	-0.044	-0.159	-0.04	-0.06	-0.033	0.067	-0.016	0.003	0.957
As	0.955	-0.052	0.131	-0.018	0.047	-0.078	-0.037	-0.104	-0.031	0.042	0.955
Se	0.261	0.119	0.385	0.091	0.746	0.085	0.074	0.031	-0.081	0.16	0.841
Rb	0.104	-0.977	-0.032	-0.032	0.003	-0.11	-0.017	0.018	0.016	-0.016	0.98
Sr	0.452	-0.259	0.155	-0.42	-0.036	-0.374	-0.012	0.12	0.054	-0.066	0.635
Y	0.995	-0.005	0.043	-0.034	0.022	-0.024	-0.006	0.016	-0.02	0.035	0.995
Zr	0.106	-0.561	-0.029	-0.787	0.028	-0.003	-0.015	0.025	-0.021	-0.035	0.949
Mo	0.905	-0.191	-0.002	0.029	-0.003	-0.136	-0.05	-0.247	-0.003	0.061	0.942
Ru	-0.23	0.162	-0.152	-0.183	-0.804	0.062	0.046	0.223	-0.021	0.111	0.851
Ag	0.072	0.08	0.151	0.084	-0.037	-0.006	-0.024	0.093	-0.895	0.121	0.869
Sn	0.003	0.05	0.967	0.03	0.065	-0.025	-0.011	0.01	-0.049	-0.004	0.945
Ba	0.006	0.016	-0.046	-0.012	-0.062	0.062	0.895	-0.112	-0.053	-0.242	0.886
La	0.918	-0.109	0.313	-0.061	0.072	-0.004	0.01	0.075	-0.018	0.032	0.968
Ce	0.972	-0.171	0.092	-0.083	0.032	-0.027	-0.013	0.042	-0.027	0.031	0.994
Pr	0.973	-0.143	0.118	-0.072	0.043	-0.025	-0.007	0.038	-0.026	0.033	0.993
Nd	0.984	-0.108	0.082	-0.058	0.038	-0.031	-0.009	0.021	-0.027	0.036	0.994
Sm	0.989	-0.094	0.034	-0.049	0.03	-0.03	-0.011	-0.009	-0.026	0.042	0.995
Eu	0.964	-0.086	0.027	-0.059	0.019	-0.029	0.212	-0.027	-0.03	-0.012	0.989
Gd	0.992	-0.069	0.034	-0.048	0.024	-0.031	-0.01	0	-0.025	0.041	0.996
Tb	0.99	-0.072	0.013	-0.052	0.034	-0.026	-0.004	0.008	-0.018	0.054	0.993
Dy	0.993	-0.061	0.02	-0.052	0.017	-0.029	-0.012	0	-0.022	0.041	0.996
Er	0.992	-0.063	0.024	-0.054	0.015	-0.023	-0.01	0.008	-0.019	0.037	0.994
Yb	0.984	-0.114	0.023	-0.077	0.022	-0.027	-0.017	0.01	-0.012	0.045	0.992
W	0.967	-0.073	-0.068	0.002	-0.001	-0.118	-0.014	0.044	0.001	0.018	0.961
Pb	0.509	-0.028	0.798	-0.059	0.121	-0.044	-0.023	-0.11	-0.058	0.016	0.933
Th	0.432	-0.756	0.078	-0.406	0.024	-0.051	-0.057	-0.115	-0.026	-0.002	0.95
U	0.779	0.07	0.147	-0.059	-0.163	-0.165	-0.168	-0.128	-0.062	-0.109	0.75
Variance	21.817	7.276	4	2.79	2.303	1.824	1.617	1.318	1.168	1.118	45.231
%Var	0.436	0.146	0.08	0.056	0.046	0.036	0.026	0.023	0.022	0.018	**0.905**

The larger subset of data was also examined using five and ten factors that can explain 60.9 and 76.4% of the total variance, respectively (Tables 7.1.3 and 7.1.4). The dominant geochemical variables contributing to the first five factors in both cases were similar to those identified for the smaller subset of data. Therefore, the five factors derived from smaller subset of data can be used as the representative factors for identification of the main geochemical associations along the Rimbey-Meadowbrook reef trend.

Factor analysis of the smaller subset reveals that approximately 44% of the total variance is explained by Factor 1. Variables strongly correlated with this factor are P, V, Cr, Fe, Mn, Co, As, Y, Mo, and REEs. The communality of each variable ranges between approximately 80 and 99%, meaning that these variables are mostly explained by the five factors, because the communalities close to 1.0 indicate that the factor analysis model successfully describes the variance in the variable. A few other variables, Li, Ga, Sr, and Pb, also contribute to the variance of this factor, but these elements fall into the moderate loading category with correlations to Factor 1 of 0.5 to 0.6.

Factor 2 explains 16.1% of the total variance in the dataset. Elements strongly correlated with Factor 2 are Al, K, Ti, Ga, Rb, Zr and Th, and the moderately correlated variables are the Sr-isotopes, mol%$CaCO_3$, Ca and Mg. The communalities of these variables range from approximately 80 to 95%. All variables strongly correlated with Factor 2, as well as the moderately correlated Sr-isotopes and mol%$CaCO_3$, exhibit negative correlation with Ca and Mg.

Factor 3 contributes 8.2% to the total variance in the dataset. Elements strongly correlated with Factor 3 are Cu, Zn, Pb and Sn with communalities of 92 to 97%.

Table 7.1.3. VARIMAX rotated factors (five factors) for the larger subset of data explaining 60.9% of the total variance. The highlighted loadings indicate dominant geochemical variables contributing to each factor (green for strong loadings, orange for moderate loadings).

Variable	Factor1	Factor2	Factor3	Factor4	Factor5	Communality
TWP	0.066	0.323	0.129	-0.334	-0.298	0.326
Type	-0.017	-0.29	-0.062	0.205	-0.013	0.131
^{13}C	-0.118	-0.205	-0.016	-0.285	0.189	0.173
^{18}O	-0.037	0.033	0.089	0.044	-0.404	0.176
CaCO$_3$	0.018	0.505	0.075	0.099	-0.388	0.421
Ca	0.014	-0.23	-0.002	-0.683	-0.24	0.578
Mg	-0.017	-0.199	-0.081	-0.658	-0.137	0.498
Li	0.412	0.587	-0.184	-0.222	-0.33	0.707
B	0.132	0.329	-0.058	-0.209	-0.206	0.215
Na	0.169	0.197	-0.181	0.009	-0.532	0.383
Al	0.151	0.916	-0.021	0.107	0.112	0.886
P	0.982	-0.001	0.001	0.013	-0.034	0.966
K	0.148	0.928	-0.025	0.119	0.084	0.905
Ti	0.111	0.916	0.018	0.127	0.043	0.87
V	0.324	0.071	0.06	0.486	-0.431	0.535
Cr	0.364	0.098	0.016	0.498	0.05	0.393
Fe	0.874	0.275	0.036	0.001	-0.025	0.841
Mn	0.925	0.175	0.024	0.044	0.011	0.889
Co	0.102	-0.057	0.18	-0.12	-0.02	0.061
Ni	0.177	0.156	-0.118	-0.216	0.086	0.123
Cu	0.014	-0.015	-0.922	-0.141	0.025	0.871
Zn	-0.02	0.011	-0.845	-0.065	-0.17	0.748
Ga	0.043	-0.002	-0.005	0.598	-0.122	0.375
As	0.837	0.047	-0.114	0.209	-0.127	0.776
Se	0.318	-0.032	-0.517	-0.213	0.277	0.492
Rb	0.125	0.914	-0.016	0.115	0.079	0.87
Sr	-0.006	-0.015	0.077	-0.024	0.024	0.007
Y	0.989	0.034	-0.051	0.029	-0.049	0.985
Zr	0.113	0.764	-0.017	0.164	-0.17	0.653
Mo	0.592	0.178	-0.004	0.062	-0.367	0.521
Ru	-0.125	0.139	0.022	0.074	0.351	0.164
Ag	0.027	-0.112	-0.193	0.282	-0.203	0.171
Sn	0.017	-0.017	-0.909	-0.117	0.04	0.843
Ba	0.048	-0.073	-0.011	0.192	0.254	0.109
La	0.868	0.113	-0.245	0.006	-0.126	0.843
Ce	0.94	0.179	-0.084	0.034	-0.103	0.935
Pr	0.955	0.159	-0.111	0.033	-0.088	0.958
Nd	0.976	0.13	-0.083	0.033	-0.066	0.981
Sm	0.985	0.117	-0.046	0.041	-0.046	0.989
Eu	0.875	0.063	-0.047	0.111	0.106	0.795
Gd	0.987	0.096	-0.044	0.038	-0.044	0.988
Tb	0.985	0.093	-0.018	0.031	-0.015	0.98
Dy	0.986	0.091	-0.032	0.041	-0.051	0.986
Er	0.984	0.093	-0.038	0.036	-0.061	0.984
Yb	0.976	0.147	-0.041	0.033	-0.071	0.981
W	0.592	0.005	0.198	-0.102	-0.012	0.401
Tl	0.074	-0.005	-0.068	0.073	-0.634	0.417
Pb	0.192	-0.054	-0.371	0.06	0.044	0.183
Th	0.411	0.699	-0.147	0.135	-0.241	0.755
U	0.639	0.105	-0.131	-0.109	-0.412	0.618
Variance	16.383	5.914	3.201	2.553	2.407	30.457
% Var	0.328	0.118	0.064	0.051	0.048	**0.609**

Table 7.1.4. VARIMAX rotated factors (ten factors) for the larger subset of data explaining 76.4% of the total variance. The highlighted loadings indicate dominant geochemical variables contributing to each factor (green for strong loadings, orange for moderate loadings).

Variable	Factor1	Factor2	Factor3	Factor4	Factor5	Factor6	Factor7	Factor8	Factor9	Factor10	Communality
TWP	0.068	0.059	0.073	0.347	-0.047	-0.034	0.016	-0.188	-0.731	0	0.707
Type	-0.017	-0.254	-0.035	-0.104	-0.356	0.483	-0.092	-0.298	0.143	0.23	0.607
^{13}C	-0.167	-0.234	-0.003	0.142	-0.002	-0.176	0.018	-0.027	-0.135	0.755	0.723
^{18}O	0.012	-0.031	0.09	-0.017	-0.129	-0.048	-0.157	0.024	-0.127	-0.637	0.475
CaCO$_3$	0.045	0.389	0.057	-0.06	-0.228	-0.053	0.009	0.234	-0.656	-0.044	0.703
Ca	0.003	-0.193	-0.036	-0.08	-0.235	-0.82	0.059	-0.218	-0.009	0.036	0.826
Mg	-0.03	-0.184	-0.077	0.139	-0.042	-0.783	-0.054	-0.124	0.118	-0.02	0.708
Li	0.389	0.427	-0.149	0.648	-0.167	-0.046	0.009	-0.033	-0.221	-0.054	0.858
B	0.084	0.184	-0.007	0.751	0.022	-0.109	0.035	0.159	-0.066	0.03	0.649
Na	0.2	0.142	-0.164	-0.035	-0.576	0.045	-0.123	-0.129	-0.291	-0.152	0.562
Al	0.155	0.961	0.014	0.094	0.037	0.028	0.021	0.015	0.037	-0.01	0.961
P	0.981	-0.042	0.014	0.112	0.017	0.024	0.034	0.018	-0.007	-0.026	0.981
K	0.157	0.959	0.014	0.117	0.043	0.033	-0.009	0.038	0.01	-0.051	0.965
Ti	0.123	0.897	0.039	0.134	0.012	0.167	-0.007	-0.059	-0.121	-0.063	0.889
V	0.274	0.105	0.119	0.28	-0.413	0.279	0.283	0.507	0.197	-0.064	0.807
Cr	0.371	0.131	0.05	-0.147	0.074	0.208	0.032	0.511	-0.074	0.102	0.506
Fe	0.859	0.274	0.047	0.093	-0.075	-0.035	0.138	0.022	-0.015	0.118	0.864
Mn	0.931	0.175	0.034	-0.063	-0.051	-0.015	0.043	0.01	-0.082	0.116	0.927
Co	0.012	-0.026	-0.008	-0.044	0.004	-0.017	0.953	-0.031	-0.033	0.037	0.915
Ni	0.168	0.056	-0.095	0.406	0.176	0.02	-0.116	-0.167	0	-0.001	0.278
Cu	0.012	-0.011	-0.942	0.114	0.049	-0.073	-0.005	0.027	0.051	-0.016	0.911
Zn	-0.007	0.008	-0.87	-0.02	-0.203	0.015	-0.024	-0.046	-0.084	-0.065	0.813
Ga	0.055	0.042	0.056	-0.125	0.003	0.151	-0.04	0.736	-0.033	-0.053	0.593
As	0.83	0.031	-0.059	0.212	-0.055	0.106	0.004	0.256	0.109	-0.072	0.836
Se	0.306	-0.006	-0.488	0.116	0.151	-0.156	-0.111	-0.049	0.133	0.35	0.548
Rb	0.131	0.967	0.022	0.075	-0.009	0.028	0.009	0	0.054	-0.036	0.964
Sr	0.006	-0.089	0.024	-0.056	0.101	0.119	0.046	-0.12	-0.238	-0.069	0.114
Y	0.99	0.007	-0.039	0.074	-0.014	0.008	0.044	0.036	-0.007	-0.028	0.991
Zr	0.14	0.656	-0.015	0.033	-0.078	0.111	-0.048	0.16	-0.563	0.023	0.815
Mo	0.557	0.135	0.045	0.413	-0.393	0.153	0.125	0.016	0.096	-0.024	0.704
Ru	-0.09	0.038	-0.008	0.025	0.532	0.267	-0.162	-0.089	-0.179	-0.177	0.462
Ag	0.014	-0.084	-0.12	0.147	-0.068	-0.061	-0.042	0.595	0.119	-0.034	0.423
Sn	0.018	-0.009	-0.931	0.081	0.074	-0.076	-0.004	0.055	0.044	-0.028	0.891
Ba	0.055	0.013	0.031	-0.275	-0.071	0.164	-0.136	-0.011	0.047	0.48	0.362
La	0.885	0.112	-0.235	-0.05	-0.127	-0.082	-0.005	0.034	-0.061	-0.052	0.884
Ce	0.953	0.164	-0.07	-0.003	-0.094	-0.031	0.009	0.021	-0.065	-0.053	0.958
Pr	0.965	0.145	-0.097	0.014	-0.077	-0.027	0.016	0.032	-0.051	-0.039	0.975
Nd	0.982	0.111	-0.068	0.045	-0.049	-0.007	0.027	0.029	-0.03	-0.031	0.989
Sm	0.987	0.093	-0.03	0.074	-0.028	0.019	0.036	0.028	-0.014	-0.019	0.994
Eu	0.88	0.084	-0.013	-0.068	-0.04	0.085	-0.04	0.007	0.011	0.234	0.852
Gd	0.989	0.068	-0.029	0.082	-0.018	0.022	0.039	0.029	-0.014	-0.024	0.994
Tb	0.986	0.065	-0.003	0.083	0.017	0.011	0.039	0.036	-0.013	-0.008	0.987
Dy	0.988	0.062	-0.017	0.085	-0.021	0.023	0.041	0.034	-0.016	-0.024	0.992
Er	0.987	0.064	-0.025	0.072	-0.032	0.013	0.042	0.031	-0.028	-0.026	0.99
Yb	0.979	0.118	-0.029	0.07	-0.046	0.011	0.048	0.023	-0.046	-0.029	0.986
W	0.512	0.011	0.05	0.048	0.031	-0.015	0.828	-0.011	-0.022	0.042	0.957
Tl	0.083	0.006	-0.019	-0.023	-0.7	-0.076	-0.065	0.081	-0.091	-0.104	0.534
Pb	0.185	-0.013	-0.373	-0.069	-0.103	0.092	0.043	0.001	0.047	0.185	0.236
Th	0.435	0.676	-0.124	-0.017	-0.313	0.089	-0.035	-0.003	-0.277	-0.019	0.846
U	0.623	0.009	-0.115	0.412	-0.272	0.002	0.078	-0.038	-0.025	-0.238	0.71
Variance	16.308	5.35	3.129	2.1	2.085	1.989	1.877	1.875	1.819	1.686	38.218
% Var	0.326	0.107	0.063	0.042	0.042	0.04	0.038	0.038	0.036	0.034	**0.764**

Factor 4 explains 5.1% of the total variance. Variables moderately associated with this factor are $\delta^{13}C$, Ca, Mg, Se and Ru. These variables are 50 to 75% explained by the selected five factors. Additionally, Ru is negatively correlated with Factor 4, while $\delta^{13}C$, Ca, Mg, and Se are positively correlated with this factor.

Factor 5 contributes only 4.7% to the total variance. Variables moderately associated with this factor are depth (TWP), $\delta^{18}O$, Li, B and Ba. The oxygen isotopic compositions are positively correlated with depth (TWP), Li and B, and are negatively correlated with Ba. The results show that only 27.7% of the variance in the $\delta^{18}O$ values is explained by the five factors. However, the ten-factor models applied to the smaller and larger subsets show stronger communalities for oxygen (80.8% and 47.5%, respectively), which is still positively correlated with Ba, but negatively correlated with $\delta^{13}C$ (Tables 7.1.2 and 7.1.4).

Generally, the only variables not associated with the five factors in the smaller data set are the dolomite type, Ni, and Ag. However, these variables appear in the results when ten factors are introduced. For the smaller subset of data, dolomite type and Sr-isotopes are moderately correlated with Factor 8, and Ag and Ni are strongly associated with Factors 9 and 10, respectively (Table 7.1.2). For the larger subset of data, dolomite type is moderately associated with Factor 6, showing negative correlation with strongly loaded Ca and Mg, and variables Ag, V, Cr and Ga are moderately associated with Factor 8 (Table 7.1.4).

7.2 Cluster analysis

Cluster analysis was used to test for geochemical similarities in groups of samples from different depths and locations along the Rimbey-Meadowbrook Reef Trend and to group samples into smaller sets for further interpretation.

Cluster observations performed on both subsets of data separated variables into groups that behave similarly. The output consisted of dendrograms with eight clusters, each of which consists of several subclusters and singletons (Figures 7.2.1). This number of clusters was decided to be the most efficient because further subdividing the sample set only identified additional outliers.

The clustering was similar in the smaller and larger data sets. Therefore, only the clusters resulting from analyzing the larger subset, which covers the entire reef trend, were plotted on a map to see if there is any geographical pattern in distribution of the clusters. However, no pattern in spatial distribution was observed (Figure 7.2.2).

The cluster centroids algorithm was used in order to identify the basis of the clustering (Table 7.2.1). A number of parameters separating the values were identified (Table 7.2.2). Even though the differences between cluster centroids were very small, this separation based on cluster centroids was the only reasonable explanation for splitting samples into different clusters.

Figure 7.2.1. Dendrogram showing clustering of matrix dolomites R1, R2, R3 and R4 along the Rimbey-Meadowbrook reef trend using the larger subset of data.
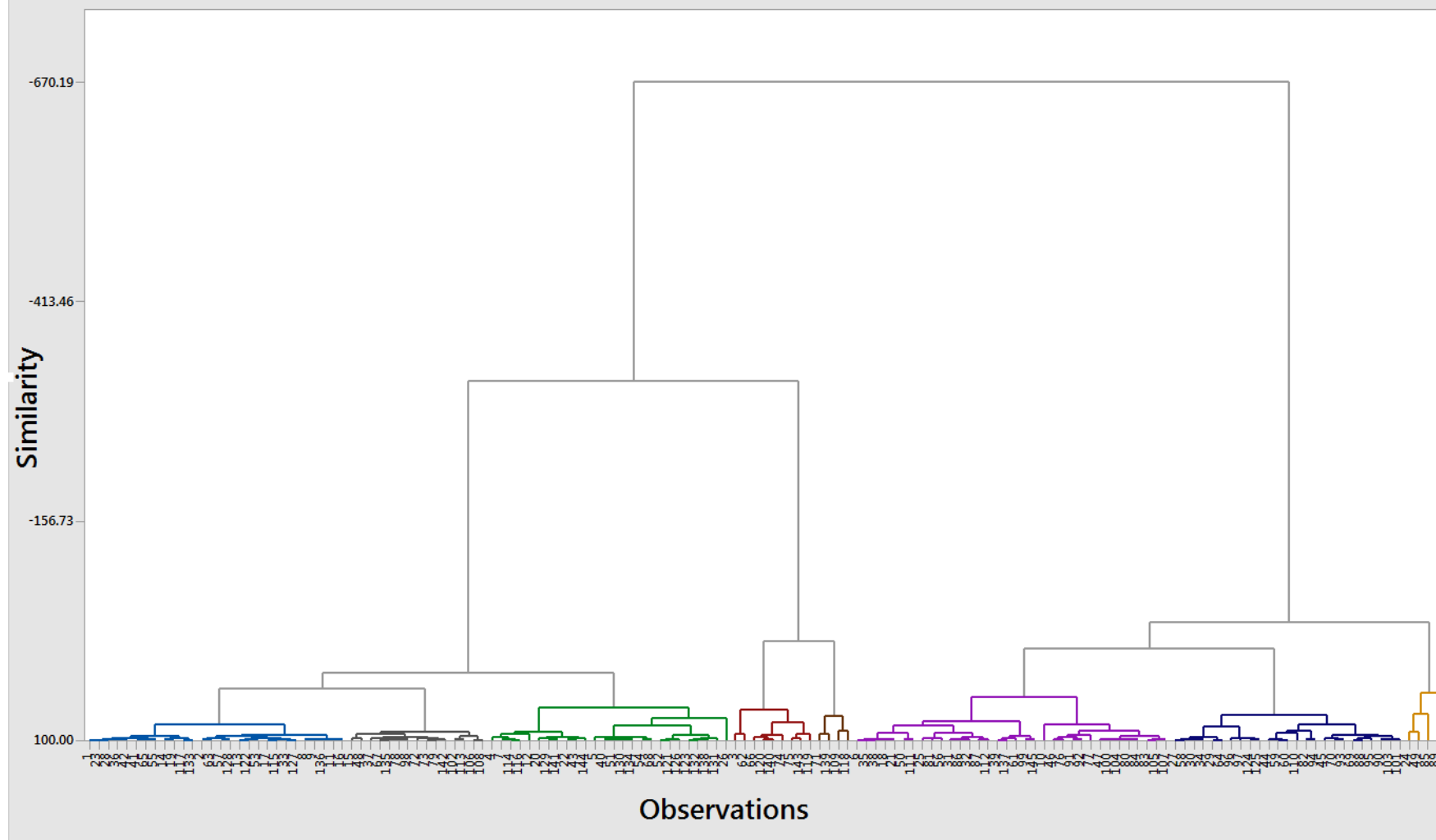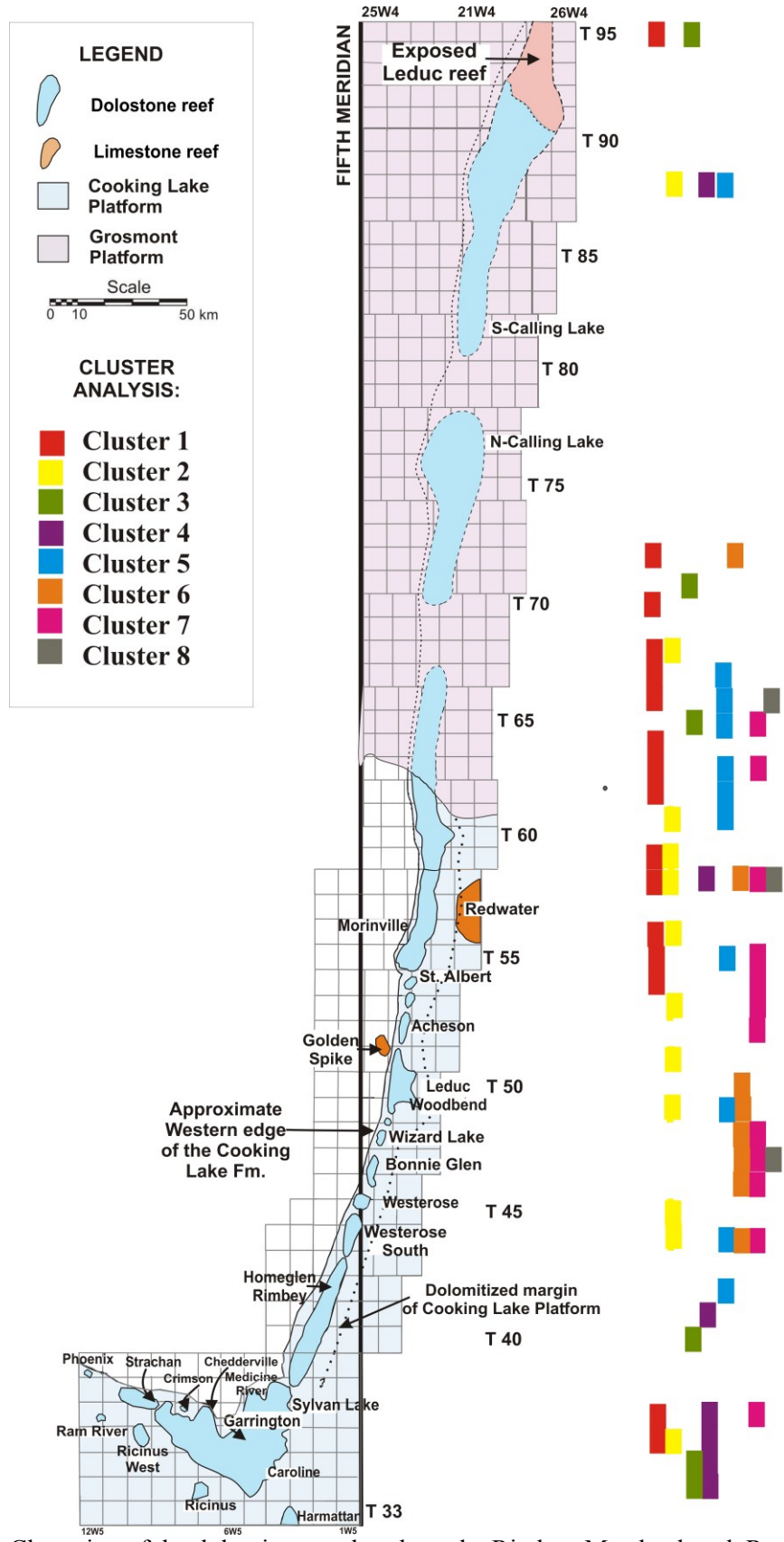
Figure 7.2.2. Clustering of the dolomite samples along the Rimbey-Meadowbrook Reef Trend.

136

Table 7.2.1. Cluster centroids illustrating the most depleted (highlighted in green) and the most elevated values (highlighted in yellow), compared to the rest of the centroids, that might have caused the clustering of the dolomite samples.

Variable	Cluster1	Cluster2	Cluster3	Cluster4	Cluster5	Cluster6	Cluster7	Cluster8	Grand centroid
TWP	57	58.4545	43	52.4286	50.2174	50.4444	49.5	53.7333	52.8207
Type	2	2.0909	3	2	2.3043	2.0741	2	2.2667	2.1655
^{13}C	2.802	2.3213	2.671	1.8564	2.3905	2.9546	2.6914	2.8855	2.61
^{18}O	-5.6667	-4.7908	-4.9245	-4.5934	-4.7659	-4.6966	-4.8713	-4.8594	-4.8058
CaCO$_3$	50.5	50.4364	49.935	51.2729	50.493	50.3152	50.4056	50.4643	50.4526
Ca	203699.91	156658.08	70175.406	119316.09	166779.67	197533.52	146629.35	184411.7	167156.88
Mg	46389.25	109485.8	37546.413	72755.384	108925.95	123075.54	99805.323	113224.15	106436.07
Li	0.8484	1.8674	0.6821	2.2411	1.929	1.5609	1.8989	1.4515	1.7022
B	2.9795	12.7016	11.8441	17.2917	14.4645	14.9502	12.7435	10.4533	12.9368
Na	373.0595	451.1438	194.8335	465.7478	519.2383	339.5339	363.1055	467.6919	425.6762
Al	320.6112	142.9667	50.4978	911.6117	95.0932	111.7853	253.5729	109.1624	174.5348
P	82.0458	121.3449	73.25	111.091	83.7146	64.9034	602.1401	161.6289	170.2508
K	276.4638	222.6702	126.2592	979.2133	162.9861	173.6485	309.4173	157.7888	236.3959
Ti	10.9139	6.5345	4.125	18.1353	4.549	2.6729	7.8578	3.8133	5.6859
V	2.3454	1.7783	9.1096	9.8836	4.1512	1.8748	4.6415	3.794	3.5504
Cr	4.3991	3.4722	18.5224	6.8383	4.5884	3.9539	7.7949	5.0779	5.2046
Fe	3151.0183	1324.8726	673.0572	3269.7272	1494.0661	1639.1955	3641.173	1872.2453	1924.7203
Mn	129.5226	99.7395	63.7592	159.0816	105.9192	94.2832	199.1036	116.4979	117.9943
Co	1.8037	1.7026	0.015	1.6204	1.1752	0.9695	2.967	21.5675	5.7009
Ni	7.0531	13.9911	0.03	9.7319	10.4708	6.7164	10.6736	10.7171	10.2546
Cu	74.5569	66.1382	2.1875	3.0527	41.0655	87.3239	5.6561	2.4422	40.784
Zn	48.7334	47.2471	3.9979	43.475	61.0002	60.3712	6.2922	16.5182	39.0862
Ga	0.1373	0.3707	1.5838	0.618	0.16	0.0491	0.5073	0.0602	0.2707
As	0.839	0.664	1.089	1.6536	0.714	0.521	1.7311	0.8789	0.8854
Rb	1.04	0.5675	0.1645	4.1581	0.4365	0.4396	1.0723	0.4435	0.7319
Sr	523.2398	66.8281	38.9709	67.2471	64.3014	63.1903	71.9105	206.1451	103.8998
Y	3.338	1.5981	0.9859	2.8484	1.6062	1.7229	6.1723	2.2983	2.4148
Mo	0.3626	0.3113	0.14	0.7258	0.7183	0.1542	0.9481	0.2888	0.4373
Ru	0.9918	1.4942	1.05	1.073	1.2416	0.9029	1.3398	0.936	1.1664
Ag	0.0238	0.1204	0.2052	0.1273	0.0583	0.0923	0.0617	0.1279	0.1002
Sn	1.233	1.4785	0.4355	0.1151	0.6979	1.9284	0.2962	0.1266	0.9123
Ba	2.769	34.8682	22.1845	8.3923	12.606	3.912	118.5159	17.3298	30.0357
La	2.4285	0.8992	0.5863	1.6964	0.8763	1.1933	2.1296	1.5644	1.3022
Ce	2.9331	1.1098	0.7153	3.4869	1.1359	1.3183	3.8468	2.1469	1.8487
Pr	0.4143	0.1667	0.0893	0.4755	0.165	0.1945	0.5736	0.2901	0.2655
Nd	1.673	0.6896	0.4386	2.1336	0.6875	0.8256	2.7964	1.2008	1.165
Sm	0.3404	0.1398	0.0575	0.5052	0.1443	0.1521	0.7121	0.2253	0.2511
Eu	0.0702	0.038	0.0089	0.1107	0.0243	0.0274	0.2303	0.049	0.0634
Gd	0.4567	0.2009	0.1275	0.5952	0.2004	0.205	0.9141	0.2989	0.3327
Tb	0.0534	0.015	0.0066	0.0725	0.0148	0.0208	0.1135	0.0305	0.0348
Dy	0.3483	0.1513	0.0944	0.4224	0.1638	0.1556	0.6931	0.2233	0.2518
Er	0.2145	0.0838	0.0269	0.1988	0.081	0.0837	0.3664	0.1102	0.1306
Yb	0.1494	0.0429	0.0217	0.155	0.0541	0.0546	0.2115	0.0748	0.0814
W	8.9482	3.2443	1.26	4.8419	1.7447	3.7576	18.5844	14.592	7.4945
Tl	0.0443	0.0264	0.0239	0.0217	0.0448	0.0314	0.0294	0.0363	0.0328
Pb	19.9002	7.2269	1.4513	17.8429	6.8101	29.7829	9.2408	5.7287	10.2694
Th	0.1909	0.1117	0.0531	0.4366	0.1383	0.0701	0.1918	0.1402	0.1397
U	0.2504	0.362	0.0437	0.2075	0.3523	0.2936	0.3474	0.2901	0.3125

Table 7.2.2. Main geochemical variables with the most elevated and the most depleted values that might have caused the clustering of the dolomite samples.

Cluster #	Elevated variables	Depleted variables
1	Ca, La	^{18}O, Ba, B
2	Ru, Ni	—
3	Cr, Ga	Ca, Mg, Fe, Mn, Cu, Pb, Zn, Li, La, Ni
4	Al, K, Ti	^{13}C
5	Na, B, Mo	—
6	Sn, Cu, Zn, Pb	As, Ga
7	Ce, Nd, Ru, Ba, P, Fe, Mn, REEs	—
8	Co, Sr, W	—

7.3 Discriminant analysis

Discriminant analysis was used to test for and identify chemical variables that distinguish groups of samples based on the predetermined parameters of geographic location and types of dolomite. Four petrographic (one to four) and four geographic groups ("1" for townships 33 – 40, "2" for townships 41 – 61, "3" for townships 62-78, and "4" for townships 79 – 95) were imposed on the dataset to distinguish chemistry based on spatial distribution and types of dolomite. Linear discriminant analysis was applied to the larger subset of data using these petrographic and geographic predictors. The results are presented in Tables 7.3.1 and 7.3.2.

A number of variables (Li, Ru, Pr, Nd, Er, W, Tl) that had significantly different discriminant function coefficients (reflecting the discriminating power of a function) for

different petrographic and geographic groups were cross-plotted against each other in order to identify the systematic relationship between these variables (Figures 7.3.1 and 7.3.2).

The difference between coefficients for the above variables ranged from 0.8 (W, (-1.3) − (-2.1)) to 90.8 (Gd, 120.5 − 211.3) in the discriminant analysis applied to the dolomite type, and from 5.4 (Ru, 3.9 − 9.3) to 62.5 (Gd, 24.6 − 87.1) in the discriminant analysis based on location. No obvious systematic relationship among the variables, representing different petrographic/ geographic groups of samples, was observed except for Li and Ru when plotted against the petrographic type, and Pr and Eu when plotted against the location (Figures 7.3.1 and 7.3.2). Discriminating by petrographic type revealed three distinct groups R1, R3 and R4 and showed an overlap with group R2 (Figure 7.3.1). Discriminating by location displayed distinct differences between samples from Location 2 and Location 3 (with a minor overlap with Location 2) and a combined sample set from locations 1 and 4 (Figure 7.3.2).

Table 7.3.1. Linear discriminant analysis based on petrographic types of dolomite. Elements highlighted in red have significantly different discriminant function coefficients.

Varialbes	1	2	3	4
Constant	-7592.1	-7613.2	-7629.3	-7647.4
13C	36.6	36.5	36	38.4
18O	-8.6	-9.2	-9.6	-10.2
CaCO3	303.6	304.1	304.3	304.7
Ca	0	0	0	0
Mg	0	0	0	0
Li	-32.4	-28.3	-26.9	-27.3
B	0.2	0	-0.1	0
Na	0.1	0.1	0.1	0.1
Al	0.3	0.3	0.3	0.3
P	0.1	0.1	0.1	0.1
K	-0.8	-0.8	-0.7	-0.8
Ti	6.4	5.8	6	6.1
V	-13.8	-13.2	-13.7	-13.9
Cr	2.8	2.8	2.7	2.5
Fe	0	0	0	0
Mn	-0.3	-0.3	-0.3	-0.4
Co	0.9	1	0.8	1.1
Ni	-0.3	-0.3	-0.3	-0.4
Cu	-0.2	-0.2	-0.2	-0.2
Zn	-0.3	-0.3	-0.3	-0.3
Ga	-41.2	-39.9	-40.4	-39.5
As	90.5	87.8	89.1	88.7
Se	-39.7	-39.7	-41.6	-44.8
Rb	143.3	140.6	131.3	132.4
Sr	0	0	0	0
Y	104.7	105.4	101.4	94.6
Zr	-385	-382.9	-382.1	-372.7
Mo	28	25.1	27.1	25.9
Ru	23.7	17.8	19.7	14.1
Ag	65.2	62.1	65.8	59.3
Sn	32.4	31.7	31	30.6
Ba	0.4	0.4	0.4	0.4
La	-131.9	-135.5	-133.9	-128
Ce	-76.2	-66.9	-69.7	-74
Pr	847.4	869.4	877	836.6
Nd	157.8	133.9	139.9	151.6
Sm	-849.3	-852.6	-838.8	-917.4
Eu	-543.2	-515.9	-562.1	-531.2
Gd	120.5	171.2	211.3	161.8
Tb	496.1	483.9	452.8	655.2
Dy	-1109.3	-1134.2	-1185	-1073.9
Er	-75.1	-68.2	-60.5	-14.7
Yb	1462.1	1444.3	1455.8	1520.6
W	-1.6	-1.7	-1.3	-2.1
Tl	270.5	203.7	231.8	235
Pb	-0.4	-0.4	-0.4	-0.4
Th	-155.8	-165.3	-169.4	-165.8
U	-68.4	-63.3	-66.8	-66.3

Table 7.3.2. Linear discriminant analysis based on geographic locations of dolomite. Elements highlighted in red have significantly different discriminant function coefficients.

Variables	1	2	3	4
Constant	-8788.4	-8655.2	-8689.5	-8286.5
13C	41	40.6	41.5	40.3
18O	11.3	9.7	11	7.5
CaCO3	346	343.4	344.2	336.2
Ca	0	0	0	0
Mg	0	0	0	0
Li	-3.7	-4.4	-3.9	-11.8
B	-2.6	-2.4	-2.5	-1.9
Na	0.1	0.1	0.1	0.1
Al	0.6	0.6	0.6	0.5
P	0.2	0.2	0.2	0.2
K	-0.9	-0.9	-0.9	-0.9
Ti	6.1	5.9	5.7	6.2
V	-14.9	-14.7	-14.8	-14.6
Cr	6	5.8	5.8	5.3
Fe	0	0	0	0
Mn	0.1	0.1	0.1	0
Co	1.4	1.4	1.6	1.4
Ni	-1	-0.9	-0.9	-0.8
Cu	-0.1	-0.1	-0.1	-0.1
Zn	0	0	0	-0.1
Ga	-54.2	-52	-52.6	-51.9
As	109.6	106.6	106.7	105.7
Se	-39.7	-39.3	-39.7	-38.8
Rb	140.3	137.3	142.3	147.2
Sr	0	0	0	0
Y	184.4	179.1	175.5	166.8
Zr	-386.8	-387.3	-386.8	-387.7
Mo	41	41	41.2	37.8
Ru	3.9	6.2	6.1	9.3
Ag	85.5	85.3	83.2	79.7
Sn	23.3	23.7	24.4	26.1
Ba	0.5	0.5	0.5	0.5
La	-185.9	-179.4	-175	-173.1
Ce	-39.1	-38.9	-37	-48
Pr	1948.3	1869	1865.8	1689.8
Nd	-148.6	-140.6	-157.1	-78.8
Sm	-1088.1	-1065.8	-1064.6	-1030.6
Eu	-716.1	-675.6	-726.6	-689.5
Gd	24.6	49.7	87.1	34.2
Tb	1661.7	1486.1	1482.6	1405.4
Dy	-1456.6	-1420.4	-1365.2	-1347.6
Er	-175.6	-218.8	-229.3	-154
Yb	1683.6	1727.2	1685	1599.5
W	-2.8	-2.8	-3.2	-2.7
Tl	-711.8	-711.8	-718.2	-469.8
Pb	-0.4	-0.4	-0.4	-0.4
Th	-421	-409.3	-401.6	-352.6
U	-72.3	-72.8	-77	-72.4
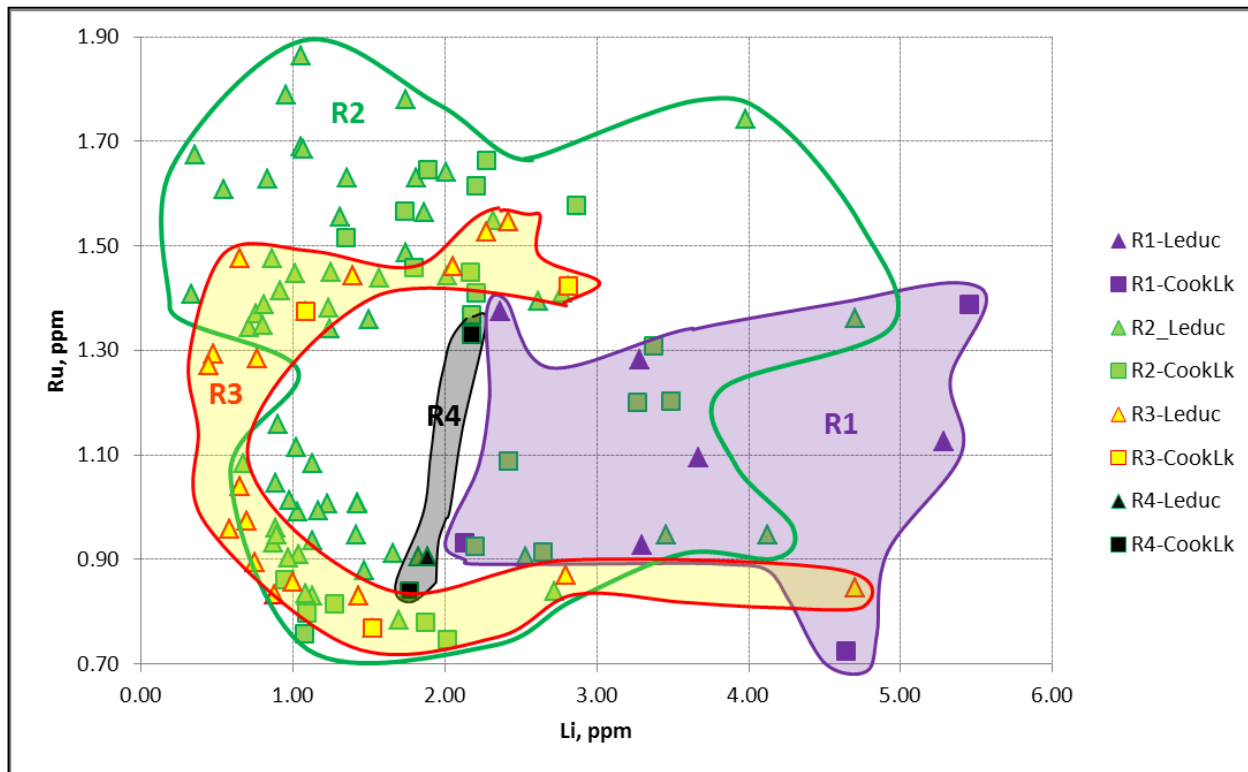
Figure 7.3.1. Cross-plot of Li vs. Ru showing distinct groups of matrix dolomites R1, R3 and R4. Note the overlap between the matrix dolomite R2 group and dolomite R1, R3 and R4 groups.
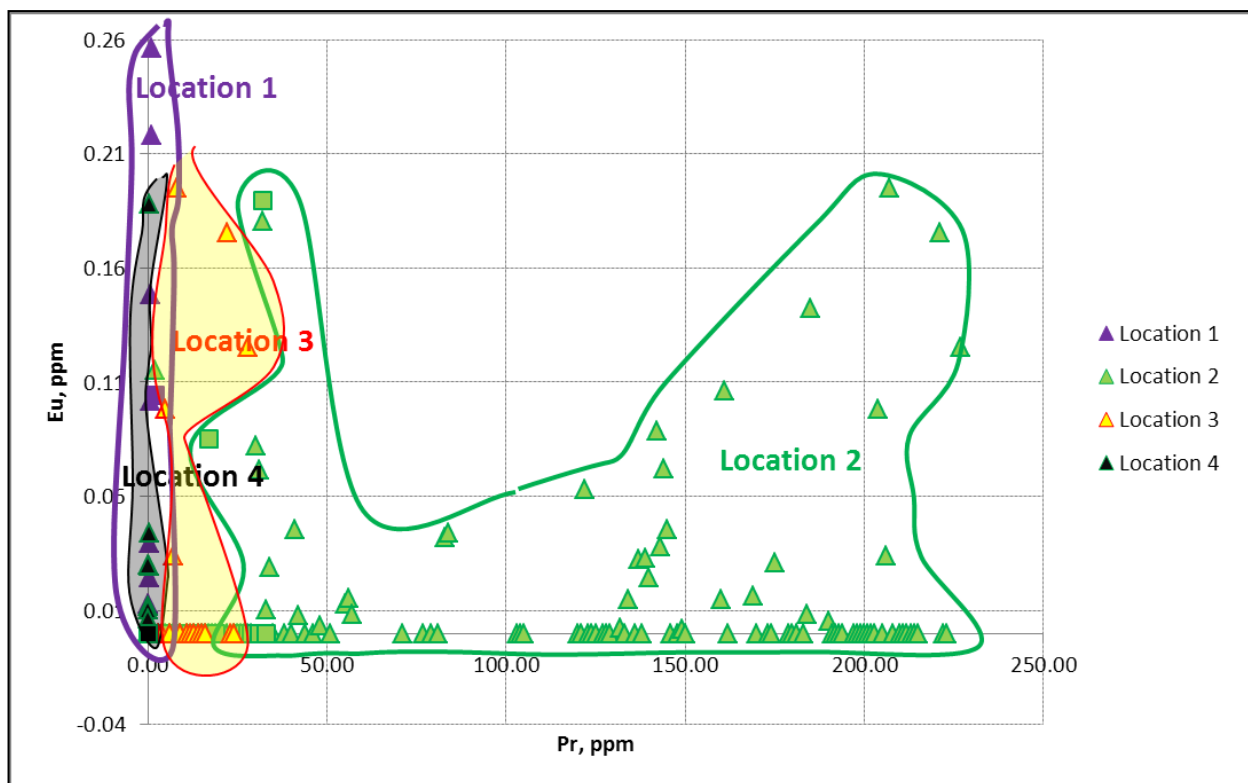
Figure 7.3.2. Cross-plot of Pr vs. Eu showing two distinct groups of matrix dolomites from Locations 2 and 3, and an overlap between matrix dolomites from locations 1 and 4.

CHAPTER 8

DISCUSSION AND INTERPRETATION

This chapter provides an interpretation of the diagenetic history of the Cooking Lake and Leduc matrix dolomites in the Rimbey-Meadowbrook Reef Trend based on the petrographic and geochemical analyses described in the preceding chapters. According to the studies by Amthor *et al.* (1993, 1994), Drivet (1993), Marquez (1994), Huebscher (1996) and Horrigan (1996), these dolomites were identified as replacement dolomites with no or very small degrees of recrystallization. However, the petrographic and geochemical data presented in Chapters 5 and 6 show that matrix dolomites R2 and R3 might have undergone 'significant recrystallization' *sensu* Machel (1997). If this is true, most matrix dolomites of the Cooking Lake and Leduc Formations could be considered 'significantly recrystallized'.

8.1 Paragenetic sequence

According to the petrography and the geochemical characteristics of matrix dolomites and later cements, these diagenetic phases can be placed in a paragenetic sequence (Figure 8.1.1). This sequence consists of four main stages distinguished by the near-seafloor diagenesis, shallow burial (less than 500 m), intermediate burial (500 to 2000m) and deep burial (more than 2000 m).

One of the earliest diagenetic events that affected the Leduc Formation reefs along with the Cooking Lake platform during shallow burial was pervasive matrix dolomitization, which was closely associated with chemical compaction (stylolite development). The dolomite replacement textures in some cases display an ambiguous timing relationship with the stylolites, which usually cross-cut all matrix dolomites (Plate 5.3.1e-f) but sometimes appear disrupted by dolomite crystals (Plate 5.3.1d). Two alternatives are possible to describe this relationship: 1) all recrystallization happened at the same time with stylolites forming at different times, and 2) all stylolites are of the same generation and the recrystallization happened in stages and to different extents. The second alternative is more likely, because there were multiple cases observed in which domains with micro-medium crystalline R2 appear enlarged to a coarser R2 and then even to R3, whereas their neighboring domains did not show any significant alteration (Plates5.1.2.2, 5.2.1a, 5.3.2b-d, and 5.3.5b). Also, the oxygen isotope values of the dolomites resulted from the early recrystallization would have retained the original compositions and would not have been so depleted in oxygen (Figure 6.2.2.3a).

Paragenetic sequence of reef trend dolostones
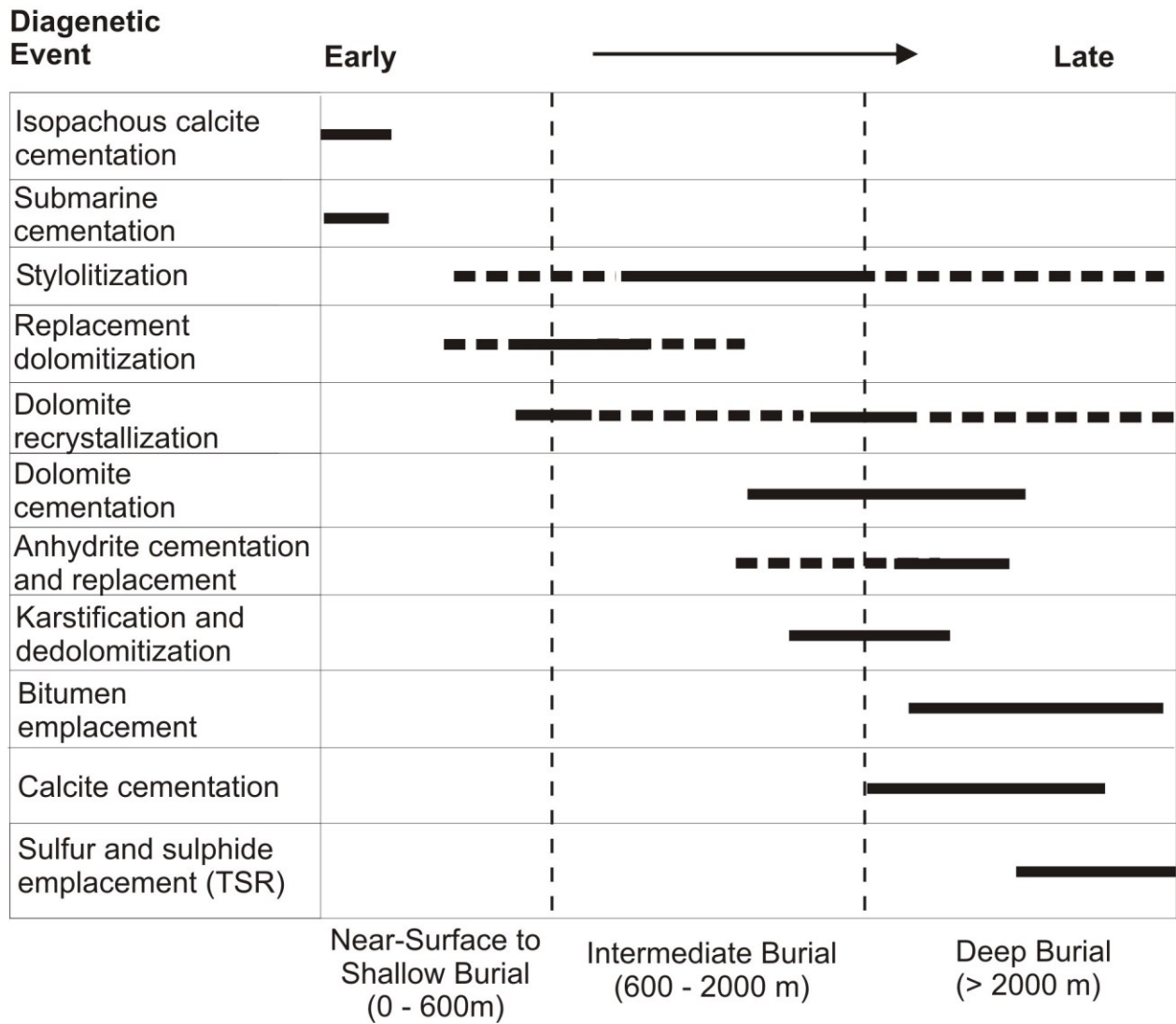
Figure 8.1.1 Paragenetic sequence for the Rimbey-Meadowbrook Reef Trend, that was compiled based on the petrographic and geochemical observations.

The next diagenetic event observed in the reef trend is dolomite cementation that occurred in stages during intermediate to deep burial. Saddle dolomite DC4, forming a distinct cluster with more negative $\delta^{18}O$ values, represents the latest phase, which postdates dolomite cements DC1 and DC2 (Figure 6.2.2.4). Some of the dolomite cements exhibit corroded crystal boundaries suggesting the presence of local dissolution of dolomites (Plates 5.2.1e and 5.2.2f).

Replacement of matrix dolomites (R1 to R4) and dolomite cements (DC1, DC2 and DC4) by anhydrite was likely contemporaneous with anhydrite cementation (Plate 5.3.2).

Carbonate dissolution due to karstification locally affected the reservoir characteristics of the Leduc Formation dolomites near the northeastern end of the reef trend, where pervasive karstification resulted in major carbonate dissolution and total elimination of sulfate minerals. This created a variety of solution-enlarged cavities ranging from a few millimetres to several centimetres, significantly enhancing overall reservoir porosity (Plate 5.1.4.2). Local calcitization of fine grained dolomites created dedolomites – remnants of the matrix largely replaced by calcite (Plate 5.1.4.1), which is typical for systems where meteoric water infiltrates dolomites.

Deep burial is marked by bitumen emplacement coating all matrix dolomites and dolomite cements (Plates 5.3.4.1 and 5.3.4.2). Precipitation of sparry calcite cements occurred some time after hydrocarbon migration. These sparry calcites locally replaced dolomite cements DC1, DC2 and DC4 (Plates 5.2.1e and 5.2.2e-f).

Thermochemical sulfate reduction (TSR) occurred during sparry calcite cementation producing H_2S, sulfide minerals, and native sulfur (Plate 5.3.5a). Some sulfides are intergrown with calcite crystals, showing that calcite cementation partly overlapped with sulfidization (Plate 5.3.5c, e), which is typical for TSR settings (Machel, 2001).

8.2. Dolomitization of the Rimbey-Meadowbrook Reef Trend

Massive dolomitization requires a sufficient source of magnesium and an effective hydrologic system capable of delivering Mg and removing calcium within a geologically reasonable amount of time. The only inexhaustible source of Mg can be seawater, or a seawater-derived formation water or brine (Land, 1985; Machel, 2004).

As discussed in Chapter 5 (section 5.3.1), most stylolites in the study area occur completely undisrupted throughout the dolomite framework deflecting around and even sometimes cutting through the dolomite crystals (Plate 5.3.1). This indicates that matrix dolomitization predates the onset of chemical compaction that starts at burial depth of 300 to 500 metres in limestones (Lind, 1993; Mazzullo *et al.,* 1995; Fabricus, 2000; Duggan *et al.,* 2001).

Fine-crystalline replacement dolomite R1 appears to be the 'least-altered' dolomite phase that is petrographically the closest to basinal dolo-mudstones and was probably formed at relatively low temperatures during relatively early diagenetic stage. This phase of dolomitization overprinted the textures and geochemistry of the precursors producing dolomicrite that was subsequently recrystallized into matrix dolomite R1 (see Section 8.3).

Most dolomitization models summarized in Machel (2004) can be ruled out for the Rimbey-Meadowbrook Reef Trend.

Seepage reflux dolomitization model was refuted by Jones and Rostron (2000) as not capable to explain matrix dolomitization on a regional scale. The hydrothermal-syndepositional model suggested by Migaszewski (1991) and later supported by Zhu

(2010) can also be ruled out based on the stratigraphic and structural constraints of the study area. The meteoric/marine mixing zone model, the topography driven and the tectonic models were eliminated by Machel (2004) as incapable of precipitating massive replacive dolostones. Amthor *et al.* (1993) and Huebscher (1996), however, considered regional-scale fluid flow to be the best explanation for the pervasive dolomitization of the reef trend, with the Cooking Lake platform beneath the Leduc buildups acting as a conduit system linking individual reefs.

The burial compaction model was previously refuted by Amthor *et al.* (1993) due to the insufficient amount of Mg derived from compaction fluids expelled from off-reef Ireton, Duvernay and Cooking Lake strata (total drainage area of 40000 km^2, which would represent a width of 100km on either side of the buildups), being only $1.1*10^{14}$ moles Mg when $4.9*10^{14}$ moles were required to dolomitize the original limestones. Funneled compaction flow, however, was advocated by Machel and Anderson (1989) as one of the alternatives for massive dolomitization of Upper Devonian reefs in Alberta. Rostron (1995) and Horrigan (1996) suggested that additional Mg could be supplied from undefined fluids derived through cross-formation flow entering the reef trend in its southwestern end similarly to the adjacent Bashaw Complex. However, the mechanism of this cross-formation flow has not been identified in the study area.

Recently, a new dynamic model, the self-accelerating dolomite-for-calcite replacement model, was proposed by Merino and Canals (2011). They suggested that this is the most effective model for dolomite replacement. However, their hypothesis is highly contentious, because it rests on an assumption that violates some basic rules of thermodynamics. Even if this model was tenable, it would not be suitable for the matrix

dolomites of the Rimbey-Meadowbrook Reef Trend due to the time required (roughly 100 my) to dolomitize the entire reef trend.

A variant of the seawater convection model (Machel, 2004) seems to be the most reasonable explanation for pervasive dolomitization due to the availability of the required large amounts of magnesium, and the efficient delivery mechanism through relatively permeable limestones (Land, 1985; Given and Wilkison, 1987). At slightly elevated burial temperatures modified seawater is an effective dolomitizing agent because of its ability to overcome the kinetic barriers present at higher temperatures (Lippman, 1973; Land 1985, 1991; Machel and Mountjoy, 1997; Hardie, 1987).

8.3 Dolomite recrystallization

8.3.1 Petrographic evidence of recrystallization

8.3.1.1. Fine-crystalline grey matrix dolomite (R1)

Fine crystalline matrix dolomite R1 is mostly present in the northern (shallow) part of the reef trend and is almost absent in the southern (deep) part. This suggests that matrix dolomite R1 was largely to completely recrystallized in the southern part of the reef trend. The local northward trend of increasing crystal sizes between townships 62 and 72 (Figure 5.5.2) is possibly associated with cross-formation fluid flow or the fluids moving upwards along fault and fracture conduit systems (see Section 8.5).

Fabric-preserving matrix dolomite such as R1 was previously interpreted to result from partial dissolution of unstable precursor phases and simultaneous precipitation of a more stable dolomite in a dolomite supersaturated fluid (Land, 1985; Sibley, 1990; Nordeng and Sibley, 1994; Sun, 1995). Dawans and Swart (1988) added that fine crystalline dolomites form from fast precipitation. As proposed by Sibley and Gregg (1987), this might have happened at relatively low temperatures of less than 50 ºC during near surface to shallow burial, as opposed to more coarsely crystalline dolomites commonly precipitating during deeper burial and at higher temperatures. Similarly, Huebscher (1996), who studied fine-crystalline dolomites of the Grosmont Formation overlying Leduc Formation reefs, also suggested that this type was probably formed syndepositionally or during very shallow burial.

8.3.1.2. Micro-medium- to macro-coarse crystalline grey matrix dolomite (R2)

Matrix dolomite R2 is present throughout the entire reef trend. Dolomite crystal sizes gradually increase with depth from about 400-500 micrometers in township 50 to about 900 micrometers in township 36 (Figure 5.5.3), which might be a result of recrystallization driven by a downdip temperature increase along the reef trend, as was suggested by crystal size – temperature covariance by Sibley and Gregg (1987). The domains with abnormally enlarged crystals (up to 1mm) in the central part of the reef chain are possibly caused by the cross-formation fluid flow or by fluids moving upwards into the Cooking Lake – Leduc aquifer along faults (see Section 8.5).

Compared to R1, the relatively large crystal size of matrix dolomite R2 may be a result of slow crystal growth and/ or lower fluid supersaturation with respect to dolomite (Sibley and Gregg, 1987; Dawans and Swart, 1988). Also, the coarser crystalline nature of this type suggests that it was formed during deeper burial and at higher than near-surface temperatures (Sibley and Gregg, 1987; Zenger and Dunham, 1988; Amthor *et al.,* 1993; Mountjoy and Amthor, 1994).

The crystal size variation between R1 and R2 was previously suggested to be controlled by the textural differences in the precursor limestones (Kaufman, 1989; Amthor *et al.,* 1993; Drivet, 1993; Marquez, 1994; Drivet and Montjoy, 1997; Wendte *et al.*, 1998; and Green and Mountjoy, 2005). However, Machel (2004) proposed that this difference might be influenced also by recrystallization of these rocks.

The textural and circumstantial considerations presented in this study suggest that both factors, precursor textures and recrystallization, are viable alternative interpretations. Nothing in the available data rules out that the regional pattern of occurrence of R1 and R2 is largely the result of depositional/ primary textural patterns.

8.3.1.3. Brown porous matrix dolomite (R3)

Brown porous matrix dolomite R3 is present throughout the entire reef trend similar to R2. However, dolomite R3 appears only in certain "patches" along the reef trend while it is absent in townships 33, 34, 37, 38, 39, 40, 45, 49, 50, 57, 60, 65, 66, and 70 (Figure 5.5.4). There is a weak trend of increasing R3 crystal sizes from 100 micrometers

near the shallow end to 750 micrometres near the deeper end of the reef trend (Figure 5.5.4), which might be a result of recrystallization driven by the downdip temperature increase along the reef trend. As with matrix dolomite R2, dolomite R3 with coarser crystals occurs in the central part of the study area, which is possibly caused by cross-formation fluid flow or fluids moving into the Cooking Lake – Leduc aquifer along faults (see Section 8.5).

The occurrence and petrographic attributes of matrix dolomite R3 were also previously considered to be controlled by precursor fabrics, such as open pore space, cements, or biochems in the limestones (Kaufman, 1989; Amthor *et al.,* 1993; Drivet, 1993; Marquez, 1994; Drivet and Montjoy, 1997; Wendte *et al.*, 1998; and Green and Mountjoy, 2005). Machel (2004) argued dolomite R3 to be a product of recrystallization or overgrowth of younger dolomite on older cores (Land, 1986, 1991; Sibley and Gregg, 1987; Sibley *et al.,* 1993). Notably, R3 is common as "halos" around vugs in the Upper Devonian Grosmont Formation near the northern end of the reef trend, which is clearly the result of recrystallization of matrix dolomites R1 and R2 (Machel *et al.,* 2012).

8.3.1.4. Textural evolution

If dolomite types R1, R2 and R3 resulted solely or mainly from a fabric - controlled replacement process, the precursor fabrics, presumably lime mudstones and lime grainstones with somewhat variable grain sizes, must have been present throughout the entire reef trend before dolomitization. This remains a viable explanation for much, if not

most, of the data. In a reef trend several hundred kilometers long, there surely were syndepositional grain size variations. On the other hand, the Grosmont data show that at least in the updip region R3 is the result of recrystallization of R1 and R2 (Machel et al., 2012).

Farther downdip it is possible that both matrix dolomites R2 and R3 are products of recrystallization of matrix dolomite R1 through the growth of coarser crystals over fine crystals via Ostwald Ripening whereby the smaller crystals dissolve and the remaining crystals enlarge at the expense of the smaller ones (Ostwald, 1897). Therefore, the theory proposed by Machel (2004) works on this sample set having fabric-preserving matrix replacement dolomite R1 pervasively recrystallized into fabric-destructive dolomite R2 and then locally recrystallized into porous dolomite R3 through Ostwald Ripening.

It is further noteworthy that matrix dolomite R1 exhibits coarser crystal sizes (30 to 62 μm) than most modern dolomites, which have crystals less than 4 micrometers in diameter (Milliman, 1974). This might suggest that even the smallest crystal size population of R1 in the Rimbey-Meadowbrook Reef Trend has undergone some Ostwald Ripening. As suggested by Huebscher (1996), this type of recrystallization may have occurred when the dolomites were still interacting with the dolomitizing fluids. McKenzie (1981) and Gregg *et al.* (1992) reported similar early, essentially syndepositional recrystallization in Holocene dolomites that formed very close to the depositional surface. However, it is questionable to apply the findings of these studies to the Rimbey-Meadowbrook Reef Trend for at least two reasons. Firstly, the Grosmont dolomites are not representative of the dolomites in the reef trend farther downdip, and secondly, the dolomites of Leduc and Cooking Lake Formations did not form syndepositionally.

Furthermore, the essentially "syndepositional" recrystallization during the early phases of dolomitization (whereby, in an apparent representation of the Ostwald step rule (Van Santen, 1984), protodolomite forms and then recrystallizes to dolomite in a series of intermediate steps, as observed by Kaczmarek and Sibley (2007, 2011, 2014) in hydrothermal experiments) is not recognizable in the rocks studied here. In any rate, this type of recrystallization would be 'insignificant' *sensu* Machel (1997), as it would not have resulted in any significant changes in crystal sizes recognizable today.

The evolution of the CL characteristics from dull orange-red in matrix dolomite R1 to brighter orange-red blotchy in dolomites R2 and R3 also suggests recrystallization. The cloudy cores of dolomite R3 exhibiting the same dull orange-red luminescence as dolomite R1 suggest that these cores resulted from recrystallization of R1 and/ or R2 with subsequent overgrowth nourished by the dissolution of finer grains, providing the current pore space if some of the dissolved material is carried away by advection.

The general distribution of matrix dolomites R2 and R3, whereby dolomite R3 is the most abundant in areas where the volume-percentage of R2 is minimal (Plate 5.5.6), also supports the notion of recrystallization of finer crystalline nonporous matrix dolomites into coarser crystalline porous matrix dolomites.

In conclusion, the petrographic data assembled in this study are consistent with recrystallization of R1 to R2 and/or R3. However, there is no apparent stepwise pattern in crystal size distribution with depth, as it was hypothesized by Land (1992). Furthermore, there is nothing in the available data to rule out that the distribution of R1, R2, and R3 is/ was not controlled by the precursor limestone textures.

8.3.2 Geochemical evidences of recrystallization

Most matrix dolomites are geochemically similar to each other and do not show any pronounced trends with depth. However, matrix dolomite R1 forms relatively tight clusters while the data points for dolomites R2 and R3 are dispersed. This is consistent with the previously reported data for most Devonian (Mattes and Mountjoy, 1980; Machel and Anderson, 1989; Qing and Mountjoy, 1989; Kaufman *et al.,* 1990; Laflamme, 1990; Patey, 1995; Hearn, 1996; Duggan, 1997; McKenzie, 1999; Keilly, 2004; Green and Mountjoy, 2005; Machel and Buschkuehle, 2008) and Mississippian (Al-Aasm and Packard, 2000) matrix dolomites across the Western Canada Sedimentary Basin.

8.3.2.1. Stoichiometry

As discussed by Land (1980, 1985), McKenzie (1981), Carballo *et al.* (1987), Gregg *et al.* (1992), Mazzullo (1992), Malone *et al.* (1994), and Kaczmarek and Sibley (2007, 2011, 2014), dolomites are considered to acquire closer to stoichiometric compositions during progressive recrystallization or slow crystal growth in the burial environment. Conversely, poorly ordered dolomites are a sign of fast growing dolomites or very young dolomites.

The position of the 015 peak in the XRD analyses of the samples studied suggests that most of the analysed matrix dolomites are of nearly ideal stoichiometric

composition with 49.25-52.11 mol % $CaCO_3$ (Figure 6.1.1), which may or may not be "primary" in the sense of being the composition of the dolomites after the initial protodolomite to dolomite conversion/ recrystallization that was previously deemed 'insignificant' (see Section 8.3.1.4).

If the dolomites in the Rimbey-Meadowbrook Reef Trend did "stabilize" through recrystallization as discussed by Kaczmarek and Sibley (2007, 2011, 2014), this process likely took place very soon after initial dolomite formation and resulted in what now appears as a single, essentially undifferentiated "stabilization process".

Only one sample, SK95-12, has a non-stoichiometric composition with significantly elevated $CaCO_3$ concentration (56.25 mol %). The reason for this feature is unclear.

8.3.2.2. Stable isotopes

Carbon isotopic compositions reflect the source of carbon involved in dolomite precipitation or recrystallization during diagenesis. Assuming that the range of equilibrium values of the Late Devonian dolomites is between +1.5 and +3.5‰ PDB, as estimated by Hurley and Lohmann (1989) and Carpenter and Lohmann (1989), and that of the Late Devonian evaporative dolomites is -5.5 to +3.5‰ PDB (Huebscher, 1996), the $\delta^{13}C$ compositions of 300 (out of total four hundred and twenty two) matrix dolomite samples R1, R2 and R3 fall within these ranges (Figure 6.2.2.1 and 6.2.2.3). This suggests that the carbon in these samples was mainly derived from seawater-dominated fluids. All of these dolomites retained the carbon signature of precursor limestones, and therefore show no signs of 'significant' recrystallization with respect to $\delta^{13}C$.

Compared to the marine reference values, matrix dolomites with elevated $\delta^{13}C$ ratios might be a result of recrystallization driven by fluids slightly enriched in $\delta^{13}C$ relative to the rock buffered fluids. This $\delta^{13}C$ enrichment can be explained by CO_2 produced in the isotopic equilibrium with methane during fermentation of organic matter (Claypool and Caplan, 1974; Irwin *et al.,* 1977). Huebscher (1996) estimated that the contribution of 5 to 10% of heavy organic carbon is required to cause a $\delta^{13}C$ enrichment of 1 to 6‰ in matrix dolomites. The source for isotopically heavy CO_2 probably is the organic rich limestones of the Majeau Lake Member. Heavier CO_2 with $\delta^{13}C$ values of up to +15‰ was also found in systems where CO_2 was in equilibrium with biogenic methane at temperatures up to 58°C (Whiticar *et al.,* 1986).

Bacterial fermentation of organic products is typically a very early process that occurs within depths up to 100 m (Figure 6.2.1; Irwin *et al.,* 1977), along with physical compaction and porosity loss in limestones (Feazel and Schatzinger, 1985). Because the Majeau Lake Formation limestones are underlain by porous and permeable Cooking Lake and Leduc carbonates and overlain by relatively impermeable Ireton shales, compaction-driven flow could have caused a downward drainage of pore fluids and lateral flow towards the Leduc reefs, as proposed by Hugo (1990) and Kaufman (1989) elsewhere in the Alberta Basin.

Compared to the marine reference values, relatively negative $\delta^{13}C$ values typically result from bacterial (BSR) or thermochemical (TSR) sulfate reduction (Machel, 2001). For samples collected in the deeper part of the reef trend, one can argue that TSR could have added isotopically depleted carbon to the matrix dolomites via recrystallization, especially where samples were selected from wells that contain sulfur and metal sulfides (pyrite and sphalerite). Significantly depleted sparry calcite $\delta^{13}C$ values also support this premise (Figures 6.2.1 and 6.2.2.1b). However, Machel and Bueschkuehle (2008) discovered that matrix dolomites had not recrystallized significantly, if at all, under the TSR conditions in the Southesk-Cairn Carbonate Complex very near the limit of the disturbed belt, structurally similar to the downdip end of the Rimbey-Meadowbrook Reef Trend. The temperatures of about 185°C were probably not hot enough to induce recrystallization of the matrix dolomites, even in the deeper end of the WCSB. This finding further suggests that elevated temperatures alone are insufficient to induce recrystallization in these matrix dolomites.

The $\delta^{18}O$ values of the matrix dolomites in the Rimbey-Meadowbrook Reef Trend are significantly depleted (-3.14‰ to -8.67‰ PDB; Figure 8.2.3) relative to the estimated Late Devonian marine (-3.0 to +0.3‰ PDB, Huebscher, 1996) and evaporative (-2.9 to +2.4‰ PDB, Huebscher, 1996) dolomite values. Therefore, one can argue that either these dolomites were formed from fluids that were not marine, or the estimated ranges of equilibrium values of the Late Devonian marine and evaporitive dolomites are not credible, or all matrix dolomites are recrystallized. The first argument is extremely unlikely considering the burial history and dolomitization models applied for this reef trend in Section 8.2. If the determinations of the $\delta^{18}O$ values for marine dolomites were wrong, then the Devonian sea water would have been much more depleted in $\delta^{18}O$ than commonly thought. If the estimated Late Devonian marine and evaporative values are correct, however, one can argue that all matrix dolomites are 'significantly recrystallized', and there is not a single unrecrystallized sample in the dataset.

The major causes for negative $\delta^{18}O$ values in ancient carbonates have been discussed in many studies (*e.g.,* Symons *et al.,* 1999; Al-Aasm and Packard, 2000; Gasparrini *et al.,* 2006; Muhsin *et al.,* 2007; Azmy *et al.,* 2009; Zhu *et al.,* 2010; Haeri-Ardakani *et al.,* 2013). The $\delta^{18}O$ depletion in dolomites of the Cooking Lake and Leduc Formations are most likely caused by oxygen isotopic exchange during recrystallization at higher temperatures (if the $\delta^{18}O$ composition of the water did not compensate for it) or in $\delta^{18}O$-depleted fluids. Temperature-induced recrystallization of matrix dolomites at depth causing this $\delta^{18}O$ depletion was previously discussed by Machel *et al.* (1996) and suggested for the deeper part of the Western Canada Sedimentary Basin in Machel and Cavell (1999).

Thus, the noted oxygen depletion in the matrix dolomites represents 'significant' recrystallization with respect to $\delta^{18}O$ *sensu* Machel (1997).

The involvement of meteoric water is commonly used to explain negative $\delta^{18}O$ values in carbonates (Land, 1986). However, the cold meteoric waters that entered the reef trend from its northeastern end likely caused dissolution and calcitization rather than recrystallization of dolomites (Figure 5.3.3; Machel *et al.,* 2012).

Sulfate reduction could be invoked as another possible cause of depletion of $\delta^{18}O$ values in the dolomites, but only if we assume that the TSR fluids changed from calcite to dolomite saturation over time and ignore Machel and Bueschkuehle's (2008) research, who did not find evidence for matrix dolomite recrystallization in TSR-reservoits. The potential for $\delta^{18}O$ depletion is supported by late sparry calcites from townships 33-35 that were interpreted as TSR calcites by Drivet (1993) and Marquez (1994).

The oxygen isotope compositions of matrix dolomites R1, R2 and R3 do not show any apparent regional or stratigraphic trends (Figure 6.2.2.8), nor are there oxygen isotopic depletion or enrichment trends associated with crystal size changes, as found in other studies (Gao, 1990; Gao and Land, 1991; Kupecz and Land, 1994). The most likely reason for this finding is that the temperature-dependent depletion in $\delta^{18}O$ was largely offset by the enrichment in $\delta^{18}O$ in the formation fluid concurrent with burial or low water-rock ratios.

Furthermore, if all studied matrix dolomites are indeed 'significantly' recrystallized and that dolomite R1 is the least altered type, one can rightly argue that the oxygen isotopic values of matrix dolomite R1 have been largely retained in later matrix

dolomites R2 and R3. The alteration of finer R1 dolomite to dolomites R2 and R3 might have occurred in fluids with similar oxygen isotopic composition and temperature.

The finding that all matrix dolomites of the Rimbey-Meadowbrook Reef Trend likely are 'significantly' recrystallized with respect to their oxygen isotope compositions, their $\delta^{18}O$ values can no longer be used for paleotemperature calculations of the process of dolomitization. However, dolomite R1, as the presumably least recrystallized dolomite type, may have retained its original isotopic composition. Therefore, the temperatures during formation of matrix dolomite R1 can be calculated assuming that the parent water had an isotopic composition relatively close to that of the Late Devonian seawater, ranging between -3 and 0‰ SMOW (Amthor *et al.,* 1993; Cummins *et al.,* 2014; Veizer and Prokoph, 2015). The isotopically heaviest R1 sample (-3.08‰ PDB), presumably closest to the unrecrystallized composition, thus yields a temperature range of approximately 37 to 49 °C (Figure 8.2.2.2). This temperature range corresponds to burial depths of approximately 200 to 900m (assuming a geothermal gradient of 30°C/km and a surface temperature of 25°C; Figure 8.2.2.3). These burial depths could have been reached at the end of the Late Devonian/ beginning of Early Carboniferous (Figure 8.2.2.3).

These paleotemperature interpretations correlate well with the ones reported in Amthor *et al.* (1993), Drivet (1993), Marquez (1994), Huebscher (1996) and Horrigan (1996). The fact that their temperature calculations stem largely from R2 dolomites suggests that at least the "least altered" R2 samples also preserve the original temperature of dolomite formation quite well. However, most matrix replacement dolomites of the Rimbey-Meadowbrook Reef Trend may have recrystallized by diagenetic fluids at elevated temperatures during subsequent burial with a reset of stable isotopic compositions. Also,
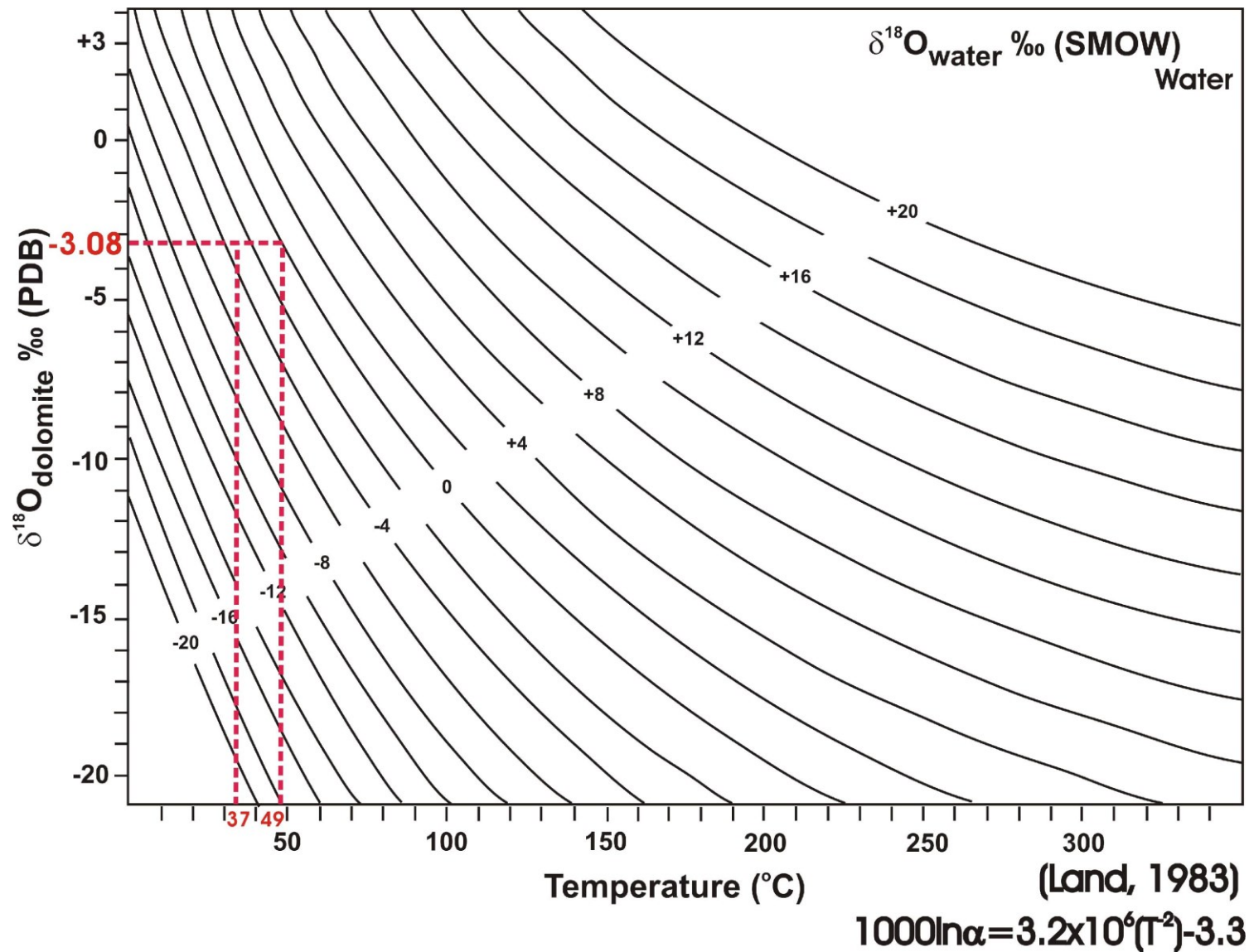
Figure 8.2.2.2. Oxygen isotopic equilibrium between parent water $\delta^{18}O$ and presumably least recrystallized dolomite R1, assuming isotope composition of the water between -3 and 0‰ SMOW, representing the lowest and highest possible values for the oxygen isotopic compositions of Late Devonian seawater based on Amthor *et al.* (1993), Cummins *et al.* (2014), and Veizer and Prokoph (2015).
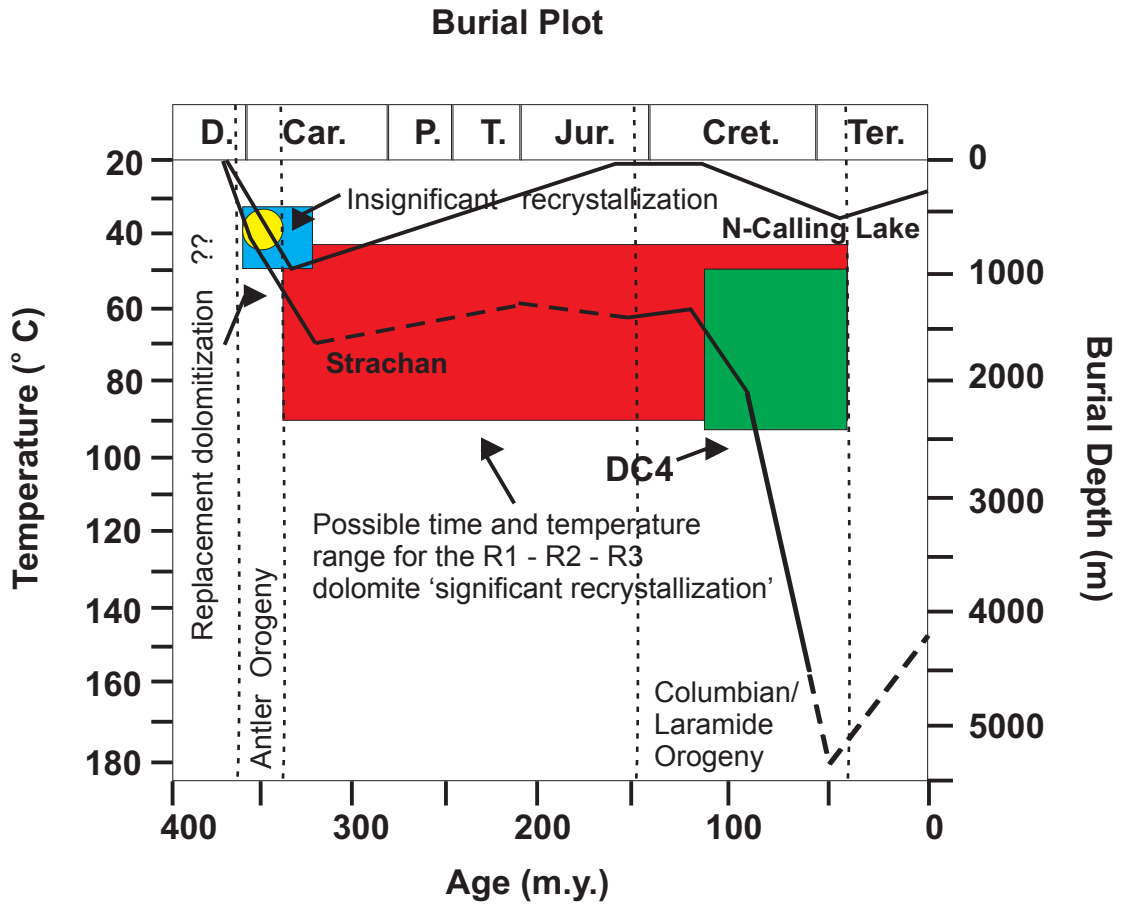
Figure 8.2.2.3. Burial history diagram for the Rimbey-Meadowbrook Reef Trend. The two burial curves represent the shallow northeast (Northern Calling Lake) and the deep southwest (Strachan) areas of the reef chain. Included are interpreted time and temperature ranges for replacement dolomitization and dolomite recrystallization. Assumed 30°C/Km geothermal gradient and surface temperatures of 25°C. Based on Amthor *et al.* (1993), Drivet (1993), Marquez (1994) and Huebscher (1996).

the isotopic similarities between matrix dolomites R1, R2, and R3 and dolomite cements DC1, DC2, and DC4 suggest that the fluids recrystallizing the matrix dolomites also formed dolomite cements (Figure 6.2.2.4). These fluids might have entered the system along faults and fractures that were reactivated during the Paleozoic in the Western Canada Sedimentary Basin (Wright *et al.,* 1994; Bottomley *et al.,* 2005). Additionally, the cross-formation fluid flow in the central part of the reef trend might have caused dolomites to recrystallize (Bachu *et al.,* 2008).

Finally, the stable isotope geochemistry did not show the stepwise progression hypothesized by Land (1992). If the dolomites in the Rimbey-Meadowbrook Reef Trend did "stabilize" from metastable Ca-rich dolomite through primary recrystallized to secondary recrystallized stoichiometric dolomite as discussed by Kaczmarek and Sibley (2007, 2011, 2014) in their four-phased model, this process likely took place very soon after initial dolomite formation and did not overprint initial stable isotope compositions. Similar early diagenetic recrystallization that happens in nature within a 1000 to 1500 years was reported by Gregg *et al.* (1992) for modern Holocene dolomites in Belize. This "initial" recrystallization was probably insignificant, yet appears to have been overprinted by the later 'significant' recrystallization identified in this study. Therefore, the multistage recrystallization described by Kaczmarek and Sibley (2007, 2011, 2014) is irrelevant to the present study, considering the age of Devonian reefs.

8.3.2.3. Strontium isotopes

Due to the insignificant fractionation by variations in the temperature and pressure conditions during precipitation and recrystallization, the $^{87}Sr/^{86}Sr$ isotopic ratio of carbonate minerals is assumed to be a reflection of the isotopic composition of the fluids (Banner, 1995). Thus, if Devonian seawater or a derivative thereof was the principle dolomitizing fluid in the Rimbey-Meadowbrook Reef Trend, the Sr-isotope ratios of the matrix dolomites should be close to the Upper Devonian marine ratio of ~0.7078 - 0.7085. Significantly higher Sr-isotope values require input of radiogenic Sr from basinal shales or metamorphic rocks.

Squeegee fluids expelled during the Laramide Orogeny are enriched in radiogenic strontium, placing them above **Ma**ximum **Sr I**sotope **R**atio of **Ba**sinal **S**hales (MASIRBAS) of 0.7120 as defined by Machel and Cavell (1999). If expelled into the foreland basin, such ^{87}Sr-enriched fluids tend to get diluted by older brines of marine origin with much lower $^{87}Sr/^{86}Sr$ ratios while moving updip, and therefore, would show a positive trend of decreasing radiogenic strontium values with decreasing depths (Machel and Buschkuehle, 2008). Additionally, Machel and Cavell (1999) showed that this type of basinal fluid flow has a very limited geographic effect, extending only for 100 to 200 km into the foreland basin. Thus, 'squeegee flow' might have only affected the dolomites of the very southern buildups of the Rimbey-Meadowbrook Reef Trend.

Most matrix dolomites examined in this study have strontium isotope ratios that are slightly enriched (up to 0.7090) compared to the theoretical Late Devonian marine value, but yet they plot below MASIRBAS, suggesting that the dolomitizing or possibly

recrystallizing fluids were intra-basinal formation waters (Figures 6.3.2 and 6.3.3). This finding is consistent with those of all earlier studies of dolomites in the Rimbey-Meadowbrook Reef Trend, which invoked Upper Devonian seawater slightly modified by interaction with basinal shales as the principal dolomitizing fluid (*e.g.* Mountjoy *et al,* 1999), with or without recrystallization.

The dolomites in the deeper parts of the reef trend might have recrystallized either before the tectonic fluid expulsion associated with the Laramide Orogeny, or recrystallization did not significantly affect the chemical composition of these matrix dolomites, which is consistent with Machel and Bueschkuehle (2008), who found that "squeegee flow" did not recrystallize the matrix dolomites in the Southesk-Cairn Carbonate.

The most elevated $^{87}Sr/^{86}Sr$ values (up to 0.7102) in the matrix dolomites of the Rimbey-Meadowbrook Reef Trend may have resulted from diagenetic interaction with siliciclastics within the study area by mixing with ^{87}Sr-rich formation waters that migrated here from neighboring siliciclastics-rich beds (McNutt *et al.,* 1987). Alternatively, such "radiogenic" signatures might also have been caused by upward-migrating fluids expelled along faults and fractures that were activated during the Late Paleozoic and Mesozoic in the Western Canada Sedimentary Basement (Wright *et al.,* 1994; Lyatsky and Pana, 2003; Bottomley *et al.,* 2005; Lyatsky *et al.,* 2005). Both alternatives, albeit speculative, are consistent with the data presented in this thesis.

In conclusion, the Sr-isotope data presented in this study are consistent with 'insignificant' recrystallization of R1, R2 and R3. However, there is no apparent stepwise correlation, as hypothesized by Land (1992).

8.3.2.4. Major and trace elements

All matrix dolomites (R1, R2 and R3) exhibit very similar Fe^{2+} (less than 3500 ppm) and Mn^{2+} (less than 200 ppm) concentrations, suggesting that all three types were formed in a similar redox environment or a low water-rock ratio system (Figures 6.4.2 and 6.4.3). Significantly elevated Fe^{2+} and Mn^{2+} concentrations in the southern (deep) and northern (shallow) parts of the reef chain, as well as the anomaly in the central part, can be related to precipitation from Fe- and Mn- enriched fluids under more reduced conditions (Frank, 1981), slower rate of precipitation or higher distribution coefficients resulting from higher temperatures (Lorens, 1981). The elevated Mn^{2+} concentrations also correlate with the CL spectroscopy data, indicating that the cathodoluminescence in the samples from the fault zones is activated by Mn^{2+}. According to Gao (1990), Barnaby and Read (1992), and Montanez and Read (1992), relatively elevated Fe and Mn values are caused by recrystallization. Fluids responsible for these local alterations of Fe^{2+} and Mn^{2+} concentrations might have been derived through the network of faults and fractures, or from the cross-formation fluid flow in the central part of the study area (see Section 8.5).

Most matrix dolomites of the study area show relatively low Sr concentrations (less than 200 ppm, Figure 6.4.4), which are similar to most ancient dolomites precipitated from marine waters (40-150 ppm, Machel and Anderson 1989). However, these values are significantly lower than the concentrations of most modern (proto-) dolomites (500 to 700 ppm) precipitated in evaporitic and marine environments (Behrens and Land, 1972; Land, 1980; Banner, 1995). This depletion could be explained by recrystallization of original dolomites by Sr-depleted fluids or by low precipitation rates (Katz and Matthews, 1977).

Clusters with significantly elevated Sr concentrations (100 – 350 ppm) in the southern and central parts of the reef chain (Figure 6.4.4) are likely a result of recrystallization by fluids expelled into the system along faults and fractures or the cross-formation fluid flow in the central part of the reef trend (see Section 8.5). Two Leduc matrix dolomite R2 samples with extremely high strontium concentrations (1346 and 4588 ppm) were probably contaminated during sample preparation.

Sodium can be used as an indicator of the degree of salinity under which dolomites are formed. Na concentrations of Leduc Formation dolomites gradually increase from about 90 ppm in the southern (deeper) end of the reef trend to about 1500 ppm in the northern (shallow) end (Figure 6.4.6), which falls into the reported range (190 to 2750 ppm) for evaporative and marine dolomites (Land and Hoops, 1973; Sibley, 1980; Humphrey, 1988). According to Veizer *et al.* (1983), sodium exhibits a positive correlation with the clay content in carbonates. Despite the fact that the samples were digested in a weak (1 M HCl) acid, there is a possibility that some siliciclastic minerals were partially dissolved during the chemical analysis (Nader *et al.,* 2007) Aluminum, as an indicator of clay content in dolomite samples, indeed shows a similar northward trend of increasing concentrations from 50 to 480 ppm (Figure 6.4.1). Significantly elevated Al concentrations (2000 to 33,000 ppm) in the southern and northern parts of the reef chain are likely due to contamination.

Copper, lead and zinc usually indicate hydrothermal influence on the dolomite systems (Leach *et al.,* 2010). The data plots for all of these elements exhibit distinct triangle-shaped patterns in the central part of the reef trend (Figures 6.4.6 through 6.4.8) suggesting that these dolomites were recrystallized by the fluids introduced into the system

along multiple faults and fractures or by a mixed fluid derived from the warm basinal brines and cross-formation fluid flow in the central part of the study area (see Section 8.5).

Rare earth elements (REE) include 15 lanthanide elements with similar ion radius and, therefore, similar geochemical characteristics. They are usually subdivided into light (LREE: La to Nd), medium (MREE: Sm to Dy) and heavy (HREE: Ho to Lu) rare earth elements, all of which are trivalent (with an exception of Ce^{+4} and Eu^{+2} in certain environments) and generally occur together in nature (Azomani *et al.,* 2013). The REE compositions of primary dolomites are usually controlled by the fluids that deposited the carbonates and can be affected by diagenesis (Schields and Stille, 2001; Azmy *et al.,* 2011). Therefore, they can be used as potential indicators of changes in fluid composition. However, several recent studies showed that some diagenetic environments, such as meteoric and mixed water setting, have no effect on composition and distribution of these elements in carbonates except in fluid-dominated systems (Nothdurft *et al.,* 2004; Barton *et al.,* 2006; Webb *et al.,* 2009). Two of these elements, Ce and La, exhibit similar clusters with elevated concentrations as on the Fe^{2+}, Mn^{2+}, Sr, Cu, Pb and Zn plots (Figures 6.4.9 and 6.4.10). These anomalies are likely associated with fluids funneled up faults and fractures or with cross-formation fluid flow in the central part, between townships 44 and 60 (see Section 8.5).

Additionally, the CL spectroscopy did not reveal CL activation by REE likely due to low concentrations of these elements – the minimum concentration required is 10-20ppm. One of the main elements of interest, which is visually indistinguishable from the Mn^{2+} activation in the CL, is Sm^{3+} that also shows orange-red cathodoluminescence (Machel *et al.,* 1991).

In conclusion, major and trace element data are generally consistent with recrystallization of matrix dolomites R1, R2 and R3. However, the relationship between these petrographic types as to which one evolved from which is not clear from the geochemical data analyzed in this study. These elements do not show any visible regional trends or a stepwise progression hypothesized by Land (1992). Similar to oxygen isotope analysis, the original elemental compositions might have been reset during recrystallization. The locations of local anomalies in the isotope versus depth cross-plots correlate with the anomalies in the TE plots. This might have been due to recrystallization driven by the same fluids. As proposed in previous section, these dolomites were recrystallized more than once. The "initial" stabilization from metastable to stable dolomite might have occured within 1000 to 1500 years after initial dolomitization (*e.g.* Gregg *et al.*, 1992). This initial recrystallization was probably insignificant and might have been overprinted by the later 'significant recrystallization'.

8.4 Statistical analysis

Factor analysis was used to examine relationships between the large number of variables in the dataset in order to reduce them to a limited number of interpretable factors with a minimum loss of information. Factor analysis revealed six dominant associations among the original variables that describe a significant amount of the variance in the dataset. The first three factors identified in all datasets are essentially identical, suggesting that these associations are valid and may represent real geochemical processes.

Approximately 44% of total variance is explained by Factor 1. Variables strongly correlated with this factor are all of the REE and redox sensitive elements (P, V, Cr, Fe, Mn, Co, As, Mo, Pb, U). Therefore, Factor 1 likely indicates dolomite recrystallization by upward-migrating REE-enriched fluids expelled along faults and fractures. The fault network in the Western Canada Sedimentary Basin was previously studied by Lyatsky and Pana (2003) and Lyatsky *et al.* (2005) and is schematically shown in Figure 8.5. The fluids ascending through fault systems might have changed the redox conditions to a more reducing state. A possible byproduct of this reaction might be Fe-sulfides that occur mainly around faults.

Factor 2 explains 16.1% of the total variance in the dataset. Variables strongly correlated with Factor 2 are elements associated with siliciclastic minerals, as well as the Sr-isotopes, mol%$CaCO_3$, Ca and Mg. Factor 2 is interpreted to reflect the presence of clays in dolomite samples. These clays might have been originally incorporated as inclusions within the dolomite crystals, but are now occurring in seams between crystals, as supported by negative correlation between the Sr-isotopes and mol%$CaCO_3$, Ca and Mg.

171

Alternatively, radiogenic Sr-isotopes might have been picked up by the dolomitizing fluids circulating through the overlaying shales.

Factor 3 contributes 8.2% to the total variance in the dataset. Variables strongly correlated with this factor are Cu, Zn, Pb and Sn. Factor 3 likely indicates the hydrothermal signal from the fluids coming upward along the faults that were reactivated during Paleozoic. It is interesting that both Factors 1 and 3 indicate the fault systems, and the variables representative for these factors (REE-Fe-Mn-Sr and Cu-Pb-Zn) show significantly increased concentrations in exactly the same locations (Figures 6.4.2-6.4.4 and 6.4.7-6.4.11). This suggests that the same faults were carrying different fluids at different times.

Variables moderately associated with factor 4 are δ^{13}C, Ca, Mg, Se and Ru. As discussed in Section 8.3.2.2, changes in δ^{13}C composition could be resulted from thermochemical (TSR) sulfate reduction or microbial fermentation of organic matter. Therefore, this factor likely indicates TSR or fermentation signals acquired during recrystallization of these dolomites.

Factor 5 of the smaller subset is correlated with depth (TWP), oxygen isotopes, Li, B and Ba. Oxygen isotopes are positively correlated with depth (TWP) indicating that this is a temperature-driven recrystallization (see Section 8.3.2.2).

Variables associated with Factor 10 (larger subset) are the negatively correlated δ^{13}C and δ^{18}O isotopes. These variables are very weakly correlated with this factor. When plotted against each other, these variables do not show a clear negative correlation, as suggested by factor analysis (Figure 6.2.2.4). However, this correlation might appear when a third variable is introduced creating a 3-dimensional plot (δ^{13}C vs. δ^{18}O vs. third variable).

Variables associated with Factor 4 (smaller subset) and Factor 9 (larger subset) are the depth and mol%$CaCO_3$. These factors indicate that the dolomites acquire more stoichiometric compositions with depth, because both variables are positively correlated with each other.

Cluster analysis was used to test for geochemical similarities in groups of samples from different depths and locations along the Rimbey-Meadowbrook Reef Trend and to group samples into smaller sets for further interpretation. However, cluster analyses performed on the dataset did not reveal any spatial relationship in sample distribution. Various algorithms with various combinations of data variables in a number of statistical programs (MINITAB, IBM SPSS, and R) showed similar distribution of clusters along the reef trend. This distribution did not show any spatial coherence and is probably due to recrystallization of the rocks during diagenesis. This recrystallization overprinted the original geochemical signatures of the rocks resulting in relatively similar clusters.

Discriminant analysis was used to test for and identify chemical variables that distinguish groups of samples based on the predetermined parameters of geographic location and types of dolomite. No obvious systematic relationship between the variables, representing different petrographic/ geographic groups of samples, was observed except for Li and Ru when plotted against the petrographic type (R1, R2, R3, and R4, Figure 7.3.1), and Pr and Eu when plotted against the geographic groups (Locations 1 to 4) discussed in Section 7.3 (Figure 7.3.2).

Discriminating by petrographic type revealed that the samples formed three geochemically distinct groups R1, R3 and R4. However, all of these groups (R1, R3 and R4) overlapped with group R2 (Figure 7.3.1). This shows that dolomites R1, R3 and R4 differ in terms of Li and Ru that are present in these samples only in very small amounts. Even though different dolomite types did not show any differences in terms of more abundant elements, this difference might appear a 3-dimentional plot.

Discriminating by location displayed distinct differences between samples from Location 2 and Location 3 (with a minor overlap with Location 2) and a combined sample set from locations 1 and 4 (Figure 7.3.2). Locations 1 and 4 formed a similar group, likely due to their values being close to the detection limit.

Multivariate statistical analysis helped to understand what processes might have driven recrystallization along the Rimbey-Meadowbrook Reef Trend. Six main processes that likely explain the associations of the variables are:

1) dolomite recrystallization by REE-enriched fluids expelled along faults and fractures;

2) dolomite recrystallization by fluids circulating through the overlaying shales;

3) dolomite recrystallization by hydrothermal fluids expelled along faults and fractures;

4) dolomite recrystallization in the presence of TSR or microbial fermentation in the system;

5) temperature-driven recrystallization;

6) stabilization to a more stoichiometric dolomite phase with depth.

8.5 Synopsis

Most dolomite samples of the Rimbey-Meadowbrook Reef Trend exhibit nearly stoichiometric compositions, with depleted $\delta^{18}O$ values and enriched $^{87}Sr/^{86}Sr$ ratios that, according to Al-Aasm and Packard (2000), can be interpreted as the result of recrystallization by "warmer" basinal fluids and re-equilibration during progressive burial. As opposed to Al-Aasm and Packard (2000), who showed spatially separated data clouds with increasing degree of 'significant' recrystallization, the present study could not identify such distinct groups. Rather, the data of matrix dolomites R1, R2 and R3 show significant or nearly total overlap for nearly all parameters investigated (*e.g.,* Figure 6.2.2.3). Dolomite cements DC1, DC2, and DC4 also overlap with matrix dolomites, but on their own they form two distinct clusters at least for some parameters (Figure 6.2.2.4).

Petrographic data presented in this study show signs of 'significant' recrystallization of dolomite R1 to dolomites R2 and/or R3 (Table 8.5). XRD data show that all dolomites are nearly stoichiometric, which may or may not be the result of recrystallization. The oxygen isotope analysis demonstrates that all matrix dolomite samples are 'significantly' recrystallized but the carbon isotope data represent 'insignificant' recrystallization, as do the Sr-isotope data. The elemental compositions show significant variation in the data that can be interpreted as resulting from 'significant' recrystallization.

None of the data from the Rimbey-Meadowbrook Reef Trend show a stepwise progression as hypothesized by Land (1992), nor do they display a trend representative of steady recrystallization with depth (Figure 1.1.3). However, these dolomites are herein

Table 8.5. An overview table showing the degree of recrystallization of matrix dolomites along the Rimbey-Meadowbrook Reef Trend for different parameters.

	'significant' recrystallization	'insignificant' recrystallization
Petrography	✔	
XRD	✔	
$\delta^{18}O$	✔	
$\delta^{13}C$		✔
$^{87}Sr/^{86}Sr$		✔
Elemental compositions	✔	

identified as 'significantly' recrystallized with respect to at least oxygen isotope ratios. Therefore, one of the possible alternatives for dolomite recrystallization described in Chapter 1 (p. 5) is "something other".

If the dolomites in the Rimbey-Meadowbrook Reef Trend did "stabilize" from metastable protodolomite to stoichiometric dolomite as discussed by Kaczmarek and Sibley (2007, 2011, 2014), this process likely took place within 1000 to 1500 years after initial dolomite formation. This initial recrystallization was probably insignificant (*sensu* Machel, 1997) and might have been overprinted by the later 'significant recrystallization'. Therefore, the multistage recrystallization described by Kaczmarek and Sibley (2007, 2011, 2014) is totally irrelevant to the present study considering the age of these rocks.

The timing of recrystallization and the exact causes of its apparent regional variability remain speculative, if not elusive. Increased temperature surely correlated with burial and major tectonic events, which also triggered or sustained major fluid flow in the basin. The two major tectonic events that might be responsible for such large scale fluid movement and subsequent recrystallization in the Alberta Basin were:

1) Antler Orogeny that occurred between the Late Devonian and Early Mississippian, and

2) Columbian/ Laramide Orogeny that occurred between the Late Jurassic and Early Tertiary.

According to paleomagnetic studies of Symons *et al.* (1999) and Lewchuk *et al.* (2000), all Middle Devonian to Mississippian matrix dolomites in the western side of the Western Canada Sedimentary Basin were remagnitized during deep burial associated with the late Laramide Orogenic event, erasing any earlier paleomagnetic signatures. They also suggested that this caused a massive fluid flow event, which recrystallized preexisting dolomites by increasing their crystal sizes, changing the crystal geometry and negatively shifting oxygen isotope values. This flow might also have resulted in saddle hydrothermal dolomite precipitation, MVT mineralization and hydrocarbon migration.

Metamorphic fluids rapidly expelled during the Laramide Orogeny were described as "squeegee flow" by Machel and Cavell (1999). However, this "squeegee flow" was not "powerful" enough to recrystallize matrix dolomites (Machel and Buschkuehle, 2008). Therefore, the dolomites of the Rimbey-Meadowbrook Reef Tend might have been

recrystallized either before the Laramide tectonic fluid expulsion (possibly during Antler Orogeny), or this recrystallization did not significantly affect the chemical composition of matrix dolomites.

This type of formation water flow driven by tectonic compression likely was channeled updip in the northward direction across the entire study area. In the central part, it may have been joined by cross-formation flow facilitated by the erosional surface of the sub-Cretaceous unconformity (Figure 8.5). This resulted in mixing of waters of meteoric origin with dense brines, especially in the places where the Ireton shales thin above Leduc buildups (Anfort, 1998; Anfort *et al*., 2001; Bachu *et al.,* 2008). This fluid mixing event might have significantly altered matrix dolomites in the region approximately between townships 44 and 60 causing orange-red zoned luminescence, depletion of $\delta^{18}O$ values and enrichment in $^{87}Sr/^{86}Sr$, trace elements and REE compositions. Additionally, this region is characterized by coarser crystal sizes.

Another meteoric water anomaly was discovered by Grasby and Chen (2005) who found that the brines discharging from the northern end of the Rimbey-Meadowbrook Reef Trend do not correlate geochemically with the deep-basin formation waters but exhibit mixed signatures of fresh water, dissolved evaporates and deeper basin brines. They proposed that subglacial meltwater intruded into the Devonian carbonates of the Rimbey-Meadowbrook Reef Trend during the Pleistocene/ early Holocene deep enough to dissolve Prairie evaporates, causing collapse features, karstification and calcitization of dolomites. The nature of these fluids was also supported by Gue (2012) and Gibson (2013), who found that fresh waters chemically altered through dissolution of evaporites are currently

Figure 8.5. Diagrammatic representation of the original flow of formation waters of the Rimbey-Meadowbrook Reef Trend (purple arrow) joined by cross-formation fluid through local breaching of the Ireton aquitard (blue and green arrows). Approximate area of mixing of connate and meteoric waters is circled on the map (modified from Bachu et al., 2008). Note the major fault systems along the reef trend, the locations of faults are taken from Lyatsky and Pana (2003) and Lyatsky et al. (2005).

179

discharging into the Athabasca river. Based on these findings, it was proposed that the present-day fluid flow in the Northern part of the reef trend does not necessarily reflect past fluid movements due to multiple changes in flow direction throughout the basin history. The modern fluid flow likely is a response to the disappearance of the glacier from the basin and probably does not represent the Laramide tectonically induced flow (Grasby and Chen, 2005).

Other fluid flow components causing recrystallization of matrix dolomites along the Rimbey-Meadowbrook Reef Trend might have been the upward-migrating fluids expelled along faults and fractures (Figure 8.5) that were activated during the Late Paleozoic and Mesozoic in the Western Canada Sedimentary Basement (Wright *et al.,* 1994; Lyatsky and Pana, 2003; Bottomley *et al.,* 2005; Lyatsky *et al.,* 2005).

CHAPTER 9

CONCLUSIONS

The objectives of this study, as originally outlined in Section 1.4, are as follows:

1. establish a paragenetic sequence from the diagenetic textures;

2. determine if there are any significant differences between the dolomites that occur in the Cooking Lake platform and the ones from the overlying Leduc reefs;

3. determine possible sources, timing and temperatures of the dolomitizing fluids from C, O, and Sr isotopes, and major and trace element compositions;

4. elucidate the origin of the dolomites and other diagenetic phases;

5. characterize the extent of dolomite recrystallization;

6. encompassing the previous points and with a reference to Figure 1.1.3, determine which theoretical alternative (steady recrystallization, stepwise recrystallization, no recrystallization, or other) applies to and/ or represents these dolomites.

All of these objectives have been successfully addressed, albeit to variable degrees, as follows.

Objective 1:

Eight textural types of dolomite were distinguished based on crystal size, crystal size distribution, and crystal geometry: fine-crystalline grey matrix dolomite (R1), medium- to coarse-crystalline grey matrix dolomite (R2), brown porous matrix dolomite (R3), mimetic dolomite (R4), unzoned dolomite cement (DC1), zoned dolomite cement (DC2), Fe-dolomite cement (DC3), saddle dolomite (DC4). According to the lithological relationship between the diagenetic features observed in the Rimbey-Meadowbrook Reef Trend and the geochemical characteristics of matrix dolomites and later cements, these diagenetic phases were placed in a paragenetic sequence.

Objective 2:

Cooking Lake and Leduc Formation dolomites did not exhibit any significant differences in petrography and geochemistry. In some areas, these two formations could not be distinguished due to the resemblance between the dolomites caused by complete dolomitization. On the geochemical cross-plots, samples from both formations were assigned different labels in order to test spatial relationships. However, the data from the Cooking Lake Formation consistently overlapped the data from the Leduc Formation. Cluster analysis did not reveal any spatial relationship in sample distribution either.

Objective 3:

Based on the geochemical analyses of samples obtained from the Cooking Lake and Leduc Formations, possible sources, timing and temperatures of the dolomitizing fluids are identified.

Fine crystalline matrix dolomite R1 is interpreted as the 'least-altered' dolomite phase that is geochemically and petrographically the closest to the initial replacive dolomite. The fluids responsible for initial dolomitization and early recrystallization are suggested to be normal to near-normal marine waters. Temperatures of formation were calculated to range between ~37 and 50 ºC. This temperature range corresponds to burial depths of approximately 200 to 900m placing dolomitization to Late Devonian – Early Carboniferous. The relative timing of R1 precipitation predates stylolitization but postdates the calcite cementation.

At least some medium crystalline matrix dolomite R2 and coarsely crystalline porous R3 are interpreted to have formed by further alteration of a microcrystalline R1 precursor at deeper burial and/or by warmer fluids. However, nothing in the available data rules out that the regional pattern of occurrence of R1 and R2 is largely the result of depositional/ primary textural patterns.

A potential source of the fluids, in which R1 recrystallized to R2 and/ or R3, is warm basinal brines forced through the rocks by compaction and possibly convection flow joined by cross-formation fluid flow in the central part of the study area. The mixing of waters of meteoric origin of the Lower Mannville and dense brines of the Cooking Lake aquifer might have affected a region between townships 44 and 60 causing depletion of $\delta^{18}O$ values and enrichment in $\delta^{13}C$, $^{87}Sr/^{86}Sr$, trace elements and REE compositions. Additionally, this region is characterized by coarser crystal sizes completely avoiding the fine matrix dolomites.

Other fluid flow components causing recrystallization of matrix dolomites might have been the upward-migrating fluids moving along faults and fractures that have been activated during Late Paleozoic.

Objective 4:

Matrix dolomites of the Rimbey-Meadowbrook Reef Trend could be described as having recrystallized during the progressive burial associated with the Antler Orogeny (Figure 8.2.2.3). The conclusion of no recrystallization in the study area made in the previous studies was found to be incorrect for at least a subset of the samples investigated in this study.

Objective 5:

The petrographic data presented in this study show signs of 'significant' recrystallization of dolomite R1 to dolomites R2 and/or R3. XRD data showed that all dolomites are nearly stoichiometric, which may or may not be a sign of 'significant' recrystallization. Stable isotope analysis demonstrates that all matrix dolomite samples are 'significantly' recrystallized with respect to $\delta^{18}O$. Major and trace element plots showed significant variation in data, which might have been a sign of 'significant' recrystallization (Table 8.5).

Early recrystallization likely occurred in matrix dolomite R1 as suggested by its coarser crystal size (30-62μm) relative to recent dolomite (commonly less than 4 μm) and depleted $\delta^{18}O$ values. This estimate places the timing of the earliest recrystallization into the Late Devonian to Early Carboniferous.

Objective 6:

Finally, petrography and geochemistry of the study area did not show the stepwise progression hypothesized by Land (1992). If the dolomites in the Rimbey-Meadowbrook Reef Trend did "stabilize" from metastable protodolomite to stoichiometric dolomite as discussed by Kaczmarek and Sibley (2007, 2011, 2014), this process likely took place within 1000 to 1500 years after initial dolomite formation. This initial recrystallization was probably insignificant and might have been overprinted by the later 'significant recrystallization'. Therefore, the multistage recrystallization described by Kaczmarek and Sibley (2007, 2011, 2014) is totally irrelevant to the present study, considering the age of Devonian reefs.

FUTURE RESEARCH

This thesis sets a number of objectives for future research projects:

1) Core wells north of township 70;

2) Sample matrix dolomites from the overlying Nisku formation in order to see if the same fluids that recrystallized Leduc dolomites affected Nisku dolomites as well;

3) Perform microdrilling on different zones of matrix dolomite R2 and R3 crystals and analyze the obtained powders for stable δ ^{13}C and δ ^{18}O and radiogenic Sr-isotopes;

4) Use clumped carbon and oxygen isotopes to calibrate the existing dataset;

5) Investigate fluid inclusions of matrix dolomites and saddle dolomite cements;

6) Use 'R' to complete Principal Component Analysis and Multi-Dimensional Scaling;

7) Use Rietveld analysis to define stoichiometry and ordering parameters from XRD.

REFERENCES

Al-Aasm, I.S., and Packard, J.J. 2000. Stabilization of early-formed dolomite: a tale of divergence from two Mississippian dolomites. *Sedimentary Geology*, **131**, 97-108.

Anderson, T.F. and Arthur, M.A. 1983. Stable isotope of oxygen and carbon and their application to sedimentologic and paleoenvironmental problems. *Stable Isotopes in Sedimentary Geology*, SEPM Short Course, **10**, 1–151.

Anderson, G.M. and Garven, G. 1987. Sulfate-sulfide-carbonate associations in Mississippi Valley Type lead-zinc deposits. *Economic Geology*, **82**, 442-448.

Anfont, S.J. 1998. Regional-scale hydrogeology of Lower Cretaceous to Middle Devonian aquifers in southeastern Alberta. M.Sc. Thesis, University of Calgary, 161p.

Anfont, S.J., Bachu, S., and Bentley, L.R. 2001. Regional-scale hydrogeology of the Upper Devonian-Lower Cretaceous sedimentary succession, south-central Alberta basin, Canada, *The American Association of Petroleum Geologists*, **85**, 637-660

Amthor, J.E., Mountjoy, E.W., and Machel, H.G. 1993. Subsurface dolomites in Upper Devonian Leduc Formation buildups, central part of Rimbey-Meadowbrook reef trend, Alberta, Canada. *Canadian Petroleum Geology Bulletin*, **41**, 164-185.

Amthor, J.E., Mountjoy, E.W., and Machel, H.G. 1994. Regional-scale porosity and permeability variations in Upper Devonian Leduc Buildups: implications for Reservoir Development and Prediction in Carbonates. *American Assosiation of Petroleum Geologist Bulletin*, **78**, 1541-1559.

Andrichuk, J.M. 1958a. Statigraphy and facies analysis of Upper Devonian reef in Leduc, Stettler, and Redwater areas, Alberta. *American Assosiation of Petroleum Geologists Bulletin*, **42**, 1-93.

Andrichuk, J.M. 1958b. Cooking Lake and Duvernay (Late Devonian) sedimentation in Edmonton area of central Alberta, Canada. *American Association of Petroleum Geologists Bulletin*, **42**, 2189-2222.

Anfort, S.J., Bachu, S., Bentley, L.R., 2001. Regional-scale hydrogeology of the Upper Devonian-Lower Cretaceous sedimentary succession, south-central Alberta Basin, Canada. *American Association of Petroleum Geologists Bulletin*, **85**, 637–660.

Azmy, K., Brand, U., Sylvester, P., Gleeson, S. A., Logand, A., Bitner, M. A. 2011. Biogenic and abiogenic low-Mg calcite (bLMC and aLMC): Evaluation of seawater-REE composition, water masses and carbonate diagenesis. *Chemical Geology*, **280**, 180–190.

Azmy, K., Knight, I., Lavoie, D., Chi, G. 2009. Origin of dolomites in the Boat Harbour Formation, St. George Group, in western Newfoundland, Canada: implications for porosity development. *Bulletin of Canadian Petroleum Geology*, **57(1)**, 81-104.

Azomani, E., Azmy, K., Blamey, N., Brand U. and Al-Aasm, I. 2013. Origin of Lower Ordovician dolomites in eastern Laurentia: Controls on porosity and implications from geochemistry. *Marine and Petroleum Geology*, **40**, 99-114.

Bachu, S. 1995. Synthesis and model of formation-water flow, Alberta Basin, Canada. *AAPG Bulletin*, **79 (8)**, 1159-1178.

Bachu, S., Buschkuehle, M., Haug, K., and Michael, K. 2008. Subsurface characterization of the Edmonton-area acid-gas injection operations. *ERCB/AGS Special Report*, **92**, 134p.

Banner, J.L., 1995. Application of the trace element and isotope geochemistry of strontium to studies of carbonate diagenesis. *Sedimentology*, **42**, 805-824.

Barfoot, G.L. and Ko, S.C.M. 1987. Assessing, and compensating for, the impact of the Leduc D-3A gas cap Blowdown on the other Golden Trend pools. *Journal of Canadian Petroleum Technology*, July-August, 28-36.

Barnaby, R.J., and Read, J.F. 1992. Dolomitization of a carbonate platform during late burial: Lower to Middle Cambrian shady dolomite, Virginia Appalachians. *Journal of Sedimentary Petrology*, **62(6)**, 1023-1043.

Barton, E.D., Bau, M., and Alexander, B. 2006. Preservation of primary REE patterns without Ce anomaly during dolomitization of Mid-Paleoproterozoic limestone and the potential re-establishment of marine anoxia immediately after the 'Great Oxidation Event'. *South African Journal of Geology*, **109**, 81–86.

Baugh, J.E. 1950. Leduc D-3 Zone Pool. *Reservoir Engineering*, **126**, 32-36.

Bein, A. and Land, L.S. 1983. Carbonate sedimentation and diagenesis associated with Mg-Ca chloride brines: the Permian San Andres Formation in the Texas Panhandle. *Journal of Sedimentary Petrology*, **53**, 243-260.

Behrens, E.W., and Land, L.S. 1972. Subtidal Holocene dolomite, Baffin Bay. Texas. *Journal of Sedimentary Petrology*, **42**, 155-161.

Berner, R.A. 1978. Rate control of mineral dissolution under earth surface conditions. *American Journal of Science*, **278**, 1235 – 1252.

Blakey, R. 2014. Late Devonian, *Paleogeography and geologic evolution of North America*. Retrieved from http://www2.nau.edu/rcb7/namD360.jpg.

Bottomley, D. J., Clark, I. D., Battye, N., Tom Kotzer, T. 2005. Geochemical and isotopic evidence for a genetic link between Canadian Shield brines, dolomitization in the Western Canada Sedimentary Basin, and Devonian calcium-chloridic seawater. *Canadian Journal of Earth Sciences*, **42**, 2059–2071.

Broughton, P. L. 2013. Devonian salt dissolution-collapse breccias flooring the Cretaceous Athabasca oil sands deposit and development of lower McMurray Formation sinkholes, northern Alberta Basin, Western Canada. *Sedimentary Geology*, **283(C)**, 57–82.

Budai, J.M., Lohmann, K.C. and Wilson, J.L. 1987. Dolomitization of the Madison Group, Wyoming and Utah Overthrust Belt. *American Association of Petroleum Geologists Bulletin*, **71(8)**, 909-924.

Burke, W.H., Denison, R.E., Hetherington, E.A.. Koepnick, R.B., Nelson, H.F., and Otto, J.B., 1982. Variation of seawater $^{87}Sr/^{86}Sr$ throughout Phanerozoic time. *Geology*, **10**, 516-519.

Carballo, J.D., Land, L.S. and Miser, D.E. 1987. Holocene dolomitization of supratidal sediments by active tidal pumping, Sugarloaf Key, Florida. *Journal of Sedimentary Petrology*, **57**, 153-165.

Carpenter, A.B. 1980. The chemistry of dolomite formation 1: the stability of dolomite. *In:* Concepts and Models of Dolomitization, *The Society Economic Paleontologists and Mineralogists Special Publications,* **28**, 111-121.

Carpenter, S.J. and Lohmann, K. C. 1989. ^{18}O and ^{13}C variations in Late Devonian marine cements from Golden Spike and Nevis reefs, Alberta, Canada. *Journal of Sedimentary Petrology*, **59**, 792-814.

Claypool, G.E. and Kaplan, I. R. 1974. The origin and distribution of methane in marine sediments. *Natural Gasses in Marine Sediments*, 99-139.

Clayton R. N., Friedman I., Graf D. L., Mayeda T. K., Meents W. F.. and Shimp N. F. 1966. The origin of saline formation waters: I. Isotopic composition. *Journal of Geophysical Research*, **71**, 3869-3882.

Clayton, R.N., Skinner, H.C., Berner, R.A. and Rubinson, M. 1968. Isotopic compositions of recent South Australian lagoonal carbonates. *Geochimica et Cosmochimica Acta*, **32**, 983–988.

Creaney, S., Allan, J., Cole, K.S., Fowler, M.G., Brooks, P.W., Osadetz, K.G., Macqueen, R.W., Snowdon, L.R. and Riediger, C.L. 1994. Petroleum generation and migration in the Western Canadian Sedimentary Basin. in Mossop, G., and Shetsen, I., eds.,

Geologic Atlas of the Western Canada Sedimentary Basin. Calgary, Canadian Society of Petroleum Geologists and Alberta Research Council, Calgary, 455-468.

Cummins, R.C., Finnegan, S., Fike, D.A., Eiler, J.M., Fischer, W.W. 2014. Carbonate clumped isotope constraints on Silurian ocean temperature and seawater δ^{18}O. *Geochimica et Cosmochimica Acta*, **140**, 241-258.

Dawans, J.M. and Swan, P.K. 1988. Textural and geochemical alteration in late Cenozoic Bahamian dolomites. *Sedimentology*, **35**, 385-403.

Degens, E.T. and Epstein, S. 1962. Relation between ^{18}O/^{16}O ratios in coexisting carbonates, cherts, and diatomites. *American Association of Petroleum Geologists Bulletin*, **46**, 534-542.

Dembicki, E.A. and Podivinsky, T.J. 2012. Heavy Oil from an Ancient Reef. GEOExPro, **9 (6)**, 42–46.

Dickson, J.A.D. 1966. Carbonate identification and staining as revealed by staining. *Journal of Sedimentary Petrology*, **36 (2)**, 491-505.

Dix, G.R. 1993. Patterns of burial and tectonically controlled dolomitization in an Upper Devonian fringing-reef complex, Leduc Formation, Peace River Arch area, Alberta, Canada. *Journal of Sedimentary Petrology*, **63**, 628–640.

Drivet, E., 1993. Diagenesis and reservoir characteristics of Upper Devonian Leduc dolostones, southern Rimbey-Meadowbrook reef trend, central Alberta. M.Sc.. thesis, McGill University, Montreal, 112p.

Drivet, E., and Mountjoy, E.W. 1997. Dolomitization of the Leduc Formation (Upper Devonian), southern Rimbey-Meadowbrook reef trend, Alberta. *Journal of Sedimentary Research*, **67**, 411-423.

Duggan, J.P. 1997. Sedimentology and diagenesis of Swan Hills Simonette oil field, west-central Alberta. M.Sc. Thesis, McGill University, Montreal, 177p.

Duggan, J.P., Mountjoy, E.W., and Stasiuk, L.D. 2001. Fault-controlled dolomitization at Swan Hills Simonette oil field (Devonian), deep basin west-central Alberta, Canada. *Sedimentology*, **48**, 301-323.

Durocher, S., and Al-Aasm, I.S., 1998. Dolomitization and neomorphism of Mississipian (Visean) Upper Debolt Formation, Blueberry Field, northeastern British Columbia: geological, petrologic, and chemical evidence. *American Association of Petroleum Geologists Bulletin*, **81**, 954-977.

Fabricius. I. L. 2000. Interpretation of burial history and rebound from loading experiments and occurrence of microstylolites in mixed sediments of Caribbean sites 999 and 1001. In: Leckie. R.M., Sigurdsson. H., Acton. G.D., Draper. G. (Eds.). *Proceedings of the Ocean Drilling Program. scientific results,* **165**, 177-190.

Feazel, C.T. and Schatzinger, R.A. 1985. Prevention of carbonate cementation in petroleum reservoirs. *SEPM Special Publication*, **36**, 97 -106.

Folk, R.L. 1962. Spectral subdivision of limestone types, in Ham, W.E., editor, *Classification of carbonate Rocks: American Association of Petroleum Geologists Memoir,* **1** 62-84.

Folk, R.L., 1965, Some aspects of recrystallization in ancient limestones. *In:* Dolomitization and Limestones Diagenesis, *SEPM Special Publications*, **13**, 14–48.

Frank, J.R., 1981. Dedolomitization in the Taum Sauk Limestone (Upper Cambrian), Southeast Missouri. *Journal of Sedimentary Petrology*, **51**, 7-18.

Friedman, G.M., l965. Terminology of crystallization textures and fabrics in sedimentary rocks. *Journal of Sedimentary Petrology*, **35**, 643-655.

Friedman, G.M., l975. The making and unmaking of limestones or the downs and ups of porosity. *Journal of Sedimentary Petrology*, **45(2)**, 379-398.

Friedman I. and O'Neil J.B. 1977. Compilation of stable isotope fractionation factors of geochemical interest. *In:* Data of Geochemistry. *US Geological Survey Professional Paper*, 440-KK, **6**.

Gao, G. 1990. Geochemical and isotopic constraints on the diagenetic history of a massive stratal, late Cambrian (Royer) dolomite, Lower Arbuckle Group, Slick Hills, SW Oklahoma, USA. *Geochimica et Cosmochimica Acta*, **54**, 1979-1989.

Gao, G. and Land, L.S. 1991. Early Ordovician Cool Creek Dolomite, Middle Arbuckle Group, Slick Hills, southwestern Oklahoma, U.S.A.: origin and modification. *Journal of Sedimentary Petrology*, **61**, 161-173.

Gasparrini, M., Bechstadt, T., Boni, M. 2006. Massive hydrothermal dolomites in the southwestern Cantabrian Zone (Spain) and their relation to the Late Variscan evolution. *Marine and Petroleum Geology*, **23(5)**, 543-568.

Gibson, J.J., Fennell, S.J., Birks, J.J., Yi, Y., Moncur, M.C., Hansen, B., Jasechko, S. 2013. Evidence of discharging saline formation water to the Athabasca River in the oil sands mining region, northern Alberta. *Canadian Journal of Earth Science*, **50**, 1244-1257.

Given, R.K. and Wilkinson, B.H. 1987. Dolomite abundance and stratigraphic age: constraints on rates and mechanisms of Phanerozoic dolostone formation. *Journal Sedimentary Petrology*, **57**, 1068-1078.

Grasby, S.E. and Chen, Z. 2005. Subglacial recharge into the Western Canada Sedimentary Basin– Impact of Pleistocene glaciation on basin hydrodynamics. *GSA Bulletin*, **117(3/4)**, 500-514.

Green, D. G. and Mountjoy, E. W. 2005. Fault and conduit controlled burial dolomitization of the Devonian west-central Alberta Deep Basin. *Bulletin of Canadian Petroleum Geology*, **53(2)**, 101-129.

Gregg, J.M., Howard, S.A., and Mazzullo, SJ. 1992. Early diagenetic recrystallization of Holocene (<3000 years old) peritidal dolomites, Ambergris Cay, Belize. *Sedimentology*, **39**, 143-160.

Gue, A. 2012. The geochemistry of saline springs in the Athabasca oil sands region and their impact on the Clearwater and Athabasca Rivers. M.Sc. Thesis, University of Calgary, 159p.

Gussow, W.C. 1954. Differential entrapment of oil and gas - A fundamental principle. *American Association of Petroleum Geologists Bulletin*, **38**, 816–853.

Haeri-Ardakani, O., Al-Aasm, I.S., Coniglio, M. and Samson, I. 2013. Diagenetic evolution and associated mineralization in Middle Devonian carbonates, southwestern Ontario, Canada. *Canadian Society of Petroleum Geologists Bulletin*, **61**, 41–58.

Hardie, L.A., 1987. Dolomitization: a critical view of some current views. *Journal of Sedimentary Petrology*, **57(1)**, 166-183.

Hearn, M. R. 1996. Stratigraphic and diagenetic controls on aquitard integrity and hydrocarbon entrapment, Bashaw Reef Complex, Alberta, Canada. M.Sc. thesis, University of Alberta, Edmonton, 135 p.

Hitchon, B. 1969. Fluid flow in the Western Canada Sedimentary Basin. Effect of geology. *Water Resources Research,* **5**, 186-195.

Hitchon, B. and Friedman, I. 1969. Geochemistry and origin of formation waters in the western Canada sedimentary basin-I. Stable isotopes of hydrogen and oxygen. *Geochimica et Cosmochimica Acta*, **33**, 1321 - 1349

Horrigan, E. 1996. Extent of dolomite recrystallization along the Rimbey-Meadowbrook Reef Trend, Western Canada Sedimentary Basin, Alberta, Canada. M.Sc. thesis. University of Alberta, Edmonton, 156p.

Huebscher, H. 1996. Regional controls on the stratigraphic and diagenetic evolution of Woodbend Group carbonates, north-central Alberta, Canada. Ph.D. thesis, University of Alberta, Edmonton, 231p.

Hugo, K.J. 1990. Mechanisms of ground water flow associated with Leduc reefs. *Bulletin of Canadian Petroleum Geology*, **38**, 307-319.

Humphrey, J.D. 1988. Late Pleistocene mixing zone dolomitization, southeastern Barbados, West Indies. *Sedimentology*, **35**, 327-348.

Hurley, N.F., and Lohmann, K.C. 1989. Diagenesis of Devonian reefal carbonates in the Oscar Range, Canning Basin, Western Australia. *Journal of Sedimentary Petrology*, **59**, 127-146.

IBM Corporation. 2013. IBM SPSS Statistics for Windows, Version 22.0. Armonk, NY: IBM Corporation.

Illing, L.V.1956. Dolomitization in relation to porosity in carbonate rocks. *American Assosiation of Petroleum Geologists, Program of 41st Annual Meeting*, 13-14.

Illing, L.V. 1959. Deposition and diagenesis of some Upper Paleozoic carbonate sediments in western Canada. *Proceedings of the Fifth World Petroleum Congress*, **1**, 23–52.

Imperial Oil Limited Geological Staff. 1950. Devonian Nomenclature in the Edmonton Area, Alberta, Canada. *American Association of Petroleum Geologists Bulletin*, **34**, 1807-1825.

Irwin, H., Curtis, C., and Coleman, M. 1977. Isotopic evidence for source of diagenetic carbonates formed during burial of organic-rich sediments. *Nature*, **269**, 209-213.

Jones, J.B., and Rostron, B.J. 2000. Analysis of flow constraints in regional-scale reflux dolomitization: Constant versus variable-flux hydrogeological models. *Bulletin of Canadian Petroleum Geology*, **48**, 230-245.

Kaczmarek, S.E., and Sibley D.F. 2007. A comparison of nanometer-scale growth and dissolution features on natural and synthetic dolomite crystals; implications for the origin of dolomite: *Journal of Sedimentary Research*, **77(5)**, 424-432.

Kaczmarek, S.E., and Sibley D.F. 2011. On the evolution of dolomite stoichiometry and cation order during high temperature synthesis experiments; an alternative model for the geochemical evolution of natural dolomites. *Sedimentary Geology*, **240(1-2)**, 30-40.

Kaczmarek, S.E., and Sibley D.F. 2014. Direct physical evidence of dolomite recrystallization. *Sedimentology*, **61**, 1862-1882.

Katz, A., and Matthews, A. 1977. The dolomitization of $CaCO_3$: an experimental study at 252–292C. *Geochimica et Cosmochimica Acta*, **41**, 297–308.

Kaufman, J. 1989. Sedimentology and diagenesis of the Swan Hills Formation (Devonian), Rosevear Field, Alberta, Canada. Ph.D. thesis, State University of New York, Stony Brook, New York, 412p.

Kaufman, J., Meyers, W.J., Hanson, G.N. 1990. Burial cementation in the Swan Hills Formation (Devonian), Rosevear Field, Alberta, Canada. *Journal of Sedimentary Petrology*, **60**, 918 – 933.

Keilly, R.A. 2004. Depositional facies and reservoir-enhancing dolomitization surrounding monadnocks in the Slave Point Formation, Dawson Field, Alberta, Canada. M.Sc. thesis, University of Alberta, Edmonton, 141p.

Kupecz, J.A. and Land, L.S. 1991. Late-stage dolomitization of the Lower Ordovician Ellenburger Group, West Texas. *Journal of Sedimentary Petrology*, **61(4)**, 551-574.

Laflamme, A.K. 1990. Replacement dolomitization in the Upper Devonian Leduc and Swan Hills formations, Caroline area, Alberta, Canada. M.Sc. Thesis, McGill University, Montréal, 138p.

Lamari, L. 2008. Assess 2.0: Image analysis software for disease quantification (www.apsnet.org).

Land, L.S. 1980. The isotopic and trace element geochemistry of dolomite: the state of the art. *In* Concepts and models of dolomitization, *Society Economic Paleontologists and Mineralogists Special Publication*, **28**, 87-110.

Land, L.S. 1983. Dolomitization: Education Course Note Series no. 24. American Association of Petroleum Geologist Education Conference, Denver, Colorado, 34p.

Land, L.S. 1985. The origin of massive dolomite. *Journal of Geological Education*, **33**, 112-125.

Land, L.S. l986. The carbon and oxygen isotopic chemistry of surficial Holocene shallow marine carbonate sediment and Quaternary limestone and dolomite. *Handbook of Environmental Isotope Geochemistry*, **3**, 191- 217.

Land, L.S., 1991. Dolomitization of the Hope Gate Formation (north Jamaica) by seawater: Reassessment of mixing-zone dolomite. *In:* Stable isotope geochemistry: a tribute to Samuel Epstein. *Geochemical Society Special Publication*, **3**, 121-134.

Land, L.S. 1992. The quantum theory of dolomite stabilization: does dolomite stabilize by 'Ostwald steps?' Proceedings of National Conference of Earth Sciences, Banff, Alberta. *Canadian Society of Petroleum Geologists Bulletin*, 2p.

Land, L.S., and Hoops, G.K. 1973. Sodium in carbonate sediments and rocks: A possible index to the salinity of diagenetic solutions. *Journal of Sedimentary Petrology*, **43**, 614-617.

Leach, D.L., Bradley, D.C., Huston, D., Pisarevsky, S.A., Taylor, R.D., and Gardoll, S.J. 2010. Sediment-hosted lead-zinc deposits in Earth history. *Economic Geology*, **105**, 593–625.

Lewchuk, M.T., Al-Aasm, I.S., Symons, D.T.A. and Gillen, K.P., 2000. Late Laramide dolomite recrystallization of the Husky Rainbow "A" hydrocarbon Devonian Reservoir, northwestern Alberta, Canada: paleomagnetic and geochemical evidence. *Canadian Journal of Earth Science*, **37**, 17-29.

Lind, I.L. 1993. Stylolites in chalk from Leg 130, Ontong Java Plateau. *In* Berger, W.H., Kroenke, L.W., Mayer, L.A., et al., *Proceedings. ODP, Sci. Results,* **130**, 673–686.

Lippman, F. 1973. Sedimentary carbonate minerals. Springer-Verlag/Berlin, New York, 228p.

Lockock, A. 2012. Recommended Method for Semi-quantitative Measurement of Aragonite – Calcite – Dolomite Mixtures by Powder X-ray Diffraction. Dept. of Earth and Atmospheric Sciences in-house report, University of Alberta.

Lomando, A.J. 1992. The influence of solid reservoir bitumen on reservoir quality. *American Assosiation of Petroleum Geologists Bulletin*, **76(8)**, 1137-1152.

Lorens, R.B., 1981, Sr. Cd, Mn and Co distribution coefficients in calcite as a function of calcite precipitation rate. *Geochimica et Cosmochimica Acta*, **45**, 553-561.

Lowenstein, T.K., Hardie, L.A., Timofeeff, M.N., and Demicco, R.V. 2003. Secular variation in seawater chemistry and the origin of calcium chloride basinal waters. *Geology*, **31**, 857–860.

Lucia, F.J. 2007. Carbonate reservoir characterization: an integrated approach. Berlin. Springer.

Lumsden, D.N., and Chimahusky. J.S. l980. Relationship between dolomite nonstoichiometry and carbonate facies parameters. *Society of Economic Paleontologists and Mineralogists Special Publications*, 28, 123-137.

Lyatsky, H.V. and Pană, D.I. 2003. Catalogue of selected regional gravity and magnetic maps of northern Alberta; Alberta Energy and Utilities Board, EUB/AGS Special Report 56, 43 p.

Lyatsky, H.V., Pană, D.I. and Grobe, M. 2005. Basement structure in central and southern Alberta: insights from gravity and magnetic maps; Alberta Energy and Utilities Board, EUB/AGS Special Report 72, 83 p.

Machel, H.G. 1985. Facies and diagenesis of the Upper Devonian Nisku Formation in the subsurface of Central Alberta. PhD. thesis, McGill University, Montreal, 392p.

Machel, H.G. 1989. Relationships between sulphate reduction and oxidation of organic compounds to carbonate diagenesis, hydrocarbon accumulations, salt domes, and metal sulphide deposits. *Carbonates and Evaporites*, **4(2)**, 137-151.

Machel, H.G. 1997. Recrystallization versus neomorphism, and the concept of 'significant recrystallization' in dolomite research. *Sedimentary Geology*, **113**, 161-168.

Machel, H.G. 2001. Bacterial and thermochemical sulfate reduction in diagenetic settings. *Sedimentary Geology*, **140**, 143-175

Machel, H.G. 2004. Concepts and models of dolomitization: a critical reappraisal. *In:* The Geometry and Petrogenesis of dolomite hydrocarbon reservoirs. *Geological Society, London, Special Publication*, **235**, 7-63.

Machel, H.G. 2005. Investigations of burial diagenesis in carbonate hydrocarbon reservoir rocks. *Geoscience Canada*, **32**, 103-128.

Machel, H.G. 2010. The Devonian Petroleum Systems of the Western Canada Sedimentary Basin – with implications for Heavy-oil Reservoir Geology. In: Chopra, S., Lines, L.R., Schmitt, D.R. and Batzle, M.L. (eds.): Heavy oils: Reservoir characterization and production monitoring. SEG *Geophysical Developments Series No. 13, Chapter 9*, 131-154.

Machel, H.G. and Anderson, J.H. l989. Pervasive subsurface dolomitization of the Nisku Formation in the central Alberta. *Journal of Sedimentary Petrology*, **59(6)**, 891-911.

Machel, H.G. and Burton, E.A. 1991. Factors governing cathodoluminescence in calcite and dolomite, and their implications for studies of carbonate diagenesis. In: Luminescence Microscopy and Spectroscopy: Qualitative and Quantitative Applications. C.E. Barker & O.C. editors. *SEPM Short Course Notes*, **25**, 37-57.

Machel, H.G. and Buschkuehle, B.E. 2008. Diagenesis of the Devonian Southesk-Cairn Carbonate Complex, Alberta, Canada: marine cementation, burial dolomitization, thermochemical sulfate reduction, anhydritization, and squeegee fluid flow. *Journal of Sedimentary Research*, **78**, 366-389.

Machel, H.G. and Cavell, P.A. 1999: Low-flux, tectonically induced squeegee fluid flow ("hot flash") into the Rocky Mountain Foreland Basin. *Bulletin Canadian Petroleum Geology* **47,** 510-533.

Machel, H.G., Mason, R.A., Mariano, A.N. and Mucci, A. 1991. Causes and emission of luminescence in calcite and dolomite. In: Luminescence Microscopy and Spectroscopy: Qualitative and Quantitative Applications. C.E. Barker & O.C. editors. *SEPM Short Course Notes*, **25**, 9-25.

Machel, H.G. and Mountjoy E.W. 1987, General constraints on extensive pervasive dolomitization – and their application to the Devonian Carbonates of Western Canada. *Bulletin of Canadian Petroleum Geology*, **22**, 269-304.

Machel, H.G., Mountjoy, E.W., and Amthor, J.E. 1996. Mass balance and fluid flow constraints on regional-scale dolomitization, Late Devonian, Western Canada Sedimentary Basin – Discussion. *Bulletin of Canadian Petroleum Geology*, **44**, 566- 571.

Machel H.G., Borrero, M. L., Dembicki, E., Huebscher, H., Ping, L., Zhao, Y. 2012. The Grosmont: the world's largest unconventional oil reservoir hosted in carbonate rocks. *Advances in Carbonate Exploration and Reservoir Analysis*, Geological Society of London Special Publications, **370**, 49-81.

Machel, H.G., Krouse, H.R. and Sassen R. 1995 Products and distinguishing criteria of bacterial and thermochemical sulfate reduction. *Applied Geochemistry*, **10**, 373-389.

Malone, M.J., Barker, P.A., and Bums, S. 1996. Recrystallization of dolomite: An experimental study from 50 to 200 °C. *Geochimica Cosmochimica Acta*, **60**, 2189-2207.

Marquez, X. 1994. Reservoir geology of Upper Devonian Leduc buildups, deep Alberta Basin. Ph.D. thesis, McGill University, Montreal, 285p.

Mattes, B.W. and Mountjoy, E.W. 1980. Burial dolomitization of the Upper Devonian Miette buildup, Jasper National Park, Albena. *In:* Concepts and models of dolomitization, *Society of Economic Paleontologists and Mineralogists Special Publication,* **28**, 259-297.

Mazzullo, S.J. 1992. Geochemical and neomorphic alteration of dolomite: a review. *Carbonates and Evaporites*, **6**, 21-37.

Mazzullo, S.J., Bischoff, W.D., and Teal, C.S. 1995. Holocene shallow-subtidal dolomitization by near-normal seawater, northern Belize. *Geology,* **23**, 341–344.

McKenzie, J.A. 1981. Holocene dolomitization of calcium carbonate sediments from the coastal sabkhas of Abu Dhabi, U.A.E: A stable isotope study. *Journal of Geology*, **89**, 185–198.

McKenzie, M.C. 1999. Carbonates of the Upper Devonian Leduc Formation, Southwestern Peace River Arch, Alberta: Indications for Tectonically-Induced Fluid Flow. M.Sc. thesis. University of Alberta, Edmonton, 131p.

McNutt R.H., Frape S.K. and Dollar P. 1987. A strontium, oxygen and hydrogen isotopic composition of brines, Michigan and Appalachian Basins, Ontario and Michigan. *Applied Geochemistry*, **2**, 495-505.

Merino E. and Canals, A. 2011. Self-accelerating dolomite-for-calcite replacement: sef-organized dynamics of burial dolomitization and associated mineralization. *American Journal of Science*, **311**, 573–607.

Migaszewski, Z.M. 1991. Devonian Dolomites from the Holy Cross Mts, Poland: A New Concept of the Origin of Massive Dolomites Based on Petrographic and Isotopic Evidence. *The Journal of Geology*, **99(2)**, 171-187.

Milliman, J.D., 1974. Marine carbonates. Springer-Verlag/Berlin, New York, 375p.

Minitab Inc. 2014. Minitab Statistical Software, version 17.1.0. State College, PA (www.minitab.com).

Montanez, I.P., and Read, J.F. 1992. Fluid-rock interaction history during stabilization of early dolomites, Upper Knox Group (Lower Ordovician), U.S. Appalachians. *Journal of Sedimentary Petrology*, **62(5)**, 753-778.

Morrow, D. W. 1998. Regional subsurface dolomitization: Models and constraints: *Geoscience Canada*, **25**, 57 – 70

Mossop, G., and Shetsen, I., eds. *Geologic Atlas of the Western Canada Sedimentary Basin. Calgary*, Canadian Society of Petroleum Geologists and Alberta Research Council, 510p.

Mountjoy, E.W and Amthor, J.E. 1994. Has burial dolomitization come of age? Some answers from the Western Canada Sedimentary Basin. *In*: Dolomites: a volume in honour of Dolomieu. *International Association of Sedimentologists Special Publication*, **21**, 203-229.

Mountjoy, E.W., Machel, H.G., Green, D., Duggan, J. and Williams-Jones, A.E. 1999. Devonian matrix dolomites and deep burial carbonate cements: A comparison between the Rimbey-Meadowbrook reef trend and the deep basin of westcentral Alberta. *Bulletin of Canadian Petroleum Geology* **42 (4)**, 487-509.

Mountjoy, E.W., and Marquez, X. 1997. Predicting reservoir properties in dolomites: Upper Devonian Leduc buildups, deep Alberta Basin. *American Association of Petroleum Geologists Bulletin*, **69**, 267–306.

Mountjoy, E.W., Qing H. and McNutt R.H. 1992. Strontium isotopic composition of Devonian dolomites, Western Canada Sedimentary Basin: significance of sources of dolomitizing fluids. *Applied Geochemistry*, **7**, 59-75.

Muehlenbachs, K. 1998. The oxygen isotopic composition of the oceans, sediments and the seafloor. *Chemical Geology*, **145**, 263-273.

Muhsin, E., Kaplan M.Y., and Selahattin, K. 2007. Petrography, Geochemistry and Origin of Lower Liassic Dolomites in the Aydincik Area, Mersin, Southern Turkey. *Turkish Journal of Earth Sciences*, **16**, 339-362.

Nader, F.H., Swennen, R., and Ellam R.M. 2007. Field geometry, petrography and geochemistry of a dolomitization front (Late Jurassic, central Lebanon). *Sedimentology*, **54**, 1093-1119.

Nesbitt, B.E., Prochaska, W., Muehlenbachs, K. and Morris, G. 1998. Paleo-fluid regimes during carbonate diagenesis in the Western Canada Sedimentary Basin. *Abstracts of the 15th International Sedimentological Congress, Alicante, Spain*, 575-576.

Nothdurft, L.D., Webb, G.E., and Kamber, B.S. 2004. Rare earth element geochemistry of Late Devonian reefal carbonates, Canning Basin, Western Australia: confirmation of a seawater REE proxy in ancient limestones. *Geochimica et Cosmochimica Acta*, **68**, 263–283.

Nordeng, S.H., and Sibley, D.F. 1994. Dolomite stoichiometry and Ostwald's step rule. *Geochimica et Cosmochimica Acta*, **58**, 191–196.

O'Connor, M.J. and Gretener, P.E. 1974. Differential compaction within the Woodbend Group of central Alberta. *Bulletin of Canadian Petroleum Geology*, **22**, 269-304.

Ostwald, W. 1897. Studien über die Bildung und Umwandlung fester Körper. 1. Abhandlung: Übersättigung und Überkaltung. *Zeitschrift für Physikalische Chemie*, **22**: 289–330.

Patey, K.S. 1995. Facies, stratigraphy, and the diagenesis of the Upper Devonian carbonates in the Obed area, West-Central Alberta, Canada. M.Sc. thesis, University of Alberta, 147p.

Potma, K, Weissenberger, J.A.W., Wong, P.K. and Gilhooly, M.G. 2001. Toward a sequence stratigraphic framework for the Frasnian of the Western Canada Basin. *Bulletin of Canadian Petroleum Geology*, **49(1)**, 37-85.

Qiang, N. 1990-1992. Unfinished PhD project, University of Alberta, Edmonton.

Qing, H. and Mountjoy, E. W. 1989. Multistage dolomitization in rainbow buildups, Middle Devonian Keg River Formation, Alberta, Canada. *Journal of Sedimentary Petrology*, **56(2)**, 237-247.

R Development Core Team. 2014. R: A language and environment for statistical computing, version 3.1.2. R Foundation for Statistical Computing, Vienna, Austria, (http://www.R-project.org).

Reeder, R.J. and Sheppard, C.E. 1984. Variation of lattice-parameters in some sedimentary dolomites. *American Mineralogist*, **69**, 520–527.

Rostron, B.J. 1995. Cross-formation fluid flow in Upper Devonian to Lower Cretaceous Strata, West-Central Alberta, Canada. Ph.D. thesis, University of Alberta, Edmonton, 201p.

Rostron, B.J., Toth, J., and Machel, H.G. 1997. Fluid flow, hydrochemistry and petroleum entrapment in Devonian reef complexes, south-central Alberta, Canada. *Basin-Wide Diagenetic Patterns: Integrated Petrologic, Geochemical, and Hydrologic Considerations*, **57**, 139-154.

Sass, E., Bein, A., and Almogi-Labin, A. 1991. Oxygen-isotope composition of diagenetic calcite in organic-rich rocks: evidence for ^{18}O depletion in marine anaerobic pore water. *Geology*, **19**, 839-842.

Searl, A., 1994. Discontinuous solid solution in Ca-rich dolomites: the evidence and implications for the interpretation of dolomite petrographic and geochemical data. *In* Dolomites, A volume in honour of Dolomieu. *International Association of Sedimentologists Special Publication*, **21**, 361-376.

Sharma, T. and Clayton, R.N. 1965. Measurement of $^{18}O/^{16}O$ ratios of total oxygen of carbonates. *Geochimica et Cosmochimica Acta*, **29**, 1347-1353.

Shields, G.A. and Stille, P. 2001. Diagenetic constraints on the use of cerium anomalies as palaeoseawater redox proxies: an isotopic and REE study of Cambrian phosphorites. *Chemical Geology*, **175**, 29 – 48.

Sibley, D.F. 1990. Unstable to stable transformations during dolomitization. *Journal of Geology*, **98**, 739-748.

Sibley, D.F., Gregg, G.M., Brown, R.G.. and Laudon, P.R. 1993. Dolomite crystal size distribution. *Carbonate Microfabrics, Frontiers in Sedimentology*, Springer-Verlag, New York, 195-204.

Sibley, D.F. and Gregg, G.M. 1987. Classification of dolomite rock textures. *Journal of Sedimentary Petrology*, **57**, 967-975.

Singh, W., Hjorleifsson, E., and Stefansson G. 2011. Robustness of fish assemblages derived from three hierarchical agglomerative clustering algorithms performed on Icelandic groundfish survey data. *ICES Journal of Marine Science*, **68(1)**, 189-200.

Smalley, P.C., Higgins, A.C., Howarth, R.J., Nicholson, H., Jones, C.E., Swinburne, N.H.M., Bessa, J. 1994. Seawater Sr isotope variations through time: a procedure for constructing a reference curve to date and correlate marine sedimentary rocks. *Geology*, **22**, 431–434.

Smith, T.M., and Dorobek, S.L. 1989. Dolomitization of the Devonian Jefferson Formation, South-Central Montana. *The Mountain Geologist*, **26(3)**, 81-96.

Sorby, H.C. 1858. On the microscopical structure of crystals , indicating the origin of minerals and rocks. *The Quarterly Journal of the Geological Society of London*, **14**, 453-500.

Sorby, H.C. 1887. On the microscopical structure of iron and steel. *Journal of the Iron and Steel Institute*, **2**, 254-288.

Sperber, C.M., Wilkinson, B.H., and Peacor, D.R. 1984. Rock composition, dolomite stoichiometry, and rock/water reactions in dolomitic carbonate rocks. *Journal of Geology*, **92**, 609-622.

Spőtl, C., and Vennemann, T. W. 2003. Continuous-flow isotope ratio mass spectrometric analysis of carbonate minerals. *Rapid Communications in Mass Spectrometry*, **17**, 1004–1006.

Stoakes, F.A., and Creaney, S., 1984, Sedimentology of a carbonate source rock: the Duvernay Formation of Central Alberta. *Canadian Society of Petroleum Geologists*, Core conference 1984, 132-147.

Symons, D.T.A., Enkin R. and Cioppa, M.T. 1999. Paleomagnetism in the Western Canada Sedimentary Basin: Dating fluid flow and deformation events. *Bulletin of Canadian Petroleum Geology*, **47(4)**, 534-547.

Sun, S.Q. 1995. Dolomite reservoirs: porosity evolution and reservoir characteristics. *American Association of Petroleum Geologists Bulletin*, **79**, l86-204.

Switzer, S., Holland, W., Christie, D., Graft, G., Heidenger, A., McAuley, R., Wierzbicki, R., and Packard, J., 1994. Devonian Woodbend-Winterburn strata of the Western Canada Sedimentary Basin, in Mossop, G., and Shetsen, I., eds., *Geologic Atlas of the Western Canada Sedimentary Basin. Calgary*, Canadian Society of Petroleum Geologists and Alberta Research Council, 165-195.

Tucker, M.E. and Wright, V.P. 1990. Carbonate Sedimentology: Oxford: Blackwell Scientific Publications, 482p.

Vahrenkamp, V.C. and Swart, P.K. 1990. New distribution coefficient for the incorporation of strontium into dolomite and its implications for the formation of ancient dolomites. *Geology*, **18**, 387-391.

Van Santen, R.A. 1984. The Ostwald step rule. *The Journal of Physical Chemistry*, **88**, 5768–5769

Veizer, J., Ala, D., Azmy, K., Bruckschen, P., Buhl, D., and Strauss, H. 1999. $^{87}Sr/^{86}Sr$, $\delta^{13}C$ and $\delta^{18}O$ evolution of Phanerozoic seawater, *Chemical Geology*, **161**, 59-88.

Veizer, J., Prokoph, A. 2015. Temperatures and oxygen isotopic composition of Phanerozoic oceans. *Earth-Science Reviews*, **146**, 92-104.

Veizer, J. 1983. Chemical diagenesis of carbonates: theory and application of trace element technique. *In* Stable Isotopes in Sedimentary Petrology, *Society of Economic Paleontologists and Mineralogists Short Course,* **10**, 3-1 to 3-100.

Waring, W.W., and Layer, D.B. 1950. Devonian dolomitized reef, D-3 reservoir, Leduc field, Alberta, Canada. *American Assosiation of Petroleum Geologists Bulletin*, **34**, 295-312.

Webb, G.E., Nothdurft, L.D., Kamber, B.S., Kloprogge, J.T., Zhao, J.-X., 2009. Rare earth element geochemistry of scleractinian coral skeleton during meteoric diagenesis: a before and-after sequence through neomorphism of aragonite to calcite. *Sedimentology*, **56**, 1433–1463.

Wendte, J., Qing, H., Dravis, J.J., Moore, S.L.O., Stasiuk, L.D., and Ward, G. 1998. High-temperature saline (thermoflux) dolomitization of Devonian Swan Hills platform and bank carbonates, Wild River area, west-central Alhena. *Bulletin of Canadian Petroleum Geology*, **46**, 210-265.

Whiticar M.J., Faber E., and Schoell M. (1986) Biogenic methane formation in marine and freshwater environments: CO_2 reduction vs. acetate fermentation-isotope evidence. *Geochimica et Cosmochimica Acta,* **50**, 693-709.

Wright, G.N., McMechan, M.E. and Potter, D.E.G. 1994. Structure and architecture of the Western Canada Sedimentary Basin; Chapter 3 in Geological atlas of the Western Canada Sedimentary Basin, G.D. Mossop and I. Shetsen (comp.), *Canadian Society of Petroleum Geologists and Alberta Research Council*, **4**, 25–40.

Zenger, D.H., and Dunham, J.B. 1988. Dolomitization of Siluro-Devonian limestones in a deep core (5,350 m), southeastern New Mexico. *In* Sedimentology and Geochemistry of Dolostones. *Society of Economic Paleontologists and Mineralogists Special Publication*, **43**, 161-173.

Zhu D., Jin, Z. and Hu, W. 2010. Hydrothermal recrystallization of the Lower Ordovician dolomite and its significance to reservoir in northern Tarim Basin. *Science China Earth Sciences*, **53(3)**, 368-381.

Appendix 1

Inventory of samples collected from the Leduc and Cooking Lake Formations along the Rimbey-Meadowbrook Reef Trend.

Leduc/ Cooking Lake Fm. sample inventory

TWN	Well ID					Pool	Original sample set	Sample ID	Depth		Stratigraphic unit	Core samples	Thin sections
	LSD	SEC	TWN	RGE	MER				(ft)	(m)			
T95	2	28	95	18	W4	Liege	Kuflevskiy	SK95-1	1274.6	388.5	Leduc	x	
								SK95-2	1276.2	389	Leduc	x	
								SK95-3	1279.5	390	Leduc	x	
								SK95-4	1281.3	390.55	Leduc	x	
								SK95-5	1282.8	391	Leduc	x	x
								SK95-6	1313.6	400.4	Leduc	x	x
								SK95-7	1363.3	415.55	Leduc	x	
								SK95-8	1365.1	416.1	Leduc	x	
								SK95-9	1366.6	416.55	Leduc	x	
								SK95-10	1418.2	432.27	Leduc	x	
								SK95-11	1419.8	432.77	Leduc	x	
								SK95-12	1426.4	434.77	Leduc	x	x
T88	3	34	88	20	W4	Orchid	Huebscher	HH88-1	1325	403.9	Leduc	x	x
								HH88-2	1334	406.6	Leduc	x	x
								HH88-3	1396	425.5	Leduc	x	x
								HH88-4	1500	457.2	Leduc	x	x
								HH88-5	1523	464.2	Leduc	x	x
								HH88-6	1530	466.3	Leduc	x	x
T72	11	4	72	23	W4	Canal	Huebscher	HH72-1	3051	930.0	Leduc	x	x
								HH72-2	3063	933.6	Leduc	x	x
								HH72-3	3071	936.1	Leduc	x	x
								HH72-4	3084	940.0	Leduc	x	x
								HH72-5	3114	949.1	Leduc	x	x
T71	15	17	71	25	W4	Smith	Huebscher	HH71-1	3013	918.4	Leduc	x	x
								HH71-2	3336	1016.8	Leduc	x	x
T70	3	28	70	24	W4	Bouvier	Huebscher	HH70-1	3448	1051.0	Leduc	x	x
								HH70-2	3506	1068.0	Leduc	x	x
								HH70-3	3518	1072.3	Leduc	x	x
								HH70-4	3528	1075.3	u. Cook. Lk.	x	x
								HH70-5	3558	1084.5	u. Cook. Lk.	x	x
								HH70-6	3568	1087.5	u. Cook. Lk.	x	x
T68	4	33	68	22	W4	Baptiste	Huebscher	HH68-1	3470	1057.7	l. Cook. Lk.	x	x
								HH68-2	3476	1059.5	l. Cook. Lk.	x	x

TWN	Well ID					Pool	Original sample set	Sample ID	Depth		Stratigraphic unit	Core samples	Thin sections
	LSD	SEC	TWN	RGE	MER				(ft)	(m)			
T67	13	17	67	23	W4	Big Coulee	Kuflevskiy	SK67-1	2942	896.7	Leduc	x	
								SK67-2	2958	901.6	Leduc	x	x
								SK67-3	3203	976.3	Leduc	x	x
T66	4	26	66	26	W4	Big Bend	Huebscher	HH66(1)-1	3411	1039.7	Leduc	x	x
								HH66(1)-2	4081	1243.9	Leduc	x	x
	6	16	66	24	W4	Steele	Huebscher	HH66(2)-1	2891	881.2	Leduc	x	x
								HH66(2)-2	3298	1005.2	Leduc	x	x
								HH66(2)-3	3421	1042.7	u. Cook. Lk.	x	x
								HH66(2)-4	3430	1045.5	u. Cook. Lk.	x	x
								HH66(2)-5	3620	1103.4	u. Cook. Lk.	x	x
								HH66(2)-6	3627	1105.5	u. Cook. Lk.	x	x
								HH66(2)-7	3677	1120.8	u. Cook. Lk.	x	x
								HH66(2)-8	3893	1186.6	u. Cook. Lk.	x	x
								HH66(2)-9	4073	1241.5	u. Cook. Lk.	x	x
T65	9	39	65	24	W4	Steele	Huebscher	HH-65-3	3456	1053.4	Leduc	x	x
	5	19	65	24	W4	Steele	Huebscher	HH65(2)-1	4013	1223.2	Cook. Lk.	x	x
								HH65(2)-2	4033	1229.3	Cook. Lk.	x	x
	12	6	65	24	W4	Bolloque	Huebscher	HH65(1)-1	3854.9	1175	Leduc	x	x
T64	3	24	64	25	W4	Bolloque	Huebscher	HH64-1	3625.8	1105.15	Leduc	x	x
T63	5	24	63	25	W4	Bolloque	Huebscher	HH63-1	3479	1060.4	Leduc	x	x
								HH63-2	3502	1067.4	Leduc	x	x
								HH63-3	3522	1073.5	Leduc	x	x
								HH63-4	3674	1119.8	Leduc	x	x
								HH63-5	3722	1134.5	Leduc	x	x
								HH63-6	3725	1135.4	Leduc	x	x
								HH63-7	4366	1330.8	Leduc	x	x
								HH63-8	4375	1333.5	Leduc	x	x
	9	36	63	25	W4	Bolloque	Huebscher	HH63-11	3449	1051.3	Leduc	x	x
								HH63-12	3456	1053.4	Leduc	x	x
								HH63-13	3461	1054.9	Leduc	x	x
T62	16	22	62	25	W4	Meadow	Huebscher	HH62-1	3690	1124.7	Leduc	x	x
								HH62-2	3695	1126.2	Leduc	x	x
								HH62-3	3701	1128.1	Leduc	x	x

TWN	Well ID					Pool	Original sample set	Sample ID	Depth		Stratigraphic unit	Core samples	Thin sections
	LSD	SEC	TWN	RGE	MER				(ft)	(m)			
								HH62-4	3710	1130.8	Leduc	x	x
								HH62-5	3720	1133.9	Leduc	x	x
T61	13	35	61	23	W4	Abee	Huebscher	B-15	3377	1029.3	Leduc	x	x
								B-16	3388	1032.7	Leduc	x	x
								B-17	3416	1041.2	Leduc	x	x
								B-18	3416	1041.2	Leduc	x	x
	1	32	61	23	W4	Abee	Huebscher	B-20	3752	1143.6	Leduc	x	x
								B-21	3762	1146.7	Leduc	x	x
								B-22	3776	1150.9	Leduc	x	x
								B-23	3807	1160.4	Leduc	x	x
	7	31	61	24	W4	Nestow	Huebscher	HH61-1	3491	1064.1	Leduc	x	x
								HH61-2	3493	1064.7	Leduc	x	x
								HH61-3	3496	1065.6	Leduc	x	x
T59	2	9	59	24	W4	Westlock	Kuflevskiy	SK59-1	3883	1183.6	Leduc	x	
								SK59-2	3885.6	1184.3	Leduc	x	x
								SK59-3	3892.1	1186.3	Leduc	x	
								SK59-4	3893.3	1186.7	Leduc	x	
T58	11	26	58	23	W4	Redwater	Kuflevskiy	SK58(1)-1	4236.2	1291.2	Cook. Lk.	x	
								SK58(1)-2	4238.6	1291.9	Cook. Lk.	x	x
								SK58(1)-3	4279.4	1304.4	Cook. Lk.	x	x
	2	5	58	25	W4	Legal	Kuflevskiy	SK58(2)-1	4623.5	1409.25	Leduc	x	x
								SK58(2)-2	4624.3	1409.5	Leduc	x	
								SK58(2)-3	4627.1	1410.35	Leduc	x	x
								SK58(2)-4	4628.4	1410.75	Leduc	x	
								SK58(2)-5	4631.7	1411.75	Leduc	x	
								SK58(2)-6	4634.9	1412.73	Leduc	x	
								SK58(2)-7	4635.4	1412.9	Leduc	x	
								SK58(2)-8	4638.7	1413.9	Leduc	x	
								SK58(2)-9	4640.7	1414.5	Leduc	x	
T57	3	21	57	24	W4	Fairydell-Bon Accord	Horrigan	EH-71	4034	1229.6	Leduc	x	x
								EH-72	4055	1236	Leduc	x	x
								EH-73	4075	1242.1	Leduc	x	x
T56	9	30	56	24	W4	Reavey	Horrigan	EH-74	4194	1278.3	Leduc	x	x

TWN	Well ID					Pool	Original sample set	Sample ID	Depth		Stratigraphic unit	Core samples	Thin sections
	LSD	SEC	TWN	RGE	MER				(ft)	(m)			
	16	24	56	26	W4	Morinville	Kuflevskiy	SK56-1	5255.5	1601.9	Cook. Lk.	x	
								SK56-2	5259.1	1603	Cook. Lk.	x	
								SK56-3	5264.0	1604.5	Cook. Lk.	x	
								SK56-4	5266.0	1605.1	Cook. Lk.	x	
								SK56-5	5279.8	1609.3	Cook. Lk.	x	
								SK56-6	5294.6	1613.8	Cook. Lk.	x	
								SK56-7	5304.7	1616.9	Cook. Lk.	x	x
								SK56-8	5310.3	1618.6	Cook. Lk.	x	
								SK56-9	5317.4	1620.75	Cook. Lk.	x	
								SK56-10	5319.7	1621.45	Cook. Lk.	x	x
T55	7	15	55	25	W4	Morinville	Horrigan	EH-75	4458	1358.8	Leduc	x	x
								EH-76	4464	1360.6	Leduc	x	x
								EH-77	4481	1365.8	Leduc	x	x
	2	16	55	25	W4	Morinville	Horrigan	EH-78	4880	1487.4	Leduc	x	x
								EH-79	5179	1578.5	Leduc	x	x
								EH-80	5330	1624.6	Cook. Lk.	x	x
	2	16	55	25	W4	Morinville	Kuflevskiy	SK55-1	4284	1305.8	Ireton	x	
								SK55-2	4326	1318.6	Ireton	x	
								SK55-3	4347	1325.0	Ireton	x	
								SK55-4	4372	1332.6	Leduc	x	x
								SK55-5	4890	1490.5	Leduc	x	x
								SK55-6	5186	1580.7	Leduc	x	
								SK55-7	5325	1623.1	Cook. Lk.	x	
	6	22	55	26	W4	Morinville	Horrigan	N-471	5125.4	1562.25	Leduc		x
								N 472	5158.1	1572.2	Leduc		x
								N-473	5427.1	1654.2	Leduc		x
	6	22	55	26	W4	Morinville	Qiang	N-470	5267.5	1605.6	Leduc		
								N-471	5131	1563.9			x
								N 472	5158	1572.2			x
								N-473	5247	1599.3			x
								N-474	5125.5	1562.3			
T54	14	18	54	25	W4	Morinville	Kuflevskiy	SK54-1	5347	1629.8	Cook. Lk.	x	x
	8	14	54	26	W4	Morinville	Kuflevskiy	SK54(2)-1	5291	1612.7	Leduc	x	
								SK54(2)-2	5294.6	1613.8	Leduc	x	
								SK54(2)-3	5301.3	1615.9	Leduc	x	
								SK54(2)-4	5306	1617.3	Leduc	x	
								SK54(2)-5	5308.6	1618.1	Leduc	x	x

TWN	Well ID					Pool	Original sample set	Sample ID	Depth		Stratigraphic unit	Core samples	Thin sections
	LSD	SEC	TWN	RGE	MER				(ft)	(m)			
T53	2	14	53	26	W4	Acheson	Horrigan	EH-65	5026.2	1532	Leduc	x	
								N-420	5069.2	1545.1	Leduc		x
	2	14	53	26	W4	Acheson	Qiang	N-426	4973.7	1516	Leduc		x
								N-425	5005.8	1525.8	Leduc		x
								N-423	5013.1	1528	Leduc		x
								N-422	5020.9	1530.4	Leduc		x
								N-421	5069.2	1545.1	Leduc		x
								N-420	5069.2	1545.1	Leduc		x
								N-419	5074.1	1546.6	Leduc		x
								N-418	5087.9	1550.8	Leduc		x
	10	4	53	25	W4	Acheson East	Kuflevskiy	K53-1	5551	1692.0	Cook. Lk.	x	
								K53-2	5560	1694.7	Cook. Lk.	x	x
								K53-3	5566.75	1696.8	Cook. Lk.	x	
T52	2	35	52	26	W4	Acheson	Qiang	N-434	?	?	Leduc		x
								N-435	?	?	Leduc		x
								N-436	?	?	Leduc		x
								N-437	?	?	Leduc		x
								N-438	?	?	Leduc		x
								N-439	5049.5	1539.1	Leduc		x
								N-440	?	?	Leduc		x
								N-441	?	?	Leduc		x
								N-443	?	?	Leduc		x
								N-444	?	?	Leduc		x
								N-446	?	?	Leduc		x
								N-447	?	?	Leduc		x
								N-450	5130.8	1563.9	Leduc		x
	15	23	52	26	W4	Acheson	Horrigan	EH-61	5037.3	1535.4	Leduc	x	x
								EH-62	5069.8	1545.3	Leduc	x	x
								EH-63	5076.2	1547.25	Leduc	x	x
								N-461	5076.7	1547.4	Leduc		x
								EH-64	5081.3	1548.8	Leduc	x	x
	15	23	52	26	W4	Acheson	Qiang	N-468	5011.4	1527.5	Leduc		
								N-467	5019.0	1529.8	Leduc		x
								N-466	5031.8	1533.7	Leduc		x
								N-465	5040.3	1536.3	Leduc		x
								N-464	5046.5	1538.2	Leduc		x
								N-462	5058.0	1541.7	Leduc		x
								N-461	5076.7	1547.4	Leduc		x
								N-459	5088.5	1551	Leduc		x
								N-458	5104.9	1556	Leduc		x

TWN	Well ID					Pool	Original sample set	Sample ID	Depth			Stratigraphic unit	Core samples	Thin sections
	LSD	SEC	TWN	RGE	MER				(ft)		(m)			
T51	9	27	51	27	W4	Golden Spike	Qiang	N-404	5567		1696.8	Leduc		x
								N-405	?		?	Leduc		x
								N-406	?		?	Leduc		x
								N-407	?		?	Leduc		x
								N-408	5847		1782.2	Leduc		x
								N-410	?		?	Leduc		x
								N-411	5853		1784.0	Leduc		
	9	22	51	27	W4	Golden Spike	Qiang	N-249	5355		1632.2	Leduc	x	
								N-248	5374		1638.0	Leduc	x	
								N-247	5558		1694.1	Leduc	x	
								N-246	5765		1757.2	Leduc	x	
								N-245	5840		1780.1	Leduc	x	
								N-244	5910		1801.4	Leduc	x	
								N-243	5995		1827.3	Cook. Lk.	x	
	6	11	51	26	W4	Leduc-Woodbend	Kuflevskiy	SK51-1	5840.5		1780.2	Cook. Lk.	x	
								SK51-2	5846.7		1782.1	Cook. Lk.	x	x
								SK51-3	5852.5		1783.9	Cook. Lk.	x	
	6	11	51	26	W4	Leduc-Woodbend	Horrigan	N-91	5771.9		1759.3	Cook. Lk.	x	x
	6	11	51	26	W4	Leduc-Woodbend	Qiang	N-97	4974		1516.1	Nisku	x	
								N-96	?		?		x	
								N-95	5727		1745.6	Leduc	x	x
								N-94	?		?	Leduc	x	
								N-92	5763.5		1756.7	Leduc	x	x
								N-91	5771.9		1759.3	Cook. Lk.		x
								N-90	?		?	Cook. Lk.	x	
								N-89	5833		1777.9	Cook. Lk.	x	
								N-88	5854		1784.3	Cook. Lk.	x	
								N-87	?		?	Cook. Lk.	x	
								N-86	?		?	Cook. Lk.	x	
								N-85	6203.5		1890.8	Cook. Lk.	x	
	8	16	51	25	W4	Whitemud	Qiang	N-196	?		?	Duverney		x
								N-195	?		?	Duverney		x
								N-194	5748		1752.0	Cook. Lk.		x
								N-193	?		?	Cook. Lk.		x
								N-191	5776		1760.5	Cook. Lk.		x
								N-189	5812.5		1771.7	Cook. Lk.		x
								N-188	5830.4		1777.1	Cook. Lk.		x
								N-187	5828.4		1776.5	Cook. Lk.		x
								N-184	5846		1781.9	Cook. Lk.		
								N-183	5849		1782.8	Cook. Lk.		x
								N-182	5851		1783.4	Cook. Lk.		x

TWN	Well ID					Pool	Original sample set	Sample ID	Depth		Stratigraphic unit	Core samples	Thin sections
	LSD	SEC	TWN	RGE	MER				(ft)	(m)			
T50	8	34	50	26	W4	Leduc-Woodbend	Qiang	N-230	4962	1512.4	Leduc	x	
								N-229	4959	1511.5	Leduc	x	
								N-104	4965	1513.4	Leduc	x	
								N-103	5191	1582.2	Leduc	x	
								N-102	5219.4	1590.9	Leduc		x
								N-101	5241	1597.5	Leduc	x	
								N-100	5258.5	1602.8	Leduc	x	
								N-99	5283	1610.3	Leduc	x	
								N-98	5269	1606.0	Leduc	x	
								N-75	?	?	Leduc	x	
								N-74	5729.9	1746.5	Leduc	x	
								N-73	5840.6	1780.25	Leduc		
								N-72	5956.9	1815.7	Leduc	x	
								N-71	5912.0	1802	Leduc	x	
								N-69	5939.2	1810.3	Leduc	x	
								N-68	5962.9	1817.5	Leduc		
								N-67	5982.5	1823.5	Leduc	x	
	8	17	50	26	W4	Leduc-Woodbend	Horrigan	N-58	5591.8	1704.4	Leduc		x
								N-324	6354.6	1936.9	Leduc		x
	8	17	50	26	W4	Leduc-Woodbend	Qiang	N-66	5394.5	1644.3	Leduc		x
								N-63	?	?	Leduc		x
								N-62	5525.5	1684.2	Leduc		x
								N-61	5531	1685.9	Leduc		x
								N-58	5591.8	1704.4	Leduc		x
								N-56	5609	1709.6	Leduc		x
								N-54	5644.5	1720.5	Leduc		x
								N-52	5691	1734.6	Leduc		x
								N-49	5741.5	1750.0	Leduc		
								N-47	5748	1752.0	Leduc		
								N-45	5803	1768.8	Leduc		x
								N-43	5832	1777.6	Leduc		x
								N-40	?	?	Leduc		x
								N-38	?	?	Leduc		x
								N-36	5966	1818.5	Leduc		
								N-329	?	?	Leduc		x
								N-328	5996	1827.6	Leduc		x
								N-33	6035	1839.5	Leduc		x
								N-27	?	?	Leduc		x
								N-26	6128	1867.8	Leduc		x
								N-327	6206	1891.6	Leduc		x
								N-326	?	?	Leduc		x
								N-16	6328	1928.8	Leduc		x
								N-15	?	?	Leduc		x
								N-14	6344.6	1933.9	Leduc		
								N-325	?	?	Leduc		x

TWN	Well ID					Pool	Original sample set	Sample ID	Depth		Stratigraphic unit	Core samples	Thin sections
	LSD	SEC	TWN	RGE	MER				(ft)	(m)			
								N-324	6354.6	1936.9	Leduc		x
								N-323	?	?	Leduc		x
								N-13	6381	1945.0	Leduc		x
								N-12	?	?	Leduc		x
								N-320	?	?	Leduc		x
								N-319	6407	1952.9	Leduc		x
	8	17	50	26	W4	Leduc-Woodbend	Amthor	A50-1	5387	1642.0	Leduc	x	
								A50-2	6098	1858.7	Leduc	x	
								A50-3	6101	1859.6	Leduc	x	
								A50-4	6108	1861.7	Leduc	x	
								A50-5	6118	1864.8	Leduc	x	
								A50-6	6133	1869.4	Leduc	x	
								A50-7	6136	1870.3	Leduc	x	
								A50-8	6147	1873.6	Leduc	x	
								A50-9	6148	1873.9	Leduc	x	
								A50-10	6153	1875.5	Leduc	x	
								A50-11	6170	1880.6	Leduc	x	
								A50-12	6178.5	1883.2	Leduc	x	
								A50-13	6183	1884.6	Leduc	x	
								A50-14	6187	1885.8	Leduc	x	
								A50-15	6189	1886.4	Leduc	x	
								A50-16	6193	1887.6	Leduc	x	
								A50-17	6196	1888.6	Leduc	x	
								A50-18	6199	1889.5	Leduc	x	
								A50-19	6203	1890.7	Leduc	x	
								A50-20	6210	1892.8	Leduc	x	
								A50-21	6212	1893.4	Leduc	x	
								A50-22	6214.5	1894.2	Leduc	x	
								A50-23	6216	1894.7	Leduc	x	
								A50-24	6218.5	1895.4	Leduc	x	
								A50-25	6224	1897.1	Leduc	x	
								A50-26	6226	1897.7	Leduc	x	
								A50-27	6229	1898.6	Leduc	x	
								A50-28	6233.5	1900.0	Leduc	x	
								A50-29	6239	1901.7	Leduc	x	
								A50-30	6243.5	1903.0	Leduc	x	
								A50-31	6247	1904.1	Leduc	x	
								A50-32	6255.5	1906.7	Leduc	x	
								A50-33	6261	1908.4	Leduc	x	
								A50-34	6262	1908.7	Leduc	x	
								A50-35	6263	1909.0	Leduc	x	
								A50-36	6274	1912.3	Leduc	x	
								A50-37	6278.5	1913.7	Leduc	x	
								A50-38	6289	1916.9	Leduc	x	
								A50-39	6299	1920.0	Leduc	x	
								A50-41	6310.5	1923.5	Leduc	x	
								A50-42	6315	1924.8	Leduc	x	

TWN	Well ID					Pool	Original sample set	Sample ID	Depth		Stratigraphic unit	Core samples	Thin sections
	LSD	SEC	TWN	RGE	MER				(ft)	(m)			
								A50-N-14	6344.6	1933.9	Leduc	x	
T49	4	10	49	26	W4	Leduc-Woodbend	Kuflevskiy	SK49-1	6304	1921.5	Cook. Lk.	x	
								SK49-2	6311	1923.6	Cook. Lk.	x	x
								SK49-3	6362	1939.2	Cook. Lk.	x	
	4	10	49	26	W4	Leduc-Woodbend	Qiang	N-83	5288	1611.8	Wabamun	x	
								N-82	5363	1634.7	Camar	x	
								N-81	5393	1643.8	Nisku	x	
								N-80	5674	1729.5	Ireton	x	
								N-79	5702	1738.0	Ireton	x	
								N-78	6347	1934.6	Cook. Lk.	x	
								N-77	6355	1937.0	Cook. Lk.	x	
								N-76	6370	1941.6	Cook. Lk.	x	
	9	30	49	25	W4	Leduc-Woodbend	Qiang	N-228	5246	1599	Leduc	x	
								N-227	5248	1599.6	Leduc	x	
								N-226	?	?	Leduc	x	
								N-225	?	?	Leduc	x	
T48	3	10	48	26	W4	Wizard Lake	Kuflevskiy	SK48-1	6734	2052.5	Cook. Lk.	x	
								SK48-2	6742	2055.0	Cook. Lk.	x	
	14	22	48	27	W4	Wizard Lake	Qiang	N-234	6436	1961.7	Leduc		x
								N-233	?	?	Leduc		x
								N-123	?	?	Leduc	x	
								N-122	?	?	Leduc	x	
								N-121	?	?	Leduc	x	x
								N-120	?	?	Leduc	x	
								N-119	?	?	Leduc	x	x
								N-118	?	?	Leduc		x
								N-117	?	?	Leduc	x	
								N-116	?	?	Leduc	x	
								N-115	?	?	Leduc	x	
								N-114	?	?	Leduc	x	
								N-113	6439	1962.6	Leduc	x	x
								N-112	?	?	Leduc	x	
								N-111	6458	1968.4	Leduc	x	x
	5	22	48	27	W4	Wizard Lake	Amthor	A48-1	5466.5	1666.2	Wabamun	x	
								A48-2	6044.9	1842.5	Leduc	x	
								A48-3	6049.1	1843.8	Leduc	x	
								A48-4	6068.5	1849.7	Leduc	x	

TWN	Well ID					Pool	Original sample set	Sample ID	Depth		Stratigraphic unit	Core samples	Thin sections
	LSD	SEC	TWN	RGE	MER				(ft)	(m)			
								A48-5	6076.0	1852	Leduc	x	
								A48-6	6086.2	1855.1	Leduc	x	
								A48-7	6087.5	1855.5	Leduc	x	
								A48-8	6094.4	1857.6	Leduc	x	
								A48-9	6102.9	1860.2	Leduc	x	
								A48-10	6115.4	1864	Leduc	x	
								A48-11	6130.8	1868.7	Leduc	x	
								A48-12	6133.9	1869.65	Leduc	x	
								A48-13	6137.1	1870.6	Leduc	x	
								A48-14	6145.6	1873.2	Leduc	x	
								A48-15	6151.5	1875	Leduc	x	
								A48-16	6153.8	1875.7	Leduc	x	
								A48-17	6157.1	1876.7	Leduc	x	
								A48-18	6160.4	1877.7	Leduc	x	
								A48-19	6163.0	1878.5	Leduc	x	
								A48-20	6166.6	1879.6	Leduc	x	
								A48-21	6167.4	1879.85	Leduc	x	
								A48-22	6181.0	1884	Leduc	x	
								A48-23	6181.2	1884.05	Leduc	x	
								A48-24	6184.3	1885	Leduc	x	
								A48-25	6185.8	1885.45	Leduc	x	
								A48-26	6190.4	1886.85	Leduc	x	
								A48-27	6195.5	1888.4	Leduc	x	
								A48-28	6200.7	1890	Leduc	x	
								A48-29	6204.0	1891	Leduc	x	
								A48-30	6207.3	1892	Leduc	x	
								A48-31	6207.9	1892.2	Leduc	x	
								A48-32	6212.5	1893.6	Leduc	x	
								A48-33	6217.1	1895	Leduc	x	
								A48-34	6220.4	1896	Leduc	x	
								A48-35	6230.2	1899	Leduc	x	
								A48-36	6235.5	1900.6	Leduc	x	
								A48-37	6245.7	1903.7	Leduc	x	
								A48-38	6255.8	1906.8	Leduc	x	
								A48-39	6262.1	1908.7	Leduc	x	
								A48-40	6481.2	1975.5	Leduc	x	
								A48-41	6492.0	1978.8	Leduc	x	
								A48-42	6493.4	1979.2	Leduc	x	
								A48-43	6502.9	1982.1	Leduc	x	
								A48-44	6510.4	1984.4	Leduc	x	
								A48-45	6515.7	1986	Leduc	x	
								A48-46	6522.2	1988	Leduc	x	
								A48-47	6525.5	1989	Leduc	x	
								A48-48	6529.8	1990.3	Leduc	x	
								A48-49	6533.7	1991.5	Leduc	x	
								A48-50	6540.6	1993.6	Leduc	x	
								A48-51	6547.2	1995.6	Leduc	x	

TWN	Well ID					Pool	Original sample set	Sample ID	Depth		Stratigraphic unit	Core samples	Thin sections
	LSD	SEC	TWN	RGE	MER				(ft)	(m)			
								A48-52	6552.7	1997.3	Leduc	x	
								A48-53	6555.0	1998	Leduc	x	
								A48-54	6566.5	2001.5	Leduc	x	
								A48-55	6571.4	2003	Leduc	x	
								A48-56	6573.7	2003.7	Leduc	x	
								A48-57	6577.0	2004.7	Leduc	x	
								A48-58	6583.3	2006.6	Leduc	x	
								A48-59	6587.8	2008	Leduc	x	
								A48-60	6589.2	2008.4	Leduc	x	
								A48-61	6592.8	2009.5	Leduc	x	
								A48-62	6606.7	2013.75	Leduc	x	
								A48-63	6610.8	2015	Leduc	x	
								A48-64	6615.7	2016.5	Leduc	x	
								A48-65	6617.4	2017	Leduc	x	
								A48-66	6630.5	2021	Leduc	x	
								A48-67	6637.1	2023	Leduc	x	
								A48-68	6642.6	2024.7	Leduc	x	
								A48-69	6646.9	2026	Leduc	x	
								A48-70	6647.7	2026.25	Leduc	x	
								A48-71	6647.7 (2)	2026.25 (2)	Leduc	x	
								A48-72	6651.8	2027.5	Leduc	x	
								A48-73	6663.3	2031	Leduc	x	
								A48-74	6666.6	2032	Leduc	x	
								A48-75	6676.4	2035	Leduc	x	
								A48-76	6679.7	2036	Leduc	x	
								A48-77	6693.7	2040.25	Leduc	x	
								A48-78	6697.8	2041.5	Leduc	x	
								A48-79	6702.7	2043	Leduc	x	
								A48-80	6705.3	2043.8	Leduc	x	
								A48-81	6707.9	2044.6	Leduc	x	
	3	22	48	27	W4	Wizard Lake	Horrigan	N-307	6354	1936.7	Ireton		x
								N-304	6543.2	1994.4	Leduc	x	x
								N-288	6628.9	2020.5	Leduc	x	x
	3	22	48	27	W4	Wizard Lake	Qiang	N-308	6354	1936.7	Ireton		x
								N-307	6354	1936.7	Ireton		x
								N-306	6518.5	1986.9	Leduc		x
								N-305	6526.5	1989.3	Leduc		x
								N-304	6543.2	1994.4	Leduc		x
								N-302	6546.5	1995.4	Leduc		x
								N-301	6549.5	1996.3	Leduc		x
								N-298	6553	1997.4	Leduc		x
								N-296	6633.5	2021.9	Leduc		x
								N-294	6564	2000.7	Leduc		x
								N-292	6594	2009.9	Leduc		x
								N-291	6598	2011.1	Leduc		

TWN	LSD	SEC	TWN	RGE	MER	Pool	Original sample set	Sample ID	Depth (ft)	Depth (m)	Stratigraphic unit	Core samples	Thin sections
								N-288	6628.9	2020.5	Leduc		x
								N-287	?	?	Leduc		x
								N-286	?	?	Leduc		x
								N-285	?	?	Leduc		x
								N-282	6692	2039.7	Leduc		x
								N-281	6693	2040.1	Leduc		x
								N-280	6704	2043.4	Leduc		x
								N-273	?	?	Leduc		x
								N-271	6909	2105.9	Leduc		
								N-270	6958	2120.8	Leduc		x
								N-266	6980	2127.5	Leduc		
	10	9	48	27	W4	Wizard Lake	Qiang	N-131	6532.1	1991	Leduc	x	
								N-130	6553.4	1997.5	Leduc	x	
								N-129	6555.7	1998.2	Leduc	x	
								N-128	6596.7	2010.7	Leduc	x	
								N-127	6624.6	2019.2	Leduc	x	
T47	3	20	47	27	W4	Bonnie Glen	Horrigan	N-215	6557.9	1998.9	Leduc	x	x
	3	20	47	27	W4	Bonnie Glen	Qiang	N-318	6077	1852.3	Nisku	x	
								N-317	?	?	Nisku	x	x
								N-316	?	?	Nisku		x
								N-315	?	?	Nisku		x
								N-314	?	?	Nisku	x	
								N-313	6140.02	1871.5	Nisku		x
								N-312	?	?		x	
								N-311	?	?		x	
								N-220	?	?		x	
								N-219	?	?		x	x
								N-218	?	?		x	
								N-217	?	?			x
								N-216	?	?			x
								N-215	6557.9	1998.9	Leduc		x
								N-214	?	?	Leduc	x	x
								N-212	6656	2028.8	Leduc	x	x
								N-213	6675.7	2034.8	Leduc		x
								N-211	?	?	Leduc	x	
	3	19	47	27	W4	Bonnie Glen	Qiang	N-199	7086	2159.8	Leduc	x	
								N-198	7091	2161.4	Leduc	x	
	16	7	47	27	W4	Bonnie Glen	Qiang	N-159	6526	1989.1	Leduc		x
								N-158	?	?	Leduc	x	
								N-157	?	?	Leduc	x	
								N-156	6574	2003.8	Leduc		x

TWN	Well ID					Pool	Original sample set	Sample ID	Depth (ft)	Depth (m)	Stratigraphic unit	Core samples	Thin sections
	LSD	SEC	TWN	RGE	MER								
								N-155	6594	2009.9	Leduc	x	x
								N-154	?	?	Leduc	x	
								N-153	?	?	Leduc	x	
								N-152	?	?	Leduc	x	
								N-151	6711	2045.5	Leduc	x	x
								N-150	6742	2055.0	Leduc	x	
								N-149	?	?	Leduc	x	
								N-148	?	?	Leduc	x	
								N-147	6855	2089.4	Leduc		x
								N-147	6855	2089.4	Leduc		x
								N-146	?	?	Leduc	x	
								N-145	?	?	Leduc	x	x
								N-144	?	?	Leduc		
								N-143	6929	2112.0	Leduc	x	
								N-142	?	?	Leduc	x	
								N-141	6904	2104.4	Leduc	x	x
								N-140	6990	2130.6	Leduc	x	x
								N-139	7029	2142.5	Leduc		x
								N-138	7049	2148.6	Leduc		x
								N-137	?	?	Leduc	x	
								N-136	?	?	Leduc	x	
								N-135	?	?	Leduc	x	
								N-134	7069	2154.7	Leduc		x
								N-133	?	?	Leduc	x	
								N-132	7085	2159.5	Leduc	x	x
T46	12	36	46	28	W4	Bonnie Glen	Qiang	N-209	6906.1	2105	Leduc	x	
								N-208	6935.6	2114	Leduc	x	
								N-207	7070.1	2155	Leduc	x	
								N-206	7094.1	2162.3	Leduc	x	
								N-205	7211.2	2198	Leduc	x	
								N-204	7519.6	2292	Leduc	x	
								N-203	7549.1	2301	Leduc	x	
								N-202	7560.6	2304.5	Leduc	x	
								N-201	7567.2	2306.5	Leduc	x	
	8	4	46	28	W4	Westerose	Horrigan	EH-23	7240.7	2207	Leduc	x	x
								EH-24	7329.3	2234	Leduc	x	x
								EH-25	7352.3	2241	Leduc	x	x
T45	1	36	45	1	W5	Westerose	Horrigan	EH-7	7365.4	2245	Leduc	x	x
	16	33	45	28	W4	Westerose	Horrigan	EH-60	6958.6	2121	Leduc	x	x

TWN	Well ID					Pool	Original sample set	Sample ID	Depth		Stratigraphic unit	Core samples	Thin sections
	LSD	SEC	TWN	RGE	MER				(ft)	(m)			
T44	11	27	44	1	W5	Westerose South	Kuflevskiy	SK44(1)-1	7378.3	2248.9	Leduc	x	x
								SK44(1)-2	7383.5	2250.5	Leduc	x	
								SK44(1)-3	7384.7	2250.9	Leduc	x	
								SK44(1)-4	7540	2298.2	Leduc	x	x
								SK44(1)-5	7543	2299.1	Leduc	x	
								SK44(1)-6	7718	2352.5	Leduc	x	
								SK44(1)-7	7719	2352.8	Leduc	x	x
								SK44(1)-8	7723	2354.0	Leduc	x	
	12	25	44	1	W5	Westerose South	Kuflevskiy	SK44(2)-1	7876	2400.6	Cook. Lk.	x	
								SK44(2)-2	7883.7	2403.0	Cook. Lk.	x	x
								SK44(2)-3	7886	2403.7	Cook. Lk.	x	
								SK44(2)-4	7888.6	2404.5	Cook. Lk.	x	x
								SK44(2)-5	7889.9	2404.9	Cook. Lk.	x	x
								SK44(2)-6	7901.4	2408.4	Cook. Lk.	x	
								SK44(2)-7	7910	2411.0	Cook. Lk.	x	
								SK44(2)-8	7914.5	2412.4	Cook. Lk.	x	x
								SK44(2)-9	8026.4	2446.5	Cook. Lk.	x	
T43	3	29	43	1	W5	Homeglen Rimbey	Horrigan	EH-8	7791.9	2375	Leduc	x	x
	11	7	43	1	W5	Homeglen Rimbey	Horrigan	EH-39	7841.1	2390	Leduc	x	x
T42	10	4	42	1	W5	Homeglen Rimbey	Kuflevskiy	SK42-1	8461.5	2579.1	Cook. Lk.	x	x
								SK42-2	8465.5	2580.3	Cook. Lk.	x	
								SK42-3	8468	2581.1	Cook. Lk.	x	x
								SK42-4	8469	2581.4	Cook. Lk.	x	
	11	25	42	2	W5	Homeglen Rimbey	Horrigan	EH-43	7969.1	2429	Leduc	x	x
	7	22	42	2	W5	Homeglen Rimbey	Horrigan	EH-19	7882.1	2402.5	Leduc	x	x
	11	3	42	2	W5	Homeglen Rimbey	Horrigan	EH-38	7841.1	2390	Leduc	x	x
T41	14	5	41	2	W5	Gilby	Horrigan	EH-51	8247.9	2514	Leduc	x	x
								EH-50	8284.0	2525	Leduc	x	x
								EH-52	8310.3	2533	Leduc	x	x
T40	10	7	40	2	W5	Homeglen Rimbey	Horrigan	EH-4	8579.9	2615.2	Leduc	x	x
								EH-5	8605.9	2623.1	Leduc	x	x
								EH-6	8627.8	2629.8	Leduc	x	x

TWN	Well ID					Pool	Original sample set	Sample ID	Depth		Stratigraphic unit	Core samples	Thin sections
	LSD	SEC	TWN	RGE	MER				(ft)	(m)			
T39	14	28	39	3	W5	Medicine River	Horrigan	EH-1	9261.7	2823	Leduc	x	x
								EH-2	9297.8	2834	Leduc	x	x
								EH-3	9333.9	2845	Leduc	x	x
	7	9	39	12	W5	Phoenix	Horrigan	EH-17	15543.4	4737.7	Leduc	x	x
								EH-18	15550.7	4739.9	Leduc	x	x
T38	8	30	38	4	W5	Medicine River	Horrigan	EH-28	10287.3	3135.6	Leduc	x	x
	6	20	38	4	W5	Medicine River	Horrigan	EH-13	10283.0	3134.3	Leduc	x	x
	16	11	38	5	W5	Sylvan Lake	Horrigan	EH-56(R2)	10075.3	3071	Leduc	x	x
T37	10	17	37	3	W5	Sylvan Lake	Horrigan	EH-29	9392.9	2863	Leduc	x	x
	16	32	37	4	W5	Sylvan Lake	Horrigan	EH-58	9783.3	2982	Leduc	x	x
								EH-59	9807.0	2989.2	Leduc	x	x
	6	30	37	7	W5	Chedderville	Horrigan	EH-16	11587.8	3532	Leduc	x	x
	10	29	37	7	W5	Chedderville	Horrigan	EH-30	11994.6	3656	Leduc	x	x
	6	14	37	7	W5	Chedderville	Kuflevskiy	SK37-1	12226.9	3726.8	Cook. Lk.	x	
								SK37-2	12228.9	3727.4	Cook. Lk.	x	x
								SK37-3	12232.8	3728.6	Cook. Lk.	x	
								SK37-4	12258.4	3736.4	Cook. Lk.	x	
								SK37-5	12260.7	3737.1	Cook. Lk.	x	x
								SK37-6	12263.3	3737.9	Cook. Lk.	x	
	11	28	37	8	W5	Crimson	Horrigan	EH-46	12138.0	3699.7	Leduc	x	x
	7	32	37	9	W5	Strachan	Horrigan	EH-21	13402.7	4085.2	Leduc	x	x
								EH-22	13491.6	4112.3	Leduc	x	x
	10	31	37	9	W5	Strachan	Horrigan	EH-31	14108.4	4300.3	Leduc	x	x
								EH-32	14167.5	4318.3	Leduc	x	x
								EH-33	14191.6	4325.7	Leduc	x	x
	5	13	37	12	W5	Ram River	Horrigan	EH-9	16558.2	5047	Leduc	x	x
								EH-10	16625.1	5067.4	Leduc	x	x

TWN	Well ID					Pool	Original sample set	Sample ID	Depth		Stratigraphic unit	Core samples	Thin sections
	LSD	SEC	TWN	RGE	MER				(ft)	(m)			
T36	8	27	36	6	W5	Garrington	Horrigan	EH-26	11755.1	3583	Leduc	x	x
								EH-27	11790.2	3593.7	Leduc	x	x
	16	25	36	6	W5	Garrington	Horrigan	EH-57	11384.4	3470	Leduc	x	x
	10	33	36	10	W5	Ricinus West	Horrigan	EH-34	14838.7	4522.9	Leduc	x	x
								EH-35	14973.2	4563.9	Leduc	x	x
								EH-36	15017.5	4577.4	Leduc	x	x
								EH-37	15291.8	4661	Leduc	x	x
	11	27	36	10	W5	Ricinus West	Horrigan	EH-44	14685.2	4476.1	Leduc	x	x
								EH-45	14730.5	4489.9	Leduc	x	x
	7	26	36	10	W5	Ricinus East	Horrigan	EH-20	14428.6	4397.9	Leduc	x	x
	15	23	36	10	W5	Ricinus West	Horrigan	EH-53	14748.8	4495.5	Leduc	x	x
								EH-54	14912.5	4545.4	Leduc	x	x
								EH-55	15067.1	4592.5	Leduc	x	x
T35	11	10	35	5	W5	Caroline	Horrigan	EH-40	11008.7	3355.5	Leduc	x	x
								EH-41	11023.8	3360.1	Leduc	x	x
								EH-42	11042.8	3365.9	Leduc	x	x
T34	6	24	34	8	W5	Ricinus	Horrigan	EH-14	14369.6	4379.9	Leduc	x	x
								EH-15	14389.3	4385.9	Leduc	x	x
	6	14	34	8	W5	Ricinus East	Horrigan	EH-11	14058.9	4285.2	Leduc	x	x
								EH-12	14064.5	4286.9	Leduc	x	x
T33	13	9	33	4	W5	Harmattan	Horrigan	EH-47	11236.7	3425	Leduc	x	x
								EH-48	11351.6	3460	Leduc	x	x
								EH-49	11374.5	3467	Leduc	x	x

224

Appendix 2

**Petrographic observations, cathodoluminescence microscopy
and spectroscopy, and image analysis of a representative set of samples.**

TWN	LSD	SEC	TWN	RGE	MER	Depth (ft)	Depth (m)	Sample ID	R1	R2	R3	R4	Dominance	Diameter, µm	C1	C2	C3	C4	Image analysis	AccuMap	Bitumen	Calcite	Anhydrite	Pyrite	Diagenesis Description	CL-microscopy Description	Spectrum, nm	Drilled
T95	2	28	95	18	W4	1282.8	391	K95-5(1)		43.9			PS-NA	150-750					39.3	2					Tight dolomite matrix - coarse to very coarse crystalline. Most crystals are Nonplanar Anhedral. There are some clusters showing a tripple junction of subhedral crystals.	Dull orange-red, slightly mottled	570	R2
								K95-5(2)			16.8		PE(PS)	150-250						50					Micro-medium zoned crystals with a lot of porosity. Some crystals reach up to 500µm. Zoning is very typical for meteoric systems. R3 crystals are replacing amphipora. Centres of some crystals are leached out. Crystal size populations are inverted in this sample.	Dull orange-red, slightly mottled	570	R3
						1313.6	400.4	K95-6		29.2	58.4		PS-NA PE(PS)	80-250 110-250					12.3					0.13	Mixed matrix - transition between R2 and R3	Mottled orange-red	570	
						1426.4	434.77	K95-12	90.79			5.14	PS-NA	40-60					0		3.75			0.32	Dense fine crystalline dolomite matrix with some bitumen coating the grains and a bit of pyrite. R4 appears in the matrix as single crystalls with sharp or sweeping exctinction.	Dull orange-red, slightly mottled	570	R1
T88	3	34	88	20	W4	1334	406.6	HH88-2		52.6	42.89		NA PE	150-250 60-500					3.99	9.5	0.5				Tight micro-medium crystalline matrix R2 crosscut by solution seams (too much clay in solution seams) with occasional coarser clusters of R2 - around 500 µm. Matrix R3 is represented by patches of medium euhedral crystals with cloudy cores and clear rims.	Dull orange-red, very mottled	570	R3
T71	15	17	71	25	W4	3336	1016.8	HH71-2	42.38		55.98		PS PS	30-100 60-120					1.19					0.51	Dense bitumen stained fine crystalline matrix R1 with some areas of micro-medium R3 crystals around the pores, some pyrite.	Dull orange-red, speckled	570	R1
T68	4	33	68	22	W4	3476	1059.5	HH68-2		54.5	34.81		PS-NA PS-NA	150-300 200-400					4.38		6.27				Tight macro-medium crystalline matrix R2 mosaic crosscut by solution seams. There are some areas with micro-coarse R3 crystals around the pores. There is some pyrite in the matrix.	R2 and R3 - dull, mottled orange-red.	570	R2
T67	13	17	67	23	W4	2958	901.6	K67-2		56.2	36.24		PS PS-PE	80-270 110-400					7.53	13.5					Karstified medium matrix R2 with patches of coarser euhedral (some subhedral) R3-like crystalls in the dissolution porosity.	R2/R3 - dull orange-red, speckled.	570	KD

226

TWN	LSD	SEC	TWN	RGE	MER	Depth (ft)	Depth (m)	Sample ID	R1	R2	R3	R4	Dominance	Diameter, μm	C1	C2	C3	C4	Image analysis	AccuMap	Bitumen	Calcite	Anhydrite	Pyrite	Diagenesis Description	CL-microscopy Description	Spectrum, nm	Drilled
T66	6	16	66	24	W4	3893	1186.6	HH66(2)-8		96.9			PS	80-175					3.11						Homogenious medium crystalline matrix R2, there is a fracture with a finer crystalline dolomite halo around it. There is a lot of brown porous dolomite (R3) in hand specimen.	Dull orange-red with a strange pattern (probably biogenic - strom).	570	R2, R3
						4073	1241.5	HH66(2)-9	10.94		39.79		PS-NA PE	40-80 50-120					0			48.8		0.47	Dedolomite. R2 is largely replaced by calcite. This is typical for systems where meteoric water infiltrates dolomites.	Dull orange-red, yellow	570 615	R2
T63	5	24	63	25	W4	3479	1060.4	HH63-1		58.4	28.87		PS PE (PS)	70-150 60-100					6.09			6.41		0.26	Dense micro-medium crystalline fairly homogeneous mosaic of R2 with some porous areas of zoned R3 crystals and some calcite and pyrite. Stylolite crosscuts matrix placing the stylolitization event after dolomitization (recrystallization).	Almost homogenious dull orange-red luminescence with no difference between R2 and R3.	570	R2
						3722	1134.5	HH63-5		61.1	31.15		PS-NA PS	200-350 200-400					7.68						Dense macro-medium crystalline mosaic of R2 with some porous R3 areas.	Homogenious dull orange-red luminescence.	570	R2
T62	16	22	62	25	W4	3710	1130.8	HH62-4			90.1		PS-NA PS (PE)	200-600 150-400					10.1						Karstified matrix R2 with dissolution boundaries - a lot of coarse euhedral (some subhedral) R3-like crystalls in the dissolution porosity.	Intracrystalline microblotchy orange-red luminescence.	570	KD
						3720	1133.9	HH62-5			78.5		PS-NA PS (PE)	150-700 150-400					21.5						Karstified matrix R2 with dissolution boundaries - a lot of coarse euhedral (some subhedral) R3-like crystalls in the dissolution porosity.	Intracrystalline microblotchy orange-red luminescence.	570	KD
T61	7	31	61	24	W4	3491	1064.1	HH61-1			81.7		PS-PE	100-500					12.2			6.12			This is a karstified sample. The finer matrix was affected by dissolution resulting in formation of coarse euhedral (some subhedral) R3-like crystalls with a lot of porosity.	Intracrystalline microblotchy orange-red luminescence.	570	KD
T59	2	9	59	24	W4	3885.6	1184.3	K59-2		64.5	31.7		PS PE	150-250 200-260					3.38		12.4				Tight macro-medium crystalline matrix R2 mosaic with some areas of micro-coarse R3 crystals associated with the pores.	Matrix R2 - dull blotchy orange-red, R3 - cores lighter red, rims dark.	570	R2, R3
T58	2	5	58	25	W4	4623.5	1409.3	K58(2)-1		40.9			PS-NA PS-NA	80-160 80-750		29.01			22.7		12.4	6.71		0.77	Tight bimodal matrix of cloudy micro-medium dolomite crystals and clear crystals that are larger in size. Dolomite cement crystals nucleating on the wall of the void (some are zoned). Late diagenetic calcite crystals (3-5mm) filling the void poikilitically. There are some dolomite cement crystals (300-600) nucleating in the calcite. these dolomite crystals are younger than calcite. There are lottle cracs in calcite that permit the fluids to go in providing Mg. There are also some bitumen and pyrite present.	Dull, slightly mottled orange-red matrix. Dolomite cements - blood red rim. Calcite - yellow.	570 615	R2, C2

TWN	Well ID LSD	SEC	TWN	RGE	MER	Depth (ft)	Depth (m)	Sample ID	R1	R2	R3	R4	Dominance	Diameter, µm	C1	C2	C3	C4	Image analysis	AccuMap	Bitumen	Calcite	Anhydrite	Pyrite	Diagenesis Description	CL-microscopy Description	Spectrum, nm	Drilled
						4627.1	1410.4	K58(2)-3		54.7			PS	80-300		27.4			2.29			15.6			4 domains, 1 is missing in the thin section but not in the hand specimen. Tight matrix R2 with a loose framework of dolomite crystals growimg on the wall upwords with huge amount of porosity in between. This dolomite is not replacing the calcite. Calcite just fills the spaces in between. The fact that these crystals look as if they are floating is an illusion, because in 3-dimentions they are connected Interlocking texture of the Dolomite cement: dense cluster of cement crystals getting into a looser cluster of cement crystals, but you can still see that most of them are touching + a bit of remnand porosity. Coarse crystalline blocky calcite cement crystals almost completely filling intercrystal pore spaces between planar-c dolomite. This calcite is a poikilitic cement that fills in the spaces between dolomite crystals and the excess calcite grows into the void.	Dull, slightly mottled orange-red matrix. Dolomite cements - blood red rim. Calcite - yellow.	570 615	R2
T56	9	30	56	24	W4	4194	1278.3	EH-74		56.9		41.98	PS-NA PS-PE	75-250 30-150		1.11			0						Dense coated with bitumen matrix R2. Large dolomite cement crystals at the rims of the pores. R4 smaller than R2 crystals with undulating extinction. The fossils are most likely amphipora, stromatoporoids. Still with dolomite size distinction of larger rim and finer core visible. However, some of the finer cores are dissolved, and there are incorporations of larger, nonplanar crystals throughout the fossils. There is also a brachiopod shell that is replaced allowing for the ghost to remain, but dolomite is grown randomly throughout it.	Biochems barely recognizable. R2 - dull, flat, some evidence of brighter core, but generally dull. Bright cement surrounding all vugs.	570	
	16	24	56	26	W4	5304.7	1616.9	K56-7		44.9	18.9		PS-NA PE	200-550 200-400					1.06				35.1		Coarse matrix R2 with patches of zoned R3 crystals. Dead oil coating extremely coarse crystalline (>4mm) anhydrite cement.The margin of the void.	Matrix R2 - dull blotchy orange-red, R3 - cores lighter red, rims dark.	570	R2, R3
T55	7	15	55	25	W4	4458	1358.8	EH-75		9.24	85.35		PS PE	200-450 200-450					5.24					0.17	Dense coarse crystalline fairly homogeneous mosaic of R2 with bitumen stain and some pyrite. Smaller crystals along the stylolite.R3 has bitumen in core, very little white rim. Zoned R3 is a product of recrystallization of R2. R3 has bitumen in core, very little white rim.	R2 - dull, flat with some light bits. R3 - mottled - generally light cores surrounded by dull red, but in cores - even lighter and smaller bits	570	R2, R3

TWN	LSD	SEC	TWN	RGE	MER	Drilled (ft)	(m)	Sample ID	R1	R2	R3	R4	Dominance	Diameter, µm	C1	C2	C3	C4	Image analysis	AccuMap	Bitumen	Calcite	Anhydrite	Pyrite	Description	Description (CL)	Spectrum, nm	Drilled
	6	22	55	26	W4	5427.1	1654.2	N-473		86.5	10.74		PS-NA PE	180-650 80-200					2.81						Matrix R2 with zones of R3 associated with pores, but they are not widespread. Mostly recrystallized, not totally.	R2 - slightly mottled (light red core, dull red interconnected rims). R3 has lighter cores.	570	R2
T54	8	14	54	26	W4	5308.6	1618.1	K54(2)-5		51.77 48.11			PS-NA PS-NA	150-800 70-500					0.12						Tight coarse crystalline bimodal matrix mosaic with some anhydrite in the sample, but it is ripped out from the section.	Flat orange-red matrix	570	R2
T53	10	4	53	25	W4	5560	1694.7	K53-2		21.08 26.04	6.44		NA PS-NA PE	80-500 500-1000 80-250					0.26	5.1			46.2		Transitioning/ gradational change from tight MXL R2 dolomite matrix to coarser R2 crystals and then to porous R3 dolomite. This is the margin of the vug and the outermost part of this domain's intercrystal porosity is cemented with coarse crystalline blocky anhydrite anhydrite poikilitically, partially filling the intercrystal pore spaces plus dead oil stain. Stylolite with unusually coarse crystalline residue (might be muscovite or illite) and a bit of dead oil in it. Anhydrite grows into the stylolite partially destroying it. Therefore, Anhydrite is younger than the stylolite. Dolomite crystals partially replaced by anhydrite.	Matrix R2 - dull blotchy orange-red, R3 - cores lighter red, rims dark.	570	R3
T52	15	23	52	26	W4	5081.3	1548.8	EH-64		41.5	4.88	48.73	PS-NA PE NA	150-350 200-270 10-20		0.96			3.92	5.1					Thin section: half matrix R2 and half allochem fill R4. R2 - stylolitized dence matrix, bitumen stained. There is a gradational change in crystal size from R2 to R3 (medium to more coarse). R4 is represented by recrystallized strom ('algal mat') and echinoderm fragments with overgrowth. Zoned dolomite cement lining the pores.	R2 and R3 - mottled, possibly skeletal fragments because quite light. R4 - slightly mottled with some bright red zones near vugs.	570	
T51	8	16	51	25	W4	5849	1782.8	N-183		41.9	34.85	8.09	PS-NA PE NA	60-120 45-110 30-60				11.4	0.57			2.29			Micro-medium R2 with areas of porous R3. Saddle dolomite and calcite cements, also some pyrite. R4 replacing a strom.	Matrix dull blotchy orange-red, R3 - cores lighter red, rims dark. C4 - blood red. Calcite - yellow.	570 615	

TWN	LSD	SEC	TWN	RGE	MER	(ft)	(m)	Sample ID	R1	R2	R3	R4	Dominance	Diameter, µm	C1	C2	C3	C4	Image analysis	AccuMap	Bitumen	Calcite	Anhydrite	Pyrite	Diagenesis Description	CL-microscopy Description	Spectrum, nm	Drilled
					27	5851	1783.4	N-182		41.4	27.7		PS-NA PE	45-120 45-110				23.9	5.5		1.06			0.42	Micro-medium R2 with bitumen in the pores. Areas of R3. Saddle dolomite and Pyrite.	Matrix dull blotchy orange-red, R3 - cores lighter red, rims dark. Cement - blood red.	570	
T48	3	22	48	27	W4	6543.2	1994.4	N-304		62.3	30.18	3.61	PS-NA PS (PE) PS-NA	200-330 80-350 20-30					3.89	8.1					Medium to coarse matrix R2 associated with blobs (crumbly). Zoned R3 crystals in areas with small pores. This sample is recrystallized, at least partially.	Matrix R2 and R3 - dull, possibly blotchy. R4 - lighter than matrix, orange-red.	570	
T47	16	7	47	27	W4	6594	2009.9	N-155		75.73 19.96			PS-NA NA	80-200 300-750					4.31	4.5					Macro- to micro-medium R2 with clasters of coarser white nonplanar crystals. Zoned pseudocement crystals growing on the walls of the pores.	Matrix R2 - flat orange-red.	570	R2
						6711	2045.5	N-151		63.25 21.07			NP PE	250-750 400-1100					15.7	5.7					Grey in hand specimen - very coarse nonplanar crystals (recrystallized matrix). White in hand specimen - very coarse crystalline PE (PS-NA in some parts) matrix. Pseudocement (zoned) at the margin. The exstinction is not completely black and white - a bit of sweeping exstinction - it is just a boarder line going towards saddle dolomite cement. Partially disrupted microstylolite that feeds into a remnant void with liquid oil coating it (visible round interfaces). Recrystallization postdates stylolite formation, postdates oil migration, that makes it late creatious in age.	Matrix - dull, blotchy orange-red. No differences between the domains.	570	R2
						?	?	N-144		51.9	26.7		PS-NA PS	300-500 300-750					21.4						Sedimentary microbreccia with nonplanar to PSNA domains. Zoned pseudocements. Very coarse crystalline R3 in parts of the section with oil flakes. Completely undisrupted stylolite never crosses the crystals - it is younger than the dolomite framework (different extinction on both sides). Different alternatives for stylolitization: stylolites formed at different times and recrystallization was one go, or they formed at one time and recrystallization happened at different times and to a different extand. This part of the rock did not get recrystallized twice - just once, it does not look like a primary texture.	R2 - flat orange-red. R3 - bright orange-red.	570	

TWN	Well ID					Depth		Sample ID	Dolomite Matrix, %						Dolomite Cement, %				Porosity, %		Diagenesis					CL-microscopy	Spectrum, nm	Drilled
	LSD	SEC	TWN	RGE	MER	(ft)	(m)		R1	R2	R3	R4	Dominance	Diameter, µm	C1	C2	C3	C4	Image analysis	AccuMap	Bitumen	Calcite	Anhydrite	Pyrite	Description	Description		
						6990	2130.6	N-140		94.7			PS-NA	200-500		0.65			4.62						Medium R2 with echinoderm fragments (single large crystals). Matrix recrystallized into PS-NA but echinoderm fragments are still there because they were farely large to begin with. Large (400-500) zoned C2 crystals.	R2 - flat orange-red. Cement - blood red zoned.	570	R2
						7085	2159.5	N-132		96.9			PS-NA	150-1000					1.02	2.13					Medium to coarse R2 zoned at the adges. Bitumen coating microvug. Pceudocement - zoned crystals that had room to grow in the open void as opposed to the others that have neighboring crystals. There are oil droplets with round interfaces in the porosity.	Matrix - flat orange-red.	570	R2
T46	8	4	46	28	W4	7352.3	2241	EH-25		73.9	.10.15		PS-NA / PS-NA	140-350 / 60-125					2.33	4	13.8				Coarse matrix R2 with bitumen filled veins, vuggy porosity, stylolitized after dolomitization (+/- recrystallization). There are areas of R2 that look like a nonporous R3 (boarder line between R2 and R3). There are a few single large crystals of echinoderms. This sample has been recrystallized, probably before bitumen emplacement.	Matrix - dull, slightly blotchy orange-red. Echinoderms- brighter orange-red.	570	
T44	11	27	44	1	W5	7378.3	2248.9	K44(1)-1		75.6			PS-NA	70-450		1.85			21.5	9.6	1.03				Medium to coarse crystalline R2 matrix with some coarse (200-550) zoned dolomite cement crystals and dead oil coating the pores. This sample has been recrystallized.	R2 - flat orange-red. Cement - blood red zoned.	570	R2
						7719	2352.8	K44(1)-7		60.2	15.34		PS-NA / PS (PE)	70-450 / 200-700					23.4	11.2	0.47				Medium to coarse crystalline R2 mosaic with patches of brown porous matrix dolomite (R3) stained with oil. This sample is greatly recrystallized.	R2 - flat orange-red. R3 - bright orange-red.	570	R2 + R3
	12	25	44	1	W5	7888.6	2404.5	K44(2)-4		73.45 14.92	.4.84		PS-NA / NA / PS-NA	70-300 / 300-700 / 70-150		0.21			5.42	8			1.16		Bimodal matrix R2 with some recrystallized echinoderm fragments (R4) and microstylolites disrupted by dolomite crystals. Anhydrite filling the remnant porosity. Large C1 cement (100-550) postdates the matrix. This sample is recrystallized.	R2 - dull, blotchy orange-red. R4 - dull. C2 - blood red.	570	R2
						7914.5	2412.4	K44(2)-8		67.1	23.55 .8.12		PS-NA / PS-NA / PS-NA	80-260 / 100-250 / 80-180					0.93	2.5				0.29	Medium R2 matrix with patches of porous R3. There is a bit of pyrite coating amphipora (R4).This sample is recrystallized.	R2 and R3 - dull, blotchy orange-red, R4 - dull	570	R2

TWN	LSD	SEC	TWN	RGE	MER	Depth (ft)	Depth (m)	Sample ID	R1	R2	R3	R4	Dominance	Diameter, µm	C1	C2	C3	C4	Image analysis	AccuMap	Bitumen	Calcite	Anhydrite	Pyrite	Diagenesis Description	CL-microscopy Description	Spectrum, nm	Drilled
T43	11	7	43	1	W5	7841.1	2390	EH-39		92.7	.5.81		PS-NA PE	80-200 150-300					1.22	7.3	0.27				Medium matrix R2, with some R3 associated with small vugs. Bitumen filled stylolitescrosscutting crystals occurred after dolomitization (recrystallization). This sample is recrystallized.	Matrix - dull, slightly blotchy orange-red with no change between R2 and R3.	570	R2
T42	10	4	42	1	W5	8461.5	2579.1	K42-1		86.8		8.66	PS-NA NA	700-400 30-62		0.12			1.97				2.41		Medium to coarse R2 mosaic with recrystallized forssils in the matrix. Coarse (250-800) dolomite C2 zoned crystals. Microfracture with anhydrite. This sample is recrystallized.	Matrix R2 - dull orange-red. C2 - blood red.	570	R2
						8468	2581.1	K42-3		42.8	.30.76.	10.16	PS-NA PE PS-NA	80-250 250-300 30-80					8.75					0.19	Medium R2 mozaic with a fine crystalline fossil ghost (amphipora) - recrystallized dolomite fabric with no proper boundaries. Some pyrite crystals. A little bit of brown porous dolomite with some oil in the porosity. There is also some dark internal sediment (either clay or a drilling mud) in the hand specimen, that i s ripped off from the thin section. There is a feeder channel for that domain with sediment. This sample is greatly recrystallized.	R2 and R3 - dull, blotchy orange-red, R4 - dull	570	R2, R4
T41	14	5	41	2	W5	8284.0	2525	EH-50		50.9	.35.18		NA PS (PE)	250-500 240-500	0.24				13.7	12.5					Coarse matrix R2 with patches of R3 around the vugs. Some vugs are filled with blocky anhydrite. Anhydrite cements the pores between R3 crystalls poikilitically. This slide is recrystallized.	R2 - mottled: bright red mottles, dull background. Can see single crystals - mottling throughout them.	570	R2
T37	16	32	37	4	W5	9783.3	2982	EH-58		97.2	.2.16		PS-NA PS (PE)	250-500 700-900		0.15			0.2	7.6	0.32				Coarse matrix R2 with faint stringers of unmesurable R4 associated with microfractures. There are zones of R2/R3 (almost R3, but not porous) around the vugs. It appears that this sample once had abundant allochems which are now mostly indistinguishable through recrystallization, bitumen, and thin section making. This sample is recrystallized.	Matrix - flat orange-red with light red blotches. R4 stringers - dull with blood red and pink cement zones.	570	R2
						9807.0	2989.2	EH-59		93.8		.5.16	PS-NA PS-NA	200-450 30-40		0.13		0.31	0.63	4.9					Medium to coarse matrix R2 with stringers and small zones of R4 which represent recrystallized allochems. It is possible that the matrix was once a strom (at least part of it). There are some dolomite cements associated with vugs (even tiny), veins andstylolites. This sample is recrystallized.	R2 - dull, blotchy orange-red, R4 - dull. C2 - blotchy like matrix. Saddle dolomite rims - blood red.	570	

| | Well ID | | | | | Depth | | | Dolomite | | | | | | | | | | Porosity, % | | Diagenesis | | | | | CL-microscopy | | |
TWN	LSD	SEC	TWN	RGE	MER	(ft)	(m)	Sample ID	R1	R2	R3	R4	Dominance	Diameter, µm	C1	C2	C3	C4	Image analysis	AccuMap	Bitumen	Calcite	Anhydrite	Pyrite	Description	Description	Spectrum, nm	Drilled
	6	14	37	7	W5	12228.9	3727.4	K37-2		99.8			PS-NA	70-400					0		0.21				Medium to micro-coarse crystalline R2 mosaic with a dead oil stain along the microfracture. Stylolites disrupted by dolomite - dolomitization (recrystallization) postdates stylolitization.	Matrix - dull, blotchy orange-red.	570	R2
						12260.7	3737.1	K37-5		83.5		5.18	PS-NA / PS-NA	62-350 / 20-40				1.83	9.46						Multiple domains: some are micro-medium, some are macro-medium. Microstylolites disrupted by dolomite (disappeare in the matrix). There some very coarse saddle dolomite - sign of warmer fluid. There is a ghost of amphipora (R4) around the vug. This sample is recrystallized.	R2 - dull, blotchy orange-red. R4 - slightly mottled.	570	R2
	5	13	37	12	W5	16558.2	5047	EH-9		44.77 38.49	9.79		PS-NA / PS-NA / PE	300-850 / 200-350 / 350-750		2.31		1.95	1.65	5.3		2.69			Bimodal matrix R2 mosaic with some zoned R3 (inclusion rich core and clear rim) around the vugs. This is ideal R3. There is some sulfur associated with porous R3. There are also saddle dolomite (infill) and vein filling calcite cements. This sample is recrystallized.	R2 - flat orange-red. R3 - bright orange-red. +Blood red and black zoned cement.	570	R2, R2 + R3
						16625.1	5067.4	EH-10		53.48 39.33			PS-NA / PS	200-400 / 300-650				0.86	6.19	4.8				0.14	Bimodal R2 matrix with nonplanar cores and planar edges, different extinction angles. There are some large-large planars crystals associated withopen vugs and veins. This sample is recrystallized (crystal growth - Oswald's ripening).	Matrix - flat orange-red	570	R2
T36	8	27	36	6	W5	11755.1	3583	EH-26		65		29.65	PS-NA	250-500	1.46			1.03	0				2.68		Micro-coarse cristalline matrix R2 with some late dolomite cements, and patches of R4. The R4 that recrystallized remnants represents no longer visible allochems. This sample is recrystallized.	Matrix R2 solid blotchy orange-red, R1 dull, saddle dolomite blood red	570	
						11790.2	3593.7	EH-27		95.9	1.52		PS-NA / PE	250-500 / 200-650					2.51						Micro-coarse cristalline matrix R2 with several crinoids with syntaxial overgrowth, zones of very fine R4 (20-30), and patches of coarse zoned R3 crystals. The zones of R4 are recrystallized allochems. There is one zone of R4 that also contains larger dolomite crystals-this was probably a strom. This sample is recrystallized.	Matrix dull, blotchy orange-red. Echinoderms lighter, distinct blotchiness. R3 dull.	570	
	16	25	36	6	W5	11384.4	3470	EH-57		92.4			PS-NA	250-750		6.32			1.27	4.4					Coarse-crystalline matrix R2 with patches of R4 which represent recrystallized allochems. It is possible that there were more allochems in this sample due to the scattered R4 within the matrix. There is a dolomite cement filled fracture. This sample is recrystallized.	Matrix dull blotchy, orange-red. Blood red cement. Cannot determine R4 patches, possibly dark, but this zone is not visible.	570	

TWN	LSD	SEC	TWN	RGE	MER	(ft)	(m)	Sample ID	R1	R2	R3	R4	Dominance	Diameter, μm	C1	C2	C3	C4	Image analysis	AccuMap	Bitumen	Calcite	Anhydrite	Pyrite	Diagenesis Description	CL-microscopy Description	Spectrum, nm	Drilled
	10	33	36	10	W5	14838.7	4522.9	EH-34		90.3			PS	250-600					9.68	4.6					Micro-coarse cristalline matrix R2 with open vugs. This sample is probably recrystallized.	Matrix blotchy orange-red, cores lighter red blotches, rims dark.		
						14973.2	4563.9	EH-35		29.8	61.68		PS-NA PS	250-260 250-400					0.62	6.1	5.94	1.94			Matrix R3 and R2, bitumen staining cross cuts both. R3 has clear outer zones, indicating interaction with fluids passing through. There is a ghost allochem in the upper right hand corner, within R2. But the R2 there is nonplanar, and looks like Ostwald's ripening of R4. There is a calcite cement associated with vugs. This sample is recrystallized.	Matrix blotchy orange-red, oil zones bright, red R3 with rich rims.	570	R2 R3
						15017.5	4577.4	EH-36		39.7	53.85		PS-NA PE	200-380 250-450					0.96	4.5	5.94				Micro-coarse matrix R2 with clusters of bitumen coated zoned R3 crystals associated with veins and bitumen rich zones. Some crystals that look to be homogenous, tend to have different extinction angles (this could be due to stress during thin section making). This sample is recrystallized.	Flat orange-red matrix; abundant blood red zoned R3 with rich rims	570	R3
						15291.8	4661	EH-37		57.6	28.73		PS-NA PE	260-900 200-600		0.98			3.43		0.36	8.33			Coarse matrix R2 with coarse planar-e R3 associated with fractures and vugs. There is a poikilitic calcite cement growing around the dolomite C2 filling the vugs. This sample is recrystallized.	Matrix dull blotchy orange-red, R3 - cores lighter red, rims dark	570	R2
	11	27	36	10	W5	14685.2	4476.1	EH-44		62	36.23		PS-NA PE	200-400 200-400		0.94			0.57		0.31				Coarse matrix R2 with bitumen coated R3 patches associated with vugs. This sample might be recrystallized.	Matrix dull, blotchy orange-red; blood red cement rims in porous zones	570	
						14730.5	4489.9	EH-45		39		59.52	PS-NA PS-NA	80-130 20-40				0.73	0.14						Matrix micro-crystalline R2 with an abundance of bitumen, oil filled stylolites, abundant zoned dolomite cement, minor calcite cement and zones of R4 (R1) (smaller than matrix). This R4(R1) is either recrystallized allochems or recrystallized mud (R1). This sample was probably predominantly mud sized to begin with. The bitumen emplacement most likely stopped recrystallization at an early stage. This sample is recrystallized.	Matrix R2 flat orange-red, R4 slightly duller (less luminescent), dolomite cement blood red-black, yellow yellow calcite.	570 615	R2
	7	26	36	10	W5	14428.6	4397.9	EH-20		97.3			PS-NA	180-300	0.18				2.54	4.7					Macro-medium crystalline matrix R2. Vugs (probably dissolved biochems) lined or filled in with coarse dolomite cements. This sample is recrystallized.	Matrix- dull, blotchy orange-red. Blood red planar-e cements surrounding and in between open vugs	570	R2

TWN	LSD	SEC	TWN	RGE	MER	(ft)	(m)	Sample ID	R1	R2	R3	R4	Dominance	Diameter, µm	C1	C2	C3	C4	Image analysis	AccuMap	Bitumen	Calcite	Anhydrite	Pyrite	Diagenesis Description	CL-microscopy Description	Spectrum, nm	Drilled
	15	23	36	10	W5	14748.8	4495.5	EH-53		62.8	25.61	8.34	PS-NA PE PS-NA	200-350 100-280 100-250				0.35	2.77	9.4	0.14				Medium matrix R2 that probably originally was R1, it now has larger crystals throughout-can faintly see previous R1ness. Right side is odd-the dolomite looks acicular. But this looks like the recrystallized R4 from large allochem, like stromatoporoid. There are ghost allochems visible with the eye, but not with the mic. There are areas of coarse R3 around vugs and some large dolomite cement. This sample used to be fossiliferous, possibly muddy matrix as well. This sample is extensively recrystallized.	Matrix R2 - blotchy, dull orange-red. R3 around vugs - dull, flat orange-red.	570	R2 + R3
						14912.5	4545.4	EH-54		95.9			PS-NA	200-280		0.28			3.85	1					Macro-medium matrix R2 (some areas smaller and lighter than others). It appears as though the allochems were dissolved, or recrystallized with crystals slightly larger than the matrix. This sample is recrystallized.	Dull, blotchy orange-red matrix, no lighter zones distinction. No rim distinction in cements.	570	
						15067.1	4592.5	EH-55		54.9		34.7	PS-NA PS-NA	130-160 10-20				10.3	2.54						Bitumen stained stylolitized micro-medium R2 mosaic. Allochems filled with R4 with zebra-like sweeping extinction. This sample is recrystallized.	R2 - dull, flat orange-red. 'Zebra'- lighter orange-red. Blood red to zoned cements.	570	R2
T35	11	10	35	5	W5	11008.7	3355.5	EH-40		70		21.93	PS PS-NA	50-120 20-30		0.62			4.31	1.6		2.03	1.08		Dense micro-medium cristalline bitumen coateded matrix. Allochems filled with smaller R4. This sample has been recrystallized, it probably began as a mud.	Dull matrix with small bright red zoned cement	570	
						11023.8	3360.1	EH-41		61.1		37.71	NA PS-NA	50-100 20-30					0				1.13	0.16	Pathces of dense micro-medium cristalline bitumen coated (pores and microfractures) mosaic with elongated cement zones. Allochems filled with slightly larger R4. There are ghost peloids and stromatoporoids. There are a few vugs filled with anhydrite . This sample has been recrystallized (possibly interrupted by oil emplacement)	Extremely dull-nonluminescent, with patches of lighter orange-red unidentifiable biochems, bright red cement	570	R2 R4
						11042.8	3365.9	EH-42	94.54			3.65	PS-NA	20-50					0		1.72		1.8		Dense micro-medium cristalline matrix with bitumen vein crosscutting through it. There are a few allochem ghosts. This sample has been recrystallized.	Dull-nonluminescent orange-red, flat	570	R1

	Well ID					Depth			Dolomite — Matrix, %						Cement, %				Porosity, %		Diagenesis					CL-microscopy		
TWN	LSD	SEC	TWN	RGE	MER	(ft)	(m)	Sample ID	R1	R2	R3	R4	Dominance	Diameter, µm	C1	C2	C3	C4	Image analysis	AccuMap	Bitumen	Calcite	Anhydrite	Pyrite	Description	Description	Spectrum, nm	Drilled
T34	6	24	34		8 W5	14369.6	4379.9	EH-14		49.3		. / 51.53	PS-NA / PS-NA	200-380 / 10-20					0	0.15					Matrix bitumen stained and veined. The larger allochems are mostly filled with hard to distinguish individual crystals R4 (zebra R4). The smaller allochems(crinoids, brachiopod shells) are recrystallized with either matrix size or larger single crystals. Some of the larger allochems (amphipora, larger crinoids) have large crystals on the outer boarders, crosscut by bitumen veins. The recrystallization on this slide was probably rapid and heterogeneous, affecting matrix and smaller allochems, before being stopped by oil emplacement.	Matrix R2 - dull flat red. Biochems - lighter orange-red at least rimmed with blood red cement if not entirely comprised of it.	570	R4
						14389.3	4385.9	EH-15				53.78 / 45.94	PS-NA / PS-NA	180-250 / 10-20					0	0.28					Bitumen stained and stylolitized matrix is represented by a strom (peloid) and many smaller biochems unrecognizable in matrix. The small allochems are recrystallized with matrix sized, cleaner crystals. The larger allochems, stromatoporoids, crinoids and peloids still retain their original textures and structures to a certain extent. They are filled with the same R4 as in the above sample. The matrix does infringe upon these allochems like in the above sample, however, both cases might be due to breaks in the allochem. This sample is less recristallized, because oil came here first, so, fluids probably infiltrated, followed oil pathway.	Matrix dull, flat red, biochems only slightly lighter (small), strom is dark too, but brighter because of pore filling blood red cement marking structure.	570	
																									[There may be several possibilities producing these two samples, 4379.9 and 4385.9.These may be recrystallized primarily in the matrix and allochems (smaller ones=center dissolved+cemented, larger ones may be less recrystallized, but unlikely), the stratigraphically higher one more because of a slightly later emplacement of oil (if oil came from below). OR, Neither sample was dolomitized until the recrystallizing fluids started passing through this reef trend prior to oil emplacement]			
	6	14	34		8 W5	14058.9	4285.2	EH-11		48.4			PS-NA	260-600					0				52.4		Dense macro-medium to micro-coarse cristalline matrix R2 crosscut by anhydrite (massive). The matrix contains some R4 lining the vugs. Most vugs filled with anhydrite as well were probably allochems. The hand specimen contains sulfur. This sample is recrystallized.	Mottled CL (minor blothiness at the top of matrix away from anhydrite)	570	R2
						14064.5	4286.9	EH-12		78.7		. / 15.23	PS-NA / PS-NA	200-350 / 200-400	0.22				0				5.87		Dense macro-medium to micro-coarse cristalline matrix R2. Ghost allochems filled with dolomite slightly larger than matrix, or dissolved or filled with anhydrite. There is some sulfur in the hand specimen. This sample is recrystallized (unless original fabric instigated these crystal sizes).	Matrix dull, slightly blotchy orange-red. Abundant small blood red cement associated with anhydrite and small fractures	570	R2

	Well ID					Depth			Dolomite Matrix, %						Dolomite Cement, %				Porosity, %		Diagenesis					CL-microscopy		
TWN	LSD	SEC	TWN	RGE	MER	(ft)	(m)	Sample ID	R1	R2	R3	R4	Dominance	Diameter, µm	C1	C2	C3	C4	Image analysis	AccuMap	Bitumen	Calcite	Anhydrite	Pyrite	Description	Description	Spectrum, nm	Drilled
T33	13	9	33	4	W5	11236.7	3425	EH-47		81.5			PS-NA	150-300		5.82			0				7.38	0.21	Dense macro-medium cristalline matrix with anhydrite rimmed by coarse (500-750) zoned crystals of C2. This sample is recristallized. R4 is represented either by fine-crystalline matrix or echinoderm fragments.	Matrix dull, blotchy orange-red with zoned cement C2 (orange). R4 slightly duller and flat, echinoderm fragments unrecognizable.	570	
												5.11	PS-NA	40-65														
						11351.6	3460	EH-48		75.5			PS-NA	200-300		0.11			0		+		24.1	0.37	Dense macro-medium cristalline matrix stained with oil rich patches covering matrix associated with anhydrite cemented veins. There are a few brachiopod shells that were preferrentially dissolved and cemented with anhydrite. This sample is recrystallized, but the allochems were probably still fine grained at the time of dissolution, so recrystallization may not have been extensive, but considerable still.	Matrix blotchy or orange-red; oil patches dull, dark red.	570	
						11374.5	3467	EH-49		81.5			PS-NA	180-500		0.25			1.3	5.69			11.3		Clear macro-medium to micro-coarse cristalline matrix, highly stylolitized, with a great amount of bitumen filled veins. There are some vugs filled with calcite cement and dolomite cement rimming these vugs. There are a few zones of R4 adjacent to bitumen veins that are difficult to distinguish (probably recrystallized allochems). This sample is recrystallized. Recrystallizaton occurred before oil emplacement because the veins cut across and into the crystals.	Dull, blotchy orange-red matrix; bitumen areas - dull dark red; calcite cement dull.	570	R2

Appendix 3

Geochemical Database

Data acquired in this study was combined with the results from the previous works.
Values highlighted in purple are acquired from the powders drilled by Kuflevskiy.
Values highlighted in orange and blue are acquired from the powders drilled by
Huebscher (1996) and Horrigan (1996), respectively.

TWN	LSD	SEC	TWN	RGE	MER	Pool	Original sample set	Depth (ft)	Depth (m)	Stratigraphic unit	Core samples	Thin sections	Sample ID	Sample type	CH₄	H₂S	CO₂	δ¹³C‰ PDB (Orig)	δ¹⁸O‰ PDB (Orig)	δ¹³C‰ PDB (SK+adj)	δ¹⁸O‰ PDB (SK+adj)	⁸⁷Sr/⁸⁶Sr	CaCO₃ mol% XRD	6/4Pb	7/4Pb	8/4Pb	Ca 31 ppm	Mg 2 ppm	Li 0.05 ppm	Be 0.1 ppm	B 2 ppm	Na 0.5 ppm	Al 0.2 ppm	Si ppm	P 5 ppm	K 6 ppm	Ti 0.09 ppm	Sc ppm	V 0.05 ppm	Cr 0.05 ppm	Fe 3.7 ppm
T95	2	28	95	18	W4	Liege	Kuflevskiy	1282.8	391	Leduc	x	x	K95-5(R2)	R2						4.48	-5.79	0.708365	49.40				158054	111301	1.50	<DL	11	192	39.9		85	183	2.81		0.82	3.21	1418
										Leduc	x	x	K95-5(R3)	R3						4.24	-5.64	0.708376	50.56				156672	108932	1.39	<DL	7	157	176		99	151	6.15		0.87	4.63	3176
								1426.4	434.77	Leduc	x	x	K95-12(R1)	R1						3.83	-4.38	0.709005	56.25				128225	50710	3.28	<DL	18	1125	1387		172	1539	37.1		4.08	10.2	5017
														calcite						3.74	-6.03																				
T88	3	34	88	20	W4	Orchid	Huebscher	1325	403.9	Leduc	x	x	HH88-1	R2	99.5	0	0.18	2.96	-7.57	2.87	-6.22	0.708234	51.2				141222	97365	4.70	<DL	38	283	716		108	705	21.1		3.47	5.23	2618
								1334	406.6	Leduc	x	x	HH88-2(R3)	R3						2.81	-6.18		50.98				163280	103782	1.40	<DL	8	241	102		38	114	5.59		2.60	3.45	7500
								1396	425.5	Leduc	x	x	HH88-3	Calcite				12.01	-14.39																						
								1500	457.2	Leduc	x	x	HH88-4	Calcite				11.28	-14.42																						
														R2				5.81	-6.67	5.60	-5.40		50.5				185006	117685	2.72	<DL	30	245	30.4		90	108	1.16		0.55	4.26	1437
								1523	464.2	Leduc	x	x	HH88-5	R2				5.46	-6.27	5.25	-5.00		50.5																		
								1530	466.3	Leduc	x	x	HH88-6	R2				5.70	-6.14	5.789	-4.631	0.708998	51.2				145999	101404	2.78	<DL	29	270	173		100	216	9.63		1.46	2.90	1962
T72	11	4	72	23	W4	Canal	Huebscher	3051	930.0	Leduc	x	x	HH72-1(R2a)	R2						2.61	-4.66		50.21				154216	112212	1.74	<DL	12	369	60.2		75	188	3.37		1.33	2.08	744
													HH72-1(R2b)	R2						2.33	-4.60		50.21				154622	111508	1.86	<DL	12	331	104		135	205	6.52		2.07	3.41	2499
								3071	936.1	Leduc	x	x	HH72-3	R2						2.84	-4.34		50.12				188059	87658	1.24	<DL	7	331	13.5		37	85	4.38		0.93	1.93	589
														Calcite						2.59	-5.13																				
								3114	949.1	Leduc	x	x	HH72-5	R2				3.74	-5.75	3.53	-4.48	0.708455	50.64				152803	110750	1.35	<DL	6	435	42.8		71	215	2.37		0.68	1.57	756
T71	15	17	71	25	W4	Smith	Huebscher	3336	1016.8	Leduc	x	x	HH71-2 (R1)	R1				1.35	-5.57	1.29	-4.16	0.709356	51.10				139621	97972	3.67	<DL	21	393	1340		147	1208	27.6		8.24	11.3	11032
																				1.23	-4.18																				
T70	3	28	70	24	W4	Bouvier	Huebscher	3448	1051.0	Leduc	x	x	HH70-1	R2				3.93	-5.97	3.72	-4.70		50.0				153528	108349	3.98	<DL	37	327	93.1		165	257	6.96		1.31	3.91	1219
								3506	1068.0	Leduc	x	x	HH70-2	R2				4.81	-5.92	4.60	-4.65	0.709201	50.5																		
													HH70-2-RPT									0.709144																			
								3528	1075.3	u. Cook. Lk.	x	x	HH70-4	R2				3.50	-5.83	3.29	-4.56		50.7																		
								3568	1087.5	u. Cook. Lk.	x	x	HH70-6	R2				4.50	-5.95	4.29	-4.68	0.708258	50.2				159195	114770	2.20	<DL	20	337	68.2		99	228	4.25		0.76	2.18	934
T68	4	33	68	22	W4	Baptiste	Huebscher	3470	1057.7	l. Cook. Lk.	x	x	HH68-1	R1				1.97	-6.43	1.76	-5.16		51.87				173896	105606	4.65	<DL	23	1253	284		214	353	15.5		34.0	4.79	2727
								3476	1059.5	l. Cook. Lk.	x	x	HH68-2	R2				1.83	-7.39	1.56	-5.95	0.708683	50.75				153164	110745	1.89	<DL	10	385	64.3		112	165	3.72		1.43	3.09	2043
										(no extr.)										1.46	-6.07																				
T67	13	17	67	23	W4	Big Coulee	Kuflevskiy	2958	901.6	Leduc	x	x	K67-2	KD						0.45	-3.92	0.708614	50.19				154493	109022	2.01	<DL	8	987	186		93	265	10.2		2.66	1.98	915
								3203	976.3	Leduc	x	x	K67-3	R1						0.93	-3.84		49.92				183954	116107	3.30	<DL	25	178	292		101	280	9.05		2.78	6.05	1321
T66	4	26	66	26	W4	Big Bend	Huebscher	4081	1243.9	Leduc	x	x	HH66(1)-2	Calcite	92.4	0	2.7			0.39	-5.094						325363	3985	1.22	<DL	3	795	317		170	268	8.06		2.47	4.50	2751
	6	16	66	24	W4	Steele	Huebscher	3298	1005.2	Leduc	x	x	HH66(2)-2	R2	93.5	0.04	1.8	2.12	-5.34	1.38	-4.35	0.708395	50.9				157000	115326	1.34	<DL	13	481	123		149	237	7.33		1.70	2.74	821
								3421	1042.7	u. Cook. Lk.	x	x	HH66(2)-3	R1				0.88	-6.92	0.67	-5.65	0.708872	51.2				150190	108212	5.45	<DL	55	775	997		377	998	26.9		3.33	6.01	2452
								3430	1045.5	u. Cook. Lk.	x	x	HH66(2)-4	R2				2.65	-5.56	2.44	-4.29		50.4																		
								3620	1103.4	u. Cook. Lk.	x	x	HH66(2)-5	R2				2.85	-5.73	2.64	-4.46		50.7				182981	116291	1.09	<DL	13	272	43.2		43	100	1.14		0.78	1.91	448
								3627	1105.5	u. Cook. Lk.	x	x	HH66(2)-6	R1				2.85	-5.73	2.64	-4.46																				
								3677	1120.8	u. Cook. Lk.	x	x	HH66(2)-7	R2				1.70	-5.37	1.49	-4.10		49.2																		
								3893	1186.6	u. Cook. Lk.	x	x	HH66(2)-8(R2)	R2				5.28	-5.86	5.13	-4.54	0.708424	50.0				146627	103693	2.27	<DL	30	337	93.5		132	230	5.12		0.77	3.24	1228
											x	x	HH66(2)-8(R3)	R3						4.46	-4.59		51.12				158219	112041	2.05	<DL	9	726	109		72	149	3.66		0.66	2.22	1276
								4073	1241.5	u. Cook. Lk.	x	x	HH66(2)-9	KD						4.80	-5.42		50.47				225713	73393	1.27	<DL	4	824	341		81	275	6.04		3.50	6.88	6428
														calcite						3.57	-6.56																				
T65	9	39	65	24	W4	Steele	Huebscher	3456	1053.4	Leduc	x	x	HH-65-3	Calcite				4.04	-12.47																						
	5	19	65	24	W4	Steele	Huebscher	4013	1223.2	Cook. Lk.	x	x	HH65(2)-1(R1)	R1				1.09	-3.54	1.04	-4.008																				
											x	x	HH65(2)-1(R2)	R2				1.18	-5.31	0.91	-4.01		50.82				182771	111982	1.87	<DL	7	593	189		2321	249	5.59		1.20	5.03	4079
								4033	1229.3	Cook. Lk.	x	x	HH65(2)-2	R2skeletal				0.86	-6.13	0.65	-4.86	0.708724					155281	96758	7.28	<DL	35	1306	541		9167	603	12.0		22.8	30.0	32978
	12	6	65	24	W4	Bolloque	Huebscher	3854.9	1175	Leduc	x	x	HH65(1)-1	R2				1.97	-6.29	2.09	-4.41		50.68				190340	121006	1.42	<DL	14	297	148		142	242	3.44		1.22	1.99	456
T64	3	24	64	25	W4	Bolloque	Huebscher	3625.8	1105.15	Leduc	x	x	HH64-1	R2	93.4	0	1.6	1.79	-5.54																						
										no extr.										1.37	-4.44	0.708503	50.86				158790	111177	1.74	<DL	8	668	124		95	222	7.06		0.64	2.47	701
T63	5	24	63	25	W4	Bolloque	Huebscher	3674	1119.8	Leduc	x	x	HH63-4	R2				1.62	-5.86	1.34	-4.30		50.53				192338	124962	1.03	<DL	5	409	94.7		93	137	3.50		0.65	5.00	962
																				1.68	-4.17																				
								3722	1134.5	Leduc	x	x	HH63-5	R2				1.40	-6.15	1.19	-4.88		50.49				190000	122154	1.13	<DL	11	344	131		70	167	4.54		0.72	4.07	1187
								4366	1330.8	Leduc	x	x	HH63-7	R2				2.85	-6.16	2.64	-4.89		50.81				179055	114036	1.42	<DL	16	256	31.2		93	167	1.74		0.96	3.91	965
								4375	1333.5	Leduc	x	x	HH63-8	R2				2.75	-4.93	3.09	-4.96		50.88				178148	110553	2.53	<DL	22	253	235		47	264	5.74		1.16	5.04	684
														Calcite				-5.64	-13.35																						
														Calcite				-5.66	-11.32																						

Sample ID	Mn	Co	Ni	Cu	Zn	Ga	Ge	As	Se	Rb	Sr	Y	Zr	Nb	Mo	Ru	Pd	Ag	Cd	Sn	Sb	Te	Cs	Ba	La	Ce	Pr	Nd	Sm	Eu	Gd	Tb	Dy	Ho	Er	Tm	Yb	Lu	Hf	Ta	W	Re	Os	Ir	Pt	Tl	Pb	Bi	Th	U
detection (ppm)	0.03	0.03	0.06	0.03	0.08	0.01	0.02	0.06	0.2	0.04	0.03	0.02	0.09	0.04	0.02	0.01	0.01	0.01	0.06	0.06	0.01	0.02	0.02	0.03	0.03	0.03	0.04	0.03	0.04	0.03	0.03	0.03	0.04	0.02	0.04	0.06	0.05	0.04	0.05	0.02	0.08	0.03	0.08	0.04	0.01	0.05	0.03		0.01	0.03
K95-5(R2)	74.7	1.48	13.3	5.19	7.80	<DL	<DL	0.21	0.4	0.21	60.7	0.87	0.11	<DL	0.16	1.36	<DL	<DL	<DL	0.31	<DL	<DL	<DL	1.81	0.45	0.32	0.06	0.28	<DL	<DL	0.10	<DL	0.08	<DL	<DL	<DL	<DL	<DL	<DL	<DL	3.44	<DL	<DL	<DL	<DL	<DL	0.68		0.03	0.36
K95-5(R3)	128	1.62	17.1	3.23	23.9	0.11	<DL	0.34	0.6	0.36	46.6	0.84	0.38	<DL	0.18	1.44	<DL	<DL	<DL	<DL	<DL	<DL	<DL	4.38	0.41	0.54	0.09	0.39	0.08	<DL	0.12	<DL	0.09	<DL	<DL	<DL	<DL	<DL	<DL	<DL	0.27	<DL	<DL	<DL	<DL	<DL	0.94		0.06	0.24
K95-12(R1)	413	3.01	17.0	3.36	4.09	0.72	<DL	0.68	0.3	6.27	129	3.91	4.36	<DL	0.11	1.28	<DL	<DL	<DL	<DL	<DL	<DL	0.34	11.9	2.89	6.98	0.93	3.85	0.86	0.22	0.99	0.14	0.73	0.14	0.40	<DL	0.32	<DL	<DL	<DL	<DL	<DL	<DL	<DL	<DL	<DL	6.12		1.12	0.21
HH88-1	66.6	2.66	11.0	2.18	6.19	0.26	<DL	0.48	0.3	3.11	82.9	3.47	1.19	<DL	1.55	1.36	<DL	<DL	<DL	0.27	<DL	<DL	0.21	18.8	1.64	2.50	0.38	1.69	0.39	0.12	0.52	0.08	0.48	0.10	0.27	<DL	0.20	<DL	<DL	<DL	15.8	<DL	<DL	<DL	<DL	<DL	4.05		0.43	0.48
HH88-2(R3)	247	1.18	6.44	1.32	1.65	<DL	<DL	0.68	<DL	0.58	39.1	1.43	0.40	<DL	0.50	0.49	0.13	0.13	<DL	<DL	<DL	<DL	<DL	7.65	0.62	1.08	0.17	0.75	0.18	<DL	0.26	<DL	0.21	<DL	0.13	<DL	0.10	<DL	<DL	<DL	1.15	<DL	<DL	<DL	<DL	0.07	8.06		0.28	0.26
HH88-3																																																		
HH88-4	101	0.49	2.77	0.39	25.1	<DL	<DL	<DL	0.3	0.08	69.8	0.37	<DL	<DL	<DL	0.84	<DL	<DL	<DL	0.49	<DL	<DL	<DL	3.06	0.32	0.41	<DL	0.21	<DL	<DL	<DL	<DL	<DL	<DL	<DL	<DL	<DL	<DL	<DL	<DL	5.54	<DL	<DL	<DL	<DL	<DL	0.70		<DL	<DL
HH88-5																																																		
HH88-6	84.8	2.10	9.20	1.12	18.5	<DL	<DL	0.37	0.3	0.49	65.7	1.77	0.73	<DL	0.61	1.41	<DL	<DL	<DL	0.08	<DL	<DL	<DL	8.61	0.96	1.40	0.20	0.80	0.17	<DL	0.22	<DL	0.19	<DL	0.13	<DL	0.09	<DL	<DL	<DL	9.91	<DL	<DL	<DL	<DL	<DL	9.43		0.19	0.28
HH72-1(R2a)	76.2	1.66	8.03	0.27	2.39	<DL	<DL	0.17	0.5	0.29	65.6	1.65	<DL	<DL	0.19	1.49	<DL	<DL	<DL	0.13	<DL	<DL	<DL	3.07	0.69	0.86	0.13	0.55	0.12	<DL	0.17	<DL	0.14	<DL	0.08	<DL	0.08	<DL	<DL	<DL	3.44	<DL	<DL	<DL	<DL	<DL	1.20		0.04	0.13
HH72-1(R2b)	107	2.01	9.72	0.80	51.6	0.11	<DL	0.40	0.2	0.38	69.4	1.74	0.31	<DL	0.45	1.56	<DL	<DL	0.40	0.23	<DL	<DL	<DL	2.95	1.00	1.17	0.17	0.69	0.13	<DL	0.20	<DL	0.16	<DL	0.10	<DL	0.10	<DL	<DL	<DL	7.49	<DL	<DL	<DL	<DL	<DL	3.72		0.05	0.17
HH72-3	55.7	0.52	1.67	0.26	1.06	<DL	<DL	<DL	<DL	0.08	4588	1.10	<DL	<DL	<DL	1.34	0.07	<DL	<DL	<DL	<DL	<DL	<DL	50.7	0.41	0.46	0.08	0.33	0.07	<DL	0.10	<DL	0.08	<DL	<DL	<DL	<DL	<DL	<DL	<DL	1.65	<DL	<DL	<DL	<DL	<DL	0.45		<DL	<DL
HH72-5	72.0	1.65	7.93	0.37	2.50	<DL	<DL	0.19	0.5	0.27	54.8	1.67	0.11	<DL	0.17	1.63	<DL	<DL	<DL	<DL	<DL	<DL	<DL	12.7	0.80	0.91	0.14	0.60	0.11	<DL	0.17	<DL	0.14	<DL	0.09	<DL	<DL	<DL	<DL	<DL	3.08	<DL	<DL	<DL	<DL	<DL	1.25		0.03	0.10
HH71-2 (R1)	252	6.49	17.0	5.80	2.00	0.51	<DL	1.82	0.4	6.53	131	3.17	0.95	<DL	2.44	1.10	<DL	<DL	<DL	0.30	<DL	<DL	0.38	11.8	1.86	4.69	0.64	2.68	0.60	0.15	0.73	0.10	0.55	<DL	0.29	<DL	0.23	<DL	<DL	<DL	57.7	<DL	<DL	<DL	<DL	<DL	20.2		0.70	0.15
HH70-1																																																		
HH70-2	90.4	1.92	9.15	0.60	4.70	<DL	<DL	0.35	0.4	0.33	131	0.84	0.17	<DL	0.39	1.74	<DL	0.08	<DL	0.10	<DL	<DL	<DL	3.71	0.39	0.40	0.06	0.24	<DL	<DL	0.07	<DL	<DL	<DL	<DL	<DL	0.10	<DL	<DL	<DL	6.86	<DL	<DL	<DL	<DL	<DL	1.63		0.05	0.12
HH70-2-RPT																																																		
HH70-4																																																		
HH70-6	96.6	1.84	8.56	2.88	4.76	<DL	<DL	0.24	0.3	0.31	52.9	1.19	0.11	<DL	0.25	1.61	<DL	<DL	<DL	0.11	<DL	<DL	<DL	3.29	0.51	0.47	0.09	0.38	0.08	<DL	0.12	<DL	0.10	<DL	<DL	<DL	<DL	<DL	<DL	<DL	5.10	<DL	<DL	<DL	<DL	<DL	1.66		0.04	0.11
HH68-1	103	3.05	11.0	36.2	1.35	0.19	<DL	0.84	0.3	1.39	79.3	1.28	0.72	<DL	10.7	0.72	0.20	<DL	<DL	0.19	0.11	<DL	0.13	7.44	0.87	2.05	0.27	1.10	0.24	<DL	0.29	<DL	0.23	<DL	0.12	<DL	0.10	<DL	<DL	<DL	3.58	<DL	<DL	<DL	<DL	0.21	4.75		0.29	1.94
HH68-2	83.8	1.97	8.74	0.67	3.37	<DL	<DL	0.31	0.5	0.18	58.9	0.44	<DL	<DL	0.43	1.65	<DL	0.16	<DL	1.81	<DL	<DL	<DL	2.68	0.27	0.43	0.04	0.19	<DL	<DL	0.06	<DL	<DL	<DL	<DL	<DL	<DL	<DL	<DL	<DL	7.83	<DL	<DL	<DL	<DL	<DL	1.91		0.05	0.27
(no extr.)																																																		
K67-2	72.9	1.56	13.0	5.63	5.34	0.11	<DL	0.33	0.3	0.89	52.5	0.51	0.37	<DL	0.28	1.64	<DL	1.09	<DL	0.39	<DL	<DL	<DL	3.07	0.53	1.20	0.14	0.56	0.12	<DL	0.14	<DL	0.10	<DL	<DL	<DL	<DL	<DL	<DL	<DL	0.15	<DL	<DL	<DL	<DL	<DL	1.74		0.22	0.65
K67-3	88.2	1.17	201	3.25	3.66	0.12	<DL	5.59	0.2	0.91	57.7	0.57	0.62	<DL	0.10	0.93	0.13	<DL	<DL	<DL	<DL	<DL	<DL	4.47	0.60	1.23	0.15	0.57	0.11	<DL	0.13	<DL	0.09	<DL	<DL	<DL	<DL	<DL	<DL	<DL	0.20	<DL	<DL	<DL	<DL	<DL	1.95		0.13	0.64
HH66(1)-2	964	2.51	5.94	3.53	21.8	0.22	<DL	0.72	0.3	1.10	336	1.94	0.25	<DL	0.26	1.01	0.16	<DL	0.23	<DL	<DL	<DL	<DL	12.6	1.69	2.41	0.32	1.24	0.24	<DL	0.30	<DL	0.23	<DL	0.14	<DL	0.10	<DL	<DL	<DL	11.5	<DL	<DL	<DL	<DL	<DL	12.2		0.16	0.73
HH66(2)-2	70.4	1.57	6.64	0.52	2.62	0.08	<DL	0.49	0.3	0.49	47.7	1.99	0.16	<DL	0.24	1.52	<DL	<DL	<DL	0.08	<DL	<DL	<DL	3.16	1.05	1.80	0.26	1.07	0.22	<DL	0.29	<DL	0.20	<DL	0.12	<DL	<DL	<DL	<DL	<DL	4.50	<DL	<DL	<DL	<DL	<DL	1.37		0.06	0.59
HH66(2)-3	85.4	2.46	9.95	3.08	5.26	0.31	<DL	1.46	0.0	4.28	81.6	3.31	1.06	<DL	0.49	1.39	<DL	<DL	<DL	0.12	0.06	<DL	0.28	11.8	2.62	3.80	0.51	2.08	0.41	0.10	0.52	<DL	0.35	<DL	0.21	<DL	0.14	<DL	<DL	<DL	9.20	<DL	<DL	<DL	<DL	<DL	4.81		0.45	0.80
HH66(2)-4																																																		
HH66(2)-5	91.0	0.58	2.52	0.56	4.81	<DL	<DL	0.18	0.2	0.11	42.9	1.23	<DL	<DL	<DL	0.80	0.05	<DL	<DL	<DL	<DL	<DL	<DL	2.44	1.01	0.89	0.13	0.54	0.10	<DL	0.14	<DL	0.10	<DL	<DL	<DL	<DL	<DL	<DL	<DL	1.08	<DL	<DL	<DL	<DL	<DL	6.52		<DL	0.12
HH66(2)-6																																																		
HH66(2)-7																																																		
HH66(2)-8(R2)	88.5	1.63	8.01	0.82	4.36	<DL	<DL	1.00	0.3	0.34	49.8	0.81	0.19	<DL	0.37	1.66	<DL	<DL	<DL	<DL	<DL	<DL	<DL	2.94	0.43	0.52	0.08	0.34	0.08	<DL	0.10	<DL	0.08	<DL	<DL	<DL	<DL	<DL	<DL	<DL	3.90	<DL	<DL	<DL	<DL	<DL	1.72		0.08	0.14
HH66(2)-8(R3)	129	1.56	8.01	4.01	6.62	0.12	<DL	0.52	0.3	0.41	49.0	1.47	0.32	<DL	0.21	1.46	<DL	<DL	<DL	0.08	<DL	<DL	<DL	32.0	0.95	1.65	0.23	0.91	0.21	<DL	0.26	<DL	0.18	<DL	0.10	<DL	0.10	<DL	<DL	<DL	1.44	<DL	<DL	<DL	<DL	<DL	5.69		0.40	0.20
HH66(2)-9	220	2.72	6.88	3.45	23.6	0.13	<DL	0.40	0.2	1.00	97.1	2.75	0.34	<DL	0.82	0.81	0.23	<DL	0.19	0.11	<DL	<DL	<DL	3.84	2.49	2.27	0.37	1.49	0.27	<DL	0.35	<DL	0.28	<DL	0.17	<DL	0.12	<DL	<DL	<DL	25.9	<DL	<DL	<DL	<DL	0.08	42.4		0.13	0.32
HH-65-3																																																		
HH65(2)-1(R1)																																																		
HH65(2)-1(R2)	487	1.75	4.42	0.82	1.16	0.24	<DL	2.18	0.6	0.96	70.1	17.97	0.27	<DL	<DL	0.78	0.43	<DL	<DL	<DL	<DL	<DL	<DL	2.63	14.12	23.5	3.06	12.7	2.32	0.56	2.86	0.34	1.94	0.40	1.09	0.12	0.66	<DL	<DL	<DL	7.12	<DL	<DL	<DL	<DL	0.13	15.4		0.91	0.51
HH65(2)-2	1464	26.3	51.4	35.8	7.86	1.05	<DL	16.4	2.3	1.94	153	82.4	0.78	<DL	9.14	0.87	<DL	0.24	<DL	0.97	0.39	<DL	0.11	10.9	23.4	47.2	7.08	37.1	9.83	2.32	12.7	1.64	9.40	1.92	4.98	0.59	2.77	<DL	<DL	<DL	212	<DL	<DL	<DL	<DL	<DL	63.8		0.84	3.15
HH65(1)-1	72.0	1.20	4.19	0.56	1.04	<DL	<DL	0.23	<DL	0.66	44.5	1.93	0.19	<DL	<DL	1.01	0.09	<DL	<DL	<DL	<DL	<DL	<DL	2.01	0.79	1.20	0.20	0.89	0.19	<DL	0.25	<DL	0.18	<DL	0.10	<DL	0.08	<DL	<DL	<DL	1.88	<DL	<DL	<DL	<DL	<DL	1.28		0.10	0.37
HH64-1 no extr.	78.1	2.95	7.68	0.23	110	0.23	<DL	0.43	0.4	0.45	56.9	1.32	0.26	<DL	0.09	1.78	<DL	<DL	0.52	<DL	<DL	<DL	<DL	2.31	1.35	1.21	0.16	0.62	0.11	<DL	0.16	<DL	0.11	<DL	<DL	<DL	<DL	<DL	<DL	<DL	7.33	<DL	<DL	<DL	<DL	<DL	5.09		0.05	0.17
HH63-4	85.8	0.68	3.70	0.34	15.3	<DL	<DL	0.11	0.2	0.27	42.7	0.93	0.12	<DL	<DL	0.99	<DL	<DL	<DL	<DL	<DL	<DL	<DL	2.39	0.69	0.88	0.11	0.45	0.08	<DL	0.12	<DL	0.08	<DL	<DL	<DL	<DL	<DL	<DL	<DL	2.13	<DL	<DL	<DL	<DL	<DL	1.25		<DL	0.13
HH63-5	71.4	6.02	4.59	1.08	7.97	<DL	<DL	0.32	0.3	0.34	49.2	0.94	0.11	<DL	<DL	0.94	0.09	<DL	<DL	<DL	<DL	<DL	<DL	2.24	0.76	0.98	0.12	0.50	0.10	<DL	0.12	<DL	0.09	<DL	<DL	<DL	<DL	<DL	<DL	<DL	15.0	<DL	<DL	<DL	<DL	<DL	3.95		<DL	0.10
HH63-7	98.5	5.27	2.80	0.24	1.14	<DL	<DL	<DL	0.4	0.16	60.6	0.67	0.10	<DL	0.28	0.95	0.38	0.44	<DL	<DL	<DL	<DL	<DL	1.30	0.47	0.56	0.10	0.31	0.07	<DL	0.10	<DL	0.07	<DL	<DL	<DL	<DL	<DL	<DL	<DL	11.7	1.76	<DL	<DL	<DL	<DL	0.50		0.18	0.25
HH63-8	76.5	2.63	3.38	0.70	1.15	0.09	<DL	0.16	<DL	0.85	73.4	0.52	0.31	<DL	0.27	0.91	0.17	<DL	<DL	<DL	<DL	<DL	<DL	3.70	0.41	0.66	0.08	0.33	0.07	<DL	0.09	<DL	0.07	<DL	<DL	<DL	<DL	<DL	<DL	<DL	13.1	<DL	<DL	<DL	<DL	<DL	1.08		0.13	0.41

TWN	LSD	SEC	TWN	RGE	MER	Pool	Original sample set	Depth (ft)	Depth (m)	Stratigraphic unit	Core samples	Thin sections	Sample ID	Sample type	CH₄	H₂S	CO₂	δ¹³C ‰ PDB (Orig)	δ¹⁸O ‰ PDB (Orig)	δ¹³C ‰ PDB (SK+adj)	δ¹⁸O ‰ PDB (SK+adj)	⁸⁷Sr/⁸⁶Sr	CaCO₃ mol% XRD	Ca (31 ppm)	Mg (2 ppm)	Li (0.05 ppm)	Be (0.1 ppm)	B (2 ppm)	Na (0.5 ppm)	Al (0.2 ppm)	Si (ppm)	P (5 ppm)	K (6 ppm)	Ti (0.09 ppm)	Sc (ppm)	V (0.05 ppm)	Cr (0.05 ppm)	Fe (3.7 ppm)
	9	36	63	25	W4	Bolloque	Huebscher	3449	1051.3	Leduc	x	x	HH63-11	R2	94.2	0	0	0.75	-6.80	0.54	-5.53	0.708525	50.38	155593	108919	1.81	<DL	10	341	239		108	257	11.3		1.34	3.46	878
								3461	1054.9	Leduc	x	x	HH63-13	R2				1.17	-6.04	0.96	-4.77		50.40	190853	123111	1.04	<DL	8	361	74.4		64	130	3.60		0.56	3.01	814
T62	16	22	62	25	W4	Meadow	Huebscher	3695	1126.2	Leduc	x	x	HH62-2	R2				1.68	-5.26	1.66	-4.28		50.38	184482	118113	1.09	<DL	6	280	156		81	188	7.08		0.87	5.70	1373
								3701	1128.1	Leduc	x	x	HH62-3	R2				1.77	-5.24	1.56	-4.29		50.84															
								3720	1133.9	Leduc	x	x	HH62-5	KD				1.85	-5.52	1.50	-4.29	0.708419	50.38	159110	113158	1.25	<DL	4	400	145		108	235	6.12		1.03	3.68	1244
														KD						1.46	-4.28																	
T61	13	35	61	23	W4	Abee	Huebscher	3377	1029.3	Leduc	x	x	B-15	Calcite				2.00	-7.14																			
								3388	1032.7	Leduc	x	x	B-16	Calcite				0.58	-12.55																			
								3416	1041.2	Leduc	x	x	B-17	Calcite				1.66	-8.64																			
								3416	1041.2	Leduc	x	x	B-18	Calcite				1.68	-10.70																			
	1	32	61	23	W4	Abee	Huebscher	3752	1143.6	Leduc	x	x	B-20	Calcite				2.17	-9.12																			
								3762	1146.7	Leduc	x	x	B-21	Calcite				1.56	-10.63																			
								3776	1150.9	Leduc	x	x	B-22	Calcite				2.90	-7.79																			
								3807	1160.4	Leduc	x	x	B-23	Calcite				2.30	-9.09																			
	7	31	61	24	W4	Nestow	Huebscher	3491	1064.1	Leduc	x	x	HH61-1	KD				0.45	-5.76	0.50	-4.96	0.708905	49.96	168032	103787	0.83	<DL	<DL	395	75.2		130	154	3.72		2.06	3.83	1420
								3493	1064.7	Leduc	x	x	HH61-2	Calcite				-2.93	-12.46																			
								3496	1065.6	Leduc	x	x	HH61-3	R2				0.99	-4.79	0.82	-4.29		50.49	184345	117676	0.97	<DL	7	282	159		72	192	5.20		1.27	6.04	1518
														Calcite				-3.29	-12.66																			
T59	2	9	59	24	W4	Westlock	Kuflevskiy	3885.6	1184.3	Leduc	x	x	K59-2(R2)	R2						0.99	-3.84		49.82	169404	118248	2.01	<DL	6	375	110		64	153	8.79		1.67	2.62	878
								3885.6	1184.3	Leduc	x		K59-2(R3)	R3						0.64	-3.43	0.708391	51.24	163755	102394	2.27	<DL	6	640	179		113	185	6.85		2.57	6.01	1991
														R3-rerun calcite						0.68	-3.34																	
														R2						9.21	12.08																	
								3893.3	1186.7	Leduc	x		K59-4	R2						1.06	-3.53	0.708310	50.12	158921	109311	2.32	<DL	7	636	116		85	175	6.47		1.47	3.49	934
T58	11	26	58	23	W4	Redwater	Kuflevskiy	4238.6	1291.9	Cook. Lk.	x	x	K58(1)-2(R2)	R2+R3						3.82	-5.87	0.708604	50.40	160299	112129	2.21	<DL	7	385	62.8		94	121	2.53		1.64	1.80	1151
								4238.6	1291.9	Cook. Lk.	x	x	K58(1)-2(R3)	R3						3.69	-6.14		50.10	147023	105230	2.42	<DL	3	468	347		161	273	11.2		2.70	6.83	1738
								4279.4	1304.4	Cook. Lk.	x	x	K58(1)-3	R2						3.87	-6.06		49.84	199797	126115	2.19	<DL	19	578	63.0		47	86	1.92		2.42	5.34	686
	2	5	58	25	W4	Legal	Kuflevskiy	4623.5	1409.25	Leduc	x	x	K58(2)-1	R2	93.7	0	3.5			2.52	-5.27		50.45	200114	122102	3.46	<DL	19	329	274		98	322	5.05		2.79	3.87	1232
								4623.5	1409.25	Leduc	x		K58(2)-1(C1)	C1						1.82	-3.46		52.12	193222	111616	1.13	<DL	5	1224	117		143	204	4.31		1.12	6.85	2490
								4627.1	1410.35	Leduc	x		K58(2)-3	Calcite						-1.82	-12.24																	
								4631.7	1411.75	Leduc	x		K58(2)-5(R2)	R2						2.4	-5.16		50.5	186253	114047	1.83	<DL	3	1551	170		56	179	4.45		1.69	3.77	2325
														K58(2)-5(R3) R3						1.99	-3.54		51.01	171265	106083	4.70	<DL	7	4124	228		72	310	10.3		1.92	6.15	2239
								4640.7	1414.5	Leduc	x		K58(2)-9	R2						1.34	-6.70	0.709968	50.42	209294	61484	1.05	<DL	<DL	237	619		133	539	18.2		3.42	5.68	2822
														Calcite						-0.66	-9.53																	
T57	3	21	57	24	W4	Fairydell-Bon Accord	Horrigan	4034	1229.6	Leduc	x	x	EH-71a(R2)	R2	91.1	0	0.23	1.30	-5.58	1.34	-4.09	0.70825	50.81	181650	125446	1.84	< D.L.	24.9	608	66.4	14.73		187.5		< D.L.	7.3	4.4	397
											x		EH-71b(R1)	R1				1.43	-4.12				50.88	161550	102546	1.58	< D.L.	14.2	388	209.5	96.70		282.3		0.19	8.8	4.7	786
T56	16	24	56	26	W4	Morinville	Kuflevskiy	5264.0	1604.5	Cook. Lk.	x		K56-3	R2						3.38	-4.47	0.708582	50.53	155252	103935	2.86	<DL	11	554	149		82	194	5.12		1.41	2.08	749
								5304.7	1616.9	Cook. Lk.	x	x	K56-7(R2)	R2						2.51	-4.61		49.84	153581	106601	1.73	<DL	12	342	39.6		69	123	2.50		1.12	1.32	831
														K56-7(R3) R3						2.69	-4.68		50.62	158727	101243	2.81	<DL	9	701	176		69	184	8.53		1.99	2.15	934
								5319.7	1621.45	Cook. Lk.	x		K56-10	R2						2.23	-4.67	0.708408	50.25	160488	110195	1.80	<DL	8	447	52.2		83	145	3.01		1.97	1.74	677
T55	7	15	55	25	W4	Morinville	Horrigan	4458	1358.8	Leduc	x	x	EH-75(R2)	R2 (+R3)	85.9	1.07	1.21						49.91	157150	98146	1.10	< D.L.	10.8	420	17.7	18.00		91.3		< D.L.	12.6	3.6	450
											x	x	EH-75(R3)	R3 (+R2)									51.34	135150	85246	0.94	< D.L.	13.7	257	12.6	27.59		96.1		0.07	11.8	3.6	467
													EH-75SK(R3)	R3 (+R2)						1.014	-3.91		50.82	181942	108467	2.80	<DL	5	2299	241		60	232	6.91		7.26	5.73	2851
	2	16	55	25	W4	Morinville	Horrigan	5330	1624.6	Cook. Lk.	x	x	EH-80	R4				4.12	-3.73	4.16	-2.24	0.70841																
	2	16	55	25	W4	Morinville	Kuflevskiy	4372	1332.6	Leduc	x	x	K55-4	R2						-0.04	-3.92	0.708288	50.43	157544	105944	2.61	<DL	11	596	75.5		100	216	3.50		2.66	2.72	1069
														R2-rerun Calcite						-0.05	-3.88																	
														Calcite						-0.25	-4.52																	
														R2-rerun2 Calcite						-0.03	-3.81																	
														Calcite						-0.24	-4.65																	
								4890	1490.5	Leduc	x	x	K55-5	R2						1.16	-4.19		49.68	190535	121307	1.66	<DL	13	576	112		40	212	2.93		0.83	2.89	639
														R2-rerun						1.31	-3.98																	
								5325	1623.1	Cook. Lk.	x		K55-7	R1-brown						4.155	-4.241	0.70841	50.23	198120	126208	2.13	<DL	32	313	12.0		63	98	0.35		0.71	4.53	1494
														R2-black						3.99	-4.311	0.70839	50.31	197925	125783	4.12	<DL	62	232	142		66	175	3.63		3.34	7.08	2600
	6	22	55	26	W4	Morinville	Horrigan	5125.4	1562.25	Leduc		x	N-471	R2				1.99	-5.65	2.03	-4.16		50.88	172450	116246	1.99	< D.L.	21.5	486	76.9	75.45		181.0		0.42	7.5	4.3	1171

Sample ID	Mn	Co	Ni	Cu	Zn	Ga	Ge	As	Se	Rb	Sr	Y	Zr	Nb	Mo	Ru	Pd	Ag	Cd	Sn	Sb	Te	Cs	Ba	La	Ce	Pr	Nd	Sm	Eu	Gd	Tb	Dy	Ho	Er	Tm	Yb	Lu	Hf	Ta	W	Re	Os	Ir	Pt	Tl	Pb	Bi	Th	U
(D.L. ppm)	0.03	0.03	0.06	0.03	0.08	0.01	0.02	0.06	0.2	0.04	0.03	0.02	0.09	0.04	0.02	0.01	0.01	0.01	0.06	0.06	0.01	0.02	0.02	0.03	0.03	0.03	0.04	0.03	0.04	0.03	0.03	0.04	0.02	0.04	0.06	0.05	0.04	0.05	0.02	0.08	0.03	0.08	0.04	0.01	0.05	0.05	0.03		0.01	0.03
HH63-11	76.7	3.37	8.15	0.46	35.7	0.17	<DL	0.83	0.6	0.80	59.4	1.53	0.43	<DL	0.22	1.63	<DL	<DL	0.35	<DL	<DL	<DL	<DL	37.8	0.79	1.26	0.16	0.66	0.14	<DL	0.20	<DL	0.16	<DL	0.10	<DL	<DL	<DL	<DL	<DL	11.3	<DL	<DL	<DL	<DL	<DL	7.43		0.07	0.21
HH63-13	75.9	1.80	3.14	0.20	25.6	<DL	<DL	0.55	<DL	0.25	50.0	1.28	0.13	<DL	<DL	0.91	0.12	<DL	0.25	<DL	<DL	<DL	<DL	1.31	0.98	1.46	0.17	0.67	0.13	<DL	0.18	<DL	0.12	<DL	0.08	<DL	<DL	<DL	<DL	<DL	6.06	<DL	<DL	<DL	<DL	<DL	2.55		<DL	0.15
HH62-2																																																		
HH62-3	85.2	0.64	4.02	0.68	2.68	<DL	<DL	0.15	0.2	0.38	56.1	1.30	0.19	<DL	<DL	0.83	<DL	<DL	<DL	0.34	<DL	<DL	<DL	1.38	0.93	1.20	0.17	0.66	0.15	<DL	0.17	<DL	0.14	<DL	0.09	<DL	0.07	<DL	<DL	<DL	4.38	<DL	<DL	<DL	<DL	<DL	0.99		0.12	0.15
HH62-5	79.6	1.80	8.39	0.73	3.92	0.08	<DL	0.45	0.4	0.55	55.8	1.68	0.17	<DL	0.27	1.45	<DL	0.06	<DL	0.17	<DL	<DL	<DL	3.38	1.30	1.63	0.21	0.84	0.16	<DL	0.24	<DL	0.17	<DL	0.11	<DL	<DL	<DL	<DL	<DL	3.95	<DL	<DL	<DL	<DL	<DL	3.46		0.08	0.14
B-15																																																		
B-16																																																		
B-17																																																		
B-18																																																		
B-20																																																		
B-21																																																		
B-22																																																		
B-23																																																		
HH61-1	119	1.89	8.37	0.82	7.12	0.07	<DL	0.58	0.6	0.31	40.2	2.49	0.21	<DL	0.25	1.63	<DL	<DL	<DL	0.04	<DL	<DL	<DL	4.06	0.76	1.29	0.20	0.83	0.19	<DL	0.27	<DL	0.25	<DL	0.18	0.12	0.12	<DL	<DL	<DL	3.32	<DL	<DL	<DL	<DL	<DL	3.47		0.11	0.20
HH61-2																																																		
HH61-3	88.5	0.64	3.67	0.61	4.44	<DL	<DL	0.17	0.3	0.58	36.9	1.74	0.63	<DL	<DL	1.01	0.07	<DL	<DL	<DL	<DL	<DL	<DL	2.12	0.65	1.07	0.15	0.64	0.13	<DL	0.19	<DL	0.16	<DL	0.11	<DL	0.08	<DL	<DL	<DL	6.51	<DL	<DL	<DL	<DL	<DL	0.67		0.09	0.22
K59-2(R2)	80.3	1.47	14.0	2.67	4.34	0.08	<DL	0.35	0.4	0.33	77.8	2.80	0.23	<DL	0.29	1.44	<DL	0.07	<DL	0.09	<DL	<DL	<DL	1.80	1.27	1.35	0.21	0.90	0.19	<DL	0.30	<DL	0.23	<DL	0.15	<DL	0.10	<DL	<DL	<DL	<DL	<DL	<DL	<DL	<DL	<DL	1.17		0.11	0.78
K59-2(R3)	109	1.65	20.5	22.3	50.5	0.11	<DL	0.76	0.5	0.54	83.6	3.30	0.82	<DL	0.31	1.53	<DL	0.07	0.15	0.70	0.18	<DL	<DL	20.1	1.81	2.50	0.35	1.48	0.30	<DL	0.42	<DL	0.33	<DL	0.21	<DL	0.16	<DL	<DL	<DL	0.55	<DL	<DL	<DL	<DL	<DL	39.0		0.32	0.90
K59-4	75.2	1.45	20.2	24.4	15.5	0.08	<DL	0.39	0.5	0.38	87.5	2.43	0.26	<DL	0.37	1.55	<DL	<DL	<DL	0.43	<DL	<DL	<DL	2.48	1.21	1.20	0.19	0.78	0.16	<DL	0.24	<DL	0.20	<DL	0.13	<DL	0.09	<DL	<DL	<DL	0.10	<DL	<DL	<DL	<DL	<DL	3.65		0.08	0.77
K58(1)-2(R2)	63.8	1.42	124	185	103	<DL	<DL	0.36	0.4	0.22	53.1	0.92	<DL	<DL	0.27	1.41	<DL	0.10	0.40	3.13	0.16	<DL	<DL	2.75	0.44	0.57	0.08	0.36	0.08	<DL	0.11	<DL	0.09	<DL	<DL	<DL	<DL	<DL	<DL	<DL	0.14	<DL	<DL	<DL	<DL	<DL	13.6		0.06	0.19
K58(1)-2(R3)	73.9	1.50	9.42	39.1	27.7	0.14	<DL	0.55	0.4	1.15	53.4	1.08	0.39	<DL	0.35	1.55	<DL	0.06	<DL	0.68	0.07	<DL	0.10	7.12	0.65	1.19	0.15	0.66	0.15	<DL	0.18	<DL	0.14	<DL	<DL	0.09	<DL	<DL	<DL	<DL	0.26	<DL	<DL	<DL	<DL	<DL	5.50		0.24	0.19
K58(1)-3	41.6	0.59	5.16	198	110	<DL	<DL	0.15	0.2	0.26	56.1	0.31	0.14	<DL	0.52	0.93	0.26	0.82	<DL	3.61	0.27	<DL	<DL	1.00	0.17	0.23	<DL	0.14	<DL	<DL	<DL	<DL	<DL	<DL	<DL	<DL	<DL	<DL	<DL	<DL	0.28	<DL	<DL	<DL	<DL	<DL	13.9		0.10	0.50
K58(2)-1	86.5	0.89	15.2	445	242	0.13	<DL	0.89	0.3	1.16	112	3.75	0.53	<DL	0.29	0.95	0.37	0.26	<DL	7.79	0.34	<DL	<DL	3.32	1.95	2.23	0.36	1.50	0.32	0.08	0.42	<DL	0.35	<DL	0.22	<DL	0.16	<DL	<DL	<DL	<DL	<DL	<DL	<DL	<DL	<DL	32.6		0.27	0.83
K58(2)-1(C1)	207	1.31	7.97	6.01	29.6	0.13	<DL	1.71	0.4	0.94	63.0	8.15	0.34	<DL	0.11	1.04	0.43	0.15	<DL	0.23	0.10	<DL	0.11	2.56	9.63	11.0	1.35	4.96	0.81	0.20	1.08	0.14	0.79	0.16	0.44	<DL	0.29	<DL	<DL	<DL	1.71	<DL	<DL	<DL	<DL	<DL	4.28		0.21	0.58
K58(2)-3																																																		
K58(2)-5(R2)	167	1.33	3.56	1.60	14.1	0.09	<DL	0.82	<DL	0.70	46.7	3.08	0.15	<DL	0.51	0.91	0.24	<DL	<DL	<DL	<DL	<DL	<DL	4.06	2.12	2.43	0.34	1.39	0.27	0.07	0.36	<DL	0.28	<DL	0.16	<DL	0.13	<DL	<DL	<DL	8.76	<DL	<DL	<DL	<DL	<DL	5.27		0.07	0.24
K58(2)-5(R3)	172	0.99	3.71	1.57	682	0.12	<DL	1.28	0.3	1.30	63.8	3.51	0.81	<DL	0.43	0.85	0.28	<DL	<DL	<DL	<DL	<DL	0.17	15.5	2.66	4.11	0.54	2.18	0.45	0.10	0.52	<DL	0.41	<DL	0.24	<DL	0.18	<DL	<DL	<DL	0.51	<DL	<DL	<DL	<DL	<DL	7.21		0.90	0.45
K58(2)-9	163	2.21	14.2	220	119	0.28	<DL	2.09	0.7	2.10	127	7.17	0.58	<DL	0.25	1.86	<DL	0.06	<DL	3.56	0.18	<DL	0.13	3.88	4.71	6.40	0.85	3.46	0.73	0.18	1.01	0.13	0.74	0.16	0.45	0.10	0.30	<DL	<DL	<DL	<DL	<DL	<DL	<DL	<DL	<DL	16.8		0.44	0.42
EH-71a(R2)	98	< D.L.	< D.L.	0.05	1.9	0.16		1.18	0.30	0.42	74.2	1.36	0.09	0.01				0.07	< D.L.	< D.L.	< D.L.		< D.L.	1.84	0.94	1.22	0.13	0.66	0.07	0.01	0.17	0.01	0.13	0.01	0.03	< D.L.	0.01	< D.L.	< D.L.	0.05						< D.L.	0.63	0.03	< D.L.	0.23
EH-71b(R1)	82	< D.L.	< D.L.	1.25	104.5	0.44		1.33	0.29	0.93	64.1	1.14	0.18	0.02				0.12	2.37	< D.L.	< D.L.		0.03	5.47	0.77	1.11	0.12	0.61	0.07	0.01	0.17	0.01	0.12	0.01	0.03	< D.L.	0.02	< D.L.	< D.L.	< D.L.						< D.L.	1.82	0.06	0.11	0.29
K56-3	84.3	1.44	12.2	58.7	33.8	<DL	<DL	0.59	0.6	0.52	81.1	2.67	0.25	<DL	0.87	1.58	<DL	<DL	<DL	1.03	0.08	<DL	<DL	3.61	0.95	0.92	0.21	0.94	0.24	<DL	0.35	<DL	0.29	<DL	0.18	<DL	0.13	<DL	<DL	<DL	0.12	<DL	<DL	<DL	<DL	<DL	5.73		0.11	1.74
K56-7(R2)	91.0	1.38	8.62	261	140	<DL	<DL	0.33	0.6	0.15	63.0	1.27	<DL	<DL	0.09	1.57	<DL	0.09	4.41	0.22	<DL	<DL	<DL	1.10	0.64	0.63	0.10	0.41	0.08	<DL	0.14	<DL	0.12	<DL	0.10	<DL	<DL	<DL	<DL	<DL	0.03	<DL	<DL	<DL	<DL	<DL	18.5		0.03	0.27
K56-7(R3)	85.9	1.40	12.2	399	245	0.10	<DL	0.51	0.5	0.71	183	2.57	0.44	<DL	0.15	1.42	<DL	0.10	7.44	0.34	<DL	<DL	<DL	5.74	2.02	2.00	0.30	1.19	0.23	<DL	0.32	<DL	0.24	<DL	0.15	<DL	0.10	<DL	<DL	<DL	0.61	<DL	<DL	<DL	<DL	<DL	30.2		0.28	0.34
K56-10	70.4	1.30	12.0	144	103	<DL	<DL	0.32	0.5	0.19	63.6	2.28	<DL	<DL	0.12	1.46	<DL	0.08	0.17	2.48	0.14	<DL	<DL	1.79	1.13	0.81	0.17	0.71	0.13	<DL	0.21	<DL	0.18	<DL	0.11	<DL	0.08	<DL	<DL	<DL	<DL	<DL	<DL	<DL	<DL	<DL	10.3		0.04	0.70
EH-75(R2)	78	< D.L.	< D.L.	3.60	3.9	0.16		1.30	0.30	0.13	59.2	2.72	0.07	0.00				0.16	< D.L.	< D.L.	< D.L.		< D.L.	2.05	1.09	1.29	0.19	0.86	0.16	0.03	0.31	0.03	0.29	0.04	0.16	< D.L.	0.12	< D.L.	< D.L.	< D.L.						< D.L.	0.86	< D.L.	< D.L.	0.58
EH-75(R3)	73	< D.L.	< D.L.	0.51	1.1	0.30		1.09	0.29	0.09	49.6	2.13	0.13	0.02				0.33	< D.L.	< D.L.	< D.L.		< D.L.	4.90	0.88	1.08	0.15	0.76	0.15	0.03	0.27	0.02	0.20	0.03	0.08	< D.L.	0.08	0.00	< D.L.	< D.L.						< D.L.	0.99	< D.L.	< D.L.	0.39
EH-75SK(R3)	138	0.94	3.10	1.73	5.07	<DL	<DL	0.64	0.3	1.06	53.2	2.17	0.56	<DL	0.27	0.87	1.02	<DL	<DL	0.14	<DL	<DL	0.14	382	1.02	1.82	0.26	1.08	0.25	0.19	0.30	<DL	0.24	<DL	0.15	<DL	0.11	<DL	<DL	<DL	4.16	<DL	<DL	<DL	<DL	<DL	10.4		0.41	0.45
EH-80																																																		
K55-4	83.2	2.06	9.45	147	79.0	<DL	<DL	0.68	0.4	0.34	92.2	0.53	0.63	<DL	0.24	1.39	<DL	<DL	<DL	9.80	0.16	<DL	<DL	2.35	0.25	0.35	0.05	0.19	<DL	<DL	0.06	<DL	0.06	<DL	<DL	<DL	<DL	<DL	<DL	<DL	5.12	<DL	<DL	<DL	<DL	<DL	15.2		0.05	0.46
K55-5	67.1	0.55	4.40	114	63.8	<DL	<DL	0.23	<DL	0.38	68.3	1.06	<DL	<DL	<DL	0.91	0.07	<DL	<DL	2.01	0.10	<DL	<DL	1.48	0.66	1.00	0.14	0.54	0.12	<DL	0.15	<DL	0.12	<DL	0.07	<DL	<DL	<DL	<DL	<DL	<DL	<DL	<DL	<DL	<DL	<DL	8.70		0.07	0.15
K55-7	102	0.54	2.34	0.69	2.05	<DL	<DL	<DL	<DL	0.08	89.9	0.40	<DL	<DL	<DL	0.93	<DL	<DL	<DL	0.13	<DL	<DL	<DL	3.29	0.28	0.37	<DL	0.19	<DL	<DL	<DL	<DL	<DL	<DL	<DL	<DL	<DL	<DL	<DL	<DL	6.03	<DL	<DL	<DL	<DL	<DL	1.38		<DL	0.21
	71.8	0.77	5.05	3.04	4.87	0.10	<DL	0.55	<DL	0.49	102	1.26	0.17	<DL	0.68	0.95	0.16	<DL	<DL	0.41	<DL	<DL	<DL	4.59	1.29	1.60	0.18	0.74	0.13	<DL	0.18	<DL	0.11	<DL	<DL	<DL	<DL	<DL	<DL	<DL	15.5	<DL	<DL	<DL	<DL	<DL	5.00		0.07	0.39
N-471	95	< D.L.	< D.L.	5.50	2.4	0.20		1.70	0.30	0.65	90.3	2.65	0.23	0.01				0.18	< D.L.	0.05	< D.L.		0.05	2.88	2.23	2.04	0.33	1.19	0.31	0.05	0.28	0.03	0.27	0.04	0.13	0.02	0.09	0.00	< D.L.	0.01						0.05	4.08	0.04	0.23	0.40

TWN	LSD	SEC	TWN	RGE	MER	Pool	Original sample set	Depth (ft)	Depth (m)	Stratigraphic unit	Core samples	Thin sections	Sample ID	Sample type	CH₄	H₂S	CO₂	Orig δ¹³C ‰PDB	Orig δ¹⁸O ‰PDB	SK δ¹³C ‰PDB	SK δ¹⁸O ‰PDB	⁸⁷Sr/⁸⁶Sr	CaCO₃ mol% XRD	6/4Pb	7/4Pb	8/4Pb	Ca 31 ppm	Mg 2 ppm	Li 0.05 ppm	Be 0.1 ppm	B 2 ppm	Na 0.5 ppm	Al 0.2 ppm	Si ppm	P 5 ppm	K 6 ppm	Ti 0.09 ppm	Sc ppm	V 0.05 ppm	Cr 0.05 ppm	Fe 3.7 ppm
								5427.1	1654.2	Leduc		x	N-473	R2				1.57	-5.37	1.61	-3.88	0.70851	51.38				113350	52446	0.67	< D.L.	8.6	282	1.6	7.54		94.4		< D.L.	8.1	3.4	405
T54	14	18	54	25	W4	Morinville	Kuflevskiy	5347	1629.8	Cook. Lk.	x	x	K54-1	R2 / R2-rerun						1.52 / 1.57	-3.94 / -3.79	0.708338	50.36				157909	108284	3.49	<DL	41	655	170		667	334	5.52		2.75	2.83	3434
	8	14	54	26	W4	Morinville	Kuflevskiy	5291	1612.7	Leduc	x		K54(2)-1	R2 / R2-rerun	66.9	0	5.6			2.76 / 2.85	-4.28 / -4.04		49.84				192789	124330	1.12	<DL	7	352	172		58	258	3.24		0.67	2.32	983
								5308.6	1618.1	Leduc	x	x	K54(2)-5	R2 / R2-rerun						0.84 / 1.01	-4.47 / -4.38	0.708540	49.38				157831	110011	1.57	<DL	10	645	31.7		115	159	2.62		1.74	2.10	800
T53	2	14	53	26	W4	Acheson	Horrigan	5069.2	1545.1	Leduc		x	N-420	R2	80	0.26	1.6	2.75	-6.65	2.79	-5.16	0.70852	50.88				111050	83746	1.22	< D.L.	13.9	682	75.9	98.60		304.4		0.77	12.7	4.2	540
	2	14	53	26	W4	Acheson	Ning	5020.9	1530.4	Leduc		x	N-422	MD, sk.	80	0.26	1.6	2.82	-5.13	2.72	-5.37	0.70806		18.064	15.541	37.483															
	10	4	53	25	W4	Acheson East	Kuflevskiy	5551	1692.0	Cook. Lk.	x		K53-1(R2) / K53-1(R3)	R2 / R3 / R3-rerun						1.21 / 1.80 / 1.82	-6.51 / -5.30 / -5.27	0.708529	51.08 / 50.91				165795 / 159427	106817 / 101812	2.16 / 1.08	<DL / <DL	9 / <DL	233 / 529	98.6 / 192		79 / 108	140 / 189	3.04 / 5.13		1.28 / 1.90	5.26 / 8.06	1419 / 3182
								5560	1694.7	Cook. Lk.	x	x	K53-2(R3)	R3						1.75	-5.31		50.84				196795	116772	1.52	<DL	9	217	72.2		51	101	2.79		2.77	3.85	3002
T52	15	23	52	26	W4	Acheson	Horrigan	5076.7	1547.4	Leduc		x	N-461 / N-461(R4)	R2 / R4	78.93	0.05	1.84	2.10	-5.92	2.14	-4.43	0.70849	50.11 / 50.58				202184 / 54150	118572 / 15946	0.87 / 0.42	<DL / < D.L.	26 / 7.6	165 / 170	24.4 / 22.0	117.96	59	39 / 122.6	0.77	0.61	4.05 / 12.5	2.30 / 4.0	748 / 287
	15	23	52	26	W4	Acheson	Ning	5019.0	1529.8	Leduc		x	N-467	MD, sk.	78.93	0.05	1.84	1.80	-5.11	1.70	-5.35																				
								5040.3	1536.3	Leduc		x	N-465	MD, sk.				1.54	-5.53	1.44	-5.77																				
								5076.7	1547.4	Leduc		x	N-461a(R4)	R4				1.88	-5.45	1.78	-5.69	0.70833		22.527	15.797	37.858															
													N-461b(R4)	R4				2.03	-5.23	1.93	-5.47	0.70813		29.257	16.15	37.573															
T51	9	27	51	27	W4	Golden Spike	Ning	5567	1696.8	Leduc		x	N-404	CC	67.3	0	2.8					0.70803		19.049	15.583	38.075															
								5847	1782.2	Leduc		x	N-408	CC								0.70809		18.93	15.594	37.906															
								5853	1784.0	Leduc			N-411	CC								0.70803		19.078	15.554	37.688															
	6	11	51	26	W4	Leduc-Woodbend	Kuflevskiy	5846.7	1782.1	Cook. Lk.	x	x	K51-2(R2) / K51-2(R4)	R2 / R2-rerun / R4 / R4-rerun						2.79 / 2.96 / 2.58 / 2.60	-4.61 / -4.55 / -4.99 / -4.93		50.47 / 50.10				163247 / 165226	107290 / 108814	2.18 / 2.17	<DL / <DL	32 / 30	272 / 341	135 / 132		74 / 68	210 / 147	4.24 / 3.99		1.34 / 1.20	5.89 / 4.34	1571 / 1590
	6	11	51	26	W4	Leduc-Woodbend	Horrigan	5771.9	1759.3	Cook. Lk.	x	x	N-91(R1)	R1				2.82	-6.44	2.86	-4.95	0.70902																			
	6	11	51	26	W4	Leduc-Woodbend	Ning	6203.5	1890.8	Cook. Lk.	x		N-85	CC				3.02	-7.03	2.92	-7.27	0.70882		18.265	15.543	37.936															
	8	16	51	25	W4	Whitemud	Ning	5748	1752.0	Cook. Lk.		x	N-194a	R4				4.31	-5.92	4.21	-6.16	0.70829																			
								5748	1752.0	Cook. Lk.		x	N-194c	filling. Dol.				2.73	-6.6	2.63	-6.84	0.70867																			
								5748	1752.0	Cook. Lk.		x	N-194d	filling. Dol.				3.03	-5.76	2.93	-6.00	0.70845																			
								5776	1760.5	Cook. Lk.		x	N-191a	MD				4.54	-7.2	4.44	-7.44																			
								5776	1760.5	Cook. Lk.		x	N-191b	MD				3.00	-6.35	2.90	-6.59	0.70850		17.944	15.5	37.499															
								5812.5	1771.7	Cook. Lk.		x	N-189a	MD				4.26	-6.51	4.16	-6.75	0.70822		18.496	15.561	37.714															
								5812.5	1771.7	Cook. Lk.		x	N-189b	MD				3.94	-6.45	3.84	-6.69																			
								5830.4	1777.1	Cook. Lk.		x	N-188	MD				5.02	-5.78	4.92	-6.02	0.70820		18.362	15.581	38.029															
								5828.4	1776.5	Cook. Lk.		x	N-187	MD				5.80	-6.68	5.70	-6.92																			
								5846	1781.9	Cook. Lk.			N-184	C4				3.61	-5.94	3.51	-6.18	0.70873		17.596	15.498	37.251															
								5849	1782.8	Cook. Lk.		x	N-183	C4				3.50	-6.42	3.40	-6.66	0.70867																			
								5851	1783.4	Cook. Lk.		x	N-182	C4				4.15	-5.53	4.05	-5.77	0.70869																			
T50	8	34	50	26	W4	Leduc-Woodbend	Ning	5982.5	1823.5	Leduc	x		N-67	R2	78.1	2.8	2.7			4.21	-5.77																			
	8	17	50	26	W4	Leduc-Woodbend	Horrigan	5591.8	1704.4	Leduc		x	N-58-a	R2	78.1	2.8	2.7	2.05	-6.07	2.09	-4.58	0.70842	49.38				124050	74546	1.32	< D.L.	14.6	288	85.9	106.01		189.7		0.55	12.1	4.4	808
												x	N-58-b	R2				2.20	-5.92	2.24	-4.43	0.70831	51.03				130350	96046	1.42	< D.L.	19.2	645	82.4	90.66		249.5		0.66	11.8	4.8	507
												x	N-58-c	R2									50.11				110750	61446	2.40	0.13	39.3	520	127.0	55.04		255.5		0.08	10.4	5.0	1880
								6354.6	1936.9	Leduc		x	N-324(R1)	R1 (R4?)				2.41	-6.41	2.31	-6.65	0.70819																			
	8	17	50	26	W4	Leduc-Woodbend	Ning	5394.5	1644.3	Leduc		x	N-66	MD	78.1	2.8	2.7	1.34	-5.8	1.24	-6.04	0.70828																			
								5525.5	1684.2	Leduc		x	N-62	MD				2.46	-4.45	2.36	-4.69	0.70823																			
								5531	1685.9	Leduc		x	N-61a	C4				2.23	-6.65	2.13	-6.89	0.70982		17.746	15.535	37.476															
								5531	1685.9	Leduc		x	N-61b	CC				1.59	-7.98	1.49	-8.22	0.71003		18.029	15.525	37.575															
								5609	1709.6	Leduc		x	N-56	MD				1.67	-5.35	1.57	-5.59	0.70861		20.249	15.817	38.304															
								5644.5	1720.5	Leduc		x	N-54	C2						-0.10	-0.24	0.70828		20.039	15.677	39.326															
								5691	1734.6	Leduc		x	N-52	MD				2.09	-5.01	1.99	-5.25	0.70847		18.199	15.537	37.700															

Sample ID	Mn	Co	Ni	Cu	Zn	Ga	Ge	As	Se	Rb	Sr	Y	Zr	Nb	Mo	Ru	Pd	Ag	Cd	Sn	Sb	Te	Cs	Ba	La	Ce	Pr	Nd	Sm	Eu	Gd	Tb	Dy	Ho	Er	Tm	Yb	Lu	Hf	Ta	W	Re	Os	Ir	Pt	Tl	Pb	Bi	Th	U
(D.L. ppm)	0.03	0.03	0.06	0.03	0.08	0.01	0.02	0.06	0.2	0.04	0.03	0.02	0.09	0.04	0.02	0.01	0.01	0.01	0.06	0.06	0.01	0.02	0.02	0.03	0.03	0.03	0.04	0.03	0.04	0.03	0.03	0.04	0.02	0.04	0.06	0.05	0.04	0.05	0.02	0.08	0.03	0.08	0.04	0.01	0.05	0.05	0.03		0.01	0.03
N-473	61	< D.L.	< D.L.	0.87	281.1	0.41		0.75	0.30	0.10	49.0	1.07	< D.L.	0.01				0.30	0.68	< D.L.	< D.L.		< D.L.	4.07	0.44	0.56	0.06	0.37	0.05	0.01	0.14	0.01	0.10	0.00	0.02	< D.L.	< D.L.	< D.L.	< D.L.	< D.L.						< D.L.	0.60	< D.L.	< D.L.	0.13
K54-1	102	2.29	18.1	603	346	0.13	<DL	4.34	0.8	1.02	102	3.06	0.20	<DL	1.75	1.20	<DL	0.26	<DL	10.6	0.66	<DL	<DL	5.30	2.35	3.04	0.43	1.83	0.35	0.09	0.49	<DL	0.30	<DL	0.15	<DL	<DL	<DL	<DL	<DL	0.19	<DL	<DL	<DL	<DL	<DL	48.8		0.42	1.08
K54(2)-1	81.6	0.81	4.95	324	182	<DL	<DL	0.47	<DL	0.86	45.0	1.84	0.13	<DL	0.23	0.83	0.13	<DL	<DL	5.76	0.29	<DL	<DL	2.26	0.87	1.19	0.19	0.78	0.17	<DL	0.22	<DL	0.17	<DL	0.11	<DL	0.08	<DL	<DL	<DL	<DL	<DL	<DL	<DL	<DL	<DL	23.6		0.11	0.36
K54(2)-5	97.2	1.28	8.57	309	171	<DL	<DL	0.45	0.7	0.15	56.4	2.58	0.13	<DL	0.19	1.44	<DL	0.15	<DL	5.33	0.27	<DL	<DL	1.33	0.97	1.04	0.16	0.71	0.15	<DL	0.24	<DL	0.21	<DL	0.15	<DL	0.10	<DL	<DL	<DL	0.11	<DL	<DL	<DL	<DL	<DL	21.6		0.06	0.37
N-420	73	< D.L.	< D.L.	2.03	3.1	0.64		1.50	< D.L.	0.34	46.2	1.00	0.11	0.01				0.33	< D.L.	0.34	< D.L.		0.00	7.97	0.63	0.70	0.09	0.41	0.08	0.00	0.13	0.01	0.09	0.01	0.04	0.01	0.02	< D.L.	< D.L.	< D.L.						0.00	#####	0.05	0.08	0.04
N-422																																																		
K53-1(R2)	115	1.86	13.2	165	95.3	<DL	<DL	0.48	0.8	0.35	71.2	1.22	<DL	<DL	0.38	1.45	<DL	0.07	<DL	2.65	0.14	<DL	<DL	2.97	0.64	0.98	0.14	0.56	0.12	<DL	0.18	<DL	0.14	<DL	<DL	<DL	<DL	<DL	<DL	<DL	4.97	<DL	<DL	<DL	<DL	<DL	13.6		0.08	0.28
K53-1(R3)	210	1.92	12.9	16.7	23.7	0.10	<DL	0.82	0.9	0.88	48.6	1.77	0.32	<DL	0.57	1.37	<DL	0.16	<DL	0.29	0.08	<DL	<DL	4.87	1.00	2.07	0.29	1.28	0.29	<DL	0.34	<DL	0.27	<DL	0.15	<DL	0.11	<DL	<DL	<DL	0.57	<DL	<DL	<DL	<DL	<DL	14.0		0.26	0.25
K53-2(R3)	127	2.20	3.66	7.24	1.29	<DL	<DL	0.48	<DL	0.42	149	0.98	<DL	<DL	0.31	0.77	0.24	<DL	<DL	1.32	0.09	<DL	<DL	1.07	0.69	1.06	0.15	0.62	0.12	<DL	0.15	<DL	0.11	<DL	0.07	<DL	<DL	<DL	<DL	<DL	4.50	<DL	<DL	<DL	<DL	<DL	8.79		0.08	0.39
N-461	89.2	0.61	2.04	0.45	1.59	<DL	<DL	<DL	<DL	<DL	42.7	1.91	<DL	<DL	0.15	0.93	0.18	<DL	<DL	<DL	<DL	<DL	<DL	1.04	0.75	0.88	0.13	0.55	0.10	<DL	0.16	<DL	0.12	<DL	0.08	<DL	<DL	<DL	<DL	1.23	<DL	<DL	<DL	<DL	<DL	<DL	0.59		<DL	1.19
N-461(R4)	61	< D.L.	< D.L.	0.53	1.7	0.10		1.16	< D.L.	0.09	19.2	0.73	0.12	0.01				0.02	0.07	0.19	0.01		< D.L.	0.92	0.36	0.44	0.05	0.27	0.03	0.00	0.08	0.00	0.07	0.00	0.01	< D.L.	0.01	< D.L.	< D.L.	0.56						< D.L.	1.37	0.08	0.05	0.01
N-467																																																		
N-465																																																		
N-461a(R4)																																																		
N-461b(R4)																																																		
N-404																																																		
N-408																																																		
N-411																																																		
K51-2(R2)	102	1.38	12.2	289	169	<DL	<DL	0.48	0.9	0.51	73.9	0.94	0.20	<DL	0.94	1.37	<DL	0.16	<DL	4.71	0.23	<DL	<DL	3.19	0.43	0.60	0.09	0.37	0.08	<DL	0.12	<DL	0.10	<DL	<DL	<DL	<DL	<DL	<DL	2.15	<DL	<DL	<DL	<DL	<DL	<DL	21.6		0.07	0.34
K51-2(R4)	117	1.50	10.2	81.9	65.6	<DL	<DL	0.46	0.8	0.46	82.0	0.84	0.18	<DL	0.21	1.33	<DL	<DL	<DL	1.33	0.09	<DL	<DL	5.54	0.47	0.75	0.10	0.43	0.10	<DL	0.13	<DL	0.11	<DL	<DL	<DL	<DL	<DL	<DL	0.28	<DL	<DL	<DL	<DL	<DL	<DL	10.2		0.10	0.16
N-91(R1)																																																		
N-85																																																		
N-194a																																																		
N-194c																																																		
N-194d																																																		
N-191a																																																		
N-191b																																																		
N-189a																																																		
N-189b																																																		
N-188																																																		
N-187																																																		
N-184																																																		
N-183																																																		
N-182																																																		
N-67																																																		
N-58-a	66	< D.L.	< D.L.	0.31	1.0	0.15		1.80	< D.L.	0.37	54.6	1.29	0.18	0.01				0.01	< D.L.	< D.L.	< D.L.		< D.L.	0.88	0.66	0.95	0.11	0.52	0.12	0.01	0.16	0.01	0.12	0.00	0.04	< D.L.	0.03	< D.L.	< D.L.	< D.L.						< D.L.	0.68	< D.L.	< D.L.	0.03
N-58-b	78	< D.L.	< D.L.	3.36	1.8	0.14		1.68	< D.L.	0.37	52.1	1.60	0.13	0.02				0.07	< D.L.	0.27	< D.L.		0.03	1.18	1.01	1.18	0.17	0.65	0.16	0.02	0.19	0.02	0.19	0.02	0.07	0.01	0.04	< D.L.	< D.L.	< D.L.						0.01	2.41	0.02	0.08	0.07
N-58-c	100	< D.L.	< D.L.	0.27	1.4	0.12		0.90	0.30	0.52	62.6	1.47	0.15	0.00				0.03	< D.L.	< D.L.	< D.L.		0.09	1.49	1.15	1.15	0.23	0.63	0.14	0.01	0.19	0.01	0.10	0.01	0.15	0.08	0.03	< D.L.	< D.L.	< D.L.						0.13	6.12	0.12	0.19	0.19
N-324(R1)																																																		
N-66																																																		
N-62																																																		
N-61a																																																		
N-61b																																																		
N-56																																																		
N-54																																																		
N-52																																																		

TWN	LSD	SEC	TWN	RGE	MER	Pool	Orig. sample set	Depth (ft)	Depth (m)	Stratigraphic unit	Core samples	Thin sections	Sample ID	Sample type	CH₄	H₂S	CO₂	δ¹³C‰ PDB (Orig)	δ¹⁸O‰ PDB (Orig)	δ¹³C‰ PDB (SK+adj)	δ¹⁸O‰ PDB (SK+adj)	⁸⁷Sr/⁸⁶Sr	CaCO₃ mol% XRD	6/4Pb	7/4Pb	8/4Pb	Ca 31 ppm	Mg 2 ppm	Li 0.05 ppm	Be 0.1 ppm	B 2 ppm	Na 0.5 ppm	Al 0.2 ppm	Si ppm	P 5 ppm	K 6 ppm	Ti 0.09 ppm	Sc ppm	V 0.05 ppm	Cr 0.05 ppm	Fe 3.7 ppm
								5741.5	1750.0	Leduc			N-49	MD								0.70829																			
								5748	1752.0	Leduc			N-47									0.70820																		
								5803	1768.8	Leduc		x	N-45	MD				2.26	-4.6	2.16	-4.84	0.70822																		
								5832	1777.6	Leduc		x	N-43	R2				2.05	-3.38	1.95	-3.62	0.70821																		
								5966	1818.5	Leduc			N-36	MD				3.05	-5.30	2.95	-5.54	0.70821																		
								5996	1827.6	Leduc		x	N-328	MD				1.63	-5.68	1.53	-5.92	0.70830		17.980	15.552	37.625															
								6035	1839.5	Leduc		x	N-33	MD				1.80	-4.44	1.70	-4.68	0.70827		20.659	15.547	37.456															
								6128	1867.8	Leduc		x	N-26	MD				3.10	-6.75	3.00	-6.99																			
								6206	1891.6	Leduc		x	N-327	MD				3.03	-6.36	2.93	-6.6	0.70841																		
								6328	1928.8	Leduc		x	N-16	MD				5.21	-4.9	5.11	-5.14	0.70822		18.578	15.565	38.016															
								6354.6	1936.9	Leduc		x	N-324a	CC-coral				2.41	-6.41	2.31	-6.65	0.70819		18.233	15.572	37.629															
								6354.6	1936.9	Leduc		x	N-324b	CC-strom				2.52	-7.8	2.42	-8.04	0.70849		18.439	15.549	37.912															
								6381	1945.0	Leduc		x	N-13	CC						-0.10	-0.24	0.70835																		
								6407	1952.9	Leduc		x	N-319	CC				4.03	-5.93	3.93	-6.17	0.70819		18.433	15.552	38.154															
	8	17	50	26	W4	Leduc-Woodbend Amthor		6289	1916.9	Leduc	x		A50-38	R2	78.1	2.8	2.7			6.28	-5.91		50.45				191454	109886	1.70	<DL	10	238	108		64	115	2.73		1.13	6.23	2342
								6299	1920.0	Leduc	x		A50-39	R2						5.56	-4.94		50.38																		
								6303	1921.2	Leduc			A50-40-1(R3)	R2+R3				4.26	-6.06	4.22	-5.08																			
								6303	1921.2	Leduc			A50-40-2(R3)	R2+R3				4.69	-5.65	4.65	-4.67																			
								6303	1921.2	Leduc			A50-40-3(R3)	R2+R3				4.54	-6.04	4.50	-5.06																			
								6303	1921.2	Leduc			A50-40-1	R2				4.58	-6.12	4.54	-5.14																			
								6303	1921.2	Leduc			A50-40-2	R2				4.77	-6.19	4.73	-5.21																			
								6315	1924.8	Leduc	x		A50-42	R2						5.42	-4.68		50.46																		
								6323	1927	Leduc			A50-43-2	R2				5.20	-6.40	5.16	-5.42																			
								6323	1927	Leduc			A50-43-1	R2				5.00	-6.20	4.96	-5.22																			
								6332	1930	Leduc			A50-44-1	R2				4.76	-7.26	4.72	-6.28																			
								6332	1930	Leduc			A50-44-2	R2				5.99	-7.45	5.95	-6.47																			
								6332	1930	Leduc			A50-44-3	R2				4.23	-6.19	4.19	-5.21																			
								6332	1930	Leduc			A50-44-1(R3)	R2+R3				5.10	-5.93	5.06	-4.95																			
								6332	1930	Leduc			A50-44-2(R3)	R2+R3				4.50	-6.48	4.46	-5.50																			
								6332	1930	Leduc			A50-44-1(R4)	R4				5.65	-6.85	5.61	-5.87																			
								6334	1931	Leduc			A50-45	dol. Ls.				2.80	-8.40	2.76	-7.42																			
								6344.6	1933.9	Leduc	x		A50-N-14(R3)	R3						5.16	-6.11		50.62				190281	99488	0.58	<DL	2	237	186		51	113	4.82		2.04	6.65	4470
								6352	1936	Leduc			A50-47-a	dol. Ls.				3.07	-7.63	3.03	-6.65																			
								6352	1936	Leduc			A50-47-1(R4)	R4				2.77	-8.66	2.73	-7.68																			
								6352	1936	Leduc			A50-47-b	dol. Ls.				5.12	-7.08	5.08	-6.10																			
								6357	1938	Leduc			A50-48-a	dol. Ls.				4.50	-6.30	4.46	-5.32																			
								6357	1938	Leduc			A50-48-b	dol. Ls.				2.20	-8.30	2.16	-7.32																			
								6378	1944	Leduc			A50-49	dol. Ls.				2.70	-7.50	2.66	-6.52																			
T49	4	10	49	26	W4	Leduc-Woodbend Kuflevskiy		6311	1923.6	Cook. Lk.	x	x	K49-2	R2						3.33	-5.98	0.708313	50.80				166986	108183	3.37	<DL	36	216	57.4		79	130	2.37		2.20	5.48	1571
								6362	1939.2	Cook. Lk.	x		K49-3	R2						3.66	-6.05	0.708344	50.10				165167	109314	3.27	<DL	52	250	67.2		60	150	2.49		1.13	4.33	1083
														R2-rerun						3.81	-5.97																				
	9	30	49	25	W4	Leduc-Woodbend Ning		5246	1599	Leduc	x		N-228	R2						3.45	-5.85		50.4				189318	112900	1.47	<DL	14	90.2	37.9		68	31	1.66		13.7	7.13	3681
													+sphalerite	C1						3.52	-6.05		50.6				182205	109465	0.94	<DL	7	87.3	108		135	51	3.68		5.64	3.36	6442
T48	3	10	48	26	W4	Wizard Lake Kuflevskiy		6734	2052.5	Cook. Lk.	x		K48-1	Calcite						5.24	-6.00						333389	11418	1.19	<DL	4	258	213		46	248	1.84		0.45	2.02	849
								6742	2055.0	Cook. Lk.	x		K48-2	Calcite						5.73	-6.37						339692	5251	0.84	<DL	3	154	171		51	174	2.20		0.37	3.32	542
														Calcite						5.58	-6.58																				
	14	22	48	27	W4	Wizard Lake Ning		6436	1961.7	Leduc		x	N-234a(R2)	R2	87.8	0	0	3.18	-6.02	3.08	-6.26	0.70830																			
								6436	1961.7	Leduc			N-234b(R4)	R4?				2.46	-6.05	2.36	-6.29	0.70832																			
								6436	1961.7	Leduc			N-234c(R4)	R4?				3.48	-4.26	3.38	-4.50	0.70822																			
	5	22	48	27	W4	Wizard Lake Amthor		6679.7	2036	Leduc	x		A48-76	R2	3.7	0	0			2.25	-4.57						207203	122424	1.13	<DL	7	398	51.8		46	170	2.59		2.56	4.93	1525
														R2-rerun						2.25	-4.48																				
													A48-76(R3)	R2+R3				2.30	-5.70	2.26	-4.72						190941	114891	0.88	<DL	5	272	65.5		58	113	3.18		1.06	3.40	1190
								6707.9	2044.6	Leduc	x		A48-81	R2						2.29	-5.06																				
														R2-rerun						2.30	-4.98																				
													A48-81(R3)	R3				2.30	-5.80	2.26	-4.82						189540	113850	0.65	<DL	5	189	54.1		53	61	2.68		1.44	4.19	1675
	3	22	48	27	W4	Wizard Lake Horrigan		6354	1936.7	Ireton		x	N-307(R4)	R4	70.3	0.03	0.6	3.91	-6.07	3.95	-4.58	0.70861	51.67				243150	115546	1.33	0.14	8.9	353	128.2	125.79		257.5		< D.L.	9.5	3.7	8051
								6543.2	1994.4	Leduc	x	x	N-304	R2									51.47				176550	112946	2.04	< D.L.	18.0	415	74.3	78.29		221.0		0.40	16.5	4.3	1103
								6628.9	2020.5	Leduc	x	x	N-288-a(R2)	R2				1.97	-6.36	2.01	-4.87	0.70825	50.41				177650	117546	2.39	0.01	19.6	379	144.3	127.59		250.2		0.61	18.9	4.8	1220
											x	x	N-288-b(R4)	R4									51.37				117750	48546	0.97	< D.L.	11.9	226	22.6	46.97		143.5		0.30	13.7	3.8	229

Sample ID	Mn	Co	Ni	Cu	Zn	Ga	Ge	As	Se	Rb	Sr	Y	Zr	Nb	Mo	Ru	Pd	Ag	Cd	Sn	Sb	Te	Cs	Ba	La	Ce	Pr	Nd	Sm	Eu	Gd	Tb	Dy	Ho	Er	Tm	Yb	Lu	Hf	Ta	W	Re	Os	Ir	Pt	Tl	Pb	Bi	Th	U
	0.03	0.03	0.06	0.03	0.08	0.01	0.02	0.06	0.2	0.04	0.03	0.02	0.09	0.04	0.02	0.01	0.01	0.01	0.06	0.06	0.01	0.02	0.02	0.03	0.03	0.03	0.04	0.03	0.04	0.03	0.03	0.04	0.02	0.04	0.06	0.05	0.04	0.05	0.02	0.08	0.03	0.08	0.04	0.01	0.05	0.03	0.05	0.03	0.01	0.03
	ppm	ppm	ppm	ppm	ppm	ppm	ppm	ppm	ppm	ppm	ppm	ppm	ppm	ppm	ppm	ppm	ppm	ppm	ppm	ppm	ppm	ppm	ppm	ppm	ppm	ppm	ppm	ppm	ppm	ppm	ppm	ppm	ppm	ppm	ppm	ppm	ppm	ppm	ppm	ppm	ppm	ppm	ppm	ppm	ppm	ppm	ppm	ppm	ppm	ppm
N-49																																																		
N-47																																																		
N-45																																																		
N-43																																																		
N-36																																																		
N-328																																																		
N-33																																																		
N-26																																																		
N-327																																																		
N-16																																																		
N-324a																																																		
N-324b																																																		
N-13																																																		
N-319																																																		
A50-38	116	0.75	2.41	1.00	1.72	<DL	<DL	0.14	<DL	0.39	56.8	0.60	<DL	<DL	0.10	0.78	0.18	<DL	<DL	<DL	<DL	<DL	<DL	2.19	0.47	0.70	0.10	0.37	0.08	<DL	0.09	<DL	0.07	<DL	<DL	<DL	<DL	<DL	<DL	<DL	13.8	<DL	<DL	<DL	<DL	<DL	3.03		0.15	<DL
A50-39																																																		
A50-40-1(R3)																																																		
A50-40-2(R3)																																																		
A50-40-3(R3)																																																		
A50-40-1																																																		
A50-40-2																																																		
A50-42																																																		
A50-43-2																																																		
A50-43-1																																																		
A50-44-1																																																		
A50-44-2																																																		
A50-44-3																																																		
A50-44-1(R3)																																																		
A50-44-2(R3)																																																		
A50-44-1(R4)																																																		
A50-45																																																		
A50-N-14(R3)	162	1.10	3.89	1.17	2.34	<DL	<DL	0.20	<DL	0.49	51.0	1.25	0.15	<DL	0.25	0.96	0.73	0.12	<DL	0.18	<DL	<DL	<DL	2.41	0.89	1.48	0.19	0.76	0.14	<DL	0.17	<DL	0.13	<DL	<DL	<DL	<DL	<DL	<DL	<DL	9.95	<DL	<DL	<DL	<DL	<DL	6.24		0.23	<DL
A50-47-a																																																		
A50-47-1(R4)																																																		
A50-47-b																																																		
A50-48-a																																																		
A50-48-b																																																		
A50-49																																																		
K49-2	63.5	1.48	12.1	24.5	16.5	<DL	<DL	0.42	1.0	0.20	97.4	1.12	<DL	<DL	0.22	1.31	<DL	0.09	0.14	0.44	<DL	<DL	<DL	3.81	1.10	0.90	0.12	0.47	0.08	<DL	0.13	<DL	0.09	<DL	<DL	<DL	<DL	<DL	<DL	<DL	2.47	<DL	<DL	<DL	<DL	<DL	6.07		0.05	0.39
K49-3	59.6	1.52	12.2	172	102	<DL	<DL	0.41	0.9	0.24	81.6	0.77	<DL	<DL	0.24	1.20	<DL	0.15	<DL	2.84	0.14	<DL	<DL	2.99	0.44	0.58	0.08	0.34	0.07	<DL	0.11	<DL	0.09	<DL	<DL	<DL	<DL	<DL	<DL	<DL	2.74	<DL	<DL	<DL	<DL	<DL	13.2		0.04	0.20
N-228	135	618	3.52	1.74	11.6	<DL	<DL	0.43	<DL	<DL	50.5	2.25	<DL	<DL	0.79	0.88	0.59	<DL	<DL	0.13	<DL	<DL	<DL	1.96	1.08	1.31	0.19	0.76	0.16	<DL	0.22	<DL	0.17	<DL	0.12	<DL	0.08	<DL	<DL	<DL	307	<DL	<DL	<DL	<DL	<DL	7.38		0.09	0.45
+sphalerite	126	1.30	3.02	2.64	293	0.22	0.15	0.80	<DL	0.40	42.5	2.73	0.17	<DL	0.56	0.78	0.80	<DL	1.81	0.12	<DL	<DL	<DL	10.2	1.16	1.82	0.30	1.36	0.30	<DL	0.39	<DL	0.27	<DL	0.15	<DL	0.10	<DL	<DL	<DL	2.76	<DL	<DL	<DL	<DL	<DL	34.0		0.22	0.49
K48-1	56.2	0.95	28.4	263	146	<DL	<DL	0.20	<DL	0.77	247	0.50	<DL	<DL	<DL	1.33	0.11	<DL	<DL	4.77	0.21	<DL	<DL	3.58	0.47	1.08	0.13	0.51	0.10	<DL	0.12	<DL	0.08	<DL	<DL	<DL	<DL	<DL	<DL	<DL	<DL	<DL	<DL	<DL	<DL	<DL	19.0		0.11	<DL
K48-2	64.3	0.88	18.7	4.89	3.50	<DL	<DL	<DL	<DL	0.51	215	0.53	<DL	<DL	<DL	1.23	0.12	<DL	<DL	<DL	<DL	<DL	<DL	2.54	0.51	1.07	0.13	0.50	0.10	<DL	0.13	<DL	0.09	<DL	<DL	<DL	<DL	<DL	<DL	<DL	<DL	<DL	<DL	<DL	<DL	<DL	1.57		0.10	<DL
N-234a(R2)																																																		
N-234b(R4)																																																		
N-234c(R4)																																																		
A48-76	89.8	0.62	1.74	0.70	10.9	<DL	<DL	<DL	<DL	0.23	59.8	1.51	<DL	<DL	0.09	1.08	0.15	<DL	<DL	0.21	<DL	<DL	<DL	0.77	0.67	0.66	0.13	0.53	0.12	<DL	0.18	<DL	0.14	<DL	0.09	<DL	<DL	<DL	<DL	<DL	10.9	<DL	<DL	<DL	<DL	<DL	2.68		<DL	0.27
A48-76(R3)																																																		
A48-81	79.2	0.62	1.82	0.62	2.56	<DL	<DL	0.36	<DL	0.25	48.5	1.44	<DL	<DL	<DL	0.96	0.14	<DL	<DL	0.13	<DL	<DL	<DL	1.23	0.63	0.76	0.13	0.53	0.12	<DL	0.17	<DL	0.12	<DL	0.08	<DL	<DL	<DL	<DL	<DL	4.19	<DL	<DL	<DL	<DL	<DL	0.84		<DL	0.27
A48-81(R3)	116	0.63	1.84	0.89	5.69	<DL	<DL	0.42	<DL	0.18	40.9	1.49	<DL	<DL	<DL	1.04	0.13	<DL	<DL	<DL	<DL	<DL	<DL	0.59	0.56	0.73	0.12	0.53	0.12	<DL	0.16	<DL	0.13	<DL	0.08	<DL	<DL	<DL	<DL	<DL	4.79	<DL	<DL	<DL	<DL	<DL	1.52		<DL	0.18
N-307(R4)	222	< D.L.	< D.L.	0.86	3.9	0.52		1.83	< D.L.	0.67	56.8	1.83	0.10	0.01				0.36	< D.L.	< D.L.	< D.L.		0.05	2.29	1.62	2.38	0.35	1.20	0.22	0.03	0.19	0.03	0.24	0.03	0.15	0.06	0.06	< D.L.	< D.L.	< D.L.						0.07	8.72	0.09	0.19	0.21
N-304	93	< D.L.	< D.L.	2.26	2.0	0.11		1.95	< D.L.	0.31	61.3	2.58	0.08	0.01				0.42	< D.L.	< D.L.	< D.L.		< D.L.	< D.L.	1.34	1.65	0.24	1.17	0.22	0.04	0.32	0.03	0.31	0.04	0.13	0.02	0.08	0.01	< D.L.	< D.L.						0.01	3.01	0.04	0.06	0.63
N-288-a(R2)	94	< D.L.	< D.L.	2.23	2.8	0.30		2.21	< D.L.	0.61	90.3	2.96	0.23	0.01				2.24	1.63	0.04	< D.L.		0.02	2.43	1.41	1.31	0.23	1.07	0.20	0.04	0.35	0.04	0.34	0.05	0.16	0.02	0.08	0.01	< D.L.	< D.L.						0.02	2.71	0.02	0.10	0.44
N-288-b(R4)	49	< D.L.	< D.L.	0.32	2.1	0.09		1.40	< D.L.	0.13	56.3	1.32	0.08	0.01				0.24	< D.L.	< D.L.	< D.L.		< D.L.	0.87	0.67	0.59	0.09	0.51	0.07	0.01	0.19	0.01	0.15	0.02	0.04	< D.L.	0.03	< D.L.	< D.L.	< D.L.						< D.L.	1.79	0.01	< D.L.	0.14

246

TWN	LSD	SEC	TWN	RGE	MER	Well ID	Pool	Orig. sample set	Depth (ft)	Depth (m)	Stratigraphic unit	Core samples	Thin sections	Sample ID	Sample type	CH₄	H₂S	CO₂	δ¹³C ‰ PDB (Orig.)	δ¹⁸O ‰ PDB (Orig.)	δ¹³C ‰ PDB (SK+adj)	δ¹⁸O ‰ PDB (SK+adj)	⁸⁷Sr/⁸⁶Sr	CaCO₃ mol% XRD	6/4Pb	7/4Pb	8/4Pb	Ca 31 ppm	Mg 2 ppm	Li 0.05 ppm	Be 0.1 ppm	B 2 ppm	Na 0.5 ppm	Al 0.2 ppm	Si ppm	P 5 ppm	K 6 ppm	Ti 0.09 ppm	Sc ppm	V 0.05 ppm	Cr 0.05 ppm	Fe 3.7 ppm
	3	22	48	27	W4	Wizard Lake	Ning		6354	1936.7	Leduc		x	N-307a	MD	70.3	0.03	0.6	4.18	-4.82	4.08	-5.06																				
														N-307b	CC				1.98	-7.76	1.88	-8.00	0.70848		18.666	15.597	38.056															
									6518.5	1986.9	Leduc		x	N-306a	MD				1.57	-5.74	1.47	-5.98																				
														N-306b	MD				1.62	-5.65	1.52	-5.89	0.70820																			
									6526.5	1989.3	Leduc		x	N-305a	R4								0.70837																			
														N-305b	R4				2.51	-4.5	2.41	-4.74	0.70823																			
														N-305c	MD				2.63	-5.2	2.53	-5.44	0.70891																			
									6543.2	1994.4	Leduc		x	N-304	R4				1.8	-5.62	1.70	-5.86	0.70834																			
									6546.5	1995.4	Leduc		x	N-302a	MD				2.18	-5.29	2.08	-5.53	0.70835																			
														N-302b	C4				2.95	-7.46	2.85	-7.70	0.70954		17.721	15.493	37.355															
														N-302c	C4								0.70970																			
									6549.5	1996.3	Leduc		x	N-301a	MD, sk.				1.58	-5.21	1.48	-5.45	0.70817																			
														N-301b	C4				3.15	-6.03	3.05	-6.27																				
									6553	1997.4	Leduc		x	N-298	MD				2.31	-6.68	2.21	-6.92	0.70873																			
									6633.5	2021.9	Leduc		x	N-296a	C4				2.21	-7.86	2.11	-8.10	0.71124		17.592	15.489	37.220															
														N-296b	CC				2.01	-8.82	1.91	-9.06	0.71177		17.537	15.492	37.129															
									6564	2000.7	Leduc		x	N-294a	MD				1.28	-5.94	1.18	-6.18	0.70867																			
														N-294b	MD, sk.				2.24	-7.18	2.14	-7.42																				
														N-294c	MD, sk.				2.24	-7.18	2.14	-7.42	0.70817																			
									6594	2009.9	Leduc		x	N-292	MD				2.64	-5.39	2.54	-5.63	0.70840																			
									6692	2039.7	Leduc		x	N-282a	MD				2.08	-4.19	1.98	-4.43	0.70821																			
														N-282c	MD, sk.				2.18	-4.34	2.08	-4.58	0.70824																			
									6693	2040.1	Leduc		x	N-281	MD, sk.								0.70840																			
									6704	2043.4	Leduc		x	N-280	MD				2.52	-5.52	2.42	-5.76	0.71174		20.060	15.664	38.117															
									6909	2105.9	Leduc			N-271	C4				2.97	-6.63	2.87	-6.87	0.70861		17.935	15.549	37.898															
									6958	2120.8	Leduc		x	N-270a	MD				4.34	-5.69	4.24	-5.93																				
														N-270b	filling dol.				3.93	-5.96	3.83	-6.20	0.70831																			
									6980	2127.5	Leduc			N-266	C4				2.84	-8.44	2.74	-8.68																				
T47	3	20	47	27	W4	Bonnie Glen	Horrigan		6557.9	1998.9	Leduc	x	x	N-215(R4)	R4	68.5	0.45	0										207650	146346	0.87	< D.L.	9.6	197	< D.L.	< D.L.		< D.L.		< D.L.	10.4	< D.L.	463
	3	19	47	27	W4	Bonnie Glen	Ning		7086	2159.8	Leduc	x		N-199	CC	74.5	0.34	0.93	1.8	-8.98	1.7	-9.22																			
									7091	2161.4	Leduc	x		N-198(R3)	R3													197914	116870	1.43	<DL	5	349	341		75	271	5.35		3.27	5.56	2874
	16	7	47	27	W4	Bonnie Glen	Ning		6526	1989.1	Leduc		x	N-159	MD	74.5	0.34	0.93	2.15	-5.13	2.05	-5.37	0.70870																			
									6574	2003.8	Leduc		x	N-156	MD				2.36	-4.64	2.26	-4.88																			
									6594	2009.9	Leduc	x	x	N-155a-grey	R2				2.36	-4.64	2.26	-4.88	0.70831	50.61	17.962	15.532	37.226	176093	4291	0.23	<DL	4	57.3	1.9		31	16	8.53		0.11	0.64	203
														N-155b-white	R2						2.17	-4.68		50.82				194386	120026	1.08	<DL	11	398	22.2		66	106	0.71		1.63	6.19	1261
									6711	2045.5	Leduc	x	x	N-151	R2				3.65	-4.49	3.46	-4.67	0.70846	50.18	21.096	15.713	38.173	189346	107489	0.90	<DL	6	267	159		125	249	5.64		1.27	8.56	1719
	?					?					Leduc	x		N-148	R2						2.39	-4.26																			
									6855	2089.4	Leduc		x	N-147	MD				2.08	-5.46	1.98	-5.7	0.70814																			
									6855	2089.4	Leduc		x	N-147	MD				2.25	-6.16	2.15	-6.4	0.70823																			
	?					?					Leduc	x		N-146	R2						2.48	-4.59																			
	?					?					Leduc	x	x	N-145	MD								0.708207		18.048	15.515	37.748															
	?					?					Leduc			N-144	R2				3.24	-4.81	3.14	-5.05																			
									6904	2104.4	Leduc	x	x	N-141	R2						2.12	-4.45																			
									6990	2130.6	Leduc	x	x	N-140	R2				1.63	-5.19	1.38	-4.42																			
									7029	2142.5	Leduc		x	N-139	MD				1.84	-4.32	1.74	-4.56	0.70824																			
									7049	2148.6	Leduc		x	N-138	MD				2.85	-4.94	2.75	-5.18	0.70837		17.939	15.466	37.23															
	?					?					Leduc	x		N-137	R2						2.09	-4.29																			
	?					?					Leduc	x		N-135	R2						1.73	-4.46																			
									7069	2154.7	Leduc		x	N-134	MD				1.84	-4.32	1.74	-4.56	0.70842																			
	?					?					Leduc	x		N-133	R2						1.88	-4.97																			
									7085	2159.5	Leduc	x	x	N-132	R2				1.86	-4.37	1.87	-4.57	0.70828	50.24				188496	105043	0.67	<DL	6	300	71.1		102	136	4.27		0.83	9.59	1250
	13	8	47	27	W4	Bonnie Glen	Amthor		6916	2108	Leduc			A47-1(R3)	R2+R3	69.3	0.16	1.44	2.70	-5.60	2.66	-4.62																			
									6929	2112	Leduc			A47-2(R3)a	R2+R3				2.20	-5.00	2.16	-4.02																			
									6929	2112	Leduc			A47-2(R3)b	R2+R3				2.30	-5.10	2.26	-4.12																			
									6929	2112	Leduc			A47-2	C1				2.60	-5.90	2.56	-4.92																			
									6940	2115	Leduc			A47-3(R3)a	R2+R3				2.30	-5.60	2.26	-4.62																			
									6940	2115	Leduc			A47-3(R3)a	R2+R3				2.20	-6.20	2.16	-5.22																			
									7011	2137	Leduc			A47-4	R2				3.30	-5.80	3.26	-4.82																			
									7011	2137	Leduc			A47-4-a	C1				2.90	-6.30	2.86	-5.32																			
									7011	2137	Leduc			A47-4-b	C1				2.90	-6.20	2.86	-5.22																			
									7015	2138	Leduc			A47-5(R3)a	R2+R3				3.30	-5.60	3.26	-4.62																			
									7015	2138	Leduc			A47-5(R3)b	R2+R3				3.10	-5.70	3.06	-4.72																			
									7015	2138	Leduc			A47-5(R3)c	R2+R3				2.90	-6.30	2.86	-5.32																			

Sample ID	Mn	Co	Ni	Cu	Zn	Ga	Ge	As	Se	Rb	Sr	Y	Zr	Nb	Mo	Ru	Pd	Ag	Cd	Sn	Sb	Te	Cs	Ba	La	Ce	Pr	Nd	Sm	Eu	Gd	Tb	Dy	Ho	Er	Tm	Yb	Lu	Hf	Ta	W	Re	Os	Ir	Pt	Tl	Pb	Bi	Th	U
(detection limit)	0.03 ppm	0.03 ppm	0.06 ppm	0.03 ppm	0.08 ppm	0.01 ppm	0.02 ppm	0.06 ppm	0.2 ppm	0.04 ppm	0.03 ppm	0.02 ppm	0.09 ppm	0.04 ppm	0.02 ppm	0.01 ppm	0.01 ppm	0.01 ppm	0.06 ppm	0.06 ppm	0.01 ppm	0.02 ppm	0.02 ppm	0.03 ppm	0.03 ppm	0.03 ppm	0.04 ppm	0.03 ppm	0.04 ppm	0.03 ppm	0.03 ppm	0.03 ppm	0.04 ppm	0.02 ppm	0.04 ppm	0.06 ppm	0.05 ppm	0.04 ppm	0.05 ppm	0.02 ppm	0.08 ppm	0.03 ppm	0.08 ppm	0.04 ppm	0.01 ppm	0.05 ppm	0.03 ppm		0.01 ppm	0.03 ppm
N-307a																																																		
N-307b																																																		
N-306a																																																		
N-306b																																																		
N-305a																																																		
N-305b																																																		
N-305c																																																		
N-304																																																		
N-302a																																																		
N-302b																																																		
N-302c																																																		
N-301a																																																		
N-301b																																																		
N-298																																																		
N-296a																																																		
N-296b																																																		
N-294a																																																		
N-294b																																																		
N-294c																																																		
N-292																																																		
N-282a																																																		
N-282c																																																		
N-281																																																		
N-280																																																		
N-271																																																		
N-270a																																																		
N-270b																																																		
N-266																																																		
N-215(R4)	99	< D.L.	< D.L.	0.19	1.0	0.09		1.84	< D.L.	< D.L.	49.1	1.68	< D.L.	0.00				0.30	< D.L.	< D.L.	< D.L.		< D.L.	0.67	0.84	0.86	0.08	0.55	0.06	< D.L.	0.11	0.00	0.12	< D.L.	0.01	< D.L.	< D.L.	< D.L.	< D.L.	< D.L.					< D.L.	1.44	< D.L.	< D.L.		0.11
N-199																																																		
N-198(R3)	144	1.20	2.59	2.23	48.7	0.13	<DL	0.80	<DL	1.65	73.2	2.26	0.22	<DL	0.53	0.83	0.37	<DL	<DL	0.20	<DL	<DL	0.21	20.9	1.16	2.27	0.34	1.41	0.32	<DL	0.38	<DL	0.27	<DL	0.15	<DL	0.11	<DL	<DL	<DL	1.89	<DL	<DL	<DL	<DL	<DL	8.68		0.36	0.19
N-159																																																		
N-156																																																		
N-155a-grey	5.07	0.49	<DL	0.59	3.37	<DL	<DL	<DL	<DL	<DL	1346	0.09	<DL	<DL	<DL	<DL	0.30	0.09	<DL	<DL	<DL	<DL	<DL	0.59	0.08	0.13	<DL	0.07	<DL	<DL	<DL	<DL	<DL	<DL	<DL	<DL	<DL	<DL	<DL	<DL	0.86	<DL	<DL	<DL	<DL	<DL	0.46		<DL	<DL
N-155b-white	83.3	0.58	0.88	1.14	1.09	<DL	<DL	<DL	<DL	0.13	46.1	0.76	<DL	<DL	<DL	0.84	0.24	<DL	<DL	0.15	<DL	<DL	<DL	1.25	0.24	0.27	<DL	0.21	<DL	<DL	0.07	<DL	0.07	<DL	<DL	<DL	<DL	<DL	<DL	<DL	9.63	<DL	<DL	<DL	<DL	<DL	0.81		<DL	0.14
N-151	83.9	0.96	3.05	1.27	2.13	<DL	<DL	0.18	<DL	0.73	44.4	1.64	0.17	<DL	0.12	1.16	0.39	<DL	<DL	<DL	<DL	<DL	<DL	2.87	1.04	1.32	0.19	0.74	0.14	<DL	0.19	<DL	0.12	<DL	<DL	<DL	<DL	<DL	<DL	<DL	7.71	<DL	<DL	<DL	<DL	<DL	4.19		0.13	0.31
N-148																																																		
N-147																																																		
N-147																																																		
N-146																																																		
N-145																																																		
N-144																																																		
N-141																																																		
N-140																																																		
N-139																																																		
N-138																																																		
N-137																																																		
N-135																																																		
N-134																																																		
N-133																																																		
N-132	87.1	0.98	2.63	0.63	1.75	<DL	<DL	0.18	0.3	0.30	41.4	1.76	0.15	<DL	<DL	1.08	0.55	<DL	<DL	<DL	<DL	<DL	<DL	1.94	0.59	0.70	0.12	0.52	0.12	<DL	0.16	<DL	0.13	<DL	<DL	<DL	<DL	<DL	<DL	<DL	3.64	<DL	<DL	<DL	<DL	<DL	2.64		0.13	0.24
A47-1(R3)																																																		
A47-2(R3)a																																																		
A47-2(R3)b																																																		
A47-2																																																		
A47-3(R3)a																																																		
A47-3(R3)a																																																		
A47-4																																																		
A47-4-a																																																		
A47-4-b																																																		
A47-5(R3)a																																																		
A47-5(R3)b																																																		
A47-5(R3)c																																																		

TWN	LSD	SEC	TWN	RGE	MER	Pool	Original sample set	Depth (ft)	Depth (m)	Stratigraphic unit	Core samples	Thin sections	Sample ID	Sample type	CH₄	H₂S	CO₂	δ¹³C ‰ PDB (Orig)	δ¹⁸O ‰ PDB (Orig)	δ¹³C ‰ PDB (SK+adj)	δ¹⁸O ‰ PDB (SK+adj)	⁸⁷Sr/⁸⁶Sr	CaCO₃ mol% XRD	6/4Pb	7/4Pb	8/4Pb	Ca 31 ppm	Mg 2 ppm	Li 0.05 ppm	Be 0.1 ppm	B 2 ppm	Na 0.5 ppm	Al 0.2 ppm	Si ppm	P 5 ppm	K 6 ppm	Ti 0.09 ppm	Sc ppm	V 0.05 ppm	Cr 0.05 ppm	Fe 3.7 ppm
								7023	2141	Leduc			A47-6(R4)a	R4				3.40	-6.70	3.36	-5.72																				
								7023	2141	Leduc			A47-6(R4)b	R4				3.10	-6.20	3.06	-5.22																				
								7023	2141	Leduc			A47-6(R4)c	R4				3.30	-5.90	3.26	-4.92																				
								7023	2141	Leduc			A47-6	R2				3.50	-5.70	3.46	-4.72																				
T46	12	36	46	28	W4	Bonnie Glen	Ning	7070.1	2155	Leduc	x		N-207(R3)	R3	74.5	0.34	0.93			3.01	-4.98		50.63				199948	118569	0.69	<DL	6	238	17.1		44	75	0.72		1.39	3.54	1235
								7567.2	2306.5	Leduc	x		N-201-R2	R2						2.98	-5.07		50.21				209393	122505	1.43	<DL	9	217	9.3		44	70	0.32		0.62	3.03	1036
													N-201-R3	R3						3.05	-5.03		50.33				195313	113732	0.87	<DL	4	98.2	43.6		45	16	1.98		1.27	5.89	2695
	8	4	46	28	W4	Westerose	Horrigan	7240.7	2207	Leduc	x	x	EH-23-a(R2)	R2	88.3	0	3.85			2.95	-5.15		50.11				192450	134546	1.71	< D.L.	16.1	485	332.4	151.46		459.6		0.39	1.3	5.8	2888
								7240.7	2207	Leduc			EH-23-b(R1)	R1									50.61				160550	107946	1.74	0.05	14.2	366	458.7	134.84		603.8		0.67	17.6	5.8	1676
								7240.7	2207	Leduc			EH-23-c(R4)	R4									51.14				141950	95846	0.79	< D.L.	10.5	350	28.4	79.31		178.9		0.48	13.5	4.2	574
								7329.3	2234	Leduc	x	x	EH-24(R4)	R4				3.39	-6.00	3.40	-4.53	0.70942	49.91				190250	129146	1.87	0.04	19.3	391	141.1	175.00		293.8		0.58	1.8	4.8	2019
																				3.45	-4.84																				
	8	4	46	28	W4	Westerose	Amthor	7239	2207	Leduc			A46-1a	R2	88.3	0	3.85	2.94	-6.14	2.90	-5.16																				
								7239	2207	Leduc			A46-1b	R2				2.99	-6.13	2.95	-5.15																				
								7239	2207	Leduc			A46-1c	R2				2.86	-6.20	2.82	-5.22																				
								7239	2207	Leduc			A46-1(R3)a	R2+R3				2.95	-6.66	2.91	-5.68																				
								7239	2207	Leduc			A46-1(R3)b	R2+R3				2.26	-5.94	2.22	-4.96																				
								7239	2207	Leduc			A46-1(R3)c	R2+R3				2.55	-5.80	2.51	-4.82																				
								7239	2207	Leduc			A46-1(R3)d	R2+R3				2.90	-6.22	2.86	-5.24																				
								7283	2220	Leduc			A46-2(R3)a	R2+R3				2.53	-5.32	2.49	-4.34																				
								7283	2220	Leduc			A46-2(R3)b	R2+R3				2.56	-5.94	2.52	-4.96																				
								7283	2220	Leduc			A46-2(R4)a	R4				3.28	-8.44	3.24	-7.46																				
								7283	2220	Leduc			A46-2-C1	C1				2.91	-7.38	2.87	-6.40																				
								7283	2220	Leduc			A46-2(R4)b	R4				3.32	-8.16	3.28	-7.18																				
								7283	2220	Leduc			A46-2(R4)c	R4				3.28	-8.45	3.24	-7.47																				
								7298	2224	Leduc			A46-3(R3)a	R2+R3				2.58	-6.38	2.54	-5.40																				
								7298	2224	Leduc			A46-3(R3)b	R2+R3				2.72	-5.82	2.68	-4.84																				
								7329	2234	Leduc			A46-4(R3)b	R2+R3				3.65	-5.72	3.61	-4.74																				
								7329	2234	Leduc			A46-4-C1a	C1				3.41	-5.81	3.37	-4.83																				
								7329	2234	Leduc			A46-4-C1b	C1				3.36	-5.64	3.32	-4.66																				
								7329	2234	Leduc			A46-4-C1c	C1				3.34	-5.98	3.30	-5.00																				
								7329	2234	Leduc			A46-4(R4)b	R4				3.18	-6.84	3.14	-5.86																				
								7329	2234	Leduc			A46-4(R4)b	R4				3.11	-6.82	3.07	-5.84																				
								7329	2234	Leduc			A46-4(R4)b	R4				3.30	-6.81	3.26	-5.83																				
								7329	2234	Leduc			A46-4(R4)b	R4				3.35	-6.80	3.31	-5.82																				
								7329	2234	Leduc			A46-4(R4)b	R4				3.42	-6.76	3.38	-5.78																				
								7351	2241	Leduc			A46-5(R2)a	R2				2.14	-5.83	2.10	-4.85																				
								7351	2241	Leduc			A46-5(R2)b	R2				2.17	-5.79	2.13	-4.81																				
	4	3	46	28	W4	Westerose	Amthor	6859	2091	Leduc			A46(1)-1(R3)	R2+R3	62	1.84	0.96	2.29	-5.93	2.25	-4.95																				
								6881	2097	Leduc			A46(1)-2(R3)	R2+R3				2.25	-5.46	2.21	-4.48																				
								6942	2116	Leduc			A46(1)-3(R3)	R2+R3				2.36	-5.58	2.32	-4.60																				
								6998	2133	Leduc			A46(1)-4(R3)	R2+R3				2.59	-5.72	2.55	-4.74																				
								7038	2145	Leduc			A46(1)-5(R3)	R2+R3				2.50	-5.59	2.46	-4.61																				
								7135	2175	Leduc			A46(1)-6(R3)	R2+R3				2.35	-5.70	2.31	-4.72																				
								7189	2191	Leduc			A46(1)-7(R3)	R2+R3				2.29	-5.53	2.25	-4.55																				
								7248	2209	Leduc			A46(1)-8(R3)	R2+R3				2.25	-5.81	2.21	-4.83																				
								7287	2221	Leduc			A46(1)-9(R3)	R2+R3				2.77	-5.46	2.73	-4.48																				
								7365	2245	Leduc			A46(1)-10(R3	R2+R3				2.88	-6.00	2.84	-5.02																				
								7365	2245	Leduc			A46(1)-11(R3	R2+R3				2.80	-5.77	2.76	-4.79																				
T45	16	33	45	28	W4	Westerose	Horrigan	6958.6	2121	Leduc	x	x	EH-60	R2	71.6	1.4	1.5	2.87	-5.67			0.70827	49.38				167750	118346	0.85	< D.L.	9.1	289	< D.L.	13.57		62.7		< D.L.	4.4	< D.L.	328
														R2						2.79	-4.43		50.36				168671	108052	0.86	<DL	5	426	13.5		109	254	1.00		1.16	4.84	1028
	16	33	45	28	W4	Westerose	Amthor	6876	2096	Leduc			A45-1(R3)a	R2+R3	71.6	1.4	1.5	1.90	-5.75	1.86	-4.77																				
								6876	2096	Leduc			A45-1(R3)b	R2+R3				2.01	-5.52	1.97	-4.54																				
								6876	2096	Leduc			A45-1(R3)c	R2+R3				2.16	-5.74	2.12	-4.76																				
								6890	2085	Leduc			A45-2(R3)a	R2+R3				2.25	-5.16	2.21	-4.18																				
								6890	2085	Leduc			A45-2(R3)b	R2+R3				2.23	-5.88	2.19	-4.90																				
								6890	2085	Leduc			A45-2(R3)c	R2+R3				2.22	-5.96	2.18	-4.98																				
								6923	2110	Leduc			A45-3(R3)a	R2+R3				2.45	-5.89	2.41	-4.91																				
								6923	2110	Leduc			A45-3(R3)b	R2+R3				2.38	-5.83	2.34	-4.85																				
								6973	2125	Leduc			A45-4(R3)a	R2+R3				2.71	-5.65	2.67	-4.67																				
								6973	2125	Leduc			A45-4(R3)b	R2+R3				2.70	-5.60	2.66	-4.62																				

Sample ID	Mn	Co	Ni	Cu	Zn	Ga	Ge	As	Se	Rb	Sr	Y	Zr	Nb	Mo	Ru	Pd	Ag	Cd	Sn	Sb	Te	Cs	Ba	La	Ce	Pr	Nd	Sm	Eu	Gd	Tb	Dy	Ho	Er	Tm	Yb	Lu	Hf	Ta	W	Re	Os	Ir	Pt	Tl	Pb	Bi	Th	U
	0.03 ppm	0.03 ppm	0.06 ppm	0.03 ppm	0.08 ppm	0.01 ppm	0.02 ppm	0.06 ppm	0.2 ppm	0.04 ppm	0.03 ppm	0.02 ppm	0.09 ppm	0.04 ppm	0.02 ppm	0.01 ppm	0.01 ppm	0.01 ppm	0.06 ppm	0.06 ppm	0.01 ppm	0.02 ppm	0.02 ppm	0.03 ppm	0.03 ppm	0.03 ppm	0.04 ppm	0.03 ppm	0.04 ppm	0.03 ppm	0.03 ppm	0.04 ppm	0.02 ppm	0.04 ppm	0.06 ppm	0.05 ppm	0.04 ppm	0.05 ppm	0.02 ppm	0.08 ppm	0.03 ppm	0.08 ppm	0.04 ppm	0.01 ppm	0.05 ppm	0.03 ppm		0.01 ppm	0.03 ppm
A47-6(R4)a																																																		
A47-6(R4)b																																																		
A47-6(R4)c																																																		
A47-6																																																		
N-207(R3)	92.2	0.63	0.84	0.80	1.50	<DL	<DL	<DL	<DL	<DL	39.4	0.91	<DL	<DL	<DL	0.97	0.15	<DL	<DL	<DL	<DL	<DL	<DL	1.04	0.31	0.35	<DL	0.25	<DL	0.08	<DL	0.07	<DL	<DL	<DL	<DL	<DL	<DL	<DL	<DL	5.27	<DL	<DL	<DL	<DL	<DL	1.31		<DL	0.20
N-201-R2	94.3	0.87	0.10	0.39	3.07	<DL	<DL	<DL	<DL	<DL	51.1	1.06	<DL	<DL	0.12	1.01	0.20	<DL	<DL	<DL	<DL	<DL	<DL	2.69	0.56	0.43	<DL	0.31	<DL	0.09	<DL	0.07	<DL	<DL	<DL	<DL	<DL	<DL	<DL	<DL	4.68	<DL	<DL	<DL	<DL	<DL	2.59		<DL	0.20
N-201-R3	163	0.56	0.55	0.83	19.4	<DL	<DL	0.21	<DL	<DL	43.1	2.09	<DL	<DL	0.13	0.83	0.46	<DL	0.26	0.15	<DL	<DL	<DL	6.78	0.86	1.22	0.19	0.79	0.16	<DL	0.23	<DL	0.18	<DL	0.11	<DL	0.08	<DL	<DL	<DL	4.27	<DL	<DL	<DL	<DL	<DL	246		<DL	0.22
EH-23-a(R2)	96	< D.L.	< D.L.	3.62	2.6	0.16		1.86	< D.L.	1.32	60.3	3.40	0.38	0.05				0.22	0.03	3.84	0.11		0.07	2.84	1.77	2.36	0.35	1.49	0.31	0.06	0.41	0.05	0.37	0.06	0.14	0.02	0.12	0.01	< D.L.	< D.L.						< D.L.	< D.L.	< D.L.	< D.L.	< D.L.
EH-23-b(R1)	78	< D.L.	< D.L.	1.75	1.9	0.38		2.11	< D.L.	1.77	42.0	1.97	0.21	0.02				0.43	< D.L.	0.04	0.00		0.12	2.98	1.00	1.36	0.23	0.86	0.20	0.04	0.34	0.03	0.23	0.03	0.09	0.02	0.08	0.00	< D.L.	0.00						0.03	2.90	0.03	0.20	0.74
EH-23-c(R4)	65	< D.L.	< D.L.	2.17	2.6	0.13		1.84	< D.L.	0.21	42.6	1.59	0.08	0.02				0.45	< D.L.	0.16	< D.L.		< D.L.	1.09	0.78	0.98	0.13	0.60	0.11	0.01	0.18	0.01	0.15	0.03	0.06	< D.L.	0.05	< D.L.	< D.L.	< D.L.						< D.L.	2.04	0.01	< D.L.	0.43
EH-24(R4)	92	< D.L.	< D.L.	1.25	1.3	0.18		0.86	< D.L.	0.53	75.6	2.88	0.33	0.04				0.17	0.05	1.07	0.05		0.02	1.76	2.36	2.66	0.35	1.32	0.23	0.04	0.34	0.04	0.28	0.04	0.13	0.02	0.09	0.01	< D.L.	0.00						0.03	5.06	0.02	0.12	0.28
A46-1a																																																		
A46-1b																																																		
A46-1c																																																		
A46-1(R3)a																																																		
A46-1(R3)b																																																		
A46-1(R3)c																																																		
A46-1(R3)d																																																		
A46-2(R3)a																																																		
A46-2(R3)b																																																		
A46-2(R4)a																																																		
A46-2-C1																																																		
A46-2(R4)b																																																		
A46-2(R4)c																																																		
A46-3(R3)a																																																		
A46-3(R3)b																																																		
A46-4(R3)b																																																		
A46-4-C1a																																																		
A46-4-C1b																																																		
A46-4-C1c																																																		
A46-4(R4)b																																																		
A46-4(R4)b																																																		
A46-4(R4)b																																																		
A46-4(R4)b																																																		
A46-5(R2)a																																																		
A46-5(R2)b																																																		
A46(1)-1(R3)																																																		
A46(1)-2(R3)																																																		
A46(1)-3(R3)																																																		
A46(1)-4(R3)																																																		
A46(1)-5(R3)																																																		
A46(1)-6(R3)																																																		
A46(1)-7(R3)																																																		
A46(1)-8(R3)																																																		
A46(1)-9(R3)																																																		
A46(1)-10(R3)																																																		
A46(1)-11(R3)																																																		
EH-60	74	< D.L.	< D.L.	1.65	2.8	0.15		0.80	< D.L.	< D.L.	44.4	0.86	< D.L.	0.01				0.26	< D.L.	< D.L.	< D.L.		< D.L.	0.78	0.41	0.44	< D.L.	0.25	< D.L.	< D.L.	< D.L.	< D.L.	< D.L.	< D.L.	< D.L.	< D.L.	< D.L.	< D.L.	< D.L.	0.05						< D.L.	< D.L.	< D.L.	< D.L.	0.09
	78.8	1.42	9.79	0.51	2.06	<DL	<DL	0.27	0.4	0.20	55.0	0.89	<DL	<DL	0.21	1.48	<DL	<DL	<DL	0.10	<DL	<DL	<DL	1.67	0.42	0.40	0.07	0.28	<DL	<DL	0.09	<DL	0.07	<DL	<DL	<DL	<DL	<DL	<DL	<DL	4.86	<DL	<DL	<DL	<DL	<DL	0.82		0.01	0.25
A45-1(R3)a																																																		
A45-1(R3)b																																																		
A45-1(R3)c																																																		
A45-2(R3)a																																																		
A45-2(R3)b																																																		
A45-2(R3)c																																																		
A45-3(R3)a																																																		
A45-3(R3)b																																																		
A45-4(R3)a																																																		
A45-4(R3)b																																																		

TWN	LSD	SEC	TWN	RGE	MER	Pool	Original sample set	Depth (ft)	Depth (m)	Stratigraphic unit	Core samples	Thin sections	Sample ID	Sample type	CH₄	H₂S	CO₂	Orig δ¹³C ‰ PDB	Orig δ¹⁸O ‰ PDB	SK δ¹³C ‰ PDB	SK δ¹⁸O ‰ PDB	⁸⁷Sr/⁸⁶Sr	CaCO₃ mol% XRD	6/4Pb	7/4Pb	8/4Pb	Ca 31 ppm	Mg 2 ppm	Li 0.05 ppm	Be 0.1 ppm	B 2 ppm	Na 0.5 ppm	Al 0.2 ppm	Si ppm	P 5 ppm	K 6 ppm	Ti 0.09 ppm	Sc ppm	V 0.05 ppm	Cr 0.05 ppm	Fe 3.7 ppm
								7022	2140	Leduc			A45-5(R3)a	R2+R3				2.86	-6.42	2.82	-5.44																				
								7022	2140	Leduc			A45-5(R3)b	R2+R3				2.99	-5.87	2.95	-4.89																				
								7022	2140	Leduc			A45-5(R3)c	R2+R3				3.01	-5.80	2.97	-4.82																				
								7089	2161	Leduc			A45-6(R3)a	R2+R3				2.87	-5.98	2.83	-5.00																				
								7089	2161	Leduc			A45-6(R3)b	R2+R3				2.75	-6.12	2.71	-5.14																				
								7118	2170	Leduc			A45-7(R3)a	R2+R3				2.62	-5.85	2.58	-4.87																				
								7118	2170	Leduc			A45-7(R3)b	R2+R3				2.56	-5.74	2.52	-4.76																				
								7118	2170	Leduc			A45-7(R3)c	R2+R3				2.51	-5.79	2.47	-4.81																				
								7159	2182	Leduc			A45-7-C1a	C1				2.57	-5.56	2.53	-4.58																				
								7159	2182	Leduc			A45-7-C1b	C1				2.57	-5.47	2.53	-4.49																				
								7159	2182	Leduc			A45-7-C1c	C1				2.68	-5.55	2.64	-4.57																				
								7159	2182	Leduc			A45-7(R4)	R4				2.57	-5.46	2.53	-4.48																				
								7207	2197	Leduc			A45-8(R3)a	R2+R3				2.44	-5.85	2.40	-4.87																				
								7207	2197	Leduc			A45-8(R3)b	R2+R3				2.54	-5.92	2.50	-4.94																				
T44	11	27	44	1	W5	Westerose South	Kuflevskiy	7378.3	2248.9	Leduc	x	x	K44(1)-1	R2	49.5	3.9	1.04			2.77	-4.80	0.708620	49.57				174045	120870	0.97	<DL	3	284	25.8		83	85	2.04		5.19	5.85	1391
														R2-rerun						2.77	-4.91																			
														R3 (+R2)						2.85	-4.804		50.13				187110	112745	0.75	<DL	4	170	64.5		57	56	1.43		3.28	3.77	1651
								7540	2298.2	Leduc	x	x	K44(1)-4	R2						2.54	-4.62		49.94				194088	117837	0.89	<DL	6	308	65.8		63	138	2.02		0.66	3.15	776
								7719	2352.8	Leduc	x	x	K44(1)-7	R2						3.53	-4.61	0.708876	49.66				166146	114718	1.02	<DL	3	311	66.1		62	158	1.81		0.54	4.18	521
								7723	2354.0	Leduc	x		K44(1)-8(R2)	R2						3.47	-4.71		49.72				196275	120395	0.89	<DL	6	449	36.9		40	111	1.16		0.58	2.05	953
													K44(1)-8(R3)	R3						3.54	-4.68		50.12				188511	112170	1.00	<DL	6	454	100		49	145	2.24		0.88	2.59	1539
	12	25	44	1	W5	Westerose South	Kuflevskiy	7883.7	2403.0	Cook. Lk.	x	x	K44(2)-2	R2	73.8	1.74	1.3			2.94	-4.81		50.12				191500	115700	0.95	<DL	6	254	65.1		363	155	2.74		1.84	1.94	984
								7888.6	2404.5	Cook. Lk.	x	x	K44(2)-4	R2						3.59	-4.61	0.708380	50.53				169283	111631	2.42	<DL	12	311	61.0		61	124	2.61		1.69	3.85	502
														R2-rerun						3.41	-4.81																			
								7889.9	2404.9	Cook. Lk.	x	x	K44(2)-5	R2						2.57	-4.67		51.17				193208	115393	2.64	<DL	38	280	151		43	207	4.27		1.06	3.76	512
								7914.5	2412.4	Cook. Lk.	x	x	K44(2)-8	R2						2.15	-5.15	0.709446	50.51				169283	111631	2.42	<DL	12	311	61.0		61	124	2.61		1.69	3.85	502
T43	3	29	43	1	W5	Homeglen Rimbey	Drivet	7791.9	2375	Leduc			D43-1(R1)	R1	74.9	6.09	2.64	2.76	-5.04																					
								7791.9	2375	Leduc			D43-1(R2)	R2				2.67	-5.06																					
								7791.9	2375	Leduc			D43-1(R3)	R3				2.68	-5.20																					
								7791.9	2375	Leduc			D43-1-C1	C1				2.02	-6.07																					
								7814.9	2382	Leduc			D43-2(R2)	R2				2.55	-4.44			0.70826																			
								7814.9	2382	Leduc			D43-2-C1a	C1				2.53	-4.07			0.70834																			
								7814.9	2382	Leduc			D43-2-C1b	C1				2.49	-4.37																					
								7814.9	2382	Leduc			D43-2-C1c	C1				2.42	-4.34																					
								8008.4	2441	Leduc			D43-3(R2)	R2				3.33	-4.73																					
								8008.4	2441	Leduc			D43-3(R3)	R3				3.34	-5.03																					
	11	28	43	1	W5	Homeglen Rimbey	Drivet	8021.6	2445	Leduc			D43(1)-1	R2	79.67	0	1.97	2.86	-4.77																					
								8021.6	2445	Leduc			D43(1)-1-C1a	C1				2.61	-5.04																					
								8021.6	2445	Leduc			D43(1)-1-C1b	C1				2.77	-4.55																					
								8021.6	2445	Leduc			D43(1)-1-C1c	C1				2.94	-5.18																					
	11	7	43	1	W5	Homeglen Rimbey	Horrigan	7841.1	2390	Leduc	x	x	EH-39	R2	77.5	3.2	2.08						50.11				91850	53946	0.76	< D.L.	10.2	255	68.5	51.53		162.6		0.53	9.9	4.2	1147
	11	7	43	1	W5	Homeglen Rimbey	Drivet	7841.1	2390	Leduc			D43(2)-1(R1)	R1	77.5	3.2	2.08	2.15	-4.39																					
								7841.1	2390	Leduc			D43(2)-1	R2				2.09	-4.76																					
								7841.1	2390	Leduc			D43(2)-1-CC	CC-Postdate dolomite cement C				1.67	-9.31																					
								7841.1	2390	Leduc			D43(2)-1-CC	CC-Distributed near sulphides				1.83	-9.51																					
T42	10	4	42	1	W5	Homeglen Rimbey	Kuflevskiy	8461.5	2579.1	Cook. Lk.	x	x	K42-1	R2						6.67	-5.66	0.708459	49.94				201167	138385	1.40	<DL	20	443	65.3		80	140	3.38		1.16	1.60	1246
								8468	2581.1	Cook. Lk.	x	x	K42-3(R2)	R2						6.85	-5.74	0.708425	50.29				182985	124098	1.17	<DL	14	333	60.6		82	139	2.86		1.28	6.15	1814
													K42-3(R4)	R4						5.10	-5.85	0.708434	49.25				176098	115612	1.77	<DL	7	1355	207		131	289	4.68		1.87	9.83	2441
								8469	2581.4	Cook. Lk.	x		K42-4																												
	11	35	42	2	W5	Homeglen Rimbey	Drivet	8290.6	2527	Leduc			D42-C1	C1				2.39	-5.57			0.70876																			
	11	25	42	2	W5	Homeglen Rimbey	Drivet	7939.5	2420	Leduc			D42(1)-1-C1a	C1				1.17	-7.05			0.70862																			
								7939.5	2420	Leduc			D42(1)-1-CC	CC-Postdate dolomite cement C				1.70	-4.83			0.70873																			
								7969.1	2429	Leduc			D42(1)-2	R2				2.36	-4.68																					
								7969.1	2429	Leduc			D42(1)-2-C1a	C1				2.19	-4.57																					
								7969.1	2429	Leduc			D42(1)-2-C1b	C1				2.11	-4.29																					
	7	22	42	2	W5	Homeglen Rimbey	Horrigan	7882.1	2402.5	Leduc	x	x	EH-19a	R2	84.5	0.17	1.35			2.40	-4.94		50.04				164350	115146	0.88	< D.L.	11.1	148	< D.L.	32.54	< D.L.			< D.L.	8.2	4.1	1558
													EH-19b(R4)	R4				2.44	-6.54	2.37	-4.86	0.70843	51.07				144650	100246	0.93	< D.L.	11.1	291	47.4	79.90		140.3		0.53	15.3	8.0	1298

Sample ID	Mn	Co	Ni	Cu	Zn	Ga	Ge	As	Se	Rb	Sr	Y	Zr	Nb	Mo	Ru	Pd	Ag	Cd	Sn	Sb	Te	Cs	Ba	La	Ce	Pr	Nd	Sm	Eu	Gd	Tb	Dy	Ho	Er	Tm	Yb	Lu	Hf	Ta	W	Re	Os	Ir	Pt	Tl	Pb	Bi	Th	U
D.L. (ppm)	0.03	0.03	0.06	0.03	0.08	0.01	0.02	0.06	0.2	0.04	0.03	0.02	0.09	0.04	0.02	0.01	0.01	0.01	0.06	0.06	0.01	0.02	0.02	0.03	0.03	0.03	0.04	0.03	0.04	0.03	0.03	0.04	0.02	0.04	0.06	0.05	0.04	0.05	0.02	0.08	0.03	0.08	0.04	0.01	0.05	0.03			0.01	0.03
A45-5(R3)a																																																		
A45-5(R3)b																																																		
A45-5(R3)c																																																		
A45-6(R3)a																																																		
A45-6(R3)b																																																		
A45-7(R3)a																																																		
A45-7(R3)b																																																		
A45-7(R3)c																																																		
A45-7-C1a																																																		
A45-7-C1b																																																		
A45-7-C1c																																																		
A45-7(R4)																																																		
A45-8(R3)a																																																		
A45-8(R3)b																																																		
K44(1)-1	94.8	1.25	8.48	30.1	25.2	<DL	<DL	0.48	1.0	0.07	40.7	2.25	<DL	<DL	0.51	0.90	<DL	0.12	<DL	0.67	0.09	<DL	<DL	1.88	0.82	0.89	0.16	0.69	0.15	<DL	0.20	<DL	0.19	<DL	0.12	<DL	0.09	<DL	<DL	<DL	2.30	<DL	<DL	<DL	<DL	<DL	2.83		0.15	0.27
K44(1)-4	102	0.64	2.05	1.72	14.6	<DL	<DL	0.16	<DL	0.27	45.6	1.80	<DL	<DL	0.23	0.89	0.11	<DL	<DL	0.42	<DL	<DL	<DL	3.68	0.82	1.05	0.17	0.68	0.15	<DL	0.20	<DL	0.16	<DL	0.10	<DL	<DL	<DL	<DL	<DL	4.67	<DL	<DL	<DL	<DL	<DL	1.31		0.09	0.18
K44(1)-7	79.8	0.64	6.36	96.2	54.1	<DL	<DL	0.18	<DL	0.29	40.5	0.84	<DL	<DL	<DL	0.95	0.11	<DL	<DL	1.64	<DL	<DL	<DL	1.03	0.35	0.45	<DL	0.31	<DL	<DL	0.08	<DL	0.06	<DL	<DL	<DL	<DL	<DL	<DL	<DL	0.18	<DL	<DL	<DL	<DL	<DL	7.11		<DL	0.32
K44(1)-8(R2)	71.5	1.20	9.21	113	72.1	<DL	<DL	0.41	1.0	0.29	45.2	1.34	0.13	<DL	0.10	1.12	<DL	<DL	<DL	1.95	0.10	<DL	<DL	1.70	0.45	0.50	0.10	0.42	0.10	<DL	0.14	<DL	0.13	<DL	0.09	<DL	<DL	<DL	<DL	<DL	0.18	<DL	<DL	<DL	<DL	<DL	8.73		0.08	0.09
K44(1)-8(R3)	80.8	0.73	1.38	0.29	5.78	<DL	<DL	0.17	<DL	0.18	41.8	0.71	<DL	<DL	0.15	1.05	0.08	<DL	<DL	<DL	<DL	<DL	<DL	1.86	0.31	0.37	<DL	0.23	<DL	<DL	0.07	<DL	<DL	<DL	<DL	<DL	<DL	<DL	<DL	<DL	2.63	<DL	<DL	<DL	<DL	<DL	1.11		<DL	0.13
	87.0	0.73	2.50	1.00	25.1	<DL	<DL	0.75	<DL	0.49	44.9	1.04	0.13	<DL	0.35	0.86	0.29	<DL	<DL	<DL	<DL	<DL	<DL	6.22	0.51	0.80	0.12	0.47	0.10	<DL	0.14	<DL	0.10	<DL	<DL	<DL	<DL	<DL	<DL	<DL	3.39	<DL	<DL	<DL	<DL	<DL	28.9		0.19	0.15
K44(2)-2	73.3	0.69	10.1	1.90	1.67	<DL	<DL	0.36	<DL	0.30	51.4	1.32	<DL	<DL	2.16	0.86	0.18	<DL	<DL	<DL	<DL	<DL	<DL	0.92	0.65	0.70	0.11	0.45	0.09	<DL	0.13	<DL	0.09	<DL	<DL	<DL	<DL	<DL	<DL	<DL	<DL	<DL	<DL	<DL	<DL	<DL	1.74		0.06	1.14
K44(2)-4	68.4	1.28	34.8	11.3	8.18	<DL	<DL	0.54	1.0	0.23	75.7	2.02	0.11	<DL	0.38	1.09	<DL	<DL	<DL	0.21	<DL	<DL	<DL	2.57	0.87	0.84	0.15	0.66	0.14	<DL	0.22	<DL	0.18	<DL	0.11	<DL	<DL	<DL	<DL	<DL	<DL	<DL	<DL	<DL	<DL	<DL	2.93		0.07	0.32
K44(2)-5	60.3	0.64	47.0	6.87	5.24	<DL	<DL	0.18	<DL	0.59	88.4	1.69	0.22	<DL	0.18	0.91	0.11	<DL	<DL	0.12	<DL	<DL	<DL	3.61	0.77	0.98	0.16	0.65	0.15	<DL	0.19	<DL	0.16	<DL	0.10	<DL	<DL	<DL	<DL	<DL	<DL	<DL	<DL	<DL	<DL	<DL	1.81		0.10	0.43
K44(2)-8	68.4	1.28	34.8	11.3	8.18	<DL	<DL	0.54	1.0	0.23	75.7	2.02	0.11	<DL	0.38	1.09	<DL	<DL	<DL	0.21	<DL	<DL	<DL	2.57	0.87	0.84	0.15	0.66	0.14	<DL	0.22	<DL	0.18	<DL	0.11	<DL	<DL	<DL	<DL	<DL	<DL	<DL	<DL	<DL	<DL	<DL	2.93		0.07	0.32
D43-1(R1)																																																	
D43-1(R2)																																																	
D43-1(R3)																																																	
D43-1-C1																																																	
D43-2(R2)																																																	
D43-2-C1a																																																	
D43-2-C1b																																																	
D43-2-C1c																																																	
D43-3(R2)																																																	
D43-3(R3)																																																	
D43(1)-1																																																	
D43(1)-1-C1a																																																	
D43(1)-1-C1b																																																	
D43(1)-1-C1c																																																	
EH-39	62	< D.L.	< D.L.	3.14	2.1	0.32		1.02	< D.L.	0.24	31.4	0.85	0.13	0.02				0.28	< D.L.	< D.L.	< D.L.		< D.L.	1.04	0.34	0.55	0.07	0.35	0.06	0.00	0.11	0.00	0.08	< D.L.	0.02	< D.L.	0.03	< D.L.	< D.L.	< D.L.						0.02	2.20	< D.L.	< D.L.	0.10
D43(2)-1(R1)																																																	
D43(2)-1																																																	
D43(2)-1-CC																																																	
D43(2)-1-CC-?																																																	
K42-1	83.4	1.03	29.0	59.3	35.6	<DL	<DL	1.05	3.2	0.19	70.0	0.80	0.12	<DL	0.08	0.96	<DL	0.08	<DL	1.14	<DL	<DL	<DL	2.26	0.53	0.52	0.08	0.31	0.06	<DL	0.08	<DL	<DL	<DL	<DL	<DL	<DL	<DL	<DL	<DL	<DL	<DL	<DL	<DL	<DL	<DL	7.27		0.03	0.06
K42-3(R2)	66.1	1.31	23.7	1.87	0.90	<DL	<DL	0.86	2.5	0.19	58.3	0.84	0.11	<DL	0.26	0.99	<DL	0.07	<DL	0.22	<DL	<DL	<DL	3.91	0.52	0.55	0.08	0.33	0.06	<DL	0.08	<DL	<DL	<DL	<DL	<DL	<DL	<DL	<DL	<DL	3.86	<DL	<DL	<DL	<DL	<DL	3.01		0.03	0.04
K42-3(R4)	101	1.22	11.8	5.05	5.40	<DL	<DL	1.06	2.3	0.86	71.9	1.02	0.24	<DL	1.00	0.84	<DL	0.10	<DL	0.18	<DL	<DL	<DL	13.7	0.75	1.17	0.16	0.64	0.14	<DL	0.16	<DL	0.11	<DL	<DL	<DL	<DL	<DL	<DL	<DL	0.75	<DL	<DL	<DL	<DL	<DL	19.6		0.19	0.06
K42-4																																																		
D42-C1																																																		
D42(1)-1-C1a																																																	
D42(1)-1-CC																																																	
D42(1)-2																																																	
D42(1)-2-C1a																																																	
D42(1)-2-C1b																																																	
EH-19a	87	< D.L.	< D.L.	< D.L.	0.9	0.46		1.49	< D.L.	0.07	49.6	1.92	< D.L.	0.01				0.04	< D.L.	< D.L.	< D.L.		< D.L.	3.29	0.83	0.93	0.09	0.63	0.07	0.02	0.19	0.01	0.14	< D.L.	0.02	< D.L.	0.05	< D.L.	< D.L.	0.06						< D.L.	0.41	< D.L.	< D.L.	0.18
EH-19b(R4)	93	< D.L.	< D.L.	2.22	7.5	6.4		2.68	0.30	0.22	65.8	2.48	0.22	0.02				0.42	< D.L.	0.33	0.02		< D.L.	82.0	0.67	0.86	0.12	0.56	0.11	0.03	0.17	0.01	0.14	0.02	0.06	< D.L.	0.03	< D.L.	< D.L.	0.05						< D.L.	2.28	0.00	0.05	0.12

TWN	LSD	SEC	TWN	RGE	MER	Pool	Original sample set	Depth (ft)	Depth (m)	Stratigraphic unit	Core samples	Thin sections	Sample ID	Sample type	CH₄	H₂S	CO₂	δ¹³C ‰ PDB (Original)	δ¹⁸O ‰ PDB (Original)	δ¹³C ‰ PDB (SK+adjusted)	δ¹⁸O ‰ PDB (SK+adjusted)	⁸⁷Sr/⁸⁶Sr	CaCO₃ mol% XRD	6/4Pb	7/4Pb	8/4Pb	Ca (31 ppm)	Mg (2 ppm)	Li (0.05 ppm)	Be (0.1 ppm)	B (2 ppm)	Na (0.5 ppm)	Al (0.2 ppm)	Si (ppm)	P (5 ppm)	K (6 ppm)	Ti (0.09 ppm)	Sc (ppm)	V (0.05 ppm)	Cr (0.05 ppm)	Fe (3.7 ppm)
	7	22	42	2	W5	Homeglen Rimbey	Drivet	7880.5	2402	Leduc			D42(2)-1	R2	84.5	0.17	1.35	1.96	-5.27			0.70856																			
	11	3	42	2	W5	Homeglen Rimbey	Horrigan	7841.1	2390	Leduc	x	x	EH-38	R2				1.78	-5.79	1.55	-4.45	0.70836	50.68				154613	108861	0.91	<DL	7	348	139		80	212	8.35		0.62	3.76	1006
																				1.63	-4.47																			
	11	3	42	2	W5	Homeglen Rimbey	Drivet	7791.9	2375	Leduc			D42(3)-1(3)	R3				1.30	-5.18																					
								7811.6	2381	Leduc			D42(3)-2-CC	CC-Postdate dolomite cement C1				0.98	-5.41																					
								7821.4	2384	Leduc			D42(3)-3(2)	R2				1.96	-4.73																					
								7821.4	2384	Leduc			D42(3)-3-C1a	C1				1.82	-4.39																					
								7821.4	2384	Leduc			D42(3)-3-C1b	C1				1.98	-4.53																					
								7821.4	2384	Leduc			D42(3)-3-C1c	C1				2.00	-4.89																					
								7821.4	2384	Leduc			D42(3)-3-CC	CC-Postdate dolomite cement C1				-1.14	-7.82																					
								7821.4	2384	Leduc			D42(3)-3-CC-	CC-Distributed near sulphides				-1.78	-7.94																					
								7841.1	2390	Leduc			D42(3)-4(2)	R2				1.59	-4.80																					
								7841.1	2390	Leduc			D42(3)-4-C1	C1				1.73	-4.81			0.70830																			
								7857.5	2395	Leduc			D42(3)-5(2)	R2				2.02	-4.44																					
								7857.5	2395	Leduc			D42(3)-5-C1a	C1				1.36	-5.37			0.70834																			
								7857.5	2395	Leduc			D42(3)-5-C1b	C1				2.01	-4.92																					
								7857.5	2395	Leduc			D42(3)-5-S	CC-Distributed near sulphides				1.23	-9.10			0.70874																			
	11	3	42	2	W5	Homeglen Rimbey	Amthor	7810	2381	Leduc			A42-1(R3)a	R2+R3				1.55	-6.24	1.51	-5.26																				
								7810	2381	Leduc			A42-1(R3)b	R2+R3				1.63	-5.98	1.59	-5.00																				
								7843	2390	Leduc			A42-2(R3)a	R2+R3				1.71	-5.61	1.67	-4.63																				
								7843	2390	Leduc			A42-2(R3)b	R2+R3				1.68	-5.79	1.64	-4.81																				
								7843	2390	Leduc			A42-2(R4)a	R4				1.84	-5.90	1.80	-4.92																				
								7843	2390	Leduc			A42-2(R4)b	R4				1.79	-5.93	1.75	-4.95																				
								7858	2395	Leduc			A42-3(R3)a	R2+R3				2.08	-5.80	2.04	-4.82																				
								7858	2395	Leduc			A42-3(R3)b	R2+R3				2.09	-5.76	2.05	-4.78																				
								7858	2395	Leduc			A42-3-CC	CC				-1.08	-9.16	-1.12	-8.18																				
								7858	2395	Leduc			A42-3(R4)	R4				1.54	-5.84	1.50	-4.86																				
T41	14	5	41	2	W5	Gilby	Horrigan	8247.9	2514	Leduc			EH-51	R2	79.7	4.5	1.82						50.77				138650	98646	1.02	0.05	10.8	540	50.9	50.12		195.8		0.61	9.8	4.4	1498
														R2						1.54	-4.65		50.49				144641	100062	0.71	<DL	2	443	29.04		108	159	1.95		0.76	3.93	973
								8284.0	2525	Leduc			EH-50a	R2				1.73	-5.81	1.85	-4.23	0.70873	51.01				161050	113946	0.95	0.09	8.5	276	37.8	55.04		136.4		0.45	12.1	5.0	1244
								8284.0	2525	Leduc			EH-50b	R2				1.48	-6.51	1.70	-4.60	0.70870	50.87				68850	53846	0.75	0.00	8.5	217	111.4	60.80		154.7		0.79	5.6	62.4	927
	14	5	41	2	W5	Gilby	Drivet	8247.9	2514	Leduc			D41-1	R2	79.7	4.5	1.82	1.57	-4.27																					
T40	10	7	40	2	W5	Homeglen Rimbey	Horrigan	8579.9	2615.2	Leduc	x	x	EH-4	R1	79.8	0	5.21						50.93				75850	52546	15.63	0.43	24.5	573	7119.5	227.00		3636.0		2.50	16.0	17.0	14049
								8605.9	2623.1	Leduc	x	x	EH-5	R1				-0.20	-7.21	-0.07	-5.12	0.71023	50.41				39850	19546	4.05	0.15	19.3	248	1511.2	326.42		1358.8		1.45	13.6	7.5	5427
																				-0.19	-5.54						124906	88333	5.29	<DL	29	317	2838		209	2678	46.1		7.37	9.88	10222
T39	1	30	39	3	W5	Medicine River	Drivet	9629.1	2935	Leduc			D39-1	CC-Postdate replacement dolom				1.98	-7.80			0.70825																			
								9819.4	2993	Cook. Lk.			D39-2	CC-Postdate replacement dolom				3.48	-5.16																						
	14	28	39	3	W5	Medicine River	Horrigan	9261.7	2823	Leduc	x	x	EH-1a	R2	77.2	0	6.08	2.41	-6.39	2.45	-4.90	0.70850	50.11				115650	78646	2.02	0.03	25.8	172	1191.9	211.44		925.9		1.07	20.6	10.6	2269
													EH-1b	R2													106650	69746	1.34	< D.L.	21.2	154	< D.L.	183.92		75.7		< D.L.	7.3	3.7	1319
													EH-1c	R2													108850	70046	1.60	0.01	29.1	258	66.0	73.82		169.7		0.83	7.2	4.8	878
													EH-1d	R2									50.64				139250	95446	4.62	0.35	64.0	445	109.4	655.77		385.4		0.74	70.5	6.3	7559
	14	28	39	3	W5	Medicine River	Drivet	9261.7	2823	Leduc			D39(1)-1	R2	77.2	0	6.08	2.33	-4.25																					
								9261.7	2823	Leduc			D39(1)-1-C1a	C1				2.75	-4.84			0.70883																			
								9261.7	2823	Leduc			D39(1)-1-CC	CC-Postdate dolomite cement C1				1.67	-4.61			0.70876																			
								9297.8	2834	Leduc			D39(1)-2	R2				3.13	-4.33																						
T38	8	30	38	4	W5	Medicine River	Amthor	10252	3125	Leduc			A38-1(R3)a	R2+R3	83.9	0	1.79	3.51	-6.02	3.47	-5.04																				
								10252	3125	Leduc			A38-1(R3)b	R2+R3				3.44	-6.47	3.40	-5.49																				
								10252	3125	Leduc			A38-1(R3)c	R2+R3				3.44	-4.98	3.40	-4.00																				
								10356	3157	Leduc			A38-2(R3)a	R2+R3				4.43	-6.77	4.39	-5.79																				
								10356	3157	Leduc			A38-2(R3)b	R2+R3				4.35	-6.77	4.31	-5.79																				
								10356	3157	Leduc			A38-2(R3)c	R2+R3				4.41	-7.07	4.37	-6.09																				
								10356	3157	Leduc			A38-2(R3)d	R2+R3				4.34	-6.76	4.30	-5.78																				
								10366	3160	Leduc			A38-3-C1a	C1				4.04	-6.53	4.00	-5.55																				
								10366	3160	Leduc			A38-3-C1b	C1				4.46	-6.39	4.42	-5.41																				
								10366	3160	Leduc			A38-3(R3)a	R2+R3				3.72	-6.48	3.68	-5.50																				
								10366	3160	Leduc			A38-3(R3)b	R2+R3				3.56	-6.76	3.52	-5.78																				

Sample ID	Mn	Co	Ni	Cu	Zn	Ga	Ge	As	Se	Rb	Sr	Y	Zr	Nb	Mo	Ru	Pd	Ag	Cd	Sn	Sb	Te	Cs	Ba	La	Ce	Pr	Nd	Sm	Eu	Gd	Tb	Dy	Ho	Er	Tm	Yb	Lu	Hf	Ta	W	Re	Os	Ir	Pt	Tl	Pb	Bi	Th	U
D.L.	0.03	0.03	0.06	0.03	0.08	0.01	0.02	0.06	0.2	0.04	0.03	0.02	0.09	0.04	0.02	0.01	0.01	0.01	0.06	0.06	0.01	0.02	0.02	0.03	0.03	0.03	0.04	0.03	0.04	0.03	0.03	0.03	0.04	0.02	0.04	0.06	0.05	0.04	0.05	0.02	0.08	0.03	0.08	0.04	0.01	0.05	0.03		0.01	0.03
(ppm)	ppm	ppm	ppm	ppm	ppm	ppm	ppm	ppm	ppm	ppm	ppm	ppm	ppm	ppm	ppm	ppm	ppm	ppm	ppm	ppm	ppm	ppm	ppm	ppm	ppm	ppm	ppm	ppm	ppm	ppm	ppm	ppm	ppm	ppm	ppm	ppm	ppm	ppm	ppm	ppm	ppm	ppm	ppm	ppm	ppm	ppm	ppm		ppm	ppm
D42(2)-1																																																		
EH-38	90.1	1.73	9.54	0.55	1.56	<DL	<DL	0.72	0.4	0.41	52.6	1.31	0.20	<DL	0.24	1.41	<DL	0.08	<DL	<DL	<DL	<DL	<DL	2.69	0.81	0.97	0.13	0.54	0.11	<DL	0.15	<DL	0.11	<DL	0.07	<DL	<DL	<DL	<DL	<DL	4.12	<DL	<DL	<DL	<DL	<DL	2.39		0.04	0.18
D42(3)-1(3)																																																		
D42(3)-2-CC																																																		
D42(3)-3(2)																																																		
D42(3)-3-C1a																																																		
D42(3)-3-C1b																																																		
D42(3)-3-C1c																																																		
D42(3)-3-CC																																																		
D42(3)-3-CC-																																																		
D42(3)-4(2)																																																		
D42(3)-4-C1																																																		
D42(3)-5(2)																																																		
D42(3)-5-C1a																																																		
D42(3)-5-C1b																																																		
D42(3)-5-S																																																		
A42-1(R3)a																																																		
A42-1(R3)b																																																		
A42-2(R3)a																																																		
A42-2(R3)b																																																		
A42-2(R4)a																																																		
A42-2(R4)b																																																		
A42-3(R3)a																																																		
A42-3(R3)b																																																		
A42-3-CC																																																		
A42-3(R4)																																																		
EH-51	93	< D.L.	< D.L.	0.92	4.4	2.3		3.30	< D.L.	0.32	54.3	1.82	0.43	0.03				0.18	< D.L.	< D.L.	< D.L.		0.05	13.2	1.32	1.20	0.20	0.70	0.16	0.03	0.22	0.02	0.16	0.02	0.09	0.04	0.05	< D.L.	< D.L.	0.01						0.06	2.24	0.04	0.14	0.30
	88.3	1.39	9.09	0.53	3.26	<DL		0.36	0.3	0.17	49.8	1.75	0.10	<DL	0.22	1.34	<DL	<DL	<DL	0.11	<DL	<DL	<DL	8.49	1.20	1.02	0.15	0.66	0.12	<DL	0.18	<DL	0.13	<DL	0.08	<DL	<DL	<DL	<DL	<DL	2.33	<DL	<DL	<DL	<DL	<DL	1.41		0.02	0.29
EH-50a	86	< D.L.	< D.L.	1.61	10.6	10.1		4.29	< D.L.	0.46	63.0	1.43	0.51	0.04				0.38	< D.L.	< D.L.	< D.L.		0.10	86.6	0.70	0.88	0.18	0.54	0.17	0.03	0.16	0.02	0.12	0.01	0.11	0.06	0.05	0.00	< D.L.	0.05						0.07	1.25	0.05	0.16	0.09
EH-50b	60	< D.L.	< D.L.	5.06	10.1	5.1		0.69	< D.L.	0.31	52.9	1.13	0.79	0.08				0.34	0.02	1.50	0.03		0.04	81.4	0.68	0.98	0.13	0.53	0.10	0.02	0.17	0.01	0.12	0.01	0.05	0.01	0.04	0.00	< D.L.	0.03						0.02	1.99	< D.L.	0.15	0.05
D41-1																																																		
EH-4	320	9.1	< D.L.	4.08	15.0	2.7		1.93	0.30	13.28	54.8	5.88	1.02	0.04				0.09	< D.L.	0.14	< D.L.		0.68	24.88	7.53	18.46	2.27	9.53	2.24	0.48	2.17	0.29	1.62	0.24	0.72	0.06	0.41	0.04	< D.L.	0.07						0.05	2.46	0.10	1.77	0.10
EH-5	179	1.8	< D.L.	4.37	6.0	1.1		1.53	< D.L.	6.29	43.6	2.39	0.39	0.03				0.32	< D.L.	< D.L.	< D.L.		0.27	12.39	2.28	4.83	0.58	2.47	0.46	0.10	0.54	0.06	0.43	0.06	0.15	0.01	0.15	0.02	0.01	0.08						0.02	0.99	< D.L.	0.40	0.08
	361	4.21	12.6	5.39	7.84	1.14	<DL	0.60	0.6	13.8	73.8	4.71	1.00	<DL	1.01	1.13	<DL	<DL	<DL	0.32	<DL	<DL	0.75	21.2	3.71	8.68	1.16	5.01	1.12	0.26	1.23	0.16	0.83	0.15	0.43	<DL	0.34	<DL	<DL	<DL	16.8	<DL	<DL	<DL	<DL	<DL	6.04		0.76	0.20
D39-1																																																		
D39-2																																																		
EH-1a	74	< D.L.	< D.L.	4.95	5.2	0.92		3.31	< D.L.	2.93	56.3	4.86	0.39	0.02				0.24	< D.L.	< D.L.	< D.L.		0.09	4.12	2.38	3.35	0.52	2.45	0.46	0.09	0.63	0.07	0.47	0.06	0.16	< D.L.	0.13	< D.L.	< D.L.	0.00						0.02	3.16	< D.L.	0.39	0.35
EH-1b	58	< D.L.	< D.L.	2.40	1.3	0.21		0.91	< D.L.	0.20	47.3	3.03	< D.L.	0.01				0.36	< D.L.	< D.L.	< D.L.		< D.L.	0.96	1.73	2.08	0.27	1.35	0.24	0.04	0.40	0.03	0.32	0.02	0.11	< D.L.	0.06	< D.L.	< D.L.	0.03						< D.L.	0.61	< D.L.	< D.L.	0.12
EH-1c	62	< D.L.	< D.L.	7.77	1.6	0.28		1.68	< D.L.	0.30	60.0	3.43	0.36	0.04				0.08	< D.L.	< D.L.	0.02		0.01	1.63	2.40	2.56	0.36	1.55	0.34	0.07	0.43	0.04	0.34	0.06	0.18	0.01	0.13	0.01	0.01	0.07						0.02	2.13	< D.L.	0.27	0.23
EH-1d	237	2.7	< D.L.	7.34	1.5	0.47		3.15	< D.L.	0.70	68.1	3.62	0.43	0.03				0.09	< D.L.	< D.L.	< D.L.		0.05	1.70	2.23	2.31	0.39	1.56	0.30	0.05	0.43	0.04	0.31	0.04	0.24	0.12	0.09	0.00	< D.L.	< D.L.						0.17	1.76	0.11	0.28	0.24
D39(1)-1																																																		
D39(1)-1-C1a																																																		
D39(1)-1-CC																																																		
D39(1)-2																																																		
A38-1(R3)a																																																		
A38-1(R3)b																																																		
A38-1(R3)c																																																		
A38-2(R3)a																																																		
A38-2(R3)b																																																		
A38-2(R3)c																																																		
A38-2(R3)d																																																		
A38-3-C1a																																																		
A38-3-C1b																																																		
A38-3(R3)a																																																		
A38-3(R3)b																																																		

TWN	LSD	SEC	TWN	RGE	MER	Pool	Original sample set	Depth (ft)	Depth (m)	Stratigraphic unit	Core samples	Thin sections	Sample ID	Sample type	CH₄	H₂S	CO₂	Original δ¹³C ‰ PDB	Original δ¹⁸O ‰ PDB	SK+adj δ¹³C ‰ PDB	SK+adj δ¹⁸O ‰ PDB	⁸⁷Sr/⁸⁶Sr	CaCO₃ mol% XRD	6/4Pb	7/4Pb	8/4Pb	Ca 31 ppm	Mg 2 ppm	Li 0.05 ppm	Be 0.1 ppm	B 2 ppm	Na 0.5 ppm	Al 0.2 ppm	Si ppm	P 5 ppm	K 6 ppm	Ti 0.09 ppm	Sc ppm	V 0.05 ppm	Cr 0.05 ppm	Fe 3.7 ppm
	8	30	38	4	W5	Medicine River	Drivet	10285.3	3135	Leduc			D38-1	R2	83.9	0	1.79	3.67	-4.06																						
								10364.0	3159	Leduc			D38-2-C1	C1				1.17	-6.21			0.70950																			
	10	23	38	4	W5	Sylvan Lake	Amthor	9872	3009	Leduc			A38(1)-1(R3)a	R2+R3	80.7	0	2.7	2.49	-5.69	2.45	-4.71																			
								9872	3009	Leduc			A38(1)-1(R3)b	R2+R3				2.55	-5.86	2.51	-4.88																			
								9872	3009	Leduc			A38(1)-1(R3)c	R2+R3				2.60	-5.79	2.56	-4.81																			
								9872	3009	Leduc			A38(1)-1(R3)d	R2+R3				2.54	-5.94	2.50	-4.96																			
								9888	3014	Leduc			A38(1)-2(R3)a	R2+R3				2.16	-5.57	2.12	-4.59																			
								9888	3014	Leduc			A38(1)-2(R3)b	R2+R3				2.91	-5.36	2.87	-4.38																			
								9888	3014	Leduc			A38(1)-2(R3)c	R2+R3				2.30	-5.81	2.26	-4.83																			
								9888	3014	Leduc			A38(1)-2(R3)d	R2+R3				2.24	-5.98	2.20	-5.00																			
	10	23	38	4	W5	Sylvan Lake	Drivet	9868.6	3008	Leduc			D38(1)-CC	CC-Postdat	80.7	0	2.7	-0.61	-7.24																				
	6	20	38	4	W5	Medicine River	Drivet	10186.9	3105	Leduc			D38(2)-1-C1	C1	58.2	6	2.43	2.78	-4.67			0.70903																		
								10249.2	3124	Leduc			D38(2)-2(R4)	R4				3.51	-4.93																				
	6	4	38	4	W5	Sylvan Lake	Drivet	9714.4	2961	Leduc			D38(3)-1(R2)	R2	76.2	3.7	1.9	1.18	-4.54																				
								9714.4	2961	Leduc			D38(3)-1(R3)	R3				1.28	-4.43																				
	16	11	38	5	W5	Sylvan Lake	Horrigan	10075.3	3071	Leduc	x	x	EH-56(R2)	R2				2.63	-6.24	2.63	-4.38	0.70843	50.87				154869	104600	1.31	<DL	5	278	216		97	255	11.0		1.15	4.88	891
																											137550	96446	1.11	< D.L.	14.4	269	32.3	254.31		109.1		< D.L.	14.1	4.1	688
	16	11	38	5	W5	Sylvan Lake	Drivet	10072.1	3070	Leduc			D38(3)-1-C1	C1				2.13	-3.96																				
								10075.3	3071	Leduc			D38(3)-2(R1)	R1				2.13	-4.29																				
								10075.3	3071	Leduc			D38(3)-2(R2)	R2				2.28	-4.48			0.70855																			
	5	11	38	10	W5	Strachan	Marquez	13871.2	4228	Leduc			M38-CC	CC	85.8	0	1.64	0.08	-6.60			0.70930																			
	15	2	38	10	W5	Strachan	Marquez	13597.9	4144.7	Leduc				SMC1				1.55	-6.88																				
								13597.9	4144.7	Leduc				SMC2				1.67	-7.87																				
								13597.9	4144.7	Leduc				SMC3				2.14	-5.51																				
								13597.9	4144.7	Leduc				SMC4				1.62	-7.44																				
								13597.9	4144.7	Leduc				SMC5				1.73	-7.59																				
								13599.2	4145.1	Leduc				SMC1				1.97	-6.46																				
								13599.2	4145.1	Leduc				SMC2				1.94	-6.59																				
								13599.2	4145.1	Leduc				SMC3				1.56	-5.86																				
								13599.2	4145.1	Leduc				SMC4				1.82	-5.87																				
								13599.2	4145.1	Leduc				SMC5				1.72	-5.55																				
								13599.2	4145.1	Leduc				SMC6				2.09	-6.54																				
								13599.2	4145.1	Leduc				SMC7				2.43	-6.07																				
T37	10	17	37	3	W5	Sylvan Lake	Horrigan	9392.9	2863	Leduc	x	x	EH-29	R2	52.7	12.3	2.21	2.22	-6.17	2.10	-4.42	0.70822	50.41				153334	107786	1.23	<DL	35	453	30.6		71	119	2.26		0.49	3.93	573
																											95650	43546	0.30	< D.L.	6.2	48	2.0	5.52		51.0		0.07	3.4	106.2	-52
	10	17	37	3	W5	Sylvan Lake	Drivet	9392.9	2863	Leduc			D37-1	R2	52.7	12.3	2.21	2.13	-4.25																				
								9392.9	2863	Leduc			D37-1-C1a	C1				1.99	-4.64																				
								9392.9	2863	Leduc			D37-1-C1b	C1				1.97	-3.96																				
	16	32	37	4	W5	Sylvan Lake	Horrigan	9783.3	2982	Leduc	x	x	EH-58	R2	80	0.08	1.24	1.83	-5.31			0.70833	50.87				120050	67846	1.01	< D.L.	12.0	271	22.9	7.42		< D.L.		< D.L.	5.7	3.5	-89
															R2						1.87	-3.68		51.01				153883	98093	1.05	<DL	<DL	245	56.2		126	142	3.11		1.13	6.40	804
	16	32	37	4	W5	Sylvan Lake	Drivet	9783.3	2982	Leduc			D37(1)-1(R2)	R2	80	0.08	1.24	1.29	-4.98																				
								9783.3	2982	Leduc			D37(1)-1(R3)	R3				1.19	-4.60																				
								9803.0	2988	Leduc			D37(1)-2(R2)a	R2				1.48	-4.64																				
								9803.0	2988	Leduc			D37(1)-2(R2)b	R2				1.70	-3.76																				
								9806.3	2989	Leduc			D37(1)-3(R2)	R2				1.51	-4.28			0.70912																			
								9812.9	2991	Leduc			D37(1)-4(R2)	R2				1.58	-4.06																				
								9812.9	2991	Leduc			D37(1)-4(R4)	R4				1.74	-4.21																				
								9849.0	3002	Leduc			D37(1)-5-C1	C1				0.31	-4.00																				
								9855.5	3004	Leduc			D37(1)-6(R2)	R2				2.17	-4.11			0.70818																			
	6	30	37	7	W5	Chedderville	Marquez	11587.8	3532	Leduc			M37-1(R3)	R3	9.78	10.2	0.65	2.28	-4.89																				
	10	29	37	7	W5	Chedderville	Marquez	11994.9	3656.1	Leduc			M37(1)-1(R2)	R2				2.37	-4.47																				

Sample ID	Mn	Co	Ni	Cu	Zn	Ga	Ge	As	Se	Rb	Sr	Y	Zr	Nb	Mo	Ru	Pd	Ag	Cd	Sn	Sb	Te	Cs	Ba	La	Ce	Pr	Nd	Sm	Eu	Gd	Tb	Dy	Ho	Er	Tm	Yb	Lu	Hf	Ta	W	Re	Os	Ir	Pt	Tl	Pb	Bi	Th	U
(D.L.)	0.03 ppm	0.03 ppm	0.06 ppm	0.03 ppm	0.08 ppm	0.01 ppm	0.02 ppm	0.06 ppm	0.2 ppm	0.04 ppm	0.03 ppm	0.02 ppm	0.09 ppm	0.04 ppm	0.02 ppm	0.01 ppm	0.01 ppm	0.01 ppm	0.06 ppm	0.06 ppm	0.01 ppm	0.02 ppm	0.02 ppm	0.03 ppm	0.03 ppm	0.03 ppm	0.04 ppm	0.03 ppm	0.04 ppm	0.03 ppm	0.03 ppm	0.04 ppm	0.02 ppm	0.04 ppm	0.06 ppm	0.05 ppm	0.04 ppm	0.05 ppm	0.02 ppm	0.08 ppm	0.03 ppm	0.08 ppm	0.04 ppm	0.01 ppm	0.05 ppm	0.03 ppm	0.05 ppm	0.03 ppm	0.01 ppm	0.03 ppm
D38-1																																																		
D38-2-C1																																																		
A38(1)-1(R3)a																																																		
A38(1)-1(R3)b																																																		
A38(1)-1(R3)c																																																		
A38(1)-1(R3)d																																																		
A38(1)-2(R3)a																																																		
A38(1)-2(R3)b																																																		
A38(1)-2(R3)c																																																		
A38(1)-2(R3)d																																																		
D38(1)-CC																																																		
D38(2)-1-C1																																																		
D38(2)-2(R4)																																																		
D38(3)-1(R2)																																																		
D38(3)-1(R3)																																																		
EH-56(R2)	67.8	1.58	9.48	0.65	2.02	0.12	<DL	0.32	0.4	0.73	44.3	1.68	0.27	<DL	0.27	1.55	<DL	<DL	<DL	<DL	<DL	<DL	<DL	2.86	0.77	1.05	0.13	0.57	0.12	<DL	0.17	<DL	0.14	<DL	0.09	<DL	<DL	<DL	<DL	<DL	4.32	<DL	<DL	<DL	<DL	<DL	2.99		0.08	0.53
	63	< D.L.	< D.L.	1.27	2.1	0.27		2.69	< D.L.	0.31	38.6	1.28	0.13	0.02				0.01	< D.L.	< D.L.	< D.L.		< D.L.	1.05	0.68	0.78	0.11	0.53	0.05	< D.L.	0.13	0.01	0.13	< D.L.	0.02	< D.L.	0.02	< D.L.	< D.L.	< D.L.						0.03	1.60	< D.L.	< D.L.	0.26
D38(3)-1-C1																																																		
D38(3)-2(R1)																																																		
D38(3)-2(R2)																																																		
M38-CC																																																		
EH-29	72.4	1.45	9.21	0.47	1.68	<DL	<DL	0.27	0.3	0.12	96.8	1.06	<DL	<DL	0.18	1.38	<DL	<DL	<DL	<DL	<DL	<DL	<DL	2.21	0.60	0.60	0.09	0.34	<DL	<DL	0.10	<DL	0.08	<DL	<DL	<DL	<DL	<DL	<DL	<DL	2.15	<DL	<DL	<DL	<DL	<DL	1.10		0.06	0.14
	9	< D.L.	< D.L.	0.40	0.76	0.03		0.59	< D.L.	0.07	19.0	0.37	0.04	0.00				0.04	< D.L.	< D.L.	< D.L.		< D.L.	0.09	0.15	0.23	0.03	0.14	0.02	< D.L.	0.06	0.00	0.04	< D.L.	0.00	< D.L.	0.00	< D.L.	< D.L.	0.01						< D.L.	0.23	< D.L.	< D.L.	0.01
D37-1																																																		
D37-1-C1a																																																		
D37-1-C1b																																																		
EH-58	71	< D.L.	< D.L.	0.73	2.80	0.29		0.67	0.30	0.13	59.2	0.94	0.16	0.01				0.33	< D.L.	< D.L.	< D.L.		< D.L.	4.21	0.56	0.80	0.07	0.42	0.06	0.00	0.11	0.00	0.12	0.00	0.00	< D.L.	0.00	< D.L.	< D.L.	0.08						< D.L.	0.51	< D.L.	< D.L.	0.06
	76.6	1.40	11.9	0.47	3.31	<DL	<DL	0.34	0.8	0.17	75.2	0.99	<DL	<DL	0.19	1.69	<DL	<DL	<DL	<DL	<DL	<DL	<DL	8.65	0.56	0.87	0.11	0.44	0.09	<DL	0.10	<DL	0.10	<DL	<DL	<DL	<DL	<DL	<DL	<DL	1.94	<DL	<DL	<DL	<DL	<DL	1.10		0.03	0.15
D37(1)-1(R2)																																																		
D37(1)-1(R3)																																																		
D37(1)-2(R2)a																																																		
D37(1)-2(R2)b																																																		
D37(1)-3(R2)																																																		
D37(1)-4(R2)																																																		
D37(1)-4(R4)																																																		
D37(1)-5-C1																																																		
D37(1)-6(R2)																																																		
M37-1(R3)																																																		
M37(1)-1(R2)																																																		

Well ID / data table:

LSD	SEC	TWN	RGE	MER	Pool	Original sample set	Depth (ft)	Depth (m)	Stratigraphic unit	Core	Thin	Sample ID	Sample type	CH₄	H₂S	CO₂	Orig δ¹³C ‰ PDB	Orig δ¹⁸O ‰ PDB	SK δ¹³C ‰ PDB	SK δ¹⁸O ‰ PDB	⁸⁷Sr/⁸⁶Sr	CaCO₃ mol% XRD	6/4Pb	7/4Pb	8/4Pb	Ca	Mg	Li	Be	B	Na	Al	Si	P	K	Ti	Sc	V	Cr	Fe
10	20	37	7	W5	Chedderville	Marquez	11618.0	3541.2	Leduc			M37(2)-1(R3)	R3	83	6.9	1.28	1.74	-4.06																					
6	14	37	7	W5	Chedderville	Kuflevskiy	12228.9	3727.4	Cook. Lk.	x	x	K37-2	R2	84.2	0	0.85			3.97	-5.92	0.708600	50.36				189126	131920	2.02	<DL	11	261	217		109	238	3.78		1.93	4.42	1481
							12260.7	3737.1	Cook. Lk.	x	x	K37-5	R2						5.92	-5.82	0.708812	49.59				187741	133321	1.07	<DL	13	327	77.2		77	167	4.13		1.18	2.05	901
11	28	37	8	W5	Crimson	Marquez	12138.0	3699.7	Leduc			M37(3)-1(R2)a	R2A	80.26	9.09	2.68	2.03	-3.84			0.70854																			
							12138.0	3699.7	Leduc			M37(3)-1(R2)b	R2B				2.00	-3.67																						
							12138.0	3699.7	Leduc			M37(3)-1-C2a	C2A				-4.83	-5.95			0.71045																			
							12138.0	3699.7	Leduc			M37(3)-1-C2b	C2B				-4.07	-5.63																						
10	11	37	8	W5	Ricinus East	Marquez	12367.0	3769.5	Leduc			M37(4)-1(R3)	R3	18.62	5.11	15.53																							
							12370.3	3770.5	Leduc			M37(4)-2(R3)	R3																											
							12373.5	3771.5	Leduc			M37(4)-3(R3)	R3																											
							12376.8	3772.5	Leduc			M37(4)-4(R3)	R3																											
							12380.1	3773.5	Leduc			M37(4)-5(R3)	R3																											
							12383.4	3774.5	Leduc			M37(4)-6(R3)	R3																											
							12460.2	3797.9	Leduc			M37(4)-7(R3)	R3				1.35	-4.03																						
7	32	37	9	W5	Strachan	Horrigan	13402.7	4085.2	Leduc	x	x	EH-21a(R2)	R2	52.8	23.1	2.53						50.64				162650	107546	0.98	< D.L.	14.0	458	< D.L.	57.03		159.5		0.51	11.2	3.8	630
												EH-21b(R1)	R1									50.11				153350	101946	0.74	0.12	8.1	304	31.4	95.50		169.1		1.00	7.9	19.8	1556
7	32	37	9	W5	Strachan	Marquez	13403.4	4085.4	Leduc			M37(5)-1(R1)	R1	52.8	23.1	2.53	3.14	-4.28																						
							13496.9	4113.9	Leduc			M37(5)-2(R1)	R1				3.19	-5.34																						
12	31	37	9	W5	Strachan	Marquez	14092.3	4295.4	Leduc			M37(6)-1(R2)	R2				2.30	-6.58																						
10	31	37	9	W5	Strachan	Horrigan	14167.5	4318.3	Leduc	x	x	EH-32	R2	27.3	64	7.16	5.03	-3.04	3.84	-4.08	0.70878	50.11				154850	107946	0.54	< D.L.	7.4	223	9.1	40.35		107.8		0.57	8.3	4.2	1581
													R2						3.78	-4.17						155959	109610	0.33	<DL	<DL	222	57.5		93	119	3.16		0.85	3.86	1292
													R2						3.71	-4.24																				
10	31	37	9	W5	Strachan	Marquez	13635.0	4156	Leduc			M37(7)-1-a	SMC	27.3	64	7.16	1.90	-8.78																					
							13635.0	4156	Leduc			M37(7)-1	MD				1.71	-5.71																						
							13635.0	4156	Leduc			M37(7)-1(R4)	R4				1.91	-8.67																						
							13635.0	4156	Leduc			M37(7)-1c	Patch				3.07	-8.31			0.70861																			
							13704.2	4177.1	Leduc			M37(7)-2b	SMC																											
							13707.5	4178.1	Leduc			M37(7)-2a	SMC																											
							13710.8	4179.1	Leduc			M37(7)-3	SMC																											
							13714.1	4180.1	Leduc			M37(7)-4	R2																											
							13717.4	4181.1	Leduc			M37(7)-5	R2																											
							13720.6	4182.1	Leduc			M37(7)-6	R2																											
							13722.3	4182.6	Leduc			M37(7)-7(R4)	R4				1.89	-7.87																						
							13722.3	4182.6	Leduc			M37(7)-7b	Patch				3.17	-7.85			0.70827																			
							13722.3	4182.6	Leduc			M37(7)-7c	Patch				3.22	-7.50																						
							13723.9	4183.1	Leduc			M37(7)-8	R2																											
							13727.2	4184.1	Leduc			M37(7)-9	R2																											
							13865.3	4226.2	Leduc			M37(7)-10a	MD				3.73	-5.46																						
							13865.3	4226.2	Leduc			M37(7)-10b(R)	R4				3.25	-6.22																						
							13865.3	4226.2	Leduc			M37(7)-10c(R)	R4				3.44	-6.47																						
							13865.3	4226.2	Leduc			M37(7)-10d	Patch				3.40	-8.53			0.70822																			
							13865.3	4226.2	Leduc			M37(7)-10-C2	C2/frac.				3.31	-8.28																						
							13865.3	4226.2	Leduc			M37(7)-10-C2	C2				3.23	-5.97																						
							14030.3	4276.5	Leduc			M37(7)-11a	MD				2.24	-6.65																						
							14030.3	4276.5	Leduc			M37(7)-11b(R)	R4				2.63	-7.38																						
							14030.3	4276.5	Leduc			M37(7)-11c	Patch				2.51	-7.45			0.70840																			
							14030.3	4276.5	Leduc			M37(7)-11-C2	C2				2.47	-6.84																						
							14030.3	4276.5	Leduc			M37(7)-11-C2	C2				2.63	-7.84																						
							14030.3	4276.5	Leduc			M37(7)-11-C2	C2				2.57	-7.01																						
							14030.3	4276.5	Leduc			M37(7)-11-C2	C2				2.57	-7.65																						
							14067.4	4287.8	Leduc			M37(7)-12(2)a	R2																											
							14067.4	4287.8	Leduc			M37(7)-12(2)b	R2																											
							14067.4	4287.8	Leduc			M37(7)-12(2)c	R2																											
							14067.4	4287.8	Leduc			M37(7)-12(2)d	R2																											
							14067.4	4287.8	Leduc			M37(7)-12C2a	C1																											
							14067.4	4287.8	Leduc			M37(7)-12C2b	C1																											
							14067.4	4287.8	Leduc			M37(7)-12C2c	C1																											
							14108.4	4300.3	Leduc			M37(7)-13(2)	R2								0.70966																			
							14107.4	4300	Leduc			M37(7)-14(2)a	R2																											

Sample ID	Mn	Co	Ni	Cu	Zn	Ga	Ge	As	Se	Rb	Sr	Y	Zr	Nb	Mo	Ru	Pd	Ag	Cd	Sn	Sb	Te	Cs	Ba	La	Ce	Pr	Nd	Sm	Eu	Gd	Tb	Dy	Ho	Er	Tm	Yb	Lu	Hf	Ta	W	Re	Os	Ir	Pt	Tl	Pb	Bi	Th	U
	0.03 ppm	0.03 ppm	0.06 ppm	0.03 ppm	0.08 ppm	0.01 ppm	0.02 ppm	0.06 ppm	0.2 ppm	0.04 ppm	0.03 ppm	0.02 ppm	0.09 ppm	0.04 ppm	0.02 ppm	0.01 ppm	0.01 ppm	0.01 ppm	0.06 ppm	0.06 ppm	0.01 ppm	0.02 ppm	0.02 ppm	0.03 ppm	0.03 ppm	0.03 ppm	0.04 ppm	0.03 ppm	0.04 ppm	0.03 ppm	0.03 ppm	0.03 ppm	0.04 ppm	0.02 ppm	0.04 ppm	0.06 ppm	0.05 ppm	0.04 ppm	0.05 ppm	0.02 ppm	0.08 ppm	0.03 ppm	0.08 ppm	0.04 ppm	0.01 ppm	0.05 ppm	0.03 ppm		0.01 ppm	0.03 ppm
M37(2)-1(R3)																																																		
K37-2	126	1.05	20.9	1080	777	<DL	<DL	1.69	3.6	0.62	62.9	7.29	0.17	<DL	0.15	0.75	<DL	0.36	0.23	21.8	1.05	<DL	<DL	9.56	9.90	6.86	1.28	5.07	0.80	0.19	0.99	0.11	0.60	0.12	0.33	<DL	0.20	<DL	<DL	<DL	0.12	<DL	<DL	<DL	<DL	<DL	83.4		0.17	0.45
K37-5	67.4	0.90	11.6	8.83	2.09	<DL	<DL	1.07	2.8	0.22	46.4	1.92	0.12	<DL	0.07	0.76	<DL	0.13	<DL	0.41	<DL	<DL	<DL	21.0	0.95	0.73	0.15	0.62	0.13	<DL	0.18	<DL	0.16	<DL	0.11	<DL	0.08	<DL	<DL	<DL	0.11	<DL	<DL	<DL	<DL	<DL	1.75		0.05	0.06
M37(3)-1(R2)a																																																		
M37(3)-1(R2)b																																																		
M37(3)-1-C2a																																																		
M37(3)-1-C2b																																																		
M37(4)-1(R3)																																																		
M37(4)-2(R3)																																																		
M37(4)-3(R3)																																																		
M37(4)-4(R3)																																																		
M37(4)-5(R3)																																																		
M37(4)-6(R3)																																																		
M37(4)-7(R3)																																																		
EH-21a(R2)	85	< D.L.	< D.L.	1.05	2.0	0.11		1.48	< D.L.	0.11	42.8	1.16	0.12	0.01				0.07	< D.L.	0.12	< D.L.		< D.L.	0.99	0.50	0.64	0.09	0.38	0.06	0.01	0.13	0.00	0.08	0.00	0.04	0.00	0.01	< D.L.	< D.L.	< D.L.						0.01	1.24	< D.L.	< D.L.	0.53
EH-21b(R1)	157	< D.L.	< D.L.	1.74	4.2	0.39		2.20	< D.L.	0.29	33.6	1.93	0.43	0.05				0.25	0.16	0.54	0.06		0.16	2.41	1.06	0.90	0.26	0.68	0.24	0.02	0.20	0.02	0.17	0.03	0.17	0.10	0.10	0.01	< D.L.	0.00						0.12	1.24	0.11	0.17	0.12
M37(5)-1(R1)																																																		
M37(5)-2(R1)																																																		
M37(6)-1(R2)																																																		
EH-32	167	< D.L.	< D.L.	1.43	13.8	37.5		3.93	< D.L.	0.18	40.7	2.41	0.26	0.04				0.32	< D.L.	< D.L.	< D.L.		< D.L.	461.1	0.92	0.87	0.18	0.79	0.15	0.11	0.25	0.02	0.18	0.03	0.08	0.01	0.08	< D.L.	< D.L.	< D.L.						0.02	3.03	< D.L.	< D.L.	0.13
	167	1.48	9.32	0.26	1.56	<DL	<DL	0.16	0.2	0.15	23.0	2.05	<DL	<DL	0.16	1.41	<DL	<DL	<DL	<DL	<DL	<DL	<DL	3.55	0.85	0.69	0.18	0.78	0.17	<DL	0.25	<DL	0.21	<DL	0.12	<DL	<DL	<DL	<DL	<DL	1.98	<DL	<DL	<DL	<DL	<DL	2.00		0.05	0.23
M37(7)-1-a																																																		
M37(7)-1																																																		
M37(7)-1(R4)																																																		
M37(7)-1c																																																		
M37(7)-2b																																																		
M37(7)-2a																																																		
M37(7)-3																																																		
M37(7)-4																																																		
M37(7)-5																																																		
M37(7)-6																																																		
M37(7)-7(R4)																																																		
M37(7)-7b																																																		
M37(7)-7c																																																		
M37(7)-8																																																		
M37(7)-9																																																		
M37(7)-10a																																																		
M37(7)-10b(R																																																		
M37(7)-10c(R																																																		
M37(7)-10d																																																		
M37(7)-10-C2																																																		
M37(7)-10-C2																																																		
M37(7)-11a																																																		
M37(7)-11b(R																																																		
M37(7)-11c																																																		
M37(7)-11-C2																																																		
M37(7)-11-C2																																																		
M37(7)-11-C2																																																		
M37(7)-11-C2																																																		
M37(7)-12(2)a																																																		
M37(7)-12(2)b																																																		
M37(7)-12(2)c																																																		
M37(7)-12(2)d																																																		
M37(7)-12C2a																																																		
M37(7)-12C2b																																																		
M37(7)-12C2c																																																		
M37(7)-13(2)																																																		
M37(7)-14(2)a																																																		

TWN	LSD	SEC	TWN	RGE	MER	Pool	Original sample set	Depth (ft)	Depth (m)	Stratigraphic unit	Core samples	Thin sections	Sample ID	Sample type	CH₄	H₂S	CO₂	Original δ¹³C ‰ PDB	Original δ¹⁸O ‰ PDB	SK+adjusted δ¹³C ‰ PDB	SK+adjusted δ¹⁸O ‰ PDB	⁸⁷Sr/⁸⁶Sr	CaCO₃ mol% XRD	6/4Pb	7/4Pb	8/4Pb	Ca 31 ppm	Mg 2 ppm	Li 0.05 ppm	Be 0.1 ppm	B 2 ppm	Na 0.5 ppm	Al 0.2 ppm	Si ppm	P 5 ppm	K 6 ppm	Ti 0.09 ppm	Sc ppm	V 0.05 ppm	Cr 0.05 ppm	Fe 3.7 ppm
								14107.4	4300	Leduc			M37(7)-14(2)b	R2																											
								14107.4	4300	Leduc			M37(7)-14(2)d	R2																											
								14107.4	4300	Leduc			M37(7)-14C2a	C2																											
								14107.4	4300	Leduc			M37(7)-14C2b	C2																											
								14145.2	4311.5	Leduc			M37(7)-15(2)	R2																											
								14148.5	4312.5	Leduc			M37(7)-16(2)	R2																											
								14151.7	4313.5	Leduc			M37(7)-17(2)	R2																											
								14155.0	4314.5	Leduc			M37(7)-18(2)	R2																											
								14158.3	4315.5	Leduc			M37(7)-19	C1																											
								14161.6	4316.5	Leduc			M37(7)-20	C1																											
								14164.9	4317.5	Leduc			M37(7)-21	C1																											
								14168.1	4318.5	Leduc			M37(7)-22	C2																											
								14171.4	4319.5	Leduc			M37(7)-23	C2																											
								14167.5	4318.3	Leduc			M37(7)-24(2)	R2				3.54	-4.57			0.70825																			
								14167.5	4318.3	Leduc			M37(7)-24-Ca	CC (TSR)				-10.29	-7.47																							
								14191.4	4325.6	Leduc			M37(7)-25(2)	R2				3.57	-4.50																							
								14191.4	4325.6	Leduc			M37(7)-25-CC	CC				-3.65	-6.62																							
								14191.4	4325.6	Leduc			M37(7)-25-CC	CC				-3.65	-6.62																							
	11	27	37	9	W5	Strachan	Marquez	12918.2	3937.5	Leduc			M37(8)-1(R3)	R3	42.57	25.3	2.95	2.56	-5.32																						
								13196.4	4022.3	Leduc			M37(8)-2(R3)	R3				3.52	-4.51																							
	10	24	37	9	W5	Strachan	Marquez	12557.9	3827.7	Leduc			M37(9)-1(2)	R2 (TSR)	85.29	0.52	2.86	2.20	-5.38																						
								12558.9	3828	Leduc			M37(9)-2(2)	R2 (TSR)				1.94	-4.23																							
	5	13	37	12	W5	Ram River	Horrigan	16558.2	5047	Leduc	x	x	EH-9a(R2)	R2	84.48	0	0.14	1.65	-9.87	2.06	-8.67	0.70888	50.68				156060	107026	0.75	<DL	<DL	452	66.7		80	115	3.18		1.05	4.36	1962
																											176450	117046	1.19	0.05	8.7	563	153.6	103.10		238.6		0.92	5.1	5.1	2753
													EH-9b(R2/3)	R2 (+R3)									50.94				174550	115646	0.86	0.03	9.6	620	42.3	52.17		180.7		0.76	7.2	5.7	1960
								16625.1	5067.4	Leduc	x	x	EH-10	R2									50.18				172350	116346	0.65	0.00	7.7	339	66.7	102.90		162.8		0.87	4.1	4.7	2335
														R2						3.12	-7.92		49.66				150590	103755	0.36	<DL	<DL	226	67.3		71	86	3.27		0.53	3.19	1860
	5	13	37	12	W5	Ram River	Marquez	16559.2	5047.3	Leduc			M37(10)-1(R2)	R2	84.48	0	0.14	1.43	-7.19																						
								16559.2	5047.3	Leduc			M37(10)-1Cal	CC (TSR)				-17.15	-7.48																							
								16625.1	5067.4	Leduc			M37(10)-2	MD				3.15	-6.42			0.70837																			
								16625.1	5067.4	Leduc			M37(10)-2C2a	C2				2.09	-7.38																							
								16625.1	5067.4	Leduc			M37(10)-2C2b	C2				2.79	-7.84																							
T36	11	6	36	3	W5	Lanaway	Drivet	9721.0	2963	Leduc			D36-1-CC-S	CC-Distribu	13.49	10.5	1.26	-6.53	-7.71																						
								9753.8	2973	Leduc			D36-2(R2)	R2				2.04	-4.08			0.70871																			
								9753.8	2973	Leduc			D36-3	C1				2.33	-4.31																							
								9760.4	2975	Leduc			D36-4	C1				1.97	-4.07																							
								9812.9	2991	Leduc			D36-5	C1				2.55	-4.00																							
	8	27	36	6	W5	Garrington	Drivet	11738.7	3578	Leduc			D36(1)-1CC-S	CC-Distributed near pores filled w				-2.58	-5.95																						
								11755.1	3583	Leduc			D36(1)-2(R1)	R1				3.71	-4.57																							
								11755.1	3583	Leduc			D36(1)-2(R2)	R2				3.64	-4.62																							
								11755.1	3583	Leduc			D36(1)-2(R4)a	R4				3.80	-4.11																							
								11755.1	3583	Leduc			D36(1)-2(R4)b	R4				3.24	-4.43																							
								11787.9	3593	Leduc			D36(1)-3(R1)	R1				3.73	-4.57																							
								11787.9	3593	Leduc			D36(1)-3(R2)	R2				3.47	-4.90																							
								11787.9	3593	Leduc			D36(1)-3(R4)	R4				3.66	-4.76																							
	16	25	36	6	W5	Garrington	Drivet	11351.6	3460	Leduc			D36(2)-1CC-S	CC-Distribu	6.5	14.6	0.9	-17.90	-8.02																						
								11384.4	3470	Leduc			D36(2)-2(R1)	R1				3.58	-4.55																							
								11440.1	3487	Leduc			D36(2)-3	C1				3.08	-5.50																							
								11446.7	3489	Leduc			D36(2)-4CC-S	CC-Distributed near pores filled w				0.26	-9.12			0.70894																			
	10	33	36	10	W5	Ricinus West	Horrigan	14973.2	4563.9	Leduc	x	x	EH-35b(R2)	R2	50.63	42	6.48			2.36	-4.72		49.91				162447	105261	0.95	<DL	3	213	174		124	224	8.26		0.88	5.88	1147
													EH-35a(R3)	R3 (+R2)						2.41	-4.63		49.38				149713	97341	0.65	<DL	<DL	184	83.4		85	125	4.58		0.77	3.48	1060
													EH-35SK-R3	R3 (+R2)									49.9				153441	98730	0.47	<DL	<DL	115	86.2		124	137	3.54		1.22	7.06	1705
								15017.5	4577.4	Leduc	x	x	EH-36(R3)	R3									50.41																			
								15291.8	4661	Leduc			EH-37	R2				1.85	-6.55	2.07	-4.74		50.18				161809	113659	1.02	<DL	20	227	60.1		65	115	3.38		0.94	6.60	728
														R2						2.08	-4.68						135950	83646	1.03	0.06	15.2	184	28.3	32.10		79.6		0.02	7.4	4.4	370
														R2						2.00	-4.99																				
	10	33	36	10	W5	Ricinus West	Marquez	14973.6	4564	Leduc			M36-1(R3)	R3	50.63	42	6.48	2.42	-4.61			0.70923																				
								15017.5	4577.4	Leduc			M36-2	CC				-2.49	-8.95			0.70854																			

Sample ID	Mn	Co	Ni	Cu	Zn	Ga	Ge	As	Se	Rb	Sr	Y	Zr	Nb	Mo	Ru	Pd	Ag	Cd	Sn	Sb	Te	Cs	Ba	La	Ce	Pr	Nd	Sm	Eu	Gd	Tb	Dy	Ho	Er	Tm	Yb	Lu	Hf	Ta	W	Re	Os	Ir	Pt	Tl	Pb	Bi	Th	U
(detection limit)	0.03	0.03	0.06	0.03	0.08	0.01	0.02	0.06	0.2	0.04	0.03	0.02	0.09	0.04	0.02	0.01	0.01	0.01	0.06	0.06	0.01	0.02	0.02	0.03	0.03	0.03	0.04	0.03	0.04	0.03	0.03	0.03	0.04	0.02	0.04	0.06	0.05	0.04	0.05	0.02	0.08	0.03	0.08	0.04	0.01	0.05	0.03		0.01	0.03
(units)	ppm	ppm	ppm	ppm	ppm	ppm	ppm	ppm	ppm	ppm	ppm	ppm	ppm	ppm	ppm	ppm	ppm	ppm	ppm	ppm	ppm	ppm	ppm	ppm	ppm	ppm	ppm	ppm	ppm	ppm	ppm	ppm	ppm	ppm	ppm	ppm	ppm	ppm	ppm	ppm	ppm	ppm	ppm	ppm	ppm	ppm	ppm		ppm	ppm
M37(7)-14(2)b																																																		
M37(7)-14(2)c																																																		
M37(7)-14C2a																																																		
M37(7)-14C2b																																																		
M37(7)-15(2)																																																		
M37(7)-16(2)																																																		
M37(7)-17(2)																																																		
M37(7)-18(2)																																																		
M37(7)-19																																																		
M37(7)-20																																																		
M37(7)-21																																																		
M37(7)-22																																																		
M37(7)-23																																																		
M37(7)-24(2)																																																		
M37(7)-24-Ca																																																		
M37(7)-25(2)																																																		
M37(7)-25-CC																																																		
M37(7)-25-CC																																																		
M37(8)-1(R3)																																																		
M37(8)-2(R3)																																																		
M37(9)-1(2)																																																		
M37(9)-2(2)																																																		
EH-9a(R2)	304	1.58	9.37	2.20	7.18	<DL	<DL	0.18	0.3	0.26	65.5	1.54	0.20	<DL	0.22	1.37	<DL	<DL	<DL	<DL	<DL	<DL	<DL	848	0.65	0.53	0.10	0.45	0.11	0.60	0.16	<DL	0.12	<DL	0.08	<DL	<DL	<DL	<DL	<DL	3.35	<DL	<DL	<DL	<DL	<DL	3.32		0.05	0.09
EH-9b(R2/3)	352	< D.L.	< D.L.	1.50	4.6	12.0		1.95	< D.L.	0.39	72.7	1.74	0.42	0.04				0.30	0.13	-1.11	0.04		0.06	294.2	0.67	0.62	0.13	0.49	0.13	0.04	0.16	0.01	0.13	0.02	0.10	0.05	0.04	0.00	< D.L.	< D.L.						0.06	2.08	0.07	0.12	0.09
EH-10	293	< D.L.	< D.L.	1.65	1.0	39.5		2.24	< D.L.	0.32	91.2	1.95	0.40	0.07				0.33	0.12	2.10	0.12		0.09	1914.6	0.67	0.65	0.11	0.52	0.12	0.18	0.19	0.01	0.13	0.02	0.05	0.01	0.05	0.02	0.05	0.10						0.02	4.59	0.07	0.10	0.02
	290	< D.L.	< D.L.	1.45	4.3	1.8		1.74	< D.L.	0.22	42.4	1.69	0.48	0.04				0.24	0.09	-1.03	0.05		< D.L.	33.5	0.61	0.56	0.10	0.41	0.08	0.02	0.14	0.01	0.11	0.02	0.06	0.01	0.03	0.00	< D.L.	0.01						0.02	1.49	0.03	< D.L.	0.06
	284	1.54	8.50	0.52	3.67	<DL	<DL	0.18	0.4	0.16	35.4	1.53	0.11	<DL	0.13	1.67	<DL	<DL	<DL	<DL	<DL	<DL	<DL	20.1	0.65	0.54	0.10	0.42	0.08	<DL	0.13	<DL	0.11	<DL	0.08	<DL	<DL	<DL	<DL	<DL	2.63	<DL	<DL	<DL	<DL	<DL	0.71		0.02	0.04
M37(10)-1(R2																																																		
M37(10)-1Cal																																																		
M37(10)-2																																																		
M37(10)-2C2a																																																		
M37(10)-2C2b																																																		
D36-1-CC-S																																																		
D36-2(R2)																																																		
D36-3																																																		
D36-4																																																		
D36-5																																																		
D36(1)-1CC-S																																																		
D36(1)-2(R1)																																																		
D36(1)-2(R2)																																																		
D36(1)-2(R4)a																																																		
D36(1)-2(R4)b																																																		
D36(1)-3(R1)																																																		
D36(1)-3(R2)																																																		
D36(1)-3(R4)																																																		
D36(2)-1CC-S																																																		
D36(2)-2(R1)																																																		
D36(2)-3																																																		
D36(2)-4CC-S																																																		
EH-35b(R2)	129	1.33	9.71	0.31	1.84	<DL	<DL	0.40	0.7	0.62	42.8	1.06	0.61	<DL	0.14	1.79	<DL	<DL	<DL	<DL	<DL	<DL	<DL	2.87	0.54	0.63	0.10	0.42	0.09	<DL	0.12	<DL	0.09	<DL	<DL	<DL	<DL	<DL	<DL	<DL	3.14	<DL	<DL	<DL	<DL	<DL	2.19		0.07	0.16
EH-35a(R3)	143	1.26	9.34	0.87	2.38	<DL	<DL	0.38	0.5	0.27	37.2	1.14	0.14	<DL	0.12	1.48	<DL	<DL	<DL	0.33	<DL	<DL	<DL	5.34	0.57	0.73	0.10	0.45	0.09	<DL	0.12	<DL	0.09	<DL	<DL	<DL	<DL	<DL	<DL	<DL	2.15	<DL	<DL	<DL	<DL	<DL	3.75		0.10	0.11
EH-35SK-R3	212	1.23	10.0	0.54	2.28	<DL	<DL	0.72	0.6	0.24	30.4	1.32	0.14	<DL	0.15	1.29	<DL	<DL	<DL	0.20	<DL	<DL	<DL	1.47	0.59	0.79	0.11	0.49	0.11	<DL	0.15	<DL	0.14	<DL	0.09	<DL	0.10	<DL	<DL	<DL	3.08	<DL	<DL	<DL	<DL	<DL	1.17		0.05	0.09
EH-36(R3)																																																		
EH-37	114	1.39	22.7	0.61	1.71	<DL	<DL	0.21	0.3	0.20	49.7	1.39	0.10	<DL	0.13	1.45	<DL	1.07	0.71	<DL	<DL	<DL	<DL	36.6	0.59	0.58	0.10	0.44	0.09	<DL	0.16	<DL	0.12	<DL	0.08	<DL	<DL	<DL	<DL	<DL	1.98	<DL	<DL	<DL	<DL	<DL	0.34		0.02	0.08
	102	< D.L.	< D.L.	0.64	2.2	20.7		1.29	0.30	0.23	59.1	1.42	0.15	0.02				0.08	< D.L.	< D.L.	< D.L.		0.03	322.5	0.60	0.62	0.13	0.55	0.09	0.03	0.17	0.01	0.12	0.02	0.11	0.04	0.03	< D.L.	< D.L.	< D.L.						0.03	0.87	0.04	0.07	0.83
M36-1(R3)																																																		
M36-2																																																		

TWN	LSD	SEC	TWN	RGE	MER	Pool	Original sample set	Depth (ft)	Depth (m)	Stratigraphic unit	Core samples	Thin sections	Sample ID	Sample type	CH₄	H₂S	CO₂	Original δ¹³C ‰ PDB	Original δ¹⁸O ‰ PDB	SK+adj δ¹³C ‰ PDB	SK+adj δ¹⁸O ‰ PDB	⁸⁷Sr/⁸⁶Sr	CaCO₃ mol% XRD	6/4Pb	7/4Pb	8/4Pb	Ca 31 ppm	Mg 2 ppm	Li 0.05 ppm	Be 0.1 ppm	B 2 ppm	Na 0.5 ppm	Al 0.2 ppm	Si ppm	P 5 ppm	K 6 ppm	Ti 0.09 ppm	Sc ppm	V 0.05 ppm	Cr 0.05 ppm	Fe 3.7 ppm
								15017.5	4577.4	Leduc			M36-2(R1)	R1				2.58	-4.85			0.70860																			
								15189.8	4629.9	Leduc			M36-3(R2)	R2				1.79	-4.70			0.70833																			
								15202.6	4633.8	Leduc			M36-4(R3)	R3				1.81	-4.58			0.70866																			
								15202.6	4633.8	Leduc			M36-4	CC (TSR)				-25.77	-8.07			0.70861																			
								15291.8	4661	Leduc			M36-5(R2)	R2				1.94	-4.90			0.70865																			
								15291.8	4661	Leduc			M36-5	CC (TSR)				-19.01	-9.01			0.70850																			
	11	27	36	10	W5	Ricinus West	Horrigan	14685.2	4476.1	Leduc	x	x	EH-44(R2)	R2	84.63	0	0.41						50.47				162390	103973	0.54	<DL	<DL	215	28.0		93	126	1.56		0.53	4.85	885
										Leduc			EH-44(R3)	R3						2.28	-4.82		50.64				166807	106281	0.45	<DL	<DL	267	22.3		59	83	0.93		0.43	5.18	1063
								14730.5	4489.2	Leduc	x	x	EH-45	R2									50.33				171250	120846	0.99	< D.L.	11.7	219	129.6	164.01		221.8		<D.L.	9.9	3.9	1000
														R2						2.72	-4.46		50.12				156396	111656	1.07	<DL	3	231	473		137	483	29.3		2.21	7.27	1188
	11	27	36	10	W5	Ricinus West	Marquez	14685.5	4476.2	Leduc			M36(1)-1(R2)	R2	84.63	0	0.41	2.39	-4.43																						
	7	26	36	10	W5	Ricinus East	Horrigan	14428.6	4397.9	Leduc	x	x	EH-20	R2	9.43	81	9.21						50.5				169950	119146	0.88	< D.L.	11.1	319	< D.L.	81.29		74.6		<D.L.	6.1	3.7	1210
	7	26	36	10	W5	Ricinus East	Marquez	14428.6	4397.9	Leduc			M36(2)-1(R1)	R1	9.43	81	9.21	2.34	-4.52																						
	15	23	36	10	W5	Ricinus West	Horrigan	14748.8	4495.5	Leduc	x	x	EH-53(R3)	R2+R3	59.3	32.6	6.8			4.89	-4.65		50.14				155585	98700	0.76	<DL	<DL	195	83.5		95	128	2.71		1.16	12.3	1617
								15067.1	4592.5	Leduc	x	x	EH-55	R4									48.18				65850	26446	0.80	< D.L.	21.1	138	< D.L.	29.76		65.2		0.11	8.4	3.5	331
	15	23	36	10	W5	Ricinus West	Marquez	15066.7	4592.4	Leduc			M36(3)-1(R1)	R1	59.3	32.6	6.8	5.11	-4.65			0.70841																			
								15066.7	4592.4	Leduc			M36(3)-1-C2	C2								0.70882																			
								15068.7	4593	Leduc			M36(3)-2(R1)	R1								0.70830																			
								15068.7	4593	Leduc			M36(3)-2-CC	CC								0.70901																			
T35	11	10	35	5	W5	Caroline	Horrigan	11023.8	3360.1	Leduc			EH-41a(R1)	R2	77.8	0	1.31						50.63				134850	85046	2.58	0.11	16.0	517	1233.2	236.99		1469.9		1.46	15.1	6.9	3588
													EH-41b(R4)	R4									50.5				117981	80859	1.88	<DL	11	394	800		133	1124	21.8		4.25	5.08	3627
																											137150	85646	2.49	0.14	14.2	441	1146.9	156.68		1274.6		1.44	13.9	7.0	4063
								11042.8	3365.9	Leduc			EH-42a(R1)	R1				0.30	-4.81	0.36	-3.08	0.70891	51.3				149534	103719	2.37	<DL	22	363	741		77	798	18.4		2.00	5.83	1460
													EH-42b(R4)	R4						0.42	-3.08						167850	112246	2.84	0.11	17.0	526	1462.1	206.78		1219.0		1.21	8.0	6.0	1839
	11	10	35	5	W5	Caroline	Drivet	11036.6	3364	Leduc			D35-1(R1)	R1	77.8	0	1.31	0.29	-3.71																						
								11036.6	3364	Leduc			D35-1(R2)	R2				0.43	-3.71			0.70834																			
T34	8	14	34	7	W5	Caroline	Amthor	13481	4109	Leduc			A34-1-C4	C4	9.96	21.3	0.57	0.13	-7.73	0.09	-6.75																				
								13481	4109	Leduc			A34-1-Cal	CC				-4.50	-8.32	-4.54	-7.34																				
								13493	4113	Leduc			A34-2(R4)a	R4				3.28	-6.62	3.24	-5.64																				
								13493	4113	Leduc			A34-2(R4)b	R4				2.67	-7.34	2.63	-6.36																				
								13493	4113	Leduc			A34-2-C4	C4				0.21	-8.71	0.17	-7.73																				
	6	24	34	8	W5	Ricinus	Horrigan	14369.6	4379.9	Leduc	x	x	EH-14	R4	54.24	0	0.48						49.91				166550	110346	1.35	0.11	27.2	208	7.2	18.31		68.0		0.02	5.9	3.9	< D.L.
	6	24	34	8	W5	Ricinus East	Marquez	14370.6	4380.2	Leduc			M34-1(R1)	R1	54.24	0	0.48	2.44	-4.91			0.70831																			
								14370.6	4380.2	Leduc			M34-2-C2	C2				1.61	-7.26			0.70920																			
								14059.2	4285.3	Leduc			M34-3(R1)	R1				1.99	-4.64			0.70865																			
								14389.6	4386	Leduc			M34-4(R1)	R1				1.83	-5.32			0.71000																			
								14389.6	4386	Leduc			M34-4-C2	C2				1.37	-6.85																						
	6	14	34	8	W5	Ricinus East	Horrigan	14058.9	4285.2	Leduc	x	x	EH-11	R2									49.37				159750	71546	0.89	0.02	13.3	188	7.3	49.87		124.7		0.69	12.5	6.7	879
														R2						2.35	-5.72		49.28				134907	91683	0.80	<DL	4	185	19.3		76	83	4.39		0.77	2.93	624
								14064.5	4286.9	Leduc	x	x	EH-12	R2									48.67				133350	86146	0.88	< D.L.	10.7	351	< D.L.	34.43		124.5		0.30	13.3	3.9	907
														R2						2.40	-4.62		49.83				142911	103751	0.81	<DL	<DL	280	26.5		71	118	1.76		0.77	3.05	520
	6	14	34	8	W5	Ricinus East	Marquez	14059.2	4285.3	Leduc			M34(1)-1-CC	CC (TSR)				-8.61	-8.77			0.70944																			
								14064.5	4286.9	Leduc			M34(1)-2(R2)	R2				2.26	-4.55																						
T33	13	9	33	4	W5	Harmattan	Horrigan	11374.5	3467	Leduc	x	x	EH-49	R2	69.4	0	3.8	2.92	-5.77	2.89	-4.42	0.70833	49.61				174450	122346	0.91	< D.L.	11.3	335	< D.L.	71.95		88.8		<D.L.	9.1	3.4	777
														R2						2.94	-4.29																				
	7	34	33	6	W5	Caroline	Drivet	13023.8	3969.7	Cook. Lk.			D33-C2a	C2	81.1	0	0.5	4.16	-8.78																						
								13023.8	3969.7	Cook. Lk.			D33-C2b	C2				3.48	-9.34			0.71087																			

Sample ID	Mn	Co	Ni	Cu	Zn	Ga	Ge	As	Se	Rb	Sr	Y	Zr	Nb	Mo	Ru	Pd	Ag	Cd	Sn	Sb	Te	Cs	Ba	La	Ce	Pr	Nd	Sm	Eu	Gd	Tb	Dy	Ho	Er	Tm	Yb	Lu	Hf	Ta	W	Re	Os	Ir	Pt	Tl	Pb	Bi	Th	U
	0.03 ppm	0.03 ppm	0.06 ppm	0.03 ppm	0.08 ppm	0.01 ppm	0.02 ppm	0.06 ppm	0.2 ppm	0.04 ppm	0.03 ppm	0.02 ppm	0.09 ppm	0.04 ppm	0.02 ppm	0.01 ppm	0.01 ppm	0.01 ppm	0.06 ppm	0.06 ppm	0.01 ppm	0.02 ppm	0.02 ppm	0.03 ppm	0.03 ppm	0.03 ppm	0.04 ppm	0.03 ppm	0.04 ppm	0.03 ppm	0.03 ppm	0.03 ppm	0.04 ppm	0.02 ppm	0.04 ppm	0.06 ppm	0.05 ppm	0.04 ppm	0.05 ppm	0.02 ppm	0.08 ppm	0.03 ppm	0.08 ppm	0.04 ppm	0.01 ppm	0.05 ppm	0.03 ppm		0.01 ppm	0.03 ppm
M36-2(R1)																																																		
M36-3(R2)																																																		
M36-4(R3)																																																		
M36-4																																																		
M36-5(R2)																																																		
M36-5																																																		
EH-44(R2)	97.7	1.26	9.27	0.19	1.71	<DL	<DL	0.21	0.6	0.13	36.2	0.78	<DL	<DL	0.11	1.61	<DL	<DL	<DL	0.10	<DL	<DL	<DL	1.37	0.37	0.32	0.05	0.22	<DL	<DL	0.07	<DL	0.06	<DL	<DL	<DL	<DL	<DL	<DL	<DL	3.79	<DL	<DL	<DL	<DL	<DL	0.13		0.02	0.04
EH-44(R3)	171	1.22	9.09	0.98	3.24	<DL	<DL	0.35	0.4	0.09	42.0	1.26	<DL	<DL	0.11	1.27	<DL	<DL	<DL	0.23	<DL	<DL	<DL	160	0.58	0.62	0.10	0.40	0.09	0.13	0.14	<DL	0.11	<DL	<DL	<DL	<DL	<DL	<DL	<DL	1.23	<DL	<DL	<DL	<DL	<DL	2.61		0.01	0.04
EH-45	100	< D.L.	< D.L.	< D.L.	1.6	0.6		1.88	< D.L.	1.01	38.0	1.08	0.03	0.01				0.32	< D.L.	< D.L.	< D.L.		< D.L.	9.82	0.60	1.02	0.09	0.56	0.05	< D.L.	0.08	0.00	0.11	< D.L.	< D.L.	< D.L.	< D.L.	< D.L.	< D.L.							< D.L.	< D.L.	< D.L.	< D.L.	0.08
	107	1.62	9.83	0.39	2.71	0.17	<DL	0.24	0.3	1.67	36.7	1.13	0.35	<DL	0.23	1.68	<DL	<DL	<DL	0.09	<DL	<DL	<DL	9.05	0.63	1.05	0.15	0.68	0.13	<DL	0.15	<DL	0.13	<DL	0.07	<DL	<DL	<DL	<DL	<DL	4.71	<DL	<DL	<DL	<DL	<DL	1.04		0.14	0.17
M36(1)-1(R2)																																																		
EH-20	130	< D.L.	< D.L.	1.78	2.3	1.0		1.58	< D.L.	0.13	40.1	1.25	0.10	0.02				0.06	< D.L.	< D.L.	< D.L.		< D.L.	16.18	0.66	1.07	0.08	0.44	0.08	< D.L.	0.12	0.01	0.10	< D.L.	< D.L.	< D.L.	0.02		< D.L.	< D.L.	0.03						< D.L.	1.10	< D.L.	< D.L.	0.04
M36(2)-1(R1)																																																		
EH-53(R3)	196	1.29	8.80	5.13	13.2	<DL	<DL	0.61	0.5	0.29	129	1.81	0.13	<DL	0.32	1.28	<DL	<DL	<DL	0.70	0.13	<DL	<DL	1925	1.23	1.71	0.22	0.92	0.27	1.32	0.24	<DL	0.19	<DL	0.12	<DL	<DL	<DL	<DL	<DL	2.23	<DL	<DL	<DL	<DL	<DL	43.8		0.15	0.12
EH-55	71	< D.L.	< D.L.	< D.L.	2.1	0.80		1.48	< D.L.	< D.L.	52.4	1.24	0.06	0.01				0.19	< D.L.	< D.L.	< D.L.		< D.L.	5.38	0.97	0.90	0.11	0.61	0.04	0.01	0.15	0.00	0.10	< D.L.	< D.L.	< D.L.	0.01	< D.L.	< D.L.	0.05							< D.L.	0.24	< D.L.	< D.L.	< D.L.
M36(3)-1(R1)																																																		
M36(3)-1-C2																																																		
M36(3)-2(R1)																																																		
M36(3)-2-CC																																																		
EH-41a(R1)	82	2.9	< D.L.	4.95	2.6	0.1		0.19	< D.L.	5.40	64.5	2.88	0.37	0.01				0.09	< D.L.	0.05	0.07		0.23	9.35	1.22	3.14	0.42	2.12	0.67	0.14	0.74	0.10	0.63	0.09	0.26	0.02	0.18	0.01	< D.L.	0.07						0.08	7.42	0.08	0.81	0.87
EH-41b(R4)	65.7	4.06	38.5	4.45	2.06	0.35	<DL	2.94	0.5	5.35	61.5	3.10	0.52	<DL	3.55	0.90	<DL	<DL	<DL	<DL	0.20	<DL	0.46	8.59	1.16	3.20	0.45	2.33	0.85	0.19	0.88	0.12	0.61	0.11	0.31	<DL	0.23	<DL	<DL	<DL	4.00	<DL	<DL	<DL	<DL	<DL	8.50		0.69	0.49
	84	3.5	< D.L.	5.47	3.1	0.3		0.72	< D.L.	5.32	67.5	3.06	0.25	0.01				0.14	< D.L.	< D.L.	< D.L.		0.29	12.05	1.33	3.27	0.46	2.12	0.78	0.16	0.89	0.11	0.60	0.10	0.24	0.03	0.19	0.02	< D.L.	< D.L.						0.16	11.13	0.06	0.87	0.97
EH-42a(R1)	70.7	1.96	10.9	1.06	2.42	0.23	<DL	1.00	0.3	3.35	68.1	1.59	0.57	<DL	0.86	1.37	<DL	<DL	<DL	0.40	<DL	<DL	0.22	7.22	0.76	1.95	0.27	1.10	0.25	<DL	0.29	<DL	0.22	<DL	0.13	<DL	0.10	<DL	<DL	<DL	6.28	<DL	<DL	<DL	<DL	<DL	2.44		0.27	0.29
EH-42b(R4)	77	< D.L.	< D.L.	1.21	3.2	0.92		2.84	< D.L.	4.22	68.1	1.84	0.61	0.05				0.47	< D.L.	< D.L.	< D.L.		0.19	5.86	0.94	2.20	0.31	1.39	0.29	0.05	0.32	0.03	0.22	0.03	0.11	0.02	0.06	0.01	< D.L.	0.00						0.05	2.16	0.02	0.31	0.30
D35-1(R1)																																																		
D35-1(R2)																																																		
A34-1-C4																																																		
A34-1-Cal																																																		
A34-2(R4)a																																																		
A34-2(R4)b																																																		
A34-2-C4																																																		
EH-14	71	< D.L.	< D.L.	1.09	0.6	0.93		0.87	0.30	0.25	72.2	0.92	0.13	0.01				0.15	< D.L.	< D.L.	< D.L.		0.11	14.05	0.52	0.63	0.19	0.47	0.17	0.01	0.13	0.01	0.13	0.02	0.14	0.08	0.01	0.00	< D.L.	0.06						0.15	0.55	0.10	0.16	0.07
M34-1(R1)																																																		
M34-2-C2																																																		
M34-3(R1)																																																		
M34-4(R1)																																																		
M34-4-C2																																																		
EH-11	77	< D.L.	< D.L.	0.66	8.7	1.2		8.33	< D.L.	0.15	245.2	1.74	0.57	0.04				0.57	< D.L.	< D.L.	< D.L.		< D.L.	21.44	0.57	0.63	0.10	0.41	0.12	0.01	0.14	0.01	0.10	0.01	0.07	0.03	0.02	< D.L.	< D.L.	0.01						0.04	1.34	0.03	< D.L.	0.17
	81.7	1.25	8.00	0.41	1.54	<DL	<DL	0.21	0.3	0.06	139	1.14	<DL	<DL	0.10	1.35	<DL	<DL	<DL	<DL	<DL	<DL	<DL	8.13	0.57	0.63	0.09	0.38	0.07	<DL	0.11	<DL	0.08	<DL	<DL	<DL	<DL	<DL	<DL	<DL	1.70	<DL	<DL	<DL	<DL	<DL	0.85		0.01	0.20
EH-12	76	< D.L.	< D.L.	0.63	1.4	0.35		2.34	< D.L.	0.13	37.6	0.96	0.12	0.02				0.01	< D.L.	< D.L.	< D.L.		< D.L.	< D.L.	0.56	0.56	0.07	0.33	0.06	< D.L.	0.10	0.00	0.08	< D.L.	0.00	< D.L.	0.00	< D.L.	< D.L.	< D.L.							< D.L.	0.35	< D.L.	< D.L.	0.12
	74.7	1.31	9.56	0.21	1.15	<DL	<DL	0.18	0.3	0.14	43.1	1.09	<DL	<DL	0.13	1.39	<DL	<DL	<DL	<DL	<DL	<DL	<DL	3.40	0.57	0.57	0.08	0.31	<DL	<DL	0.09	<DL	0.07	<DL	<DL	<DL	<DL	<DL	<DL	<DL	1.39	<DL	<DL	<DL	<DL	<DL	0.58		0.01	0.26
M34(1)-1-CC																																																		
M34(1)-2(R2)																																																		
EH-49	98	< D.L.	< D.L.	0.29	1.1	0.25		2.95	< D.L.	0.21	51.0	1.76	< D.L.	0.01				0.00	< D.L.	< D.L.	< D.L.		< D.L.	1.08	1.07	0.99	0.09	0.54	0.06	< D.L.	0.14	0.00	0.11	< D.L.	< D.L.	< D.L.	0.03	< D.L.	< D.L.	< D.L.							< D.L.	< D.L.	< D.L.	< D.L.	0.01
D33-C2a																																																		
D33-C2b																																																		

TWN	Well ID	Pool	Original sample set	Depth (ft)	Depth (m)	Stratigraphic unit	Core samples	Thin sections	Sample ID	Sample type	Gas composition CH₄	H₂S	CO₂	Original δ¹³C ‰ PDB	δ¹⁸O ‰ PDB	SK+adjusted δ¹³C ‰ PDB	δ¹⁸O ‰ PDB	⁸⁷Sr/⁸⁶Sr	CaCO₃ mol% XRD	6/4Pb	7/4Pb	8/4Pb	Ca	Mg	Li	Be	B	Na	Al	Si	P	K	Ti	Sc	V	Cr	Fe
						Standard			NBS - 18 (1)							-4.92	-22.92																			
						Standard			NBS - 18 (2)							-4.91	-23.21																			
						Standard			NBS - 18 (3)							-5.03	-22.91																			
						Standard			NBS - 18 (4)							-5.15	-23.04																			
						Standard			NBS - 18 (5)							-4.96	-22.92																			
						Standard			NBS - 18 (6)							-5.2	-22.86																			
						Standard			NBS - 19 (1)							1.99	-2.29																			
						Standard			NBS - 19 (2)							2	-2.31																			
						Standard			NBS - 19 (3)							1.94	-2.15																			
						Standard			NBS - 19 (4)							1.95	-2.2																			
						Standard			NBS - 19 (5)							1.98	-2.3																			
						Standard			NBS - 19 (6)							1.94	-2.18																			